

N 68-35985

FACILITY FORM 602

(ACCESSION NUMBER)
515
(PAGES)
/

(THRU)
(CODE)
31
(CATEGORY)

NASA CONTRACTOR REPORT



NASA CR-66678-6

NASA CR-66678-6

GPO PRICE \$ _____

CFSTI PRICE(S) \$ _____

Hard copy (HC) _____

Microfiche (MF) _____

653 July 65

MARS HARD LANDER CAPSULE STUDY

Volume IV Capsule Point Designs and Supporting Analysis

Prepared by

GENERAL ELECTRIC
RE-ENTRY SYSTEMS

for Langley Research Center



31 JULY 1968

NATIONAL AERONAUTICS AND SPACE ADMINISTRATION-WASHINGTON, D. C.

MARS HARD LANDER CAPSULE STUDY

**Volume IV
(Book #2)**

CAPSULE POINT DESIGNS AND SUPPORTING ANALYSIS

Distribution of this report is provided in the interest of information exchange. Responsibility for the contents resides in the author or organization that prepared it.

Issued by Originator as General Electric Document No. 68SD952-6 (Vol. IV, Book 2)

PREPARED UNDER CONTRACT NO. NAS 1-8098 BY

GENERAL  ELECTRIC

RE-ENTRY SYSTEMS
3198 Chestnut Street, Philadelphia, Pa. 19101

**FOR
LANGLEY RESEARCH CENTER**

NATIONAL AERONAUTICS & SPACE ADMINISTRATION

FOREWORD

The Mars "Hard Lander" Study Final Report is divided into four volumes and bound in eight books. The titles of the volumes and a brief description of the contents of each book are presented below.

VOLUME I - SUMMARY (CR-66678-1)

Volume I contains a summary of the study activity, the conclusions reached, and a description of a possible design implementation suggested by the study results.

This study indicates that meaningful scientific payloads of approximately 1500 pounds can be placed on the Mars surface, survive for several months, and transmit more than a hundred million bits of data to Earth.

In addition, the study provided data which shows that a smaller Capsule of 700 to 900 pounds has the ability to transmit approximately 10 million bits of imagery and additional scientific surface data.

VOLUME II - MISSION AND SCIENCE DEFINITION (CR-66678-2)

Volume II contains a description of the 'reference' mission plans, both direct entry and out-of-entry, the mission analyses conducted to define the reference plans, the assumed Mars models considered, and the science definition tasks accomplished to select entry and surface science packages/measurement sequences specifically designed to satisfy LRC's scientific goals.

VOLUME III - CAPSULE PARAMETRIC STUDY (CR-66678-3, -4)

A discussion of the analysis and results derived in determining the Capsule subsystems' design characteristics parametrically is provided for the range of assumed Mars Models and the reference mission plans. The synthesis of these subsystems into complete Capsule systems is presented in terms of Capsule performance, total imagery data obtainable, and surface lifetime.

CR-66678-3 presents the Capsule System Parametric Synthesis and Entry and Retardation Subsystem Studies. CR-66678-4 presents both studies of the Lander and Re-entry Subsystems and Appendices associated with the Parametric Study.

VOLUME IV- CAPSULE POINT DESIGNS AND SUPPORTING ANALYSES (CR-66678-5, -6, -7, -8)

Volume IV contains a presentation of the detailed Capsule 'Point Designs', and their supporting analyses, derived to identify specific hardware approaches, weights, and system configurations; and confirm the correctness of the parametric results. In addition to the Capsule's engineering and design details, the results include development status, probability of success, and constraints imposed on the Orbiter by the Capsule mission.

CR-66678-5 contains a definition of the Capsule Point Design Requirements and descriptions of Point Designs 1 and 2. CR-66678-6 contains descriptions of Point Designs 3 and 4 and CR-66678-7 of Point Designs 5 and 6. CR-66678-8 provides additional information on Impact Attenuation, Surface Environment Definition, Effects on Point Designs due to Variations in Assumed Design Parameters as well as the Effects of a Lander on the Mariner Orbiter.

TABLE OF CONTENTS

BOOK 2

Section	Page
5 POINT DESIGN 3	5-1
5.1 Mission Sequence	5-1
5.2 Capsule System Design Description	5-9
5.2.1 Science Data Reference	5-11
5.2.2 Capsule System Configuration	5-12
5.2.3 Capsule Systems Weight	5-12
5.2.4 Functional Block Diagrams	5-17
5.2.5 Power Profiles, Point 3 Design	5-18
5.3 Pre-Entry Systems.	5-25
5.3.1 Canister	5-25
5.3.2 Pressure and Venting System	5-32
5.3.3 Separation Subsystem	5-36
5.3.4 Environmental Control	5-46
5.3.5 De-orbit Propulsion System	5-49
5.3.6 Electrical Equipment - Pre-entry	5-53
5.3.7 De-orbit System	5-55
5.3.8 Pre-entry Systems Weight	5-59
5.4 Entry Systems	5-60
5.4.1 Configuration	5-60
5.4.2 Heat Shield	5-64
5.4.3 Aeroshell and Structure	5-72
5.4.4 Lander/Aeroshell Separation	5-79
5.4.5 Entry Systems Equipment	5-79
5.4.6 Retardation Subsystem	5-79
5.4.7 Roll Control Subsystem	5-104
5.4.8 Entry Systems Weight	5-106
5.5 Lander Systems	5-107
5.5.1 Configuration Constraints and Descriptions	5-107
5.5.2 Science Payload Equipments	5-113
5.5.3 Telecommunications	5-127
5.5.4 Electrical Power Equipment	5-172
5.5.5 Environmental Control	5-187
5.5.6 Deployment Mechanisms	5-192
5.5.7 Lander Container Structure	5-203
5.5.8 Impact Attenuation and Structure	5-209
5.5.9 Mass Property and Inertia Data	5-229
5.6 Constraints Imposed on Orbiter	5-231
5.7 Probability of Success - Point Design 3	5-236
5.7.1 Introduction	5-236
5.7.2 Results	5-236
5.7.3 Capsule Analysis	5-237
5.7.4 Orbiter Support Analysis	5-246
5.8 References	5-247

TABLE OF CONTENTS (Continued)

Section	Page
6. POINT DESIGN 4	6-1
6.1 Mission Sequence	6-1
6.2 Capsule System Design Description	6-9
6.2.1 Science Data Reference	6-12
6.2.2 Capsule System Configuration	6-13
6.2.3 Capsule System Weight	6-13
6.2.4 Functional Block Diagrams	6-17
6.2.5 Power Profiles Point Design 4	6-23
6.3 Pre-entry Systems	6-26
6.3.1 Canister	6-26
6.3.2 Pressure and Vent System	6-34
6.3.3 Separation Subsystem	6-38
6.3.4 Environmental Control	6-48
6.3.5 De-orbit Propulsion Equipment.	6-51
6.3.6 Electrical Equipment, Pre-entry	6-55
6.3.7 De-orbit System	6-57
6.3.8 Pre-entry Systems Weight	6-61
6.4 Entry Systems	6-62
6.4.1 Configuration	6-62
6.4.2 Heat Shield	6-66
6.4.3 Aeroshell and Structure	6-71
6.4.4 Lander/Aeroshell Separation	6-80
6.4.5 Entry Systems Equipment	6-80
6.4.6 Retardation Subsystem	6-82
6.4.7 Roll Control Subsystem	6-106
6.4.8 Entry Systems Weight	6-107
6.5 Lander Systems	6-109
6.5.1 Configuration Constraints and Description	6-109
6.5.2 Science Payload Equipments	6-116
6.5.3 Telecommunications	6-130
6.5.4 Electrical Power Equipment	6-176
6.5.5 Environmental Control	6-189
6.5.6 Deployment Mechanisms	6-194
6.5.7 Lander Container Structure	6-203
6.5.8 Impact Attenuation and Structure.	6-211
6.5.9 Mass Property and Inertia Data	6-227
6.6 Constraints Imposed on Orbiter	6-231
6.7 Probability of Success, Point Design 4	6-235
6.7.1 Introduction	6-235
6.7.2 Results	6-235
6.7.3 Capsule Analysis	6-236
6.7.4 Orbiter Support Analysis	6-244
6.8 References	6-245

LIST OF ILLUSTRATIONS

Figure		Page
5.1-1	Operational Flight Sequence From Separation to Impact	5-5
5.1-2	Landed Operation	5-7
5.2.2-1	Mars Hard Lander, Point Design 3	5-15
5.2.4-1	Electrical System Signal and Power, Functional Block Diagram . . .	5-19
5.2.5-1	Power Profile, Point Design 3	5-23
5.3.1-1	Aeroshell/Canister Clearances	5-26
5.3.1-2	Inboard Profile, Point Design 3	5-27
5.3.1-3	Canister Field Joint	5-30
5.3.1-4	Required Ring Inertia for Stability as a Function of Critical Load . .	5-31
5.3.2-1	Pressure and Venting System, Block Diagram	5-33
5.3.2-2	Flow Rate and Differential Pressure vs Time After Lift-off	5-35
5.3.3-1	Separation Subsystem, Block Diagram	5-38
5.3.3-2	Hot-Wire Tension Bolt	5-41
5.3.3-3	Capsule Separation Adjustment Spring Assembly	5-41
5.3.3-4	Aft Canister Ring	5-43
5.3.3-5	Forward Canister Ring	5-44
5.3.4-1	Super Insulation Requirements to Maintain 310° R on Compart- ment Wall and Heat Shield	5-47
5.3.4-2	Transit Mode Power and Insulation Requirements for Varying Canister Areas	5-48
5.3.5-1	Monopropellant System Schematic	5-52
5.3.5-2	De-orbit Propulsion Structure	5-54
5.3.5-3	Thrust Cone Separation	5-55
5.3.7-1	Spin and Roll Control Subsystem, Block Diagram	5-57
5.4.1-1	Aeroshell Geometry, Point Design 3	5-62
5.4.2-1	Cold Wall Convective and Radioactive Heat Flux Histories, Point Design 3	5-66
5.4.2-2	Heat Shield Thickness Requirements, Point Design 3	5-68
5.4.2-3	Surface and Backface Temperature Histories, Point Design 1	5-69
5.4.2-4	Temperature Gradients Through the Shield, Point Design 1	5-70
5.4.3-1	Axial Deflection - Aeroshell 2A vs Radial Distance	5-73
5.4.3-2	Axial Bending Moment (M_x) - Aeroshell 2A vs Radial Distance	5-73
5.4.3-3	Shell Transverse Shear - Aeroshell 2A vs Radial Distance	5-74

LIST OF ILLUSTRATIONS (Continued)

Figure	Page
5.4.3-4 Axial In-Plane Load - Aeroshell 2A vs Radial Distance	5-74
5.4.3-5 Axial Honeycomb Facing Stress - Aeroshell 2A vs Radial Distance . .	5-75
5.4.3-6 Performance Characteristics of 2024-T4	5-76
5.4.3-7 Mechanical Design Yield Strength for 2024-T4.	5-76
 5.4.4-1 Lander Installation Into Aeroshell	 5-80
5.4.5-1 Entry Systems Instrumentation.	5-81
5.4.6-1 Pilot Deployment Trajectory Study, Point Design 3	5-85
5.4.6-2 Point Design 3 Main Parachute Trajectory in VM-8 Atmosphere . . .	5-88
5.4.6-3 Retardation Deployment Sequence	5-93
5.4.6-4 Altitude Marking Radar, Functional Block Diagram	5-96
5.4.6-5 Geometry of AMR Return Signal	5-98
5.4.6-6 Pattern through Axis and Plane of Antennas on Aeroshell	5-99
5.4.6-7 Roll Pattern, Radar Antenna on Aeroshell	5-100
5.4.6-8 E and H Patterns of Antenna on Vehicle Body	5-102
 5.5.1-1 General Assembly, Point Design 3	 5-111
5.5.2-1 Water Vapor Detector, Block Diagram	5-117
5.5.2-2 Wind Velocity Sensor	5-121
5.5.2-3 Alpha Back Scatter Instrument	5-122
5.5.2-4 High and Low Speed TV Cameras	5-124
5.5.2-5 Silicon Photo-Voltaic Cell Spectral Response	5-125
5.5.2-6 Rotary Potentiometer Clinometer	5-125
 5.5.3-1 Telecommunications Subsystem, Functional Block Diagram	 5-128
5.5.3-2 Reference Orbit Communication Parameters	5-134
5.5.3-3 Available Data Rate vs Time with Adverse Tolerances	5-134
5.5.3-4 Relay and Beacon Link, Block Diagram	5-135
5.5.3-5 400 MHz Antenna Pattern	5-143
5.5.3-6 Receiving Antenna Pattern and Configuration	5-144
5.5.3-7 Transmitting Antenna Pattern and Configuration	5-145
5.5.3-8 400 MHz Transmitter, Block Diagram.	5-146
5.5.3-9 Duplexer and Antenna Selector	5-148
5.5.3-10 Beacon Receiver	5-149
5.5.3-11 Orbiter 400 MHz Radio Subsystem	5-151
5.5.3-12 S-band Transponder, Functional Diagram	5-153
5.5.3-13 X30 Module of the Transmitter Exciter, Block Diagram	5-155
5.5.3-14 Data Handling System	5-160
5.5.3-15 Operation of Command Storage Control Unit	5-163
5.5.3-16 Command Word Format	5-164
5.5.3-17 Command Detector	5-165

LIST OF ILLUSTRATIONS (Continued)

Figure	Page
5.5.3-18 Entry Data Storage Routine	5-168
5.5.4-1 Electrical Power Subsystem, Point Design 3, Block Diagram	5-173
5.5.4-2 Battery Redundancy Circuit	5-175
5.5.5-1 90-Day Lander Heater Power Requirements for Thermal Battery Control, Minimum Environment	5-188
5.5.5-2 90-Day Lander Heater Power Requirements for Thermal Battery Control, Maximum Environment	5-189
5.5.5-3 90-Day Lander Payload Temperature Response, Minimum Environment.	5-190
5.5.5-4 90-Day Lander Payload Temperature Response, Maximum Environment.	5-191
5.5.6-1 Camera Deployment, Including Wind Velocity and Temperature Transducers.	5-193
5.5.6-2 Operation of Alpha Back Scatter Deployment Mechanism.	5-196
5.5.6-3 Solar Array (Basic Scheme).	5-199
5.5.6-4 Solar Array (Alternate Scheme)	5-202
5.5.7-1 Structure	5-205
5.5.7-2 Three Conditions Used for Preliminary Loading Analysis (Multi-directional)	5-207
5.5.7-3 Typical Interaction Radial Loads Between Torus and Cylinder, Edge-on Condition	5-207
5.5.7-4 Typical Interaction Moment Between Torus and Cylinder, Edge-on Condition	5-208
5.5.7-5 Typical Interaction Shear Flow Between Torus and Cylinder, Edge-on Condition	5-208
5.5.8-1 Lander Attenuation, Point Design 3.	5-212
5.5.8-2 Gross Cross-sectional Area vs Stroke	5-214
5.5.8-3 Effective Cross-sectional Area vs Stroke	5-214
5.5.8-4 Design Guide for Reduction in Honeycomb Properties for Non- axial Impacts	5-215
5.5.8-5 Comparison of Crushing Stress vs Angle-of-Impact for Static and Dynamic Loading.	5-215
5.5.8-6 Stroke Efficiency vs Bulk Density	5-217
5.5.8-7 Crushing Planes for Stroke Analysis	5-217
5.5.8-8 Typical Crush-up Condition Analyzed for Multi-directional Lander Showing Sway and Slope Angle Effects	5-218
5.5.8-9 Stroke Efficiency	5-218
5.5.8-10 Crushable Honeycomb Properties	5-220
5.5.8-11 General Internal Geometry for Point Design 3.	5-220
5.5.8-12 Layup Honeycomb Attenuator (Multi-direction)	5-225
5.6-1 Capsule/Bus Interface	5-233

LIST OF ILLUSTRATIONS (Continued)

Figure		Page
6.1-1	Operational Flight Sequence from Separation to Impact.	6-5
6.1-2	Landed Operations	6-7
6.2.2-1	Mars Hard Lander, Point Design 4	6-15
6.2.4-1	Point Design 4 Functional Block Diagram.	6-19
6.2.5-1	Point Design 4 Power Profile.	6-24
6.3.1-1	Aeroshell/Canister Clearances	6-27
6.3.1-2	Point Design 4 Inboard Profile	6-29
6.3.1-3	Canister Field Joint	6-32
6.3.1-4	Required Ring Inertia for Stability as a Function of Critical Load. . .	6-33
6.3.2-1	Pressure and Venting Subsystem Block Diagram	6-35
6.3.2-2	Flow Rate and Differential Pressure vs Time After Lift-off	6-37
6.3.3-1	Separation Subsystem Block Diagram	6-40
6.3.3-2	Hot-wire Tension Bolt	6-43
6.3.3-3	Capsule Separation Adjustable Spring Assembly	6-43
6.3.3-4	Aft Canister Ring	6-44
6.3.3-5	Forward Canister Ring	6-45
6.3.4-1	Super Insulation Requirements to Maintain 310° R on Compart- ment Wall and Heat Shield	6-49
6.3.4-2	Transit Mode Power and Insulation Requirements for Various Canister Areas.	6-50
6.3.5-1	Monopropellant System	6-54
6.3.5-2	De-orbit Propulsion Installation	6-56
6.3.5-3	Thrust Cone Separation.	6-57
6.3.7-1	Spin and Roll Control Subsystem Block Diagram	6-59
6.4.1-1	Aeroshell Geometry Point Design 4.	6-65
6.4.2-1	Cold Wall Convective and Radiative Heat Flux Histories Point Design 2B	6-68
6.4.2-2	Point Design 2B, Heat Shield Thickness Requirements	6-70
6.4.2-3	Surface and Backface Temperature Histories, Point Design 2B	6-72
6.4.2-4	Temperature Gradients Through the Shield Point Design 2B ESM 1004AP.	6-73
6.4.3-1	Axial Deflection, Aeroshell 2A vs Radial Distance	6-75
6.4.3-2	Axial Bending Moment (M_x), Aeroshell 2A vs Radial Distance	6-75

LIST OF ILLUSTRATIONS (Continued)

Figure	Page
6.4.3-3 Shell Transverse Shear, Aeroshell 2A vs Radial Distance	6-76
6.4.3-4 Axial In-plane Load, Aeroshell 2A vs Radial Distance	6-76
6.4.3-5 Axial Honeycomb Facing Stress, Aeroshell 2A, vs Radial Distance. .	6-77
6.4.3-6 Point Design 2A Shield-Structure Interface Temperature	6-79
6.4.4-1 Lander Installation in the Aeroshell.	6-81
6.4.5-1 Entry System Instrumentation.	6-83
6.4.6-1 Point Design 4 Pilot Deployment Trajectory Study	6-86
6.4.6-2 Point Design 4 Main Parachute Trajectory in VM-8 Atmosphere . . .	6-88
6.4.6-3 Retardation System Sequence of Events	6-95
6.4.6-4 Altitude Marking Radar Functional Block Diagram.	6-98
6.4.6-5 Geometry of AMR Return Signal	6-99
6.4.6-6 Pattern Thru Axis and Plane of Antennas on Aeroshell	6-101
6.4.6-7 Roll Pattern Radar Antenna on Aeroshell	6-102
6.4.6-8 E and H Plane Patterns of Antenna on Vehicle Body	6-104
6.5.1-1 General Assembly, Point Design 4	6-113
6.5.2-1 Water Vapor Detector, Block Diagram	6-121
6.5.2-2 Wind Velocity Sensor	6-122
6.5.2-3 Alpha Back Scatter Instrument	6-123
6.5.2-4 High and Low Speed TV Cameras	6-125
6.5.2-5 Silicon Photo-Voltair Cell Spectral Response	6-129
6.5.2-6 Rotary Potentiometer Clinometer	6-129
6.5.3-1 Telecommunications Subsystem, Functional Block Diagram	6-131
6.5.3-2 First Orbit Pass Communication Parameters	6-136
6.5.3-3 Available Data Rate vs Time with Adverse Tolerances, Entry Pass and Nominal Orbital Passes	6-137
6.5.3-4 Available Data Rate vs Time with Adverse Tolerances, First Orbiter Pass, -3.4 hr Period Error	6-138
6.5.3-5 Available Data Rate vs Time with Adverse Tolerances First Orbiter Pass, +3.4 hr Period Error.	6-139
6.5.3-6 Relay and Beacon Link, Block Diagram	6-141
6.5.3-7 400 MHz Antenna Pattern	6-148
6.5.3-8 Circularly Polarized S-band Antenna (90° Coverage)	6-149
6.5.3-9 Calculated Approximate 90° S-band Antenna Pattern	6-150
6.5.3-10 400 MHz Transmitter, Block Diagram.	6-151
6.5.3-11 Duplexer and Antenna Selector	6-153
6.5.3-12 400 MHz Receiver, Block Diagram	6-153
6.5.3-13 Orbiter 400 MHz Radio Subsystem	6-156
6.5.3-14 S-band Transponder, Functional Diagram	6-158
6.5.3-15 X-30 Module of the Transmitter Exciter, Block Diagram	6-160

LIST OF ILLUSTRATIONS (Continued)

Figure		Page
6.5.3-16	Data Handling System	6-165
6.5.3-17	Operation of Command Storage Control Unit	6-168
6.5.3-18	Command Word Format	6-169
6.5.3-19	Command Detector, Block Diagram	6-170
6.5.3-20	Entry Data Storage Routine	6-173
6.5.4-1	Electrical Power Subsystem Block Diagram, Point Design 4 . . .	6-177
6.5.4-2	Battery Redundancy Circuit	6-179
6.5.5-1	90-Day Lander Heater Power Requirements for Thermal Battery Control, Minimum Environment	6-190
6.5.5-2	90-Day Lander Heater Power Requirements for Thermal Battery Control, Maximum Environment	6-191
6.5.5-3	90-Day Lander Payload Temperature Response, Minimum Environment	6-192
6.5.5-4	90-Day Lander Payload Temperature Response, Maximum Environment	6-193
6.5.6-1	Camera Deployment Including Wind Velocity and Temperature Transducers	6-195
6.5.6-2	Operation of Alpha Back Scatter Deployment Mechanism	6-198
6.5.6-3	Solar Array (Basic Scheme)	6-201
6.5.6-4	Solar Array (Alternate Scheme)	6-204
6.5.7-1	Structure	6-205
6.5.7-2	Three Conditions Used for Preliminary Loading Analysis	6-209
6.5.7-3	Typical Interaction Radius Loads Between Torus and Cylinder, Edge-on Condition	6-209
6.5.7-4	Typical Interaction Moments Between Torus and Cylinder, Edge-on Condition	6-210
6.5.7-5	Typical Interaction Shear Flow Between Torus and Cylinder, Edge-on Condition	6-210
6.5.8-1	Lander Attenuation, Point Design 4	6-214
6.5.8-2	Gross Cross Sectional Area vs Stroke for the Multi-directional Lander	6-216
6.5.8-3	Effective Cross-section Area vs Stroke	6-216
6.5.8-4	Design Guide for Reduction in Honeycomb Properties for Non-axial Impacts	6-217
6.5.8-5	Comparison of Crushing Stress vs Angle of Impact for Static and Dynamic Loading	6-217
6.5.8-6	Stroke Efficiency vs Bulk Density	6-219
6.5.8-7	Crushing Planes for Stroke Analysis	6-219
6.5.8-8	Typical Crush-up Condition Analyzed for Multidirectional Lander Showing Sway and Slope Angle Effects	6-220
6.5.8-9	Illustration of Stroke Efficiency	6-220

LIST OF ILLUSTRATIONS (Continued)

Figure	Page
6.5.8-10 Crushable Honeycomb Properties	6-222
6.5.8-11 General Internal Geometry for Point Design 4	6-222
6.5.8-12 Layup of Honeycomb Attenuator (Multi-directional)	6-225
6.6-1 Capsule/Bus Interface.	6-233

LIST OF TABLES

Table		Page
5.1-1	Mission Sequence of Events - Point Design 3	5-1
5.2-1	Comparative Weight Summary of Minimum Mission Systems	5-11
5.2-2	Science Weight Summary	5-13
5.2-3	Weight and Inertia Composition - Point Design 3	5-17
5.3.1-1	Interface Ring Loads	5-29
5.3.3-1	Separation Spring Data	5-46
5.3.5-1	Performance, Weight, and Envelope Data	5-50
5.3.7-1	Spin and Roll Control Requirements, Point Design 3	5-56
5.3.8-1	Pre-entry Systems Weight Summary, Point Design 3	5-59
5.4.1-1	CONSEP Results for Point Design 3	5-61
5.4.1-2	Point Design Loads	5-63
5.4.2-1	Entry Conditions and Geometry of Point Designs 1 through 6	5-65
5.4.2-2	Thermophysical Properties of ESM Materials	5-67
5.4.2-3	Shield Thickness Requirements for Point Designs 1 through 6	5-71
5.4.3-1	Final Aluminum Honeycomb Requirements for Aeroshells	5-72
5.4.3-2	Point Design Entry Data	5-78
5.4.6-1	Pilot Parachute Design Parameters	5-87
5.4.6-2	Main Parachute Design Parameters	5-87
5.4.6-3	Point Design 3 Parachute Trajectory Parameters	5-89
5.4.6-4	Functional Parameters	5-103
5.4.6-5	Radar Altimeter Parameters	5-103
5.4.6-6	Retardation System Weight Breakdown	5-104
5.4.7-1	Spin and Roll Control Subsystem Fixed Hardware Weight, Point Design 3	5-105
5.4.7-2	Spin and Roll Control Subsystem, Point Design 3 Parameters.	5-106
5.4.8-1	Entry System Weight Summary, Point Design 3	5-106
5.5.2-1	Entry Science Payload	5-114
5.5.2-2	Surface Science Payload	5-119
5.5.2-3	Typical Camera Specifications	5-126
5.5.3-1	Design Summary	5-129
5.5.3-2	Telecommunications Sequence	5-131
5.5.3-3	Measurements List	5-132
5.5.3-4	Data Transmitted	5-132
5.5.3-5	Design Control Tables - Relay (Landed) and Beacon	5-136
5.5.3-6	Entry Link Design Control Table	5-138
5.5.3-7	Data Transferable After Impact Plus 2.5 Min (Bits/10 ⁷)	5-139
5.5.3-8	S-Band Design Control Table	5-141
5.5.3-9	Receiver Performance Parameters	5-157
5.5.3-10	Exciter Performance Parameters	5-158
5.5.3-11	Entry Data	5-167
5.5.3-12	Landed Science (Non-Imaging)	5-169
5.5.3-13	Physical Characteristics	5-171
5.5.4-1	Electrical Equipment Hardware Matrix, Point Design 3	5-178
5.5.9-1	Weight Summary	5-226

LIST OF TABLES (Continued)

Table		Page
5.5.9-2	Detailed Weight Breakdown ~ Subsystems and Components	5-227
5.6-1	Major Subsystem Changes	5-232
5.6-2	Orbiter Propulsion Summary	5-235
5.7.2-1	Mission Success Probability, Point Design 3	5-236
5.7.3-1	Reliability Estimates, Point Design 3 Components	5-241
5.7.3-2	Reliability Summary, Point Design 3 Capsule System and Subsystem	5-244
6.1-1	Mission Sequence of Events, Point Design 4	6-1
6.2-1	Comparative Weight Summary of Minimum Mission Systems	6-11
6.2-2	Science Weight Summary	6-12
6.2-3	Weight and Inertia Composition, Point Design 4	6-17
6.3.1-1	Interface Ring Load	6-31
6.3.3-1	Separation Spring Data	6-47
6.3.5-1	Performance, Weight and Envelope	6-52
6.3.7-1	Spin and Roll Control Requirements	6-58
6.3.8-1	Pre-entry System Weight Summary, Point Design 4	6-61
6.4.1-1	CONSEP Results for Point Design 4	6-62
6.4.1-2	Point Design Loads	6-64
6.4.2-1	Entry Conditions and Geometry of Point Designs 1 through 6	6-67
6.4.2-2	Thermophysical Properties of ESM Materials	6-69
6.4.2-3	Shield Thickness Requirements for Point Designs 1 through 6	6-74
6.4.3-1	Final Aluminum Honeycomb Requirements for Aeroshells	6-77
6.4.3-2	Point Design Entry Data	6-78
6.4.6-1	Pilot Parachute Design Parameters	6-87
6.4.6-2	Main Parachute Design Parameters	6-90
6.4.6-3	Point Design 4 Parachute Trajectory Parameters	6-90
6.4.6-4	Retardation System Weight Breakdown	6-105
6.4.6-5	Functional Parameters	6-105
6.4.6-6	Radar Altimeter Parameters	6-106
6.4.7-1	Spin and Roll Control Subsystem Fixed Hardware Weight, Point Design 4	6-107
6.4.7-2	Spin and Roll Control Subsystem Parameters, Point Design 4	6-108
6.4.8-1	Entry System Weight Summary, Point Design 4	6-108
6.5.2-1	Entry Science Payload	6-118
6.5.2-2	Surface Science Payload	6-126
6.5.2-3	Typical Camera Specifications	6-128
6.5.3-1	Design Summary	6-130
6.5.3-2	Telecommunications Sequence	6-133
6.5.3-3	Measurements List	6-134
6.5.3-4	Data Transmitted	6-135
6.5.3-5	Design Control Tables - Relay (Landed) and Beacon	6-140
6.5.3-6	Data Transferable After Impact Plus 2.5 Min ⁽¹⁾	6-142
6.5.3-7	Entry Link Design Control Table	6-145
6.5.3-8	S-band Design Control Table	6-147

LIST OF TABLES (Continued)

Table		Page
6.5.3-9	Receiver Performance Parameters	6-162
6.5.3-10	Exciter Performance Parameters	6-163
6.5.3-11	Entry Data	6-172
6.5.3-12	Landed Science (Non-imaging)	6-174
6.5.3-13	Physical Characteristics	6-175
6.5.4-1	Point Design 4 Electrical Equipment Hardware Matrix	6-182
6.5.9-1	Weight Summary	6-227
6.5.9-2	Detailed Weight Breakdown, Subsystems and Components	6-228
6.6-1	Major Subsystem Changes	6-232
6.7.2-1	Mission Success Probability, Point Design 4	6-235
6.7.3-1	Reliability Estimates, Point Design 4 Components	6-240
6.7.3-2	Reliability Summary, Point Design 4 Capsule System and Subsystem	6-243

5. POINT DESIGN 3

5. POINT DESIGN 3

5.1 MISSION SEQUENCE

The operational flight sequence for the interval from start of separation operations to impact is illustrated by fig. 5.1-1. This profile depicts the sequence of events for the out-of-orbit mission of Point Design 3. A more detailed sequence of events, from launch to mission completion, is shown for this mission in table 5.1-1. Fig. 5.1-2 illustrates the landed operations for the first full diurnal cycle.

Point Design 3 is an out-of-orbit mission with a nominal interplanetary flight time of 244 days and a Mars orbital flight of up to 30 days before Capsule separation. The Lander Capsule is stabilized by spin-up prior to de-orbit propulsion ignition and roll control during entry. Deceleration is accomplished by parachute, which is actuated at 20,000 ft by a radar altimeter. The Capsule is programmed to relay the data real time to the Orbiter that remains in synchronous orbit for three full diurnal cycles. Entry and surface science and surface imaging is performed at the beginning of the first cycle with data transmitted real time to the Orbiter for relay to Earth. Surface science and surface composition measurements will be continued throughout the first cycle with data stored while the Orbiter is not in periapsis communication range. Science data will be sent by direct S-band link to Earth on a daily basis. When the Orbiter returns to periapsis range it will signal the Lander and stored data will be transmitted for relay to Earth. Imaging and surface science measurements will be repeated with real time transmission to the Orbiter. Solar cell deployment occurs 1-1/2 days after landing.

Measurement and transmission modes will be repeated for the three days the Orbiter remains in support. The Orbiter then changes for a different ephemeris for separate mission activities.

The Lander continues to perform surface meteorology measurement with direct transmission to Earth by S-band T/M, for remainder of mission. Solar cells recharge the batteries for the power required in operations after the third day. The Lander includes a direct link command receiver to permit Earth to transmit variations in established sequence as desired.

TABLE 5.1-1. MISSION SEQUENCE OF EVENTS - POINT DESIGN 3

Item	Event	Time
A.	<u>Launch to Impact</u>	
1.	Launch	TL
2.	First mid course maneuver (if required)	TL + 30 days
3.	Second mid course maneuver (if required)	TL + 234 days
4.	Mars orbit insertion	TL + 244 days
5.	Start final Capsule diagnostic checkout	To (Entry-24 hr)

TABLE 5.1-1. MISSION SEQUENCE OF EVENTS - POINT DESIGN 3 (Continued)

Item	Event	Time	
6.	Complete diagnostic checkout	To + 120 min	
7.	Update programmers complete	To + 20 hr	
8.	Turn on Lander power, T/M, sequencer and diagnostic data	T1 (To + 21.7 hr)	
9.	Canister separation	T2 (T1 + 5 min)	
10.	Spacecraft maneuvers to Capsule separation attitude	T2 + 10 min	
11.	Capsule separates from Spacecraft	T3 (T2 + 10.1 min)	
12.	Initiate spin stabilization	T3 + 0.5 sec	
13.	Ignite de-orbit propulsion	T3 + 30 min	
14.	Terminate de-orbit propulsion	T3 + 30.3 min	
15.	Initiate de-spin	T3 + 30.5 min	
16.	Separate thrust cone	T3 + 30.6 min	
17.	Turn power and T/M off	T3 + 30.7 min	
18.	Turn on mass spectrometer for warmup	T4 - 15 min	
19.	Turn on T/M (low data rate), initiate accelerometer and pressure sensor readings	T4 - 60 sec	
20.	Entry	T4 (T3 + 119 min)	
21.	Mach 5 - initiate mass spectrometer, water vapor, and temperature sensor readings. Turn on radar altimeter	<u>VM-8</u>	<u>VM-9</u>
		T4+255 sec	T4+217 sec
22.	Deploy parachute (20 kft)	T4+288 sec (Mach 1.86)	T4+394 sec (Mach 0.6)
23.	Aeroshell separation	T4+298 sec	T4+404 sec
24.	Jettison parachute	T4+451 sec	T4+629 sec
25.	Impact - force sensed and transmitted to Spacecraft (with redundant storage)	T5(T4+452.5 sec)	T5(T4+630 sec)

TABLE 5.1.-1. MISSION SEQUENCE OF EVENTS - POINT DESIGN 3 (Continued)

Item	Event	Time
B.	<u>Landed Operations</u>	
1.	Diagnostic and stored entry data transmitted to Orbiter (low data rate)	T5 + 0.1 min
2.	Lander comes to rest - up direction sensed	T5 + 2 min
3.	Initiate hatch cover and boom deployments	T5 + 2.1 min
4.	Switch to high data rate transmission mode	T6 (T5 + 2.5 min)
5.	Initiate stored diagnostic, entry, and impact data transmission to Orbiter	T6 + 0.1 min
6.	Initiate imagery, meteorology, and inclinometer measurements and transmit to Orbiter for relay to Earth	T6 + 0.2 min
7.	Repeat items 5. and 6.	T6 + 8.5 min
8.	Turn off Imagery and T/M systems	T6 + 20 min
9.	Repeat surface science measurements (excluding Imagery) at 20 min intervals and store data	--
10.	Initiate surface composition (alpha scatter) measurement cycle and store data	T7 (T5 + 1 hr)
11.	Complete initial surface composition cycle	T7 + 5 hr
12.	Repeat surface composition measurements every 3 hr for one day period only	--
13.	Transmit stored science data direct to Earth by S-band T/M System	T8
14.	Receive signal that Orbiter is returning to range	T9 (T6 + 24.5 hr)
15.	Turn on T/M system (high data rate) and transmit stored science data to Orbiter	T10 (T6 + 24.6 hr)
16.	Perform imagery and surface science measurements and transmit data to Orbiter for relay to Earth	T10 + 0.1 min
17.	Repeat items 15. and 16.	T10 + 8.5 min
18.	Turn off imagery and T/M systems	T10 + 20 min
19.	Deploy solar array	T11 (T5 + 36 hr)

TABLE 5.1-1. MISSION SEQUENCE OF EVENTS - POINT DESIGN #3 (Concluded)

Item	Event	Time
20.	Repeat measurement and transmission cycles (items 13. thru 18.) for two additional days while Orbiter is in support	--
21.	Continue science measurement (no imagery) at 1 hr intervals with daily transmission direct to Earth for duration of mission*	

*Command receiver provides capability for Earth to signal variations in sequence.

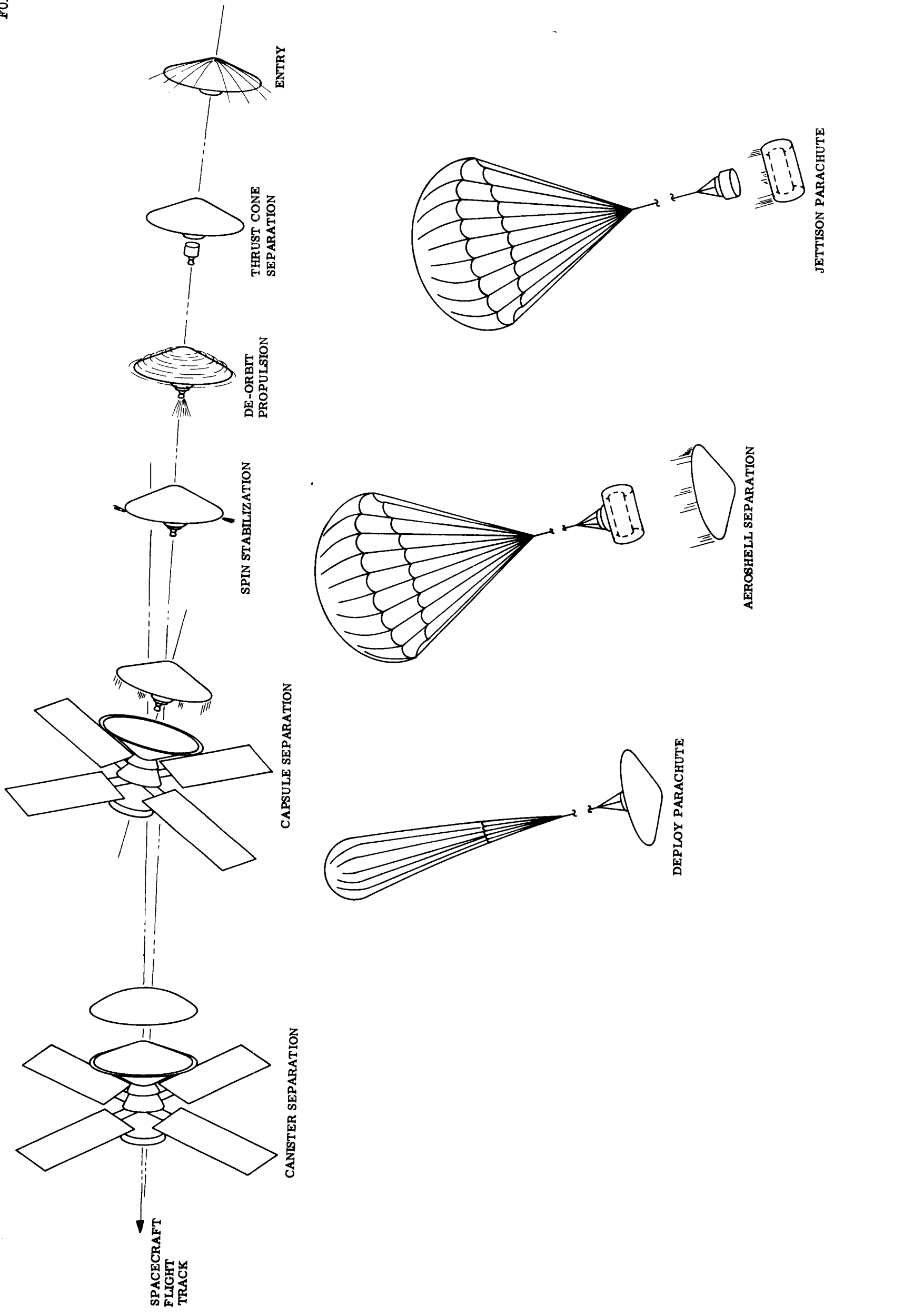


Figure 5.1-1. Operational Flight Sequence from Separation to Impact

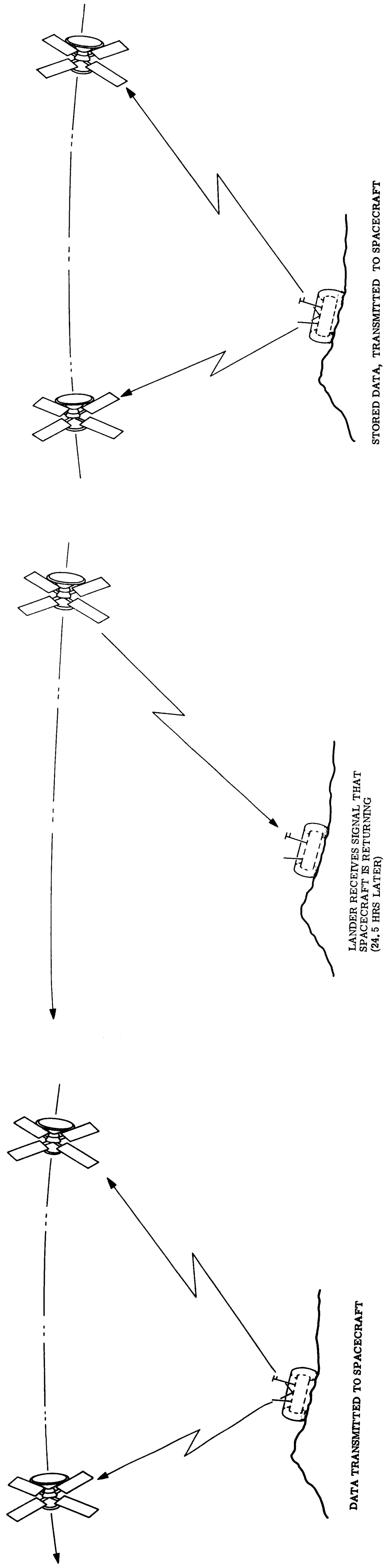


Figure 5.1-2. Landed Operation

5.2 CAPSULE SYSTEM DESIGN DESCRIPTION

A basic difference in the direct entry system and the out-of-orbit entry system in a given point design pair is that the ballistic entry parameter ($W/C_D A$) for the direct entry vehicle (20.8 kft/sec entry velocity and 25° path angle) is approximately 0.75 the value appropriate for the out-of-orbit entry system (15 kft/sec and 16° at entry). Direct entry systems entering at a path angle increased to 40° require a ballistic parameter about 0.4 smaller than the out-of-orbit vehicle.

The allowable or limiting ballistic coefficient is determined for the different entry mission modes by selecting the best combination of aeroshell drag area, parachute deployment, size and landing load attenuation in the deceleration profile to Lander touchdown. The entry system velocity must be reduced to Mach 2 before parachutes are deployed and this deceleration increment must occur at a sufficiently high altitude that the Capsule Lander System can be decelerated by parachute to the acceptable touchdown velocity increment. In this study, the ballistic entry parameter limit is determined for each entry mode based on parachute deployment in the VM-8 Mars model atmosphere (lower altitude at Mach 2) and parachute sizing for descent in the VM-7 atmosphere, the model having the lowest atmospheric density at the surface.

The effect of the limiting ballistic coefficient is that the direct entry Capsules are designed with considerably larger base diameter and heavier aeroshells than the slower entry, out-of-orbit vehicle of the point design pair. The design approach taken for each vehicle in the particular design pair is the same and the system weight difference in the launch configuration, separation and entry is primarily due to the entry shell size because it directly affects the weight of aeroshell structure and heat shield, and the canister (larger size and inertial loading).

The aeroshell designs selected for each of the six Capsule point designs incorporate blunt body, sphere cone shell structures with ablative heat shields using elastomeric formulations such as GE's ESM 1004 X at 16 lb/ft³ density for the out-of-orbit vehicles and ESM 1004 AP at 35 lb/ft³ density for the direct entry vehicles. The selected entry system structure and shield design is an extension of ICBM technology and the integrity of the approach in either soft bonded shields or film adhesive shields has been proved. The shield materials referenced are typical of the application but the exact formulation required would be specified in a more detailed engineering phase of a Mars mission program.

The Lander System of the Capsule is retained within the aeroshell by a tension strap arrangement and released by burning the wire wrap of the hot-wire bolts with 30 msec of 10 to 15 amp current. It is separated from the aeroshell by the parachute drag differential. The preferred release, separation and deceleration sequence is initiated with an altimeter. G-level switch and timing units as well as an axial g-level and base pressure measurements approach have been considered for the parachute deployment device. The altimeter approach is preferred because it can be used to delay parachute opening (below Mach 2) to match the descent time of the Lander to the view time available for communication with the Orbiter before and after landing. The requirement for shortening the descent time is most necessary if the flight was made in a VM-9 type atmosphere.

The Lander contains the instruments, power, sequencing, telemetry, and communication equipment to perform the surface science operations. The equipment is contained within a torroidal rim-stiffened cylinder equipped with a deep ring of phenolic glass, honeycomb structure sized and positioned to attenuate the landing loads by mechanical crush-up of the honeycomb material. The first point design pair developed for the minimum surface lifetime mission were prepared with both omni-directional and multi-directional Landers to develop the weight and size difference in the out-of-orbit and direct entry vehicles due to the design approach taken for impact attenuation. The difference in the weight of attenuation material between omni- and multi-landing (522 and 287 lbs, respectively) is the difference in the omni- and multi- Lander total weights (weight suspended on parachute) of 858 and 623 lb.

The weight statement of table 5.2-1 summarizes the comparison of the out-of-orbit and direct vehicles and the influence of Lander type for the minimum lifetime mission. The comparison is based on the first design pair data but the results are typical of like comparison studies of the other design pairs.

The pre-entry systems of the Capsule consist of the canister and internal adapter, attitude control and the de-orbit maneuver hardware. The prime function of the Canister is to encapsulate the Capsule system and maintain a physical, biological barrier to prevent contamination of the Capsule during:

1. The terminal sterilization cycle
2. Post sterilization operations in the ground environment
3. Launch and powered flight
4. The cruise and up to the sequence for Capsule-Orbiter separation.

The canister design approach for the six Capsule designs is a semi-monocoque construction in minimum manufacturing gauge (0.012), 7075 aluminum. The rear shell of the canister assembly contains the Capsule-to-Orbiter adapter within the sterilized envelope and connections to the Orbiter are made outside this envelope. The forward shell is released by applying 24 amps for 30 msec to the four hot-wire bolts of the V-ring type clamp segments. The shell is separated by two mechanical springs with a velocity of 2 ft/sec.

The adapter provides the structural transition between the Capsule and the Orbiter and contains the equipment for separating the flight systems. The Capsule is released by applying 48 amps to four explosive nuts and is separated at approximately 1 ft/sec by four springs.

Both spin-despin and three axis control systems were studied for Capsule attitude control for the deorbit maneuver, for entry path angle control, and for vehicle control up to Lander separation from the aeroshell. The six point designs have been detailed with spin/de-spin for pre-entry flight and roll control during entry. The final system would be selected after more detailed error analyses are made and the principle trade-offs in landing site location, data communication and trajectory design are completed.

Based on the baseline missions data, the out-of-orbit entry vehicles require a velocity increment of 235 meters/sec and the direct vehicles 45 meters/sec. Both solid propellant systems and liquid propulsion systems have been detailed in the point designs. The liquid systems are more easily adapted to de-orbit maneuver changes as weight and velocity requirements are modified. In the low impulse requirements range, the liquid systems have disproportionate weights for the propulsion hard parts compared to the total and, generally, the liquid systems applicable to these study vehicles are about three times heavier and require considerably larger packaging volumes than the solids. Both systems have been designed into the Capsules and the pertinent trades and the engineering details in each design application are given in Section 5.3 of this volume. In all six design applications the de-orbit maneuver system is arranged to be jettisoned before entry by release of preloaded, hot-wire bolts of the thrust cone and separation by mechanical springs.

The following sections give the engineering details of the out-of-orbit entry Capsule of the second design pair prepared in this study. The surface lifetime is for more than 90 days with a solar panel and battery electric power supply and with both relay and direct transmission to Earth capability. The Orbiter is assumed unavailable for data relay after the third day and thereafter all data is transmitted directly to the DSN stations. This is the third Capsule (Point Design 3) in the list of six point designs.

TABLE 5.2-1. COMPARATIVE WEIGHT SUMMARY OF MINIMUM MISSION SYSTEMS

Aeroshell base diameter	Out-of-Orbit Entry		Direct Entry	
	8.3 ft	8.3 ft	12.7 ft	11.4 ft
Lander type - weight (lb)	Omni-858	Multi-623	Omni-858	Multi-623
Retardation weight (lb)	228	172	228	172
Aeroshell and Propulsion (lb)	329	329	465	389
	---	---	---	---
Capsule weight at separation from spacecraft (lb)	1415	1124	1551	1184
Capsule weight at entry (lb)	1246	955	1480	1127
Ballistic entry coefficient $\frac{(lb)}{ft^2}$	15.2	11.7	7.9	7.3
Capsule weight at launch (lb)	1626	1335	1882	1463

5.2.1 SCIENCE DATA REFERENCE

The weight of the sensors selected and a baseline reference of the atmospheric data acquired from entry to impact in the maximum flight time range of atmospheres

is shown on table 5.2-2. Pressure and temperature readings are taken at both the stagnation and the base region of the aeroshell. The atmospheric density profile is determined from the vehicle aerodynamic data and the measured deceleration profile of the Capsule.

The landed science consists of meteorological data and surface imagery taken with (Philco) facsimile cameras that take four scenes of low resolution data and four nested scenes of high resolution data. The low resolution scenes are each $35^\circ \times 50^\circ$ segments imaged with $1/10^\circ$ Instantaneous Field of View (IFOV) and the high resolution scenes are $5^\circ \times 5^\circ$ segments imaged with $1/100^\circ$ IFOV. The total data acquired in four high and four low scenes (63 gray shades) is $6 \times 10^6 + 4.2 \times 10^6$ or 1.02×10^7 bits. A typical data summary for the surface operations is included in table 5.2-2.

The surface imagery data is transmitted twice in the first day, after landing and at periapsis passage of the Orbiter. A third set of four scenes is transmitted at the next day's periapsis and the fourth set on the third day. The total imagery data transmitted is 4.08×10^7 . Thereafter, the Orbiter changes to a new ephemeris and the relay link is discontinued. Meteorology data is sent direct each day on S-band to the Earth DSN.

5.2.2 CAPSULE SYSTEM CONFIGURATION

The Capsule for Point Design 3 is a multi-directional Lander containing the minimum surface science with a surface lifetime of more than 90 days. It will be delivered to the Martian surface in an out-of-orbit mode. Telecommunications initially will be accomplished by a UHF relay to the Orbiter and later by a direct link S-Band system. A 25 ft^2 solar array will provide the power for the extended lifetime period of performance. A liquid monopropellant propulsion system is used to de-orbit the entry vehicle. Parachute deployment will be initiated by a radar altimeter. Fig. 5.2.2-1 shows the Point Design 3 Capsule configuration.

5.2.3 CAPSULE SYSTEMS WEIGHT

The weight and inertias of this out-of-orbit entry Capsule with a 90° day surface lifetime is given in table 5.2-3. In this design approach, the Lander is designed for multi-directional landing. This Lander weighs 934 lb with considerably more mission capability than the minimum mission Landers Point Designs 1 and 2A (see sections 3.2 and 4.2) that weigh 858 lb. The difference is basically that the omni-Lander has 522 lb of mechanical crush-up compared to 406 lb in the 934 lb multi-Lander. This Capsule design is compatible with a 10 ft flight shroud and has about the same weight at entry and landing as the minimum mission out-of-orbit design. The weights at separation and at launch are approximately 200 lb heavier, which is due directly to the weight of a liquid propulsion system over a solid. Table 5.2-3 shows the composition of the Capsule and the weights and inertias for key mission events of launch, separation, entry and landing. The weight, balance and inertia detailed statements are given for the pre-entry systems in Section 5.3, the entry systems in Section 5.4 and the Lander in Section 5.5.

TABLE 5.2-2. SCIENCE WEIGHT SUMMARY

Entry Science	Pounds	Data Load (bits)	
		VM-8*	VM-9*
Pressure	3.0	1.3×10^4	2.7×10^4
Temperature	1.5	5.7×10^3	2.0×10^4
Composition	8.0	8.6×10^3	10.2×10^3
Density	2.0	1.1×10^5	2.0×10^5
Water vapor (Ducting)	1.0	7.5×10^1	3.75×10^2
Total	15.5	1.37×10^5	2.57×10^5
Landed Science			
Pressure	1.4	1.35×10^3	
Temperature	2.0	2.7×10^3	
Wind	5.0	4.9×10^3	
Moisture	10.0	1.77×10^3	
Photo imaging	4.8	1.02×10^7	
Clinometer	2.6	7.0×10^1	
Soil sampler	9.5	3.0×10^4	
Total	35.3	1.02×10^7	

*Time from entry to impact in VM-8 = 460 secs
in VM-9 = 1251 secs

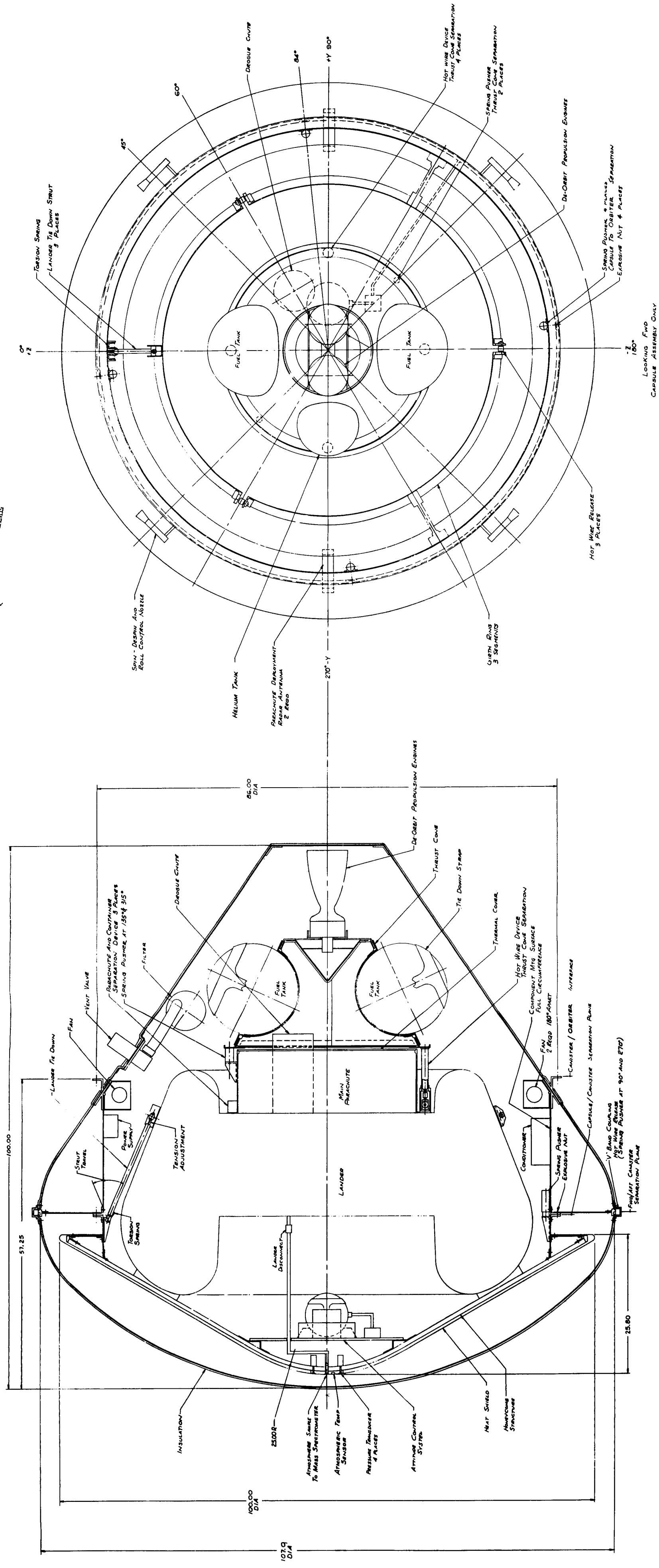


**Figure 5.2.2-1. Mars Hard Lander,
Point Design 3**

TABLE 5.2-3. WEIGHT AND INERTIA COMPOSITION - POINT DESIGN 3

Capsule Systems	Weight (lb)	Roll	Pitch (slug-ft ²)	Yaw
Lander	934			
Aeroshell	162			
Retardation	228			
Propulsion (liquid)	300			
Canister and Thermal Blanket	222			
Capsule at launch	1846	152	187	187
Capsule at separation	1624	120	133	133
Capsule at entry	1324	115	82	82
Landed system	934	72	59	59

5.2.4 FUNCTIONAL BLOCK DIAGRAMS

The Functional Block Diagram, fig. 5.2.4-1 is the complete system delineation of events from launch until the end of the mission. Each functional component is located with respect to functional criteria.

The horizontal axis can be considered a relative time axis with each mission phase occupying a discrete time segment. Each segment, however, does not represent a linear time scale since the total cumulative length would become unreasonable. The time axis, then, indicates the sequence of events rather than the time at which they occur. Whenever components operate in multiple events, either the primary event or the typical mode of operation is indicated. Although the component location indicates the relative beginning of the event, the duration, repetitive rate or the stop time of the event is not indicated.

The vertical axis is used to group the components by subsystem. The subsystem groupings, indicated on both the right and left hand borders, are maintained throughout the drawing. Therefore, for any given event, all components within the system used to perform that event will be shown within the same vertical time boundaries designated at the borders, and the components within a given subsystem are aligned from top to bottom in order of the first function of operation.

The inter-relationship of the components has been separated into four classifications as indicated on the drawing: (1) Unregulated Power; (2) Regulated Power;

(3) Signals; and (4) Data. For clarity, components are shown with the most meaningful functions indicated. For example "ON/OFF" signals are often considered to originate by correct power switching and are thus designated by a power flow line rather than a signal line. Furthermore, each individual line may carry one or more similar functions, such as different power levels.

The components are represented by uniform blocks with a common notation. The electrical reference designator is assigned in accordance with MIL-STD-16. The component's name is listed below and the location of the component is noted by the appropriate letter abbreviation at the extreme right of the block.

The electrical connections between individual components and between subsystems is designed such that it allows the appropriate operations to be performed. By referring to Point Design 3 Block Diagram, fig. 5.2.4-1, it can be seen that for a particular event, such as UHF transmission, there exists a specific group of components that must operate. These components are linked by several of the function lines. The sequence of events and flow of data can be traced as shown below. The appropriate type of power is switched through the power controller. This signal is supplied by the Lander programmer which initiates the power controller switching of all components required for the transmission of the data whether in the electrical, telecommunication or scientific payload subsystem. The correct interconnections then allow data flow from the science subsystem to the telemetry subsystem.

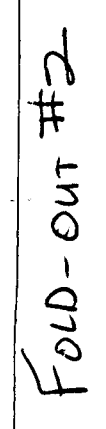
Although other events require a different series of components, the relationship of component functional line designations to events is similar. A separation event is preceeded by the Lander programmer signalling the power controller which turns the stepping switch and connects the capacitor discharge circuit. These then supply the pulse loads as required.

Similar interconnections exist for all other events and the same scheme of functional operations is carried throughout the drawing. These component/subsystem relationships then become the foundation for the harnesses that physically supply the required electrical interconnections.

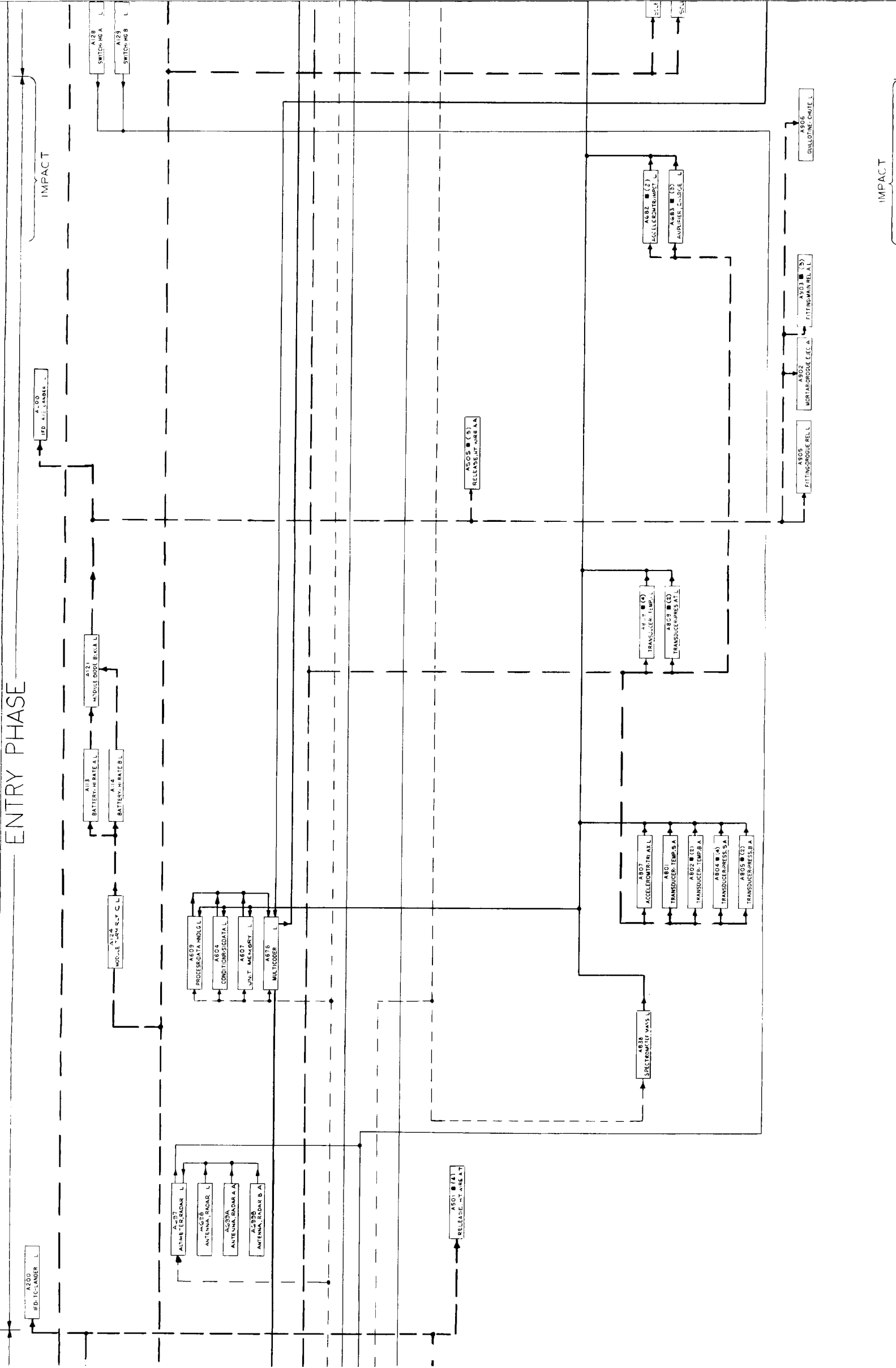
5.2.5 POWER PROFILES, POINT DESIGN 3

The power profile, as illustrated in fig. 5.2.5-1, represents the power demand sequence on the operational battery and solar array. By relating these demands to the event times, the curves reflect the mission sequence of events since each pulse is the power required by all the components operating at the event.

Superimposed on a continuous level of power are the various events. The operational battery is activated prior to Capsule/Spacecraft separation. It then supplies the required power for telemetry transmission during de-orbit and entry. In addition, entry science data is transmitted until impact. The radar altimeter also increases the power demands during this period.



ENTRY PHASE



ENTRY PHASE

Fold-out #1

After impact, the UHF relay link transmits the stored data with a real time imagery period. The meteorological sampling period begins at 20 min intervals with clinometer readings every six hr. The surface composition instrument represents the relatively high continuous power level during the first day. The diurnal day concludes with another UHF relay transmission of stored data and real time imagery.

Days 2 and 3 are identical with meteorological sampling every 20 min and a UHF relay link transmission of stored data and real time imagery.

After the fourth day and for the duration of the 90 day mission the solar array, which has been deployed, will supply power during the day and charge the battery for night operation. This day 4 sequence can be seen to consist of a meteorological sampling period every hour with a direct link transmission period to earth of both the stored data and real time imagery.

5.3 PRE-ENTRY SYSTEMS

5.3.1 CANISTER

5.3.1.1 Design Constraints

Canister design constraints for Point Design 3 were as follows:

1. Maximum diameter less than specified in Section 2.3.1 (103.9 in.)
2. Withstand an internal pressure
3. Withstand the inertial loads of launch and powered flight
4. Provide adequate clearance between the aeroshell heat shield and canister
5. Provide a separation and field joint as one and the same joint
6. Provide support for the entry system.

Diameter constraints on the maximum allowable canister diameter were fully described in Section 2.3.1 and were imposed by the internal envelope available for the Capsule System installation.

Due to the requirement to maintain biological integrity within the internal portion of the canister, it was necessary to evaluate the effects of an internal pressure on the shape, material, and construction of both the forward and aft canisters. Inertial loading of the canister during flight and handling conditions, including equipment loadings on the aft canister, was a constraint which was traded off against the differential pressure to determine the more severe loading environment for the canister structure.

A driving influence on the canister size was the allowance necessary for clearances between the entry system and canister. This clearance has been estimated to be 1.9 in., as shown in fig. 5.3.1-1, to allow for Capsule System dynamic excursions.

The field joint for the canister could be combined with the device used for in-flight separation or it could be entirely separated. Maximum leak tightness was an overriding criteria in either case.

The entry system must be supported within the Capsule System and a means of support had to be designed. This design also considered that, in addition to support, it must have the capability of withstanding and transferring the entry system inertial loads through the structure and to the Capsule bus interface to the bus adapter ring.

5.3.1.2 Canister Structural Description

The forward canister for Point Design 3 is a hemispherically shaped minimum gauge aluminum shell making a tangent at its maximum diameter through a quarter torus section,

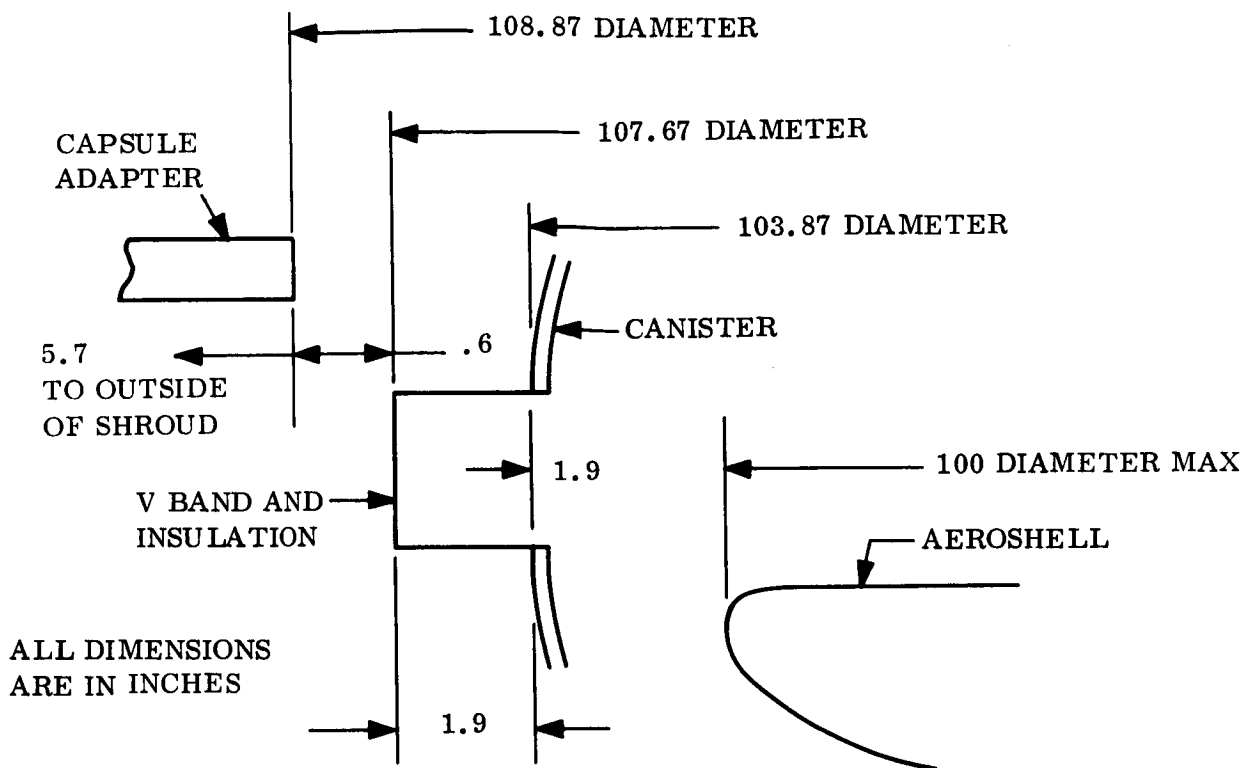


Figure 5.3.1-1. Aeroshell/Canister Clearances

fig. 5.3.1-2. This structure has been designed to act as a pressure vessel and the torus section provided to eliminate the inboard kick loads and minimize shell bending at the field joint ring due to the internal pressure. The minimum gauge aluminum material is more than adequate to withstand the pressurization and inertial loads imposed on it. The hemispherical shape has been proven in previous analyses (Voyager Phase B Study) to be considerably stiffer from a dynamics standpoint than a conical shape.

The forward canister has been designed such that there will be no yielding under design load conditions and no failure under ultimate design load conditions. This includes the transient and steady state loads encountered under the conditions of handling, transportation, sterilization, pre-flight, powered flight, transit and separation.

Inertial loading conditions were determined to be less severe than the internal pressurization condition in the design of the canister and the field joint ring. This can be seen in table 5.3.1-1 where the running loads on the interface ring are tabulated for both inertial and pressure loading conditions. As a result, the pressure loading condition determined the desired construction, material, and thickness to be used in the structural design of both the forward and aft canister.

FOLDOUT FRAME

FOLDOUT FRAME

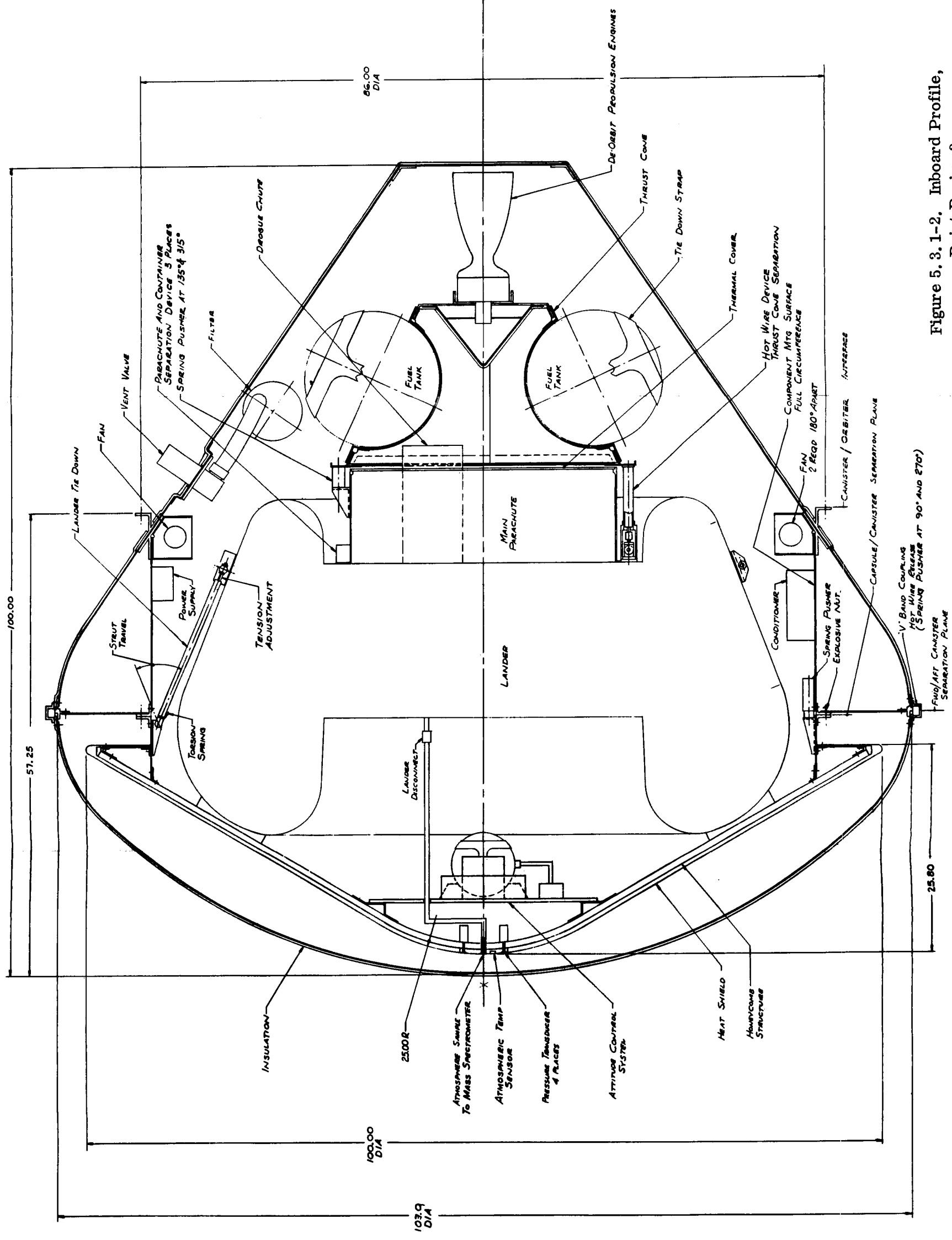


Figure 5.3.1-2. Inboard Profile, Point Design 3

TABLE 5.3.1-1. INTERFACE RING LOAD

Load Condition	Vertical Load W_V (lb/in.)	Inboard (horizontal) Load W_H (lb/in.)
C	1.06	0.38
E	1.92	0
F	0.30	1.92
C&E	2.98	0.38
C&F	1.38	2.27
M	27.85	0 0.5 psi skin pressure
N	55.7	0 1.0 psi skin pressure

Minimum sheet gages were the overriding constraint on the thicknesses selected for the canister design. Stiffeners to rigidize the shell for dynamic and ground handling loads have been provided. The limit pressure condition for the canister is 1.0 psid internal pressure and the structure is adequate to withstand a 1.7 psid burst pressure, which results in a safety factor of 1.7 on the limit pressure.

The field joint rings for the forward and aft canisters provide a seat for the band-clamp, which holds the canister halves together, resist the loads imposed by the internal pressure and the band clamp, and provide for the pressure tight sealing of the canister assembly. The aft canister ring slides under the forward mating ring and has an internal leg, as shown in fig. 5.3.1-3, which is connected to a bulkhead, joining the ring with the internal adapter. This arrangement provides a torque box in the aft canister increasing both its stiffness and structural load carrying capability.

The combined inertia of the forward ring, aft rings and bulkhead is more than adequate to insure structural stability of the field joint under the critical load condition. Figure 5.3.1-4 shows a plot of the required inertias for ring stability as a function of critical load in lb/in.

Structurally, the aft canister is sized for the internal pressure which dictates the same minimum sheet gage as the forward canister. The aft canister is essentially conical in shape with the forward end, a quarter torus, making a tangent with the maximum diameter and the conical afterbody as shown in fig. 5.3.1-1. Stiffening members are located between the adapter-to-canister ring and the end bulkhead ring. These members also act as supports for the electrical equipment and vent system equipment in the aft canister.

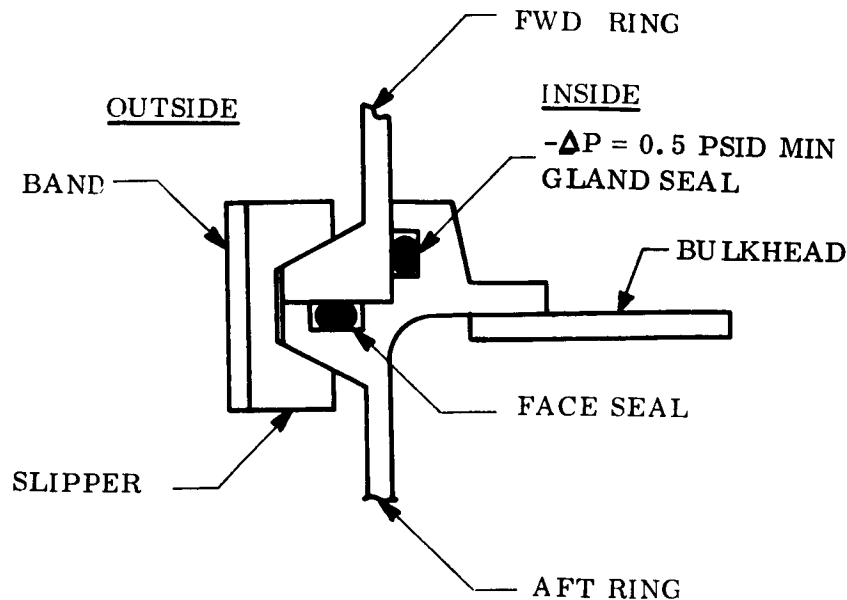


Figure 5.3.1-3. Canister Field Joint

5.3.1.3 Internal Adapter

The adapter for Point Design 3 is designed to support the entry vehicle and transfer loads introduced by the entry system to the Capsule bus interface ring. This adapter is internal to the sterilization canister and interfaces with it at the aft canister ring. The adapter picks up the entry vehicle at four points and attaches to the Capsule bus interface ring through the canister skin.

Structurally, the internal adapter is a cylindrical aluminum shell with longitudinal stiffeners as shown in fig. 5.3.1-2. The shell and stiffeners have been sized such that the section modulus and working area are more than adequate to withstand the bending moment and axial loads which the structure will experience. The inertial loads used in determining the necessary section properties of the cylindrical skin and stiffeners were 6 g's limit in the axial direction and 2 g's limit in the lateral direction.

The forward ring, at the entry vehicle interface, attaches to a lateral interconnection to the aft canister interface ring. Lightning holes have been placed in the cylindrical structure to allow for free passage of heated gases between the canister and adapter during heat sterilization cycles. The lateral interconnection, or bulkhead, provides support for the aft canister ring as well as the adapter.

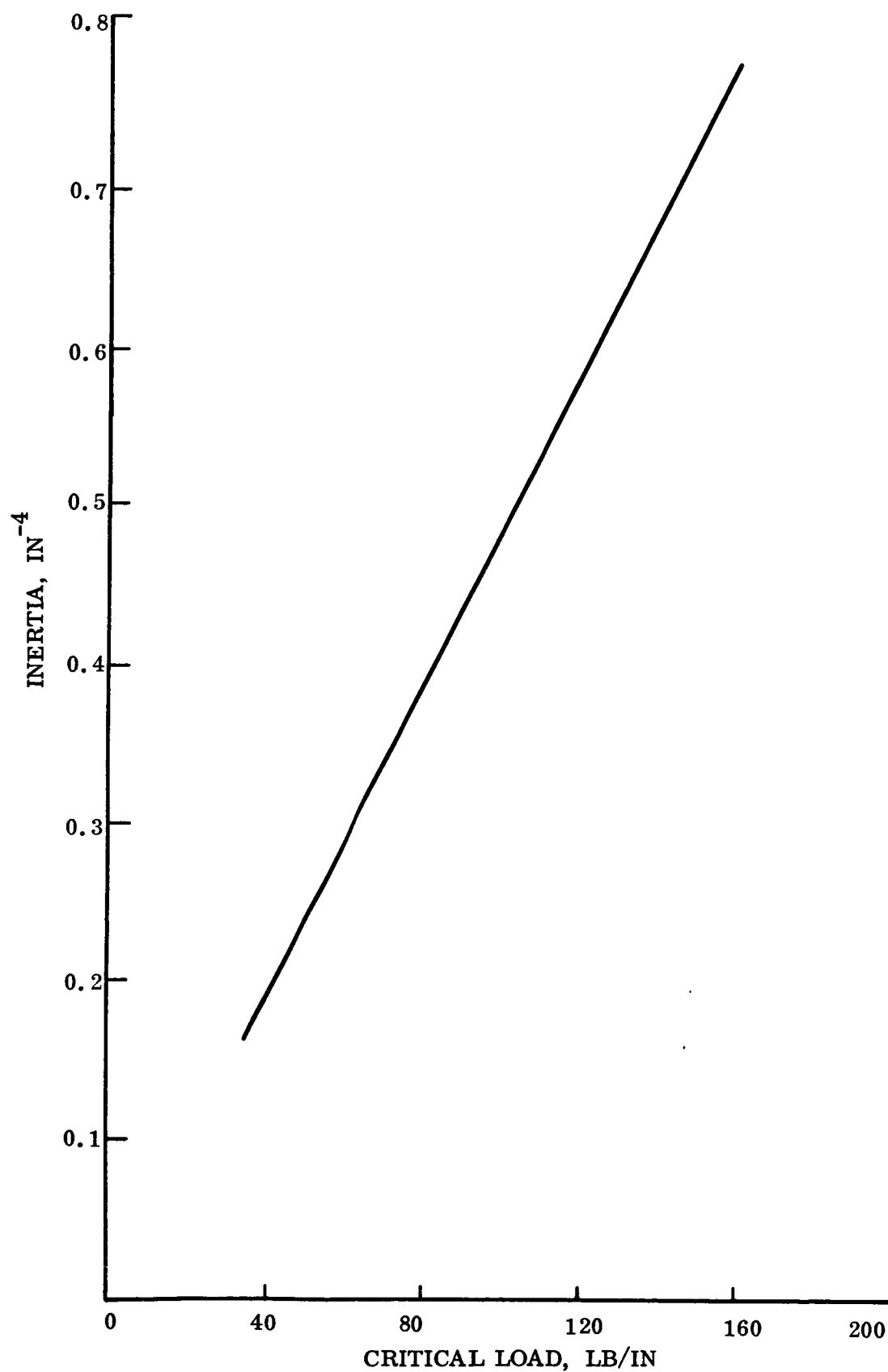


Figure 5.3.1-4. Required Ring Inertia for Stability as a Function of Critical Load

The spring-pusher housing is located on the inside of the adapter at the interface with the entry system. This device provides the separation force necessary to eject the entry system from the bus. Separation forces are reacted through the adapter skin and stiffeners.

5.3.2 PRESSURE AND VENTING SYSTEM

The basic function of the Pressure and Venting (P&V) System for Point Design 3 is to prevent recontamination of the capsule by maintaining a minimum specified differential pressure (ΔP) between the canister and the ambient environment. This positive ΔP is maintained from sterilization until prior to canister separation.

5.3.2.1 Design Constraints

The P&V System has been designed to meet the following constraints:

1. Provide inlet and outlet ports into the canister for sterilization
2. Provide circulation of air during sterilization
3. Provide pressure relief due to temperature variations
4. Maintain a positive ΔP between 0.5 and 1.0 lb/in.² differential (psid) between the canister and ambient atmosphere from sterilization until exit from Earth's atmosphere
5. Vent 70 ft³ of internal air during ascent to maintain ΔP below 1 psid
6. Evacuate all entrapped gases to ambient space vacuum.

5.3.2.2 System Description

The primary function of the P&V System is to vent the internal canister during sterilization, after sterilization and during flight to prevent the internal pressure from exceeding 1 psid. This is accomplished using a combination relief valve with a solenoid override which opens at a nominal pressure of 15.6 psia with increasing pressure and closes at a nominal pressure of 15.3 psia with decreasing pressure. A biological filter is installed upstream of the valve to filter out any bacteria flowing upstream. Relief of a pressure buildup due to a temperature increase is accomplished using the same valve described above.

The block diagram for Point Design 3 is shown on fig. 5.3.2-1. During sterilization, the P&V System provides for inlet and exit of sterilized gas (and decontaminating gases if used) by using a manually operated inlet valve connected to the sterile, filtered air supply, and electrically opening the vent valve for use as the outlet port. Since the gas will pass through the biological filter, it must be pre-filtered to prevent clogging of the "prime flight filter". Two circulating fans are used to speed up the heating and cooling cycles and to eliminate hot spots. These fans are used only during sterilization and their power will be provided by GSE. After sterilization, the make-up gas supply

is connected to the manually operated valve. The canister is vented after launch and throughout powered flight until the canister reaches 0.5 psia. The canister remains pressurized at ~ 0.5 psia less leakage, after exiting the earth's atmosphere until prior to canister separation; at which time, the vent valve will be electrically opened to evacuate the canister to near space vacuum.

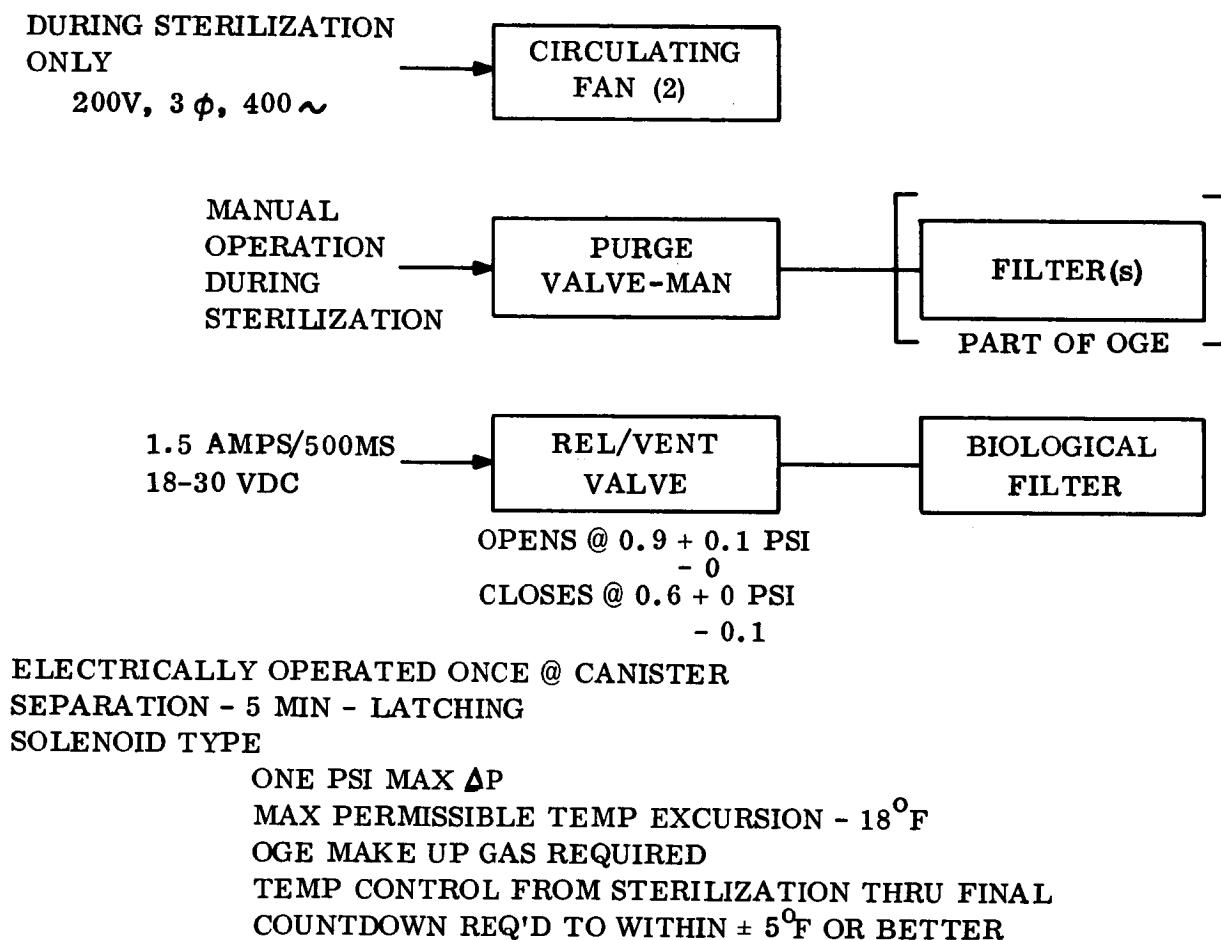


Figure 5.3.2-1. Pressure and Venting System, Block Diagram

To minimize the possibility of backflow during venting, the exit port from the canister is shaped as a convergent nozzle. It has been shown that in a convergent nozzle, flow separation does not occur. Thus, the possibility of gas flow upstream during venting is almost nil. This fact would preclude the entry of bacteria during the venting process when the valve is open.

5.3.2.2.1 Canister Venting

The vent valve is used to vent the canister during power flight. Its size is determined by the amount of gas and maximum permissible ΔP . For Point Design 3 there is an initial volume of 70 ft^3 of air and the maximum allowable ΔP is 1 psid, as

discussed in Section 5.3, Volume III. The nominal fill pressure will be 15.45 psia at 70° F. From the P&V parametric study, the vent area required for 70 ft³ of air is 0.75 in.²; and assuming a C_D for the valve of 0.7, gives a required valve aperture equivalent to a 1.07 in.² circular orifice.

The valve is a spring-loaded, pilot-operated relief valve with a latching, override solenoid, and a position-indicating switch. This valve design permits its use for relief, venting, purging and evacuation. The proposed design will be similar to Sterer P/N 19260, Pneumatic and Pressure Control Valve Assembly. The basic changes required to the valve relate to operating pressure and orifice area. The reference valve weighed 3.0 lb and it is estimated that the proposed valve will weigh 4.0 lb. Electrical power required for the solenoid is 1.5 amps at 30 VDC at 70° F for 1/2 sec maximum. A sketch of the proposed valve is found below:

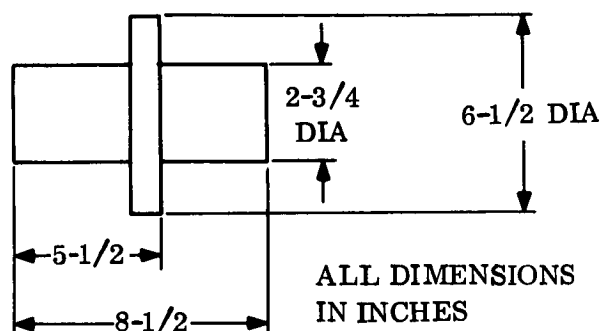


Fig. 5.3.2-2 shows the approximate ΔP time history for a valve that opened and remained opened. Obviously, this method will not meet the requirement for maintaining the $\Delta P > 0.5$ psid. The relief valve will act as a controller and it is expected that the valve will close in the cross hatched portion of the curve. The valve will be set to open at $0.9^{+0.1}_{-0}$ psid on increasing pressure and to close at $0.6^{+0}_{-0.1}$ psid on decreasing pressure. The valve will most likely cycle several times during the first 20 sec and remain open until L. O. +90, after which time it will remain closed until opened prior to canister separation.

The biological filter is used to prevent bacteria migration into the Capsule through the vent valve. The filter is installed in series with the valve and upstream of it. The filter is required to filter bacteria (0.3 microns) in the backward direction while presenting a low pressure drop to the air being vented. The filter size is governed by the maximum flow, the pressure drop and the differential pressure (ΔP). The maximum calculated flow for Point Design 3 (70 ft³ of air) was 0.116 lb/sec or 91 scfm. For the 1 psid ΔP system and a specified pressure drop of 0.1 psi, a filter area of approximately 2.6 sq ft is required. Using Pall Corp's Ultipor 0.9 medium, an element size of 6.6 in. long x 2.5 in. diameter is obtained. The filter assembly will be 7.6 in. long x 3.0 in. diameter and will weigh approximately 1 lb.

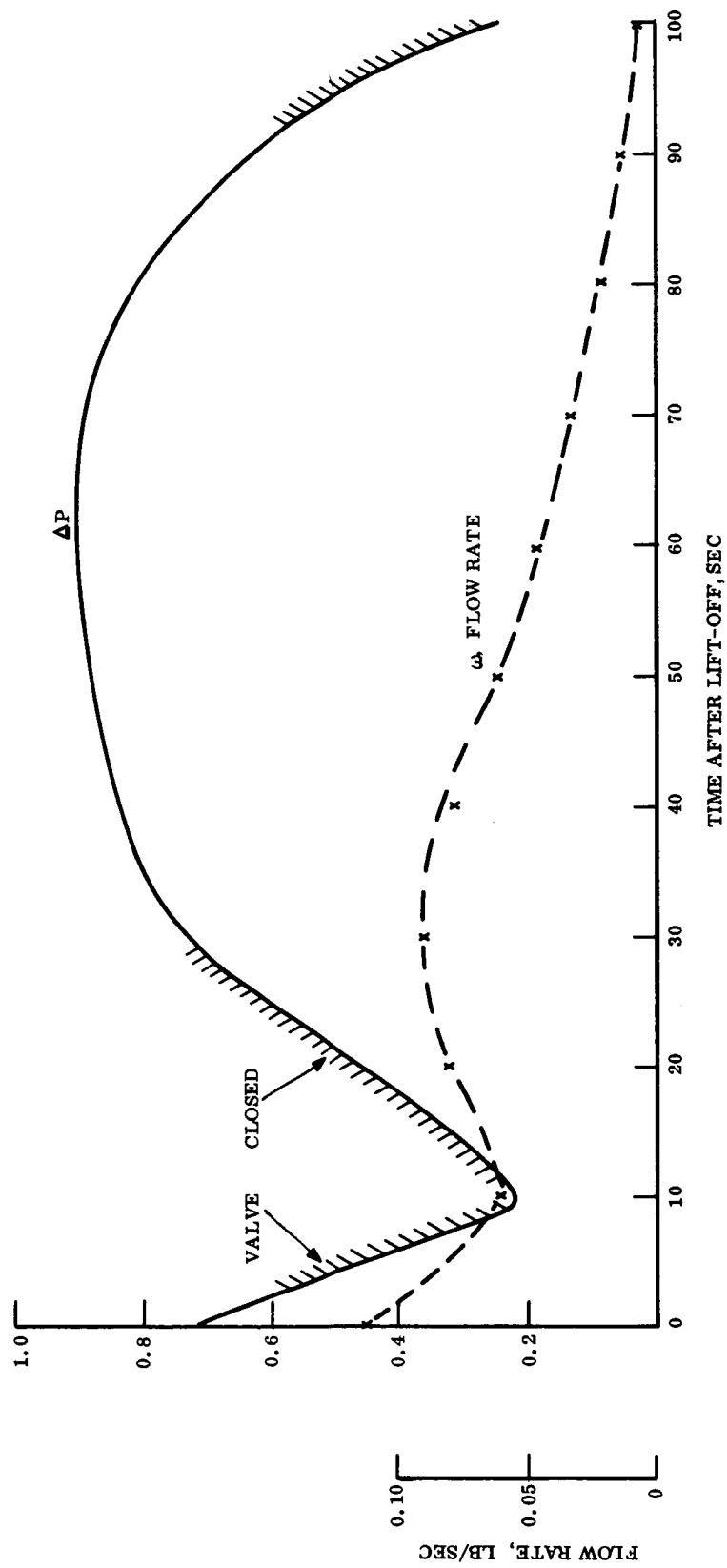


Figure 5.3.2-2. Flow Rate and Differential Pressure vs Time after Lift-off

The choice of Ultipor 0.9 was made because it presents a lower pressure drop than Ultipor 0.15, while satisfying the filtering requirements. It has a catalog rating of 100 percent removal of 0.08 micron particles in dry air. The filter can be decontaminated with ETO and has a temperature rating of 350° F in air.

To maintain the necessary flow, the filter housing requires 1-1/8 in. ports and will be connected to the vent valve with 1-1/8 in. aluminum tubing.

5.3.2.2.2 Canister Sterilization

During canister sterilization, air will be introduced into the canister to speed up heating or cooling through the manually operated valve. Using 5/8 in. tubing and a valve with an area of 0.25 in.², 5.4 cfm of air can be introduced at 1 psid (15.7 psia); thus, the canister air will be changed four plus times in one hour.

Two fans, Rotron Mfg. Co. type AXIMAX 1, with a delivery of 19 cfm at 1 in. H₂O s.p. will be used to circulate air during sterilization, thus reducing warmup times, eliminating hot spots, and insuring that the entire capsule reaches sterilization temperature.

Power required for the fans will be provided by OGE and will be as follows: 200 V, 3φ, 400 ~ ; 0.1 amp line current per motor. Fan size is 1.75 in. diameter x 1-1/2 in. long and weight is 4 oz.

5.3.3 SEPARATION SUBSYSTEM

5.3.3.1 Design Constraints, Functions and Requirements - Point Design 3

The Separation Subsystem performs the following pre-entry functions:

1. Separation of the forward canister
2. Separation of the Capsule assembly
3. Separation of the thrust cone assembly
4. Separation of the aeroshell.

The subsystem has been designed to meet the following requirements in addition to the usual environmental criteria.

1. Provide field and separation joints for the canister
2. Eject the forward canister at 2.5 ± 0.3 fps
3. Maintain a pressure-tight joint from sterilization through exit from the Earth's atmosphere for a maximum internal pressure of 1.67 psid. Pressure-tight is defined as leakage which results in less than 0.002 psi drop/hr at 70° F

4. Maintain maximum attainable pressure tightness during space cruise where outside temperature may be as low as -300°F
5. Maintain sterility of Capsule
6. Separation shall not produce debris or loose objects
7. Attach the Capsule at four points
8. Eject the Capsule at 1.5 ± 0.25 fps separation velocity from the Orbiter with tip-off rates of $< 0.5^{\circ}/\text{sec}$ to the Capsule. Orbiter pitch inertia is the same as Capsule's
9. Separation shall not cause collision with any of the remaining payload
10. Attach and separate the thrust cone at 1.0 fps minimum
11. Attach and release the aeroshell
12. Provide electrical separation as required
13. Optimum reliability and subsystem performance is paramount to mission success. Use proven concepts.

Other system constraints - electrical power, distribution, timing and signal lock-out shall be provided by the EP&D Subsystem.

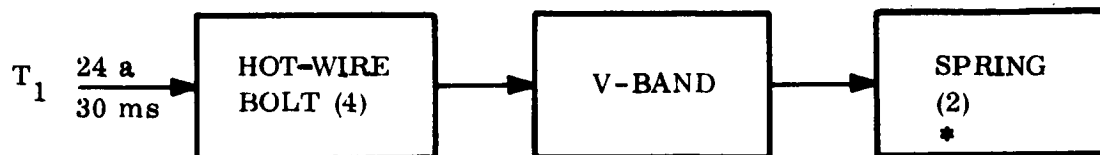
5.3.3.2 General Subsystem Description - See Block Diagram, fig. 5.3.3-1

The canister halves are joined by a V-band assembly consisting of independent slippers attached to a strap. The band is made in four equal segments joined by hot-wire tension bolts. The hot-wire bolt is a nonpyrotechnic, mechanical device consisting of a turnbuckle coupling which separates when an electrical signal is applied to a hot-wire element which kept the turnbuckle together. The forward canister is ejected using two helical coil compression springs. The rings, to which the V-band clamps, perform double duty by providing the groove and sealing surfaces for the O-ring type pressure seal. After separation, the V-band segments remain attached to the aft canister via springs and lanyards. The canister is completely evacuated by the P&V Subsystem prior to separation.

The Capsule assembly is separated from the Orbiter approximately 10 min after canister separation. The Capsule is attached to the adapter at four points by explosive nuts, but a hot-wire type of coupling is also being investigated. The Capsule is ejected at 1.4 fps nominally, by four helical coil compression springs.

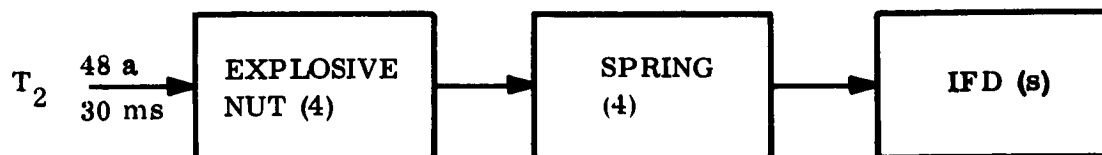
The thrust cone assembly is attached to the Lander/aeroshell assembly through four hot-wire bolts. Two helical coil compression springs identical to those used for

FWD CANISTER SEPARATION

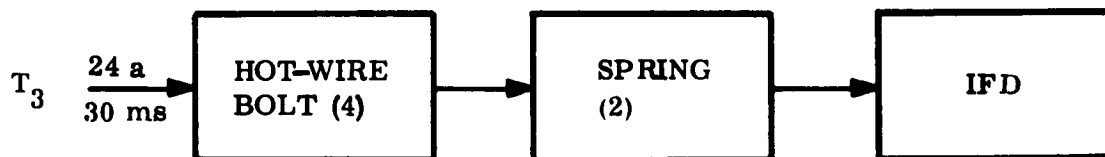


* 4 SPRINGS FOR POINT DESIGNS 2A, 2B, 4, 6

CAPSULE SEPARATION



THRUST CONE SEPARATION



AEROSHELL SEPARATION

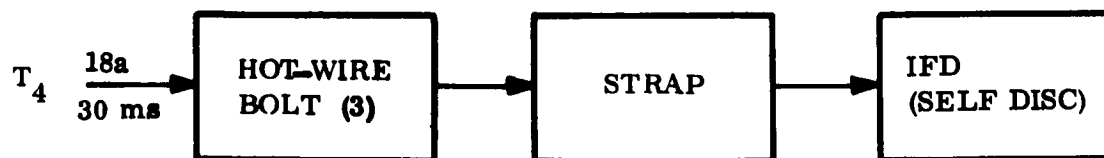


Figure 5.3.3-1. Separation Subsystem Block Diagram

canister ejection are used to eject the thrust cone at 1.9 fps nominally. The thrust cone is separated after the de-orbit function is completed.

The aeroshell is attached to the Lander by a strap assembly retained by three hot-wire tension bolts and released after parachute deployment. This system is described in more detail in Section 5.4.4.

Canister

1 V-band assembly	7.3
4 hot-wire bolts	0.8
2 springs	0.2
2 spring housings	0.7

Capsule

4 explosive nuts	1.0
4 springs	0.8
4 spring housings, adjustable	1.4

Thrust Cone

4 hot-wire bolts	1.0
2 springs	0.2

Aeroshell

1 strap	1.2
3 hot-wire bolts	0.6
TOTAL	15.2 lb

The following sections discuss the detail designs.

5.3.3.2.1 Canister Separation

The selection of the separation method for the canister is governed by the requirement for a sterile, pressure-tight joint for a large, flexible structure. This basic requirement limits the separation joint design to one that can apply a continuous distributed force, such as flexible shape charge, various types of MDC or primer cord, V-bands, closely spaced bolted joint, "pyro fuze" joint system or a thermal heat pad joint system. The V-band system was selected because of its simplicity, reliability,

low separation shock, lack of debris, tolerance to temperature environment, elimination of the need for a field joint, and it presents a tortuous path for microbial access to the separation interface.

The band must meet the following specific requirements:

1. Contain proof pressure without yielding
2. Provide the necessary clamping force without yielding
3. Contain the burst pressure without breaking
4. Make allowance for creep at low temperature over a nine month period.

The V-band assembly is made in four segments, with the strap material being 2024T86 Aluminum, 1 in. wide x 0.040 in. thick. The slippers, which are attached to the band by clips, are made of 7075T73 Aluminum. The band is preloaded to 1180 lb ± 10 percent in order to sustain all loads, allow for creep during cruise, and allow for tension variations during assembly. (See Appendix B, Volume III for load and stresses in band.)

The V-band segments are held in tension by the four hot-wire bolt* assemblies. The choice of four points for attaching and torquing was made to maintain nearly uniform tension on the entire band and to facilitate band disengagement. The hot-wire bolt is a mechanical separation device which utilizes the reduction of tensile strength property of a material upon heating to actuate. Upon application of 6 amps for 30 msec the hot-wire element breaks and separation occurs. The hot-wire bolt consists of two separate studs connected by a segmented coupling. The coupling is held together by the hot-wire element, so that tension can be carried by the mechanism.

The required preload can be applied through 3/8 in. diameter thread and a 0.69 inch O.D. coupling (see fig. 5.3.3-2) made of 17-4 PH, Cond 1050 stainless steel with an ultimate load capacity of 8000 lb tension. Nine turns of 0.014 in. diameter 302 stainless wire form the hot-wire element. The segments of the coupling are retained so that there is no debris. This unit is ideal for long service in space because of its all metal design. The band will separate if any of the four bolts operate.

The forward canister is ejected by two helical coil compression springs. The springs provide 35 lb of initial force each and have a working stroke of 2 in. They will impart a velocity of 2.7 ± 0.25 fps to the canister. The springs are of 302 stainless steel, stressed at 90,000 psi and are retained with the aft canister, in an adjustable subassembly (see fig. 5.3.3-3). Tip-off rates will be less than $2.0^\circ/\text{sec}$ about any axis. Center of gravity offsets are expected to be minimal since the forward canister is of symmetric construction.

*(The hot-wire bolt is a GE-RS proprietary design.)

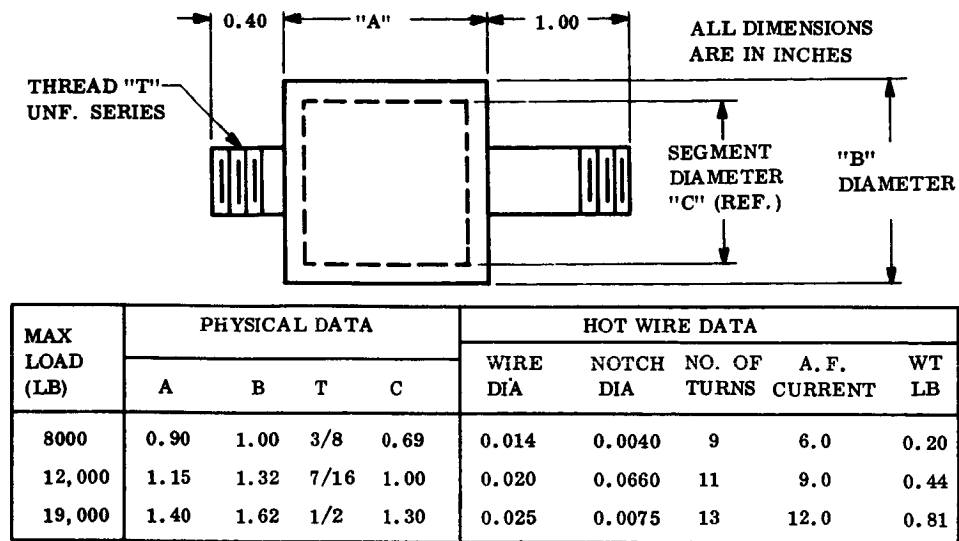


Figure 5.3.3-2. Hot-Wire Tension Bolt

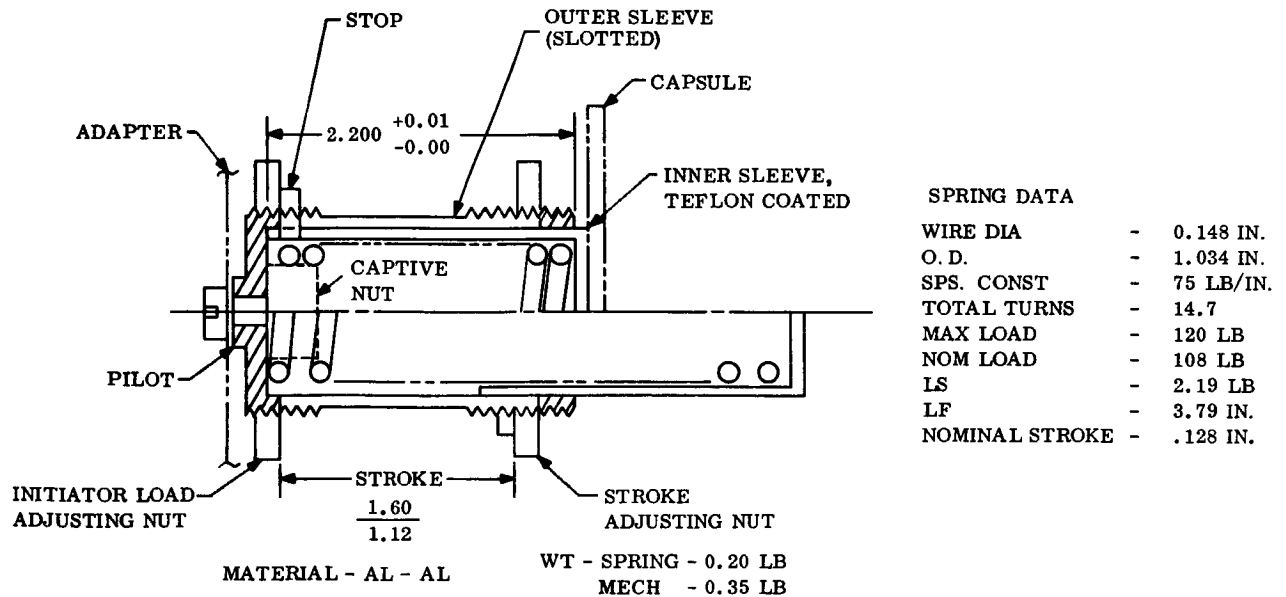


Figure 5.3.3-3. Capsule Separation Adjustment Spring Assembly

The canister separation joint seal utilizes two silicone rubber O-rings to attain a pressure-tight seal. The O-rings are used in two different modes to enhance sealing capabilities; one O-ring being a face seal and the other a gland seal (see fig. 5.3.1-3). This arrangement utilizes the axial and radial clamping forces of the V-band and closes off the clearances resulting from manufacturing tolerances, while retaining a machinable and structurally sound ring design. The basic cross-section is depicted in the figs. 5.3.3-4 and -5 for the Point Design 3 ring. The face seal O-ring is nominally 0.139 in. diameter and is compressed from 0.014 to 0.041 in. The force necessary to compress this O-ring using 50 durometer silicone is from 1.2 to 12.0 lb/linear in. The gland seal is nominally 0.210 in. diameter and is compressed from 0.015 to 0.045 in., or 7 to 22 percent. The radial force to compress this ring is from 1 to 16 lb/linear in. The radial clamping force available if the nominal axial clamping force of 45.1 lb/in. is attained is,

$$FR = FN (\text{TAN}) = 45.1 (\text{TAN } 20^\circ) = 16.4 \text{ lb/in.}$$

which is adequate.

Silicone rubber material was selected because it has the best low temperature properties -- rated to -80°F for seals, but doesn't harden until -150 to -180°F according to Dupont. Therefore, it is expected that the seal will degrade during the space cruise. If it is mandatory that a seal be maintained, thermal insulation could be applied to the band to keep the temperature above -150°F .

The ability of the separation joint to inhibit the penetration of bacteria is further enhanced by the tortuous path which they must follow to gain entry into the Capsule. The slipper is in full contact with the ring except for a $1/4$ in. gap between the 5.75 in. long slippers, or a total of 96 percent of the circumference is covered by the slippers. The band, of course, covers the entire circumference except at openings for the hot-wire bolts, which probably will be about $1-1/2$ in. long each, or 94.5 percent band coverage.

5.3.3.2.2 Capsule Separation

The main consideration for Capsule separation and ejection was the stringent tip-off rate requirement. To meet this requirement, it is necessary that the impulse generated by the separation device be either very low or nearly the same at all points. Likewise, the ejection system must have controlled force and energy, with low variances; and lastly, c.g. offsets, and ejection system force axes must be controlled.

Separation devices that meet the above needs are ball locks, collet releases, and explosive nuts. The latter was chosen because of compactness and ease of use and installation. All of the above utilize pressure cartridges for operation, and for high reliability dual cartridges will be used. This introduces the problem of wide impulse variance as a function of gas pressure (a function of cartridge design, simultaneity, and number of cartridges firing).

5-43

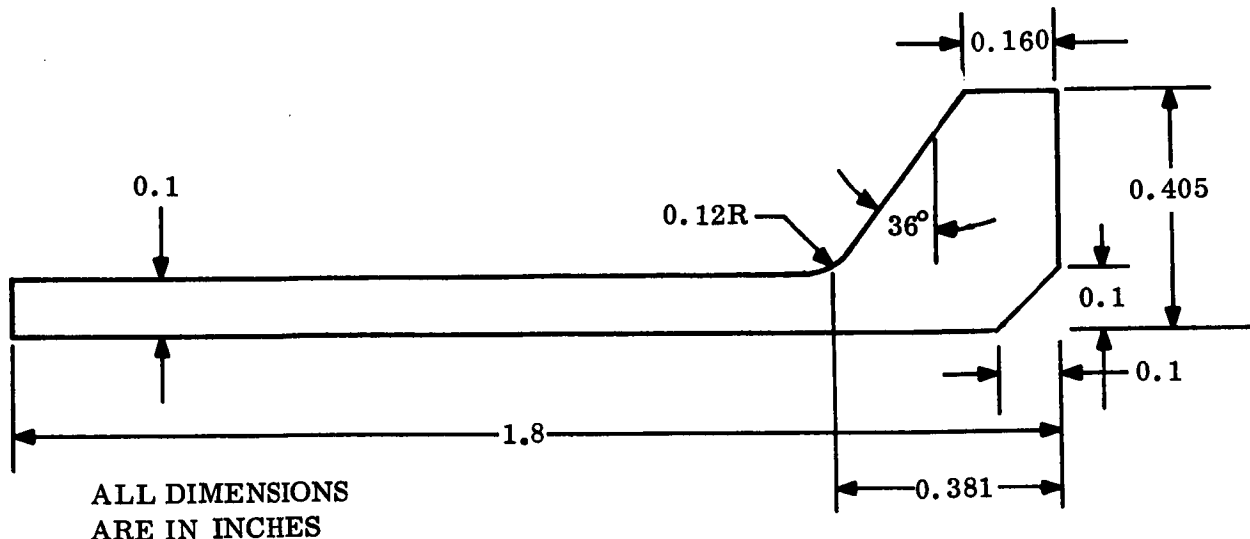


Figure 5.3.3-5. Forward Canister Ring

A non-pyrotechnic device, similar to the hot-wire tension bolt discussed previously, will be very seriously considered, because of obvious advantages. The main drawback is that it is new and needs further development.

The ejection systems available are pneumatic pistons, pyrotechnic thrusters, reaction systems and springs. Springs were selected for their obvious simplicity. To minimize tip-off rates, the energy and force of the ejection system must be controlled. A guide/roller system may also be required if rates are too high. The proposed solution uses preset springs in an energy package, with selective assembly and gives a maximum tip-off rate of $0.36^\circ/\text{sec}$ when the maximum and minimum spring forces are combined with the worst case c.g. offset.

The Capsule is attached to the adapter by four $1/4$ in. explosive nuts, each having dual cartridges. The explosive nut is of the captive type, with all loose pieces contained within the unit. The gas generated by the squibs is also contained. The choice of an explosive nut was made because of reliability, capability for dual squib initiation, low weight, and high load carrying ability. The $1/4$ in. nut can carry the full load of a $1/4$ in. 160,000 psi ultimate tensile strength bolt, which is 3600 lb. The applied limit load is 2900 lb and therefore, there is ample margin. Four nuts were selected, based on the four pick-up points on the structure.

Capsule ejection is accomplished by four helical coil compression springs. The springs exert a 108 lb force each, and have a working stroke of 1.28 in. The springs are stable ($L/D < 5$) and will impart a separation velocity of 1.4 ± 0.15 fps to the Capsule. Thus, the Capsule will acquire a positive ΔV of 0.70 fps, whereas the forward canister was ejected at 2.7. Tip-off imparted to the Capsule will be $0.36^\circ/\text{sec}$, obtained by trimming and selecting the springs. The Orbiter will acquire a negative or retrograde ΔV of $3/4$ fps and a tip-off rate $0.36^\circ/\text{sec}$ as a result of Capsule separation. It was assumed that this small motion was not detrimental to the mission. (See Volume IV, Appendix B for tip-off analysis.)

The spring assembly is shown in fig. 5.3.3-3. It provides for adjustment of initial load - one turn of the adjustment nut gives approximately a 2 lb load change - provides for adjustment of total stroke, retains the spring at the end of the stroke and provides a locating pilot. The inner sleeve is coated with teflon on both inner and outer surfaces to reduce friction. Operation of the spring over the inner 80 percent of its total possible stroke assures nearly constant spring rate.

The following summarizes the recommended spring design. (See table 5.3.3-1 for spring detail data.)

Spring material - National Standard NS-355 stainless steel

Ultimate tensile strength = 330,000 psi for up to 0.159 in. wire

Torsional shear - 45 percent x ultimate tensile strength = 148,000

Initial load - 108 lb at 0.16 in. from solid

Final load - 12 lb at 1.44 in. from solid

Max load - 120 lb at solid height

Max stroke, X_m - 1.60 in.

Operating stroke - $1.60 - 20 \text{ percent } (1.60) = 1.28$:

Energy required - 25.5 ft-lb

Energy available - $\frac{(108 + 12)}{2} \frac{(1.28)}{12} (4 \text{ springs}) = 25.6 \text{ ft-lb}$

Control spring rate to 75 (± 3 percent) lb/in.

Adjust spring to 108 (± 2) lb initial load

Install springs, so that diametrically opposite springs have an initial load within 0.5 lb.

IFD's for electrical separation will be self disconnect type or electrically actuated, hot-wire type, depending on size and location on the vehicle.

TABLE 5.3.3-1. SEPARATION SPRING DATA

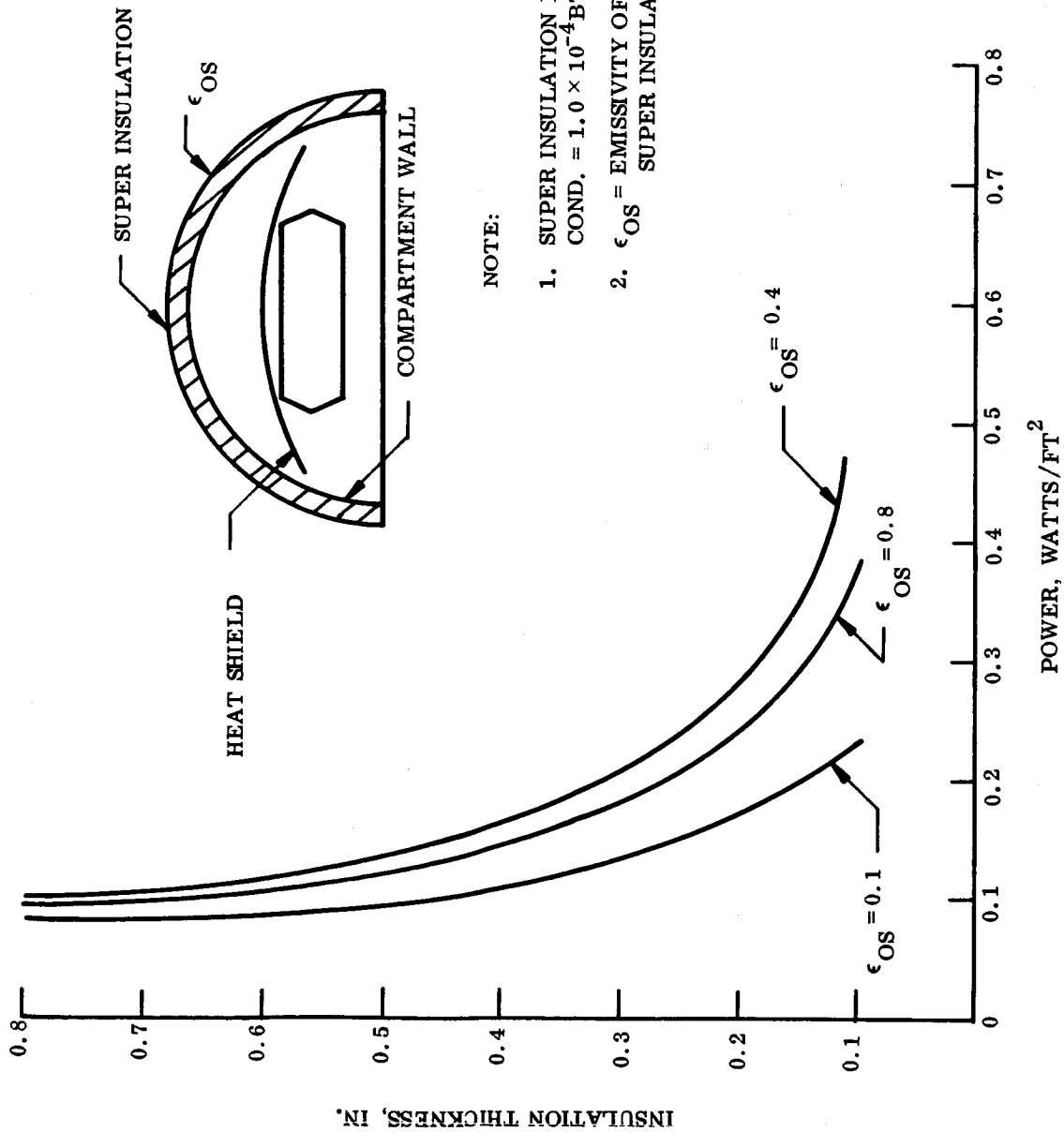
	Canister	T/C	Capsule
Wire diameter (in.)	0.107	0.107	0.148
Mean coil diameter (in.)	1.07	1.07	1.034
Number of springs	2	2	4
Component length (in.)	1.29	1.29	2.35
Solid height (in.)	1.09	1.09	2.19
Free length (in.)	3.29	3.29	3.79
Total weight (lb)	0.17	0.17	0.80
Number of active coils	8.4	8.4	12.7
Stress (lb/in. ²)	90,000	90,000	110,000
Nominal ΔV (fps)	2.5	2.5	1.5

5.3.3.2.3 Thrust Cone Separation

The thrust cone is attached to the aeroshell/Lander through a hot-wire bolt to a male fitting, which is internal, and pinned to a female fitting on the Lander cover. The hot-wire separation occurs as described for the canister. The thrust cone is ejected at 1.9 fps using two helical coil compression springs identical to the ones used for canister separation. The springs remain with the thrust cone. IFD's for electrical separation will probably be of the spring self-disconnect type.

5.3.4 ENVIRONMENTAL CONTROL

Thermal control of the Lander components during interplanetary travel will be accomplished by insulating the Lander from the space environment and using heater power from the spacecraft to control the Lander temperatures. The insulated blanket will be a multi-radiation barrier type composed of a number of layers of either aluminized mylar or aluminum foils separated by an insulating material. An effective thermal conductivity of 1×10^{-4} Btu/hr-ft-°R was selected for this type of insulation. Definition of the insulation details and heater power requirements will be dependent on the surface radiative properties, payload allowable temperatures and canister surface area. A low emissivity coating (EoS = 0.1) on the outside insulation surface will be utilized to maintain minimum heat loss through the canister. From fig. 5.3.4-1 insulation and heater power requirements can be determined on a unit surface area basis for a compartment temperature requirement of 310°R. Total heater power can be evaluated from fig. 5.3.4-2 at the design values.



NOTE:

1. SUPER INSULATION EFFECTIVE THERMAL COND. = 1.0×10^{-4} BTU/HR-FT °R
2. ϵ_{OS} = EMISSIVITY OF OUTER LAYER OF SUPER INSULATION

Figure 5.3.4-1. Super Insulation Requirements to Maintain 310°R on Compartment Wall and Heat Shield

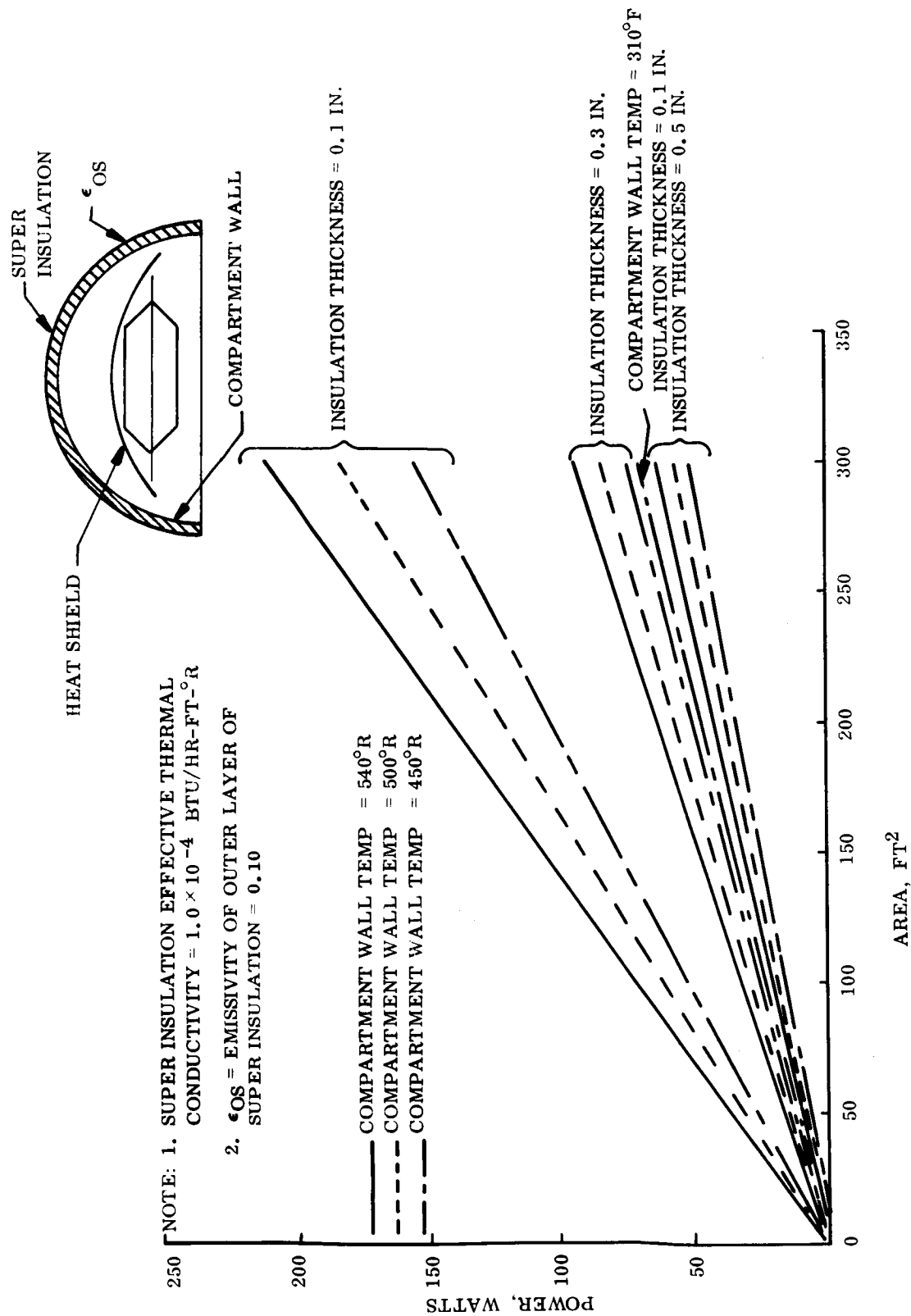


Figure 5.3.4-2. Transit Mode Power and Insulation Requirements for Varying Canister Areas

5.3.5 DE-ORBIT PROPULSION SYSTEM

5.3.5.1 Design Constraints

The design constraints for the de-orbit propulsion system for Point Design 3 were as follows:

1. De-orbit weight of 1350 lb (less propulsion)
2. Velocity increment 235 meters/sec
3. Liquid monopropellant system
4. Burn time of approximately 60 sec.

5.3.5.2 Systems Description

5.3.5.2.1 De-Orbit Propulsion Equipment

The selected propulsion equipment for the Mars Hard Lander Point Design 3 is a liquid monopropellant system conforming to the requirements presented below. This section presents the performance data and system description of the selected de-orbit propulsion equipment.

The de-orbit propulsion system must impart a velocity increment of 235 meters/sec to a 1350 lb vehicle for out-of-orbit planet entry at 15.3 kft/sec and a path angle of 16° . The vehicle weight does not include the propulsion system weight. Thrust termination is required and the system must be aligned to within $\pm 2^\circ$ with respect to the principal axis.

The performance, weight, and basic envelope data is presented in table 5.3.5-1. The propellant weight shown in the table is useful propellant weight. Inert weights consist of thrust chambers, valves, tanks, plumbing, residual propellants, gas, and structure.

Additional monopropellant systems were sized to show variability obtainable between burn time and weight; the weight change primarily due to an increase or decrease in quantity of thrust chamber assemblies. The 600 lb thrust system was selected because of the burn time constraint.

The monopropellant system will not require component development since it will use existing components. No significant changes to component function or reliability are anticipated due to the effects of the heat sterilization requirements. This is based on the heat sterilization program conducted by Martin Marietta on a bipropellant liquid system and the assumption that similar components will perform similarly when exposed to sterilization cycles. However, the cost advantage of using existing components is offset by the sterilization requirements. This is because of the additional testing at the subsystem level (i. e., pressurization assembly, propellant feed assembly, etc.) and system level that is required for verification of the above assumptions. To date,

TABLE 5.3.5-1. PERFORMANCE, WEIGHT, AND ENVELOPE DATA

Parameter	Per Require- ments	F = 100 (lb)	F = 100 (lb)
ΔV (meters/sec)	235	235	235
Payload weight (lbm)(less propulsion)	1350	1350	1350
Total Propulsion System weight, (lbm)	261	199	225
Propellant weight (lbm)	153	147	150
Propulsion Inert weight (lbm)	108	52	75
TCA	43.2 ^(*)	5.9 ^(*)	21.6 ^(*)
Controls (valves, filters, lines, etc.)	18.6	8.3	12.6
Structure	14.0	6.7	9.8
Propellant Tankage	10.9	10.5	10.7
Pressurant Tankage and Gas	16.3	15.6	15.9
Residual Propellant	4.7	4.5	4.6
Mass fraction (propellant wt/total wt)	0.59	0.74	0.67
Propellants	Anhydrous Hydrazine		
I_{sp} (specific impulse), vacuum, (sec)		240	
Nozzle Expansion Ratio		40	
Total Impulse (lbf-sec)	36739	35322	35919
Burn Time (sec)	61	353	120
Thrust (lbf)	600	100	300
Number of thrusters	2	1	1
Max Chamber Pressure (psia)	200	200	200
Approximate Dimensions (spherical diameter, in.)			
Fuel tank 1	17.0	16.7	16.8
Fuel tank 2	17.0	16.7	16.8
Gas tank	13.0	12.8	12.9

(*) Based on weight published by Walter Kidde or Rocket Research Corp.

no system subjected to heat sterilization has flown; therefore, the element of uncertainty involved requires additional testing.

A representative schematic diagram for a monopropellant propulsion system is presented in fig. 5.3.5-1. It is a regulated-gas pressure-fed system utilizing anhydrous hydrazine (N_2H_4) as the monopropellant. Helium gas, stored at 3600 psia, is used as the pressurant. Squib valves isolate the propellant and pressurant supplies until the system is required, at which time they are actuated. At maneuver completion, squib valves are again actuated to positively shut-down the system.

Components are grouped together and connections are welded to eliminate external leakage. Functional groups are joined by field brazed joints where welding is not practical. Squib valves are used, where feasible, to eliminate solenoid-operated valves and assure high system reliability. Each of the major functional groups (pressurization, propellant feed, and thrust chambers) is described below.

The helium gas is stored at 3600 psia in a 6A1-4V titanium alloy spherical tank. Two parallel squib-operated gas isolation valves are used to maintain the helium in the tank until the system is required for the de-orbit maneuver. Immediately downstream to the squib valves is a filter to remove particulate matter which might be generated by the squib valve actuation and be contained within the system. High pressure gas is fed to the pneumatic regulator providing regulated gas at a pressure of approximately 320 psia to the propellant feed system. A normally-open squib valve is provided to positively shut down the gas system at maneuver completion. The propellant tank system is protected from over-pressurization by a burst-disc and relief-valve unit. All pressurization system components, except the tank, will be tray mounted as a single all-welded unit.

Two propellant tanks will be required. The tanks are spherical, fabricated from 6A1-4V titanium alloy and contain butyl-rubber bladders which collapse, when pressurized, around a standpipe to assure positive propellant expulsion. The tank discharge line feeds two parallel squib-actuated isolation valves. A manually-operated fill and drain valve is located in the common line. The squib valves are similar to those in the pressurization system in that they isolate the propellant until required and provide a redundant system. Downstream of the squib valves is a filter to trap particles generated by squib valve actuation. Normally open squib valves are provided in series to provide redundancy in the positive shutoff mode. All valves and filter will be tray mounted and welded together to minimize leakage.

Two 300 lb thrust chambers will be required since there are no qualified thrust cone assemblies between 300 and 2000 lb thrust. Decomposition of the hydrazine is accomplished in a catalyst bed made from Shell 405 catalyst. Decomposed hydrazine at a temperature of approximately $1800^{\circ}F$ discharges through the nozzle to provide the desired thrust.

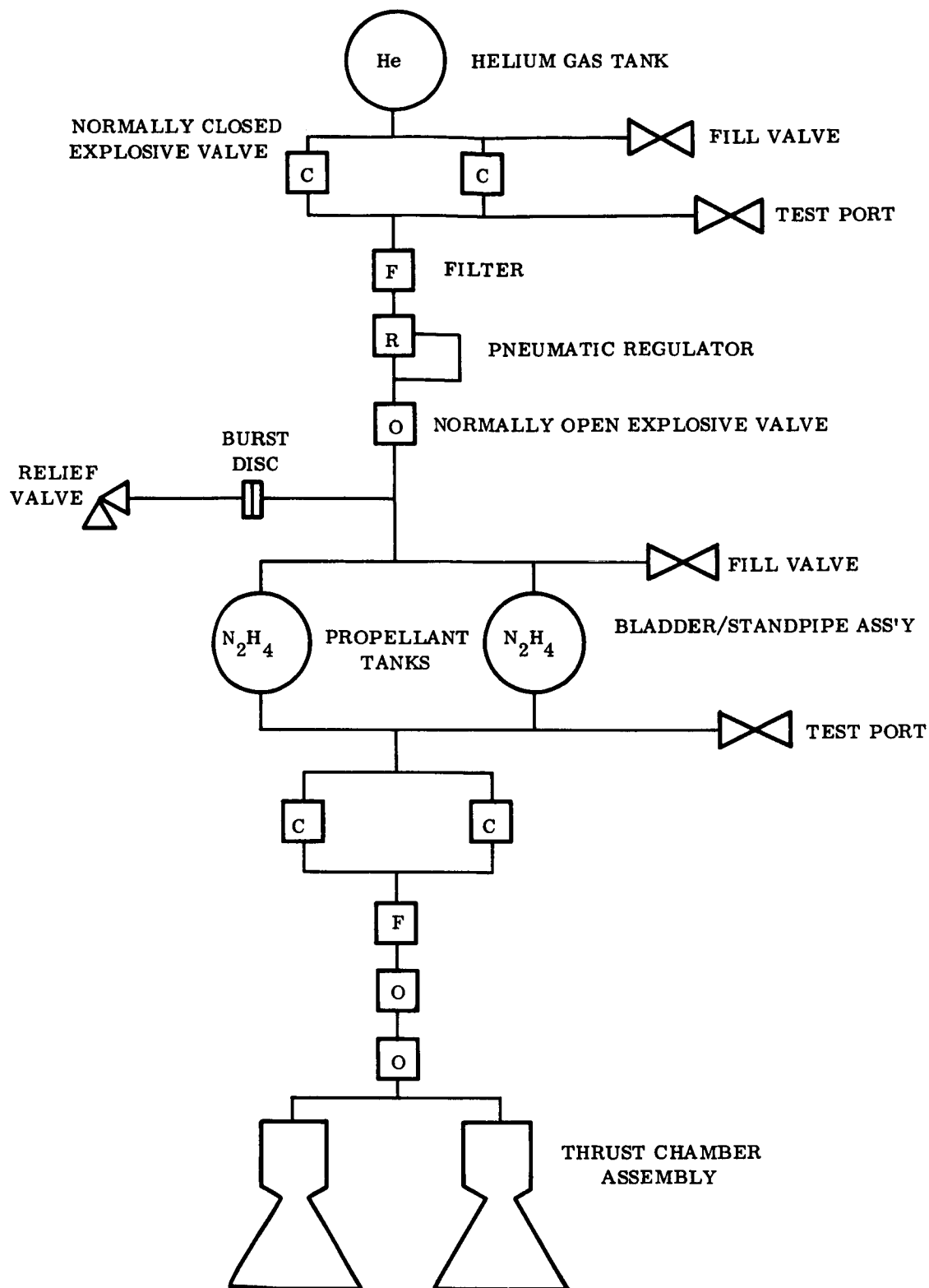


Figure 5.3.5-1. Monopropellant System Schematic

5.3.5.2.2 De-Orbit Structure

The de-orbit propulsion system for Point Design 3 is supported by an aluminum sheet metal thrust cone which is attached to the Lander cover by means of four tubular struts. Fig. 5.3.5-2 depicts the complete assembly and the associated attachments.

The thrust cone structure is a built-up sheet metal structure designed to hold and support the two fuel tanks, gas tank and thrust chambers. Structurally, it consists of sheet stiffened by full depth ribs and angles. Openings, which serve as saddles for the tanks, have been cut in the sheet. The tanks are held in place by skull caps, as shown in fig. 5.3.5-2, which are fastened to fittings on the cone structure. The cone structure is attached to the four tubular struts through a T-shaped ring. This ring takes the shear loads due to lateral loading conditions and redistributes them to the tubular struts. The ring also tends to stiffen the cone for torsional forces which occur during spin and despin.

The four struts are aluminum tubes which act as short columns taking the loads introduced by the cone structure and propulsion engine, redistributing them as four point loads into the Lander structure. The struts are attached to the Lander as shown in fig. 5.3.5-3, through a hot-wire bolt to a male fitting that fits into and is pinned to a female fitting on the Lander cover. The lower end of the column is threaded to match a threaded preload sleeve which, when tightened, puts tension in the hot-wire bolt. The de-orbit engine and all of the structure is released when the hot-wire bolt separates.

5.3.6 ELECTRICAL EQUIPMENT - PRE-ENTRY

The canister is equipped with electrical/electronic equipment which provides status monitoring during cruise, preseparation check-out, arming, electrical disconnection, separation initiations and separation event monitoring.

Commands from the Orbiter CC&S Subsystem are sent to the canister via hardwire where decoding takes place in the canister dual programmer. Signal from the programmer operate the power controller which contains redundant capacitor discharge energy storage units. Energy from these capacitors provide electrical initiation.

All canister equipment is powered from a sterilized dual silver-zinc secondary battery. This battery is similar in design to the Lander battery and its development is described in Volume III, Section 4.3.1. This provides an independent energy source for operation when the Orbiter solar arrays are pointed away from the Sun, e.g., maneuver and separation attitude, for separation event monitoring after Lander disconnection, and to avoid sending initiation energy across an interface.

Thermal batteries located on the thrust cone provide high level currents for the electrical initiation events associated with spin, de-boost and de-spin. These are ignited from the Lander through thermal relay modules which protect the operational battery against initiation circuit faults. The thermal batteries are used in redundant pairs with diode blocking for isolation.

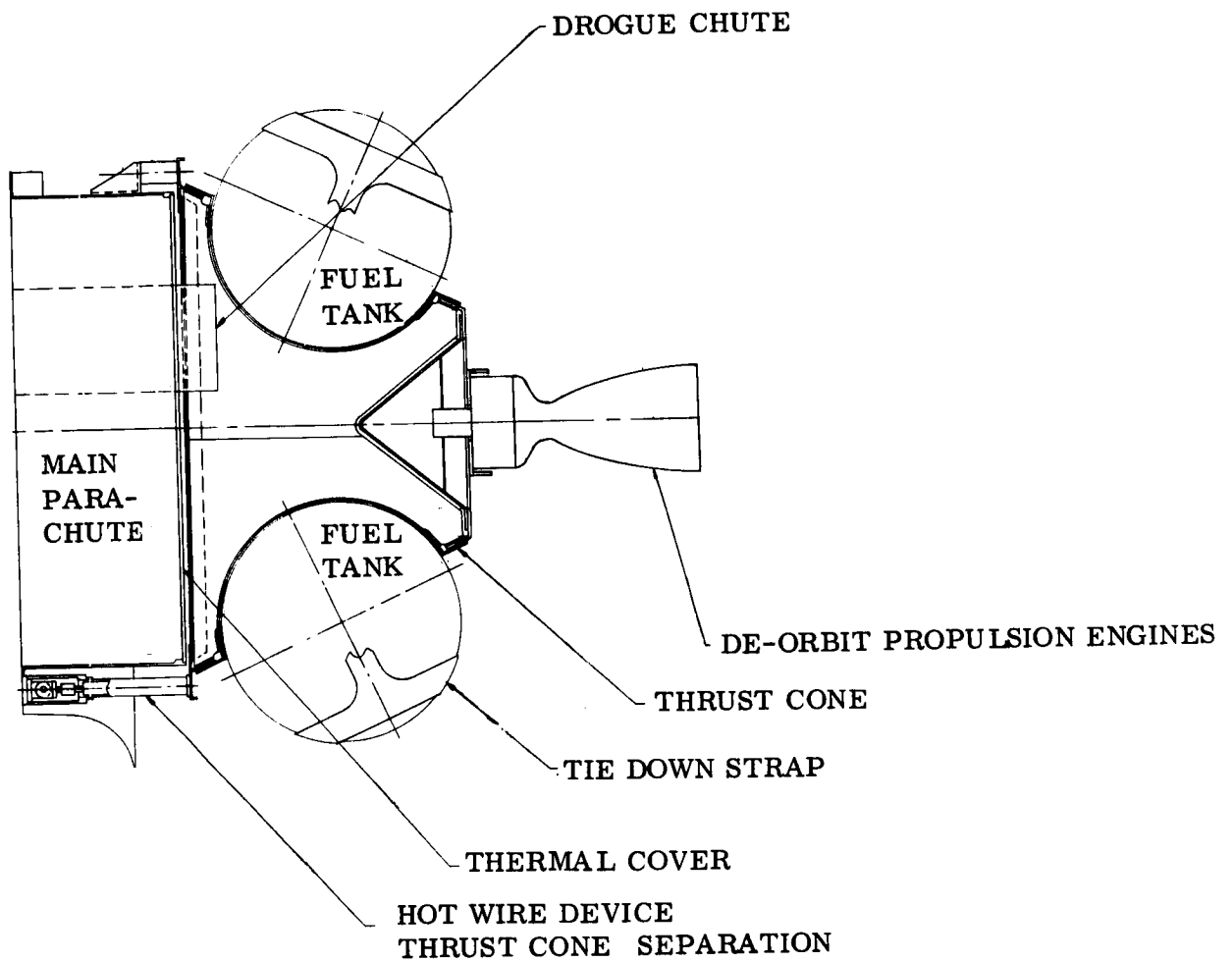


Figure 5.3.5-2. De-orbit Propulsion Structure

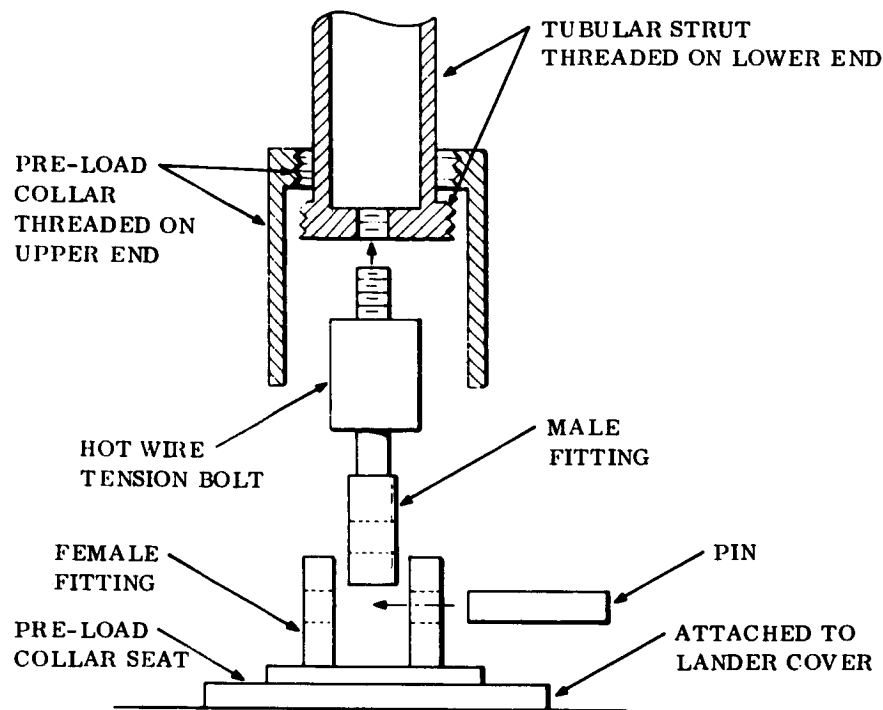


Figure 5.3.5-3. Thrust Cone Separation

5.3.7 DE-ORBIT SYSTEM

5.3.7.1 Spin Control Subsystem

The subsystem configuration for Point Design 3 performs attitude control for the de-orbit system and roll control for the entry system. By combining these functions, the overall equipment design is simpler, weighs less, and, since fewer components are needed, is more reliable. In the following discussion, reference will be made to the entry system description, Section 5.4.7, where appropriate.

5.3.7.1.1 Spin Requirements

The most important requirement for the spin control subsystem is to control the Capsule attitude during firing of the propulsion system so that the error in direction of the velocity increment (ΔV) will not cause excessive entry path angle or down range dispersions. Errors will be caused by thrust misalignment of the propulsion engine, center-of-mass offset of the Capsule, separation tip-off rates, and by other sources to be discussed later. The spin control subsystem provides a combination of gyroscopic stability and cyclical averaging to reduce the effect of these error sources to less than 2.1° , 3-sigma error on the ΔV orientation.

Another requirement for the subsystem is to control the Capsule attitude at the beginning of entry into the atmosphere so that a large initial angle-of-attack, or even backward entry, is avoided. Since the initial angle-of-attack can be as large as 40° , the requirement is met by maintaining until entry the same inertial orientation established for de-orbit propulsion firing. Again, the gyroscopic stability of the spin control performs this function.

The requirements for roll control during entry are discussed in Section 5.4.7 under entry systems. Additional requirements and constraints for spin control are summarized in table 5.3.7-1. These requirements determine the required torque level and impulse.

5.3.7.1.2 Description of the Spin Control Subsystem

The spin control subsystem consists of a small monopropellant hydrazine reaction control, a single rate gyro, and an electronic assembly. A block diagram is shown in fig. 5.3.7-1. The rate gyro measures Capsule roll rate which is compared with the output of the roll rate generator. When the spin command is given, the high rate (50 rpm) mode is used for spin-up for engine firing. When the de-spin command is given, the low rate (5 rpm) mode is used for both de-spin and entry roll control. When the error voltage is larger than the preset threshold, the valve drivers operate the appropriate valve to generate corrective roll torques.

TABLE 5.3.7-1. SPIN AND ROLL CONTROL REQUIREMENTS,
POINT DESIGN 3

Capsule weight	1700 lb.
Roll inertia	120 sl-ft ²
P/Y inertia	133 sl-ft ²
Moment arm	46 in.
Separation rate	0.5 deg/sec
CM offset	0.3 in.
Nozzle alignment error	0.5 deg
Velocity increment	771 ft/sec
Time, separation to entry	4700 sec
Entry spin rate	5 rpm
Entry roll torque	14.5 ft-lb
Entry roll impulse	620 ft-lb/sec

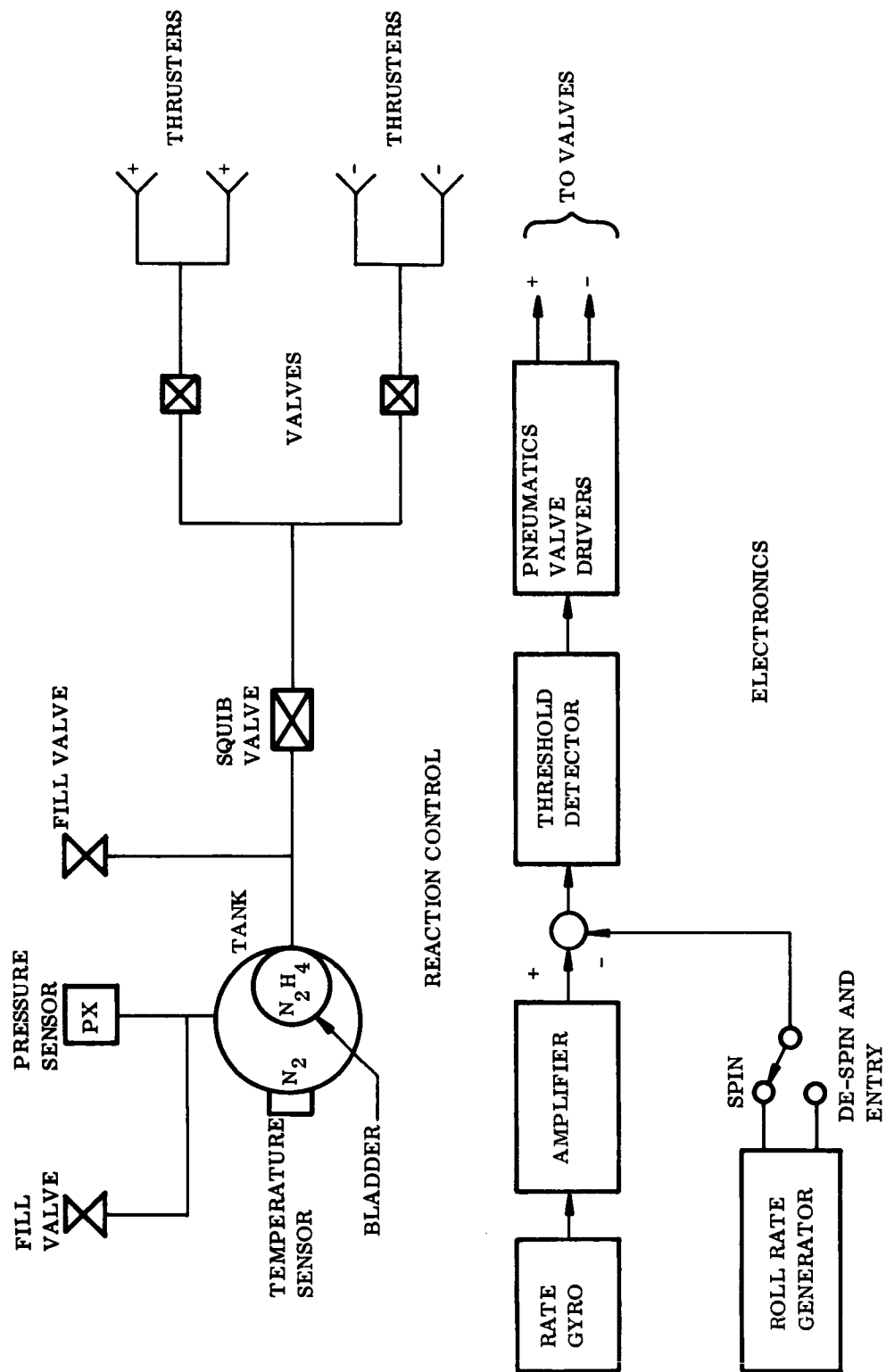


Figure 5.3.7-1. Spin and Roll Control Subsystem, Block Diagram

Reaction control is provided by a blow-down hydrazine system using nitrogen as a pressurant. An aluminum tank (less than 8 in. diameter) is used. Its size is chosen so that the initial gas pressure of 400 psi is reduced to 300 psi when all of the hydrazine has been expelled. This limits the thrust decrease to approximately 25 percent. All control torques are provided as couples. The system is sealed off until Capsule separation by the explosive squib valve shown in fig. 5.3.7-1.

Power requirement for the gyros and electronic assembly is 5 watts. When one of the valves is energized, an additional 2 watts is required. The size of the combined gyro and electronics is 5 x 6 x 3 in.

The operational sequence of the subsystem is as follows:

1. The spacecraft orients the Capsule in the proper direction for firing the de-orbit propulsion engine. The gyros and electronics are energized just prior to separation. The high rate mode of operation is commanded.
2. At 1.5 sec after separation, the explosive squib is fired, initiating spin-up.
3. A spin rate of 50 rpm is reached 25 sec after spin-up is started. This rate is maintained during propulsion firing.
4. After propulsion firing, and prior to entry, the low rate mode of operation is commanded. The subsystem remains in this mode throughout entry.

5.3.7.1.3 Spin Control Subsystem Performance

The pointing accuracy of the spin control subsystem is, of course, directly dependent on the accuracy with which the spacecraft orients the Capsule prior to separation. Two major additional errors are introduced by the Capsule separation subsystem and the spin control subsystem. These errors are the tip-off error and the coning error during propulsion firing.

The tip-off error is caused by the Capsule angular rate uncertainty at separation. This rate produces an attitude deviation from the separation spacecraft attitude proportional to the time interval from separation to spin-up command. It is estimated that the separation tip-off rate can be held to less than $0.5^\circ/\text{sec}$. For spin-up occurring 1.5 sec from separation, this creates an angular error of 0.75° , 3-sigma.

The coning error is caused by the upsetting torque created by the propulsion thrust not acting through the Capsule center of mass. Gyroscopic action reacts to the torque by producing spiralling increase in the attitude error. To maintain a required ΔV orientation error, the spin rate must be increased as the propulsion thrust level is made larger. For the selected spin rate of 50 rpm, the ΔV orientation error will be held to less than 0.75° , 3-sigma.

An error analysis, including these and other error sources, was described in Volume III, Section 5.2.5. The overall error in ΔV orientation is estimated to be 2.1° , 3-sigma.

The attitude error of the Capsule at entry into the atmosphere is dependent on the stability of the spinning Capsule from the time of propulsion burnout to entry. To use spin stabilization during this period, the problem of energy dissipation, which could lead to attitude divergence, must be considered. Since a vehicle is stable about the axis of maximum moment of inertia, even with energy dissipation, the majority of the point designs will present no problem since their roll (spin) axis inertia is much larger than that of the pitch/yaw axes. However, Point Design 3 has a roll inertia slightly less than that of the other axes. Since this is an out-of-orbit mission with a relatively short flight time prior to entry, the possible attitude divergence is probably small enough not to create a significantly large inertial angle-of-attack. This potential problem should be examined further if significant body flexibility or other energy dissipation means are present.

5.3.8 PRE-ENTRY SYSTEMS WEIGHT

The weights of those items contained within the pre-entry systems for Point Design 3 are listed in table 5.3.8-1. (The attitude control system is carried in the entry system weight summary, table 5.4.8-1.) Total pre-entry system weight for Point Design 3 including contingencies, is 522 lb.

TABLE 5.3.8-1. PRE-ENTRY SYSTEMS WEIGHT SUMMARY
POINT DESIGN 3

Equipment	Weight (lb)
<u>Thrust cone assembly</u>	<u>299.7</u>
• Structure	30.0
• Propulsion system (less propellant)	108.0
• Propellant	153.0
• Separation system	1.2
• Electrical	7.5
<u>Canister assembly</u>	<u>221.9</u>
• Shell	45.5
• Internal structure	41.9
• Separation rings	25.9
• Separation system	12.2
• Pressure and venting system	6.0
• Electrical power and distribution	53.4
• Thermal blanket	16.8
• Hardware and miscellaneous	20.2
Pre-entry System Total	521.6

5.4 ENTRY SYSTEMS

5.4.1 CONFIGURATION

5.4.1.1 Constraints

Constraints for Point Design 3 were placed on the following parameters:

1. Ballistic coefficient
2. Entry system weight
3. Maximum aeroshell diameter
4. Entry angle and velocity
5. Payload weight and volume
6. Powered flight and entry loads
7. Materials and construction techniques

The design goal was to achieve a vehicle design with a ballistic coefficient of 14 lb/ft². This had to be achieved within the envelope constraints discussed in Volume IV, Section 2.3.1, which limited the Capsule system maximum diameter to 103.9 in. and the entry system diameter to 100 in., as shown in fig. 5.3.1-1.

Entry system weight was an important parameter, since along with the half cone angle and basic diameter it determined the final ballistic coefficient achieved for a given design. It must be pointed out that the ballistic coefficient was the over-riding criteria, since it was this factor that had the most effect in heating rates, trajectories, and loading and determined the retardation system deployment regime. Table 5.4.1-1 shows a tabulation from the Configuration Selection Program (CONSEP) for Point Design 3. It can be seen from looking at this table that for a fixed base diameter of 100 in. and a varying half cone angle of 50 to 70°; the ballistic coefficient varies from 20.61 down to 13.95 for a change of greater than 25 percent, while the weight change is only 21 lbs (less than 1.5 percent). This points up the fact that the ballistic coefficient is the important factor and must be held constant.

Internal clearances between the canister and the aeroshell limit the aeroshell diameter to 100 in. Additionally, the aeroshell could not be so small as to adversely affect the packaging of the Lander system. Working with both the 100 in. diameter and the packaging volume necessary for the Lander, Point Design 3 configuration was evolved.

The entry angle and entry velocity along with the ballistic coefficient, base diameter and bluntness ratio were important factors in determining the thickness of heat shield material necessary for this out-of-orbit mission.

TABLE 5.4.1-1. CONSEP RESULTS FOR POINT DESIGN 3

Cone Angle (deg)	$W/C_D A$ (lb/ft ²)	Entry Weight (lb)	R_B (in.)
50	20.61	1313	50
60	16.40	1302	50
65	15.00	1297	50
70	13.95	1292	50

$$\frac{R_N}{R_B} = 0.5$$

The payload weight was an important factor for determining internal shell loads and for sizing the retardation system, since it was this weight which contributed greatly to the total decelerator load.

The critical loading conditions for the entry system in the out-of-orbit mode were conditions J, K, O and P as shown in table 5.4.1-2. It was based on these conditions and the entry heating environment that the aeroshell structure was selected. Also important in selection of the material and construction of the aeroshell was ease of fabrication, cost, and light weight.

5.4.1.2 Description

Geometrically, Point Design 3 is a blunt sphere-cone vehicle with a bluntness ratio (R_N/R_B) of 0.5. The spherically shaped nose has a radius of 25 in. making a tangent with a frustum of a cone with a half angle of 60° and a base diameter of 100 in. as shown in fig. 5.4.1-1.

The heat shield is an elastomeric shield material ESM1004X with a tapering thickness from the stagnation region to the end of the skirt. Density of this selected heat shield material is 16.0 lb/ft³. Corner heating effects were accounted for in the design and protection has been provided in the form of a peripheral edge protection. To protect against the possibility of backface heating around the edge of the entry vehicle, the backface, for a short distance, is coated with a heat shield material.

The aeroshell structure is an aluminum honeycomb shell with a core thickness of 0.75 in. and facing sheets 0.020 in. thick to form a total shell thickness of 0.79 in. In the aft end of the aeroshell is a torque box structure made up of webs and rings with periodic ribs to provide internal stiffness. This structure tends to stiffen the

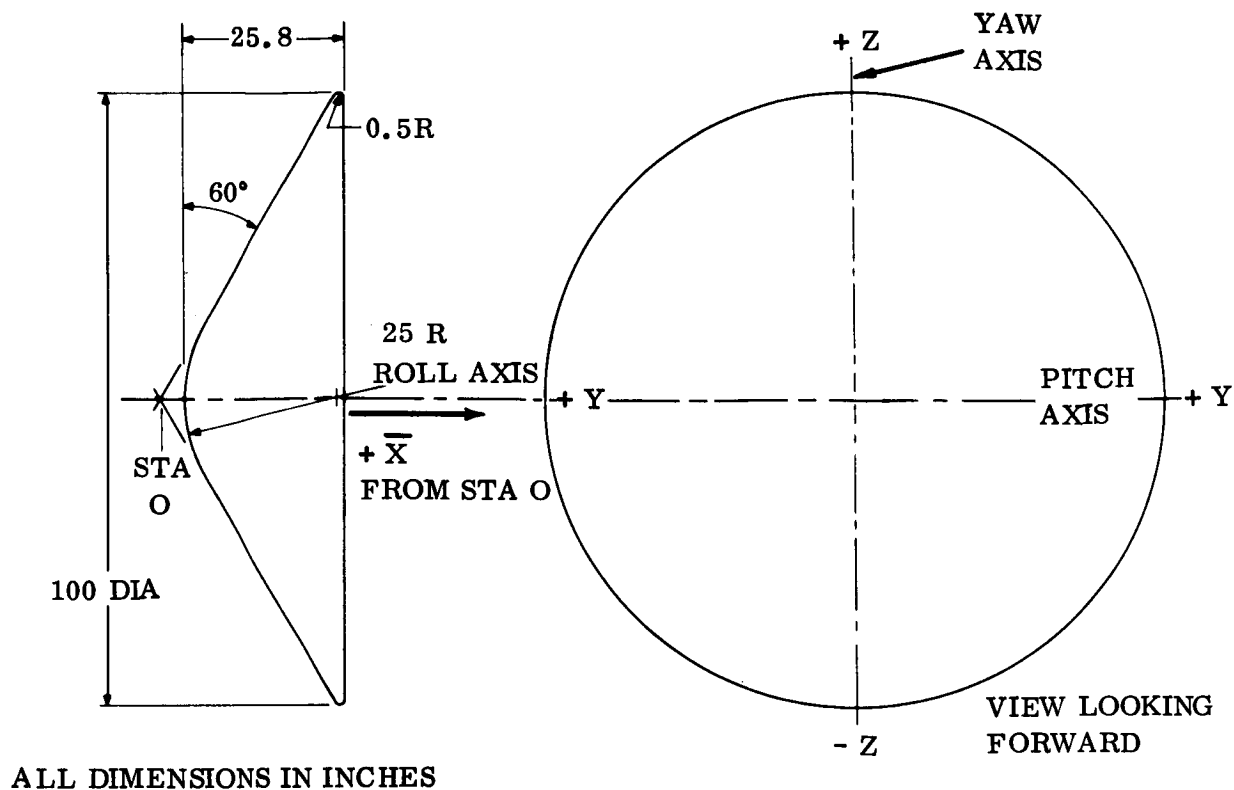


Figure 5.4.1-1. Aeroshell Geometry, Point Design 3

shell and minimize local shell bending and rotation, as well as provide a load path for the Lander loads introduced by securing the Lander into the aeroshell. The combined spin, despin, and roll control nozzles are mounted on the aft web of the torque box. Separation forces, which occur at separation from the adapter and at Lander release, are taken in the longitudinal web of the box.

The Lander is held in by a strap arrangement which consists of strap, or belly-band, which runs completely around the Lander (see fig. 5.3.1-2), hot-wire device, T-bolt, tie-down strap and torsion spring. The load in the tie-down strap is sufficient to overcome the rotational forces due to spin and de-spin and thus restrain and Lander from moving during these events.

The forward portion of the Lander sits in a phenolic glass honeycomb saddle which has a teflon lining between it and the Lander to eliminate the possibility of adhesion of the saddle and Lander to each other during the long space flight while under the tie-down load.

Pressure sensors a temperature sensor and an air intake which leads into the mass spectrometer located in the Lander, are located in the hose of the aeroshell.

TABLE 5.4.1-2. POINT DESIGN LOADS

Letter	Condition	Limit Load (Gx)	Acceleration (Gn)	Remarks
A	Ground handling	2.0	2.0	
B	Band Clamp	N/A	N/A	83 lb/in radial
C	First stage burnout	5.2	2.0	
D	Second stage burnout	4.0	2.0	
E	Axial vibration	+6.0 -3.0	---	
F	Lateral vibration	---	±2.0	
G	Canister separation	Negligible	Negligible	
H	Entry systems separation	Negligible	Negligible	
I	Thrust cone separation	Negligible	Negligible	
J	Entry (max Gx)	5.5	Negligible	Out-of-Orbit 320° interface
		12.7	Negligible	Out-of-Orbit 250°F interface
		48.0	Negligible	Direct Entry 200°F interface
K	Parachute opening	10.0	---	
L	Impact	1000.0	---	
M	Canister pressure	N/A	N/A	$\Delta P = 0.5$ psi at 275°F
N	Canister pressure	N/A	N/A	$\Delta P = 1.0$ psi at Ambient
O	Spin	N/A	N/A	50
P	Sterilization	N/A	N/A	

5.4.2 HEAT SHIELD

At the heating rates expected for the out-of-orbit Point Design 3 mission described in table 5.4.2-1, the most efficient materials on a weight basis are, in general, members of the low density charring ablator class. Thus, because of the relatively mild Martian entry environment where total surface recession is small in most cases and thermal insulation is of prime importance, the low density charring ablator, ESM 1004X was selected to be a design solution for the Mars Hard Lander heat protection system for out of orbit entry modes.

The basis for selection of this material was:

1. Minimum system weight
2. Maximum flexibility to accommodate non-design conditions
3. Fewer anticipated fabrication and development problems than with other approaches
4. Sensitivity to the sterilization/decontamination and low temperature/hard vacuum environments can be circumvented by proper material formulation.

ESM 1004X (16 lb/ft³ density) was selected as the preferred shield material for out-of-orbit Point Design 3 mission since no surface melting is anticipated, even for the steep angle entries of 16° nom (+2°) into the VM-8 atmosphere. However, ESM 1004X is not the most efficient shield material in the flight regime where surface melting occurs.

It has been shown in Volume III, Section 3.1.2 that the maximum heat shield thickness requirement is dictated by the shallowest entry angle path attainable. The heating histories which include both convective heating and equilibrium and non-equilibrium radiative heating for Point Design 3 are shown in fig. 5.4.2-1 for the stagnation point and end of skirt locations.

Employing the thermo-physical properties described in table 5.4.2-2 and the convective and radiative heat flux histories shown in fig. 5.4.2-1, the heat shield thickness requirements were generated, using the techniques described in Volume III, Section 3.1.2 and are shown for Point Design 3 in fig. 5.4.2-2. The shield thickness requirements are those required to hold the design bondline temperature to 600° F with a safety factor of 1.0. In lieu of a detailed evaluation to justify a statistical safety margin it is suggested that a safety factor of 1.2 be applied to the shield thickness requirements presented for Point Design 3. This would result in a margin of about 200° F on the backface temperature. Analysis has shown that one of the most significant factors which affects the estimation of the shield thickness to the lower limit on entry path angle results in a safety margin of about 10 percent for Point Design 3 when compared to the nominal entry condition.

The backface and frontface temperature histories of the shield material for Point Design 1 are shown in fig. 5.4.2-3. Fig. 5.4.2-4 shows the thermal gradients through the ESM material at selected times in the Martian entry corresponding to peak surface

TABLE 5.4.2-1. ENTRY CONDITIONS AND GEOMETRY OF POINT DESIGNS 1 THROUGH 6

Point Design	Mission Entry Mode	Entry Velocity (kft/sec)	Entry Angle (deg)	Ballistic Coefficient (lb/ft ²)	Aeroshell Base Diameter (ft)	Half Cone (deg)	Rn/Rb
1	Out-of-Orbit	15.3	14	14	8.33	60	0.5
2A	Direct	20.8	16	7	12.7	60	0.5
2B	Direct	20.8	16	7	11.4	60	0.5
3	Out-of-Orbit	15.3	14	14	8.33	60	0.5
4	Direct	20.8	16	7	12.7	60	0.5
5	Out-of-Orbit	15.3	14	14	10.0	60	0.5
6	Direct	20.8	16	7	14.0	60	0.5

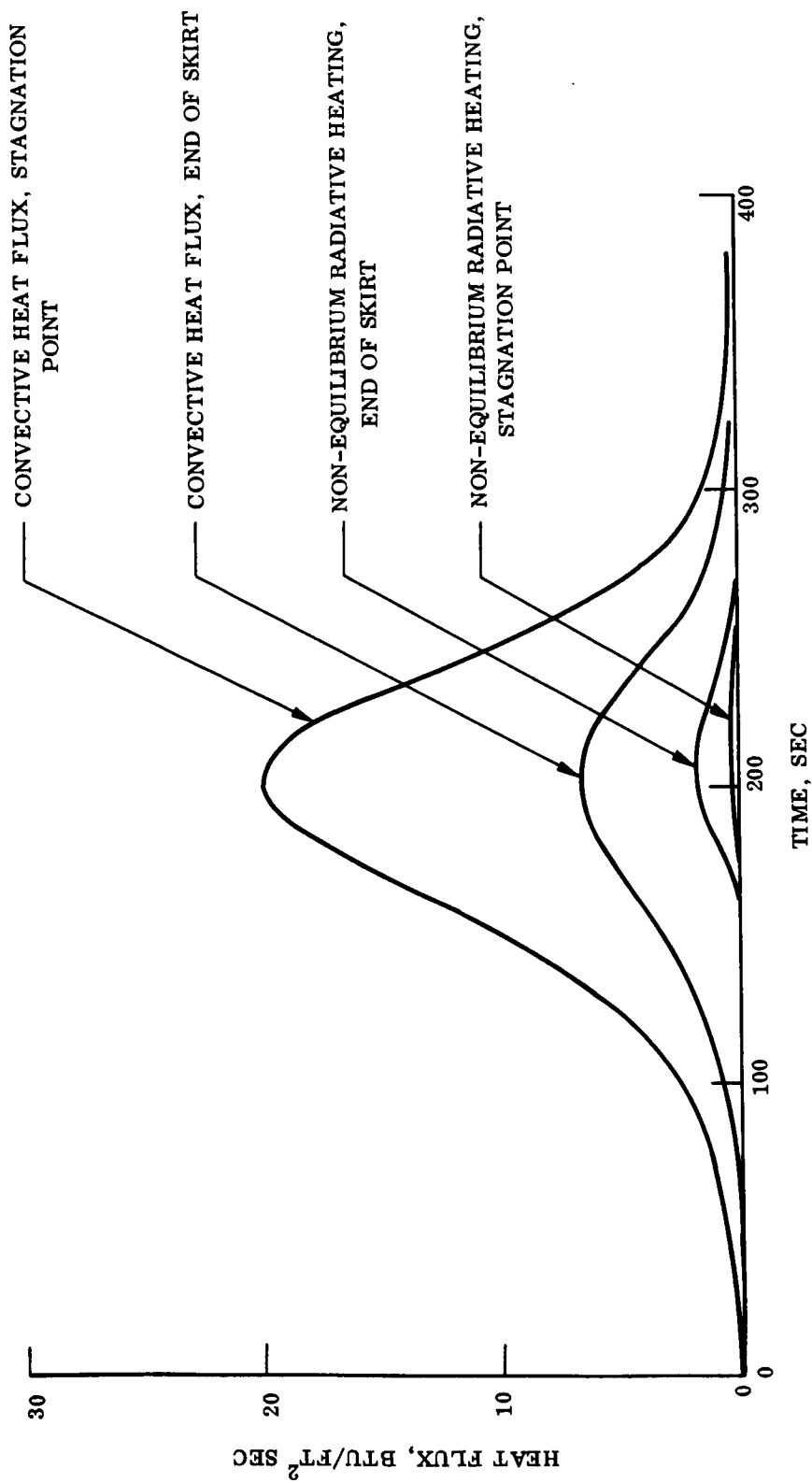


Figure 5.4.2-1. Cold Wall Convective and Radiative Heat Flux Histories, Point Design 3

TABLE 5.4.2-2. THERMOPHYSICAL PROPERTIES OF ESM MATERIALS

		ESM 1004X	ESM 1004AP
Virgin density (P_v lb/ft ³)		16.6	35.0
Char density (P_c lb/ft ³)		6.7	14.0
Pyrolysis gas specific heat (Cpg Btu/lbP)		.4	0.384
Molecular weight of injected species (Mg)		24.5	24.5
Order of reaction (N)		2	2
Pre-exponential factor (A sec ⁻¹)		15000	30000
Activation Energy (E Btu/lb mole)		44700	47500
Heat Decomposition (HGF)	1335°R	0	50
(Btu/lb gas generated)	1460°R		45
	1710°R		1000
	1960°R		2610
Specific Heat (Cp)			
(Btu/lb °R)	600°R	0.31	0.305
	710°R	0.33	0.360
	1210°R	0.44	0.44
	2075°R	0.44	0.44
Conductivity (k) Virgin	610°R	0.0000115	0.0000237
(Btu/ft - sec R)	800°R	0.0000170	0.0000220
	1335°R	0.0000220	0.0000210
	1710°R	0.0000260	0.0000231
Char	1335°R	0.0000740	0.0000777
	1710°R	0.0000850	0.0000855
	2210°R	0.0001000	0.000104

For the decomposition reaction described by the following Arrhenius type equation:

$$\frac{1}{W_o} \frac{dw}{dt} = \frac{(W-Wf)^N}{(W_o)} A e^{-\delta E/RT}$$

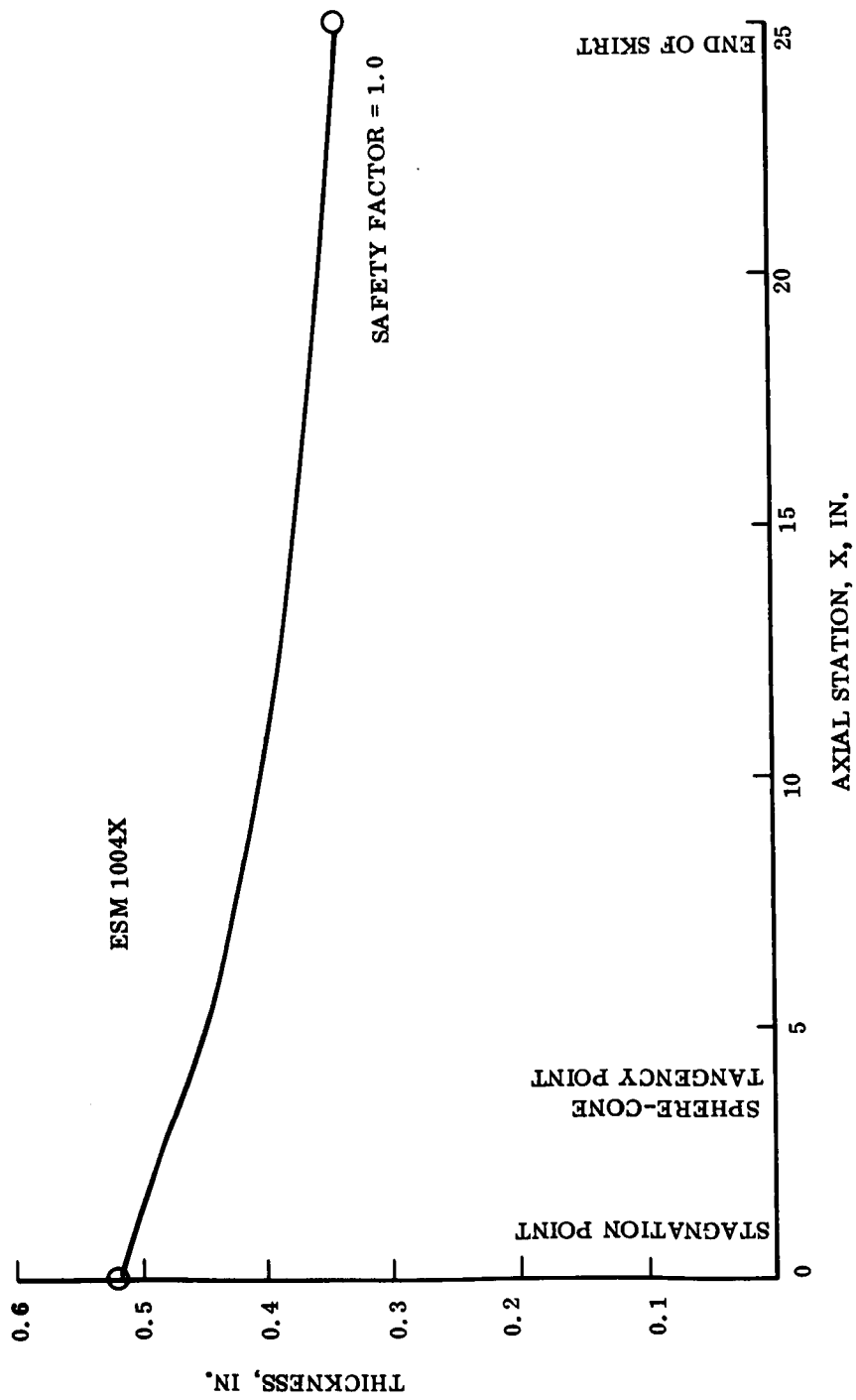


Figure 5.4.2-2. Heat Shield Thickness Requirements, Point Design 3

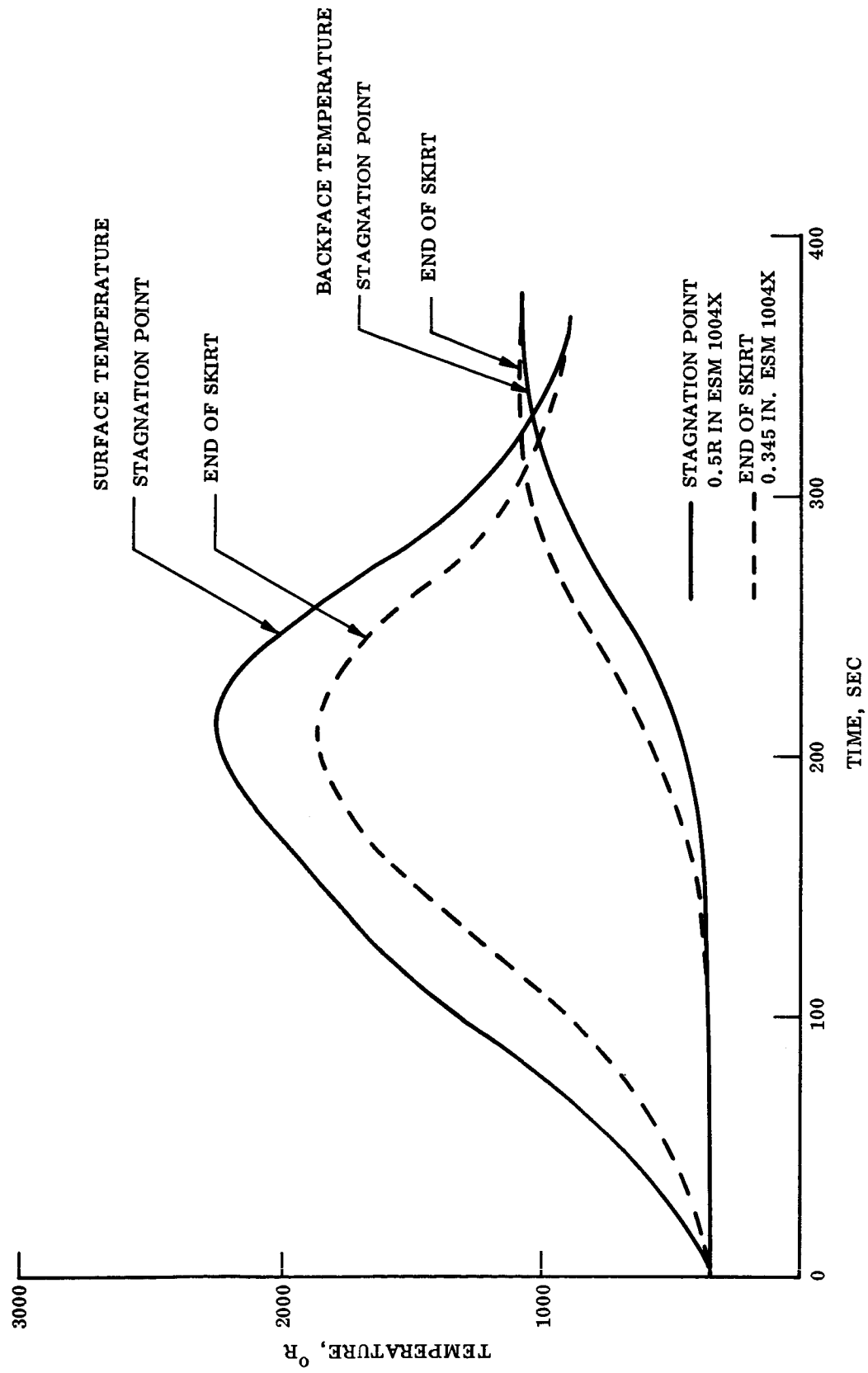


Figure 5.4.2-3. Surface and Backface Temperature Histories, Point Design 1

ESM 1004X

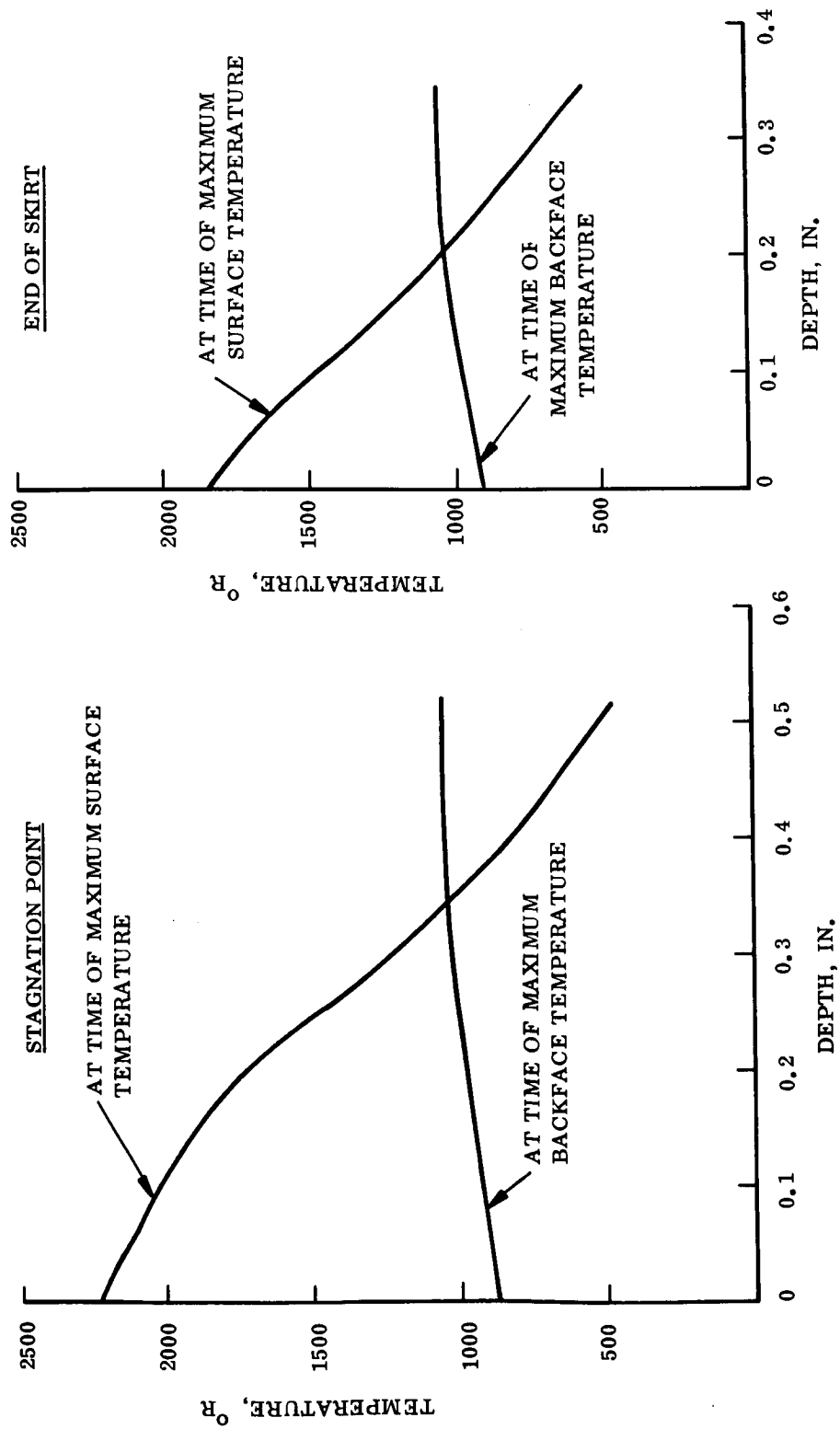


Figure 5.4.2-4. Temperature Gradients through the Shield, Point Design 1

temperature and peak bondline temperature. These results are presented for entry into the VM-3 atmosphere. Shield thickness requirements for Point Design 3 are shown in table 5.4.2-3. Since the entry conditions and shield requirements for Point Design 3 are very similar to those of Point Design 1, the thermal gradients and temperature histories presented for Point Design 1 in figs. 5.4.2-3 and 5.4.2-4 are representative for Point Design 3.

Since the total heat load on the afterbody of the sphere-cone is expected to be small compared with the forebody, an ablating material for thermal protection is unnecessary, and a high emissivity coating would be an adequate protection. An analysis * indicated that for Voyager the peak cold wall heat flux on the afterbody was small, the resultant temperature rise being only 256° F.

The current design for the ESM 1004X heat shield allows for ease of fabrication, handling, and final assembly. The heat shield material is designed to be fabricated in panel sections using maximum panel sizes, from a fabrication standpoint, of approximately 10 ft². Additional advantages of the segmented shield are that it allows for 100 percent inspection, does not require the aeroshell during manufacturing operations, and allows for finish machining prior to being bonded to the aeroshell.

Design considerations have also taken into account the necessity for steps between the segmented panels both longitudinally and circumferentially. These steps were determined by both the bond and heat shield thickness tolerances.

Corner heating effects have been taken into consideration at the base of the entry vehicle and a peripheral edge protection of ESM 1004AP is provided around the corner of the heat shield at the base of the aeroshell. To protect against the possibility of backface heating around the edge of the entry vehicle, the exposed aeroshell structure at the base and inboard on the vehicle is coated with ESM 1004X.

TABLE 5.4.2-3. SHIELD THICKNESS REQUIREMENTS FOR POINT DESIGNS 1 THROUGH 6

Point Design	Mission Entry Mode	Shield Material	Shield Thickness Requirements with 1.2 Safety Factor	
			Stagnation Point	End of Skirt
1	Out-of-Orbit	ESM 1004X	0.624	0.415
2A	Direct	ESM 1004 AP	0.367	0.275
2B	Direct	ESM 1004 AP	0.372	0.288
3	Out-of-Orbit	ESM 1004X	0.624	0.415
4	Direct	ESM 1004 AP	0.367	0.275
5	Out-of-Orbit	ESM 1004X	0.617	0.407
6	Direct	ESM 1004 AP	0.360	0.263

*McDonnell Astronautics Voyager Capsule Phase B Final Report F694, Vol II, Part B, 31 August 1967

5.4.3 AEROSHELL AND STRUCTURE

The aeroshell for Point Design 3 is an aluminum honeycomb shell 0.79 in. thick. It is comprised of a 3 lb/ft³ core 0.75 in. thick with 0.020 in. thick 2024 aluminum facing sheets bonded on with HT424 bond. This shell material has been selected for light weight, ease of fabrication, and much lower cost than other types of honeycomb materials. It has been designed to take the axial, bending, and shear loads encountered during powered flight and planetary entry.

The detailed analysis of the aeroshell to withstand the entry inertial loads and aerodynamic pressure loadings has been performed by MULTISHELL, a GE computer program. The inputs to this program to perform the analysis consist of the entire aeroshell configuration, upon which are imposed the inertia and pressure loadings. Output from the program consists of the shell internal stresses, moments, shear, inplane shell loads and, in addition, the complete shell deformations. These deformations include all local discontinuity deformations of the shell. Figs. 5.4.3-1 through -5 present the deflections, moments, shear, in plane load and stress distributions for Point Design 2A. The distributions for Point Design 3 are similar.

Approximate structural analysis was performed to determine the initial core and facing thicknesses to be used in the computer program. Upon completion of the first MULTISHELL analysis, any necessary changes to the structural material gages were made to result in small positive margins of safety for all of the elements of the shell as shown in table 5.4.3-1.

TABLE 5.4.3-1. FINAL ALUMINUM HONEYCOMB REQUIREMENTS
FOR AEROSHELLS

Point Design	Honeycomb		Minimum Safety Margin	Facing Material
	Facing Thickness	Core Thickness		
1	0.020	0.75	0.50	2024-T4
2A	0.025	1.50	0.09	7075-T6
2B	0.025	1.50	0.15	7075-T6
3	0.020	0.75	0.65	2024-T4
4	0.025	1.50	0.09	7075-T6
5	0.020	0.75	0.21	2024-T4
6	0.030	1.50	0	7075-T6

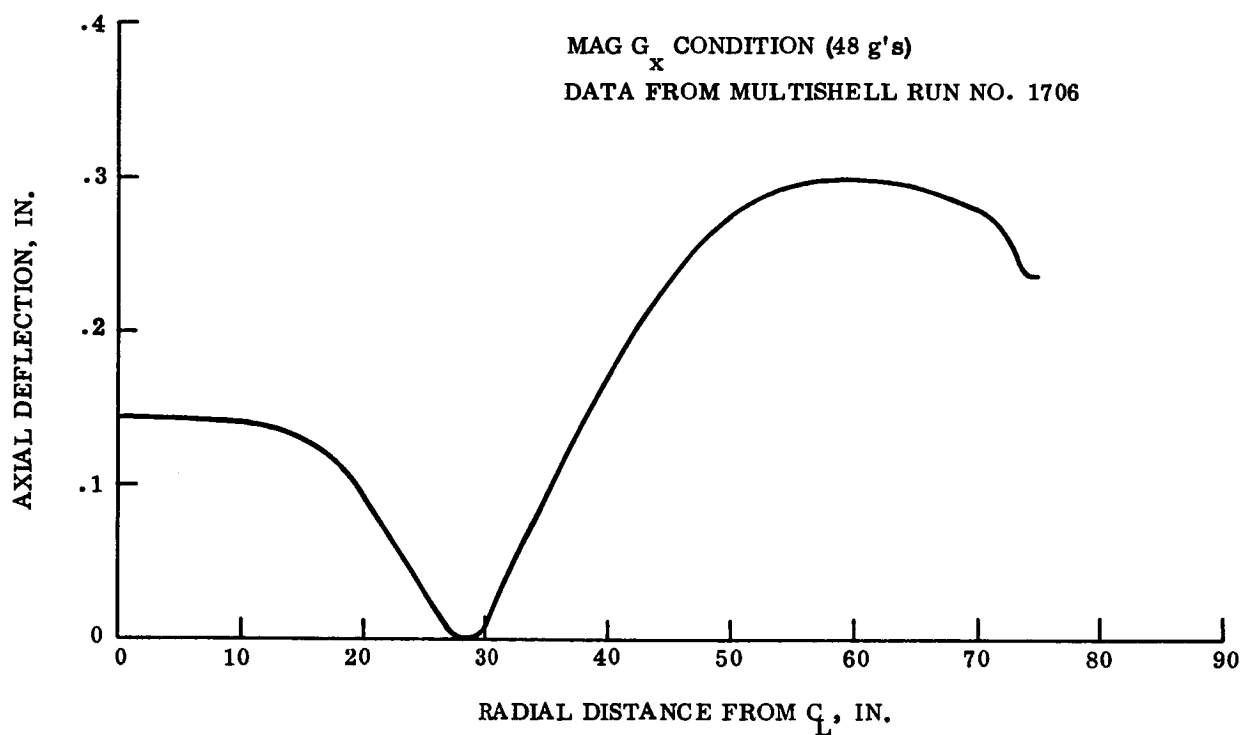


Figure 5.4.3-1. Axial Deflection - Aeroshell 2A vs Radial Distance

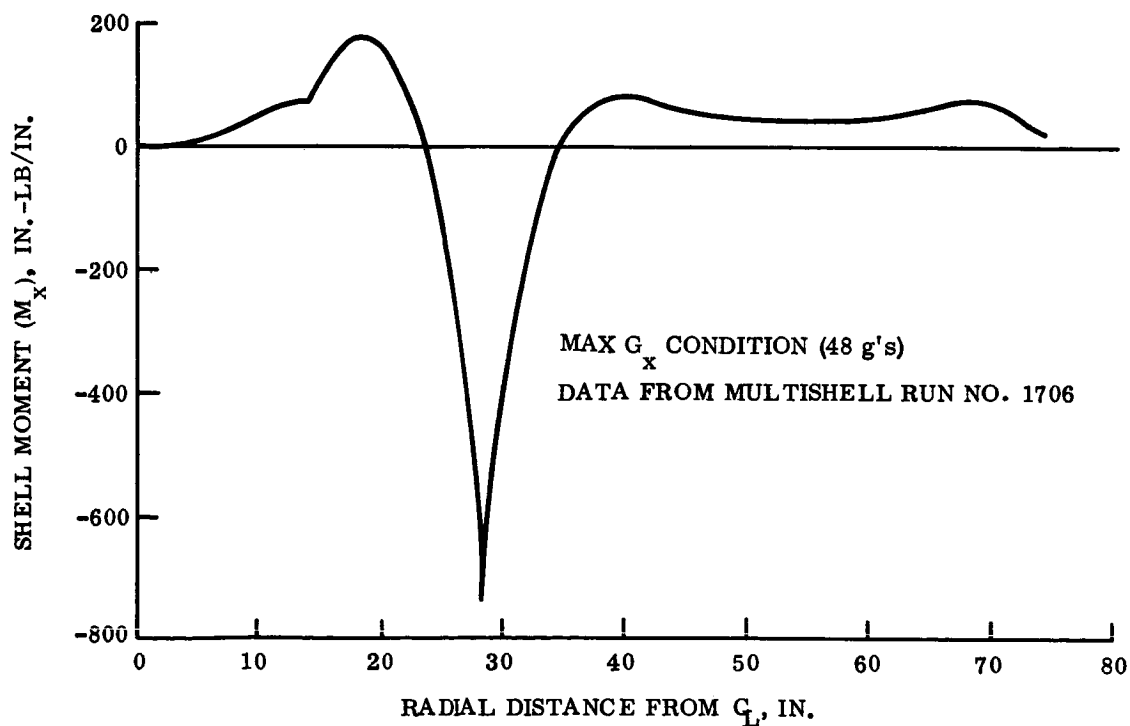


Figure 5.4.3-2. Axial Bending Moment (M_x) - Aeroshell 2A vs Radial Distance

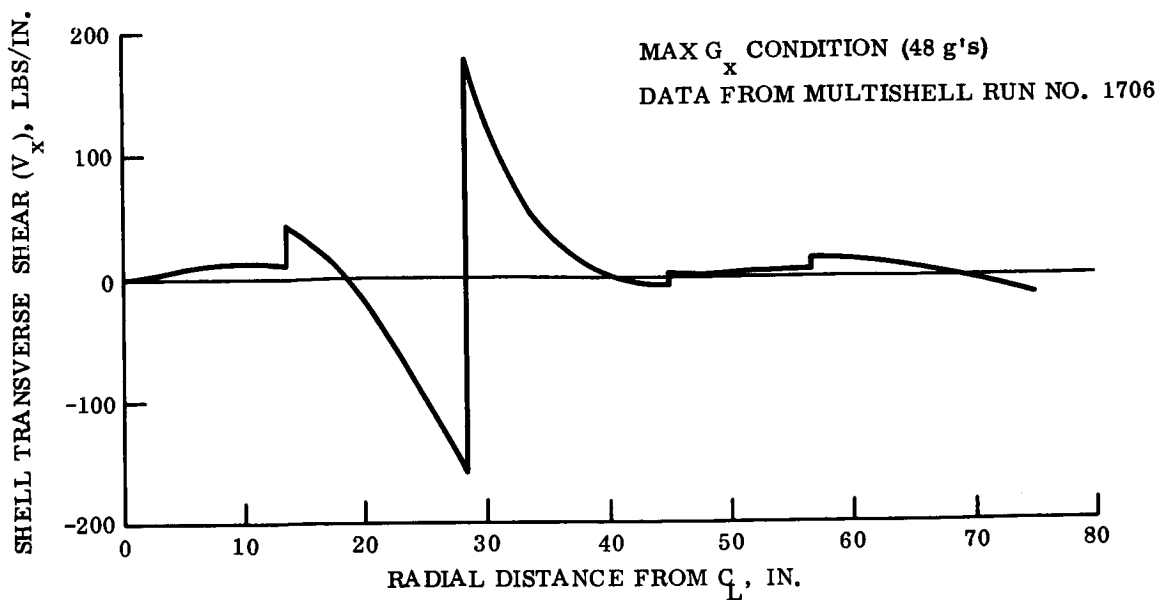


Figure 5.4.3-3. Shell Transverse Shear - Aeroshell 2A vs Radial Distance

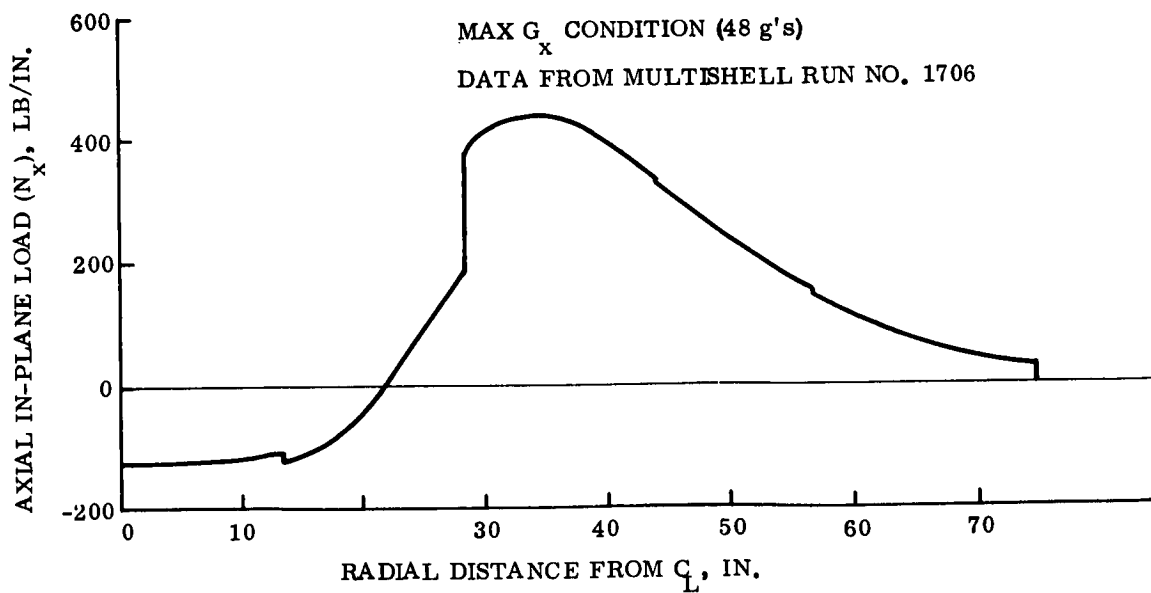


Figure 5.4.3-4. Axial In-Plane Load - Aeroshell 2A vs Radial Distance

Analysis of Point Design 3 indicates that the shell bending is critical and that aluminum honeycomb is just as efficient as titanium honeycomb, lighter than stainless steel honeycomb and easier to fabricate than both materials. The aluminum honeycomb is just as efficient as the titanium or steel honeycomb because local shell bending is the critical loading condition and the minimum gage is no longer the controlling factor. This local shell bending is induced by the loading of the aeroshell internally by the Lander and the aerodynamic pressure externally.

The heat shield structure interface temperature is only 200°F at the time of maximum loading (12.7 g's limit) and the loadings are lower at times of higher temperatures. At a temperature of 320°F the acceleration is reduced to 5.5 g's limit. The temperature at parachute deployment, at the heat shield structure interface, can be 600°F since at this time the loading on the aeroshell is negligible.

Figure 5.4.3-6 shows the relative load imposed on the aeroshell, the interface temperature and the yield strength of 2024-T4 Aluminum as a function of time from entry. The maximum load occurs 40 sec after peak heating for this out-of-orbit condition. At this time the heat shield structure interface temperature is 325°F. When parachute deployment occurs (348 sec from entry), the load has reduced 25 percent of the maximum value while the interface temperature has increased to 600°F. The total time at elevated temperature, prior to parachute deployment, is 150 sec or 2.5 min. The allowable tensile and compressive yield strengths for the 2024-T4 aluminum that have been plotted are a percentage of the allowable room temperature strength. These allowables are for the 1/2 hr (30 min) temperature exposure data from MIL Handbook 5 and are also shown in fig. 5.4.3-7.

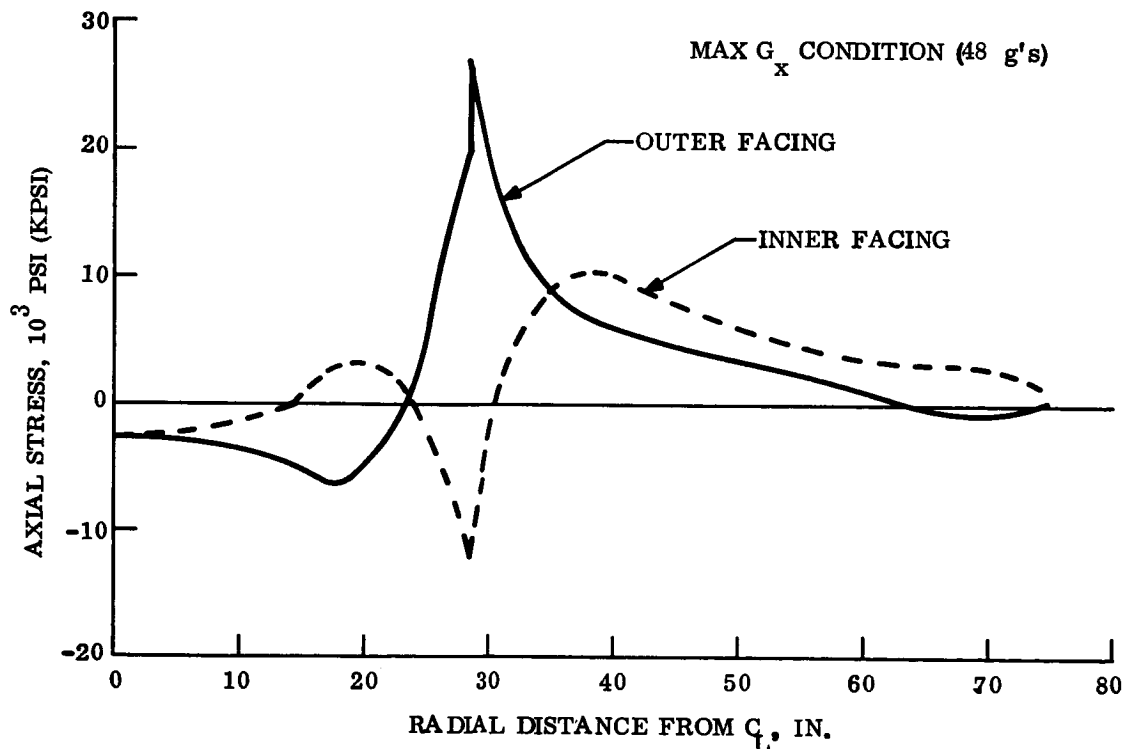


Figure 5.4.3-5. Axial Honeycomb Facing Stress - Aeroshell 2A vs Radial Distance

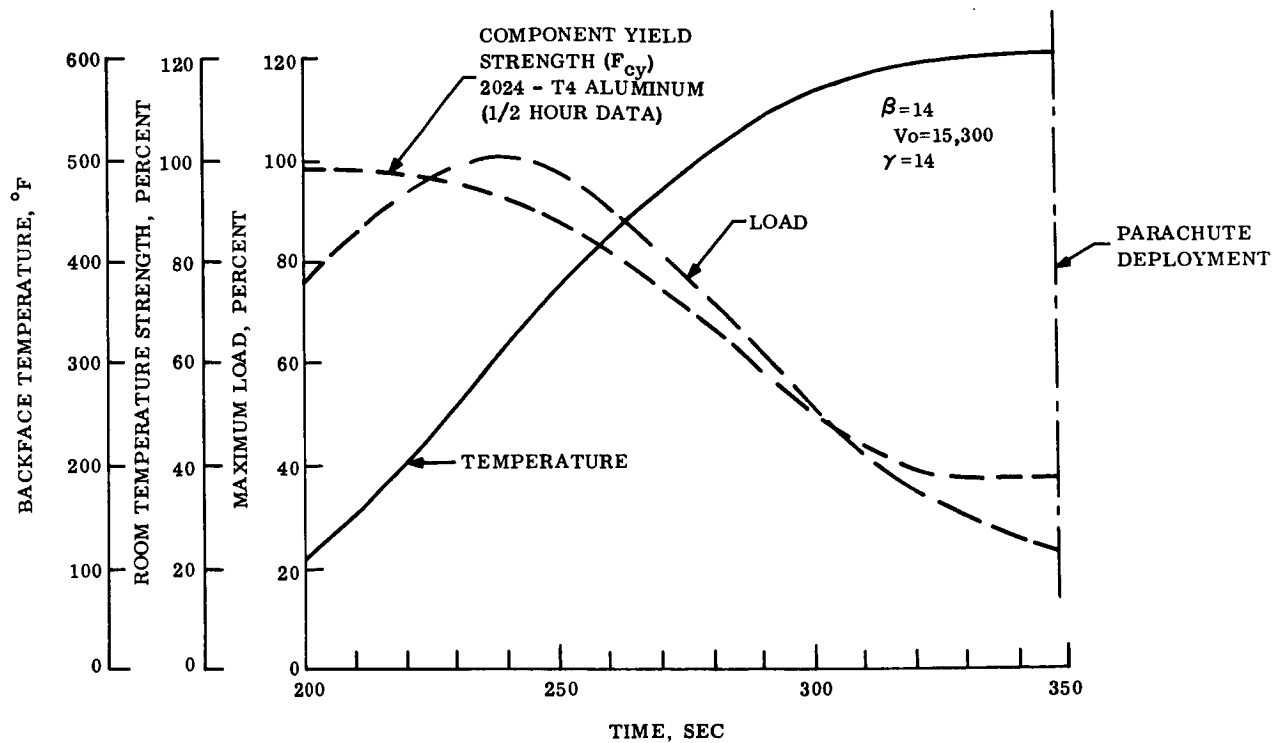


Figure 5.4.3-6. Performance Characteristics of 2024-T4

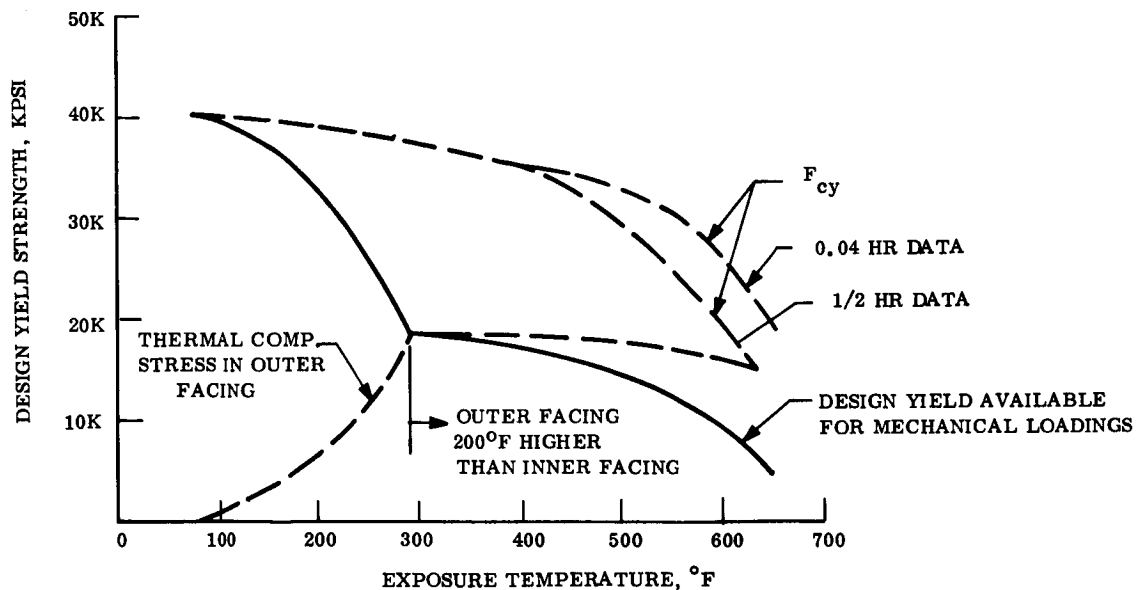


Figure 5.4.3-7. Mechanical Design Yield Strength for 2024-T4

At an elevated temperature of 600°F the allowable stresses for a 30 min exposure indicate a compressive yield strength 37 percent of room temperature strength compared with loads that are 25 percent of the maximum values.

For Point Design 3, the temperature of the aluminum honeycomb at time of maximum loading and the thermal stress levels due to the differential temperature between the outer and inner facing becomes significant. In order to consider these effects, the modified design allowable yield curve of fig. 5.4.3-7 was used for 2024-T4. The aluminum, 2024-T4 was used for the out-of-orbit designs because of the retention of strength to 600°F. The 0.04 hr data was derived using the Larson parameter T (C + log t) to represent the maximum time from the start of heating to parachute deployment (144 sec). The thermal stress due to the temperature differential between the outer and inner facing was calculated using the following equation:

$$S_f = \frac{\alpha \Delta T}{\left[\frac{1}{E_1} + \frac{1}{E_2} \right]} (1 - \gamma)$$

where:

α = Coefficient of thermal expansion

ΔT = Differential temperature between inner and outer facing

E_1 and E_2 = Modulus of elasticity in outer and inner facing respectively

γ = Poisson's Ratio

The final design curve shown in fig. 5.4.3-7 is the compression yield minus the thermal stress level. For additional conservatism, the allowable strength was reduced to γ_2 of the design values shown in fig. 5.4.3-2. Three conditions were evaluated for the out-of-orbit Point Design 3, as shown below.

Condition	G_x	Outer Facing (deg F)	Inner Facing (deg F)
1	12.7	200	70
2	5.5	320	120
3	1.375	600	400

Point Design 3 configuration parameters are presented in table 5.4.3-2. The honeycomb core and facing thickness requirements and minimum margins of safety are presented in table 5.4.3-1. The critical condition was No. 1 above, when the outer facing was 200°F.

TABLE 5.4.3-2. POINT DESIGN ENTRY DATA

Point Design	Entry Weight (lb)	Diameter (in.)	Radius To Bearing Load (in.)	Radius To Box Structure A (in.)
1 (out-of-orbit)	1246	100.0	27.0	41.5
2A (direct)	1480	152.4	32.0	44.0
2B (direct)	1127	135.6	27.0	37.0
3 (out-of-orbit)	1324	100.0	31.0	41.5
4 (direct)	1558	152.4	31.0	44.0
5 (out-of-orbit)	1530	120.0	32.5	42.5
6 (direct)	1766	168.0	31.0	46.5

The aluminum honeycomb weight is 0.82 lb/ft^2 of surface area (including bond) compared with 0.48 lb/ft^2 for titanium honeycomb and 0.69 lb/ft^2 for stainless steel honeycomb.

At the maximum base diameter is a box structure which extends forward into the aeroshell. This box structure is composed of a circular radial web and cylindrical longitudinal web with periodic ribs joined together by a ring at the base and tied into the aft ring of the aeroshell and a frustum ring internal and forward in the aeroshell. The cylindrical longitudinal web extends beyond the maximum base diameter of the aeroshell to provide a support for the entry system separation device. At this point is the mating interface with the internal adapter.

This box-like outer structure of the aeroshell acts as a torque box and restrains the rotation of the outer edge of the aeroshell. The construction of this torque box structure and the radial distance from the point of application of the load due to the payload bearing against the honeycomb shell determines the magnitude of the shell bending loads. With the torque box structure made very stiff, to allow very little torsional rotation, the maximum honeycomb shell bending moment and highest facing stresses would occur in the outer portions of the aeroshell. A reduction in the torsional box stiffness results in the maximum shell bending moment shifting to the center portion of the aeroshell. The ideal situation is where some rotation is allowed such that the shell bending is reduced over the entire shell and the moments are of the same order of magnitude in the center and outer portions.

5.4.4 LANDER/AEROSHELL SEPARATION

The Lander is attached to the aeroshell by a strap assembly retained by three hot wire tension bolts. The strap assembly, shown in fig. 5.4.4-1, consists of a strap bellyband which runs completely around the Lander. As a part of the strap are cushioning pads and a teflon spacer to eliminate the possibility of damage to the crush-up material. The strap is in three segments connected by three hot wire tension bolts. In the middle of each segment is a fitting which is attained by a T-bolt to the tie-down strap. The tie-down strap is attached to a fitting on the box structure in the aft end of the aeroshell. A torsion (or mousetrap) spring is also attached to this fitting and fits around the tie-down strap. Tension is placed in the entire assembly, to obtain the required restraining loads for the Lander, by torquing the T-bolt to a predetermined torque.

In order to separate the system, which occurs after parachute deployment, a current of 6 amps for 30 msec is fed to the hot-wire bolts, causing them to separate. At this instant the torsion springs snap the tie-down strap and attached segments of the bellyband outboard and clear of the Lander, which is extracted from the aeroshell by the parachute.

5.4.5 ENTRY SYSTEMS EQUIPMENT

With the exception of the four pressure and one temperature transducer for stagnation region measurements, all of the entry science instruments and support equipment (13.0 lb of the basic 15.5 lb package of instruments) is incorporated in the Lander module (fig. 5.4.5-1).

5.4.6 RETARDATION SUBSYSTEM

The retardation subsystem requirements are so similar for all of the point designs that a single subsystem design approach appears to be adequate. The design evolved for Point Design 3 will permit deployment and proper landing impact velocity to meet the required conditions of the mission. These are: deployment at speeds not greater than Mach 2; terminal velocity on main parachute at altitude not less than 6 kft and a vertical descent velocity in least dense atmosphere (VM-7) of 100 fps.

5.4.6.1 Retardation Performance

5.4.6.1.1 Mortared Pilot Parachute Selection

The use of a mortared pilot extraction parachute was selected over direct mortar ejection of the main parachute. The size of mortar required to directly eject such a large mass from the decelerating vehicle would take more weight than the selected arrangement. Furthermore, a more orderly deployment of the large diameter main parachute is ensured by using the pilot parachute extraction technique.

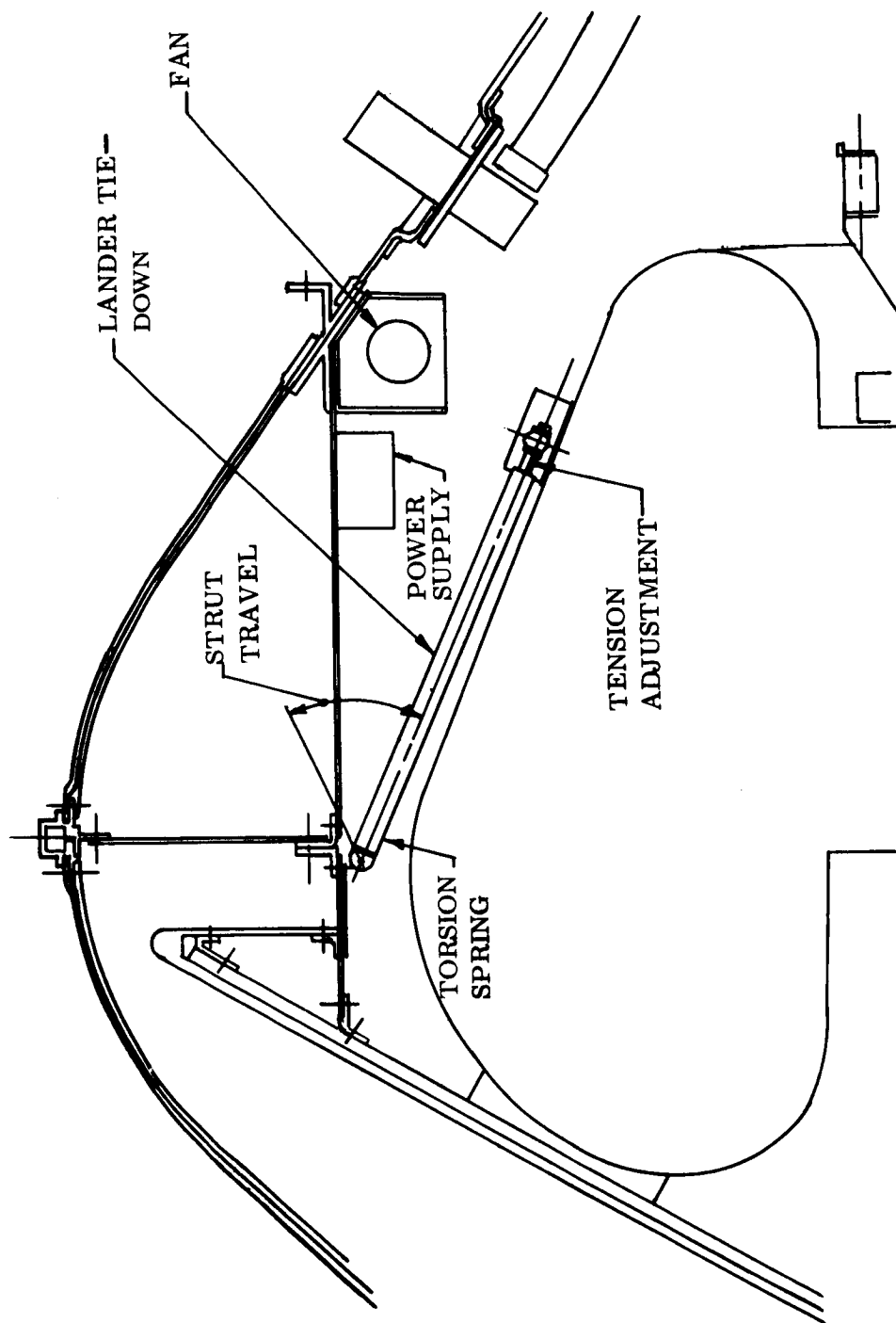


Figure 5.4.4-1. Lander Installation into Aeroshell

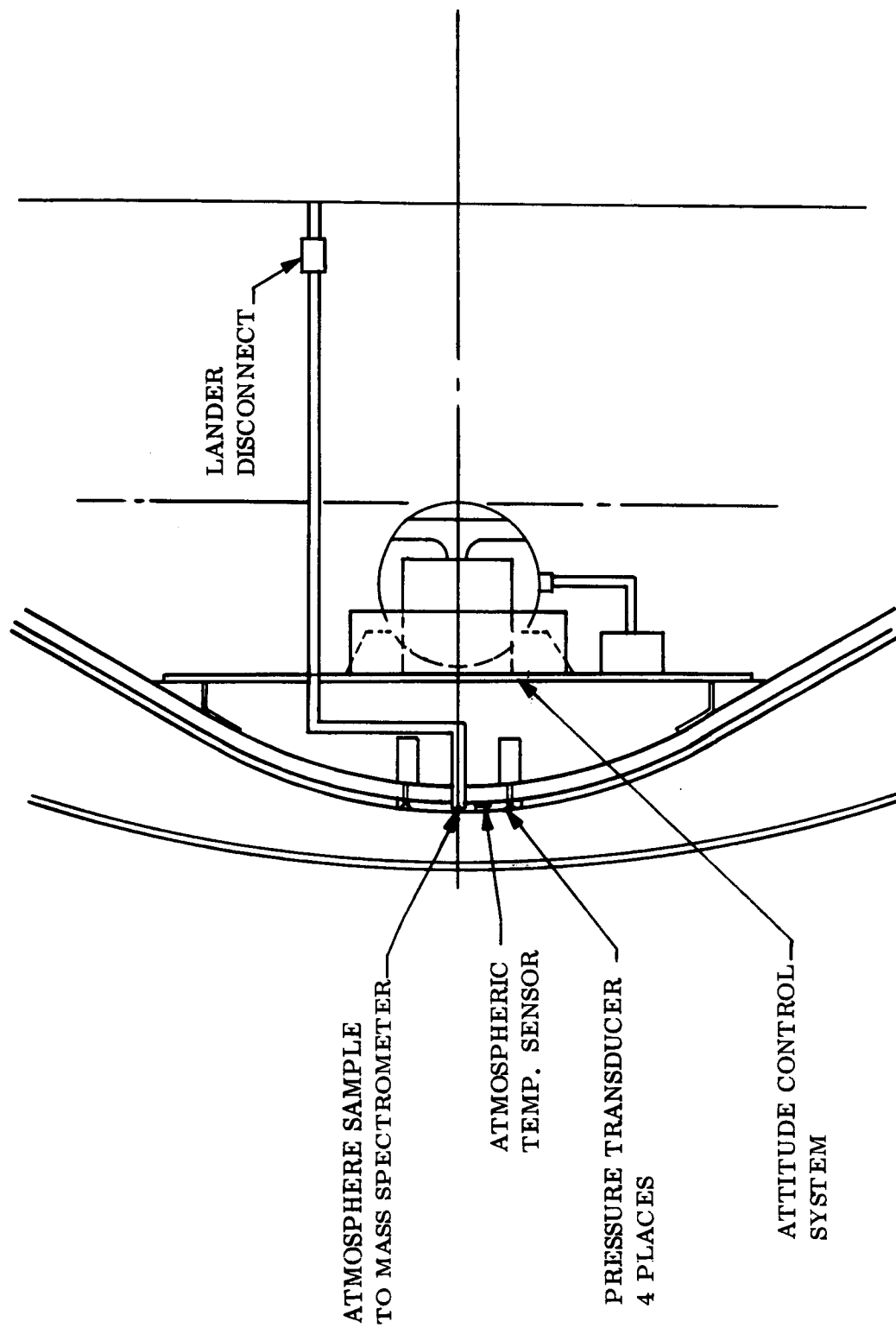


Figure 5.4.5-1. Entry Systems Instrumentation

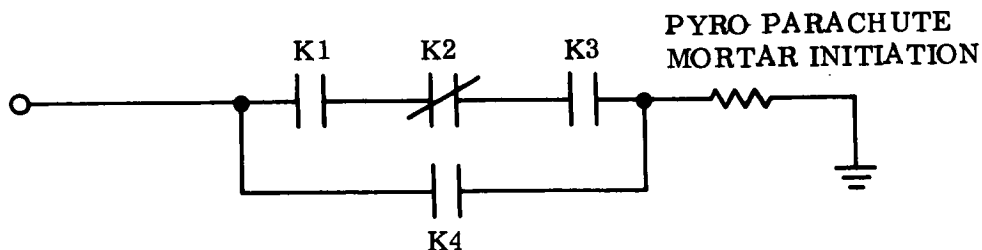
5.4.6.1.2 Trajectory Considerations

It is desired, for optimum Lander impact, to minimize descent time on the main parachute while insuring that the main parachute will be at equilibrium terminal velocity at the time of its separation. Deployment based on the use of a radar altimeter alone to deploy at a set altitude does not accomplish this. For the case where Mach 2 occurs at 11 kft, in the VM-8 atmosphere, deploying at 11 kft in the VM-7 or VM-1 atmospheres would result in reaching terminal velocity on the main parachute at lower altitude than in the VM-8 case, even though the initial deployment would be below Mach 2.

Deploying on Mach No. alone would produce high altitude deployment and a long descent time on the main parachute if the atmosphere is dense (i.e., VM-9). If the deployment sensing coupled a Mach 2 gate with a time gate and an altitude gate, deployment below Mach 2 and minimum parachute descent time would be assured. The logic for this combination is discussed below; further trajectory investigations would be necessary to optimize a point design.

Parachute deployment will be programmed to occur between 11 k and 20 kft. A 20 kft signal from the radar altimeter would enable parachute deployment. On receipt of the Mach 2 signal, the timer would be started. If the 20 kft signal were received before the preset time-out, parachute deployment would occur. This would indicate a rare atmosphere. If Mach 2 did not occur until receipt of the 11 kft signal from the radar altimeter, this would indicate very rare atmosphere, such as VM-8. If the Mach 2 signal were received and time-out of the timer occurred prior to the 20 kft signal from the altimeter, this would indicate a dense atmosphere such as VM-9 or -10. In this case, parachute deployment initiation is delayed until the 11 kft signal from the altimeter. In any case, deployment would be initiated at 11 kft.

The following schematic clarifies this deployment logic.



- K1 - Closes at Mach 2 signal
- K2 - Opens at end of timer time-out
- K3 - Closes at 20 kft signal
- K4 - Closes at 11 kft signal

5.4.6.2 Parachute Design

The modified Ringsail parachute configuration, as tested in the PEPP program, was selected for the parachute design. To assure reliable deployment, a single large diameter main canopy deployed by an extraction pilot parachute was selected. The main parachute will be deployed with one stage of reefing to minimize opening loads and parachute weight. The technique of reefing is a proven and commonly used method of controlling parachute inflation and loads. It has been used in numerous applications in the past with complete success in all sizes of parachutes including Ringsail parachutes of the size that would be required for the Hard Lander of this study.

The single large diameter main canopy was selected over a cluster of smaller parachutes. More complexity is involved in deploying clustered canopies. The use of a cluster would increase the development risk for this application. Providing reefing with clustered canopies is much more complex than in the case of a single canopy because of the interactions of the clustered canopies. This interaction problem created a great deal of difficulty in applying reefing to the clustered parachutes used in the Apollo development. None of the inflation problems encountered in the Apollo development should be experienced in applying reefing to a single main parachute design investigated here.

With a reefed stage, the deployment loads experienced by the main canopy will be low enough to allow the use of lightweight parachute construction. Analyses substantiating the materials and construction selected are presented in Volume III under Parachute Deceleration. The parachute system weights used were calculated using the RESSEP program, which is described in Volume III, Appendix A.

Parachute design drag performance was based on results obtained in the PEPP program. A constant value for C_D of 0.52 was used. Other test data on Ringsail parachutes indicates a higher value for C_D should be obtainable. This would cause a reduction in parachute size, weight and opening loads. The use of $C_D = 0.52$ should therefore be conservative.

Available test data indicates that the Ringsail parachute inflation will follow the performance curve of figs. 4-49 and 4-50 of "Performance of and Design Criteria for Deployable Aerodynamic Decelerators", ASD-TR-61-579 (referred to as the parachute handbook). This data was used for this preliminary design analysis. The parachute inflation characteristic was assumed to be linear with time for each stage of deployment, i.e., C_D increases linearly with filling time. This is a good assumption for a first cut design analysis and is fairly representative of test data.

5.4.6.3 Design Trajectory Example

The purpose of the trajectory study was to verify that the selected point design could function under the worst case deployment conditions and meet the established design requirements of parachute deployment at Mach No. ≤ 2.0 and reach main parachute full open terminal velocity at approximately 6 kft.

In some of the worst case point design trajectories investigated, the main parachute does not reach terminal velocity until altitude is down to almost 4 kft. When further work is done to finalize a planned vehicle design and the re-entry trajectory, the deployment altitude of the parachute system can be adjusted to reach terminal velocity at 6 kft.

The worst design conditions for the parachute occur in the rarest atmosphere represented by VM-8. The trade-off studies indicate that the vehicle will not decelerate to Mach 2 until approximately 11 kft altitude. For all other atmospheres, Mach 2 occurs at a higher altitude. Parachute performance was designed to meet the worst case deployment conditions of the VM-8 deployment. The study made included the extraction and deployment of the main parachute by the pilot parachute.

The pilot parachute deployment occurred at 11 kft, Mach 2, and $q = 20$ psf. The trajectory of the pilot parachute extracting the main parachute was examined and compared to the trajectory of the vehicle, now minus the weight of parachutes. This study was used to determine the point of start of main parachute reefed inflation where the main parachute skirt has been deployed. The results of this study are shown in fig. 5.4.6-1 and the parameters selected for use in the Point Design 3 study are listed in table 5.4.6-1.

5.4.6.3.1 Parachute Staging Design and Trajectory

Parachute reefing and duration of the reefed stage were optimized using existing computer programs to produce opening loads for both main parachute stages to be within the strength capability of the suspension lines and minimize altitude loss during deployment.

The analysis to establish reefing ratio is based on a simultaneous solution of the following equations for the two stage main parachute deployment.

$$F_1 = C_{D1} S_1 \cdot X_1 \cdot q_1$$

$$F_2 = C_{D2} S_2 \cdot X_2 \cdot q_2$$

$$q_2 = \frac{W_1 \cdot LF_1}{C_{D1} A_1}$$

where:

subscripts:

$C_D S$ = effective drag - ft^2

1 = stage one

F = opening force - lb

2 = stage two

X = opening shock factor

q = dynamic pressure - psf

W = Weight in local gravity - lb

LF = force along Z axis in local gravity - 'g's

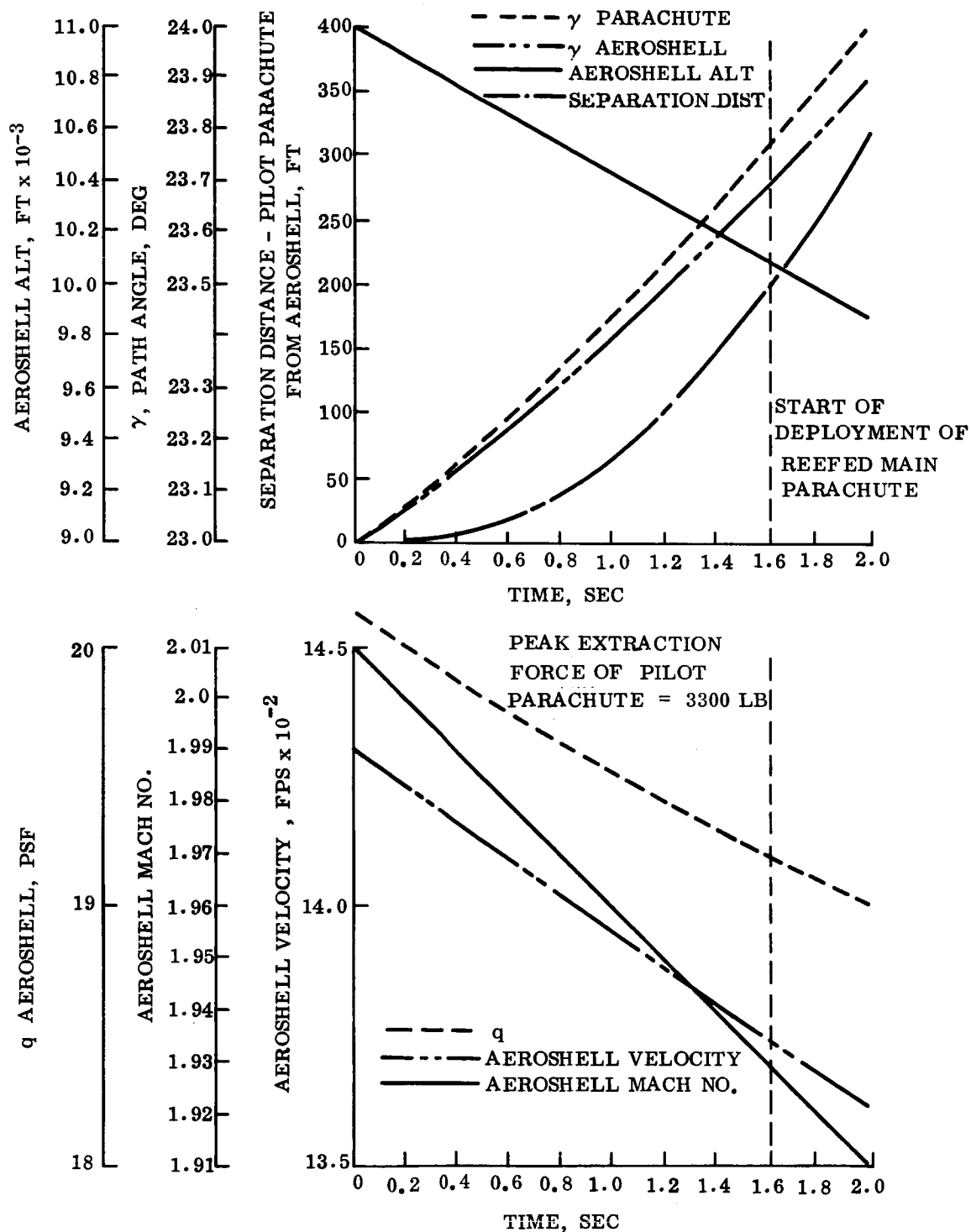


Figure 5.4.6-1. Pilot Deployment Trajectory Study, Point Design 3

The quantities C_{gS_2} , q_1 , X_1 , X_2 , LF_1 and W_1 must be known. Without accurate performance data on a given design, assumptions must be made for X_1 , X_2 , and LF_1 . If the correct characteristics are used, the performance can be verified in a computer trajectory analysis with a program designed to vary the C_{DS} during parachute inflation.

Optimum reefing should produce equal opening load peaks for both stages. However, a reefed design can be satisfactory if other objectives are met and the peak loads are not balanced. In this case, if the opening forces are within the structural capability of the parachute and the total altitude loss during deployment is not excessive, the performance will meet the requirements.

In the staging study below, values were selected based on past experience and data. Reefing ratio was selected, using the approach described above, to produce equal stage loads. In the trajectory study, fill time was based on data from the parachute handbook (ASD-TR-61-579) and C_{DS} growth was assumed to be linear with time. The disreef opening force from the trajectory analysis (shown on fig. 5.4.6-2) came out lower than the reefed opening force. By iteration, the opening forces in the reefing ratio selection analysis and the trajectory analysis could be made to come out equal. However, at this point, the exercise would be academic. Slight changes in the disreef fill time, or some non-linearity in C_{DS} growth, or a combination of the two could significantly affect the resulting disreef open force. At this point, there is higher confidence that the reefed opening force is correct than there is in the disreef opening force.

In the hardware development program, the reefing line length to produce the desired reefing ratio will be selected based on the best available data. After first test data is obtained, necessary adjustments would be made to obtain the desired reefed performance based on data from the actual system. There is high confidence that required reefed performance can be achieved with little difficulty.

The PEPP Program demonstrated satisfactory inflation characteristics in Mach 2 deployment in a rare atmosphere. With reefing, inflation will proceed in the same manner as without reefing until the point where the reefing line restricts and delays full inflation. In all cases, a reefing design must be verified in the parachute development test program.

The parameters selected for the staging study are shown for Point Design 3 in table 5.4.6-2.

The parachute trajectory was calculated by computer using the established or calculated parameters shown in table 5.4.6-3.

The results of this trajectory study are shown on fig. 5.4.6-2. These calculations are conservative inasmuch as the aeroshell or Lander drag area is not considered as part of the retardation drag area after main parachute deployment.

TABLE 5.4.6-1. PILOT PARACHUTE DESIGN PARAMETERS

Atmosphere = VM-8
Initial deployment altitude = 11,000 ft
Weight being decelerated by pilot parachute = 193 lb
Vehicle weight minus the parachutes = 969 lb
Path angle below horizontal = 23.0°
Pilot parachute fill time = 0.24
Linear pilot parachute inflation with time assumed
Pilot parachute $D_o = 15.7$ ft
Pilot parachute $C_D = 0.52$
Pilot parachute $C_D S = 101$ ft ²
Pilot parachute opening shock factor = 2.0
Average wake reduction effect during pilot parachute extraction = 0.85
Aeroshell $D_o = 8.34$ ft
Aeroshell $C_D = 1.46$

TABLE 5.4.6-2. MAIN PARACHUTE DESIGN PARAMETERS

Main parachute full open $C_D S = 6587$ ft ²
Initial reefed deployment $q = 19.22$ psf
Reefed stage opening shock factor = 2.0
Disreef opening shock factor = 0.5
Axial deceleration at disreef ≈ 7 g's Martian
Total weight being decelerated = 1162 lb
Main parachute $C_D = 0.52$

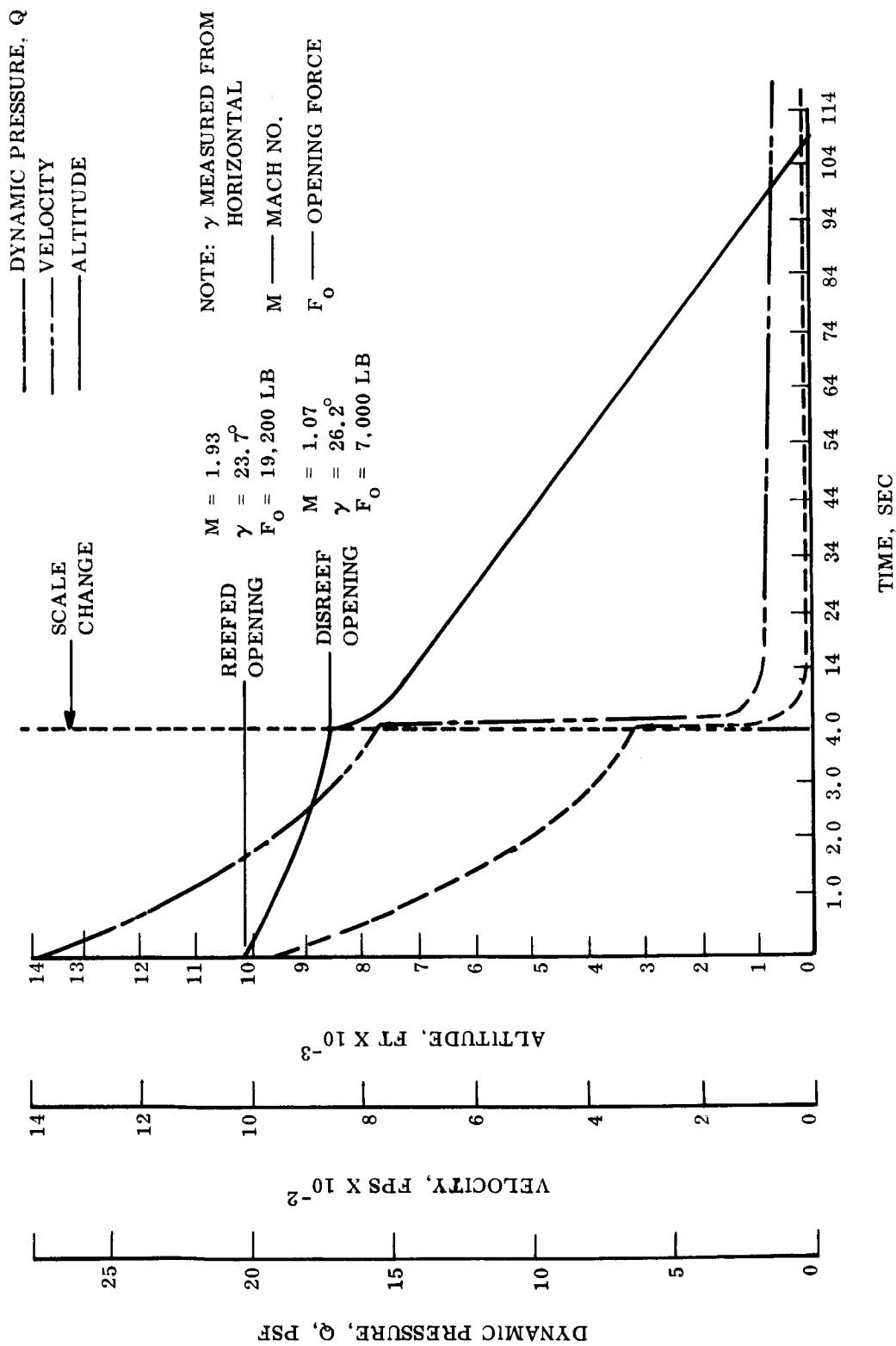


Figure 5.4.6-2. Point Design 3 Main Parachute Trajectory in VM-8 Atmosphere

TABLE 5.4.6-3. POINT DESIGN 3 PARACHUTE
TRAJECTORY PARAMETERS

Atmosphere = VM-8

Total weight being decelerated = 1162 lb

Initial deployment altitude = 10,108 ft

Initial velocity, reefed deployment = 1377 fps

Initial path angle = 23.7°

Linear reefed opening inflation with time assumed

Reefing ratio = 7.74 percent

Reefed filling time = 0.16 sec

Total time of reefed stage = 4.0 sec

Main parachute D_o = 127 ft

Main parachute C_D = 0.52

Main parachute full open $C_D S$ = 6587 ft^2

Main parachute full open fill time = 3.04 sec

Linear full opening inflation with time assumed

5.4.6.4 Hardware Description and Function

The basic hardware concepts selected for Point Design 3 have been previously used, tested and proven in other programs. The mortared parachute deployment is a commonly used technique and the thermal cover concept and deployment arrangement has been used by GE on the 698 BJ program and the Maneuvering Ballistic Re-entry Vehicle program. The method of main parachute release has also been verified on these programs using explosive nuts. The parachute designs selected for the point designs of this study are based on the designs and results to date of the NASA PEPP program. The aeroshell release and fall-away is similar to the re-entry heat shield separation used by GE in the A45 program.

5.4.6.4.1 Pilot Parachute Mortar Thermal Cover

The thermal cover provides the means for securing the pilot extraction parachute in the mortar prior to mortar deployment. It also anchors one end of the main parachute

thermal cover and provides thermal protection from wake heating to the pilot parachute, mortar gas source, and the pull away electrical disconnect. The cover will be secured to the mortar tube by a break cord or shear pins until mortar firing. A bag handle on the pilot parachute deployment bag will be secured to the thermal cover in a recess within the cover. Thus, the thermal cover will also provide a mass to assist in stripping the deployment bag from the pilot parachute during deployment.

5.4.6.4.2 Pilot Extraction Parachute

The pilot extraction parachute will be similar in design to modified Ringsails tested in the NASA PEPP program. All parachute lines and materials will be sterilizable dacron. Presently, lightweight construction is envisioned using 1.1 oz cloth and 300 lb suspension lines. In a development program, an investigation would be made to determine the suitability of utilizing 0.8 oz material in the lower panels near the skirt to save weight. The pilot parachute will be pressure packed to a 40 lb/ft³ density or slightly higher.

5.4.6.4.3 Pilot Parachute Riser Line

The pilot extraction parachute will be provided with a riser line to provide a minimum length of six aeroshell base diameters to the skirt at parachute inflation. This line will also be used to provide a mouth lock for the pilot parachute bag and to extract the main parachute bag for main deployment. It will attach to two fittings, one at each end of the main parachute thermal cover, for extraction and deployment of this cover. The end of this line, at the main parachute bag, will be used to form a tuck bight through a locking loop of the three tie-down straps securing the main parachute in its compartment.

5.4.6.4.4 Main Parachute Compartment Thermal Cover

The main compartment thermal cover provides thermal protection for the main parachute pack from re-entry wake heating. It is deployed by the pilot extraction parachute and permanently attached to the pilot parachute riser. This cover can also serve as a mounting point for spring pushers to jettison the de-orbit propulsion and thrust structure. The cover will be aluminum with necessary reinforcement to sustain the loads of deployment. All edges will be rounded to prevent damage to the pilot parachute riser line. The outside surface will be covered with thermal protective coating to preserve the cover's structure and control main parachute temperature from re-entry wake heating.

5.4.6.4.5 Main Parachute, Two Stage Deployment, Modified Ringsail - 15 Percent Geometric Porosity

The main parachute will be a single large diameter parachute with one stage of reefing. Existing design hermetically sealed reefing line cutters, manufactured by Technical Ordnance Products Co., will be used. The parachute will be made of sterilizable dacron material, in lightweight construction similar to the constructions tested in the PEP Program. At present the parachute would be made of 1.1 oz cloth with 300 lb suspension lines, since deployment q will be 20 psf or less. In a development program to optimize weight and volume, the use of 0.8 oz cloth in the lower panels near the skirt would be investigated. A higher weight, lower mechanical porosity material is needed in the crown

area to the facilitate initial reefed deployment. If added strength is required, 1.6 oz material will be used in the crown area. The main parachute will be pressure packed to 38 to 40 lbs/ft³ density. Parachute reefing will be established to produce approximately equal opening loads at each stage of deployment to a level that utilizes the full structural strength capability of the suspension lines, considering appropriate design derating factors. The reefed stage time will be set as short as possible to minimize altitude loss during this stage and provide a high opening velocity for rapid full open inflation. The trajectory in the VM-8 atmosphere, where Mach 2 occurs at the lowest altitude, will be used to determine staging time and reefing ratio. The opening loads in any other atmosphere will be lower than those for the VM-8 atmosphere as the deployment is presently envisioned.

5.4.6.4.6 Main Parachute Attachment Riser

The attachment risers will connect the main parachute at the suspension line confluence to the three tie-down fittings at the bottom of the parachute compartment. At main parachute release, the parachute compartment, including the mortar, will remain with the main parachute.

5.4.6.4.7 Parachute Compartment Including Mortar

The parachute compartment will be an aluminum sheet metal fabrication to confine the parachute and provide thermal protection from re-entry wake heating. The outside surface of the compartment will be provided with the required thermal protective coating. The attachment and tie-down fittings will be attached to the rim at the bottom of the compartment. The pilot parachute mortar will be built into one side of the compartment. It will consist of a mortar tube and a sabot for the pilot parachute to seat against. The gas for mortar ejection will enter through tubing at the bottom of the mortar under the sabot. The area on each side of the mortar will be used for mounting the gas source for mortaring and the pull-apart electrical disconnect to separate the power supply from the mortar pyrotechnic. The side of the parachute compartment opposite the mortar will provide a slotted projection to receive a tang on the main thermal cover that secures that end of the thermal cover.

5.4.6.4.8 Parachute Attachment and Tie-down Fittings

Three fittings, one for each of the three risers, are attached to the parachute compartment at the bottom flange and will be provided with two pins for webbing attachment. One pin will attach the main parachute risers, and the second pin will attach tie-down straps that secure the main parachute in a position such that it does not put a load on the main parachute thermal cover by pressing against it. The three tie-down straps will secure the main parachute using a locking loop and a tuck bight formed by the pilot parachute riser.

5.4.6.4.9 Mortar Pyro Gas Generator or Compressed Gas Supply

The gas for mortar ejection can be provided by either a pyro gas generator or a compressed gas supply. The compressed gas supply can be provided at a slight weight

increase over the gas generator. Standard components are available from Conax Corp. (Conax Eager Paks) for the compressed gas supply. It would consist of a small hermetic cylinder (10 to 15 in.³ capacity) containing compressed nitrogen at 3000 psi and a pyro valve that fires, piercing the cylinder allowing flow through a connecting tube. This arrangement offers several advantages. There is no hot gas to damage fabrics or components used for mortaring. There will be less problem of pyro development for the Mars mission in that the valve uses a standard squib and does not need the special gas generating materials. Reaction forces and performance will be more predictable. The compressed gas can be readily sterilized, where this may be a problem with the gas generator materials.

5.4.6.4.10 Pull-Apart Electrical Disconnect

This component consists of an electrical connector, half of which is mounted captive to the main parachute compartment. As the main parachute releases, i.e., the parachute compartment is pulled away, the two halves of the connector are separated. This component has been used successfully in a number of GE vehicle designs in the past.

5.4.6.4.11 Parachute Compartment Separation Required

The parachute compartment will be secured to the payload by three explosive nuts, each having dual cartridges, attached to bolts passing through the attachment and tie-down fittings. These will be similar to the explosive nuts used for Capsule separation described in Section 5.3.3. The main parachute tie-down and deployment loads will be carried by these separation devices.

5.4.6.4.12 Radar Altimeter

A radar altimeter, described in para 5.4.6.6, will be used to sense altitude for parachute deployment and main parachute release above the surface. Where altitude sensing alone may not be adequate for all possible atmospheres, the altimeter would be coupled with the Mach 2 sensor, providing gates to establish the correct point for parachute deployment.

5.4.6.5 Sequence of Retardation Subsystem Events

The series of deployment events described are depicted in fig. 5.4.6-3.

On receipt of the signal from the radar altimeter for parachute system deployment, power from the vehicle power supply will be applied to the mortar pyro initiation. Mortar firing will release and deploy the pilot parachute thermal cover and the pilot parachute. After stripping off the pilot parachute, the pilot parachute deployment bag and attached thermal cover free-fall away.

As the pilot parachute is being deployed, the main compartment thermal cover will be deployed by the snatch force of the pilot parachute. One end of the main thermal cover is released by the pilot parachute cover separation. The main cover is attached to the pilot parachute riser at two points for deployment and retention to the riser. As the

FOLDOUT FRAME

FOLDOUT FRAME

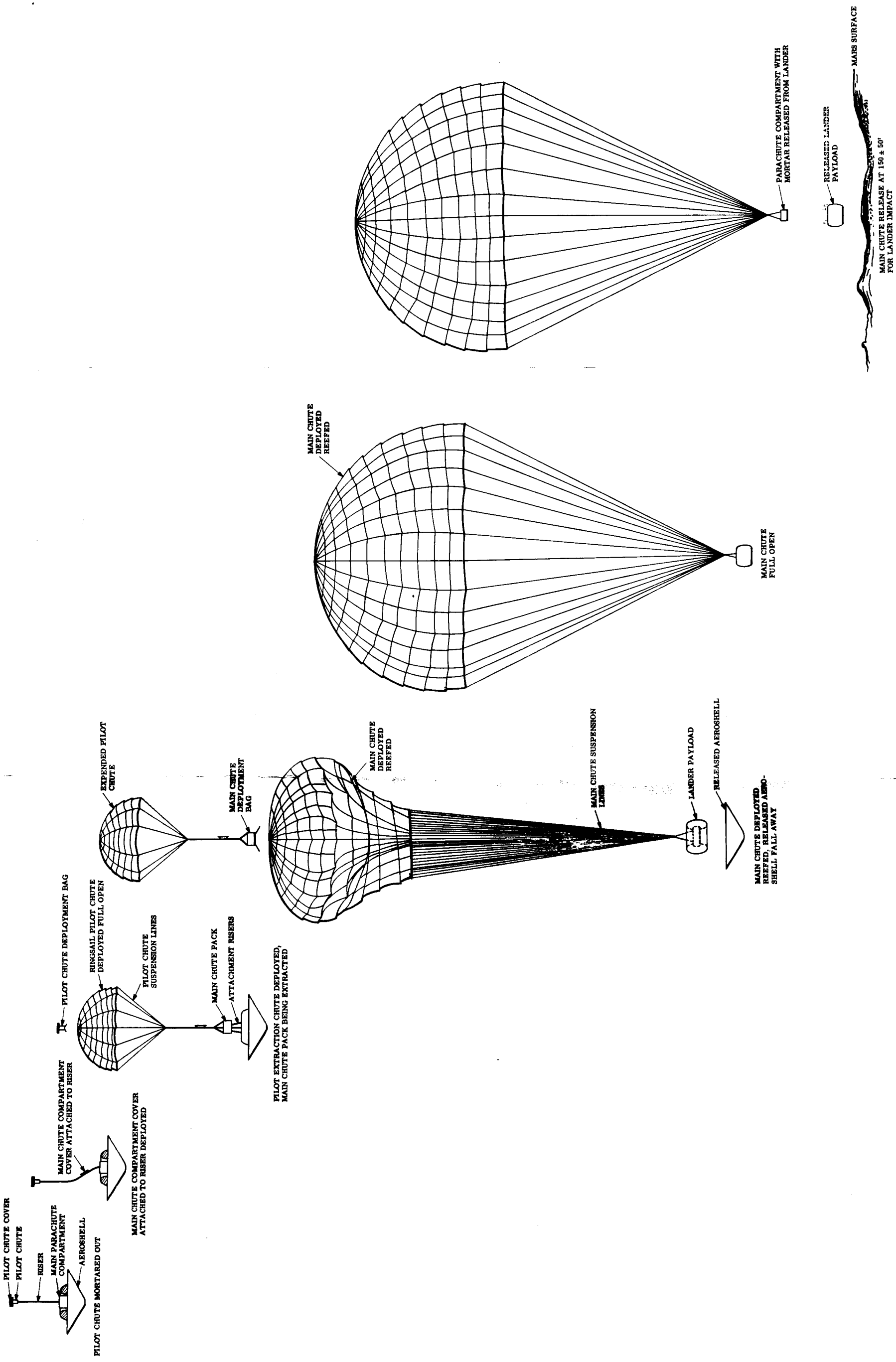


Figure 5.4.6-3. Retardation Deployment Sequence

cover is rotated out by the pull from the pilot parachute, the hold down tang on the edge of the cover opposite the mortar will rotate out of a slot in the main parachute compartment, completely releasing the cover.

The snatch force of the main compartment thermal cover on the pilot parachute riser will pull out the tuck bight securing the main parachute tie-down straps. This releases the main parachute pack for deployment. Further pull force on the pilot parachute riser will be applied to the main parachute bag handles for main parachute extraction and deployment.

The main parachute is extracted and deployed in a reefed condition by the pilot parachute. During this deployment, the mechanically initiated pyro time delay reefing line cutters are actuated. As the drag of the reefed main parachute develops, the aeroshell is released and allowed to free-fall away. After time-out of the redundant reefing line cutters, the cutters actuate, severing the reefing line. This event permits main parachute full open deployment.

When the descending Lander is 150 ± 50 ft from the surface, a signal will be sent from the radar altimeter to apply power from the vehicle power supply to the explosive nuts. This will cause release of the parachute compartment/mortar assembly from the Lander. The Lander will free-fall to surface impact. The jettisoned main parachute will collapse and spill to one side due to the sudden release of loading from the suspension lines while the parachute was fully inflated.

5.4.6.6 Radar for Deceleration Events

The function of the radar altimeter is to mark the altitude (about 20 kft) at deploy the Lander deceleration parachute and the altitude (150 ± 50 ft) at which the parachute is separated from the Lander before touchdown. In addition to providing these essential marks, the radar provides a continuous altitude signal for correlation with atmospheric profile measurements.

5.4.6.6.1 Altitude Marking Radar (AMR) Description

The AMR is a time domain radar. That is to say, it is a non-coherent, pulse type radar which utilizes an early-late gate range tracking method. Fig. 5.4.6-4 shows a functional block diagram of the AMR. None of the redundancy is shown.

The transmitter, a triode oscillator operating at 1 GHz, is pulsed by the modulator with a pulse length which depends on altitude. Initially, in Mode 1, the pulse length is $0.7 \mu\text{sec}$ and remains so until about 5 kft altitude, whereupon, in Mode 2, the pulse length is changed to $0.18 \mu\text{sec}$. This will give an accuracy of approximately 45 ft on the remaining ranges.

The duplexer is provided along with the proper gating to enable the use of one antenna for both transmission and reception.

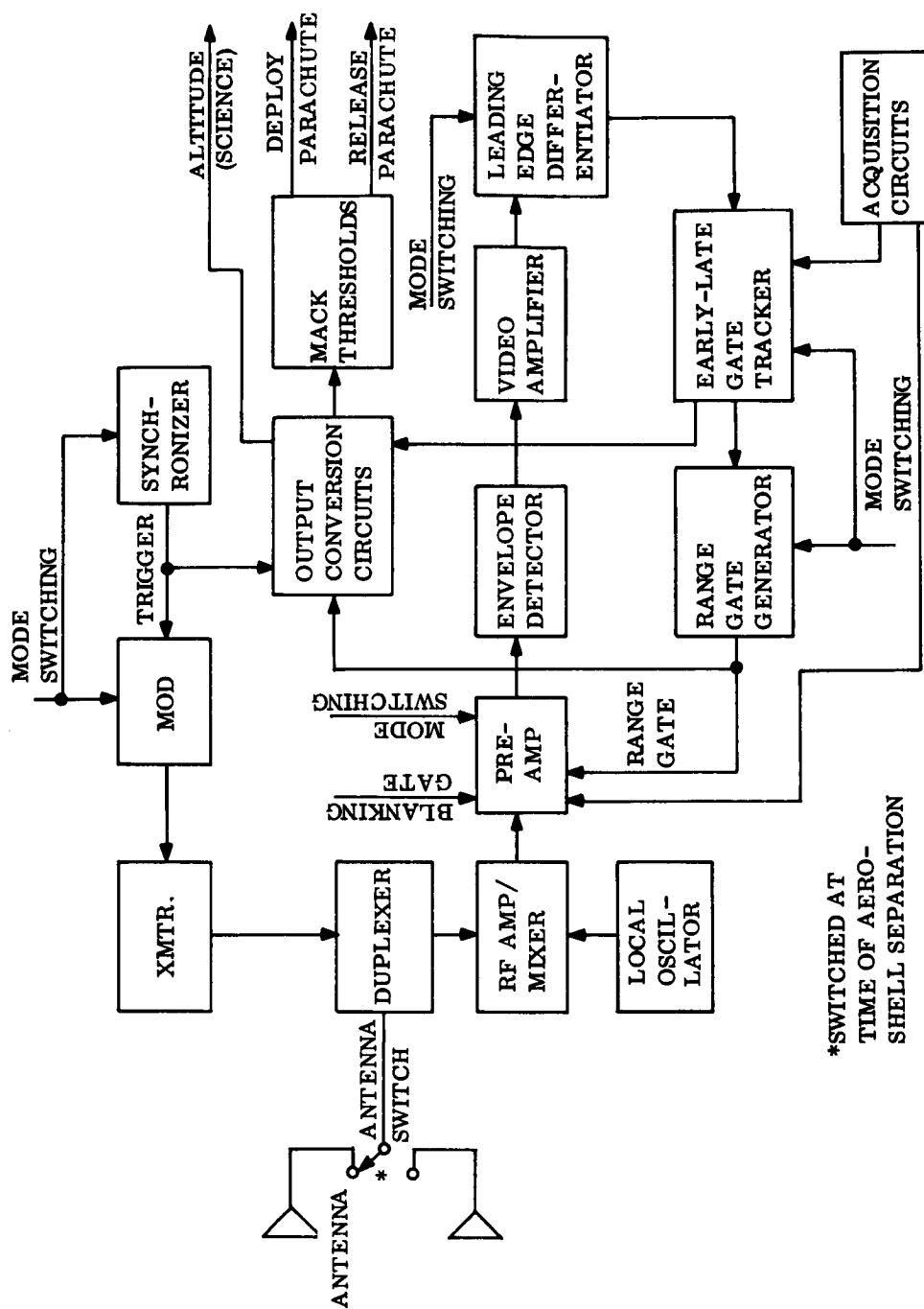


Figure 5.4.6-4. Altitude Marking Radar, Functional Block Diagram

After translation in frequency by the local oscillator the return signal is amplified, filtered, detected and enters the range tracking circuits. Because of the extent of the target and the width of the radar antenna pattern, the return is much wider than the transmitted signal; tracking of the leading edge of the return is desirable to determine altitude. To facilitate the early-late tracking approach, the target return is passed through a leading edge differentiator (delay line) whose output is a pulse of approximately the transmitted pulse width and whose position corresponds to the nearest point of the target return. Fig. 5.4.6-5 shows how the return pulse is formed. In that idealized diagram the time intervals correspond to:

t_1 = Time that leading edge of pulse hits the surface

t_2 = Time that trailing edge of pulse hits the surface.

During this time the reflected power increases linearly until the entire pulse illuminates the surface. The returned power then decreases from this level due to reflection from more distant points within the beam. If this pulse shape, passed through a μ sec delay line, is subtracted from the original, ideally one gets a non-zero output during the leading edge buildup, with a negligible output (and the opposite polarity) for the trailing edge. The resulting narrow pulse is time discriminated in a split gate range tracker whose output controls the time position of the range gate.

The range gate is used to gate the preamplifier on at the proper range, enhancing the signal-to-noise ratio.

In the output conversion circuits, the time delay between the trigger and the range gate is determined and converted to an analog voltage to give a continuous altitude signal.

5.4.6.6.2 Antennas

The AMR is used both prior to and after separation from the aeroshell. The attitude of the Lander can vary over a wide range requiring a broad beam antenna to obtain signal returns for the expected orientations. This is accomplished before aeroshell separation by an antenna with a toroidal pattern (roll symmetrical), and after aeroshell separation by a broad beam (roll symmetrical) pattern.

The 1GHz radar antenna system on the aeroshell will consist of a two antenna array. The two antennas will be identical, but they will be located 180° apart on the shell on an 88 in. diameter. They will be fed in phase with equal amplitude signals from a hybrid. Each antenna, in turn, will be a two slot element array. The slots will be oriented with their long (4 in.) dimensions along a cone element and they will be end to end. The slot closest to the vehicle nose will be fed a signal that is advanced by 60° in phase but equal in amplitude to that which feeds the rear slot. This will cause the peak amplitude of the pattern to occur at an angle of 60° with respect to the vehicle axis (see fig. 5.4.6-6). The polarization will be linear and orthogonal to the vehicle axis. The gain, which is optimized for a 15 to 40° re-entry angle, will average 0 dB or greater over any cone of 10° half-angle within the range of angles from 50 to 75° with respect to nose-on (see fig. 5.4.6-7). The elements will be dielectric loaded, cavity backed, slots 2 in. wide and

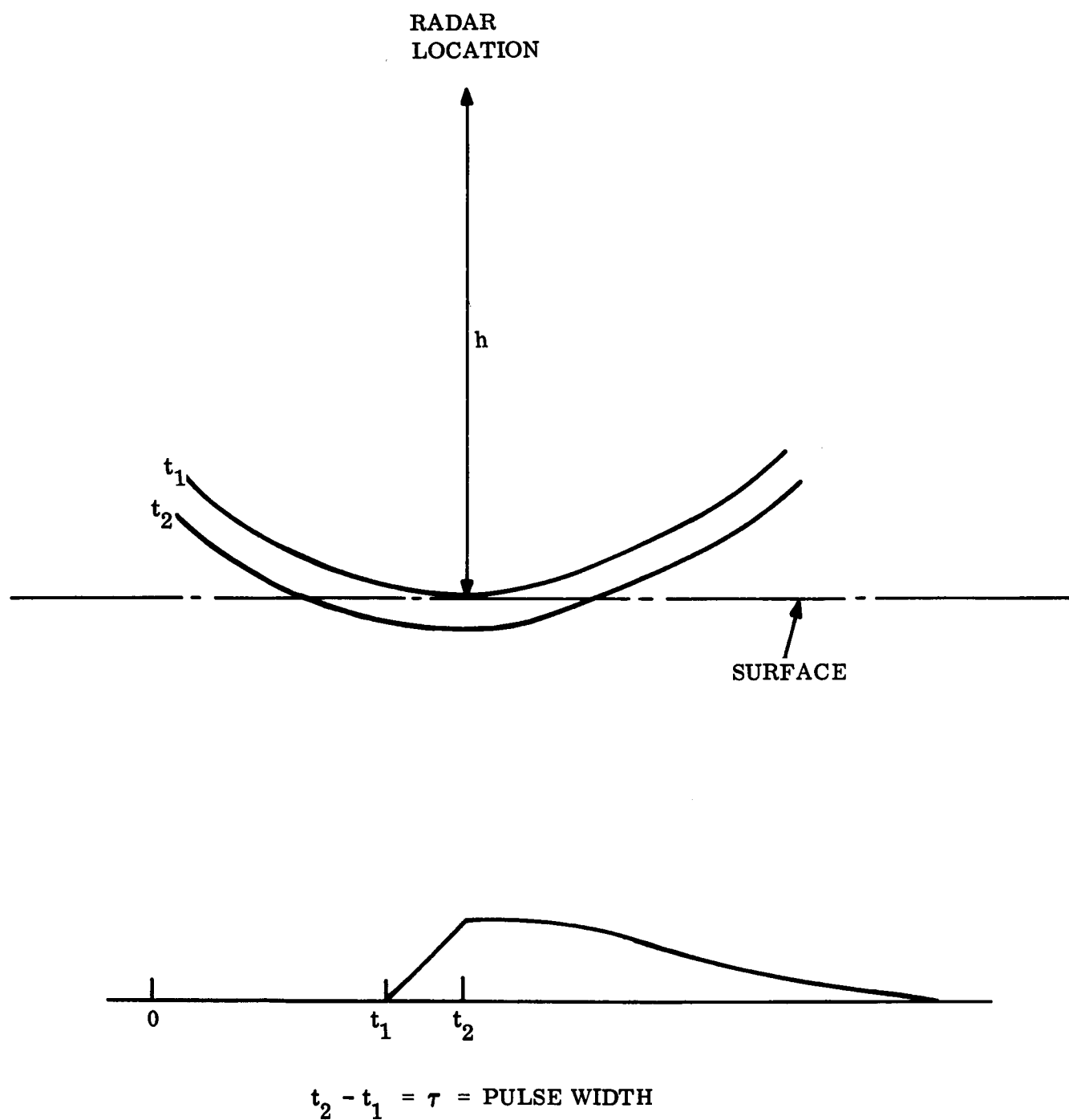


Figure 5.4.6-5. Geometry of AMR Return Signal

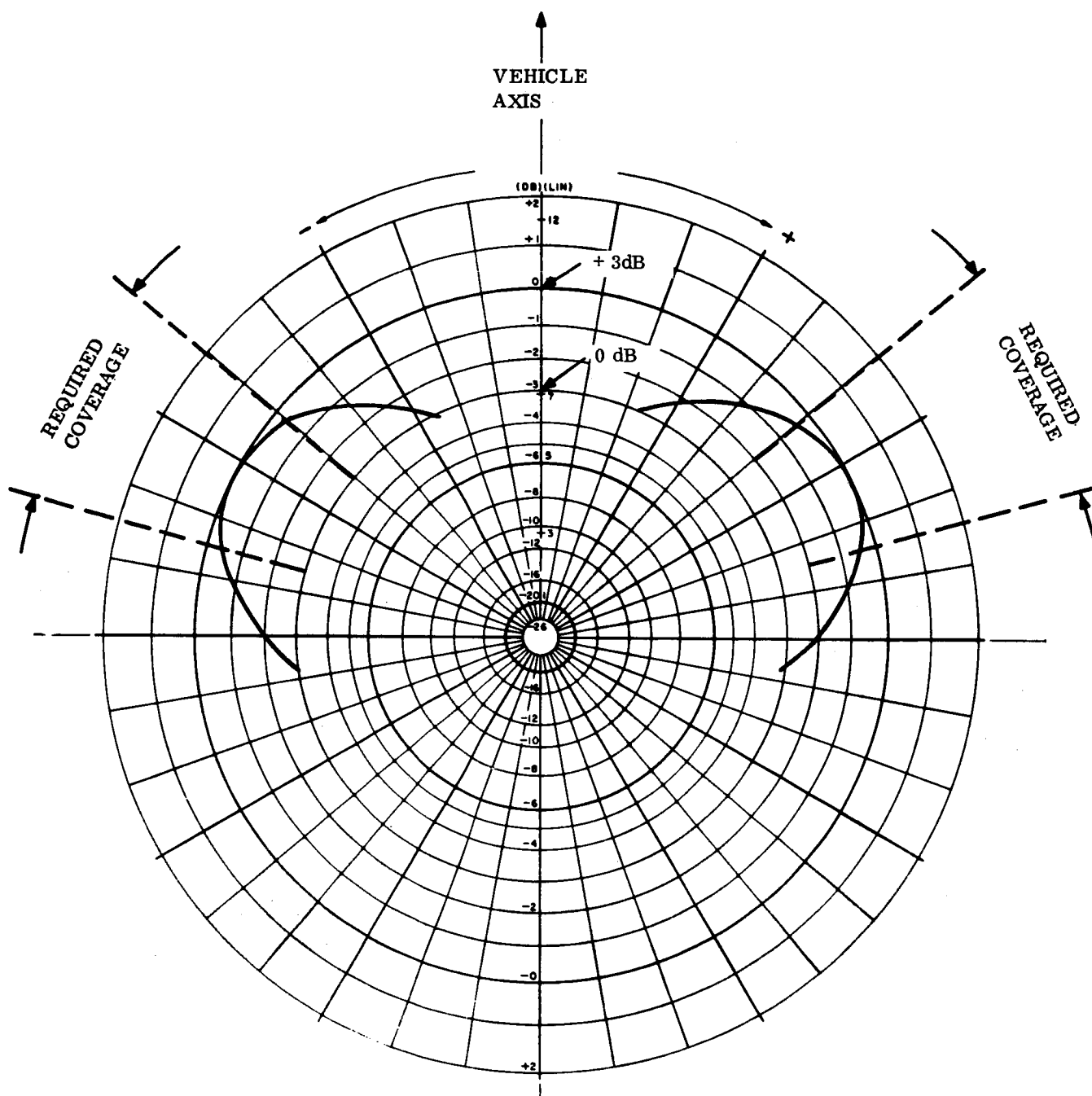


Figure 5. 4. 6-6. Pattern through Axis and Plane of Antennas on Aeroshell

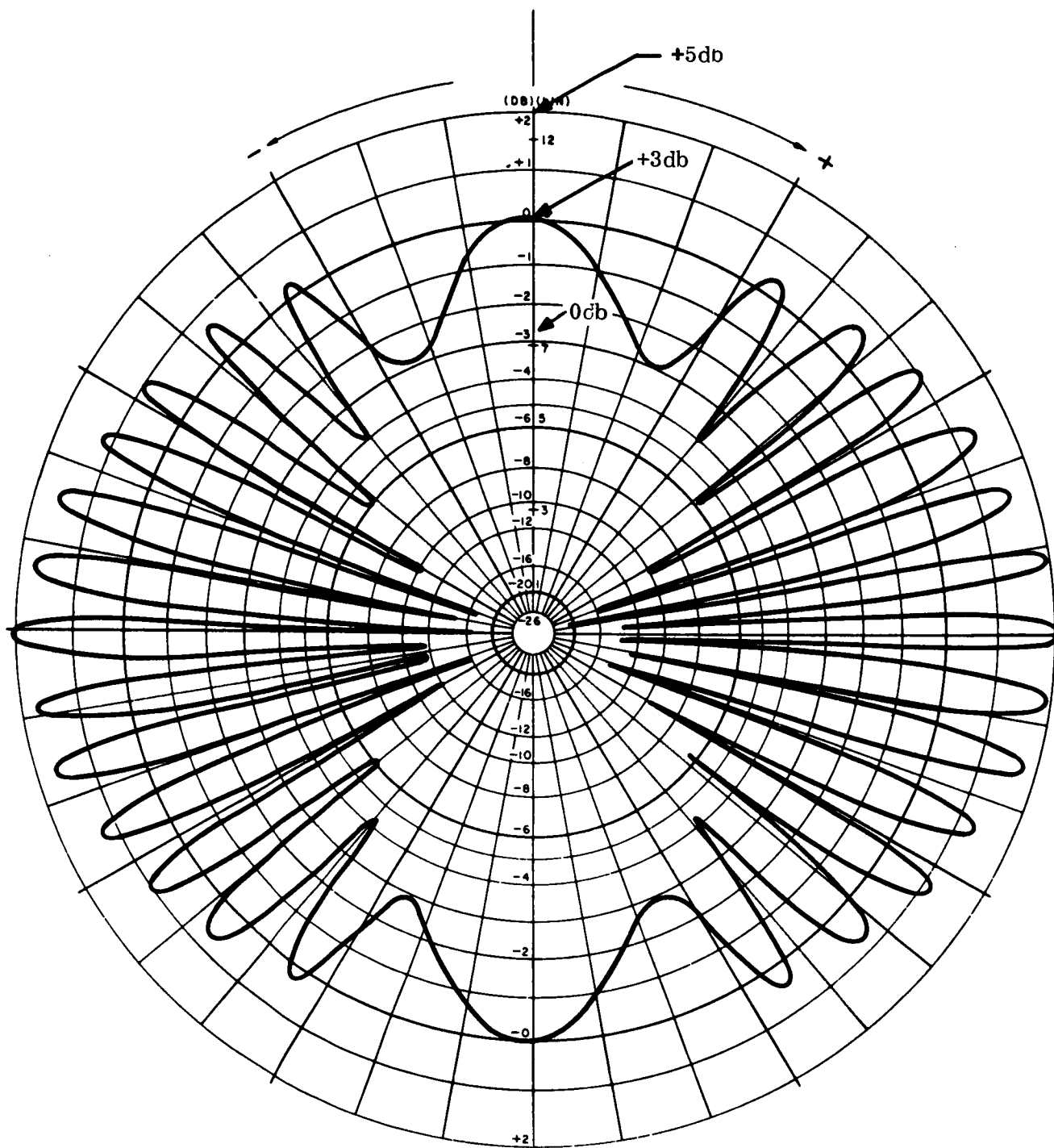


Figure 5.4.6-7. Roll Pattern, Radar Antenna on Aeroshell

2-1/2 in. deep. The cavities will be probe fed by a hybrid power divider with an additional length of transmission line in one output leg to account for the required 60° phase shift. An 8 x 2 in. quartz window will be required through the ablation shield to permit proper operation after the re-entry charring of the shield. The antenna system will weigh 5-1/2 lb exclusive of the cable feed system. The input VSWR will not exceed 3:1 ratio for this antenna system for all ablation and re-entry plasma conditions. It will handle 50 watts of input power.

The antenna system for the body of the Lander will be a simple, single slot located on the downward facing surface. It will be 6 in. long by 1 in. wide with 3 in. deep backing cavity. It will be loaded with dielectric and weigh 1 lb. It will produce a pattern with linear polarization and a major lobe of about 5 dB of gain in the downward direction (see fig. 5.4.6-8). Everywhere within the required coverage angle (within 40° of the vehicle forward axis) the gain is +2 dB or greater. The input VSWR will be less than 1.5:1 ratio for this antenna and it will handle 50 watts of input power.

Switchover from one antenna to the other occurs at aeroshell separation and requires a signal from the guidance and control sequencer to shut down the transmitter, switch the antennas, and repower the transmitter. The radar begins functioning again about 4 to 6 sec after aeroshell release. At this time the aeroshell will be near in range and must be discriminated against during the reacquisition of the desired target return. This is accomplished with a receiver blanking gate of 5 to 6 μsec duration effectively blanking out any target within 2500-3000 ft of the vehicle. This blanking gate is removed after the surface is reacquired and the normal range gate is functioning.

5.4.6.6.3 Parameters of the AMR

Table 5.4.6-4 lists the functional and physical parameters of the radar.

The calculation for SNR is based on the assumption that the surface reflectivity coefficient is $\sigma_o = -10.0$ dB.

$$SNR = \frac{\sigma_o P G^2 \lambda^2 C \tau}{64 \pi^2 L H^3 R T_o F B}$$

where:

C = Speed of light

k = Boltzman's constant

T_o = 290° K

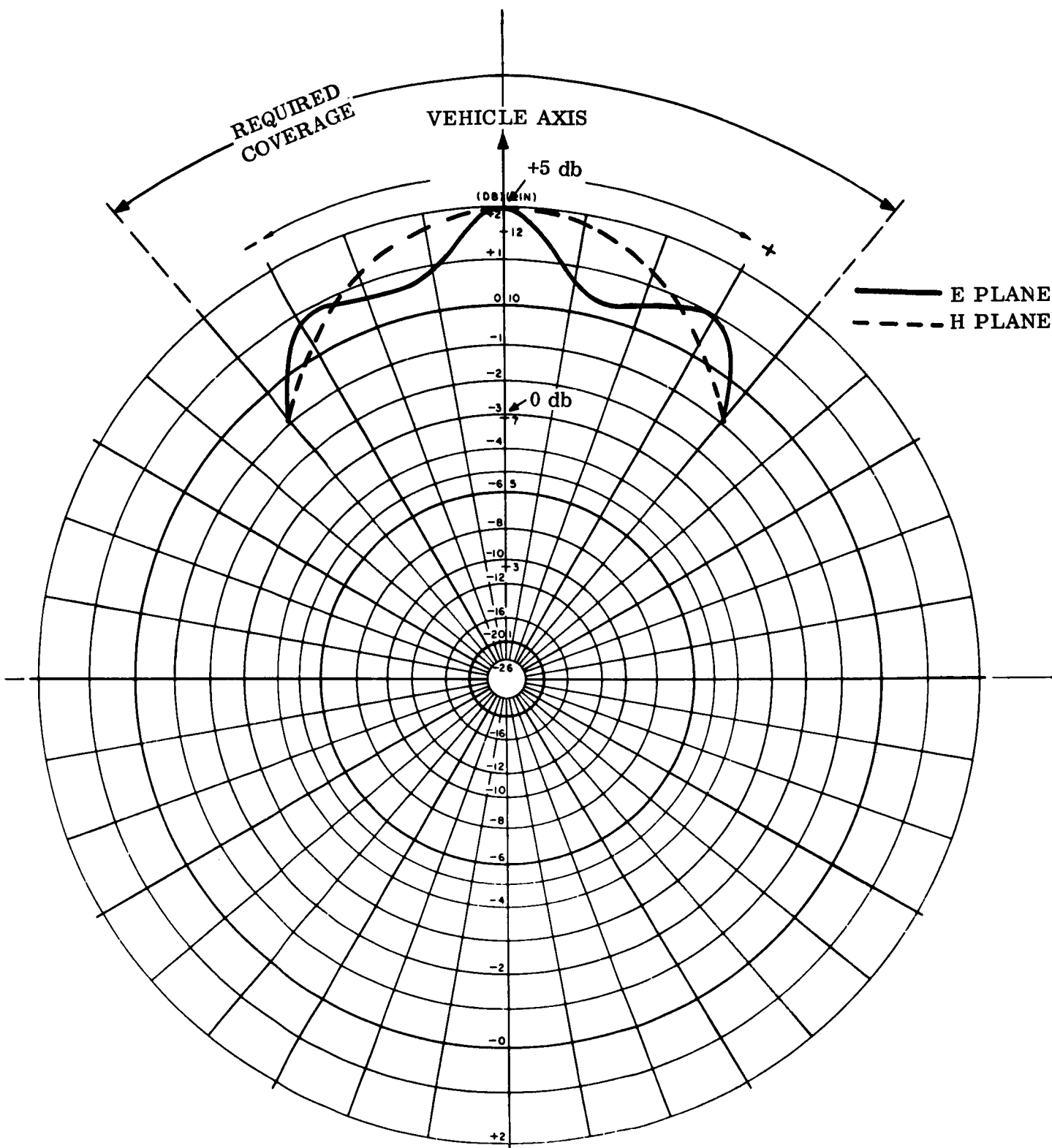


Figure 5.4.6-8. E and H Patterns of Antenna on Vehicle Body

TABLE 5.4.6-4. FUNCTIONAL PARAMETERS

Parameter	Symbol	Value
Peak power	P	50 watts
Frequency	f	1.0 GHz
Wavelength	λ	0.3 meters
Antenna gain	G	0.0 dB
Pulse length	τ	0.7 μ sec (long range) 0.18 μ sec (short range)
Repetition frequency	PRF	1000 Hz
Noise figure	F	6 dB
System losses	L	6 dB
IF bandwidth	B	2.1 MHz (long range) 8.2 MHz (short range)
Acquisition sweep time	Taq	2 sec
Single pulse signal to noise ratio	SNR	+7.1 dB (long range at 20 kft) 13.1 dB (short range at 5 kft)
Probability of detection single sweep	Pd	> 0.95
Accuracy		1% \pm 175 ft (long range) 1% \pm 45 ft (short range)

5.4.6.6.4 Radar Altimeter Parameters

Table 5.4.6-5 shows the weight, volume, and location of the components of the radar altimeter. These weights are excluded from the retardation weight table but are included in the entry system and Lander weights.

TABLE 5.4.6-5. RADAR ALTIMETER PARAMETERS

Item	Location	Weight (lb)	Volume (in. ³)	Power (watts)
Electronic	Lander	15.0	500	20
Antenna (1) (parachute release)	Lander	0.5	18	—
Antenna (2) (atmospheric profile)	Aeroshell	5.5	80	—

5.4.6.7 Retardation Subsystem Weight

The subsystem equipment weight for Point Design 3 is tabulated in table 5.4.6-6.

TABLE 5.4.6-6. RETARDATION SYSTEM WEIGHT BREAKDOWN

Component	Weight (lb)
Pilot parachute mortar thermal cover	1.5
Pilot extraction parachute (modified Ringsail)	7.0
Main parachute compartment thermal cover	7.0
Main parachute, two stage deployment (modified Ringsail)	188.0
Main parachute attachment riser (three legs)	2.0
Parachute compartment including mortar	15.0
Parachute attachment and tie-down fittings (3)	2.0
Mortar pyro gas generator or compressed gas supply	3.0
Pull-apart electrical disconnect	0.2
Explosive nuts (3)	2.5
Total Subsystem Weight	228.2

5.4.7 ROLL CONTROL SUBSYSTEM

The roll control function for Point Design 3 is performed by the de-orbit equipment described in Section 5.3.7. A single monopropellant hydrazine control is used, in conjunction with a rate gyro, to perform both the functions of spin and entry roll control.

5.4.7.1 Roll Control Requirements

At very low dynamic pressures, blunt bodies can be made unstable at zero angle-of-attack by spin, contrary to the generally accepted trend. This phenomenon occurs after peak pressure where the pressure is decreasing with time. The effect here is that in the terminal steady state condition the vehicle will diverge to a trim angle-of-attack (dependent on configuration, spin rate, ballistic coefficient, and inertial properties) and follow a helical flight path.

The effects of this divergence may or may not be significant depending on requirements. Specific items that would be affected are base pressure measurements, radar altimeter measurements, vehicle ballistic coefficient (increases at angle-of-attack), and communication aspect angle.

In order to insure stability in this region a maximum roll rate must not be exceeded. However, roll torques will develop during entry due to built-in and ablation induced

asymmetries. An estimate of this roll torque and the total roll impulse during entry was listed in table 5.3.7-1.

The Capsule will tend to spin-up under the action of this roll torque and it is necessary to provide sufficient roll control torque and impulse to prevent Capsule roll rate from exceeding a maximum limit. The list of fixed hardware is given in table 5.4.7-1 for a total fixed weight of 10.3 lb. The weight of the remainder of the subsystem (hydrazine, pressurant, and tankage), also is included in table 5.4.7-2. Total subsystem weight is 14.7 lb. The control torque and impulse provided for roll control is listed in table 5.4.7-2.

TABLE 5.4.7-1. SPIN AND ROLL CONTROL SUBSYSTEM FIXED HARDWARE WEIGHT, POINT DESIGN 3

	Quantity	Weight (lb)
Rate gyro	1	1.0
Spin electronics	1	2.4
Fill valve	2	0.5
Squib valve	1	0.5
Pressure sensor	1	0.5
Temperature sensor	1	0.25
Valves	2	0.6
Thrusters	4	1.0
Tubing, fittings	-	1.05
Supports	-	2.50
Total Weight		10.3

TABLE 5.4.7-2. SPIN AND ROLL CONTROL SUBSYSTEM,
POINT DESIGN 3 PARAMETERS

Time, separation to spin-up	1.5 sec
Spin rate	50 rpm
Spin-up time	25 sec
Roll thrust	3.3 lb
Roll torque	29.3 ft-lb
Impulse requirements	
spin despin	322 lb-sec
roll control	162 lb-sec
Weight of hydrazine	
spin despin	1.4 lb
roll control	0.7 lb
Tank weight	1.9 lb
Pressurant weight	0.4 lb
Fixed hardware weight	10.3 lb
Total Subsystem Weight	14.7 lb

5.4.8 ENTRY SYSTEMS WEIGHT

A summary weight statement for the items comprising the entry system weight (less Lander and pre-entry systems weight) for Point Design 3 is shown in table 5.4.8-1. Total entry system weight for this point design is 390 lb.

TABLE 5.4.8-1. ENTRY SYSTEM WEIGHT SUMMARY,
POINT DESIGN 3

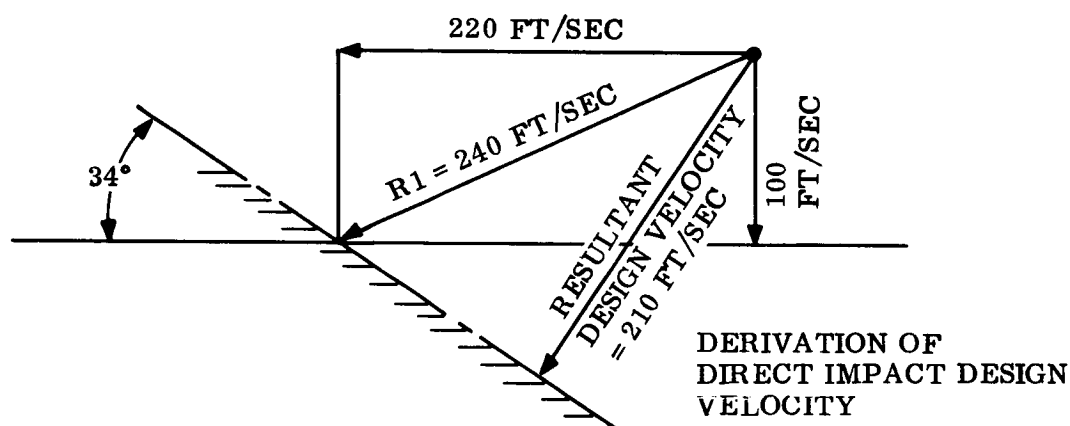
Item	Weight (lb)
Aeroshell skin	51
Miscellaneous structure	41
Heat shield	39
Separation system	1.8
Attitude control	14.7
Retardation	228.2
Harness and cabling	6.2
Entry science	2.5
Radar altimeter antenna	5.5
Total Entry System Weight	389.9

5.5 LANDER SYSTEMS

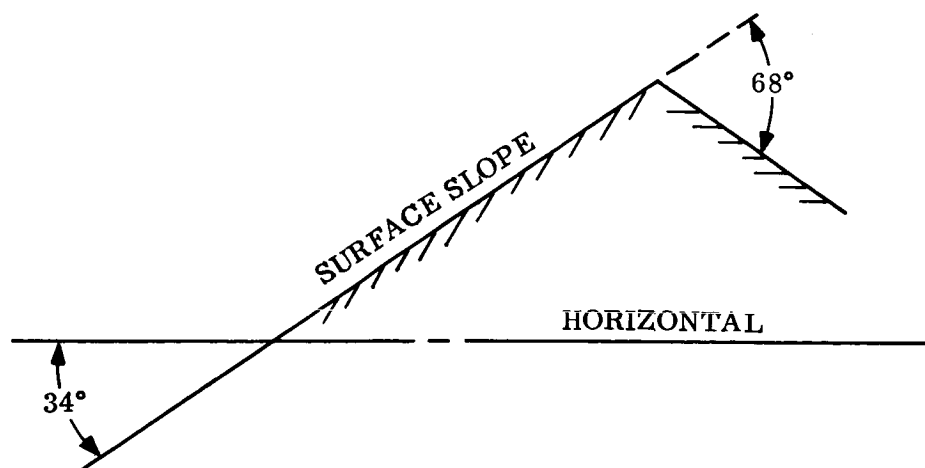
5.5.1 CONFIGURATION CONSTRAINTS AND DESCRIPTIONS

5.5.1.1 Constraints and Design Parameters for Point Design 3

1. Maximum horizontal velocity of Lander at impact due to winds: 220 ft/sec.
2. Maximum vertical velocity of Lander at impact: 100 ft/sec. This was selected based on the optimization of the deceleration and impact attenuation subsystems.
3. Maximum resultant direct impact design velocity: 210 ft/sec.



4. Surface characteristics (to NASA/LRC requirements)
 - a. Surface slopes: zero to $\pm 34^\circ$ relative to horizontal, with abrupt slope changes of $\pm 68^\circ$ forming hills (or valleys), as shown in the following sketch:



- b. Continuous slopes: as long or longer than the base diameter of the Lander.
 - c. Maximum surface rock diameter: 5.0 inches.
5. Maximum total Lander design g-level: 1000. This was selected for point design, as a compromise between conflicting influences of structure and impact attenuation system design, volume for aeroshell packaging and weight.
 6. Vehicle attitude and impact design: Multi-directional design with attenuation capability for the maximum design velocity and g-level, on the prime impact side and round the edge to approximately 70° . The remainder of the impact attenuation system on the back face and edges has been designed for 100 ft/sec impact velocity at maximum g-level. The geometry of the system is shown in Section 5.5.8.
 7. Landed temperature conditions assumed for environmental control design:
 - a. Ambient: -152°F to $+114^\circ\text{F}$ (to specification*)
 - b. Component tolerance (non-operating): -40°F to $+160^\circ\text{F}$ except for battery where the allowable temperature range is $+50^\circ\text{F}$ to $+80^\circ\text{F}$.
 8. Surface mechanical properties:
 - a. Bearing capacity: 6 psi to infinity
 - b. Coefficient of friction: up to 1.0.

(Infinite strength surface assumed as the limiting design case for impact attenuation).
 9. Geometrical, weight, and c. g. constraints:
 - a. Packaging objective: approximately 40 lb/ft^3 in central cylinder of payload container.
 - b. Center of gravity: on or forward of horizontal center line of Lander container.

5.5.1.2 Lander Description

5.5.1.2.1 Configuration

The Lander concept is a doughnut shaped vehicle, with a central circular flat pack payload container. Either side of the vehicle may be face up after landing.

* Mars Engineering Model Parameters for Mission and Design Studies. Langley Research Center, May 1968.

It utilizes a completely passive landing system. The configuration of Point Design 3 is illustrated in fig. 5.5.1-1, general assembly of Lander.

The central container, a short, large diameter cylinder with a 'D' shaped edge structure, houses all the science and supporting subsystem equipment. A deep ring phenolic glass impact attenuation system is bonded to the edge structure of the payload container. Provision is made for science instruments and other equipment to be deployed from the Lander. The degree and type of deployment necessary varies between point designs and is discussed in detail in Section 5.5.6 for Point Design 3.

Depending upon the vehicle mission, electrical power and telecommunication subsystems vary between point designs. These subsystems and other vehicle equipment for Point Design 3 are discussed in detail in the following Lander sections.

Point Design 3 carries a minimum science payload and subsystem and equipment for an operational surface lifetime in excess of 90 days. It is designed with an multi-directional landing capability.

5.5.1.2.2 Science Payload

Science instrument payload installed is listed and discussed in Section 5.5.2. The Lander carries the majority of the entry science as well as the surface science, to avoid duplication of supporting subsystems and instruments and for flexibility of data acquisition and storage.

Provision is made for deployment of cameras, wind measuring instruments, temperature transducers, the alpha backscatter instrument head and solar arrays. The cameras, wind velocity and temperature instruments are housed in a central bay, which is the full width and depth of the Lander payload container. They are mounted on short spring-loaded swinging booms primarily provided for camera deployment. The wind velocity instrumentation requires secondary spring-loaded arms, which unfold at right angles to a spring-loaded extension of the camera booms when the booms are deployed, to provide correct relative location. Deployment of equipment from this bay is substantially automatic following selection and jettison of the bay door on the uppermost and exposed side of the Lander. With the current provision for four separate cameras and deployment booms and the capability to deploy all four from either side of the Lander for high and low resolution imaging, some boom deployment and sequencing will be necessary, but can be kept relatively simple.

A gravity-sensing device determines the uppermost side of the Lander and releases the upper door. Doors are spring-loaded and secured with bolts incorporating hot-wire devices.

The alpha backscatter instrument is located in a separate full depth bay and the instrument head can be deployed downward onto the planet surface, through whichever side of the Lander constitutes the underside. To facilitate this operation with a minimum of rotational movement of the instrument head, the alpha backscatter instrument is installed on its side in the bay. Sensing for operation of inward hinging doors enclosing the alpha backscatter instrument bay is by the gravity device provided for the camera bay doors.

Each of the solar arrays, also located in individual bays, can be deployed in either direction from the flat surfaces of the Lander container. Sensing, door release, and direction of operation is again controlled by the gravity device.

A full detailed description of the deployable instruments, and equipment and mechanical operations, with illustrations, is given in Section 5.5.6.

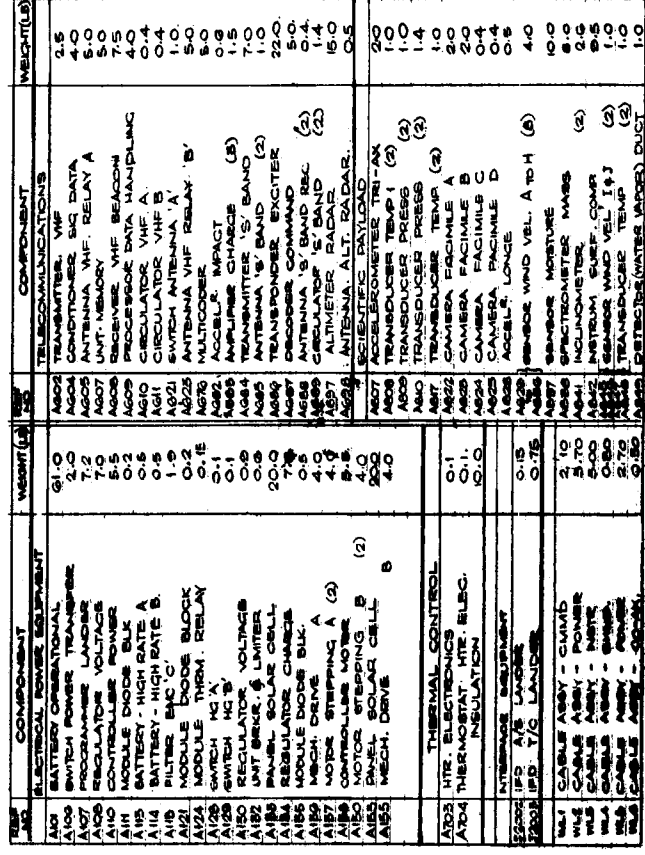
The remainder of the payload (science and supporting subsystems) is housed in other compartments formed by the inner framework of the payload container. Access to this equipment is available through either the top or bottom bolted covers of the container, or by removal of the inner framework from the Lander, complete with all equipment. The installation is compact to achieve low weight and volume, but consistent with requirements for assembly, service and operational functions.

5.5.1.2.3 Lander Support Subsystems

To perform the 90 day plus mission of Point Design 3, a telecommunications link is designed to provide a relay link for transmission of imagery data for the periapsis passage of the Orbiter immediately after impact on the surface of the planet and at the end of each succeeding diurnal cycle for a period of three days. The telecommunications system consists of a 400 MHz transmitter with a dual power amplifier output stage, memory with 180,000 bit storage capacity and the appropriate signal conditioning and data handling equipment. For the extended mission time for this point design a direct link telecommunications system and a command link with its associated decoding and data handling capability has been incorporated in the design. The direct link provides the capability for obtaining meteorological data for the extended mission time. A radar altimeter has been included to provide a more accurate altitude sensing for parachute deployment and subsequent parachute release prior to Lander impact. The antenna for parachute release is located in the base of the Lander whereas the antenna for parachute deployment is located in the aeroshell.

The electrical power and distribution equipment, located in the Lander, provides all the primary power required of the Lander and the appropriate programming and sequencing functions. The main power source for this mission is a solar array/battery system. The battery was sized for a three day mission and weighs approximately 68 lb. This battery was sized based on a 30 watt-hour/lb rating. The solar array is 25 ft² and provides the required power for the telecommunication and science equipment.

Surface science equipment consists of the minimum science package including equipment to measure wind velocity, surface temperature, and pressure, alpha backscattering, imagery, a clinometer and moisture detector. Imagery data will be taken and transmitted to the Orbiter during the periapsis passage for each of the four available transmission periods, and will be transmitted real-time. Additionally, stored entry and surface science data, diagnostic, and real time surface science data is alternately transmitted between the picture taking sequence.



5-111/5-112

Environmental control, primarily an insulation problem, is achieved by the use of honeycomb panels with fiberglass core for the outer shell of the Lander container; coupled with the application of thick layers of foam on exposed surfaces, such as the sidewalls of the camera bay. Batteries, which are the component most sensitive to the cold environment are maintained at a working temperature by a combination of heat dissipated from other components and an individual electric heater.

A complete description of science and Lander subsystems including structural and mechanical components is given in the sections following, together with detailed weight information.

5.5.2 SCIENCE PAYLOAD EQUIPMENTS

5.5.2.1 General

The various instruments carried by the Hard Lander to Mars may be classified into two general categories. They are the entry phase instruments, which require no special compatibility with unusually high deceleration loading, and the landed phase instruments which must survive the extreme loads and shocks encountered during impact and maintain their calibration and state of operability. In most cases, the entry phase instrumentation can be rather well defined in terms of the state-of-the-art; however, certain devices, such as the water vapor detector, will require some development before a device is available that will fulfill the scientific requirements of the measurement. The landed phase instrumentation includes a "minimum" science payload and certain other devices that may feasibly be carried by the Lander. In this group of instruments there are several devices that do not physically exist at the present. Others in this group are at some point in their development that provides sufficient confidence in their design to consider them in this mission even though serious doubts exist concerning their ability to withstand the high shock impact of the Hard Lander. For these designs, additional shock attenuation can be considered for isolating the instrument from the extreme environment. However, this additional weight and volume appears prohibitive at the present time.

The section provides a brief summary of the scientific instrumentation selected for inclusion in the point designs. Detailed descriptions of the equipment and the studies performed in their selection have been given in previous sections (2.3.3 and 2.3.4) of this volume. Considerations used for identifying the implementation approaches best suited for the missions have been discussed in Volume II, Section 4.0.

5.5.2.2 Entry Science Payload

5.5.2.2.1 Tri-axial Accelerometer

The tri-axial accelerometer is mounted at the entry system center of gravity. Several varieties are currently available, however the "magnetic force balance" type seems to have the most desirable characteristics. Table 5.5.2-1 shows the mechanical and electrical characteristics of an accelerometer currently in use on various military programs. Also shown are the sequencing, sampling, and data format requirements for the accelerometer. No significant problems are foreseen in sterilizing the device.

TABLE 5.5.2-1. ENTRY SCIENCE PAYLOAD

Instrument (Lander)	Weight	Volume	Power Req'mts	Location	Sampling Schedule	Data Format
Mass Spectrometer	8 lbs	2 x 7 x 14 in.	7 watts	Internal near surface. Re-quires port through heat shield	Initiates near Mach 5 Terminates at impact	50 (8) bit words per sample (2 sec scan, 8 sec readout) 50 bits/sec readout
Resistance Thermometer	0.5 lb each	1 in. dia x 2 in. long	1 watt each	Two on base of vehicle	Initiates at Mach 5 Terminates at impact	1 sensor output channel 1 sample/sec
Variable Capacitor Pressure Transducers	0.5 lb each	2 in. dia x 2 in. long	1 watt each	Two on base of vehicle	Initiates at beginning of entry Terminates at impact	1 sensor output channels 1 sample/sec
Tri-Axial Accelerometer (1 Dual Scale)	2 lb	2.8 x 1.8 x 2 in.	4 watts	Located at body c.g. with one axis aligned to vehicle vertical axis	Initiates at beginning of entry Terminates impact	8 bits/sample/axis 10 samples/sec 72 bits/sec total Automatic scale switching
Water Vapor	1 lb (ducting only)	Detector located in sur-face science package	N/A	Ducting located same as mass spectrometer ducting	Initiates near Mach 5 Terminates at impact	1 sample/15 sec 2 seven bit (parallel) channels 1 eleven bit (parallel) channels

TABLE 5.5.2-1. ENTRY SCIENCE PAYLOAD (Concluded)

Instrument (Aeroshell)	Weight	Volume	Power Req'mts	Location	Sampling Schedule	Data Format
Stagnation Temperature Transducer (1)	0.5 lb	1 in. dia x 2 in. long	1 watt	See text	Initiates at beginning of entry Terminates at aeroshell ejection	1 sensor output 1 sample/sec
Stagnation Region Pressure Transducer (4)	0.5 lb each	2 in. dia x 2 in. long each	1 watt each	Behind nose of aeroshell (See text)	Initiates at beginning of entry Terminates at aeroshell ejection	1 sensor output 1 sample/sec

5.5.2.2.2 Temperature Transducer

Atmospheric temperature measurements during the entry phase are performed by three temperature transducers. These are platinum resistance thermometers. One is located in the stagnation region of the aeroshell and measures the stagnation temperature from the beginning of entry down to aeroshell ejection. The other two thermometers are located on the base of the Lander system and are used during the subsonic region of flight primarily during parachute descent. Table 5.5.2-1 shows the physical and electrical characteristics of the resistance thermometers and its data collection profile. The exact configuration and design of the stagnation transducer will depend upon a large number of variables. The definition of the transducer design parameters will require preflight testing of the thermal characteristics of either scale model or prototype vehicles.

5.5.2.2.3 Pressure Transducers

Variable capacitance pressure transducers located on the aeroshell and on the base of the entry system measure atmospheric pressure profiles. The four transducers arrayed about the stagnation region perform the dual function of measuring pressure and angle of attack. These transducers are located just behind the heat shield and are exposed to the external environment via ducting leading through the beryllium cap of the heat shield. The pressure transducer located on the base of the Lander system measures base pressure from supersonic through subsonic flight regimes. Table 5.5.2-1 lists the characteristics of these transducers and also shows the sampling schedule and data format.

5.5.2.2.4 Mass Spectrometer

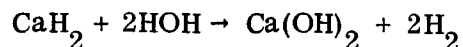
The measurement of atmospheric composition by mass spectrographic techniques requires acquisition of a sample from the atmosphere. This acquisition must be performed without exposure to contamination from gaseous materials exuded by the heat shield or other sources. The ducting leading from the mass spectrometer to the external environment terminates in the nose area that contains the beryllium plug which serves to minimize the probability of contamination from heat shield outgassing products. This same ducting also delivers atmospheric samples to the water vapor detector located in the entry payload and must be disconnected when the aeroshell is separated from the Lander at parachute deployment.

Table 5.5.2-1 shows the physical, electrical, and data collection characteristics of the mass spectrometer.

5.5.2.2.5 Water Vapor Detector

At present the chemical/radiological water detector is in the concept development stage. Since this device will also be used during landed operations it must be designed for high shock survival. Fig. 5.5.2-1 shows, in block diagram form, the design of the water vapor detector. Table 5.5.2-1 shows the physical and electrical characteristics of the detector. The ducting leading from the nose for entry data is disconnected at aeroshell separation and a second port is opened for landed operations.

The basic operating principle is that when calcium hydride comes in contact with water (in either liquid or vapor form) the following reaction takes place:



When the hydride is labelled with tritium, the gaseous effluence contains the radioactive tritium. This element may be quantitatively detected by its radiation and thus the amount of water entering into the reaction may be determined. Radiation shielding of this system will present no problems since tritium emits 18 KeV beta particles that are stopped by the chamber walls. Present laboratory tests have demonstrated the device at 1 part/million with definite indications of feasibility for operation of 1 part/billion.

5.5.2.3 Surface Science Payload

5.5.2.3.1 Pressure Transducer

Unlike the pressure transducers included in the entry payload, the surface pressure transducer must be able to withstand high level shock loading. This requirement

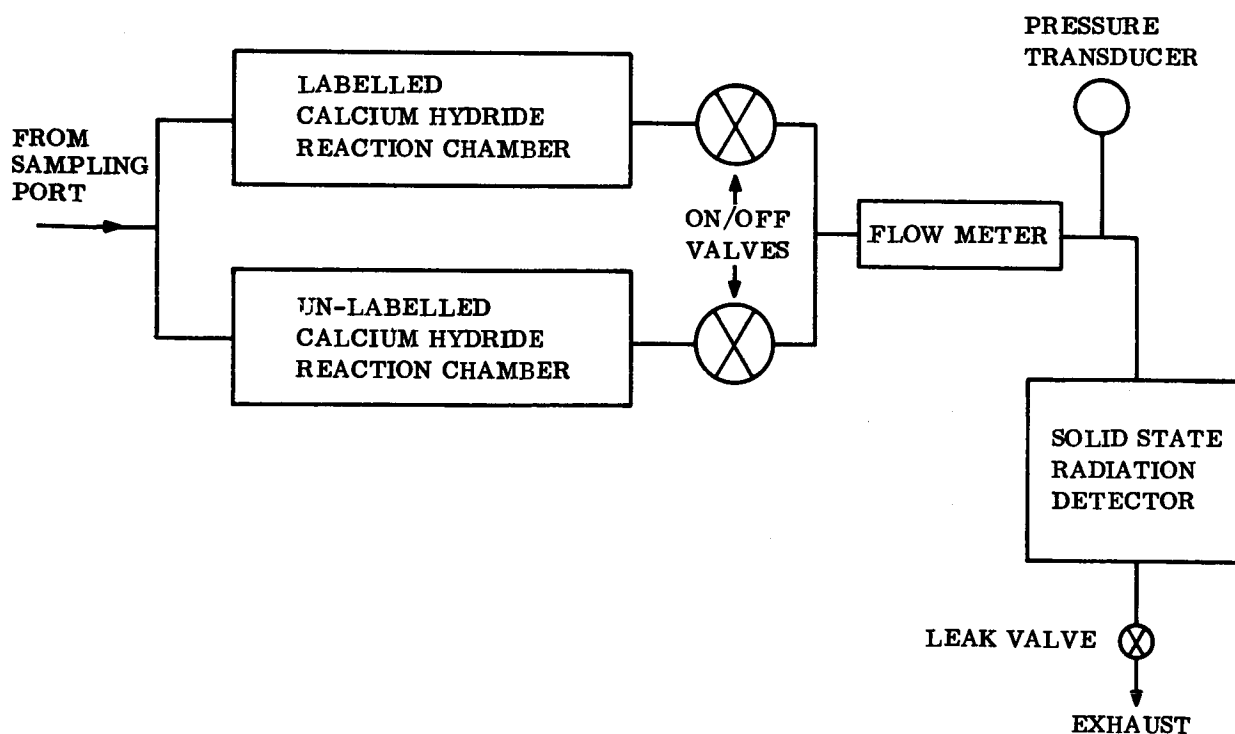


Figure 5.5.2-1. Water Vapor Detector, Block Diagram

necessitates either an extension to the state-of-the-art in low pressure transducers or provisions for reducing impact loading much below 1000 g's. The added weight and volume for this shock compatibility or attenuation is not included in the component weight or volume shown in table 5.5.2-2.

5.5.2.3.2 Temperature Transducer

Atmospheric temperature is measured by a set of platinum resistance thermometers. They are deployed following impact with the camera booms to obtain free stream data with minimum Lander-induced perturbations. Such devices have been designed to withstand rather high g-loading and thus no serious problems are expected as a result of a rough landing. The ultimate physical design of the thermometers will deal with minimization of direct solar heating since this can be a serious measurement problem. A solar shield is required to accomplish the task of decoupling the resistance element from the solar flux. See table 5.5.2-2 for transducer characteristics.

5.5.2.3.3 Wind Velocity Sensor

Although an acoustic velocity sensor has not yet been built for planetary exploration application, the changes required to modify existing designs intended for terrestrial applications appears straightforward. The design approach used for point design evaluation consists of five magnetostrictive transducers (fig. 5.5.2-2) mounted on the boom supporting the TV camera system. A microminiaturized electronics package produces the necessary ultrasonic pulses that drive the transducers and also measures the transit time for each pulse to travel from one transducer to the next. No problem is foreseen in fabricating the required electronics and transducers to meet the sterilization and shock environment requirements. Care must be taken, however, to assure reasonably good rigidity in the transducer supporting arms during the measurement since motion of the transducers may be misinterpreted to signify motion of the medium (atmosphere). Table 5.5.2-2 shows the anticipated physical and electrical characteristics of the wind velocity sensor.

5.5.2.3-4 Water Vapor (Moisture) Detector

The chemical/radiological water vapor detector has not been hardened for the extreme environments that will be encountered during the entry and landing phase of the mission. However, since the design is inherently mechanically simple, it is expected that a device with the physical characteristics shown in table 5.5.2-2 can be developed and tested in time for a 1973 mission to Mars. Operating experience (laboratory) in the low (parts/million) and high (parts/billion) range has demonstrated that water vapor sorption-desorption by materials used in the sampling system could be the major factor toward limiting the response and detection sensitivity in this and lower concentration regions. This would also be of special importance for water detectors based on physical principles, especially at lower operating pressures, where sorption-desorption by the detector supporting hardware could contribute significantly to a non-representative water environment around the detector. It is felt that water sorption-desorption can be controlled by appropriate materials selection, by minimizing exposed surfaces, and by operating these surfaces at temperatures consistent with the level of water concentration to be sensed.

TABLE 5.5.2-2. SURFACE SCIENCE PAYLOAD

Instrument (Lander)	Weight	Volume	Power	Location	Deployment/ Orientation	Mission Profile	Data Format/ Requirements
Pressure Transducer (2)	0.7 lb each	2 in. dia, 2 in. long each	1 watt each	Internal near skin of vehicle	Port through skin to am- bient environ- ment either top or bottom No deployment	Operates con- tinuously after impact	3 samples/hr each 1% accur- acy Two channels total
Resistance Thermometer (4)	0.5 lb each	1 in. dia, 2 in. long each	1 watt each	One on each camera boom	Deployed above Lander on camera booms One on each boom	Same as above	3 samples/hr each 1% accur- acy Four channels total
Wind Velocity Transducer (2)	2.5 lbs each	25 cubic in. prior to deploy- ment each	3 watts each	One on each of two camera booms	Boom deploy- ment above vehicle on camera booms	Same as above	3 samples/hr 6 channels Each channel consisting of 11 parallel bits Total of 66 bits/sample
Moisture Detector (1)	10 lb	60 in. ³	5 watts	Mounted internal to Lander	Pneumatic tubes de- ployed as part of camera booms	Same as above	3 samples/hr 2 seven bit (parallel) channels 1 eleven bit (parallel) channel

TABLE 5.5.2-2. SURFACE SCIENCE PAYLOAD (Concluded)

Instrument (Lander)	Weight	Volume	Power	Location	Deployment/ Orientation	Mission Profile	Data Format/ Requirements
Surface Composition (Alpha backscatter) (1)	9.5 lb	5.5 x 7.5 x 4.5 in.	5 watts	Internal to vehicle	Must be de- ployed so that sensor head rests on sur- face of planet top or bottom deployment controlled by clinometer	Deploy 3 hr after impact First readout 1 hr after impact 2nd readout 3 hr after impact then readouts every 3 hr thereafter	1 sample/3 hr 130 channels 14 bits (parallel) each 130 channels 12 bits (parallel) each 3 channels 7 bits (parallel) each
Photo- imaging (4)	4.8 lb total	1 to 2 in. dia 9 to 12 in. long each	6-10 watts total	One on each of four booms de- ployed above Lander	Boom deploy- ment 36 in. Height > 18 in. One boom/ camera	4 frame sweeps on high resolu- tion and 4 frame sweeps on low resolutions in sequence Operation time time coincident with transmis- sions	Flexible to meet maximum trans- mission capability of Lander. Period from 1 sec to 8 hr/ picture. Total ⁷ bits between 10 ⁸ and 10 ⁹
Clinometer (2)	1.3 lb each	2 in. dia x 3 in. long	3 watts	Two in- ternal to Lander mounted with long dimension parallel to vertical axis of Lander	N/A	Sampled imme- diately after impact then once every 3 hr	1 sample/3 hr 2 channels 7 bits (parallel) per channel

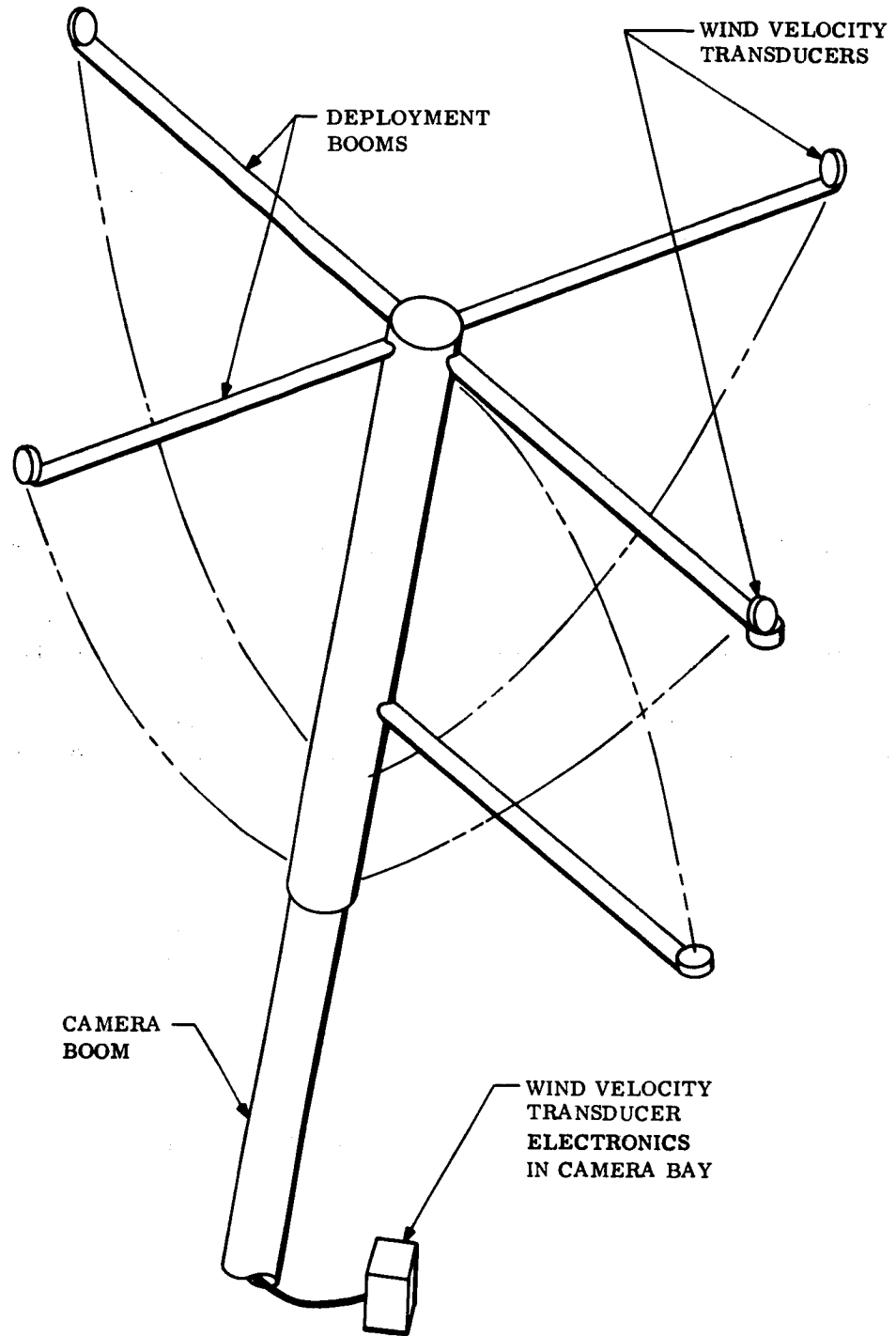


Figure 5.5.2-2. Wind Velocity Sensor

The device will remain in the Lander during operation and gas sampling will occur through a vent tube in a camera boom. The key interface requirements are shown in table 5.5.2-2.

5.5.2.3.5 Alpha-Backscatter Spectrometer

An alpha-backscatter spectrometer suitable for operation on Mars is being considered for development by the University of Chicago (Turkevitch). Such a device will most probably not use the isotope source (Cm^{242}) used in the Surveyor spectrometer and the source selection will be one of the prime considerations for any future designs. Mechanically, with the possible exception of the deployment mechanism, the spectrometer will probably be able to meet the requirements of a rough landing. Figure 5.5.2-3 shows the Surveyor alpha-spectrometer for reference purposes. Reduction of the overall dimensions of the sensor head are anticipated since the Martian atmosphere will interfere with the measurement. This reduction will result in shorter particle path lengths and correspondingly smaller interference with the measurement.

The head, which must be deployed to come in contact with the surface of the planet, is mounted on a swivel bracket so that deployment either "up" or "down" will be possible. The existence of surface protuberances in the field of view will introduce errors. A calibration sample is exposed to the bottom of the sensor head when in the stowed position, thus providing a reference source for data interpretation. Table 5.5.2-2 gives the physical and electrical parameter estimates for the proposed device. The deployment will be carried out in two stages; i.e., partial deployment toward surface for background counting and full deployment for composition measurement.

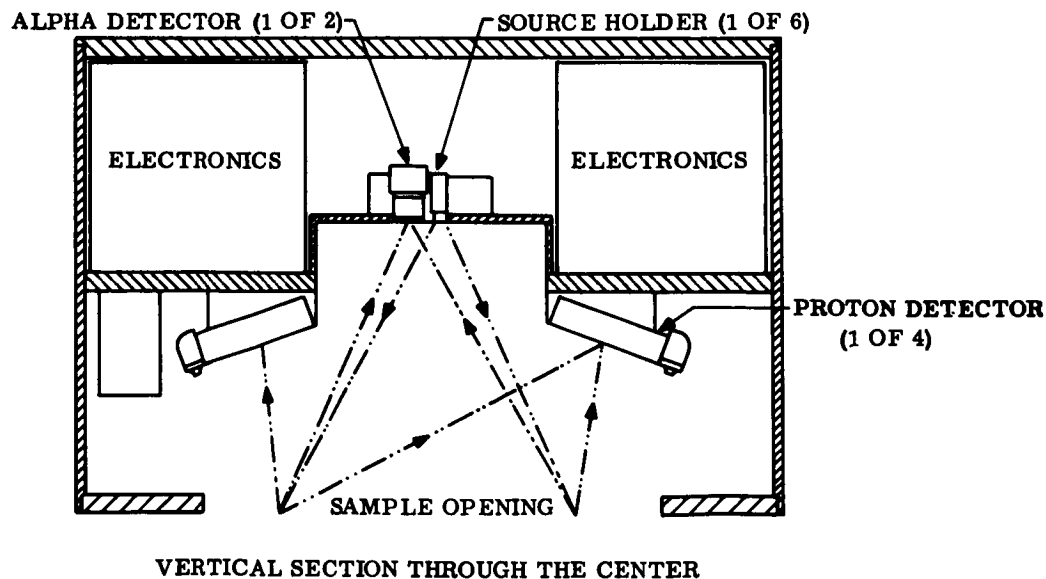


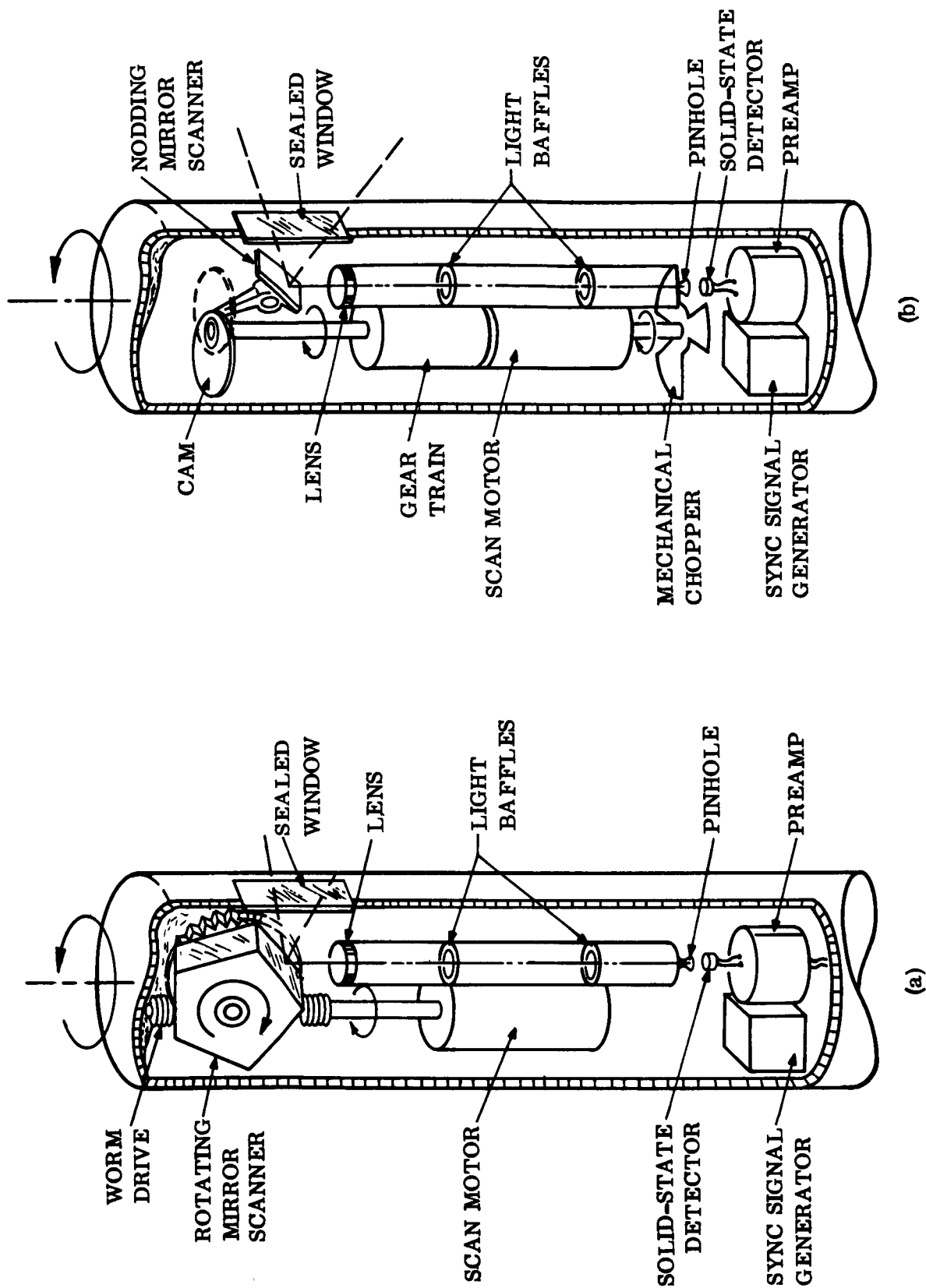
Figure 5.5.2-3. Alpha Backscattering Instrument

5.5.2.3.6 TV Cameras

The high and low resolution cameras are installed on individual hinged masts, although it may be possible to combine them within one casing. Figure 5.5.2-4 shows the basic elements that each contains. Neither of the two versions shown contain the azimuthal drive motor. The high speed version (fig. 5.5.2-4) has a 5-sided mirror that rotates unidirectionally. The preferred video rate for this version is not well defined and can be from 10 kHz to 100 kHz depending on circumstances. The incident light passes through the window and is reflected from the mirror onto the silicon cell detector. The solid state amplifier amplifies the resulting electrical signal to $\pm 5V$ maximum, the output signal leads from the camera housing carry this signal to the processing electronics. The slow speed version (that can take up to 4 hr for a full panoramic sweep) has a nodding mirror activated by a cam. The light beam is deflected via this mirror onto the silicon cell after being chopped by a small light chopper placed in front of the cell. This latter addition enables the same basic amplifier to be used for both the high speed and low speed versions. The silicon cell response is shown in fig. 5.5.2-5. The dimensions of the camera unit that contains all the mechanical drive mechanisms and all the electronics for the video and synchronizing signals varies with the full design specification; normally, however, these will be between 1 and 3 in. diameter and between 6 and 16 in. long. Total weights of the cameras as described can again vary from 1/2 to 6-1/2 lb. (See table 5.5.2-3)

5.5.2.3.7 Clinometer

The clinometer proposed for the 1973 Hard Lander will require development. Specifications for the design are not complete; however, the parameters shown in table 5.5.2-2 are based on engineering estimates for the conceptual design shown in fig. 5.5.2-6. The potentiometer housings could also include any electronics required to operate the system. Location of the instrument in the Lander is not critical.



ROTATING MIRROR FOR
RAPID SCANNING MODE

NODDING MIRROR FOR
SLOW SCANNING MODE

Figure 5.5.2-4. High and Low Speed TV Cameras

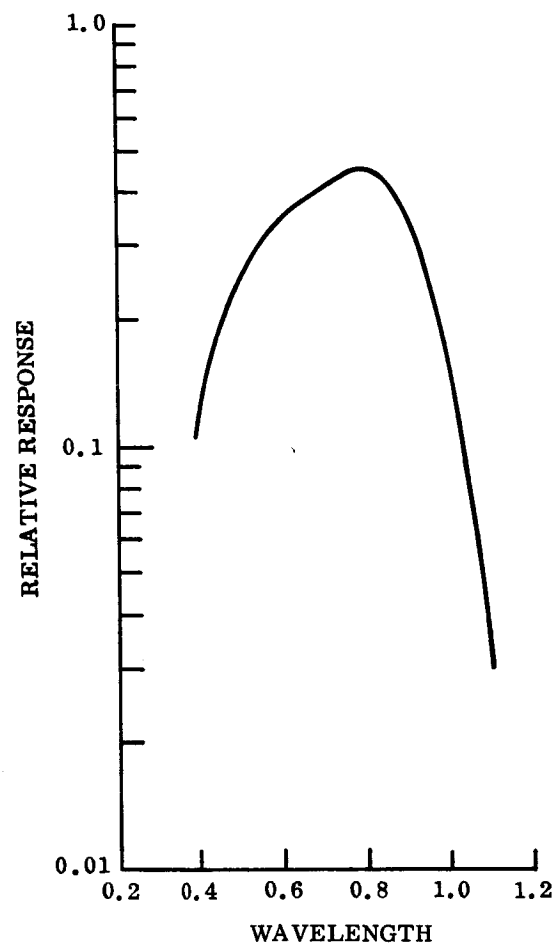


Figure 5. 5. 2-5. Silicon Photo-Voltaic Cell Spectral Response

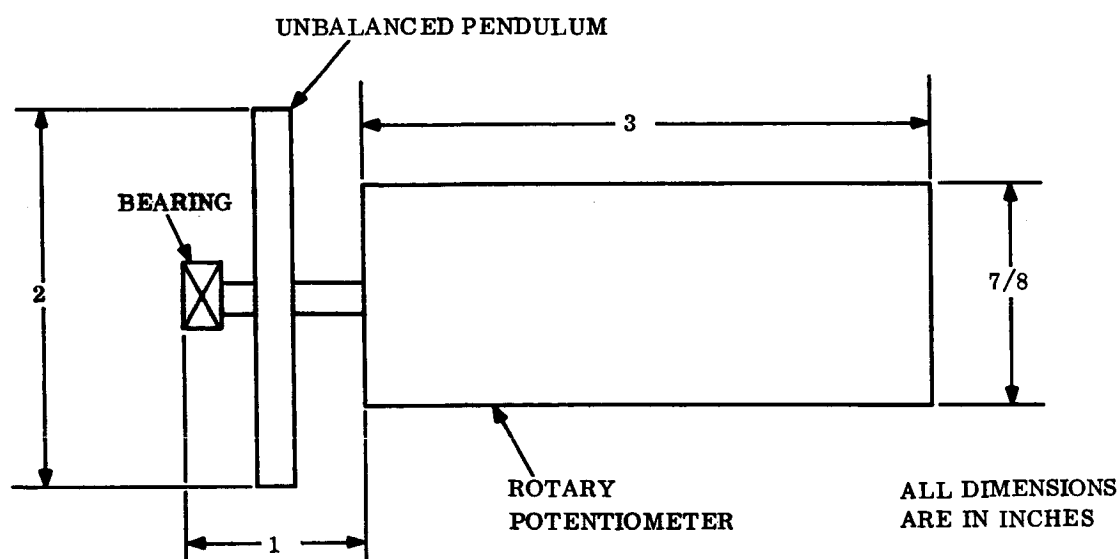


Figure 5. 5. 2-6. Rotary Potentiometer Clinometer

TABLE 5.5.2-3. TYPICAL CAMERA SPECIFICATIONS

Model Identification	CM	SL	NP	SS	SM
Special Feature	small size, small power	rugged	high speed	adjustable performance	high resolution
Field of view	9° x 360°	50° x 360°	25° x 360°	10° x 10° to 90° x 360°	1° x 1°
Resolution	0.1 in. @ 6 ft	0.1 in. @ 6 ft	1 in. @ 100 ft	0.1 in. @ 1 ft to 0.1 in. @ 60 ft	1 micron @ 3/4 in.
Frame time	1/2 min	7 min	2 1/2 sec	30 sec to 10 hr	1 sec
Sensitivity range	0.1-1000 ft-L	0.3-3000 ft-L	1.5000 ft-L	0.001-5000 ft-L	10-10,000 ft-L
Size	1 in. dia x 6 in. long	1.5 in. dia x 10 in. long	2.5 in. dia 11 in. long	3 in. dia x 18 in. long	3 in. dia x 15 in. long
Weight	0.4 lb	3.5 lb	5.5 lb	6.5 lb	6 lb
Power	1 W	10 W	150 W	15 W	4W
Temperature (of the environment)	-10°F to +150°F	-40°F to +180°F	-10°F to +125°F	-45°F to +145°F	-45°F to +145°F
Pressure (external)	1 ATM	10 ⁻⁹ Torr	1000 psi	1 mb	1 mb
Shock and Vibration	1000 g	3500 g	100 g	300 g	50 g

5.5.3 TELECOMMUNICATIONS

5.5.3.1 Summary

The telecommunications subsystem consists of:

1. A hardwire data link for Lander/Capsule checkout prior to separation from the spacecraft
2. A relay communications link to provide Lander/Capsule entry data and high data rate imagery after landing
3. A direct S-band data link to provide engineering and scientific data during the extended mission via the Deep Space Net (DSN)
4. A UHF beacon link to detect Orbiter presence for relay communications
5. An S-band command link for detecting and decoding commands for control of the Lander subsystems.

A functional block diagram of the Telecommunication Subsystem is shown in fig. 5.5.3-1. The communication link characteristics are summarized in table 5.5.3-1.

To support the high data requirement for imagery, the data will be relayed to Earth via the Orbiter, with communication to the Orbiter taking place during a periapsis pass to take advantage of the relatively short line-of-sight range. Data is stored in the Orbiter and subsequently transmitted to Earth. Non-coherent frequency shift keying with Manchester coding is chosen for the modulation technique to minimize acquisition time. After landing, the link is designed to operate at a 160 bps data rate, the optimum from the standpoint of achieving maximum total data transmission. At this rate, it is feasible to transfer 8.1×10^7 bits in a period of 8.5 min with maximum adverse link tolerance, 46° worst case Lander tilt, and reference Orbiter-Lander line-of-sight parameters. To accomplish this data transfer requires 50 watts of transmitter power, the maximum allowable to avoid antenna breakdown at Mars surface pressure. It is assumed that the Orbiter will be provided with the capability to record data at this high rate. If this is not the case, the total data transferable (and the transmitter power) scale down approximately proportional to the actual recording rate.

Data requirements prior to and during entry are relatively modest, but communication ranges are more severe. It was determined that the same transmitter and receiver used for imagery data after landing can be used at a lower data rate for entry data. This minimizes equipment and complexity on both the Orbiter and Lander.

Because of the varying communication parameters due to atmosphere uncertainty and possible vehicle tilt, the amount of data transferable via the relay link immediately after impact varies widely, but because of the compensating effect of the parachute deployment radar, relay communications immediately after impact are feasible at

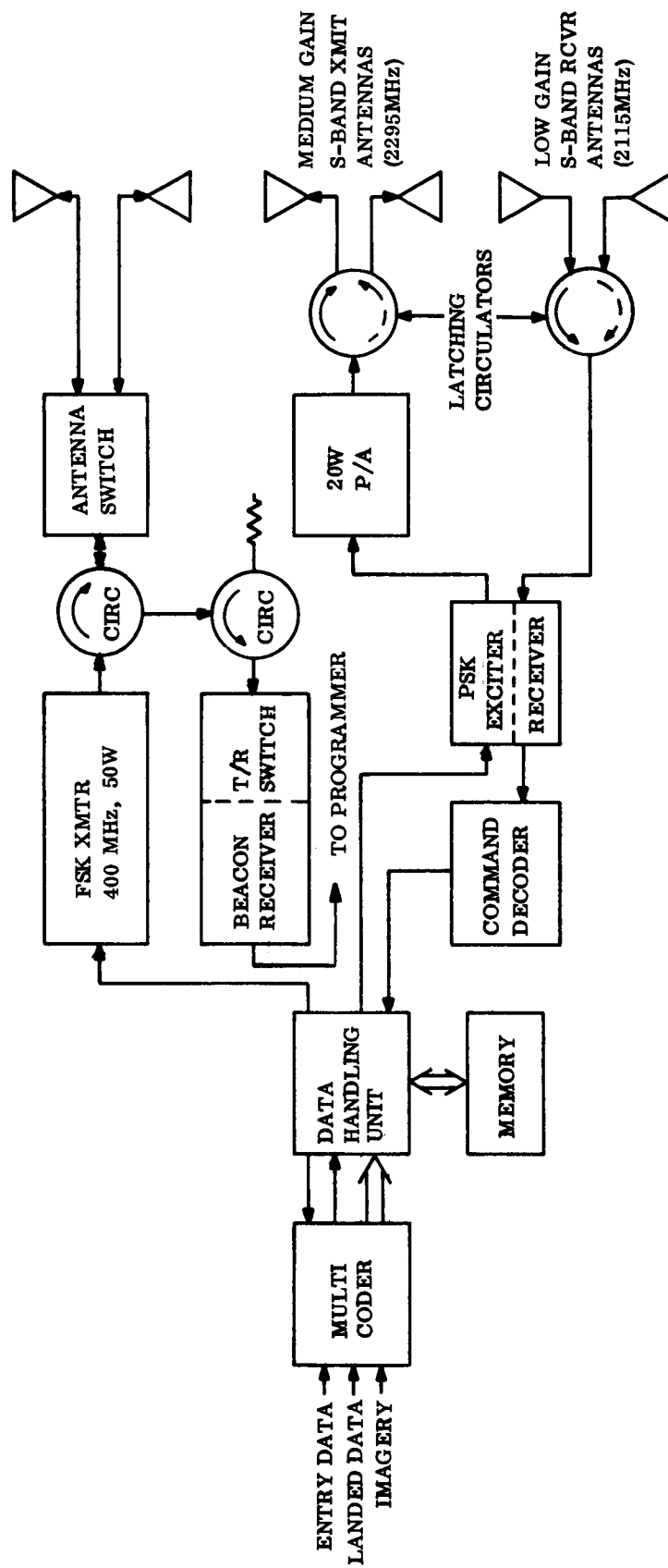


Figure 5.5.3-1. Telecommunications Subsystem, Functional Block Diagram

TABLE 5.5.3-1. DESIGN SUMMARY

Phase	Link	Data Rate (bps)	Transmission Time	Total Data (bits)
Post-separation	400 MHz FSK, relay	1090	30 min	2.0×10^6
Entry	400 MHz FSK, relay	1090	450 to 630 sec (1)	0.49 to 0.69 $\times 10^6$ (1)
Post-impact, set-up	400 MHz FSK, relay	1090	2.5 min (2)	0.16×10^6 (2)
Post-impact, Orbiter pass	400 MHz FSK, relay	160×10^3	10.4 min	0 to 10.3×10^7 (4)
Periapsis pass	400 MHz FSK, relay	160×10^3	20.5 min (3)	8.1×10^7
Post-relay (daily)	S-Band, PSK direct	24	1.6 hrs (5) 1750 sec (6) 133 sec (7)	138,000 (5) 42,000 (6) 3184 (7)
(1) Atmosphere dependent (2) Data during this period may be lost because entry antenna may be underneath Lander. (3) Includes maximum beacon turn-on time error of 12 min and 8.5 min minimum effective transmission interval. (4) Atmosphere and tilt dependent. (5) Antenna limited (6) Average daily. Limited by solar array size (7) Nominal data transmission time				

the high data rate. In fact, the total data in excess of 3.3×10^7 bits may be transferred under maximum adverse tolerance conditions for Lander tilts less than 46° .

A beacon link is provided to detect Orbiter presence. The Orbiter beacon transmitter and Lander beacon receiver are turned on prior to nominal periapsis by the time of arrival uncertainty as indicated in Section 5.5.3.4.2. The beacon link then essentially measured receives signal strength and initiates data transmission when link conditions capable of supporting the established data rate are indicated. By using the same antennas for the beacon and data links much of the potential differences between beacon and data links are removed. The remaining uncertainty in the beacon link is 9.2 dB resulting in worst case early turn-on of 12 min when the beacon link is designed to trigger at the latest time possible as determined by worst case data link performance.

After the first few days, when the Orbiter is no longer available, data is transmitted directly to Earth via DSN facilities. The nominal data load for this phase is 3184 bits. By using a 20 watt (minimum) S-band transmitter and receiving with the 210 ft dish in the listen-only mode, with a 12 Hz receiver bandwidth, the direct link can support this nominal data load with reserve capacity throughout the 90 day mission. This is accomplished using a vertically oriented helix antenna which provides about 1.6 hr Earth coverage time (at 24 bits/sec) with maximum adverse tolerance and the worst case pointing error of 17° at the nominal 10°N latitude. That is, irrespective of power supply limitations, the daily capacity is 138 kbits. Latitude errors of 4° can be accommodated with no loss in nominal data. If errors in excess of 4° are expected, the antenna must be designed with wider beamwidth and a corresponding degradation in available bit rate will result.

An S-band command link is provided. Commands at the rate of 0.5 bits/sec are feasible throughout the 90 day mission by using an 85 ft antenna and 100 kw transmitter. (To share the 210 ft dish would disastrously degrade the direct data link because of losses in additional r-f equipment.) For command reception a wide-band antenna with extended Earth viewing time is provided to provide a wide command window.

The landing orientation ambiguity necessitates duplicate antennas for the relay and direct links. Antenna selection is by semiconductor switches in the 400 MHz system and by electrically controlled latching circulators in the S-band system.

5.5.3.2 Telecommunications Sequence

Prior to separation, Lander power is turned-on for final checkout (table 5.5.3-2). Except for a momentary check of transmitter power, transmitter operation within the canister is avoided. During this interval, data is transferred via hardwire to the Spacecraft. Immediately after separation r-f transmission is initiated for event monitoring and engineering diagnostic measurements.

During entry and for 2.5 min after impact, scientific and engineering diagnostic data are transmitted at the low data rate. The high data rate is then used to transmit imagery for a period dependent on the atmosphere characteristics, i.e., entry time. (See para 5.5.3.4.)

The beacon link is turned on early by a time equal to the total Orbiter arrival time uncertainty. The beacon link will trigger high rate transmission of stored scientific and engineering data and imagery. The beacon link trigger occurs 0 to 12 min early because of link parameter tolerances.

The command receiver and direct link transmitter are turned-on by a stored command with the nominal data transmission time being 2.2 min.

5.5.3.3 Data Requirements

Table 5.5.3-3 is a list of measurements for the entry, landed (relay) and post-relay mission phase. Table 5.5.3-4 gives the corresponding data transmitted. During entry, real time data is interleaved with data delayed by 70 sec to avoid loss of data during blackout. The combined data dictates a 1.09 kbps data rate. Prior to entry, only engineering diagnostic data is transmitted. Immediately after landing, imagery is transmitted at the high data rate. Imagery and surface science data are transmitted at the high data rate on subsequent Orbiter passes. The period required to relay the total data of 8.1×10^7 bits is 506 sec with surface science and engineering diagnostic data requiring approximately 0.4 sec and the rest of the period devoted to transmission of imagery data. For redundancy purposes, the stored surface science and engineering diagnostic data are read out of memory and transmitted at the beginning and middle of each 506 sec period. In the post-relay phase, data requirements are reduced a nominal 3184 bits with flexibility available via commands.

TABLE 5.5.3-2. TELECOMMUNICATIONS SEQUENCE

Phase	Duration	Communications
Pre-separation	15 min	Low rate/hardwire
Post-separation	30 min	Low rate
Entry	452 to 629 sec	Low rate
Post impact	2.5 min	Low rate
Post-landing	(see table 5.5.3-7)	High rate
Orbit period	~ 25 hr	None
Beacon turn-on	Periapsis uncertainty	None
Beacon early trigger	0 to 12 min	High rate
Periapsis pass	8.5 min	High rate
Post-relay	≈ 4 hr	Receive commands
Post-relay	2.2 min	Direct link

TABLE 5.5.3-3. MEASUREMENTS LIST

	Pre-impact	Post-impact (relay)	Post-relay
Diagnostic data (50 channels) (6 channels)	X	X	X
Scientific Data			
Pressure	X	X	X
Stagnation pressure	X		
Temperature	X	X	X
Stagnation temperature	X		
Water vapor	X		
Tri-axial accelerometer	X		
Wind velocity		X	X
Moisture		X	X
Surface composition		X	
Clinometer		X	X
Imagery		X	
Stored data		X	

TABLE 5.5.3-4. DATA TRANSMITTED

Source	Entry	Landed (relay)	Post-relay
Science	194 2/3 bps	34600 bits	2134 bits (3)
Diagnostic	350 bps	26250 bits	1050 bits (3)
Stored	544 2/3 bits (1)	100,000 bits (2)	----
Imagery	---	$\sim 8.1 \times 10^7$ bits	----
Total data/day	---	8.1×10^7 bits	3184 bits (3)
Data transmission time	452 to 629 sec	8.5 min	2.2 min
Data rate	1.09 kbps	160 kbps	24 bps
(1) Science and diagnostic data delayed by 70 sec			
(2) Data stored during entry			
(3) Based on a 1/hr sampling rate			

5.5.3.4 Link Designs

5.5.3.4.1 Landed (Relay)

The fundamental constraints for the landed telecommunication imagery and stored data relay links are that maximum data is to be transferred, transmitter power is to be kept below 50 watts to avoid antenna breakdown, and the maximum permissible bit error probability is 4×10^{-3} (Orbiter to Earth link is 1×10^{-3} , giving an overall maximum bit error probability of 5×10^{-3}). Additionally, the link must be tolerant of Lander attitude (tilt) uncertainty due to surface slopes and crush-up variance, and must also be tolerant of landing site uncertainty. Finally, the Lander size necessitates that the antenna be of minimum size.

These constraints are satisfied by the non-coherent, frequency shift keyed (FSK), Manchester coded, 400 MHz link. Transmission during Orbiter periapsis passes minimizes range, and the use of non-coherent FSK with Manchester coding minimizes acquisition time. The antenna size is minimized by sacrificing bandwidth with essentially no degradation in link performance. The need for pointing or steering mechanisms is avoided by using an antenna with beamwidth wide enough to accommodate Lander tilt uncertainties.

The data optimization is described in Volume III. Resulting available data rates vs time for the reference orbit, fig. 5.5.3-2, are repeated in fig. 5.5.3-3 for worst case adverse link tolerances. These results do not consider possible antenna distortion resulting from ground reflections or specific Lander configuration. Fig. 5.5.3-4 is the relay/beacon block diagram, and table 5.5.3-5 contains the design control table. In this table, the 1000 km range and 0 dB transmit antenna gain are reference values and yield an allowable data rate of 190 kbps with worst case adverse tolerances. For such high data rates relative to the frequency uncertainty, the available data rate is proportional to the gain over range squared ratio (G/R^2), which is the basis of fig. 5.5.3-3. Fig. 5.5.3-3 includes gain and range as determined from Lander to Orbiter line-of-sight range and look angle and Lander tilt. Both positive and negative tilts in the Orbiter plane and tilt perpendicular to the Orbiter plane are considered. The reference condition of zero tilt shows a very sharp peak as the Orbiter passes overhead. This is the result of minimum communication range and maximum antenna gain. When the Lander is tilted in the Orbiter plane, the peak gain is pointed off vertical and tends to counteract the bit rate loss resulting from increasing range. The net effect of in-plane tilt is a lower peak data rate and longer available transmission time at near peak data rates. On the other hand, pure out-of-plane tilt lowers the gain and, hence, available data rate at all times.

Optimization is accomplished by examining the communication time as a function of bit rate for positive and negative in-plane tilt and for out-of-plane tilt. The maximum total data that can be transmitted with confidence at a specific bit rate is the product of bit rate and minimum communication time for the three tilt conditions considered. The bit rate yielding the largest maximum total data transmitted is the optimum bit rate.

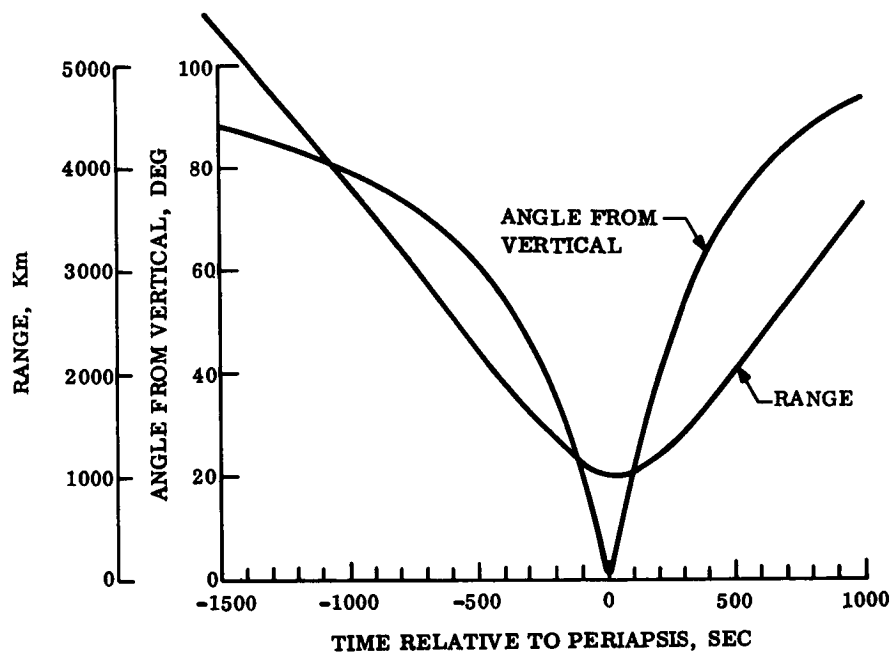


Figure 5.5.3-2. Reference Orbit Communication Parameters

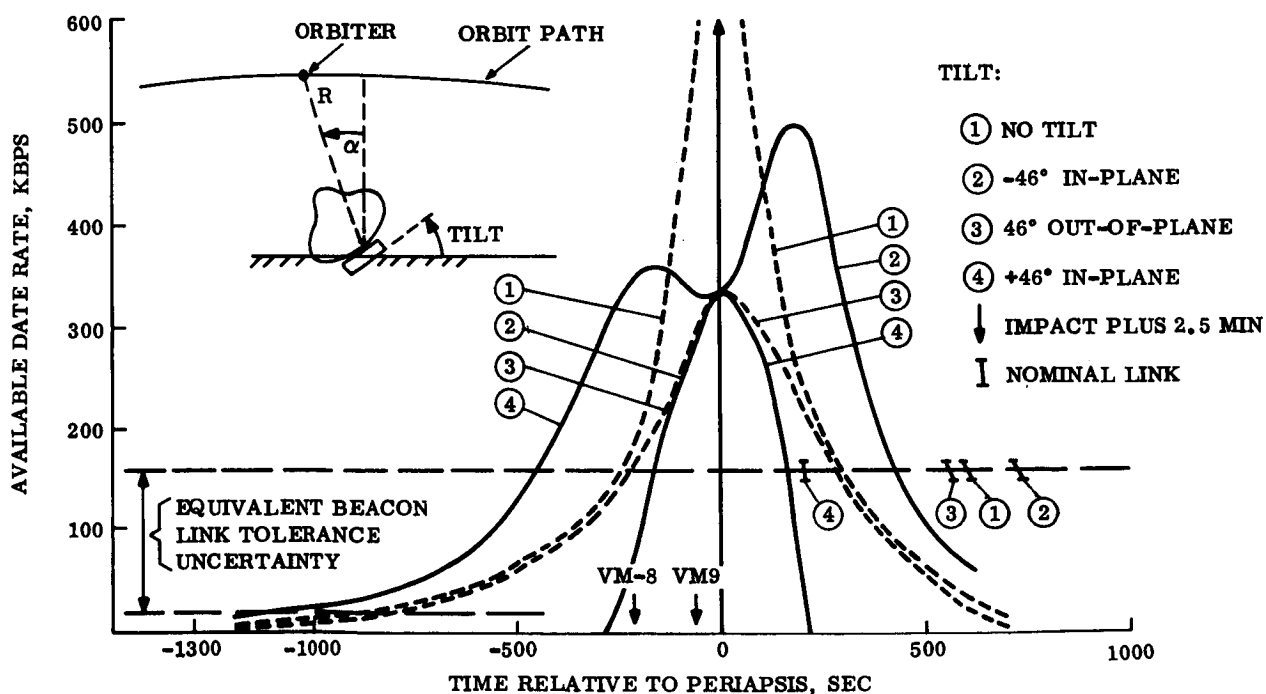


Figure 5.5.3-3. Available Data Rate vs Time with Adverse Tolerances

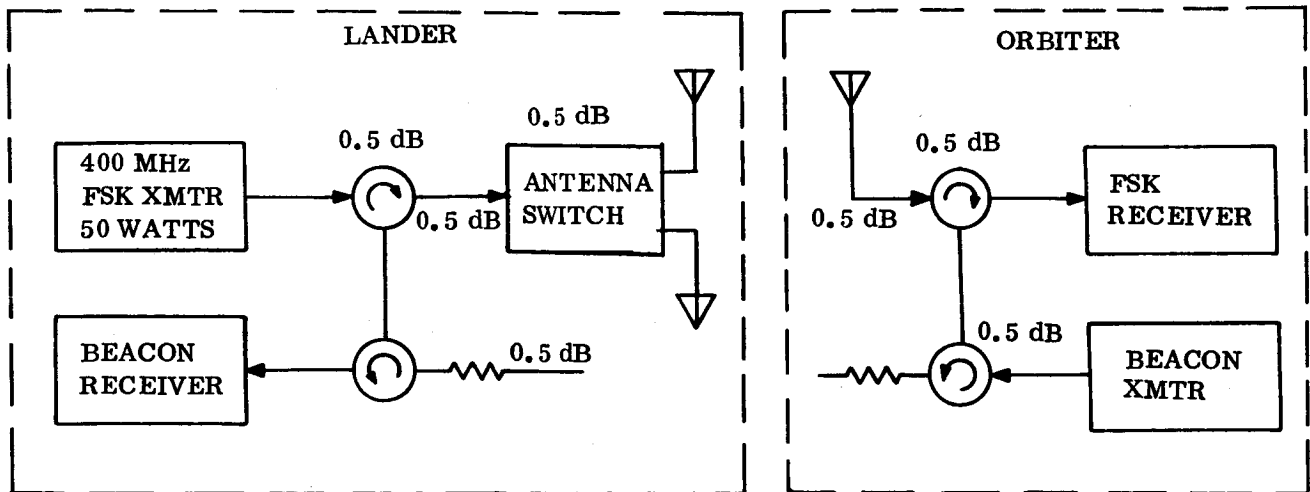


Figure 5.5.3-4. Relay and Beacon Link, Block Diagram

The maximum data transferable per pass for worst case tilt of 46° and the maximum adverse link tolerances is 8.1×10^7 bits at an optimum bit rate of 160 kbps. The effect of tilt on maximum data transferable is small, e.g., maximum data with zero tilt is 9.1×10^7 bits at an optimum rate of 350 kbps whereas 8.1×10^7 bits may be transferred at the optimum rate of 160 kbps in the case of 46° tilt.

In fig. 5.5.3-3, transmission at a given rate is allowable under maximum adverse link tolerances when the available data rate is equal to or greater than that rate. For 160 kbps the allowable transmission times for positive 46° in-plane tilt, 46° out-of-plane tilt, and negative 46° in-plane tilt are 610, 506, and 590 sec respectively. However, the three cases do not have a common 506 sec period requiring transmission for longer than 506 sec to assure a coverage. Transmission must be initiated 506 sec before the end of allowable period for the $+46^\circ$ in-plane tilt and continue 506 sec beyond the start of the allowable period for -46° tilt. Thus, transmission should begin 350 sec before overhead pass and continue until 340 sec after overhead pass, a total time of 690 sec which is about three min longer than the minimum time to transmit the data. Of course, if transmission is initiated by internal timing, the transmission time must be lengthened by the uncertainty in time of an overhead pass.

TABLE 5.5.3-5. DESIGN CONTROL TABLES - RELAY (LANDED) AND BEACON

Parameter	Nominal Values and Worst Case Tolerances					
	Relay (landed)			Beacon Link		
	Nominal	+ Tolerance	- Tolerance	Nominal	+ Tolerance	- Tolerance
Modulation technique	FSK	--	--	AM	--	--
Frequency (MHz)	400	--	--	400	--	--
Transmitter power (watts)	50	--	--	0.83	--	--
(dBm)	47.0	0.0	1.0	29.3	0.0	1.0
Transmit circuit loss	-1.5	0.2	0.4	-1.5	0.2	0.4
Transmit antenna gain	0.0(1)	0.5	0.5	2.0	0.0	0.5
Transmit antenna pointing loss	0.0	0.0	0.0	-1.0	1.0	0.0
Range (km)	1000(1)			1000(3)		
Space loss	-144.5	--	--	-144.5	--	--
Polarization loss	-1.0	1.0	0.5	-1.0	1.0	0.5
Receiving antenna gain	2.0	0.0	0.5	-0.8(3)	0.5	0.5
Receiving antenna pointing loss	-1.0	1.0	0.0	0.0	0.0	0.0
Receiving circuit loss	-1.0	0.2	0.4	-2.0	0.2	0.4
Total received power (S) (dBm)	-100.0	2.9	3.3	-117.7	2.9	3.3
Effective noise temperature ($^{\circ}$ K)	650	--	--	724	--	--
Receiver noise power						
spectral density (N/B)	-170.5	0.0	1.0	-170.0	0	1.0
Bit rate, 1/T (bps/dB)	190K/	--	--	--	--	--
	52.8					
Frequency uncertainty (kHz)	20.0(4)	--	--	16.0(5)	--	--
I-F bandwidth (kHz)	780.0	--	--	25.0	--	--
Required S/N/B	64.2(6)	0.0	2.0(6)	47.0	1.0	1.0
Required ST/N/B	11.4(6)	0.0	2.0(6)	3.0(2)	1.0	1.0
Threshold data power (dBm)	-106.3	0.0	3.0	-123.0	1.0	1.0
Margin	6.3	2.9	6.3	5.3	3.9	5.3

- (1) Reference values
- (2) Signal-to-noise ratio in i-f bandwidth
- (3) Values chosen correspond to G/R^2 ratio required by relay link to support 160 kbps data rate.
- (4) Transmitter stability ± 10 ppm; Receiver stability ± 5 ppm; Doppler ± 4 kHz
- (5) Same as (4) except only positive doppler need be considered.
- (6) Nominal signal-to-noise ratio is theoretical value. 2dB adverse tolerance is allowed to account for practical performance degradation, e.g., non-ideal bit sync. Required ST/N/B from Vol. III, Section 4.2.3.

5.5.3.4.2 Beacon Link

A beacon transmitter on the Orbiter and a beacon receiver on the Lander comprises the beacon link. The beacon and data links are duplexed on the same antenna so that r-f path losses will be nearly identical and weight and space conserved. The narrowband antenna characteristic forces the beacon link to operate at essentially the same frequency as the relay link so that the two links must time share the antennas. To accomplish this, the Orbiter beacon transmitter must transmit, for example, for an interval of 1 sec and then listen for 10 sec to see if the Lander is transmitting. When the Lander received signal strength is above a pre-set threshold level, data transmission will be initiated after a 1 sec delay. The Orbiter will sense Lander transmission and cease beacon transmission.

The beacon link received signal strength is proportional to link antenna gain divided by range squared and, hence, is indicative of relay link available data rate. Ideally the link could detect exactly when the 160 kbps data rate can be supported which would lower the required transmission time to 506 sec which is the minimum necessary to transmit the data. Unfortunately, the beacon link does have a range of tolerances which must be considered. To aid in minimizing the range of tolerance, the beacon transmitter power will be closely controlled (i.e., within 1 dB), and its signal will be AM modulated to eliminate the noise bias uncertainty. The maximum beacon link uncertainty is 9.2 dB, a factor of 2.9 in range (see table 5.5.3-5). This uncertainty will cause the relay transmitter to turn on early, since the link is designed such that transmission will be triggered in time to complete data transfer under worst case adverse tolerance conditions.

5.5.3.4.3 Entry

Although there is a wide variation in the line-of-sight range and look angle during the entry phase due to the uncertainty of the atmosphere, communications can be maintained throughout entry. The normalizing effects of parachute deployment by radar enable relay communications at the high data rate for all atmospheres with 3.3×10^7 bits being transferable for worst case link tolerance and Lander tilts of less than 46° .

Entry data is transmitted via the same link as landed data by keying at the 1090 bit/sec data rate. However, this requires that the Orbiter receiver be capable of receiving either data rate. The design control table for the entry link is shown in table 5.5.3-6. The link has a margin over adverse tolerance of 13.8 dB at the 1000 km reference range with 0 dB transmit antenna gain, or a worst case range limitation of 4890 km. The antenna provided has a minimum gain of zero dB over a range of $\pm 80^\circ$ with respect to the rear-looking Lander roll axis. The reference mission range and look angle profiles indicate an approximate maximum range of 2480 km (VM-8 at parachute deployment) and maximum look angles of 63° (at parachute deployment). Look angle is the angle to Orbiter with respect to the velocity vector. Any variation between the velocity vector and roll axis due to coning or swing on the parachute, will degrade the communication angle. Swing in excess of 17° at this time could cause

TABLE 5.5.3-6. ENTRY LINK DESIGN CONTROL TABLE

Parameter	Relay (Entry) Nominal	Adverse Tolerance
Modulation technique	FSK	--
Frequency (MHz)	400	
Transmitter power (watts)	50	
(dBm)	47.0	1.0
Transmit circuit loss	-1.5	0.4
Transmit antenna gain	0.0 (1)	0.5
Transmit antenna pointing loss	0.0	0.0
Reference range (km)	1000 (1)	
Space loss	-144.5	
Polarization loss	-1.0	0.5
Receiving antenna gain	2.0	0.5
Receiving antenna pointing loss	-1.0	0.0
Receiving circuit loss	1.0	0.4
Total received power (S) (dBm)	-100.0	3.3
Effective noise temperature ($^{\circ}$ K)	650 $^{\circ}$	
Receiver noise power spectral density (N/B)	-170.5	1.0
Modulation loss	N/A	
Data power (dBm) S_D	-100.0	3.3
Bit rate, 1/T (bps/dB)	1090/30.4	--
Frequency uncertainty	20.	--
IF bandwidth (kHz)	660. (3)	--
Required S/N/B	50.4 (2)	2.0 (2)
Required ST/N/B	20.0 (2)	2.0 (2)
Threshold data power (dBm)	-120.1	3.0
Margin	20.5 (4)	6.3
<p>(1) Reference values.</p> <p>(2) Nominal signal-to-noise ratio used is theoretical value. Two dB adverse tolerance is allowed to account for practical performance degradation, e.g., non-ideal bit sync. Required ST/N/B from Vol. III, Section 4.2.2.1.</p> <p>(3) Bandwidth is same as required by high bit rate.</p> <p>(4) This margin, less the adverse tolerances, is available as protection against multipath. At the maximum range during entry, the margin is reduced to 12.2 dB.</p>		

the link margin to decrease momentarily below the adverse tolerance level. As the Lander descends and the Orbiter begins to overtake the Lander, the look angle improves and more swing is allowable.

Times of impact plus 2.5 min for the extreme atmospheres VM-8 and VM-9 are indicated in fig. 5.5.3-3. Table 5.5.3-7 gives the data that can be transferred at the high data rate with the worst case adverse tolerance and with nominal link geometry. The amount of data transferred is the bit rate (160 kbps) times the time remaining with allowable bit rates greater than 160 kbps.

During the entry phase, signals transmitted from the Lander may be reflected from the planetary surface toward the Orbiter. These multipath signals may interfere with the desired signal which is received on the line-of-sight path from the Lander. As shown in Volume III, Section 4.2.3, the slow fading environment is most detrimental to the communication link performance. The conditions for slow fading occur near impact. Based upon the maximum range during entry, the minimum margin over worst case tolerances is 5.9 dB. The tolerable signal-to-interference level to allow fading loss for less than 99 percent of the time is about 10.0 dB for the 5.9 dB margin. If this level proves to be a problem, another Orbiter receiver can be added with an i-f bandwidth to match the transmitted data rate yielding an additional margin of approximately 6 dB.

TABLE 5.5.3-7. DATA TRANSFERABLE AFTER IMPACT PLUS 2.5 MIN
(Bits/10⁷)

Atmosphere Model	No Tilt	-46° In-Plane	46° Out-of-Plane	+46° In-Plane
<u>(Adverse Tolerances)</u>				
VM-8	8.3	10.3	8.0	6.1
VM-9	5.5	7.5	5.2	3.3
<u>(Nominal Parameters)</u>				
VM-8	13.2	15.0	12.6	7.0
VM-9	10.4	12.2	9.8	4.2

5.5.3.4.4 Direct

The direct link was constrained to a power of 20 watts (minimum) in order to capitalize on the high shock TWT. Steered antennas were ruled out because of complexity and size/deployment limitations. To establish direct communications throughout the 90 day mission with a 4/31/74 landing date, requires use of a 210-ft DSN receiving facility. A vertically oriented antenna is used. For the reference case of 10°N latitude, the antenna has a beamwidth of 33°. The antenna provides a gain and beamwidth approximately equivalent to the optimum in the sense of maximum daily data transfer. (See parametric data, Volume III.)

For the direct link, split phase coded data phase modulates the S-band carrier for transmission to the DSN station. The 210 ft antenna with the listen-only feed is utilized and a receiving system temperature of 28° K is achieved by restricting operation to elevation angles exceeding 20° (rather than the worst case temperature of 55° K).

The modulation index is selected so that carrier and data channel thresholds occur at the same input power. The carrier channel threshold is set by the carrier phase lock loop bandwidth ($2B_{LO}$) and the required signal to noise ratio (SNR) in that bandwidth while the data channel threshold is set by the product of the data rate, (R_b) and the ratio of data energy per bit to noise spectral density (E/N_o). As the modulation index is adjusted so that the carrier channel power is decreased, the power in the data channel increases, allowing a higher data rate to be achieved; however, as the SNR in the carrier loop is reduced, the VCO phase jitter is increased, thereby degrading the data channel performance. For a given set of values of carrier loop bandwidth and data rate, there is an optimum modulation index which will result in the best performance. For this link the modulation loss for the optimum modulation index is 3.4 dB.

The required data channel E/N_o was taken to be 7.4 dB based on the following assumptions:

Theoretical E/N_o for $P_e^b = 5 \times 10^{-3}$	5.2 dB
Filter loss	0.5 dB
Carrier jitter loss	0.8 dB
Subcarrier jitter loss	0.2 dB
Bit sync jitter loss	0.2 dB
Margin	0.5 dB
Total	<u>7.4 dB</u>

Table 5.5.3-8 summarizes the direct link design. The range shown is the worst case for the 90 day mission. The transmit circuit loss includes 0.5 dB for the latching circulator (used as an antenna switch, see fig. 5.3.5-1), 0.4 dB transmit filter loss, and 0.4 dB cable losses.

The link can support a data rate of 24 bits/sec and is able to transmit the nominal data load of approximately 3184 bits in about 2.2 min. The total daily capacity is limited by the 1.6 hr. Earth viewing time to 138k bits.

5.5.3.4.5 Command

The command link utilizes the DSN S-band command capability at a one sub-bit per second rate. To provide coverage for the 90 day mission duration requires the use of a 100 kw transmitter and an 85 ft. antenna.

TABLE 5.5.3-8. S-BAND DESIGN CONTROL TABLE

Parameter	Data		Command	
	Nominal	Adverse Tolerance	Nominal	Adverse Tolerance
Modulation technique	PSK		PSK	
Frequency (MHz)	2295		2115	
Transmitted power (w/dBm)	20/43	0.7	100KW/80.0	
Transmit circuit loss (duplexer)	-1.3	0.4	0	0
Transmit antenna gain	13.0	0.4	51.0	0.5
Transmit antenna pointing loss	-2.0		0.1	
Maximum range (km)	380x10 ⁶		380x10 ⁶	
Space loss	-271.3	-	-270.7	
Polarization loss	-0.1		-0.1	
Receiving antenna gain	61.0		5.0	0.5
Receiving antenna pointing loss	0.0	0.3	-3.0	
Receiving circuit loss	0.0		-2.1	0.5
Total received power(s) (dBm)	-157.7	1.8	-139.5	1.5
Effective noise temperature (°K)	28		1750	
Receiver noise power				
Spectral density (N/B)	-184.1		-166.2	1.1
Carrier Performance				
Carrier modulation loss (dB)	-3.8		-0.9	0.1
Received carrier power	-161.5	1.8	-140.4	1.6
Carrier APC noise BW (2B _W)	12/10.8		20/13	0.2
Hz/dB				
Threshold SNR in 2B _{LO}	10		8.5	1.0
Threshold carrier power	-163.3		-144.7	2.3
Performance margin	1.8	1.8	4.3	3.9
Data Performance				
Data modulation loss (dB)	-3.4		-12.0	0.4
Data power (dBm)	-161.1	1.8	-151.5	1.9
Bit rate, 1/T (bps/dB)	24/13.8		1 SBPS/0	
Required S/N/B (total power)	24.6		11.3	
Required ST/N/B (data power)	7.4		11.3	
Threshold data power (dBm)	-162.9		-154.9	1.1
Performance margin	1.8	1.8	3.4	3.0

Table 5.5.3-8 contains the command link design control table. It shows that the link is capable of operation at maximum range in the presence of maximum adverse tolerance. A receiver noise figure of 8.0 dB is used with receiver circuit loss allowances as follows:

Latching circulator	0.5 dB
Receiver filter	1.2 dB
Cable	0.4 dB
	<hr/>
Total	2.1 dB

The signal to noise ratio used in the table yields a bit error probability of 10^{-5} . The time available for transmission of commands is approximately 4 hrs. minimum under the worst case 46° tilt during the 90 day lifetime. This minimum time occurs during the early portion of the mission.

5.5.3.5 Equipment Descriptions

5.5.3.5.1 Antennas (400 MHz)

The configuration of the wide beam 400 MHz antenna is that of a pill box 8 in. in diameter and 2 in. deep. The top surface of the box is flush with the vehicle outer surface and has two orthogonal slots, 2 in. wide and 8 in. long (dividing the top of the box into four quarters). The slots are tuned with capacitors to match the input and provide circular polarization. The bandwidth of this antenna is about 2 MHz. The estimated pattern is shown in fig. 5.5.3-5. Since the lander diameter is on the order of a wavelength, the available ground plane is not large, indicating that the actual antenna pattern will vary somewhat from that shown.

5.5.3.5.2 S-Band Antennas

The S-band receiver and transmitter are operated on different antennas in order to match the beamwidth requirements associated with the command and telemetry functions. The command antenna is required to have a broad beamwidth in order to increase the assurance of establishing the command link. The telemetry antenna is required to have as narrow a beamwidth as possible, consistent with the antenna system selected, in order to obtain as high a data rate as is practical.

The command antenna and its associated antenna pattern is shown in fig. 5.5.3-6. The wide beamwidth antenna is a one turn helix mounted in a conical cup. The 3 dB beamwidth of this antenna is approximately 120° with a peak gain of 5 dB. The antennas are mounted on each side of the Lander. However, if the configuration is such that a sufficiently clear area is not available, the command antenna will have to be deployed automatically upon sensing of the Lander orientation to select the antenna on the upward side of the Lander.

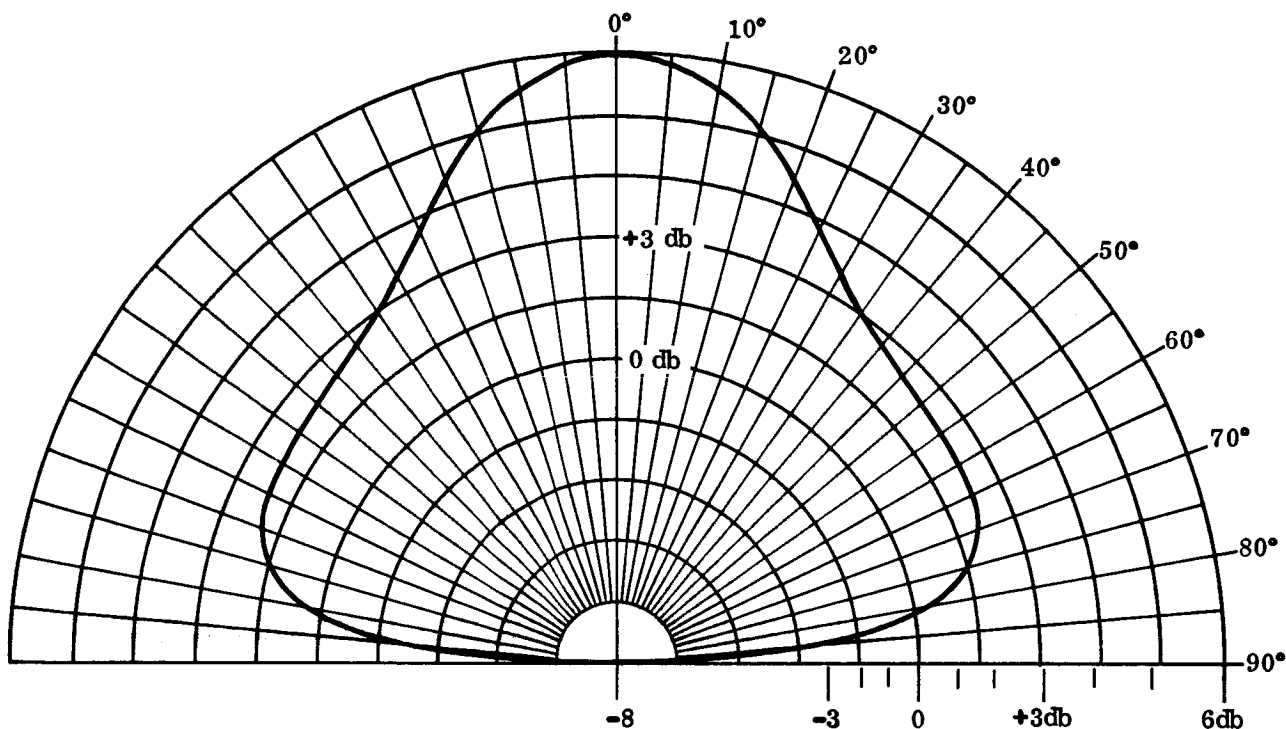


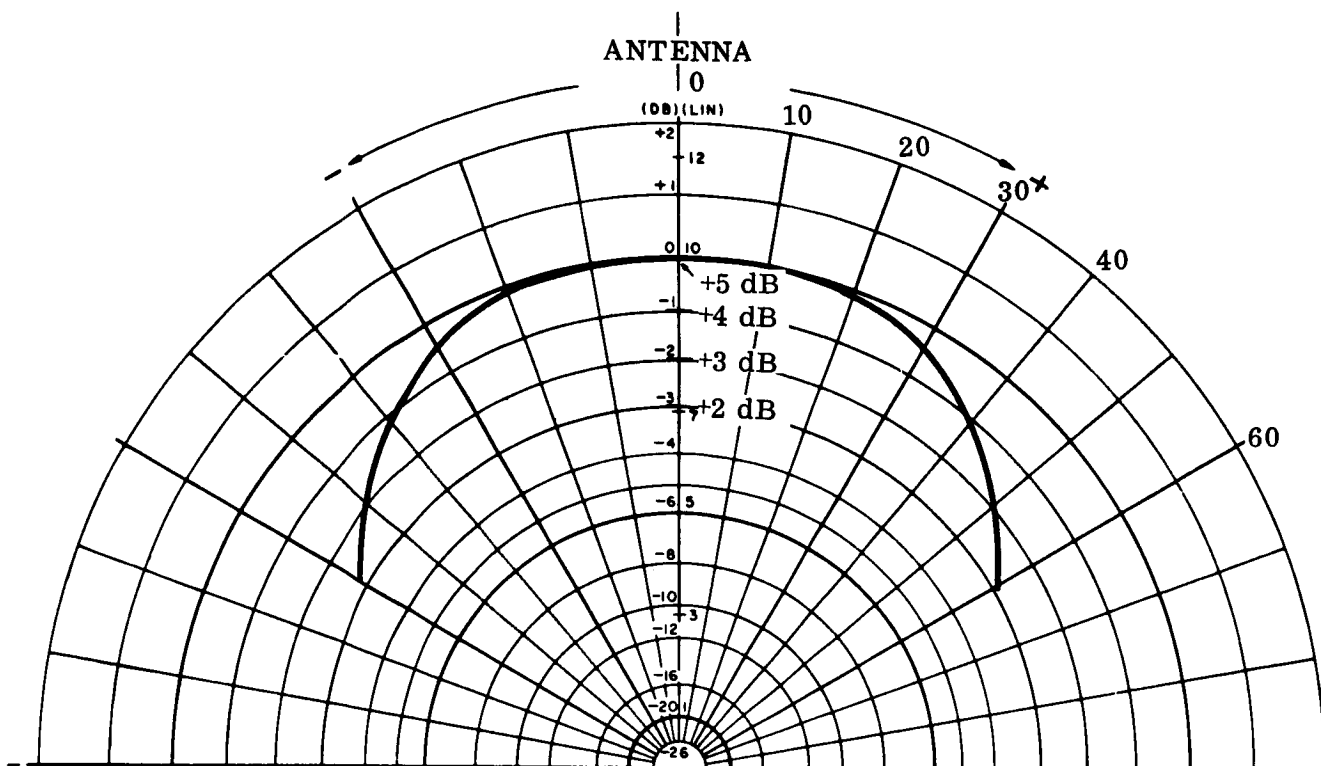
Figure 5.5.3-5 400 MHz Antenna Pattern

The transmitter antenna is also a helical antenna. Its configuration and pattern are shown in fig. 5.5.3-7. This antenna has a minimum of 11 dB over a 33° beamwidth. In order to utilize the narrow beamwidth, this antenna is required to be vertically oriented, and, in order to remove obstructions from the beam, it is deployed above the Lander. This antenna is deployable in only one direction. Therefore, two antennas are provided to account for the uncertainty in which side is visible. The antenna selection is accomplished automatically once the orientation of the Lander is determined.

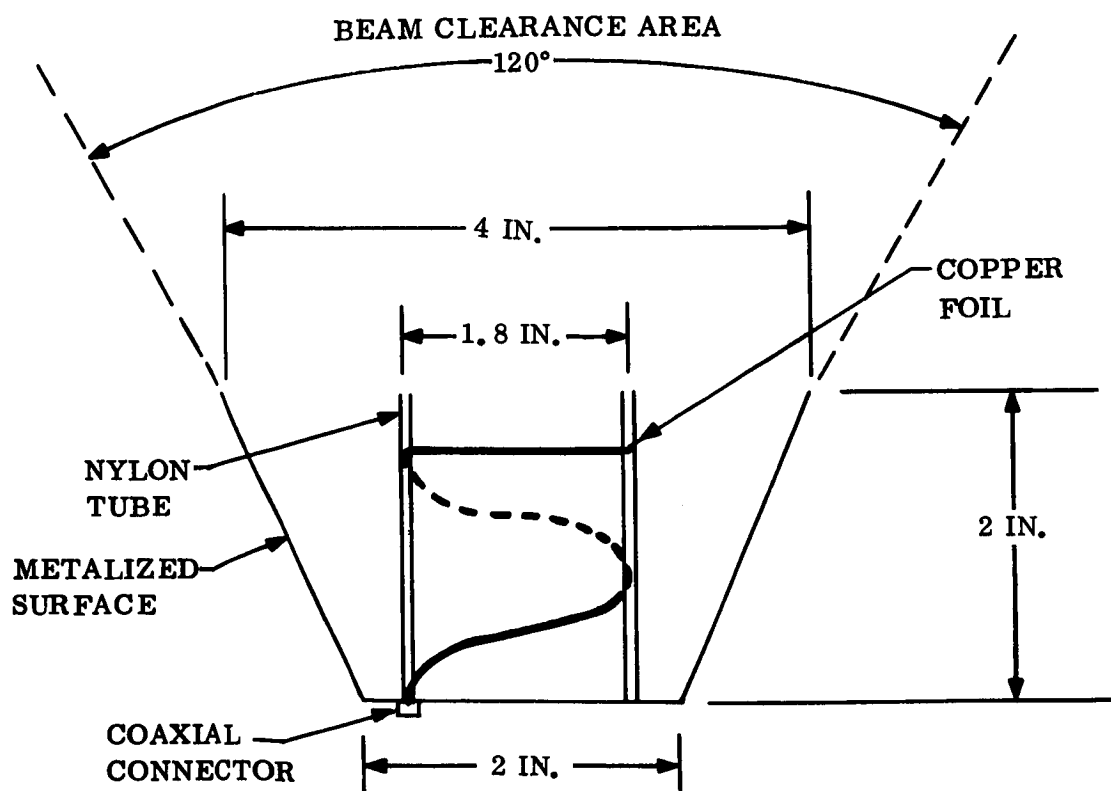
5.5.3.5.3 400 MHz FSK Transmitter

A block diagram for the FSK transmitter is shown in fig. 5.5.3-8. The frequency shift keyed modulation is produced by switching between two stable crystal oscillators operating at 25.0375 MHz and 24.9625 MHz, respectively. Multiplying these signals by a factor of 16 produces transmitter output signals at 400.6 MHz and 399.4 MHz, respectively. The multiplier chain will be constructed at a low signal level in order that filtering and multiplier inefficiencies do not adversely affect the overall efficiency.

The power amplifier chain consists of amplifier stages to produce a total gain of about 47 dB; approximately 10 dB of this will be excess gain to be used for AGC. The final amplifier stage consists of two 2N5178's operating in push-pull. These transistors are each rated for 50 watts output at 500 MHz with a dissipation rating of 70 watts at 25° C.



A. ANTENNA PATTERN



B. ANTENNA CONFIGURATION

Figure 5.5.3-6. Receiving Antenna Pattern and Configuration

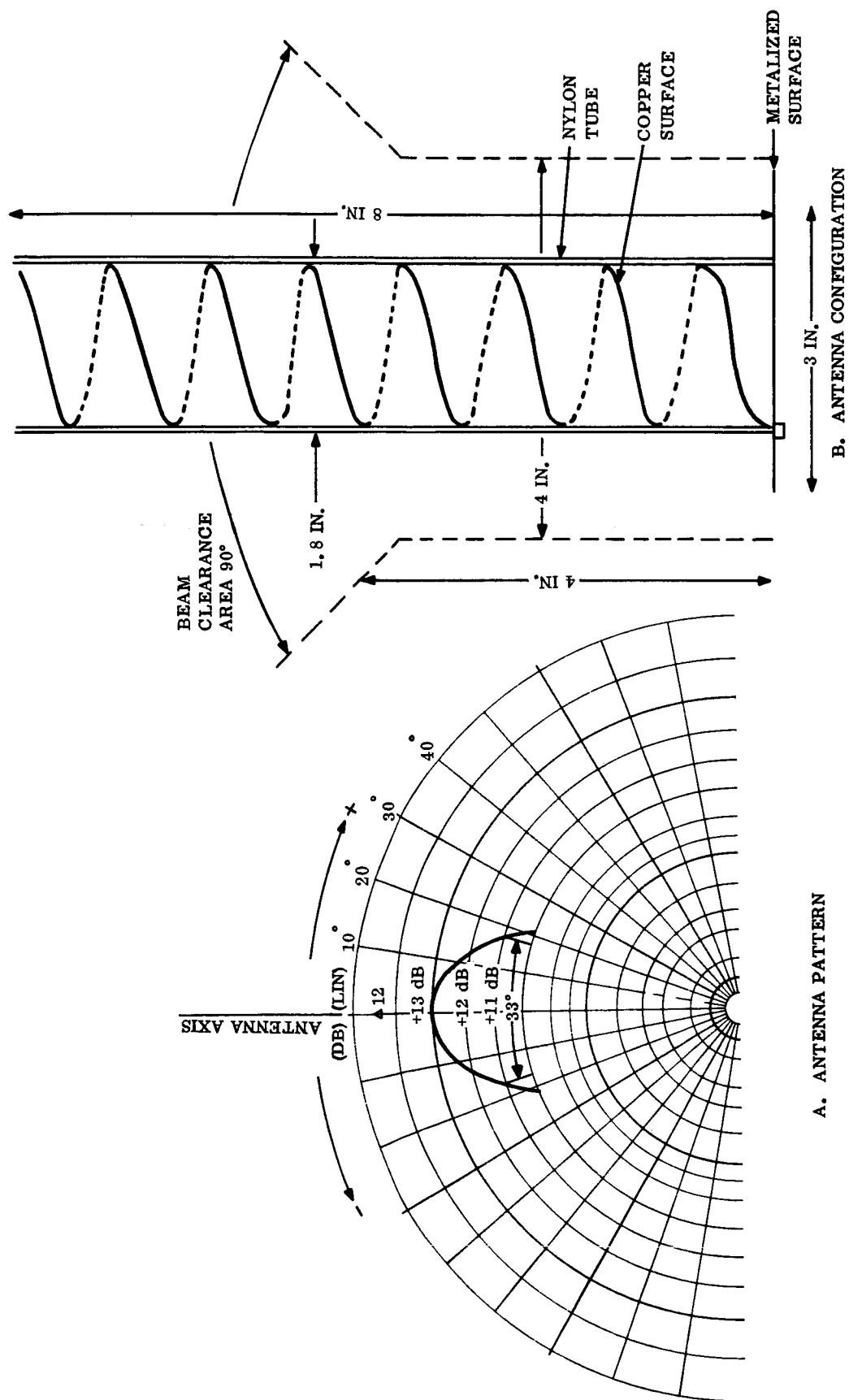


Figure 5.5.3-7. Transmitting Antenna Pattern and Configuration

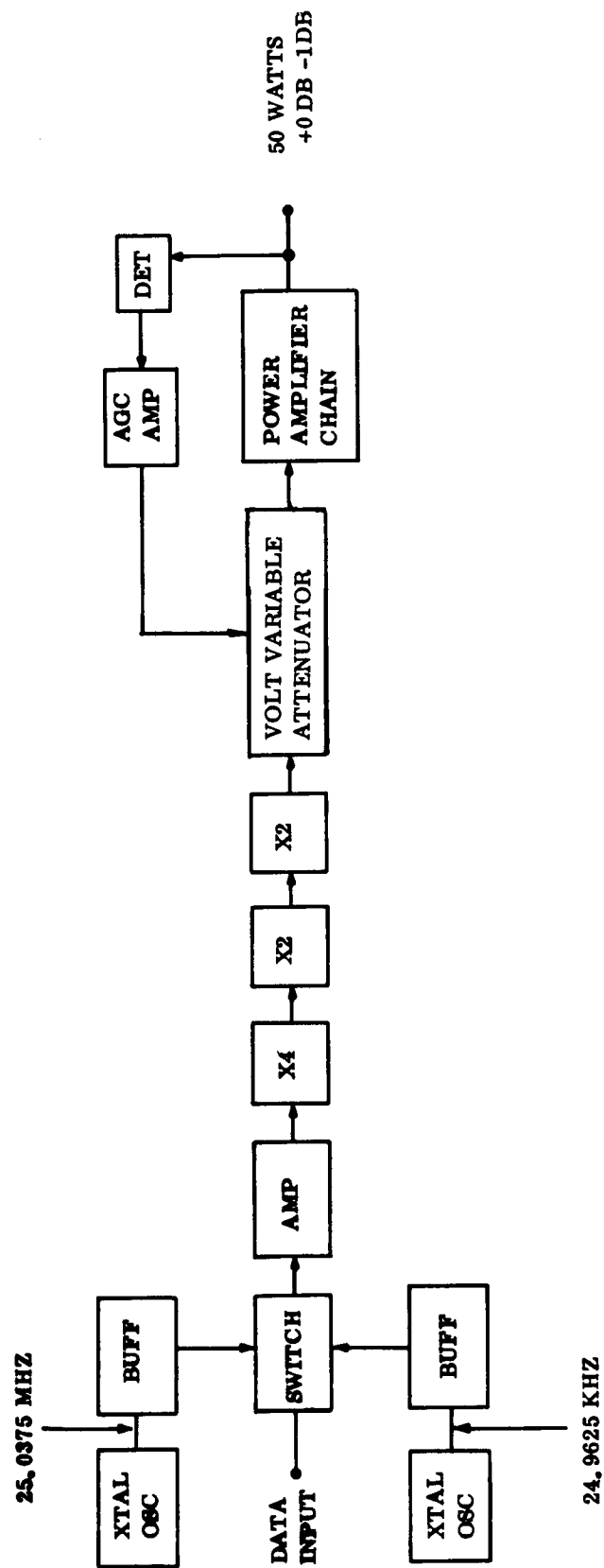


Figure 5.5.3-8. 400 MHz Transmitter, Block Diagrams

The output power level of the transmitter will be controlled at 50 watts ± 0 , -1 dB throughout the temperature environment by means of an AGC circuit consisting of a detector for output sampling, a high gain amplifier, and a voltage variable attenuator located at the low level input to the 400 MHz power amplifier chain.

The transmitter oscillator stability will be 10 PPM over a temperature range of -40°C to $+70^{\circ}\text{C}$ with negligible warmup time at any temperature. Aging will be 1 PPM per year. The state-of-the-art in temperature compensated crystal oscillators has reached a point where stabilities in the order of 1 PPM or better can be achieved for considerable periods of time, however, to account for degradation which may result from shock such as deformation of the crystal structure or holder, a stability of 10 PPM is considered conservative.

No serious problems are anticipated in the sterilization of the transmitter or in the high shock levels expected. Several years ago GE/RS designed and constructed a VHF 50 watt transmitter which was successfully sterilized and subjected to multiple shock impacts at levels of 5000 g's for approximately 500 μ . The transmitter was potted with Dow Corning XR-6-3700 silicon potting compound. (The complete results of these tests are reported in GE TIS #66SD2002 entitled "Fifty Watt Solid State FM Transmitter for Deep Space Communications", by Julius Shatas.

5.5.3.5.4 Duplexing Circuit

The duplexing arrangement used for the 400 MHz transmitter and receiver, shown in the fig. 5.5.3-9, consists of two circulators connected as a 4-port circulator and a receiver T/R switch. The circulators protect the transmitter against large reflections and provide receiver isolation. In the normal receive mode the T/R switch is biased to pass the received signal. When the transmitter is turned on the circulator provides 20 dB receiver isolation, and the T/R switch is biased to reflect the leakage power back into the circulator where it is dissipated in a load. The T/R switch will be located in the receiver and the 4-port circulator near the transmitter.

The T/R switch considered is a Hylelectronics model SU175, and the circulators are similar to the Melabs HB5 series.

The antenna terminal of the duplexing circuitry is connected to the antenna switch as shown in the block diagram. This solid state switch is used to select one of two antennas according to Lander orientation. A solid state switch is selected because of its reliability and potential to withstand the shock environment. The switch considered is Hylelectronics model SU176.

5.5.3.5.5 400 MHz Beacon Receiver

The purpose of the beacon receiver is to sense when the relay link can support the high data rate. This is accomplished by looking for reception of a preset signal level. When the expected signal level is detected the 400 MHz transmitter is energized after a sec delay.

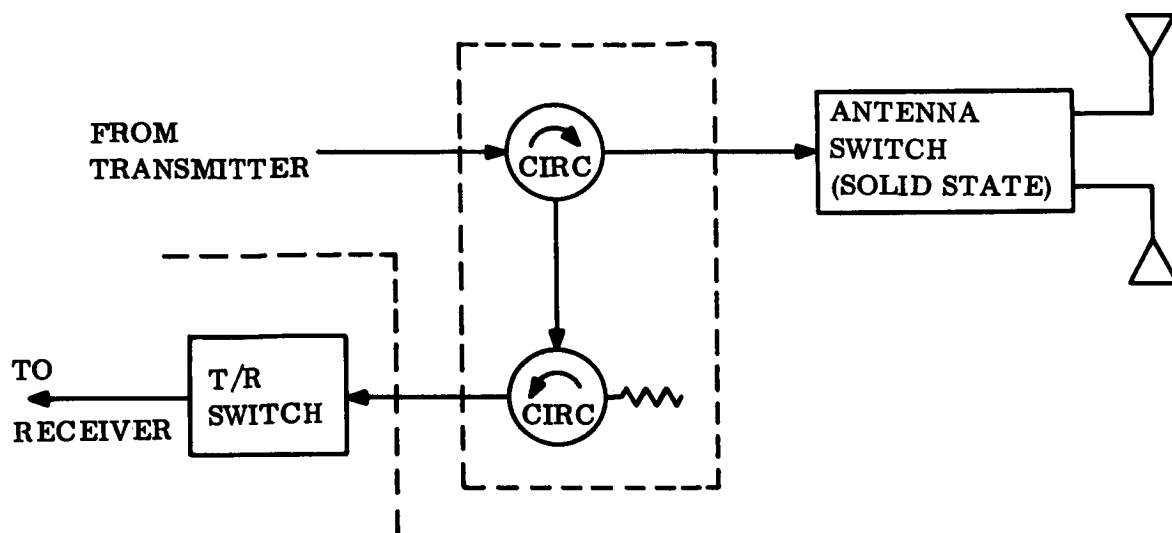


Figure 5.5.3-9. Duplexer and Antenna Selector

The receiver shown in fig. 5.5.3-10 receives an amplitude-modulated signal of 400 MHz which is amplified in the low noise pre-amplifier and converted to the first i-f frequency. After amplification a second conversion takes place, resulting in a second i-f signal at 3.0 MHz. The second mixer is fed to a band pass filter which reduces the overall noise level at that point to prevent limiting in the 3.0 MHz i-f amplifiers which follow. The signal is then filtered in a band pass filter with a noise bandwidth of 25 kHz. The filter is a 4-pole crystal filter with variations of not more than ± 0.1 dB across the 18 kHz passband. After filtering, the signal is detected and the demodulated signal filtered in a tone filter with a pass band of about 100 Hz. At this point the signal is fed to a threshold detector.

The threshold is set for a nominal signal-to-noise ratio of 3 dB in the 25 kHz bandwidth which is equivalent to 27 dB in the 100 Hz final detection bandwidth. Allowing 3 dB for modulation loss and 6 dB for detection loss leaves a signal-to-noise ratio at threshold of 18 dB with a corresponding probability of false alarm on the order of 10^{-26} , implying false alarm is essentially impossible.

In order for the receiver to provide indication of signal strength the total gain of the receiver must be stable over a wide temperature range. This is achieved from the receiver front end to the output of the second i-f by means of an AGC circuit referenced to the receiver noise generated in the receiver front end. With a high gain AGC loop, gain variations with temperature can be kept to ± 0.5 dB, excluding effects of changes in the referenced noise level.

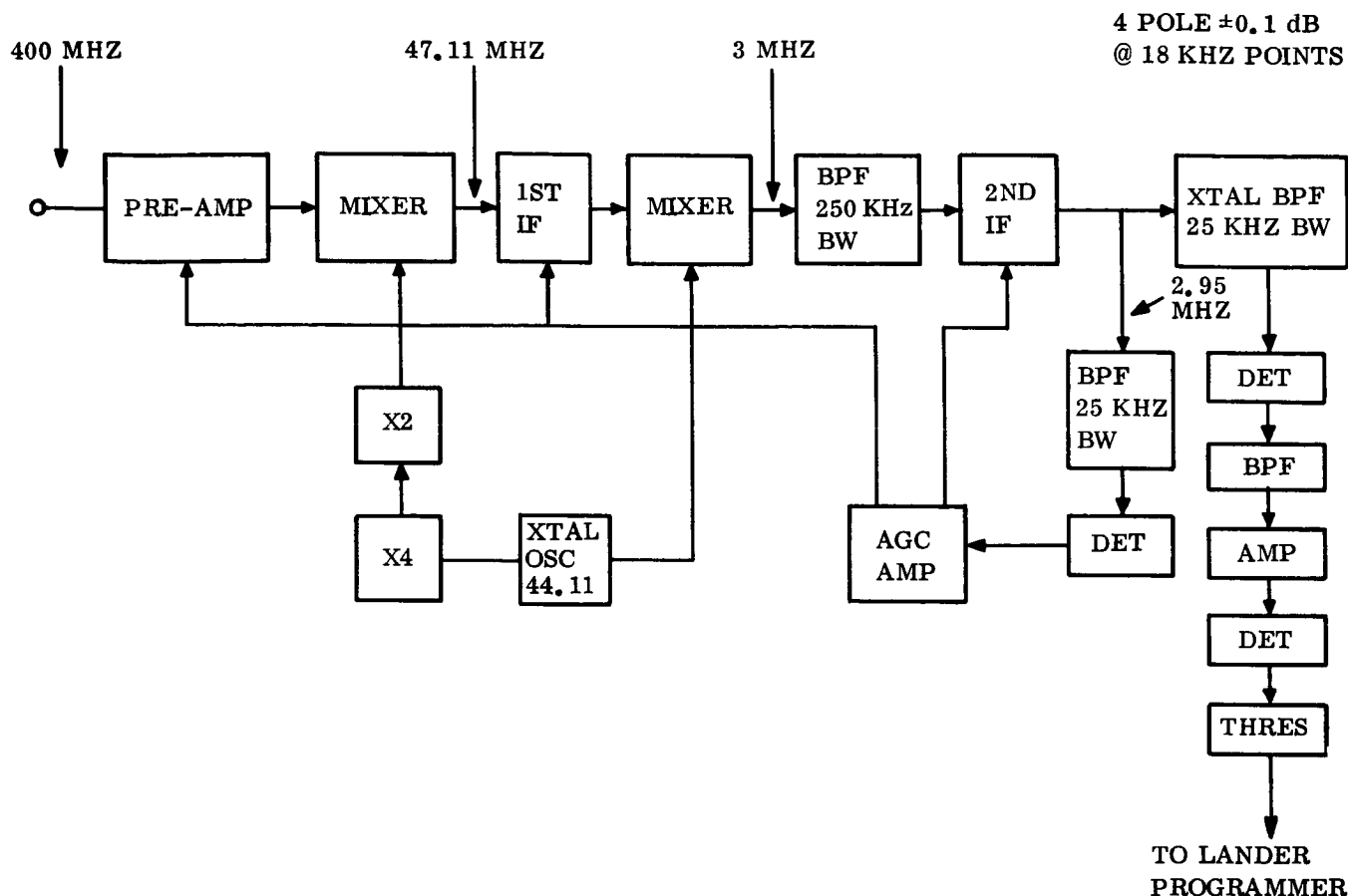


Figure 5.5.3-10. Beacon Receiver

The remaining gain of the receiver which falls outside the AGC loop, that is, from the output of the second i-f to the threshold detector must be kept within ± 0.5 dB for a total receiver gain variation of ± 1 dB. This includes ripple (± 0.1 dB) in the pass band of the 25 kHz bandwidth crystal filter, changes in the detectors and threshold circuit and variations in gain of amplifiers used outside the AGC loop.

The noise figure of the receiver is 5 dB referenced to the input of a pre-selector filter at the pre-amplifier front end. Since the receiver AGC circuit is referenced to front-end receiver noise, variations in noise figure will cause the receiver gain to vary. Thus the noise figure will be required to remain constant to within ± 0.5 dB over the operating temperature range. The transistor anticipated for use in the pre-amplifier circuit is a KMC-K5001 specified at a noise figure of 1.4 dB at 400 MHz. If the noise figure of the transistor circuit is optimized at room temperature, the noise figure increases 0.4 dB at both temperature extremes. Since the optimum noise figure for this transistor is obtained with a 3:1 mismatch at the input, any temperature effects on the circuit affect the overall noise figure.

If the device noise figure changes from 1.4 to 1.8 dB, then 0.6 dB variation allowance remains for the rest of the front end circuit if the overall noise figure is to remain at a fixed value $-0, +1$ dB. This is accomplished by temperature compensating the front end circuitry and having sufficient gain at the front end to override noise contributed by the following stages such as the first mixer.

The effective receiver temperature is given by:

$$T_e = (N-1) 290^\circ + \frac{T_a}{L} + (1 - \frac{1}{L}) T_L$$

where N is the receiver noise figure, T_a is the antenna noise temperature, T_L is the temperature of the receiving circuit loss components, and L is the numeric loss factor (greater than one). The receiver loss is 2 dB (two circulators at 0.5 dB, one antenna switch at 0.5 dB, and 0.5 dB of cable losses). Using an antenna temperature of 70°K, a loss temperature of 200°K, and N = 5 dB yields

$$T_e = (3-1) 290 + \frac{70}{1.51} + (1 - \frac{1}{1.51}) 290^\circ = 724^\circ\text{K}.$$

5.5.3.5.6 Orbiter 400 MHz Radio Sub-System

Figure 5.5.3-11 shows a simplified block diagram of the Orbiter 400 Mhz equipment. The duplexing circuitry including the two circulators and T/R switch is identical to that in the Lander vehicle.

The beacon transmitter consists of a stable crystal oscillator operating at 25 MHz, a times 16 multiplier chain to 400 MHz, and amplifies to achieve the desired output level. The square wave tone oscillator 100 percent amplitude modulates the transmitter output.

The receiver, with an overall noise figure of 4 dB, is similar to the beacon receiver used on the Lander except for the output detectors. The second i-f output drives the FSK demodulator having two wideband filters followed by independent opposite polarity detectors with which are summed to form the detected, Manchester coded signal.

In the Lander transmitter, binary data having an NRZ format and bit rate R_b is bi-phase modulated on a square-wave subcarrier with frequency R_b to produce a Manchester coded signal. This signal modulates the frequency shift key (FSK) transmitter. The reconstructed signal (detected by the Orbiter FSK detector) is fed to the bit sync detector which generates a square-wave subcarrier at frequency R_b to convert the reconstructed signal back to the NRZ format. This signal is detected in a matched filter.

5.5.3.5.7 S-Band Transponder

The transponder consists of a phase-lock receiver, and a solid-state exciter, and performs the following functions:

1. Receives and demodulates an r-f signal from the DSN via the Lander antenna.

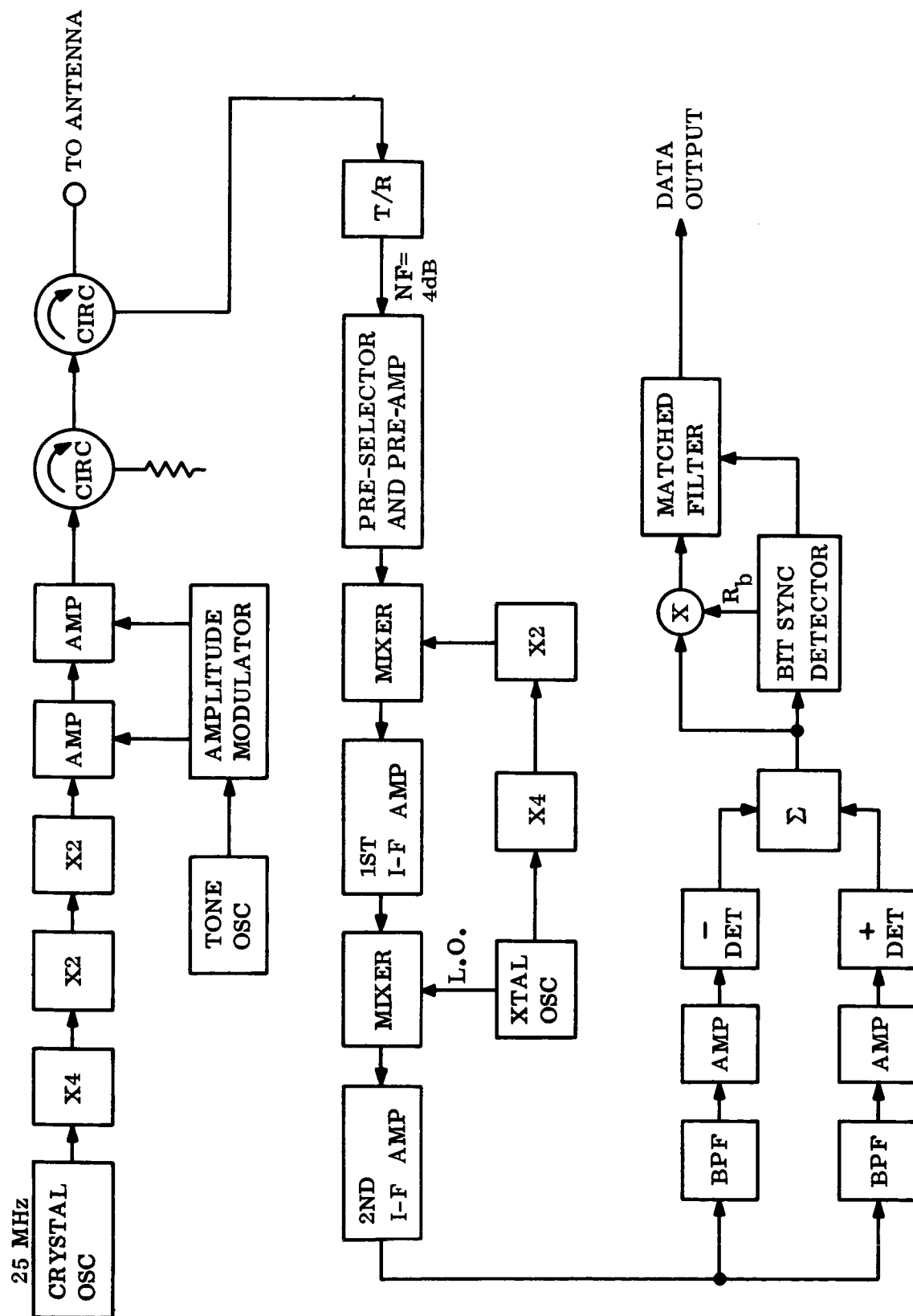


Figure 5.5.3-11. Orbiter 400 MHz Radio Subsystem

2. Provides coherent translation of the frequency and phase of the received signal by a 240:221 ratio for coherent two-way Doppler tracking.
3. Provides a turnaround ranging channel which demodulates the range code to baseband and conditions it for modulation on the transmitted signal.*
4. Generates a stable r-f carrier at a level suitable for driving the power amplifier.
5. Modulates the carrier with the telemetry (and ranging) signal.

The transponder has the same basic configuration as the Mariner C transponder; however, minor modifications directed at obtaining greater reliability and improved performance have been considered. The basic Mariner C design is selected for its proven reliability and demonstrated performance. A complete description of that design is presented in the Motorola document "Final Report, S-Band Transponder, Mark I, 20-Cycle Bandwidth" dated July 31, 1964.

A condensed description of transponder operation and brief discussion of modifications under consideration are presented in the following paragraphs. Improvements in these areas are being made in the updating of the transponder design for Mariner '69 by Philco. Fig. 5.5.3-12 is a block diagram of the transponder for reference during the ensuing discussion.

A. Receiver Description

The receiver is the familiar phase-lock design with a nominal noise figure of 8 dB and a carrier threshold sensitivity of -153 dBm. The characteristics are essentially those of the Mariner C receiver. The noise bandwidth of the carrier tracking loop is adaptive to the received signal level, and varies from 20 Hz at receiver threshold to 233 Hz for strong signal inputs. This provides capability for tracking high Doppler rates at strong signal strength, and preserves the narrow bandwidth desirable near threshold. The loop transfer characteristics at threshold are patterned after the mathematical model:

$$H(s) = \frac{1 + \left(\frac{3}{4\beta_L} \right) s}{1 + \left(\frac{3}{4\beta_L} \right) s + \left(\frac{9}{32\beta_L^2} \right) s^2}$$

where $2\beta_L$ is the two-sided loop noise bandwidth.

*The question of whether or not the link can support the ranging signal-to-noise ratio requirement was not considered, but the transponder has the capability to provide this function.

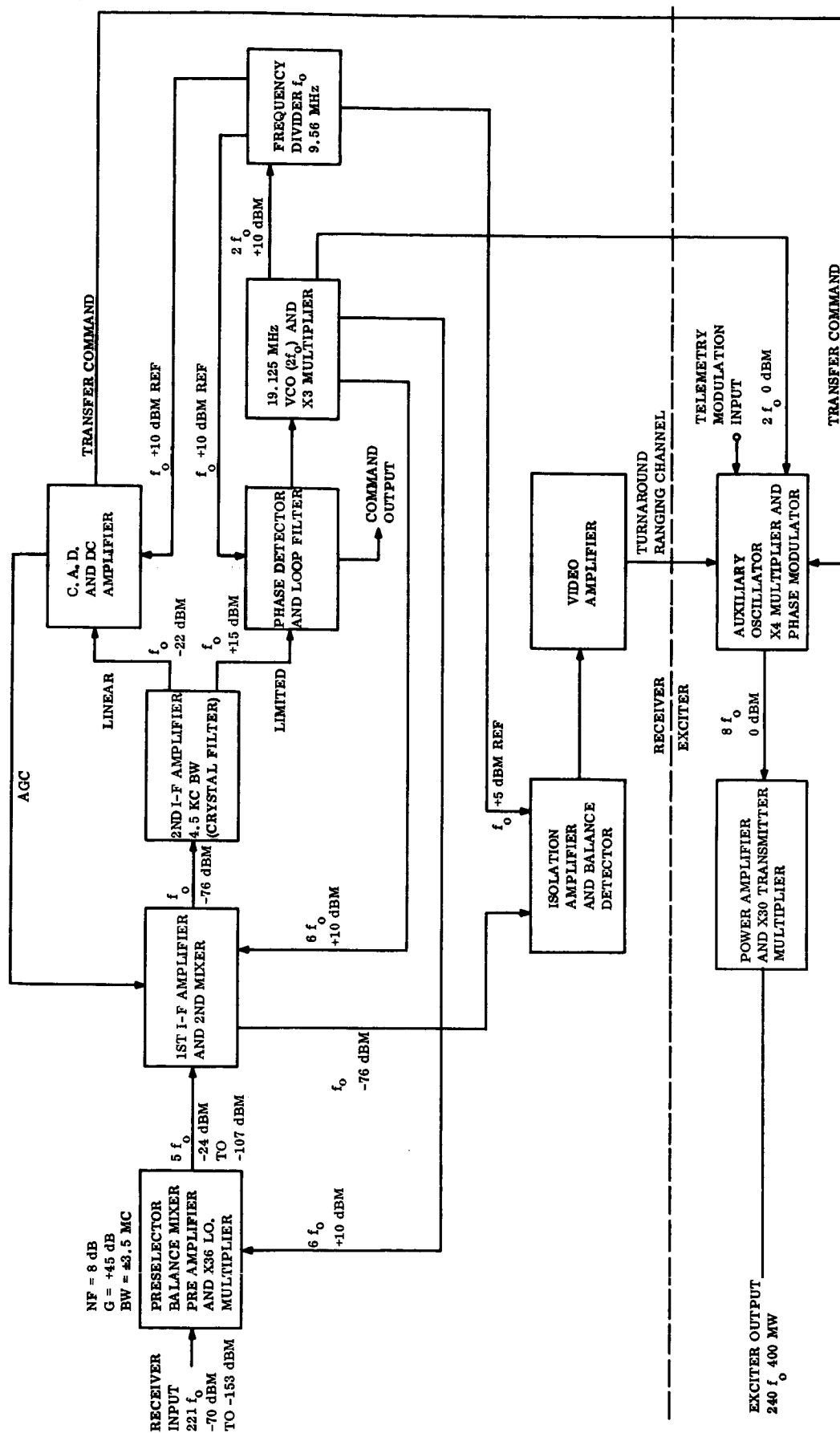


Figure 5.5.3-12. S-band Transponder, Functional Diagram

A coherent AGC system which responds only to the received carrier level provides an accurate analog of received signal strength for telemetry purposes. In addition, it serves as an indication of receiver lock, and as such, controls the selection of the signal source for the transponder exciter. When the receiver is phase-locked to a signal from the DSN, the exciter derives its source from the coherent receiver voltage controlled oscillator (VCO). Alternately, when the receiver is out of lock, as indicated by the absence of receiver AGC, the exciter is automatically switched to derive its source from a stable auxiliary crystal oscillator.

Demodulation of command information on the received signal is an auxiliary function of the phase detector in the carrier tracking loop. By virtue of the phase relationships necessary for receiver lock and the bandwidth established, the command subcarrier appears at the carrier loop error point. After suitable conditioning, this information is passed on to the command subsystem.

Because of the position of the command spectrum and the adaptive characteristic of the transponder carrier loop, some filtering of the command signal can occur when the received signal strength is high. Distortion of the command spectrum introduced by the proposed carrier loop design does not adversely affect the performance of the Command Subsystem. Also, analysis has shown the command spectrum will not adversely affect the transponder performance or the performance of the DSN receiver, Doppler, or ranging subsystems.

B. Receiver Modifications

The most significant modification under consideration for the receiver is the development of a low noise r-f mixer with a nominal noise figure of 8 dB. Advances in the state-of-the-art since completion of the Mariner design indicate this goal can be obtained with a substantial improvement in reliability. The diode contacts used in the present mixer package are recognized as a weak area. The X36 Local Oscillator (LO) multiplier would be redesigned as part of the mixer package in a configuration which reduces LO spurious outputs.

Other minor modifications which would be made include:

1. Modification of the first i-f amplifier to extend its dynamic range and reduce its noise figure.
2. Modification of the frequency divider to eliminate potential instabilities in the current design.
3. Modification of the AGC dc amplifier to improve the temperature stability of the current design.
4. Modifications when necessary to withstand high shock environment.

C. Exciter Description

The exciter portion of the transponder generates a stable S-band modulated carrier at a level which is suitable for driving the power amplifiers. The signal source for the carrier may be either the coherent receiver VCO or the stable self-contained auxiliary crystal oscillator. Two modules, the auxiliary oscillator and the X30 multiplier, are used. The auxiliary oscillator module contains the alternate crystal oscillator, an X4 multiplier, and the exciter phase modulator. The modulator accepts preconditioned telemetry and ranging signals and modulates them on the carrier at indices up to 4.0 radians peak when converted to S-band. The modulator bandwidth extends from dc to 2 MHz. The X30 multiplier module amplifies the modulated signal and multiplies it by a factor of 30 to provide the S-band output.

D. Exciter Modifications

The development of a new X30 multiplier for the exciter is considered essential. The current design exhibit excessive nonharmonic spurious outputs under certain conditions of temperature and supply voltage. These spurious outputs can cause false lock when the turnaround ranging channel is open. An alternate approach which does not exhibit these instabilities has been under development at Motorola for some time. Its operation is essentially as follows.

The X30 multiplier is required to convert a 0 dbm signal at 76.5 MHz to a 26 dBm signal at 2295 MHz. Fig. 5.5.3-13 is a block diagram of the alternate design being considered. The input signal is coupled through an isolation amplifier to an X2 varactor multiplier chain. The varactor multiplier chain requires a nominal input of 2 watts at 153 MHz to produce 0.5 watt of output power at 2295 MHz. The X5 varactor multiplier is a lumped constant circuit with a three section helical resonator filter at the output.

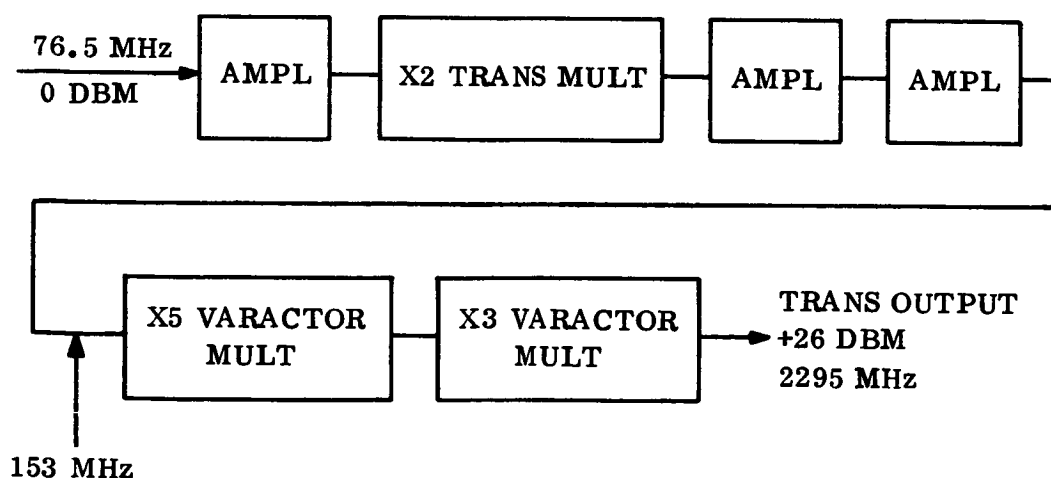


Figure 5.5.3-13. X30 Module of the Transmitter Exciter, Block Diagram

The X3 varactor multiplier is a distributed constant, strip transmission line circuit which contains a three-section interdigital bandpass output filter. The basic configuration has been successfully employed in the LEM transponder to produce 1.4 watts at S-band, and the Apollo Block II transponder to deliver 0.6 watt. A similar design produces 0.2 watt in the FM transmitter of the Apollo Block II system. This design has demonstrated reliable, stable, and efficient operation over extended temperature ranges. A 3 dB bandwidth of 90 MHz at the output frequency is being realized on the Apollo hardware with a dc to r-f efficiency of nearly 15 percent.

All spurious harmonic outputs are down 60 dB at the transmitter output terminals with no evidence of the parametric instabilities which can cause "ring-around" or "false-lock" problems in the transponder.

Additional modifications to the exciter would include changes in the auxiliary oscillator module to obtain improved oscillator stability and to reduce the variations in sensitivity of the phase modulator. This transponder module has already been redesigned for the Lunar Orbiter transponder and the improvement verified. The development of low noise oscillators for both the auxiliary oscillator and the VCO is also planned. These oscillators would allow the use of narrower tracking bandwidths in both ground and flight receivers. Performance parameters of the receiver and exciter are listed in tables 5.5.3-9 and -10.

E. S-Band Power Amplifier

The power amplifier consists of a TWT/power supply package designed by Watkins Johnson/JPL for high shock environment. This high impact tube was shock tested at 9600 g's for 0.5 msec duration.

F. Advantages of the TWT

1. The most significant argument in favor of the TWT over other power amplifiers is the fact that it is presently being used in nearly all the major space programs and has been flight proven. It shows a MTBF in excess of 50,000 hr which enhances the reliability of the telecommunication system.
2. The TWT has a nominal gain of 30 dB which eliminates the requirement for high output powers from the exciter.
3. The efficiency of a TWT is greater than 40 percent at the present and is being continually improved. Efficiencies higher than 45 percent now appear feasible.
4. The TWT is essentially a wideband device; i.e., at S-band frequencies, bandwidths well in excess of 10 MHz are possible. This provides good phase linearity over the bandwidth needed for turnaround ranging.

TABLE 5.5.3-9. RECEIVER PERFORMANCE PARAMETERS

Parameter	Value
Center frequency	2113 MHz nominal
Noise figure	8 ± 1 dB
Strong signal carrier tracking bandwidth	233 cps ($2\beta_{LSS}$)
Threshold carrier tracking bandwidth	20 cps ($2\beta_{Lo}$)
Threshold sensitivity	-153 dBm ± 1 dB
Dynamic range	-70 dBm to threshold
Tracking range	± 3.0 parts in 10^5 (for r-f signals > -120 dBm)
Carrier tracking loop threshold transfer function (model)	$H(s) = \frac{1 + \left(\frac{3}{4\beta_{Lo}} \right) S}{1 + \left(\frac{3}{4\beta_{Lo}} \right) S + \left(\frac{9}{32\beta_{Lc}^2} \right) S^2}$
Carrier tracking loop pre-detection filter bandwidth	4.5 kHz
AGC loop bandwidth	0.33 Hz to 0.85 Hz
Ranging channel i-f bandwidth (3 dB)	3.3 MHz
Video limiter rise and fall time	70 nsec
Ranging channel video bandwidth (3 dB)	100 Hz to 2 MHz
Input VSWR	1.3:1 max

TABLE 5.5.3-10. EXCITER PERFORMANCE PARAMETERS

Parameter	Value
Output frequency	2295 MHz nominal
Output power	+26 dBm \pm 0.5 dB
Output VSWR	1.3:1 max
Auxiliary oscillator frequency stability	1 part in 10^5 per year
Phase stability	Residual PM less than 9 deg peak in a 20 Hz phase coherent receiver
PM modulator dynamic range	0 to 4 radians peak
PM modulator linearity	Within \pm 7 percent of straight line
PM modulator sensitivity	1 radian per volt \pm 2 percent
PM modulator bandwidth	0.5 dB BW dc to 1 MHz 3.0 dB BW 1.8 MHz min
PM modulator input impedance	1000 ohms resistive

5. The physical size and weight of the TWT lend the device to high density packaging. The sizes of present devices are being reduced to the extent that the dimensions of an overall power amplifier package are determined by the size of the power supply and not the device.
6. The TWT is capable of stable operation at elevated temperatures which might occur in the absence of r-f drive. Without r-f drive all the dc power is dissipated through the collector.

G. Disadvantages of the TWT

1. Of most concern to the radio subsystem is the noise generated by the tube. Since the TWT has a wideband circuit, it generates noise at the receiver frequency. This is troublesome in duplexed configurations as the noise from the TWT degrades the equivalent noise figure of the receiver connected to the duplexer. Therefore, to use the TWT a filter must attenuate this noise to a sufficiently low level.

2. To minimize the external magnetic field of the TWT, complicated field balancing techniques are required to cancel the effects of the beamforming magnetic field along the full length of the tube.

5.5.3.5.8 Data Handling System

A. Functions

The data handling and storage subsystem provides encoding, time multiplexing, sequencing information and storage of the capsule's engineering and science data, and storage and execution of on-board command functions. The data handling and storage subsystem controls the programming, data collection, formatting, and data transmission as a function of the mission phase from interplanetary cruise through post impact operations. The subsystem also detects the composite command base-band from the receiver and stores these commands or transfers them to the programmer.

B. Summary Description

The functional block diagram of the data handling subsystem is presented in fig. 5.5.3-14. All analog signals, (0-5v), are multiplexed by the analog gates. The formatting of the data is determined by the data handling unit. The fixed formats are selected, as a function of mission phase, by a mode select command from the Random Access Memory.

The analog to digital (A/D) encoders sample the analog signals and perform the digital conversion many times faster than the word rate. Using the fast conversion and a 9 bit analog-to-digital converter (ADC), the transmitted number of conversion bits per scientific data source can be made 9 bits or less depending on the source's accuracy requirements. The engineering signals are encoded to 7 bits.

Multicoder

The Multicoder will have four modes of operation, each controlled by the data handling unit pulse lasting the duration of each mode. The number of data channels per mode are defined below: All analog inputs are high level (0 to +5 vdc).

1. Entry Mode

- a. 60 analog inputs, 9 bit resolution, 1 sample/sec
- b. 3 analog inputs, 9 bit resolution, 3 samples/sec
- c. 50 digital groups, 8 bit parallel occurring in 50 serial words on command from the multicoder at the rate of 5 groups/sec
- d. 2 digital words, 7 bit parallel, 7 sample/10 sec
- e. 1 digital word, 11 bit parallel occurring in two words, 1 sample/10 sec

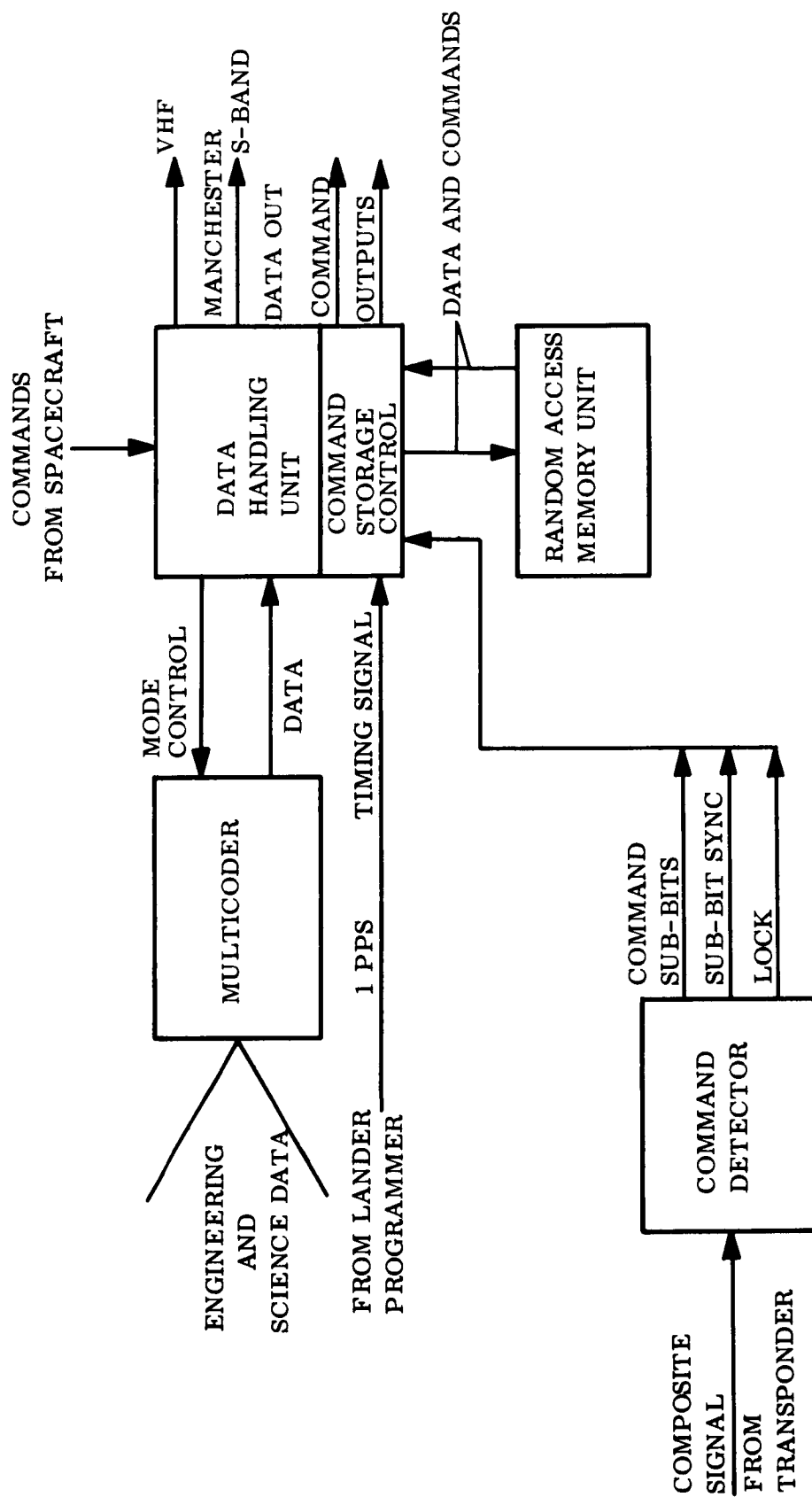


Figure 5.5.3-14. Data Handling System

2. Landed Mode #1

- a. 58 analog inputs, 7 bit resolution, 1 sample/20 min
- b. 6 digital words, 11 bit parallel, 2 lines, 3 words/line, 1 sample/20 min
- c. 1 digital word, 11 bit parallel, 1 sample/20 min
- d. 130 digital words, 14 bit parallel sequential on multicoder command, 1 sample/20 min
- e. 130 digital words, 11 bit parallel sequential on multicoder command, 1 sample/20 min
- f. 3 digital words, 7 bit parallel sequential on multicoder command, 1 sample/20 min
- g. 2 digital words, 7 bit parallel, 1 sample/20 min

3. Landed Mode #2

- a. 14 analog inputs, 7 bit resolution, 1 sample/20 min
- b. digital inputs, b, c and g of Landed Mode #1

4. Landed Mode #3

- a. One of four TV inputs, 6 bit resolution, 27000 SPS (160,000 bps)

Data Handling Unit

The data handling unit (DHU) accepts commands from the command storage control unit to determine in which mode the multicoder will operate. It decodes these commands and controls the multicoder functions by supplying pulses on one of four mode lines. The data from the multicoder is routed by the DHU either to the random access memory unit to the UHF transmitter or to the S-band transmitter. During entry, data from the multicoder is interleaved with delayed data from the random access memory unit.

The DHU also conditions the signals from the multicoder and memory going to the transmitters.

Commands from the spacecraft via handwire are routed through the DHU to the command storage unit and then to the memory.

Random Access Memory Unit

The random access memory unit (RAMU) is used to provide storage for digital words from the multicoder (7 bits/length) and to store command words (21 bits length).

The telemetry storage has two modes:

1. Store data serially and read out serially 70 sec later.
2. Store data and read out at a fixed rate at some later time.

Both of these modes are used in entry data collection as shown in fig. 5.5.3-18. Mode 2 is also used for collection of landed serial and engineering data and playback during orbiter passes.

Data will be inputted and outputted in a 21 bit format. Readout will be destructive with a restore mode option for Mode 1 as required.

Command Storage Unit

The command storage unit (CSU) (part of the DHU) accepts commands from either the spacecraft via hardwire or from the command detector. The commands and time labels are stored in the memory. The unit examines sequentially each command location in the memory fig. 5.5.3-10. It does not pass a command time word until that time agrees with the vehicle clock time. When agreement occurs it jumps to the next location which should be a command and outputs it to the Lander programmer (See para 5.5.4.2).

The commands in the memory can also control the sequence of examination of the CSU. Thus, a fixed sequence of operations can be addressed by commanding the CSU to that memory location. At the end of this sequence (e.g., data gathering) a command would be present which would send the CSU back to the memory location following the jump command. By using auxiliary registers (part of the random access memory) and decoding functions to control the CSU, the CSU became a versatile general purpose program machine.

For a mission of 24 hr with experiments requiring data gathering every 20 min, 3 hr and 6 hr, the specific actions at each sampling time need be stored only once with time increment and return commands at the end of these sequences.

The timing signals for the CSU are provided by the Lander programmer.

The actions on the vehicle can be controlled by the parallel output from the command storage control unit. The unit scans the memory and executes the commands stored therein when the time of the commands agrees with the vehicle time. This is shown in fig. 5.5.3-15.

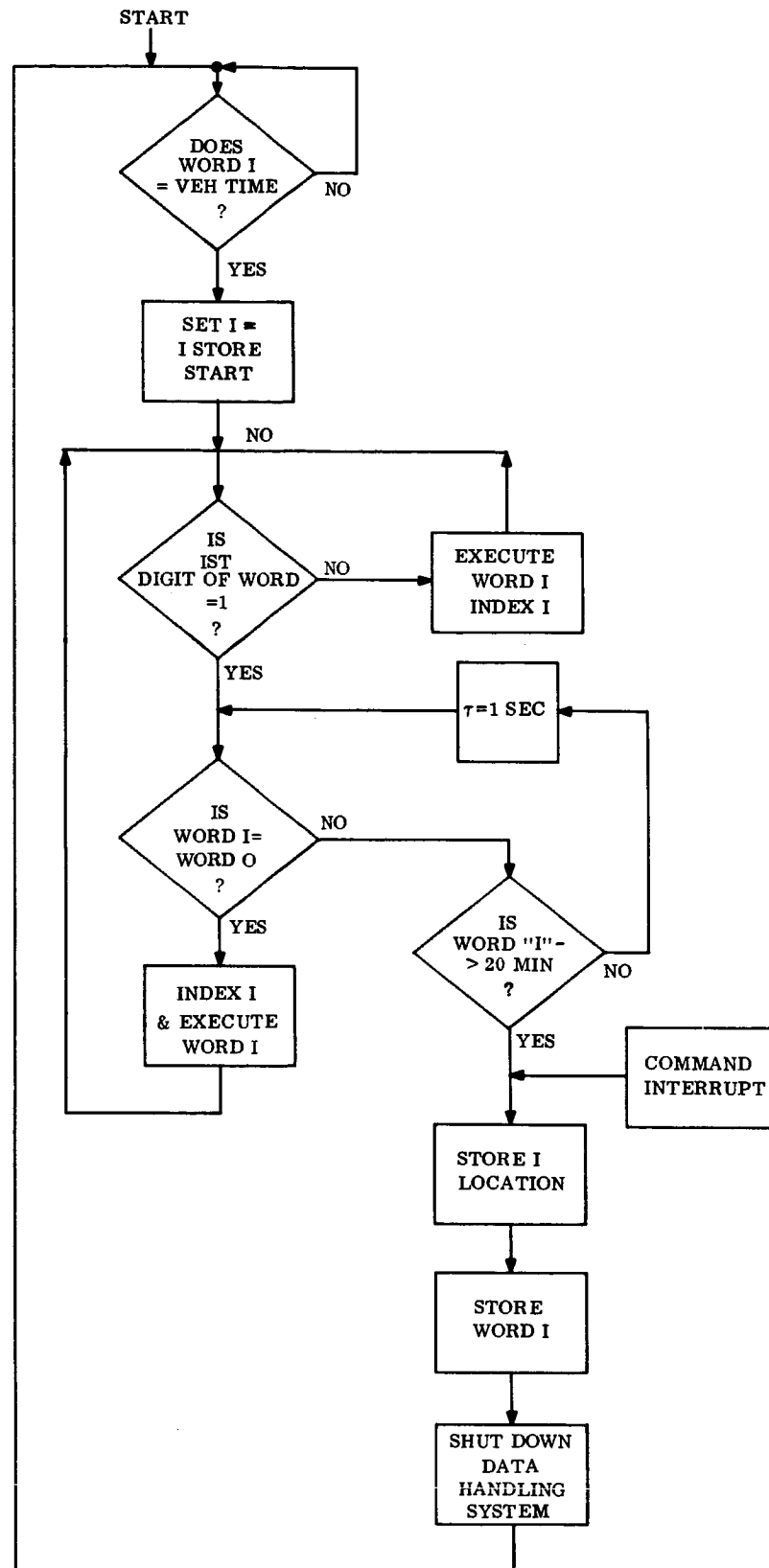


Figure 5.5.3-15. Operation of Command Storage Control Unit

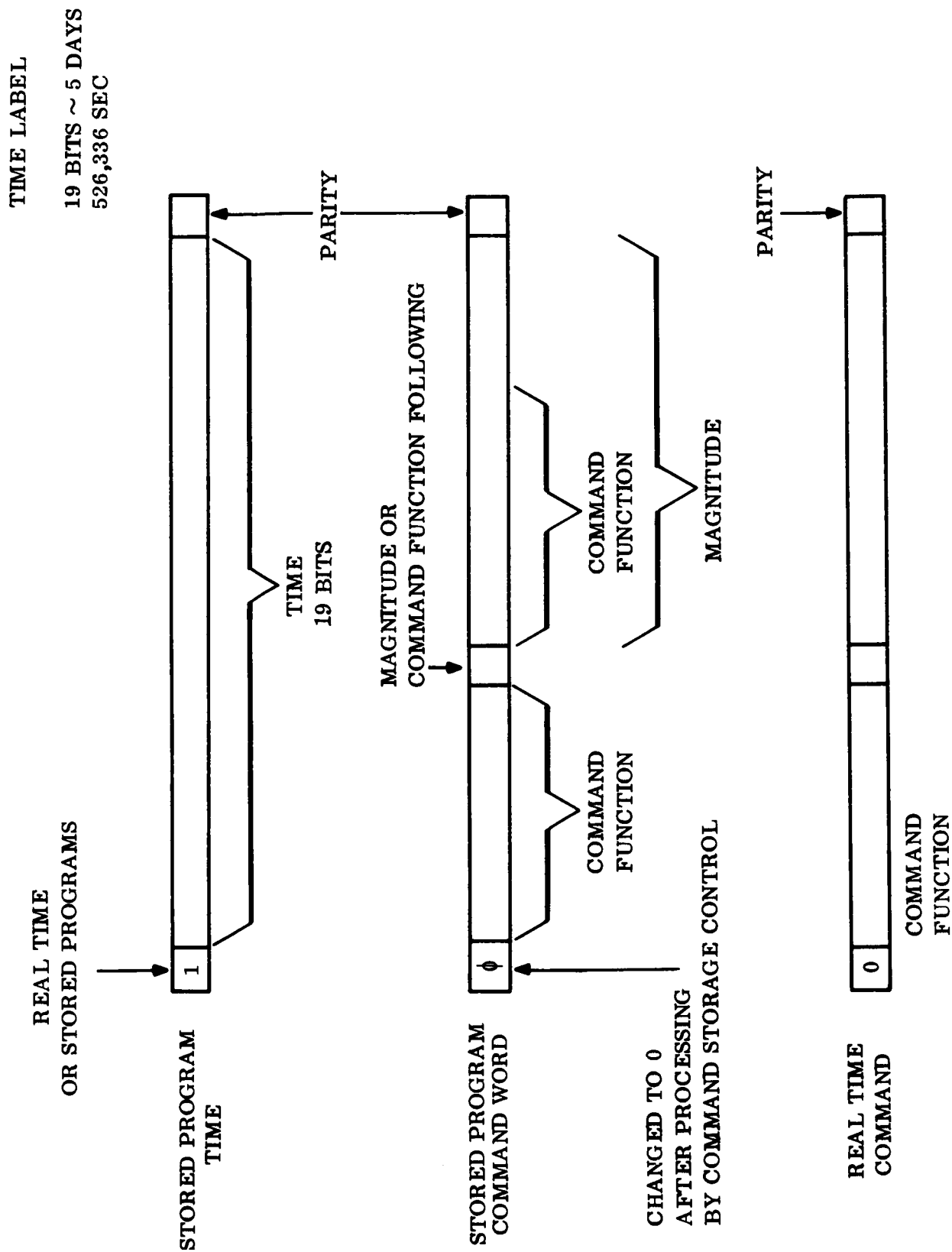


Figure 5.5.3-16. Command Word Format

The presence of a lock signal from the command detector causes the command storage control unit to cease sequential search of the memory and accept command sub bits. The command words as shown in fig. 5.5.3-16 include a six sub-bit preamble which is used for word sync purposes. The six sub-bit sequence is 111000; it is impossible for this sequence to occur in any other place without at least two errors. The command storage control unit checks the command bits after conversion from sub-bits for parity, if parity checks, the word is stored or executed and the word is transmitted to Earth via the direct link. If parity does not check, a unique 21 bit word is transmitted to Earth and nothing is stored.

The command detector, the command storage control unit, and the random access memory comprise the command group of the data handling subsystem. The command detector accepts the modulated subcarrier signals from the transponder, determines sub-bit sync and sub-bit values which are inputted to the command storage control unit. The command storage control unit (if a real time command is decoded) outputs a parallel word of 8 bits to the programmer or stores the word (if a stored program command is decoded) in the random access memory unit.

A block diagram of the command detector is shown in fig. 5.5.3-17. Note that the output of the command detector is sub-bits, each command bit being composed of two sub-bits. When the execute word is received that word is decoded. If it is a RT command it is shifted out to the programmer. If it is a stored program command it is stored in the memory (usually in a location given by a previous RT command).

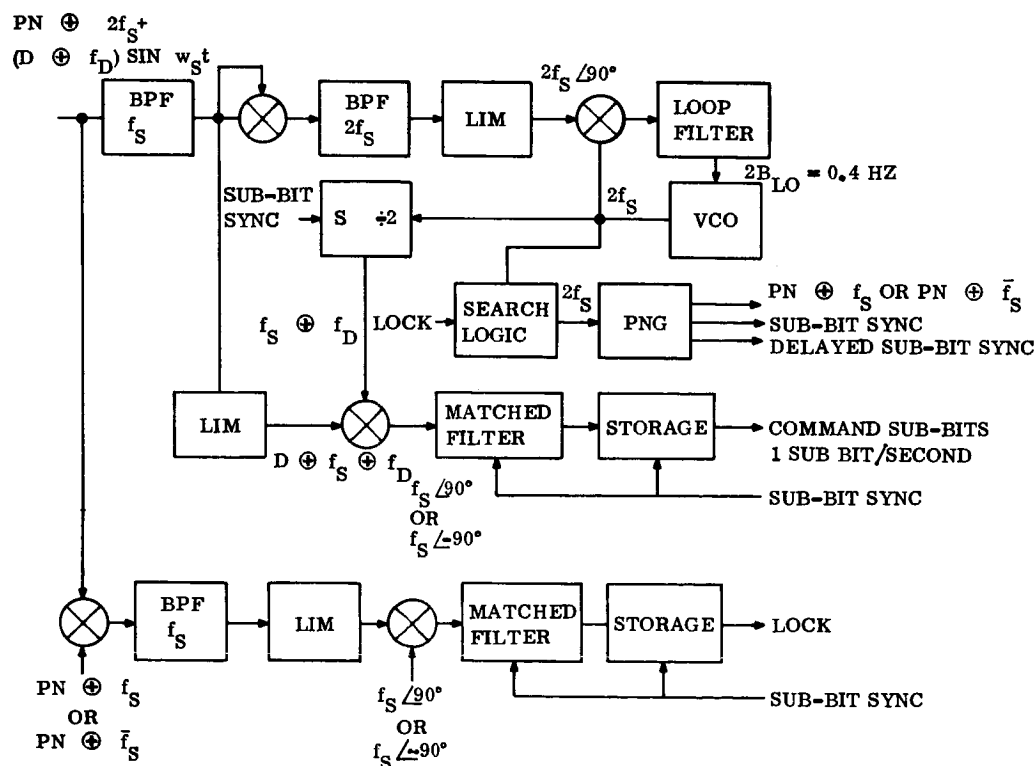


Figure 5.5.3-17. Command Detector

This subsystem will be shut down to conserve power when the time between commands is more than twenty minutes. A separate set of registers will be used to store the time at which the data handling system shall begin functioning and also the memory location of the next command. The flow chart in fig. 5.5.3-15 shows how the command storage unit checks the time until next command execute and shuts the system down until this time is reached on the vehicle clock.

C. Data Handling Versus Mission Phase

Interplanetary Cruise - The Capsule's data handling equipment is assumed de-energized during interplanetary cruise. Monitoring of thermal control and the Capsule's electrical power subsystem is performed by the spacecraft's data handling subsystem.

Capsule Checkout - The Capsule checkout mode is initiated sufficiently prior to separation to determine the status of the Capsule and its payload and to allow for corrective action. Under control of the programmer and command storage unit, Capsule checkout is accomplished with data begin transferred to the spacecraft via hardware.

Capsule Separation and Engine Fire - From Capsule separation to engine fire (approximately 20 min), the Capsule is transmitting at 1090 bps. Only engineering data is monitored. The received data on the spacecraft is detected and stored for delayed transmission to Earth over the high data rate link.

Capsule Entry - Upon initiation of entry, data transmission is resumed at 1098 bps composed of 544 $\frac{2}{3}$ bps real time and 544 $\frac{2}{3}$ bps delayed. The entry data rate requirements are shown in table 5.5.3-11. A rate of 350 bps is assumed for engineering data. The data is stored in the random access memory at a 544 $\frac{2}{3}$ bps rate. Essentially, the memory will act in two modes; one, as a delay line with a 70 sec delay, and two, as a memory in which 100 k bits of entry data are stored. Each word in the memory is 7 bits. The operation of the random access memory during entry is shown in fig. 5.5.3-18.

Post Impact Relay - Upon impact the buffer readout is temporarily halted. The buffer will contain 100 k bits of entry data. Engineering data is continued to be read out at 1090 bps until completion of the setup period. Upon completion of the setup period, the imaging data collection and transmission begins. The landed measurement requirements are given in table 5.5.3-12.

Landed Operations - The picture taking operation performed after impact is repeated one Martian day later when the Obiter is in view. Camera operation can be repeated in later days by commanding such activity from Earth.

Data for the first several days will be collected on a twenty minute period with the data collection routine loaded into the memory, controlling these actions. For

TABLE 5.5.3-11. ENTRY DATA

Sensor	Accuracy (%)	Sampling Rate (SPS)	Bits/Sample	No. of Channels	bps	Time
Pressure transducer (2) 0 - 0.3 psia	1	1	9	2	18	Post chute deployment
Resistance thermometer (2) 100° - 300° K	0.2	1	9	2	18	
Mass spectrometer (readout 8 bits at a time)	—	N/A	8	N/A	40	1 hr before entry to impact
Accelerometer, triaxial (dual scale)	1	3	8	3	72	1 hr before entry to impact
Stagnation temperature	0.25	1	9	1	9	1 hr before entry to impact
Stagnation pressure (4)	0.25	1	9	4	36	1 hr before entry to impact
Water vapor	N/A	1/15	7 (parallel)	2	14/15	1 hr before entry to impact
		1/15	11 (parallel)	1	11/15	
Engineering measurement	—	1	7	50	350	1 hr before entry to impact

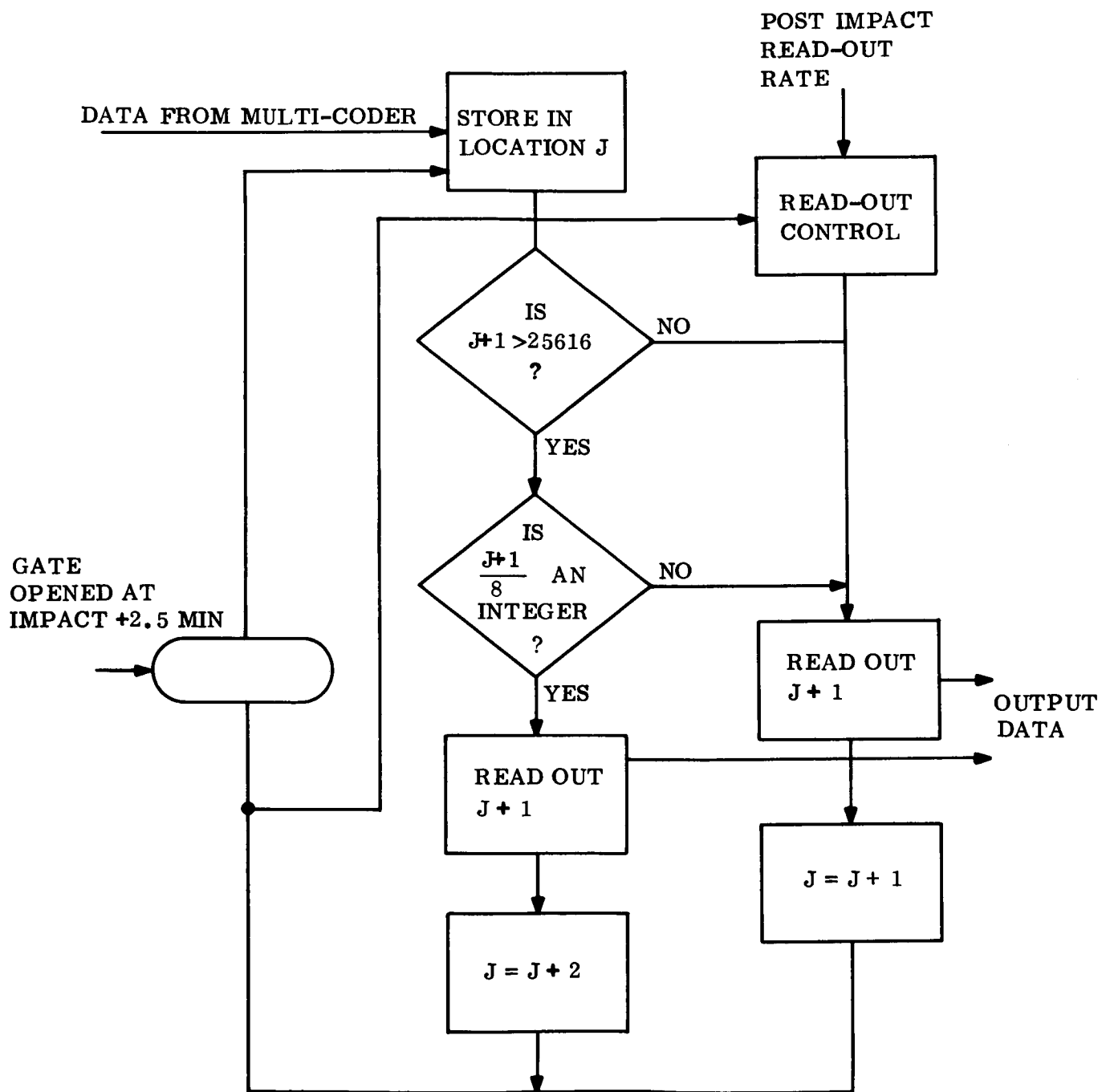


Figure 5.5.3-18. Entry Data Storage Routine

TABLE 5.5.3-12. LANDED SCIENCE (NON-IMAGING)

Sensor	Accuracy	Sampling Rate	Bits/Sample	Number of Channels Per Sensor	Number of Bits Per Hr
Pressure transducer (2)	1%	3/hr* 1/hr**	6	2	36* 12**
Thermometer (4)	1%	3/hr* 1/hr**	6	2	72* 24**
Wind velocity (2)	3%	3/hr* 1/hr**	11 (parallel)	6	66* 22**
Moisture	—	3/hr* 1/hr**	7 (parallel) 11 (parallel)	2 1	75* 25**
Surface composition*	Less than 256 counts/energy slot in 3 hr	1/3 hr	14 (P) 12 (P) 7 (P)	130 130 3	1133*
Clinometer (2)	1%	1/6 hr	7 (P)	2	14/6
Engineering measurements	—	3/hr	7	50*	1050*
	—	1/hr 3/hr	7	6**	42** 126*

*Relay mode, only

**Direct link mode

direct link operation 6.4 k bits science and 3.1 k bits engineering data will be collected each day. This data will be read out by command (RT or SP) each day when the Earth is within the transmitting antenna beamwidth.

If the relay link is used, 34.6 k bits of science and 26.3 k bits of engineering data will be accumulated and transmitted.

To conserve power and extend the life of the Lander, the system can be shut down except for the two registers, clock and time comparison circuitry which require 1/4 watt. During this time (~ 5 days), no transmission or data gathering functions will be performed.

5.5.3.5.9 Physical Characteristics

Table 5.5.3-13 summarizes the physical characteristics of telecommunications equipments. The key to development status is:

1. No modification required (off-the-shelf)
2. Modify (e.g., for high shock)
3. Redesign (basic equipment exists but redesign for new frequency, detection technique, etc.)
4. New design (specify new design using established techniques)
5. New development (employs near-future state-of-the-art techniques).

TABLE 5.5.3-13. PHYSICAL CHARACTERISTICS

Component and Quantity	Size (in.)	Weight (Based on 1000 g's) (lb)	Power	Sterilizable (125°C)	Max Shock (present information)	Development Status	Remarks
UHF Transmitter	30 in. ³ 1.5 x 4 x 5	2.5	150 w	yes		4	
UHF Antenna (2)	8 dia. x 2	1	-	yes		4	2 required 1 will be used
UHF Circulators (2)	6 in. ³ 2.5 x 2.5 x 1	0.4	-	yes		3	2 required in close proximity
UHF Antenna Switch	1.1 in. ³ 2 x 1.5 x 0.375	1.0	0.25A @ 3.5 V and 10 micro-A @ 28V	yes	3000 g's, 3 ms	1	Interchange voltages to switch antenna - Power during xmit and receiver
Beacon Receiver and T/R Switch	21 in. ³ 5.4 x 3.6 x 1.1	1.3	0.5 watts and 0.06A @ 1.2V	yes		4	0.06A @ 1.2V required during 400 MHz transmit periods
Multicoder	104 in. ³ 3.5 x 4.3 x 7	5	15 watts	yes		3	Power required during data sampling periods only (see text)
Data Handling Unit	100 in. ³ 4 x 5 x 5	4	3 w	yes		4	
Thin Film Memory	88 in. ³ 4 x 4 x 5.5	5	6 w	yes		4	180000 bit capacity, random access
Signal Conditioner	4 x 5 x 7	4	8 w	yes		2	50 channels only
Three Axis Impact Accelerometer	1.3 x 1.3 x 0.8	0.6		yes	10,000 g's	1	
Charge Amplifier (3)	1.25 x 2 x 3	0.5	1.2 w ea.	yes	representative unit passed 2000 g test	1	2 required connected to in accelerometer by coax cables
S-Band P/A	300 in. ³ 10 x 12 x 2.5	7	89 w	yes	9600 g's	2	
S-Band Antenna, receive (2)	4 dia. x 4	0.2	-	yes		4	2 required - 1 used
S-Band Antenna, trans (2)	8 dia x 3	0.5	-	yes			
S-Band Latching Circulator (2)	2 x 2.5 x 1.25	0.7	pulse 2A, 28V, 1ms	yes	3000 g's for 3 ms	3	must be vertically oriented pulse to switch antennas
Transponder: Exciter Receiver	700 in. ³	22	15 w 12 w	yes		2	
Command Decoder	153 in. ³	5	2 w	yes		2	

5.5.4 ELECTRICAL POWER EQUIPMENT

The power equipment provides electrical energy, power switching, charge control, voltage control and electrical distribution. Figure 5.5.4-1 illustrates this equipment. Note that the electrical energy flow, power, signals and data which takes place between subsystems is shown in the Functional Block Diagram, Section 5.2.4.

5.5.4.1 Operation

Commands are received via hardwire connection to OSE for post sterilization check, via hardwire from the spacecraft through the telecommunications subsystem during interplanetary cruise and Martian orbit and from the telecommunications subsystem after landing. These commands enter the programmer as a 21 bit word where they are decoded into operation signals for the relays which switch the power feeder lines. The programmer also contains a multichannel hardwire program section which provides an additional independent operation of the spin, de-boost, and landing sequences for mission assurance. These programs have programmable start times and, once initiated, proceed with the execution of a fixed program sequence. A single command, regardless of origin, may signal the operation of either a single load or a group of loads as required.

All operation signals from the programmer go to the power controller where power switching takes place. The components which require independent switching, such as the payload scientific instruments, have separate electrical power feeders. Other components which are always used as a group, such as the engineering diagnostic instrumentation, share a single feeder. The power controller can accept energy from the operational battery, from the high rate batteries, from the spacecraft or from ground power, and switch this power to the appropriate load or loads. The line contactor is used to select and control which of these power sources supplies the power controller.

The operational battery provides all Lander electrical energy except the high rate pyrotechnic and hot-wire initiations. This secondary silver-zinc battery is charged from raw spacecraft power prior to separation. Power from the operational battery feeds the unregulated loads directly. This battery is equipped with extra cells and semiconductor bypass for redundancy.

5.5.4.1.1 Battery Redundancy Considerations

To enhance reliability three alternatives have been investigated.

If two batteries were flown, each capable of providing the minimum mission duration objectives a considerable weight penalty would be suffered. An alternative route would be to provide two batteries which would each provide half the desired output. This method would increase the battery weight about 25 percent, because of the lower power to weight ratios of smaller batteries, and ensure that half the mission objective would be achieved even if one battery failed.

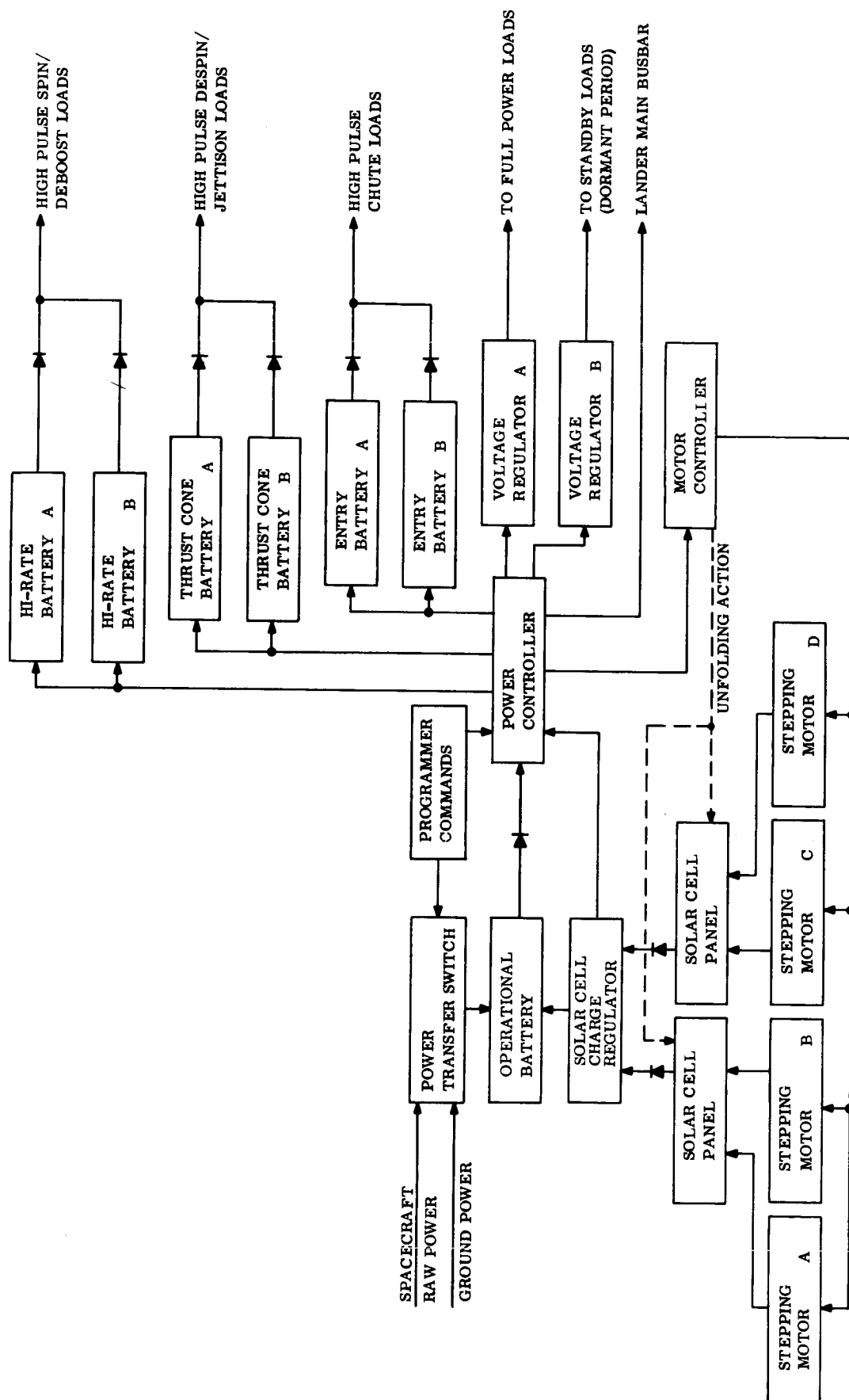


Figure 5.5.4-1. Electrical Power Subsystem, Point Design 3, Block Diagram

The method adopted to provide adequate redundancy is to carry redundant cells. The logic in this approach is that it is usual if failure should occur for only one or at most two cells to fail. If these can be replaced by reserve cells considerable savings will result.

The circuit shown in fig. 5.5.4-2 incorporates diodes on the charging side having a tightly controlled zener regulating level, e.g., 2.05 volts, and very low dynamic impedance. The diode on the discharge side of the circuit has a low forward voltage. Three redundant cells in the battery are connected through the controller to be added in series when needed as directed by the programmer.

If, during charge, a cell fails open circuit or high resistance, the zener voltage of that cell will be exceeded. The cell will be bypassed. If the cell fails short circuit or low resistance the cell will carry the charge current. A slight loss may result in charging a bad cell. Because each Zener protective voltage level will be equal to its cutoff voltage, the arrangement gives added protection against overcharging. If a cell fails on discharge, the diode in the discharge circuit will conduct and bypass the failed cell, avoiding driving the cell negative. Whichever way the cell fails it will always be bypassed.

Switching in new cells through the controller is achieved by low voltage sensing in the programmer. The low voltage is caused by the loss of a cell plus the diode drop as it switches in. Two cells would therefore be switched in for the first cell failure to compensate for diode voltage drop. A nominally higher voltage than the original battery would then result. If the second cell failed only one other cell would be switched.

A redundant system has been provided which allows for the failure of two cells in a battery. The additional weight approximates 20 percent of the original battery. This includes cells, diodes, programmer and controller modifications.

The need for high current capability during initiation operations is met by three pairs of thermal batteries. These provide power for spin/de-boost operations, de-spin/entry operation and parachute/aeroshell operations. In each case two batteries are available for redundancy. The batteries are activated separately from the canister or operational battery and the output is switched to the initiators via the power controller. These activation circuits are equipped with thermal relays to protect the operational battery.

During the extended mission, electrical energy is obtained via the conversion of solar energy through photovoltaic semiconductor arrays. These solar cell panels are stored under tension to provide shock hardening and are unfolded as described in Section 5.5.6 for use after the completion of a day's photo imagery. During illumination, the solar array powers the loads and recharges the secondary silver-zinc battery used during entry and prior to solar cell deployment. Since the battery is large, as required to meet the first few days operating requirements, a high charging efficiency results.

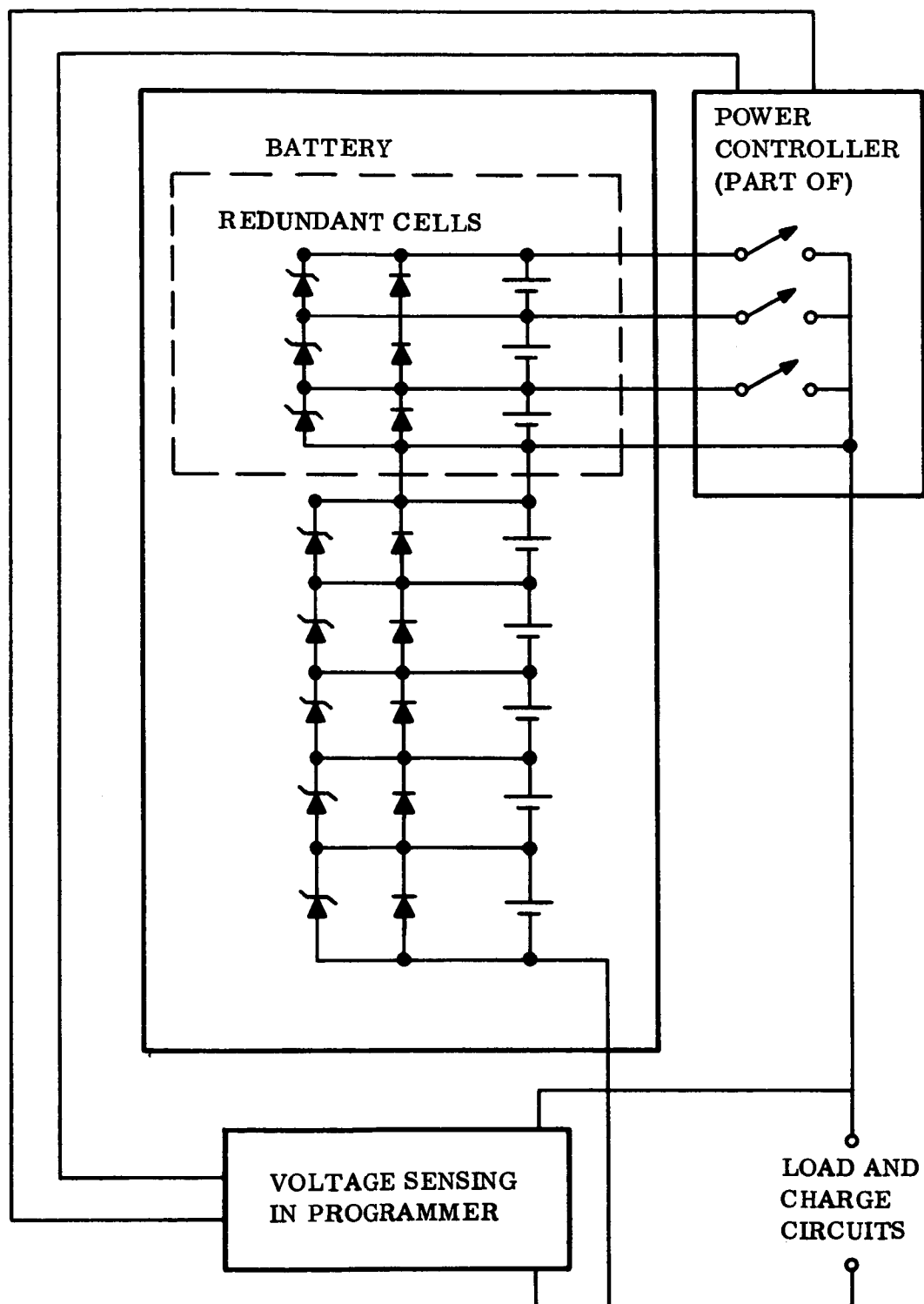


Figure 5.5.4-2. Battery Redundancy Circuit

A buck-boost regulator is used to assure the fullest possible utilization of the available solar power.

The scientific payload, r-f equipment, diagnostic instrumentation, data processing equipment, and sequencing components will require voltage regulation. To minimize weight, to obtain the high efficiency needed on the extended mission and to permit noise control, a single central voltage regulator should be used. However, the high degree of energy conservation required would not permit stand-by losses of such a large regulator on a continuing basis. For this reason two regulators are used, a small unit for the timer and receiver which are operated through the dormant periods, and a larger unit which handles all other loads. In addition, it is recognized that selected small loads in the scientific instruments may require special high accuracy regulation.

Battery charging on the spacecraft is controlled by redundant equipment located in the canister. This equipment uses solid state switching circuitry with time ratio control for high efficiency.

The Mars Hard Lander electrical system utilizes direct current power sources and distribution as well as steady-state sensing of pressure and temperatures. Programming, sequencing and power switching are performed for durations of a minute or longer with synchronization accuracies in the order of 0.1 sec. Safing and arming are performed manually. Conditioned and regulated power are processed at a low audio frequency. Initiation and electromechanical operations are performed with the application of electrical energy for durations of a few msec to a few hundred msec.

Electromagnetic compatibility equipment is designed to provide protection over a broad spectrum. This includes low repetition rate pulse-transients through the r-f frequencies used for telemetry.

Data processing, encoding, and multiplexing involve kilocycle and higher frequencies. The camera electronics with imagery represents the highest data bit rate.

UHF and S-band are used for telemetry, providing the highest frequency equipment aboard the probe system.

These needs describe the spectrum of electrical energy which must be distributed by the cables and harnessing.

Since the Lander will carry a number of different scientific equipments as payload, it is desirable to make arrangements permitting the mission to continue should electrical difficulties arise in a limited area. This feature is provided through a breaker and limiter unit which provides electrical protection to each payload item. Should an electrical fault develop, the load element is disconnected or current limited so that the remainder of the mission may continue.

5.5.4.2 Component Description

Each component is described in detail in this section. Table 5.5.4-1 lists the electrical equipment of Point Design 3 by name, location, weight, size and power level together with electrical reference designators. The equipment situation is indicated by capability to withstand 125° C sterilization temperature, prior shock level accomplished, and development status. The development status is shown by the same numerical code defined in para 5.5.3.5.

5.5.4.2.1 A101, Operational Battery

Function: Provides energy source for all aeroshell and Lander electrically operated equipment, except high rate initiation loads, from the time of aeroshell release through the mission completion.

Type: Manually-activated heat-sterilizable silver-zinc secondary battery sealed with high pressure emergency rupture disk.

Rating: 1771 watt hr each, 28v nom, ± 18 percent load profile per Section 5.2.5

5.5.4.2.2 A113, A114 High Rate Batteries

Function: Provide energy source for multiple high rate initiation type loads.

Type: Remotely-activated, electrically-initiated, thermal type primary battery.

Rating: 1000 watts peak power output. Maximum activated stand 3 min.

5.5.4.2.3 A106 Line Contactor

Function: Power transfer of aeroshell Lander systems from ground power to spacecraft power to internal batteries and solar array.

Type: Electromechanical latch type line power contactor.

Rating: Contact rating - 20 amp
Interrupt capacity - 250 amp
Pull-in time - 100 msec max
Pull-in power - 0.3 watt max
Contact configuration - later
Operating life - 100,000 cycles
Dielectric withstand capability - 1500 v for 1 min

5.5.4.2.4 A107 Lander Programmer

Function: Provide all sequencing, timing, signals, synchronization and clock functions within the Lander and aeroshell.

TABLE 5.5.4-1. ELECTRICAL EQUIPMENT HARDWARE MATRIX, POINT DESIGN 3

Component and Quantity	Size (in.)	Weight (lb)	Power (watts)	Sterilizable (125°C)	Mass Shock (g's) (present information)	Development Status
Operational Battery (A101)	12.2 × 6.1 × 12.2	67.6	Source	Yes	2,000	5
Power Transfer Switch (A106)	2.5 × 2.5 × 5.0	2.0	5.6	Yes	400	3
Lander Programmer (A107)	8.8 × 7.7 × 3.5	7.2	12.0	Yes	400	4
Voltage Regulator A(A108)	5 × 6 × 8	7.0	250.0	Yes	1,000	3
Power Controller L(A110)	3.5 × 5 × 7	5.5	15.0	Yes	700	5
High Rate Battery A & B (A114) (A113)	2 dia. × 3	0.5	Source	Yes	15,000	1
EMC Filter C(A115)	3 × 3.75 × 5.5	1.9	--	Yes	5,000	2
Diode Blocking Module C(A121)	1.5 × 1.5 × 2.5	0.2	13.6	Yes	20,000	2
Thermal Relay Module C(A124)	1.5 × 1.5 × 2.5	0.15	3.0	Yes	50	4
Hg Switch A and B (A128) (A129)	1 dia. × 2.5	0.1	--	Yes	50	4
Voltage Regulator B(A130)	2.5 × 3 × 4	0.9	27.0	Yes	1,000	3

TABLE 5.5.4-1. ELECTRICAL EQUIPMENT HARDWARE MATRIX, POINT DESIGN 3 (Continued)

Component and Quantity	Size (in.)	Weight (lb)	Power (watts)	Sterilizable (125°C)	Mass Shock (g's) (present information)	Development Status
Breaker and Limit Unit (A132)	2 × 2 × 3	0.6	1.0	Yes	10,000	2
Solar Cell Panel A(A133)	18 × 4.5 × 16.5	20.0	Source	Yes	50	4
Charge Regulator (A134)	4 × 5.4 × 10	7.8	2644	Yes	1,000	3
Diode Blocking Module S(A135)	2 × 2 × 3.5	0.5	83	Yes	20,000	2
Drive Mechanism A and B (A136)	4 dia. × 6	4.0		Yes		
Stepping Motor A, B, C, (A150) and D(A152) (A151)	2.5 dia. × 3.5	2.0	0.36	Yes	2,000	3
Motor Controller (A138)	3 × 4 × 4.5	1.3	0.72	Yes	700	5
Solar Cell Panel B(A153)	18 × 4.5 × 16.5	20.0	Source	Yes	100	4
Pin Puller (A158) (A159)		0.3		Yes		
Aeroshell/Lander IFD (J2002)	1.83 dia. × 1.52	0.16	--	Yes	2,000	3

TABLE 5.5.4-1. ELECTRICAL EQUIPMENT HARDWARE MATRIX, POINT DESIGN 3 (Continued)

Component and Quantity	Size (in.)	Weight (lb)	Power (watts)	Sterilizable (125°C)	Mass Shock (g's) (present information)	Development Status
Thrust Cone/ Lander IFD (J2003)	2.5 dia. × 2	0.75	--	Yes	2,000	3
Command Cable Assembly (WL1)	14C × 8 ft	2.1	--	Yes	2,000	3
Power Cable Assembly (WL2)	16C × 28 ft	3.7	--	Yes	2,000	3
Instrumentation Cable Assembly (WL3)	50C × 40 ft	3.0	--	Yes	2,000	3
Shielded Cable Assembly (WL4)	1C × 24 ft	2.1	--	Yes	2,000	3
Power Cable Assembly (WL5)	10C × 20 ft	2.7	--	Yes	2,000	3
Coaxial Cable Assembly (WL6)	1C × 24 ft	0.5	--	Yes	2,000	3

Type: Solid-state digital circuitry using majority logic and redundancy back up features.

Rating: Channels:
In-flight check-out
Powered flight program
Diagnostics cycle
Maneuver mode control
Preseparation program
De-boost sequence
Entry sequence
Set-up mode control
Surface science sequence
Photography cycle
Solar array unfolding and leveling
Vehicle clock

5.5.4.2.5 A108 Voltage Regulator

Function: Provide control and correction for electrical potential variations. Also, provide various potential levels required to operate aeroshell and Lander electronics.

Type: D-c isolated solid-state inverter transformer-rectifier with time ratio control and feedback regulation.

Rating: Output - 250 watts
Voltage levels - later
Transient recovery time - later
Regulation - See Volume III, table 4.3.1-4
Input - 23 to 33 vdc

5.5.4.2.6 A110 Power Controller (Lander)

Function: Provide distribution center equipment and all power switching for the aeroshell, thrust cone, and Lander electrical loads. Receives commands with proper time sequences and synchronization from the Lander Programmer A107.

Type: Electromechanical relay, switch and contactor construction

Rating: Number of switched loads - 100
Contact rating - 40 amps, max
Pull-in time - 10 to 100 msec
Pull-in power - 0.5 watt each
Feeder buses - 50

5.5.4.2.7 A121, A135 Diode Blocking Modules

Function: Prevent reverse power flow between various energy sources.

Type: Solid-state single crystal silicon semiconductor diode with redundancy.

Rating: PIV - 75 volts
Recovery time - NA
Forward current - 10 to 75 amp

5.5.4.2.8 A115 Electromagnetic Compatibility Filters

Function: Suppress spurious and conducted electromagnetic interference.

Type: Lumped parameter networks with nonlinear and lossy type circuit elements.

Rating: A115 - r-f band pass rejection
Number of bands - later
Center frequencies - later (UHF)
Attenuation - later
Dielectric withstand - 1500 volts

5.5.4.2.9 A124 Thermal Relay Module

Function: Provide system protection against faulted squib firing circuits.

Type: Bimetallic heat operated latch type switching element.

Rating: Interrupt capacity - 100 amp
Trip level $I^2 R t$ - later

5.5.4.2.10 A128, A129 Switch Hg

Function: Detect upwards direction and enable proper deployment circuits.

Type: Potted mercury switch, 3 pole

Rating: Current rating - 1 amp
Voltage rate - 250 vdc
Dielectric withstand - 1500 v, 1 min

5.5.4.2.11 A130 Voltage Regulator

Function: Provide control and correction for electrical potential variation at high efficiency for standby usage. Also, provide various potential levels required to operate the standby Lander electronics.

Type: D-c isolated solid-state inverter transformer-rectifier with time ratio control.

Rating: Output - 27 watts
Input - 23 to 33 vdc

5.5.4.2.12 A132 Breaker and Limiter Unit

Function: Protect the electrical system against non-vital load faults

Type: Circuit breaker, thermal relays, and limiting resistors in selected groups.

Rating: Circuits - 20
Trip levels - 30 ma to 2 amp

5.5.4.2.13 A133, A153 Solar Cell Panels

Function: Conversion of solar photon energy into electrical energy for the extended mission. Powers Lander loads and recharges batteries during the illuminated period.

Type: Flat stacked panels containing N/P silicon 2 ohm-cm photovoltaic cells 8 mils thick, 1 x 2 cm. Each panel unfolds to 12.5 ft² including frames. The sub-panels are joined through a series of spring loaded pantograph links.

Rating: $P_{initial}$ - 100 watts/panel at AM028 and 1AU
 P_{ave} - 19.1 watts/panel in application
 V_{out} - 42.4vdc
 I_{out} - 0.454 amp

5.5.4.2.14 A134 Charge Regulator

Function: Controls the flow of power from the solar array to the storage battery and electrical system during illumination.

Type: Buck-boost inverter regulator which power optimizes for different illumination levels together with battery temperature and pressure compensations to the charge regime.

Rating: VA_{max} - 110 volt-amp
Voltage control - $\pm 1/2$ percent

5.5.4.2.15 A136, A155 Drive Mechanism

Function: Provides translational motion of the solar panel so the unfolding base is level with the top of the "flat pack" vehicle and panel clears the crush-up material.

Type: Rack and pinion gear with brushless d-c motor drive

Rating: Later

5.5.4.2.16 A137, A150, A151, A152 Stepping Motor

Function: Move or release mechanical stops which control limits on the solar panel unfolding. Enables approximate leveling of the solar array in two axes.

Type: d-c torque motor

Rating: Later

5.5.4.2.17 A138 Motor Controller

Function: Switches and applies power to the drive mechanism and stepping motors in the proper direction and amount to achieve the desired deployment.

Type: Electromechanical relay, switch and contactor construction

Rating:	Number of loads	6
	Contractor rating	5 amp max
	Pull-in time	50 msec
	Pull-in power	0.3 watt each

5.5.4.2.18 A158, A159 Pin Pullers

Function: Release the stowed solar array to initiate unfolding.

Type: Pyrotechnically operated

Rating: Later

5.5.4.2.19 J2002, P2002 Inflight Disconnect, Aeroshell/Lander (connector, electrical: electromechanically disconnected)

Function: Provide remotely operable, electrical disconnection between the aeroshell and the Lander vehicle during Martian entry flight.

Type: Hot-wire operated push-off type collet lock-unlock connectors with crimp insertable cuperic contacts and 360° RFI shielding.

Rating:	Circuits	10 pins
	Wire sizes	later
	Operate time	less than 100 msec
	Operated signal	3.5 amp for 50 msec

Safe level	1 amp, 1 watt, for 5 min
Release impulse	later
Reliability	0.995 at 90 percent confidence each device

5.5.4.2.20 J2003, P2003 Inflight Disconnect - Thrust Cone/Lander
(connector, electrical; electromechanically disconnected)

Function: Provides remotely operable electrical disconnection between aeroshell and the Lander vehicle during Martian entry flight.

Type: Hot-wire operated push-off type collect lock-unlock connectors with crimp insertable cuperic contacts and 360° RFI shielding.

Rating:

Circuits	59 pins
Wire sizes	later
Operate time	less than 100 msec
Operated signal	3.5 amp for 50 msec
Safe level	1 amp, 1 watt, for 5 min
Release impulse	later
Reliability	0.995 at 90 percent confidence each device.

5.5.4.2.21 WL1 - Lander Command Cable Assembly

Function: Provides command and signal distribution from the Lander programmer to various receiving equipment.

Type: Copper conductor electrical cable insulated with Kapton and teflon (HF +1/2 T) in a wrapped construction. Cable connectors of NAS 1599 type and modified in selected cases to permit high density inserts and rear insertion construction.

Rating: Later

5.5.4.2.22 WL2, WL5, - Lander Power Cable Assemblies

Functions: Provide electrical power distribution throughout the Lander, from the power controller and batteries to the various loads.

Type: Copper conductor electrical cable insulated with Kapton and teflon (HF + 1/2 T) in a wrapped construction. Cable connectors of NAS 1599 type and modified in selected cases to permit high density inserts and rear insertion construction.

Rating: Later

5.5.4.2.23 WL3 - Lander Instrumentation Cable Assembly

Function: Distributes data from sensors and payload instruments to data conditioners, encoders and telecommunication equipment in the Lander.

Type: Copper conductor electrical cable insulated with Kapton and teflon (HF + 1/2 T) in a wrapped construction cable connectors of NAS 1599 type and modified in selected cases to permit high density inserts and rear insertion construction.

Rating: Later

5.5.4.2.24 WL4 - Shielded Lander Cable Assembly

Function: Provides coaxial transmission of signals and high frequency energy through the Lander.

Type: Copper conductor electrical cable insulated with Kapton and teflon (HF + 1/2 T) in a wrapped construction cable connectors of NAS 1599 type and modified in selected cases to permit high density inserts and rear insertion construction.

Rating: Later

5.5.4.2.25 WL6 Coaxial Cable Assemblies

Function: Carries i-f power to the antenna and signals from the antennas to the receiver.

Type: RG 58

Rating: Zc 50 ohms

5.5.5 ENVIRONMENTAL CONTROL

The mission weight and reliability constraints are such that the environmental control system complexity and design margins must be the minimum possible. In line with this objective, a semi-passive method of thermal control utilizing an insulated payload, optimum surface radiative coatings, and local electrical heaters was selected to satisfy the thermal control requirements.

The Lander configurations present an ideal approach for providing the necessary payload thermal insulation. The 1-1/2 in. thick honeycomb container structure will be utilized, thereby eliminating any additional space requirements for the insulating material. A low thermal conductivity core material (phenolic glass) with foam insulation packed cells will be utilized to control the Lander temperature response. Detailed insulating tradeoffs are presented in the parametric data (Section 4.4, Vol. III). By adding the foam insulation the heat transfer losses are reduced to a conduction mode only with a relatively high thermal resistance. This is desirable since the radiative and convective heat losses between the honeycomb face sheets could be considerable, based on:

1. Radiation across the cell ends could be significant with a possible outside surface temperature of -60°F and an inside structural temperature of 50°F .
2. Although a reduced atmosphere exists, by minimizing the heat transfer coefficient some convection losses could be present in the air space, thereby contributing to the overall heat loss.

This conceptual design produces a shell around the payload which has a thermal conductance value of $0.36 \text{ Btu/hr} - ^{\circ}\text{F-ft}^2$. Therefore, the payload has sufficient thermal isolation that its minimum temperature will not fall below -40°F , the lower allowable limit for all of the payload components except the battery. To maintain the battery at or above its minimum operation temperature of 50°F , it is thermally isolated from the payload with an insulated package which contains an electrical heater. This heater is thermostatically controlled to turn on when the battery falls below 50°F .

A transient solution was performed to determine the temperature response of an isothermal payload and battery in the Martian environment. Appropriate conduction and radiation was considered based on the Lander configuration. For minimum heat leak, a low surface emissivity of $E_{\text{OS}} = 0.1$ was assumed. Results of this analysis are shown in figs. 5.5.5-1 through -4. Figs. 5.5.5-1 and -2 show the battery temperature response and heater power necessary to maintain the battery at 50°F . The temperature response of the payload for the minimum and maximum environments are shown in figs. 5.5.5-3 and -4 respectively. These show that no heater power is required to maintain payload temperature above -40°F .

The transmitter temperature response was studied as a function of daily transmission power with the resulting analysis indicating that no protection in the form of thermal storage material is required to prevent overheating. The specified power level of 32.5 watt-hr/day will only produce an 18°F temperature rise resulting in a peak temperature of 138°F .

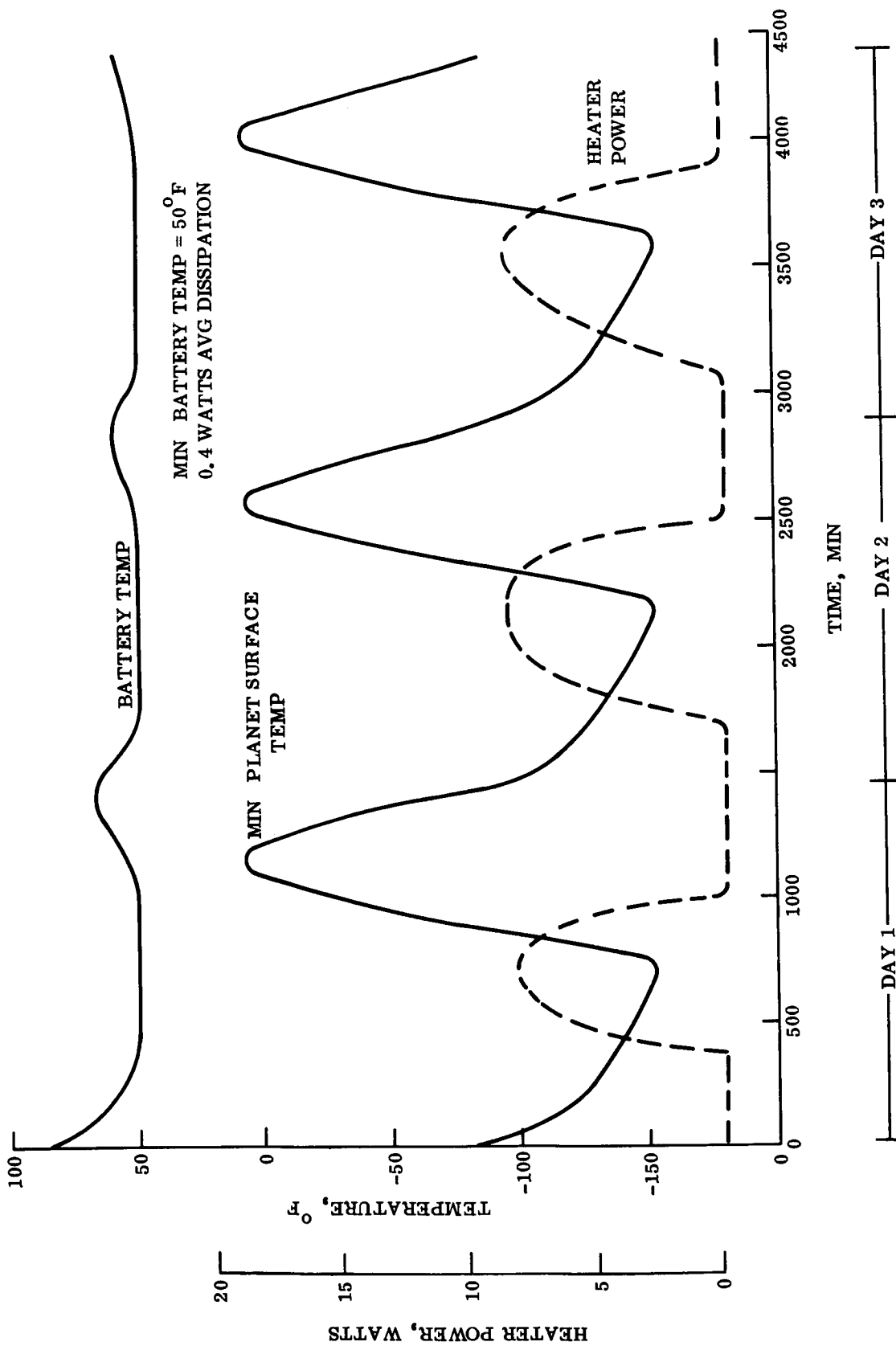


Figure 5.5.5-1. 90-Day Lander Heater Power Requirements for Thermal Battery Control, Minimum Environment

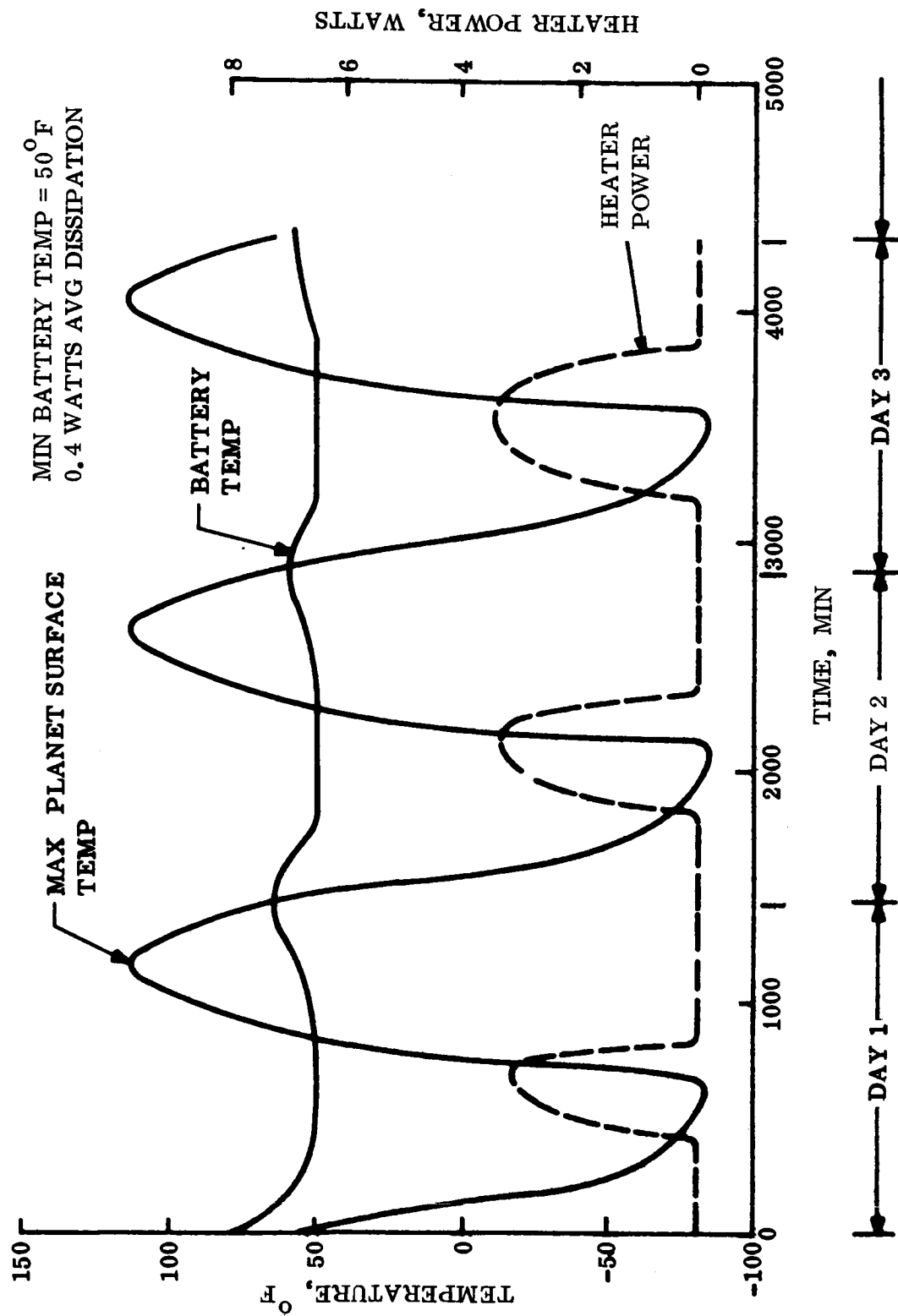


Figure 5.5.5-2. 90-Day Lander Heater Power Requirements for Thermal Battery Control, Maximum Environment

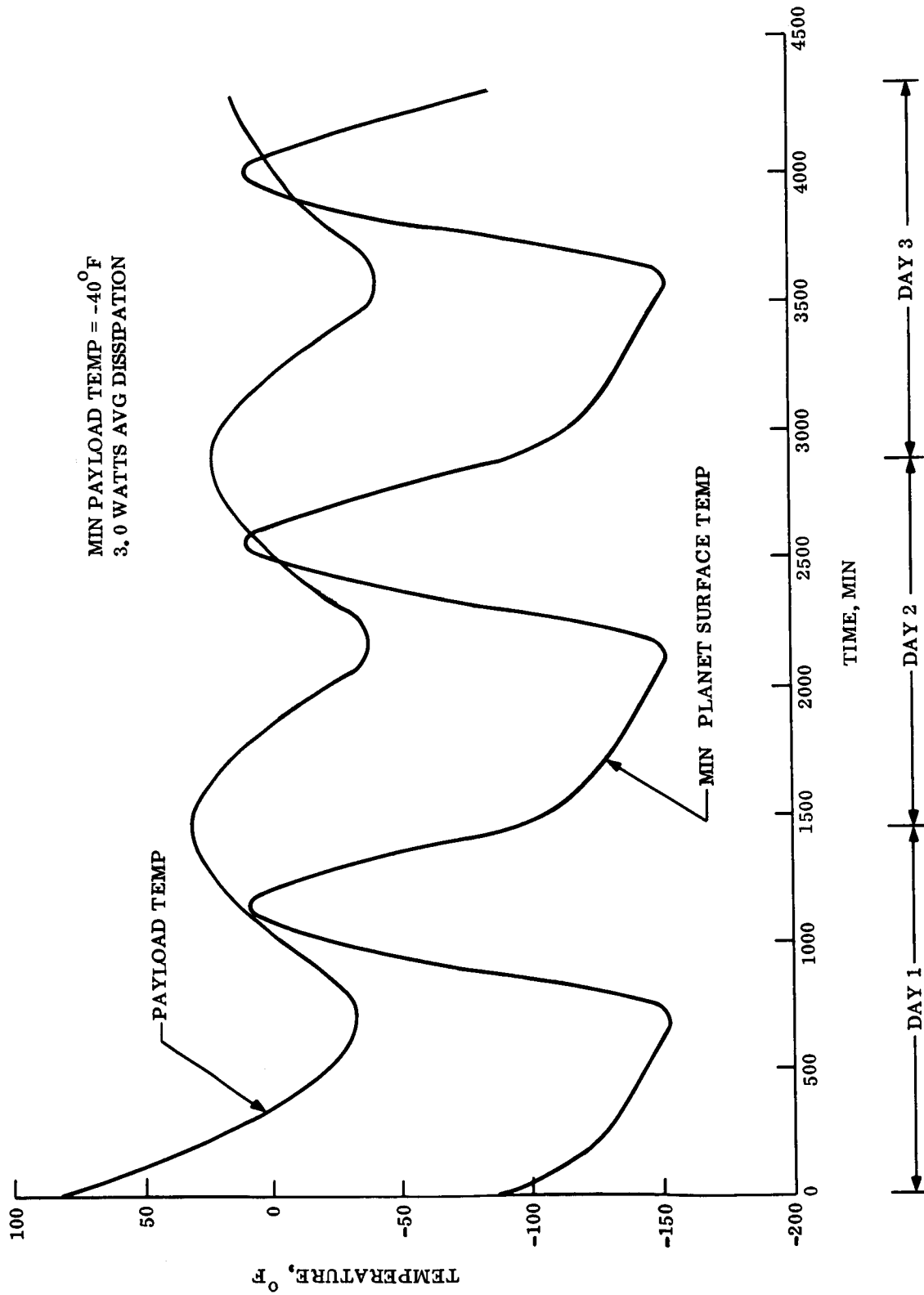


Figure 5.5.5-3. 90-Day Lander Payload Temperature Response, Minimum Environment

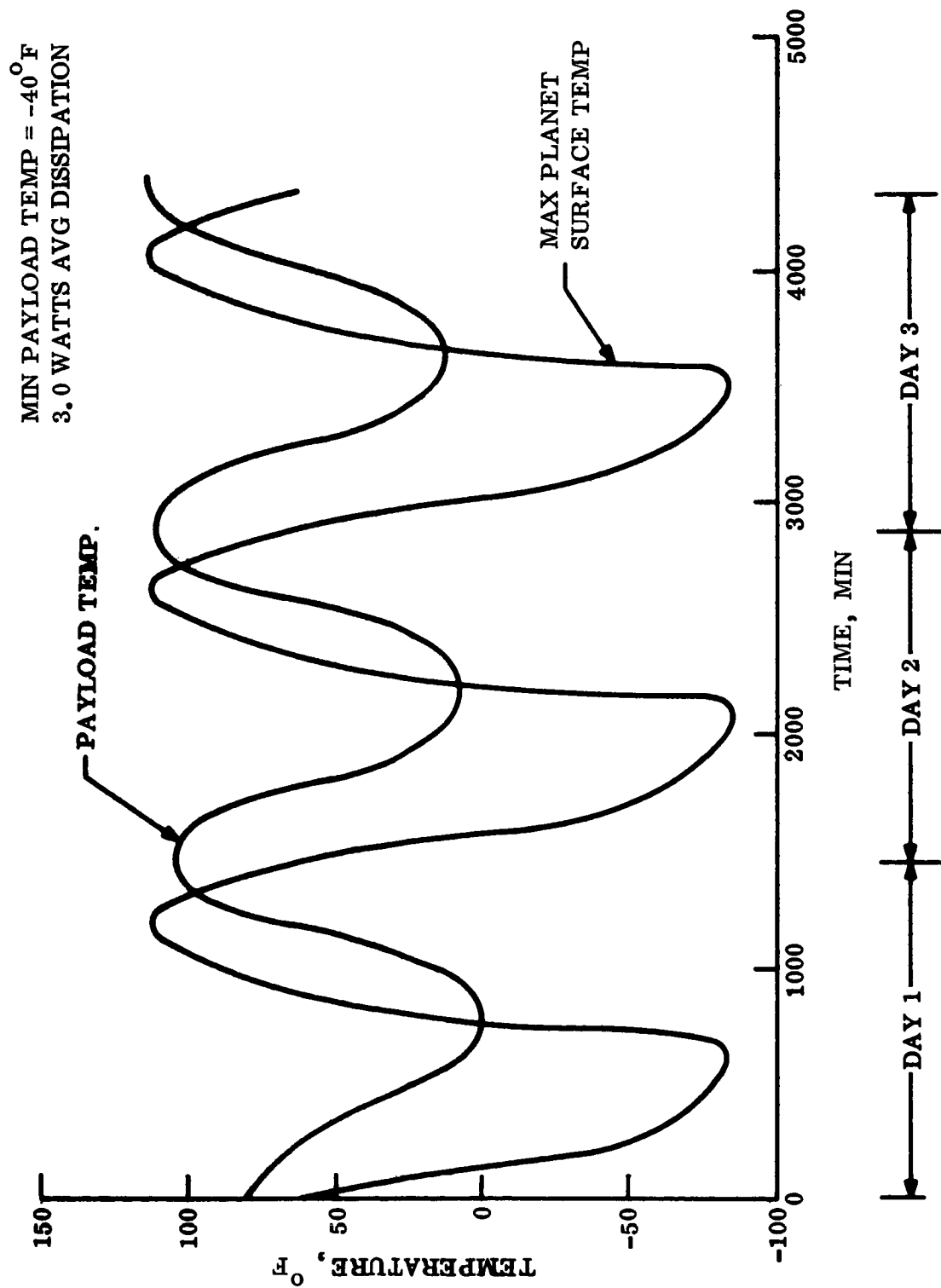


Figure 5.5.5-4. 90-Day Lander Payload Temperature Response, Maximum Environment

5.5.6 DEPLOYMENT MECHANISMS

In the landed position either side of the vehicle may be uppermost, so provision has been made for the deployment of instruments and equipment from both sides of the flat pack container. However, to avoid unnecessary duplication of the instruments, the actuating mechanisms have, in general, been designed for two way operation. A g-sensing device will determine the direction of deployment operation.

Instruments deployed in Point Design 3 are: four cameras (two high and two low resolution), ten wind velocity transducers (two sets of five), four temperature transducers and one surface composition (alpha back scatterer) instrument head. All except the alpha back scatterer are located in a central bay the full width and depth of the Lander container, as shown in fig. 5.5.1-1. The alpha back scatterer is located in an individual full depth bay, also shown on the drawing.

5.5.6.1 Camera Installation, Deployment and Mechanism

The camera(s) and swinging boom(s) installation and associated mechanism is shown in detail in fig. 5.5.6-1.

Each of the four cameras is mounted on the free end of pivoted tubular booms. The booms are aluminum alloy material approximately 36 in. long and 2 in. outside diameter. They rotate through approximately 90° in either direction, as shown from the installed horizontal position so that when erected, two are side by side at opposite edges of the Lander, one with a high and one with a low resolution camera. This arrangement of relatively short swinging booms, with the capability to erect four cameras on either side of the Lander and take pictures over the edge of the Lander in segments shown in the insert on the drawing, was selected as the most satisfactory compromise between the need for simple and stable erection devices and mechanism and the requirement for adequate azimuth and vertical angles of uninterrupted vision. Deployment design with telescoping (not hinged) tubes, cannot easily be made to work in two directions, and investigations proved that unless the number of cameras was doubled, the telescopes had to be many feet in length, to provide adequate vertical angles of vision over the edge of Lander and impact attenuation system. Deployment booms of such length pose serious problems regarding camera stability. Stowed, the cameras and booms lie horizontally across the Lander in a block of four. Saddles on the inside of the jettisonable doors covering the camera bay clamp the booms securely to withstand the 'g' forces imposed, in particular during the landing phase. The booms are spring-actuated to move through 90° in either direction from the stowed position by a single torsion spring around the hinge pivot, which is restrained in a neutral setting when the bay doors are assembled. Release and jettison of the camera bay door from the uppermost exposed side of the Lander unclamps the boom(s) and releases one end of the torsion spring to pick up a lever on the boom and effect its rotation. Thus, boom operation is automatic once the appropriate cover door has been jettisoned. All four booms are individually operated by the same spring-loaded principal; the two lying deepest in the Lander from the exposed side are restrained to move until the two uppermost

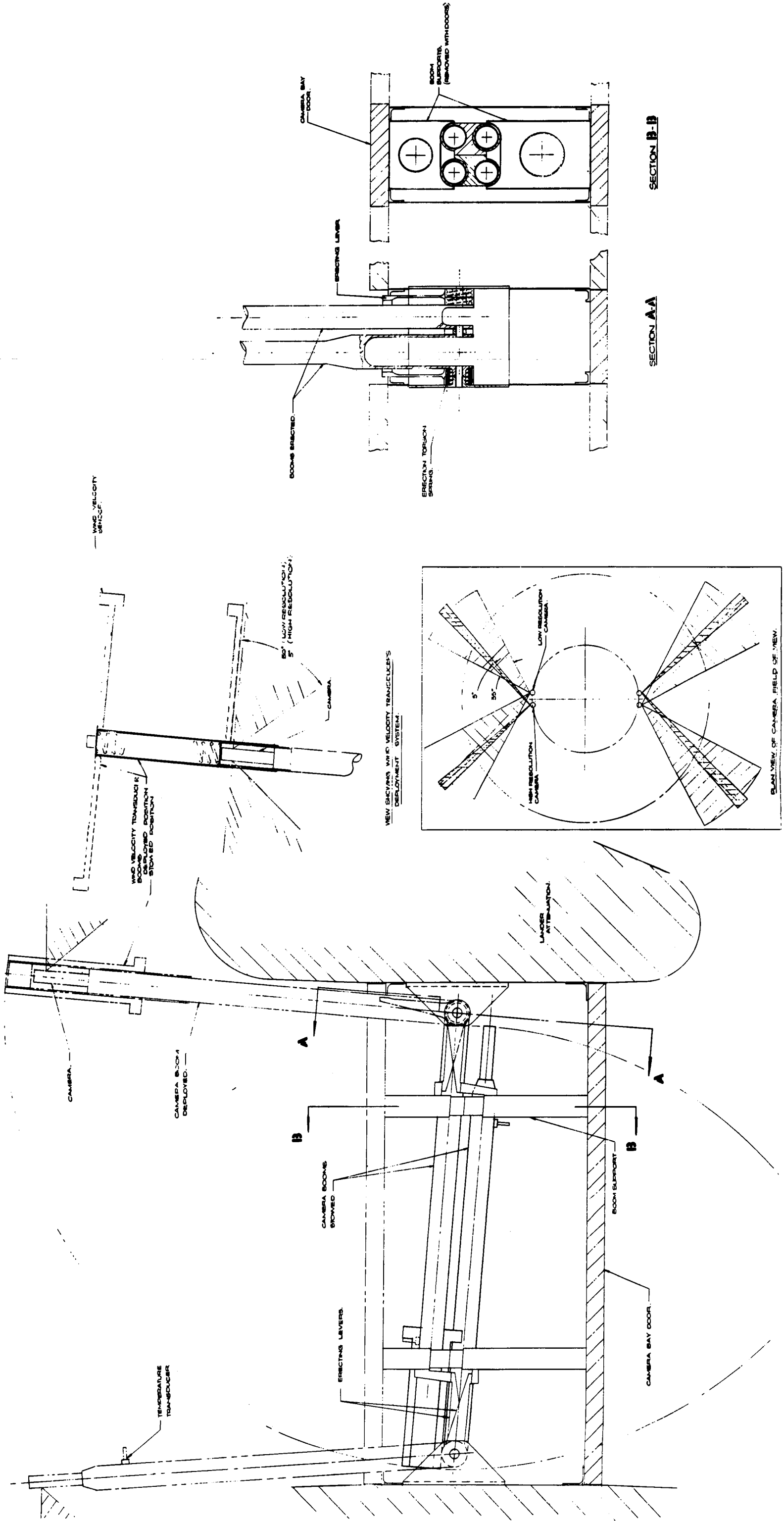


Figure 5.5.6-1. Camera Deployment, Including Wind Velocity and Temperature Transducers

ones are deployed and are unlocked by the final motion of the upper booms. This is a simple and automatic sequencing for the four boom arrangement. The cover door(s) are secured with bolts incorporating a hot-wire release and jettisoned by springs with sufficient force to ensure that they fall clear of the Lander.

5.5.6.2 Wind Velocity and Temperature Transducers

Five wind velocity transducers constitute a set necessary to obtain wind measurement data. Four are mounted in a plane at 90° to each other on a 2 ft pitch circle diameter, the fifth is mounted below one of the other four to provide a vertical reading. As stated in Section 5.5.2 the instruments are acoustic devices requiring unimpeded line of sight between each sensor. In the arrangement shown in fig. 5.5.6-1 the transducers are attached to the ends of spring-loaded arms, which are mounted on a telescoping extension of the camera booms and unfold when the boom triggers a release mechanism as it locks into the erected position.

The weight involved in the installation of a set of wind velocity transducers is very small and two sets have been provided on two camera booms for redundancy.

A temperature transducer is mounted directly on each of the four camera booms at the base of the camera.

5.5.6.3 Surface Composition (Alpha Back Scatter)

Although this instrument has not been completely designed, analysis has provided preliminary weight, volume, deployment and other requirements. The installation and deployment approach herein is based on a conceptual design which is illustrated in fig. 5.5.6-2. The Surveyor alpha back scatter instrument has been referred to and utilized to some extent.

The instrument sensor head is installed on its side in the bay provided in the Lander container. The head will be firmly clamped against a pivot bar, in the stowed position, by a soil calibration sample holder extended across the bay and secured to the vertical side walls. When the calibration phase of the alpha back scatter instrument is completed the sample holder will be moved away from the back scatter instrument head either linearly along the bay or by rotation. The function will be performed by a pin pulling device and spring-loaded mechanism. The instrument head is now free to rotate through 90° due to its offset c.g. and the force of gravity and drop through the bottom side of the Lander attached by the control cord and wire bundle provided.

Low friction guides will be installed on either side of the instrument head from the bay sidewalls to ensure that the head rotates and exits from the Lander with a smooth controlled motion.

Assuming that the head is prevented from being lowered completely clear of the Lander, it can operate equally well within the bay provided the surface is in good contact with the ground.

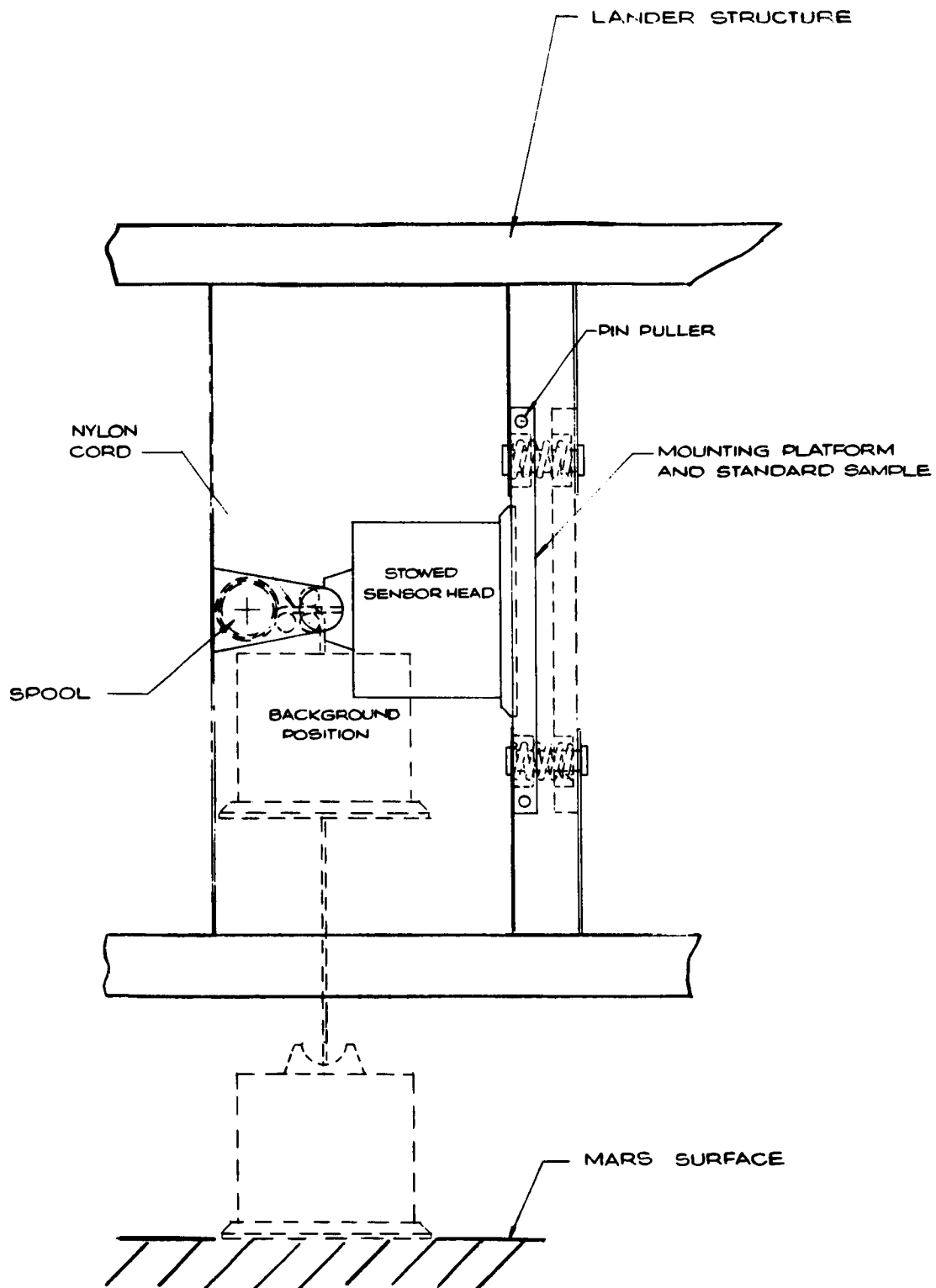


Figure 5.5.6-2. Operation of Alpha Back Scatter Deployment Mechanism

Covers over the bay provided in the Lander have been studied, but jettisonable or sliding doors are not desirable because of possible interference with the instrument head or jamming in the event of landing damage. Consequently, two inward opening hinged doors will be provided on either side of the Lander.

5.5.6.4 Solar Panels

Solar arrays have been installed in blocks in individual bays in the Lander. The combined deployed area of the arrays is 25 ft². Two installed arrangements are discussed which have been investigated to a preliminary design stage and have promise regarding feasibility. Other designs will continue to be investigated. Considering the two arrangements currently suggested, the basic scheme illustrated in fig. 5.5.6-3 utilizes two blocks of solar panels which are mounted in a compressed and locked condition vertically in approximately the center of full depth bays in the Lander container. The design is such that each block of solar panels can be deployed from either side of the Lander, whichever is uppermost. Deployed in either direction, the pantograph linkage between the solar panels in a stack, coupled with levers and a set of lazy tangs at each end of the stack, ensures that the solar cells on each panel face uppermost. Solar cells on one side of a panel only permit a shock cushioning material to be bonded to the other side; this separates the solar panels and protects the cells in the stacked condition, against the rigorous conditions imposed during landing. Stacked panels seem to be the most convenient arrangement for compact stowage and good deployment potential with the flat-pack Lander and selected impact attenuation system and this basic design offers a two directional deployment capability from each stacked pack.

To minimize the size of the bay required in the Lander for each pack and to facilitate the deployment of the array over the deep ring impact attenuation to a substantially horizontal position, deployment of the pack is in two stages. First, when the door on the exposed side of the Lander has been selected by the g-sensing device and released, the array is free to move to the surface of the Lander still in the stacked condition. The motive force is a compression spring. Compression springs are located on both sides of the stacked pack, between the pack and the cover doors. These springs can also function to jettison the door when the door attachments have been released.

When the stacked solar array is at the end of its vertical movement, locked and protruding from the surface of the Lander, a clamp compressing the panels into the stack is released with a hot-wire device. A one-twelfth horsepower electric motor mounted on the bottom of the stack drives through a gear box to actuate the lazy tang linkage at the bottom of the stack. This second stage action both raises and deploys the set of solar panels in one movement sideways over the impact attenuation to the final horizontal deployed position. Two motors are installed, one for each direction of deployment of the stack; thus, either one is operative to drive the solar array through this second stage to full deployment.

An assembly of 20 subpanels constitute a stacked array and each subpanel is approximately 7 × 11 in. Each panel, complete with structural backing, is 0.25 in.

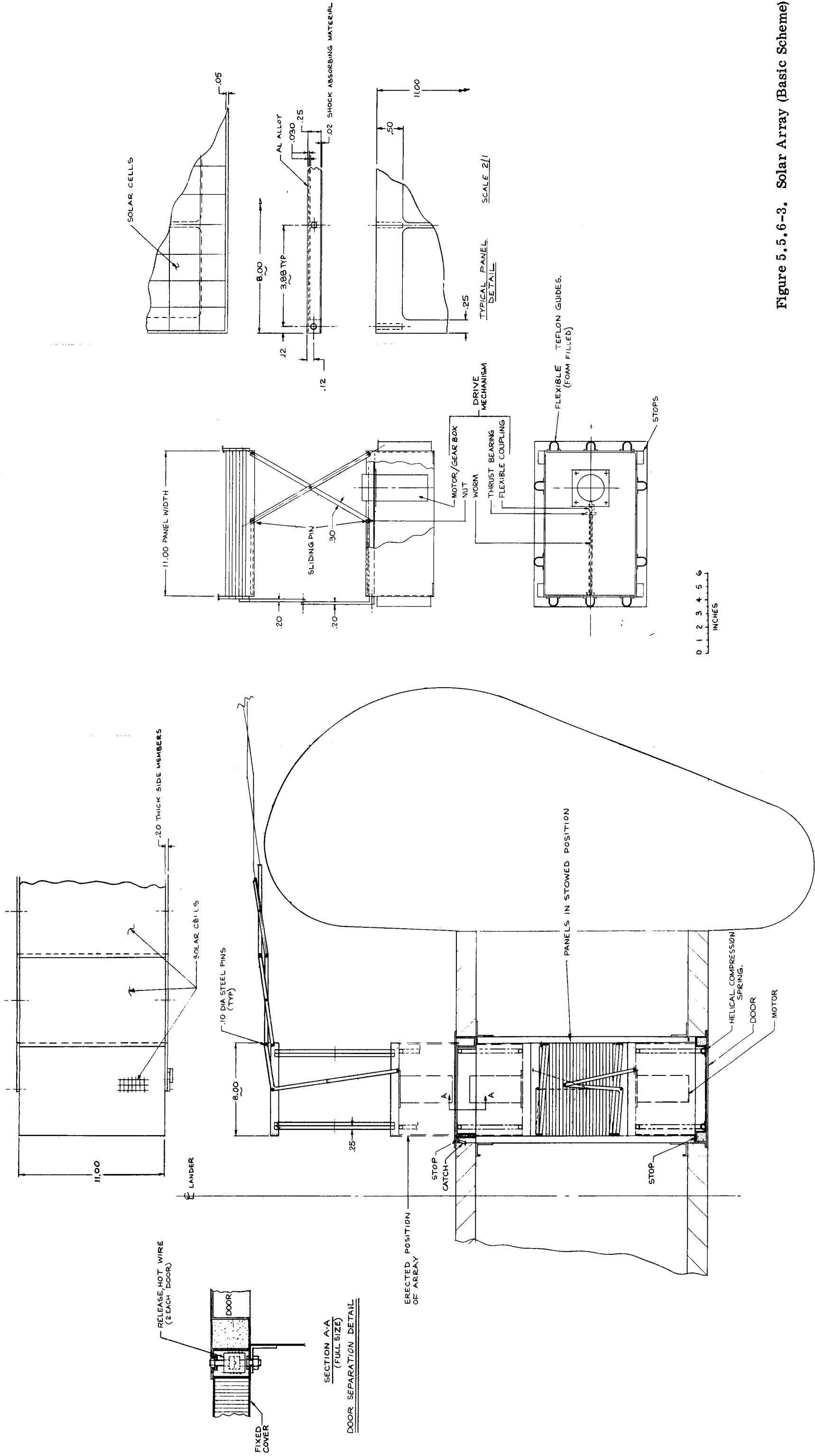


Figure 5.5.6-3. Solar Array (Basic Scheme)

deep based on the assumption that 0.025 in. maximum thickness solar cells with insulation will be bonded to a flanged metal base plate. The side links of the pantograph system are also 0.25 in. deep and required to be 0.20 in. thick at the center pin joint where bending is at maximum. It is intended that these links shall be steel, probably forgings. Pins are 1/8 in. diameter. It is recognized that this basic arrangement of solar array extends some distance over the edge of the Lander; however, it can be made quite rigid and if necessary the free end can be provided with extending feet to rest on the ground.

The second arrangement of solar array presented as an alternative provides the same total area of deployed solar array divided into four stacked blocks of panels of reduced depth on each side of the Lander container. The advantages are that each array deployed would not extend so far over the edge of the Lander; arrays can be deployed at 90° to each other in plan instead of 180° as for the basic scheme, with the possibility of increased electrical efficiency; that other equipment could be mounted underneath a solar array stack in the Lander, in other words, there is the possibility of more flexibility between solar arrays and other equipment in a tightly packed Lander; that loads on the solar arrays could be reduced, giving a potential saving in array weight. The severe disadvantage is that for a given total area deployed from one side of the Lander the installed area of solar cells doubles with a consequent appreciable increase in cost weight and volume. With this alternative proposal, which is only illustrated as a sketch scheme in fig. 5.5.6-4, the design principals, methods of actuation and deployment can be virtually the same as for the basic design.

5.5.6.5 Direct Link Telecommunication Antennas

With the installation of a direct link telecommunication subsystem, additional antennas are required. These have been located in the body of the Lander as shown in fig. 5.5.1-1. Details of the antennas are specified in Section 5.5.3.

Consistent with the principle that the Lander can settle on either side, duplicate S-band antennas have been provided to operate from both surfaces of the flat pack container. The location and installation is preliminary and subject to verification based on the antenna design and pattern definition, which is beyond the scope of the present program. If deployment is required the design can incorporate this capability.

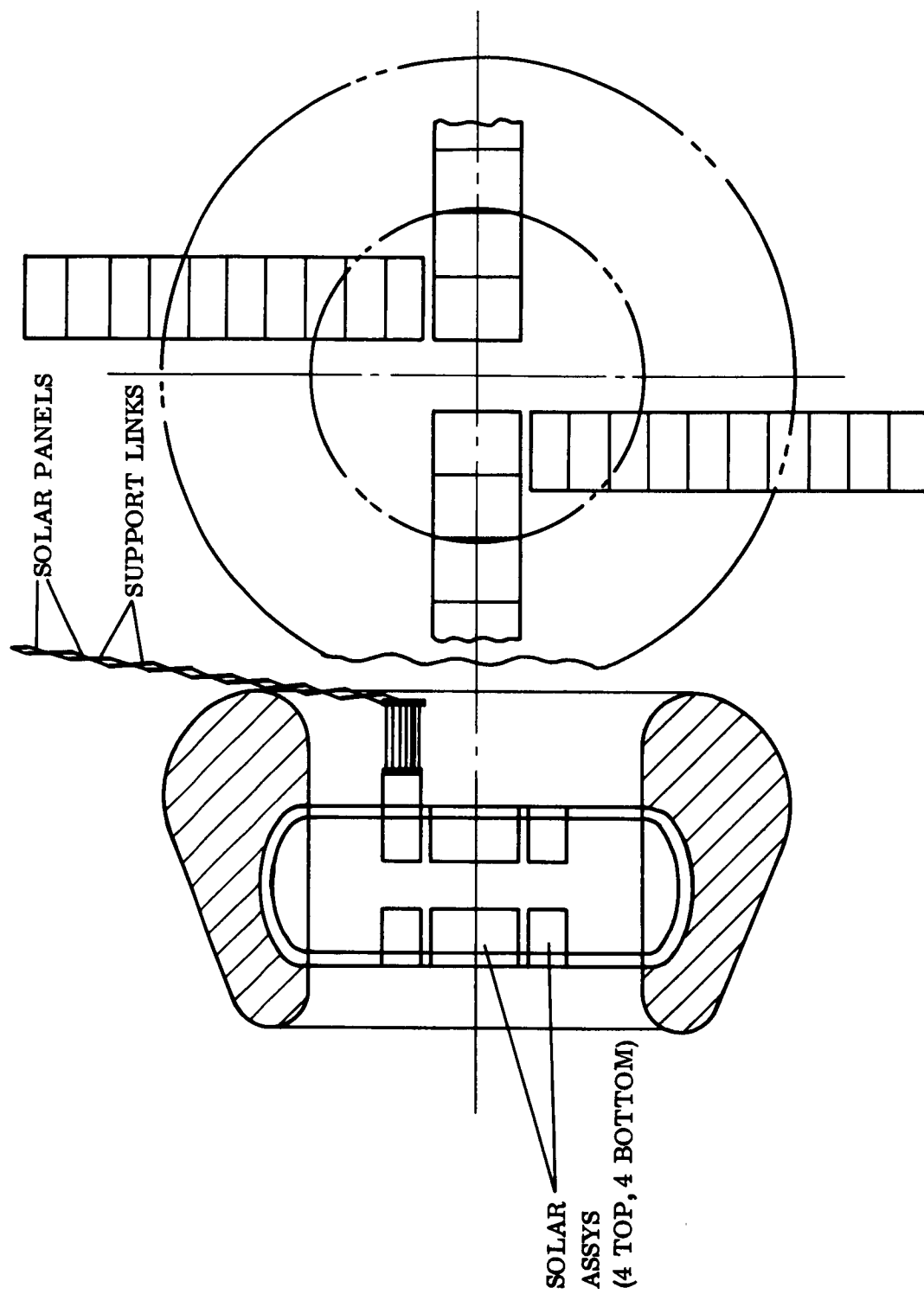


Figure 5.5.6-4. Solar Array (Alternate Scheme)

5.5.7 LANDER CONTAINER STRUCTURE

The flatpack configuration for the landed payload container illustrated in fig. 5.5.7-1, was selected on the basis that it offers a good compromise between structural efficiency and all other design constraints, notably packaging and deployment of experiments. The following requirements and criteria were imposed for the design of this structure:

1. Design weight - 900 lb. This is used for structural design purpose and is based on total Lander weight less the material which is crushed during primary impact.
2. Local pressures and inertia loads resulting from impact up to 1000 g.
3. Limit design factor - 1.0.
4. Ultimate design factor - 1.25.

Based on the requirements and constraints which are present, a design has been evolved which has the following significant features:

1. A full-depth inner space frame module to contain most instrumentation and sub-systems. This module can be removed from or inserted into the flatpack as a bench sub-assembly.
2. Individual components can be added or removed from the top or bottom of the space frame while installed in the container.
3. A dual purpose space frame which acts as primary structure and component support.
4. Jettisonable and hinged doors for deployment of camera and alpha back scatter, respectively.
5. A primary structure consisting of a D-shaped toroid section supporting the impact attenuator, combined with the inner space frame.

The container consists of three basic elements: the D-shaped toroidal edge structure, the inner space frame, and the top and bottom covers and doors. (See fig. 5.5.7-1.) This complete assembly is designed to withstand the forces generated by initial impact at 1000 g's and any forces resulting from subsequent impact after rebound.

The D-shaped edge structure acts as a primary load path for distribution of impact attenuator loads. The outer shell of this section is tied to the cylindrical wall with radial aluminum sheet nose ribs, stiffened and spaced approximately every 5 in. around the circumference. These radial members transfer some of the loading to the internal cylindrical web and allow the section to act as a heavy ring frame, transferring load into the upper and lower cylindrical edge rings. Local loading up to 950 psi imposed by the crushing honeycomb is resisted by the outer shell of the D-shaped section which is a 1-1/2 in. thick fiberglass honeycomb (3/16 in. cells) core with 0.08 in. aluminum face sheets. The cylindrical section is an 0.08 in. lightened and stiffened cylindrical shell. Except for items such as cable harnesses, it is not proposed to utilize the edge structure for packaging, and therefore, some structural deformation is tolerable.

The full depth cross members of the inner space frame stiffen the container against deformation from the cylindrical shape and resist bending of the flatpack, as well as providing component support. Two main cross members form the camera bay. These beams have 0.06 in. aluminum alloy webs, extruded alloy channel beams, and Z-section vertical stiffeners. There are seven secondary cross beams at right angles to the main beams. These are of similar but lighter construction of aluminum alloy. Top and bottom angle rings, 0.06 in. thick, and vertical angles at the junctions of the main and secondary beams and at the free ends of these beams complete the assembly. The inner space frame is attached to the D-section through the vertical flanges of top and bottom angles.

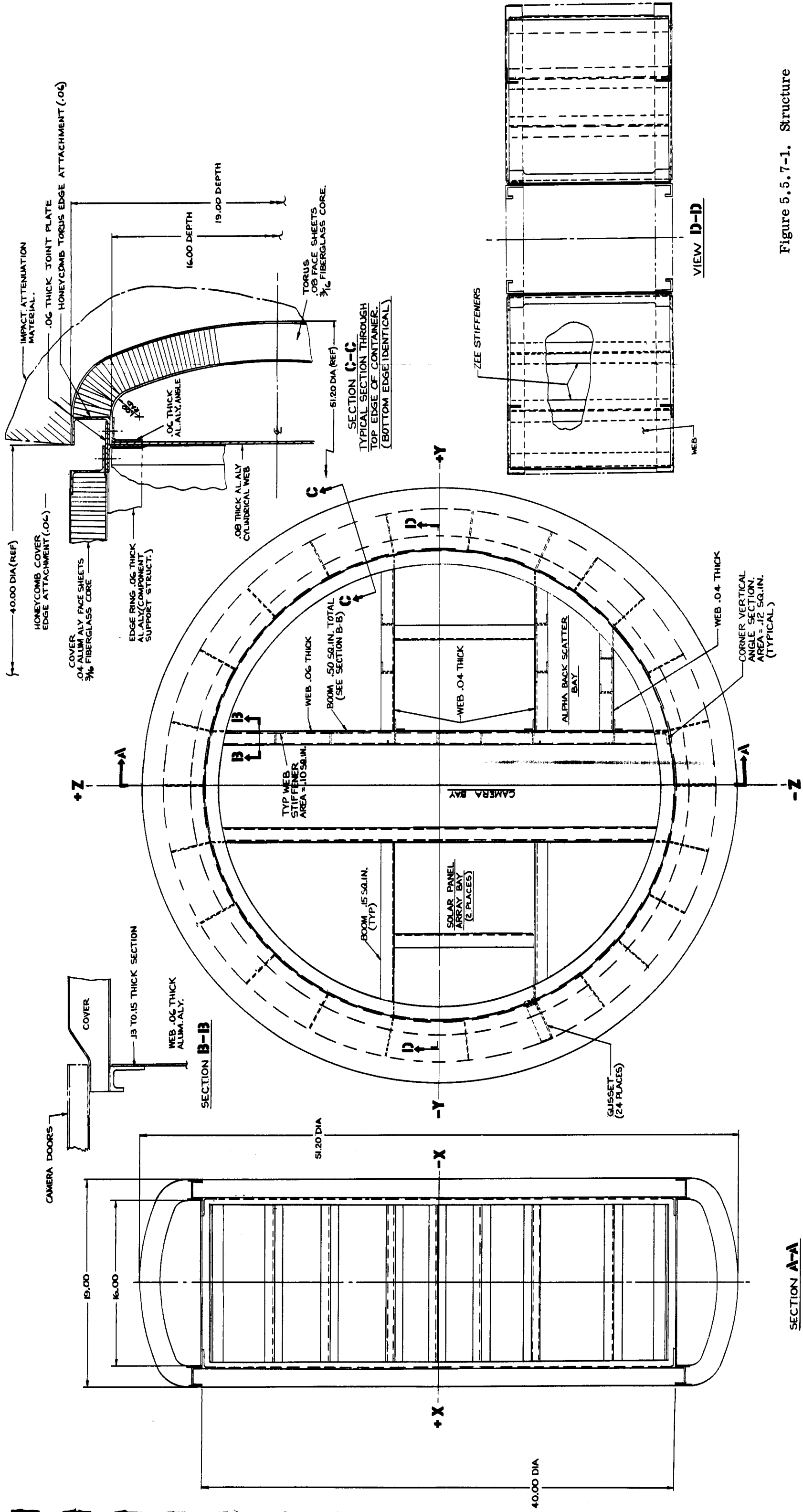
The top and bottom covers are considered secondary structure. They are 1.35 in. thick fiberglass honeycomb panels with 0.04 in. aluminum face sheets. A Z edge section is inserted for attachment. The edge members of the D-section, the inner space frame, and covers, when bolted together form strong rings at the top and bottom surface of the container.

Thick honeycomb panels with fiberglass core have been selected for the construction of the outer shell of the container as a means of satisfying both structural and thermal requirements. A possible alternative for the container outer shell could be reduced depth honeycomb panels with foam on the inner side. Additional investigation will consider fiberglass facing sheets for all honeycomb panels used as a strength-to-weight trade-off. Surfaces of the full depth cross beams, which are exposed when the camera and alpha back scatter bay doors are jettisoned, are thermally insulated with a layer of foam to the full depth of the beam vertical stiffeners. The foam is covered with plastic coating to maintain integrity on landing impact.

A preliminary analysis, for critical loading points of three conditions shown in fig. 5.5.7-2, has been made and used to formulate the estimated weight of the container. Typical torus cylinder interface loads, for the edge impact condition illustrated, are shown in figs. 5.5.7-3 through -5.

FOLDOUT FRAME

FOLDOUT FRAME



SECTION A-A

SECTION B-B

SECTION C-C
TYPICAL SECTION THROUGH
TOP EDGE OF CONTAINER.
(BOTTOM EDGE IDENTICAL)

VIEW D-D

Figure 5.5.7-1. Structure

PLAN VIEW (COVERS REMOVED FOR CLARITY)

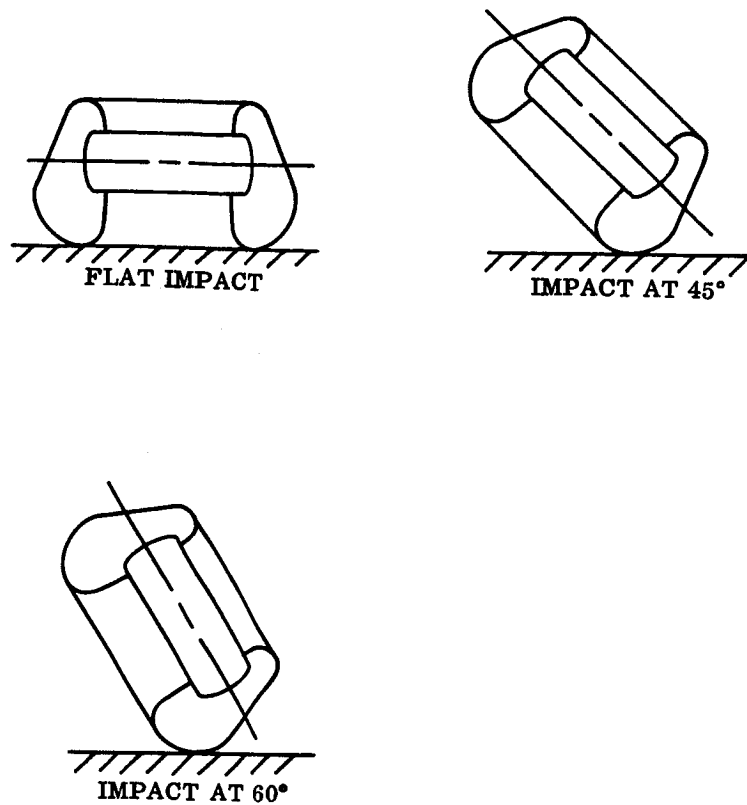


Figure 5.5.7-2. Three Conditions Used for Preliminary Loading Analysis (Multi-directional)

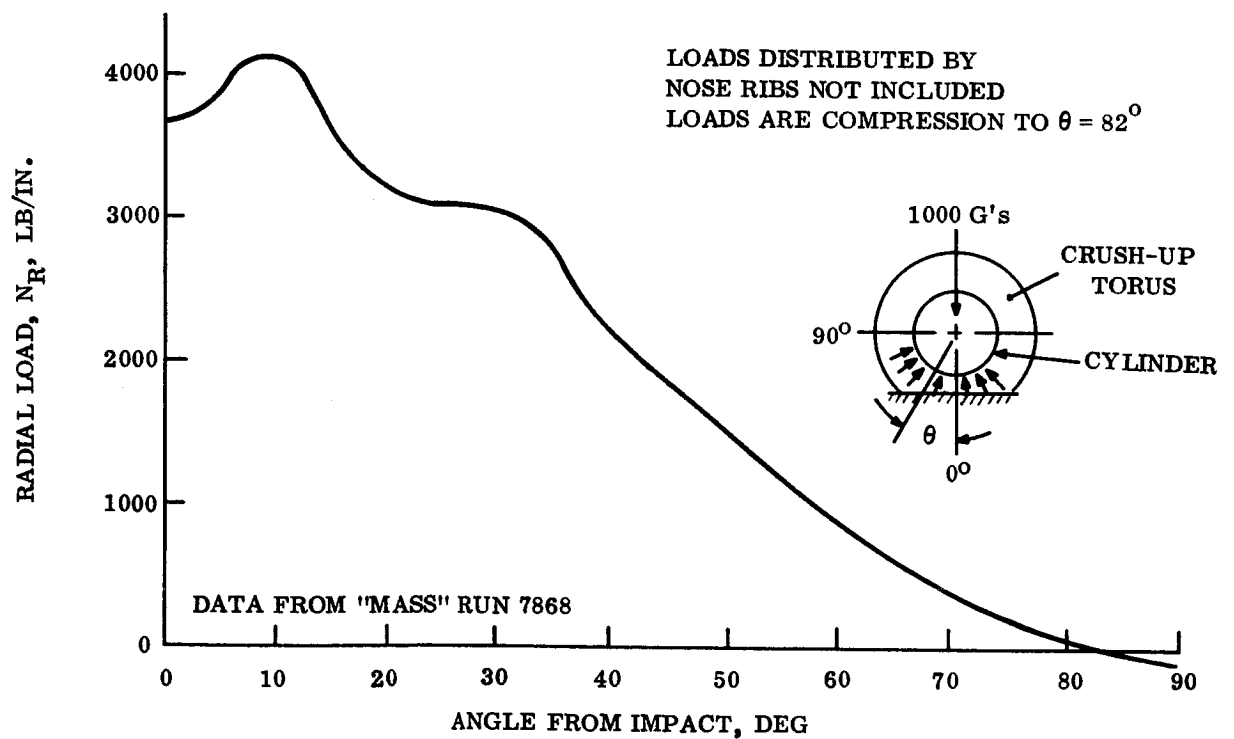


Figure 5.5.7-3. Typical Interaction Radial Loads Between Torus and Cylinder, Edge-on Condition

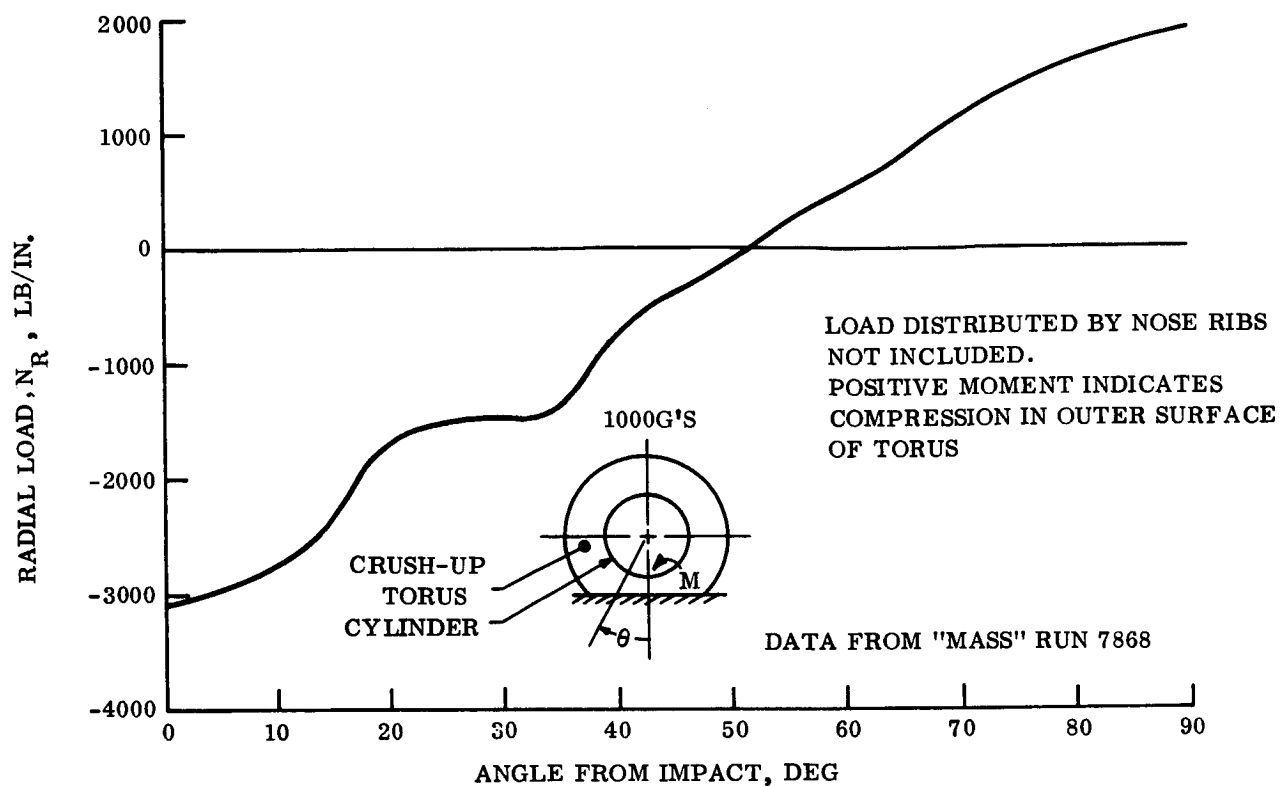


Figure 5.5.7-4. Typical Interaction Moment Between Torus and Cylinder, Edge-on Condition

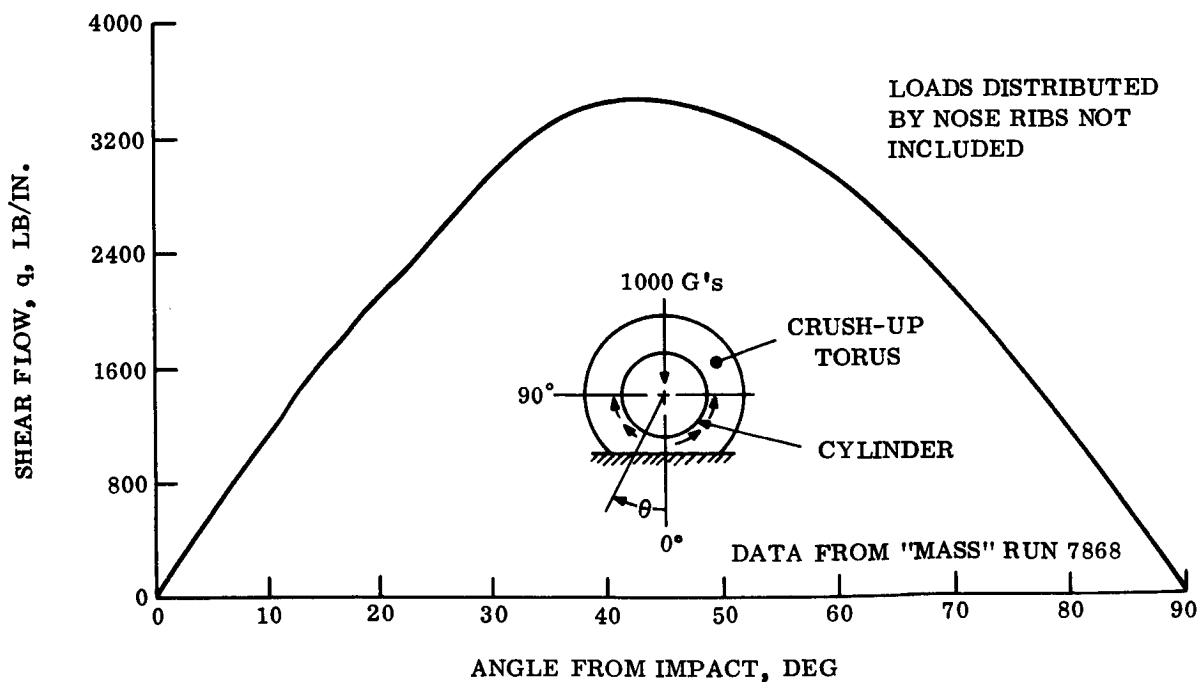


Figure 5.5.7-5. Typical Interaction Shear Flow Between Torus and Cylinder, Edge-on Condition

5.5.8 IMPACT ATTENUATION AND STRUCTURE

5.5.8.1 Attenuation Requirements and Criteria

5.5.8.1.1 Gross Vehicle Response

The mechanical crush-up impact attenuation system is designed to provide sufficient stopping distance to decelerate the Lander within the allowable g-limits while dissipating the impact kinetic energy. At the same time the acceleration pulse must have a sufficient rise time and be essentially broad and flat. The honeycomb phenolic fiberglass material inherently behaves in a manner which produces this behavior.

5.5.8.1.2 Response of Individual Components

Initial studies have been performed to determine the feasibility of further attenuating the impact acceleration levels experienced by individual components carried by the Lander. These are reported in Volume IV, Appendix A. The conclusions drawn from this appendix indicate that it does not appear feasible to obtain significant reductions with shock mounts or by component mounting stiffness tailoring. These devices are of primary use in minimizing g-level amplification effects.

5.5.8.1.3 Angular Accelerations: Their Effect on Components

It appeared that if the Lander impacts on one edge, there was the possibility that high angular accelerations might produce high loading on components located at the outer extremity of the container. This situation is studied in Appendix IV-A. The conclusion reached is that such high angular acceleration g's will not occur.

5.5.8.1.4 Selection of Phenolic Honeycomb as the Reference Material for Impact Attenuator Design

Phenolic honeycomb was selected as the reference material for this study for the following reasons. Both balsa wood and phenolic honeycomb are feasible materials for the size and weight vehicles being examined herein. Both materials can function at the operating g-levels anticipated with a Hard Lander system. However, the balsa wood can be adversely affected by exposure to the sterilization cycle. In past tests, balsa wood has split after being subjected to dry heat sterilization. Careful control of the wood moisture content can, however, probably eliminate this problem. Balsa wood has the added disadvantage that its material properties have been known to vary from ± 15 to ± 50 percent. This is significant since balsa, being a natural material, cannot be further developed to a significant extent. Phenolic honeycomb, on the other hand, has been improved in the past and this trend can be expected to continue.

5.5.8.2 Environmental Definition and Interpretation

Appendix IV-B contains the detailed account of the specification used in the point design. Included are discussions of surface strength, friction, slopes and rocks. The wind specification for the point designs is also elaborated upon.

In brief, the point design is capable of impacting an infinitely hard surface with friction, 5 in. rocks and slopes up to and including 34° from the horizontal. The prevailing wind, blowing against the surface slope is the extreme value of 220 fps. Should the surface strength be less than attenuator stress, some penetration will be experienced but this is estimated as a few inches by the analysis in Appendix IV-B.

The important effect of a parachute sway angle (of up to 40° from the local vertical) was also examined. The chief result is that the sway angle couples with the surface slopes to require higher angles of the Lander to be analyzed for the initial impact condition. The significance is that an increment in honeycomb attenuator thickness over that thickness necessitated by a non-swaying vehicle must be incorporated on the Lander sides to allow for the swaying effect on vehicle orientation at touchdown. Details are given in Appendix IV-B.

5.5.8.2.1 Secondary Impacts of the Lander Vehicle

The combined environmental conditions of extreme wind, parachute sway and varying surface slopes warranted an investigation of post impact vehicle motion. In particular, the probability and significance of secondary impacts was reviewed. Appendix IV-B contains the dynamic analysis for the secondary impact problem as well as an initial probability estimate of the likelihood of occurrence of this event.

The statistical analyses were performed for the purpose of ascertaining the probability of experiencing a secondary impact velocity less than or equal to a chosen value. In particular, the value of 100 fps was investigated because this was the velocity used to size the top side of the multi-directional Lander. Based upon the limited first order approximation used, the following trends are indicated. For the extreme wind velocity of 220 fps the Lander flips over about 92 percent of the time and hits the second time on its top side.

In light of the new Mars Mission Specification (1968) of a design wind velocity of 110 fps, another probability estimate may be made. For this wind velocity, (but the same slope and sway angle variations) the Lander will flip over only about 25 percent of the time. Given that the Lander does flip, the secondary velocity will be 100 fps or less 81 percent of the time. If the analysis were adjusted to account for the new definition of surface slope of 20° (as contained in the Mars Mission Specification - 1968) this 81 percent figure would improve considerably. The foregoing brief summary identifies the surface wind specification as a critical design parameter.

5.5.8.3 Effect on Point Design Due to Perturbation in the Design Parameters

Appendix IV-C delineates the effects on the impact attenuation system design due to variations in the reference condition. These parameters in which perturbations are especially significant are also identified.

In general, lower wind and descent velocities, flatter slopes, softer surfaces, smaller rocks, lessened parachute sway, higher component g-tolerance and lower Lander weights than the corresponding design value enhance the point design integrity. Increases in velocities, slopes and parachute sway angle tend to compromise the

design integrity. Higher Lander weights than in the design condition and lower component g-tolerance tend to compromise the adequacy of the design.

Small increments in effective rock size are deleterious but, after a point, the rock becomes a large outcrop and is more of a hard surface than a penetrating hazard. It is noted that since the design is based on an infinitely hard surface no problem arises with an increase in surface hardness above that used in design computations.

Appendix IV-C also encompasses variations in honeycomb material properties. Specific comments identify the effects of variations in crushing density, specific energy, stroke efficiency, effective geometry and crush-up behavior.

5.5.8.4 Impact Attenuation Design Approach

The attenuation system design approach for Capsule Point Design 3 is now described. Fig. 5.5.8-1 is a sketch of the deep ring geometry for the Point Design 3 multi-directional Lander. In the design, the attenuation material is phenolic fiberglass honeycomb (3/16 in. cell size) of the type developed by GE-MSD under contract to the JPL. This material is of the hexagonal cell variety with parallel cells which can be wrapped with (R/t) radius to thickness ratios of greater than five. It is the reference material selected for use in this study and is currently used in the JPL drop testing program. This material is readily available from Honeycomb Products Inc. in densities of 4 to 12 pcf. The particular density used in the point design will be determined by the design conditions, especially Lander weight and allowable rigid body g-level. The performance of this thin dipped phenolic material varies depending upon its axial orientation with respect to the impact load vector. This is a key design factor investigated in the point design computation. The requirements of multi-directionality results in analyses of the Lander for various cutting plane orientations ranging from forward-flat on to aft-end-first (for a secondary impact). Requirements of multi-directionality lead to some weight penalties since material which is fully effective in one touchdown orientation may be of less or no value when other orientations are examined. Past analyses and judicious application of the specifications have indicated that three critical crush-up conditions must be analyzed. These are 0° (forward) impact, 90° (side-on) impact, and an intermediate surface slope impact. The intermediate slope has been taken as 34° for point design purposes. It is apparent that to adequately handle all of the highly probable impact conditions special attention must be directed toward the crush-up lay-up because of the material's variable effectiveness. For point designs this honeycomb lay-up is produced by cutting and segmenting the attenuator material to produce near-radial cell axis orientations with respect to the internal toroidal container structure. At the same time this segmented approach allows more efficient wrapping of the container. Refer to Section 5.5.8.5 for details. The same varying effectivity is also complicated by a geometric effect produced by the curvature of the Lander as seen in plan. The net result is that the area-stroke characteristics are direction dependent in a complex relationship. This means that the force stroke history is direction dependent and that, depending on the direction of impact the stroke (and thus the thickness) required will be different.

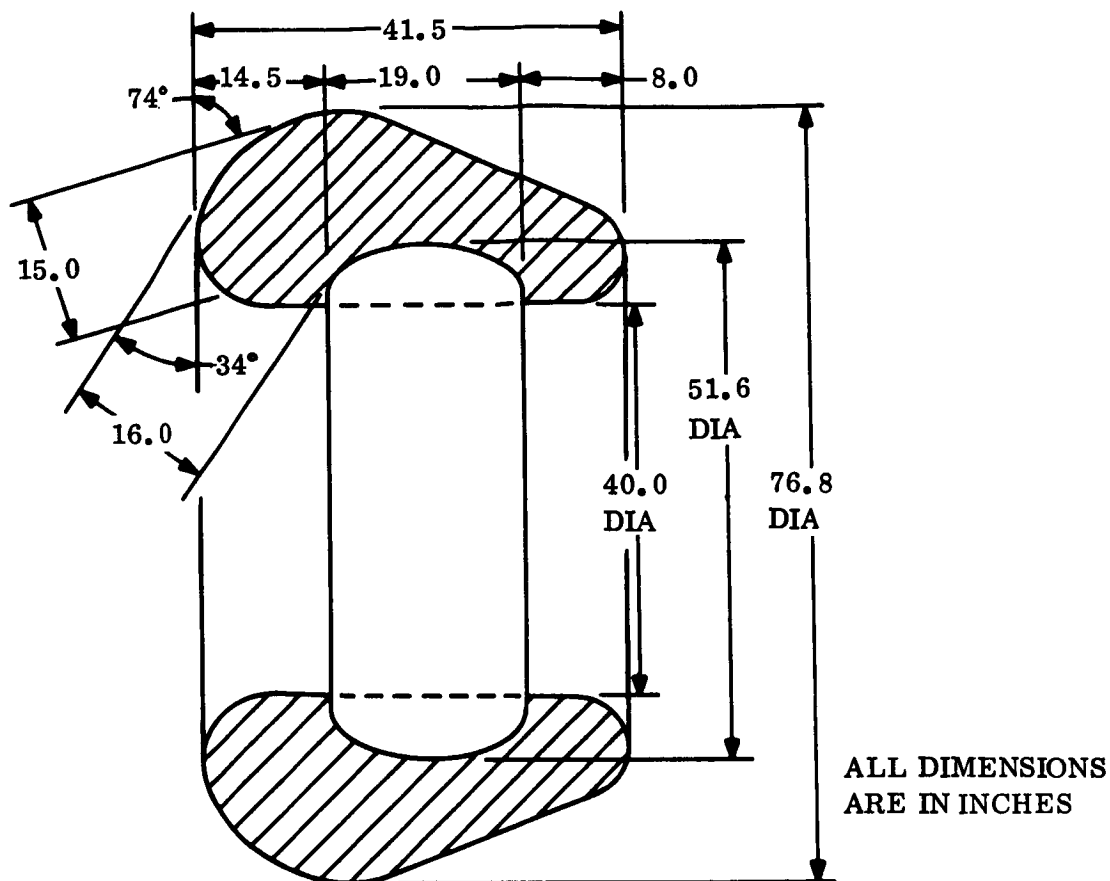


Figure 5.5.8-1. Lander Attenuation, Point Design 3

An additional geometric effect, distinct from that of crush-up directionality also enters the analysis. This is, for a given direction of impact a variable amount of honeycomb material is actively being crushed. Some material may be oriented in such a way that it experiences shearing forces. Because of this localized condition, bond line shear failures can result with little or no crush-up action. Such failures could occur without providing sufficient stroke capability. For this effect detailed design must ensure that sufficient material is working in each specific direction. Finally, attention must be directed toward the location of crush-up propagation. It is desired that the fracturing progress from the outside in and not from the payload to the extremity of the attenuator. Design details of the container/honeycomb interface and slight precrushing of the attenuator can eliminate this problem.

5.5.8.4.1 Analytical Details

With the above background point design analysis takes the following form. A series of CRUSH (geometrical program) runs were made for each prototype point design. The results were of the form of gross crushed cross-sectional area against stroke for various angles encompassing the operational map as defined in the specification. The geometric results were used to perform a direct graphical analysis of several multi-directional prototype shapes. The conclusions drawn from this thorough study provide the underlying logic for a computer assisted procedure to size the attenuator for point design purposes.

In fig. 5.5.8-2 plots of crushed area against stroke for a nominal size deep ring multi-directional Lander are produced. It is emphasized that this figure is for gross area with no directionality effects included. In fig. 5.5.8-3 plots of effective sectional area are provided. These plots were generated in the following manner. The phenolic material loses 2 percent of its strength per degree of obliquity between the longitudinal cell axis and the normal to the crushing plane.

The design guide for this reduction is fig. 5.5.8-4. This design guide is based upon test results summarized in fig. 5.5.8-5.

The data to support this procedure are reported in ref. 5-1. In addition, a 20 percent reduction is incorporated to account for the effect of curvature (in plan). The analysis also assumes that the active area encompasses all cells lying within 30° of the normal to the impacting plane examined and that all others are not actively crushed.

After examining various cutting planes for the Lander prototypes it was found that for the multi-directional Lander three principal strokes need be computed: dead on, side-on (90°) and 45° angular cutting plane. Actually, for sizing purposes there is small difference by passing the cutting plane at 34° or 45° . This is shown in fig. 5.5.8-2. From data similar to that in fig. 5.5.8-2 the principal strokes can now be computed by equating Lander normal kinetic energy to the absorbed energy due to crushing. For the prime (0° impact) case, it was found from analyzing several prototype multi-directional Landers that

$$\begin{aligned} \text{energy absorbed} &= \frac{1}{2} \frac{W}{g} (V_N)^2 = 0.77 \text{ WGS} \\ S_{(0^\circ)} &= 0.65 \frac{(V_N)^2}{gG} \approx \frac{0.6 (V_N)^2}{gG} \end{aligned}$$

where V_N is the impact velocity component normal to the plane, g is the gravitational constant and G is the allowable deceleration level in g-units. As described in Appendix IV-B it is assumed that the velocity component parallel to the plane is absorbed by surface sliding. This is why the normal velocity component is used in the stroke sizing computations. For the 45° and 90° side-on cases the same procedure applied to several cases yields on the average

$$\begin{aligned} S_{45^\circ} &= \frac{(V_N)^2}{gG} \approx \frac{0.6 (V_N)^2}{gG} \\ S_{90^\circ} &= \frac{0.5 (V_N)^2}{gG} \end{aligned}$$

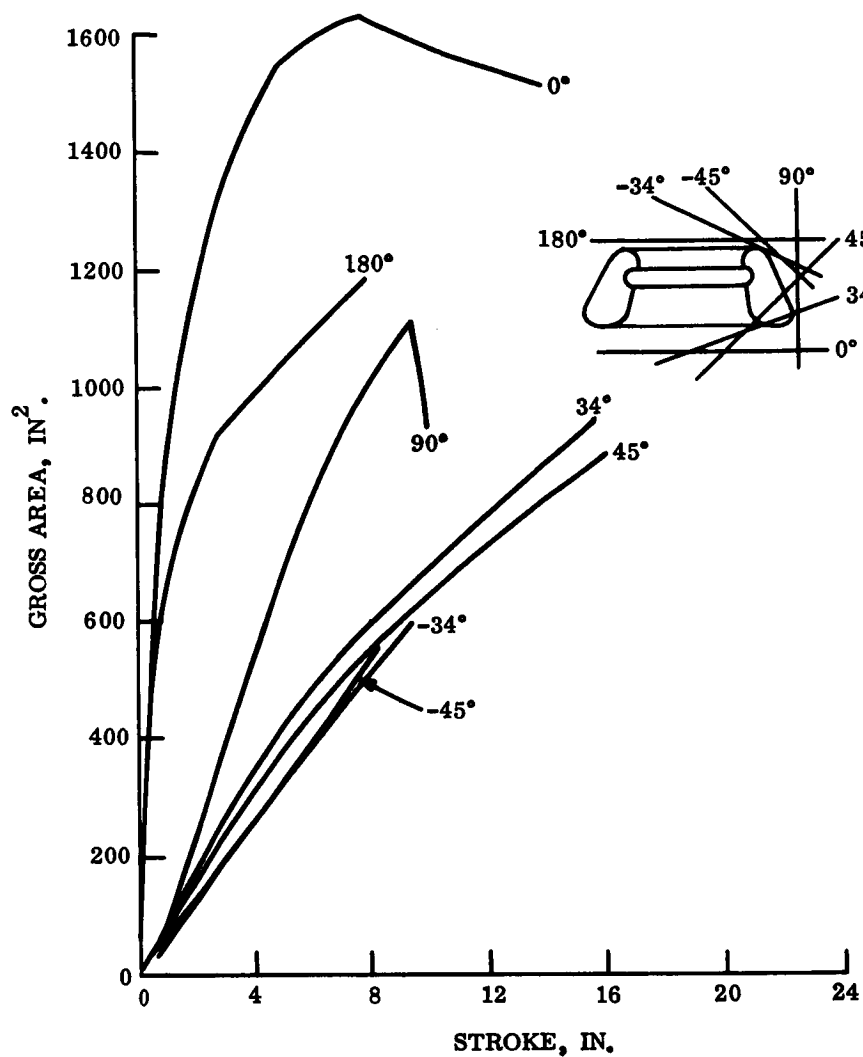


Figure 5.5.8-2. Gross Cross-sectional Area vs Stroke

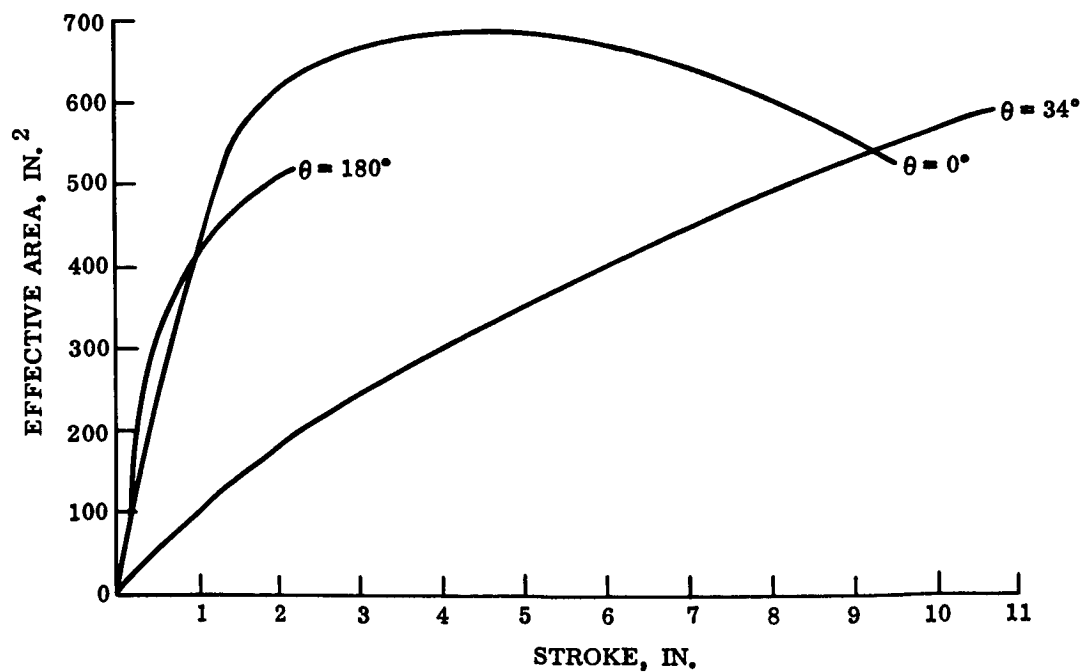


Figure 5.5.8.3. Effective Cross-sectional Area vs Stroke

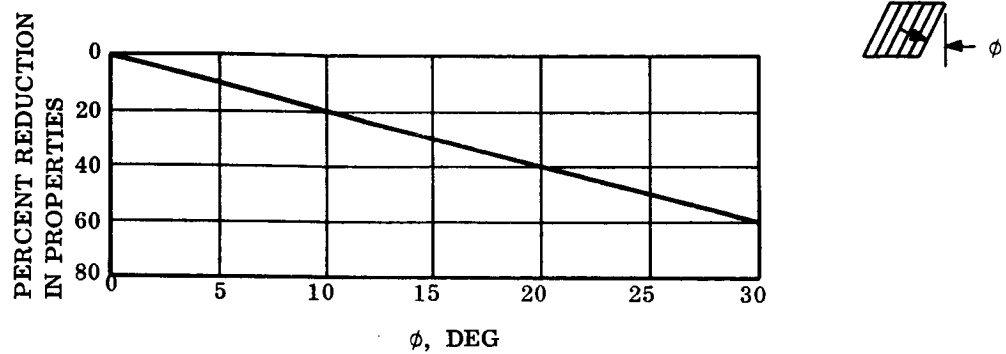


Figure 5.5.8-4. Design Guide for Reduction in Honeycomb Properties for Non-axial Impacts

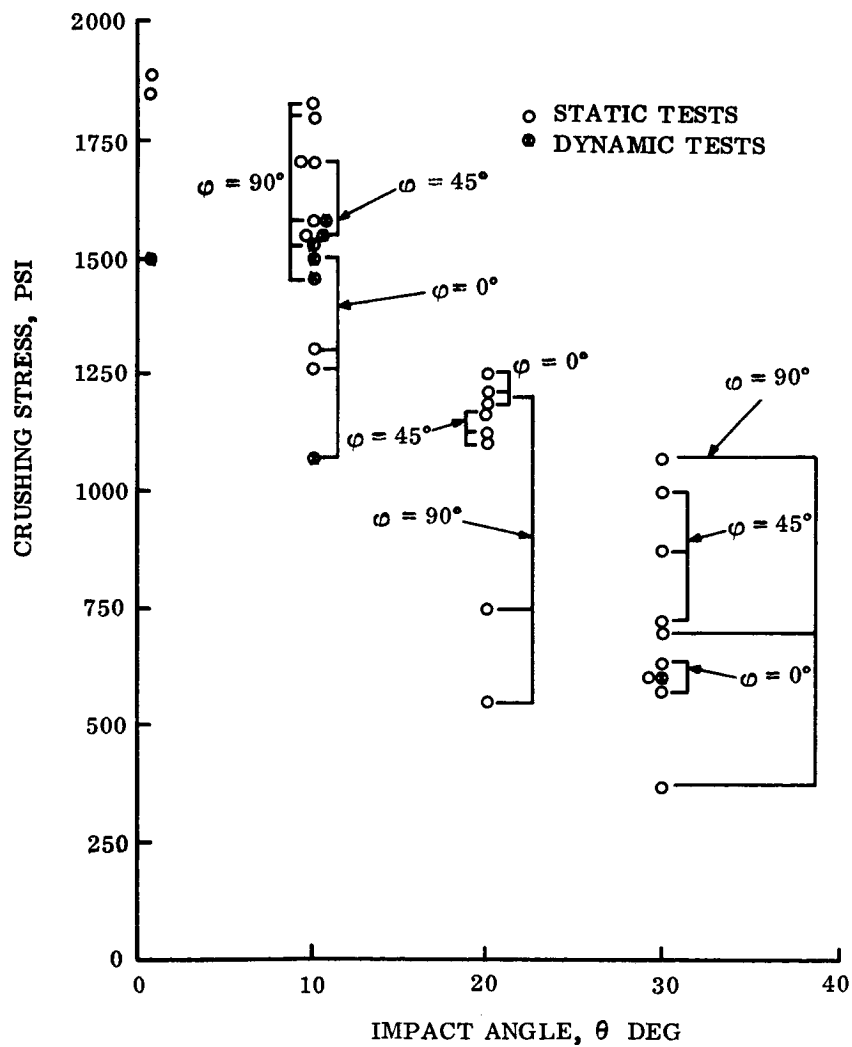


Figure 5.5.8-5. Comparison of Crushing Stress vs Angle-of-Impact for Static and Dynamic Loading

It should be realized that although these strokes are sufficient to limit the deceleration they will not necessarily be experienced. The reasoning for this statement is as follows. For the moment neglect parachute sway. The multi-directional Lander is operational for slopes up to and including 34° (fig. 5.5.8-7). This means that crushing planes from 0° through 34° must be examined. From this viewpoint only a crushing plane at 90° does not enter the analysis. If parachute sway is introduced fig. 5.5.8-8 is appropriate. From this last figure extreme conditions of slope and sway angle are apparent. The net effect is that more crushing planes must be investigated. When it is recalled that the Lander will experience a rotational motion during crush-up, it is likely that the theoretical strokes provided around the circumference, which are conservatively based on a continuing direct constant penetration, will not be expended.

With the three principal strokes known, the principal contributing factors to the attenuator thickness computation are known. Provision must still be made for stroke efficiency, a factor of safety, and rock protection dimensions. These are handled as follows. Ref. 5-1 contains data on honeycomb stroke efficiency. For the point design this efficiency is about 0.8 (see fig. 5.5.8-6 for data). Stroke efficiency is defined as that fraction of total honeycomb thickness which will actually crush-up when impacted. This effect occurs because some of the total thickness provided is lost as accumulated crushed material builds up. See fig. 5.5.8-9.

Therefore, corresponding to the three stroke values (S_i for $i = 0^{\circ}, 45^{\circ}, 90^{\circ}$) just derived, one must provide associated thicknesses (t_i) of

$$t_i = \frac{S_i}{0.8}$$

However, due to the possibility of rock or other outcroppings, these thicknesses must be compared to $S_i + 5$ in. and the larger value used in design. Therefore the design thickness is the greater of the following two expressions. (ref. Appendix IV-B.)

$$t_i = \frac{S_i}{0.8}$$

$$t_i = S_i + 5$$

With the three thicknesses known, the attenuation system may be sized and the volume of crush-up material computed.

For multi-directional point designs this was accomplished by fitting a smooth curve through the three key points and considering that the upper side is sized by the following expression.

$$t_{aft} = \frac{V^2}{gG} \times 12 + 5 \text{ in.}$$

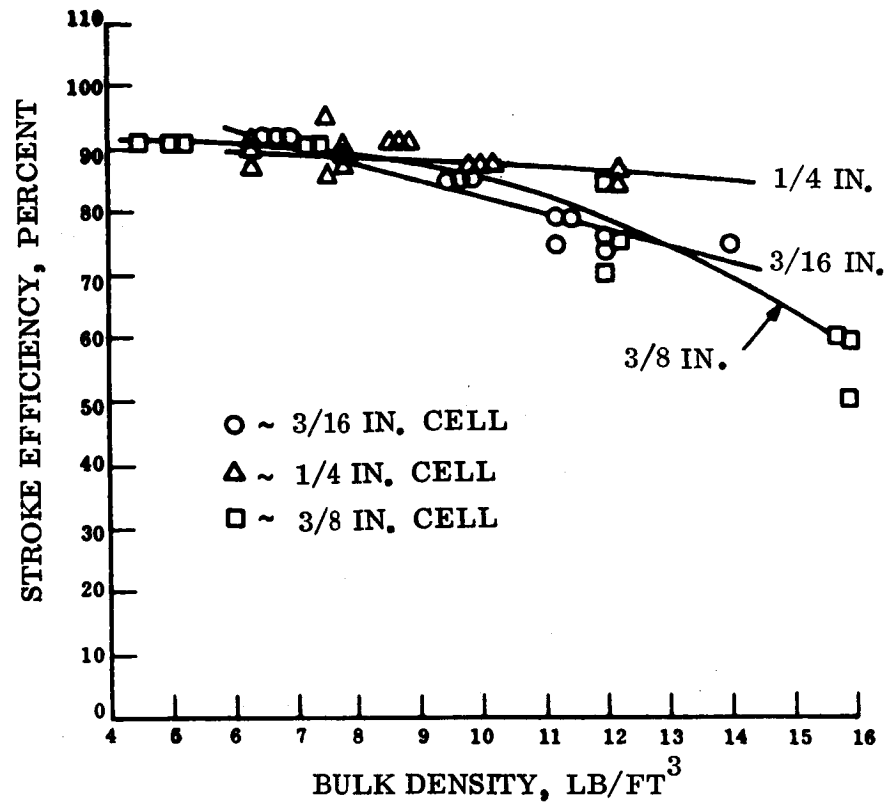


Figure 5.5.8-6. Stroke Efficiency vs Bulk Density

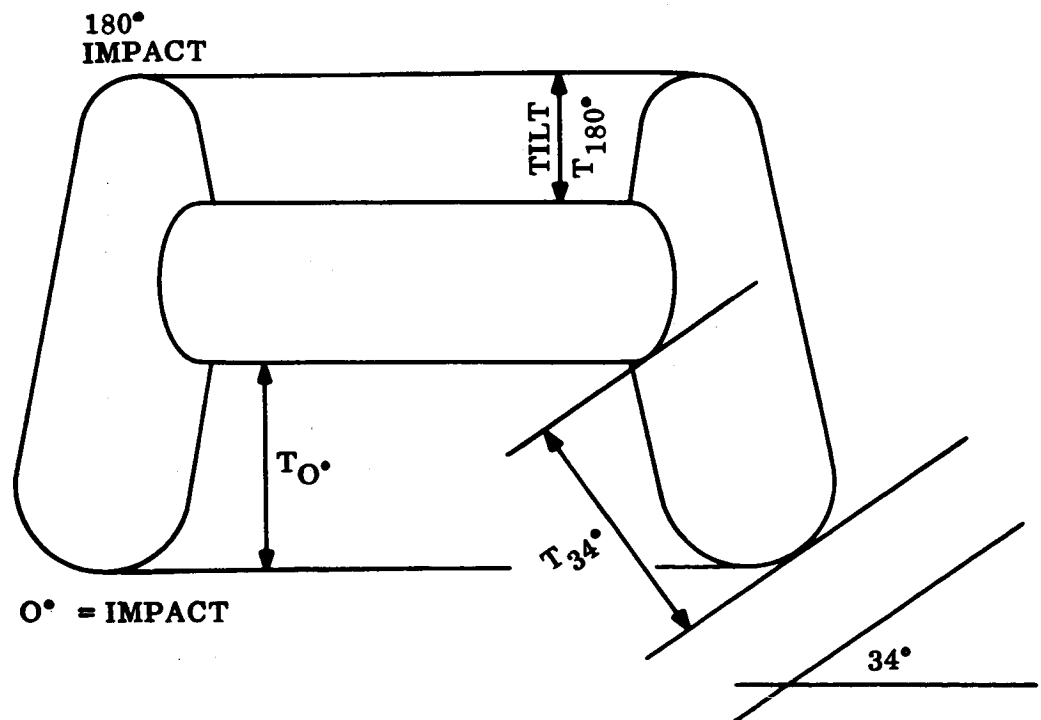


Figure 5.5.8-7. Crushing Planes for Stroke Analysis

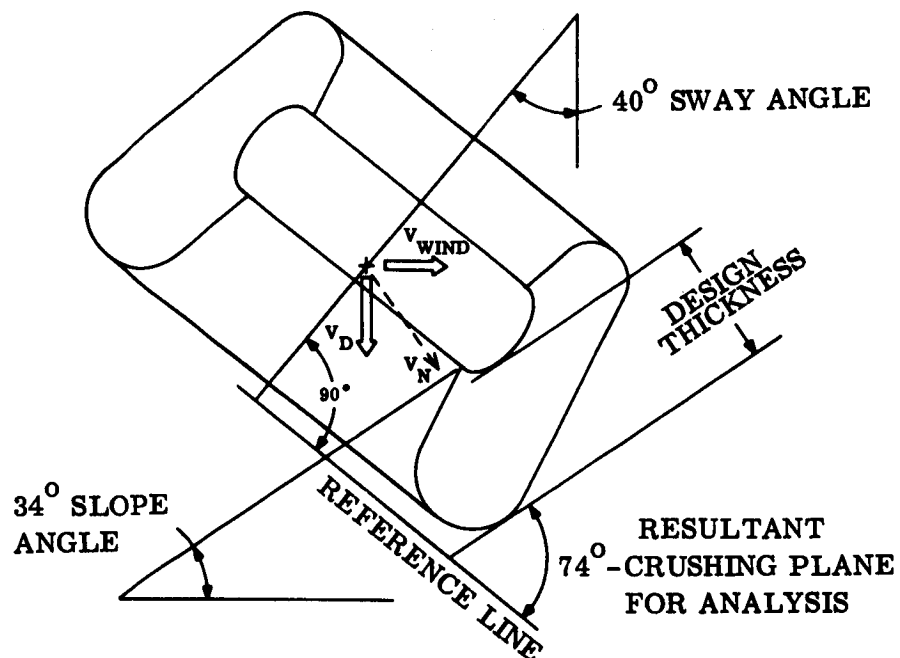


Figure 5.5.8-8. Typical Crush-Up Condition Analyzed for Multi-directional Lander Showing Sway and Slope Angle Effects

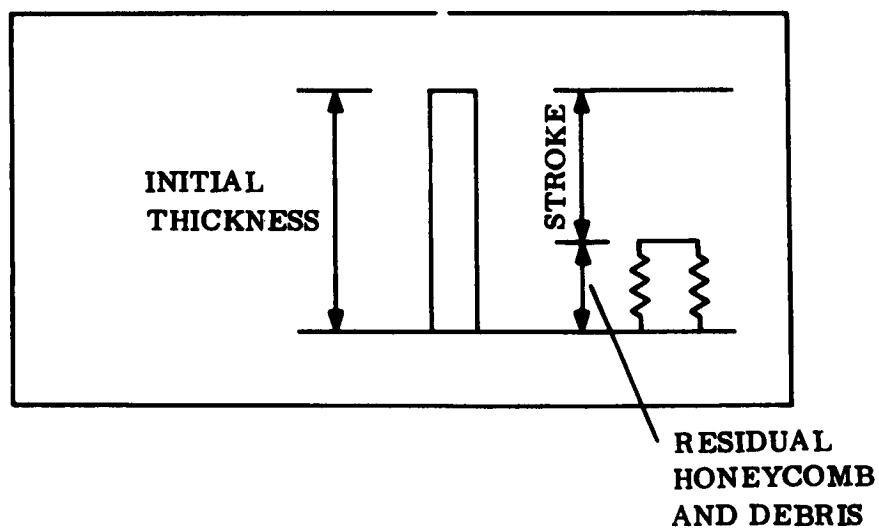


Figure 5.5.8-9. Stroke Efficiency

which is valid for a triangular 'g' versus stroke history. For purposes of the point design the velocity used in this expression was 100 fps. The implications of using this velocity, which may be produced in a secondary rebound impact are discussed in Appendix IV-B.

Another design quantity is the material density to be used to limit the g-loading to the desired values. This density for the 3/16 in. phenolic honeycomb is related to the specific energy and crushing stress as shown in fig. 5.5.8-10. For minimum attenuator weight a density greater than 11.85 pcf should not be used since the maximum specific energy and crushing stress occur at this value. This establishes an upper limit on the useful density. A lower bound on the density is determined from previously reported experimentation in ref. 5-1. It is shown that honeycomb densities below four pcf are erratic in behavior and this density is consequently a lower bound on the feasible materials for design use.

The density selection for use in point design is made by selection of a crushing stress according to the formula

$$\sigma = \frac{WG}{A}$$

where W is Lander weight, G is allowable deceleration level and A is the cross sectional area corresponding to the progression of the stroke to that point at which the peak g-loading is experienced. The area A is determined via a computer code and used to find the corresponding crushing stress. With this crushing stress the appropriate density from the relation in fig. 5.5.8-10 is read off and used in the attenuator design.

Options in the two different computer design codes were constructed based on this information. The codes allow the input of the point design conditions of touchdown velocity, size, landed subsystem weight, g-tolerance, and surface rock specification in order to obtain attenuation sizing, volume and weight, crushing stress, and material density for a given point design. The computer calculated volume and weight are then verified by planimeter computations using the exact cross sectional areas. The geometry used in the program is sketched in fig. 5.5.8-11, the input geometry includes interior and exterior diameter and inside container height. A program option yields complete sizing dimensions of the Lander as well as geometric checks for compatibility with aeroshells of different cone angles for initial installation feasibility computations.

5.5.8.4.2 Point Design 3 Particulars for Impact Attenuation System

When the foregoing criteria were applied to Point Design 3 the impact attenuation system was defined as 406 lb of 3/16 in. cell size phenolic fiberglass honeycomb. The honeycomb volume was 50.8 ft³; the density was 8 pcf. The other conditions were:

$$V_D = 100 \text{ fps descent velocity}$$

$$V_H = 220 \text{ fps wind velocity}$$

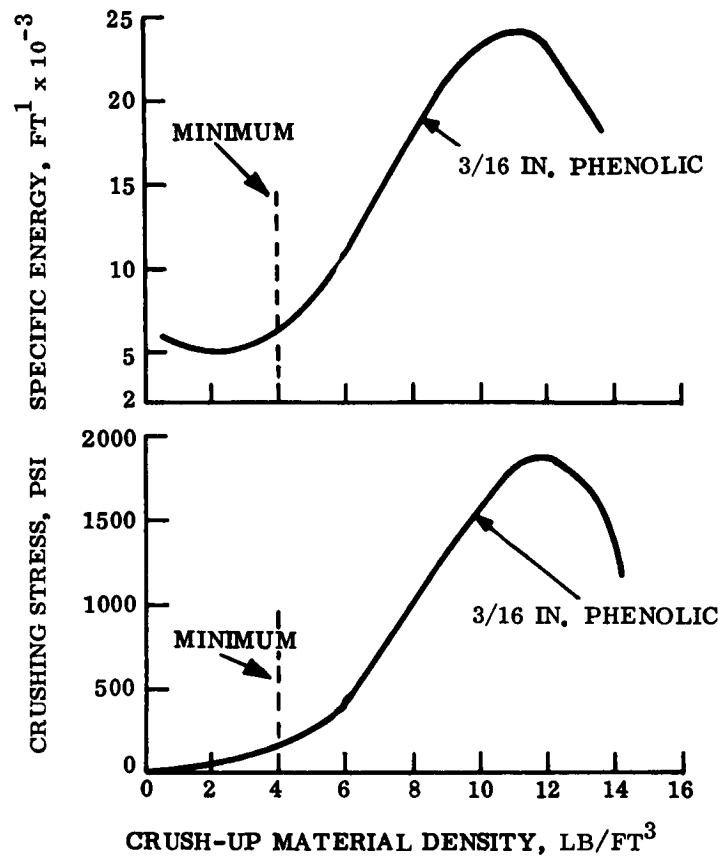


Figure 5.5.8-10. Crushable Honeycomb Properties

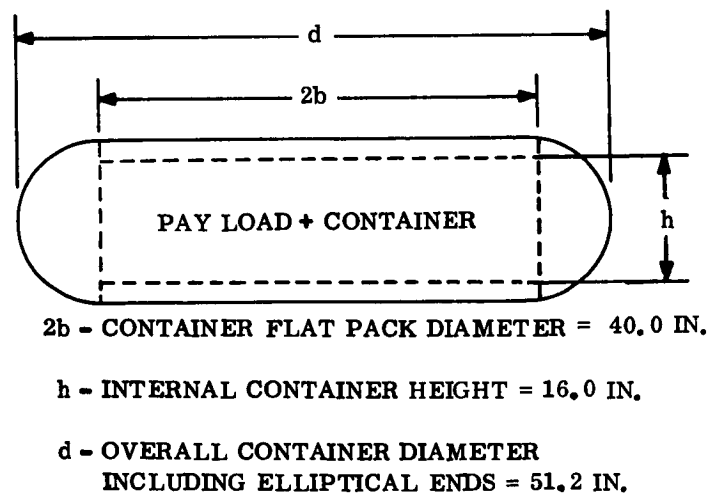


Figure 5.5.8-11. General Internal Geometry for Point Design 3

Multi-directional capability clearance and protection 5 in. rocks

1000 g (rigid body) capability

The honeycomb thicknesses are shown in outline form in fig. 5.5.8-1.

5.5.8.5 Detailed Design

Another detail in the point designs is the utilization of a face sheet over the honeycomb to excapsulate it. The potential factors which necessitate this facing are five:

1. Prevention of the honeycomb cells from filling with loose surface debris.
2. Facilitation of sliding. The sliding mechanism is used to absorb the impact velocity component parallel to the surface.
3. Enhancement of the structural integrity of the attenuator.
4. Distribution of or spreading of concentrated loads produced by surface protrusions.
5. Confinement of crush-up fragment which might provide an undesirable background for surface measurements.

Experimentation has shown that loose surface (sand, loam, dust, etc) tend to fill up the impacting cells quite quickly. This filling will interfere with pure crushing action and for this reason is undesirable. However, for surfaces presenting this potential hazard, the major energy absorber is the ground with a reduced amount of honeycomb attenuator crushing or no crush-up at all. From this viewpoint, therefore, the first consideration for a cover may not produce a compelling argument.

The smooth surface presented by a cover would certainly provide better sliding behavior than the exposed open cells of a honeycomb. On anything less than a very hard terrain of low relative roughness this is an important factor. Moreover, in the point design analyses lateral sliding motion are counted on to absorb the horizontal component of the impact velocity vector.

The structural strength of the attenuator is favorably affected by use of a facing plate. The facing lessens the tendency to shear off entire chunks of the attenuator thereby thwarting the desired crush-up behavior. A wrap around membrane also allows more of the attenuator to participate in the energy absorbing process than if no cohesive member was used.

More important than this last argument, however, a face sheet produces a spreading action of possible localized loads produced by rocks and other surface protrusions. This lessens the possibility of local punctures or intrusions which could circumvent the crush-up process. The spreading of loads is important if the design assumptions are to be reasonably accurate. Moreover, a thin cover protects the outermost cell edges and minimizes local shear deformations which could cause lateral failures produced by the surface friction.

Finally, encapsulation of the honeycomb prevents stray honeycomb fragments from reaching the surface and interfering with surface science measurements and other scientific experiments (alpha backscattering, for example).

If an encapsulation device is used, the determination of its thickness can be made as follows. Strength will not govern the design since the facing is not required to perform a major structural function. Instead, the facing must be designed to be sufficiently thin so that it can be contoured to fit the doubly curved Lander geometry. The actual lay-up is a detailed design manufacturing problem. A piecewise lay-up of extremely light gauge material is one possible design choice. The lower limit on gauge is determined by the criteria that the membrane itself must not be so light that it is easily punctured by surface abrasion.

Finally, two other design details remain. First, cross deformation effects are investigated for two conditions. The first is excessive stroke requirements which produce thickness sufficiently large (> 24 in.) to lead to impulsive buckling of the honeycomb cells without crushing behavior. If such strokes are indicated, the attenuator is segmented further to eliminate buckling and promote crushing of the attenuator. Second, gross shear failures must also be considered. This possible mode involves the breaking off of an entire piece of material without crushing deformation. Where analysis indicates that gross shear is a possibility, radial metallic strips welded to the payload container can be used to take out the shear in excess of what can be carried laterally by the honeycomb cells. These elements, while resistant to shear, are sufficiently slender so that they buckle when impacted along their length and thereby crush-up with the phenolic honeycomb materials.

Past experience indicates that the double curvature introduced in this Lander concept can be wrapped effectively by segmenting the honeycomb into pieces which are then bonded together. In this way the longitudinal axis of the honeycomb cells can be made near-radial with the payload contained structure. The wrapping proceeds around the Lander circumference and then outward until the desired thicknesses are provided.

5.5.8.6 Honeycomb Lander Fabrication

The principal operations involved in the fabrication of the honeycomb crush-up system include the segmenting and cutting of the honeycomb material so that it may be properly oriented as shown in fig. 5.5.8-12, the bonding of the honeycomb segments to one another, and the bonding of the honeycomb to the aluminum substructure and the external protective covering.

5.5.8.6.1 Adhesive Selection

For proper bond action suitable adhesives must be selected. Adhesive bond systems are required for two distinctly different joints: honeycomb-to-honeycomb and metal-to-honeycomb. While these configurations present separate joining problems the bonded joints must nevertheless have the same cure cycle. There are, however, modified epoxy-phenolic adhesives suitable for temperatures of -200°F to 900°F . A representative example of such a product is the HT 424 adhesive manufactured by

the Bloomingdale Department of the American Cyanamid Corporation. These adhesives may be formulated to be r-f transparent as required. The properties of this class of adhesive are such that the bonds formed are stronger than the weakest material comprising the joint. In fact, shear and bending tests will fail the honeycomb interface of the bond.

5.5.8.6.2 Honeycomb-to-Honeycomb Joints

In fabricating the Lander, there are a large number of possible variations at the interface between the honeycomb segments. The selected desirable approach is to bond flat surfaces of honeycomb together utilizing a space-filling adhesive as needed to fill gaps between points contacts.

5.5.8.6.3 Honeycomb-to-Aluminum Joints

Previous development testing (ref. 5-2) has identified adhesive suitable for bonding phenolic fiberglass honeycomb to aluminum.

Previous GE-MSD efforts have, furthermore, identified adhesives for this bond which have cure cycles compatible with the adhesives used for honeycomb to honeycomb joints. As an example, adhesives of the H424 high-temperature resin family produced by the Bloomingdale Department of the American Cyanamid Corporation are feasible. (For aluminum-to-honeycomb joints HT 424 F, in particular, has been tested by GE-MSD as reported in ref. 5-2. For honeycomb-to-honeycomb bonds HT 424 is indicated.)

5.5.8.6.4 Tooling and Fixtures

Phenolic fiberglass honeycomb material of the densities in this Lander point design can be cut to size and shape with moderate ease. Heavier or lighter densities should also work well. Standard shop equipment with metal cutting tools may be used throughout.

Tool steel routers and mills may be used. For rough cutting the honeycomb segments a carbide tipped band saw blade is preferred. For final thickness and taper large inertia sanding wheels are used. Specialized wood fixtures can be designed for many of the sizing and contour cutting operations. For curing operations a standard circulating air furnace provides a rotating spit fixture for the assembly cure cycle.

5.5.8.6.5 Lander Fabrication

The Lander fabrication sequence proceeds according to the following steps:

1. Preparation of container structure surface. This includes final finishing to produce proper dimensional tolerances special treatment of apertures and holes. After all finishing the structure is surface-treated with a chemical reagent (much as Alodine 1200) to promote good adhesive bonding.

2. Preparation of exterior shell interior surface. This includes final shaping of the impact attenuator encapsulating structure (skin). This surface is also surface treated prior to adhesive bonding.
3. The raw honeycomb crush-up material is then rough cut to size with proper attention to the designed lay-up and resultant cell wall orientation.
4. The rough cut surface is then checked for dimensional accuracy and secondary trimming or sanding is performed.
5. A preliminary fit-up of the honeycomb to the subsystems container is made. This is done by using shims to allow for adhesive bond thicknesses.
6. The epoxy adhesive is then prepared according to the manufacturer's specifications.
7. The bonding of the honeycomb segments to the container structure and to one another is then begun. For this purpose a rotating spit device to hold the container, along with the associated jigs and fixtures for temporary support during curing are used. The exact fixture details must be determined during the manufacturing development period. However, in general, these are wooden forms which can be snapped in and out of position.
8. The assembly, which is now fully mated, is subjected to the proper cure cycle determined by the adhesive and also the specified strength level to be attained. The lay-up of the honeycomb is shown in fig. 5.5.8-12.
9. The exterior facing plate is now attached, held in position by jigs, and cured. Because of the double curvature of this element it must be laid up in pieces in a manner comparable to the lay-up of conventional toroidal metallic shells.

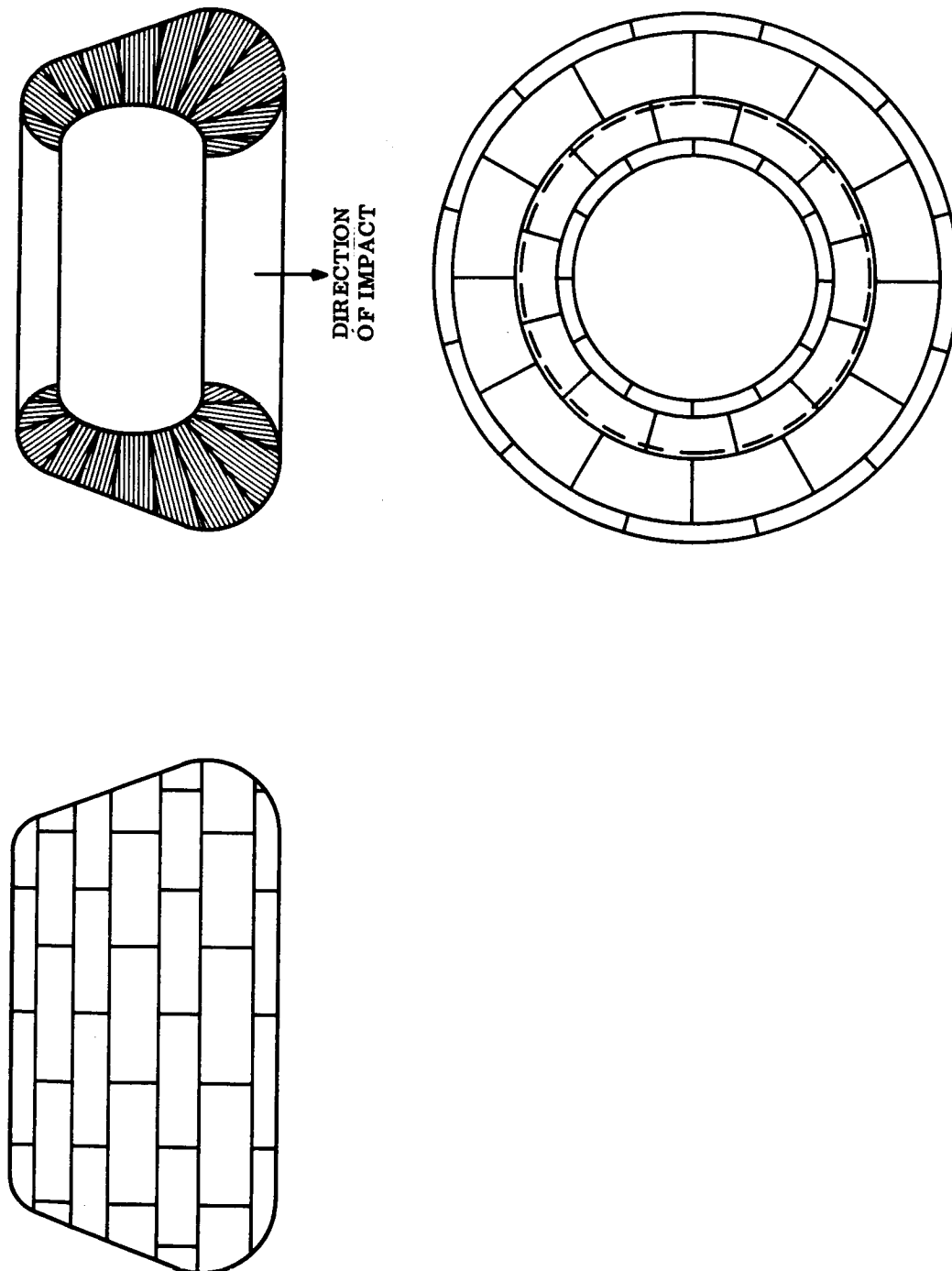


Figure 5.5.8-12. Layout of Honeycomb Attenuator (Multi-direction)

5.5.9 MASS PROPERTY AND INERTIA DATA

Following is a summary weight statement for the complete Lander, table 5.5.9-1, and a detailed weight breakdown of the payload subsystems and components, table 5.5.9-2.

TABLE 5.5.9-1. WEIGHT SUMMARY

Lander Systems and Equipment - Point Design 3	Weight (lb)	Total (lb)
Lander (Complete)	--	933.5
Structure	180.0	
Attenuation	406.0	
Electrical Power Equipment	160.5	
Telecommunications	80.0	
Environmental Control	25.0	
Scientific Payload	48.3	
Interface Equipment	0.9	
Cables and Harness	12.8	
Deployment Cameras	10.0	
Deployment "Alpha" Back Scatter	10.0	
Total		933.5
c.g.'s ('X' CG Datum - Apex of Heat Shield Cone)	Gross Inertias in Slug/Ft ²	
<u>X</u> <u>Y</u> <u>Z</u>	<u>Roll</u>	<u>Pitch</u> <u>Yaw</u>
39.0 0.22 0.59 (in.)	72.3	58.9 58.7

TABLE 5.5.9-2. DETAILED WEIGHT BREAKDOWN ~ SUBSYSTEMS AND COMPONENTS

Lander Subsystems	Weight (lb)
<u>Electrical Power</u>	
<u>Equipment</u>	(160.45)
A101 Battery, Operational	67.60
A106 Switch, Power Transfer	2.00
A107 Programmer, Lander	7.20
A108 Regulator, Voltage	7.00
A110 Controller, Power	5.50
A113 Battery, High Rate 'A'	0.50
A114 Battery, High Rate 'B'	0.50
A115 Filter, EMC 'C'	1.90
A121 Module, Diode Block	0.20
A124 Module, Thermal Relay	0.15
A128 Switch, Hg 'A'	0.10
A129 Switch, Hg 'B'	0.10
A130 Regulator, Voltage	0.90
A132 Unit Breaker and Limiter	0.60
A133 Panel, Solar Cell and Linkage	20.00
A134 Regulator, Charge	7.80
A135 Module, Diode Block	0.50
A136 Mechanical Drive	4.00
A137 Motor, Stepping	2.00
A138 Control, Motors	1.30
A150 Motor, Stepping	2.00
A151 Motor, Stepping	2.00
A152 Motor, Stepping	2.00

TABLE 5.5.9-2. DETAILED WEIGHT BREAKDOWN ~ SUBSYSTEMS AND COMPONENTS (Continued)

Lander Subsystems	Weight (lb)
A153 Panel, Solar Cell and Linkage	20.00
A155 Mechanical Drive	4.00
A158 Pin Puller	0.30
A159 Pin Puller	0.30
<u>Telecommunications</u>	(80.0)
A602 Transmitter, UHF	2.50
A604 Conditioner, Signal Data	4.00
A605 Antenna, UHF Relay A	1.00
A607 Unit, Memory	5.00
A608 Receiver, UHF Beacon	1.30
A609 Processor, Data Handling	4.00
A610 Circulator, UHF A	0.40
A611 Circulator, UHF B	0.40
A621 Switch, Antenna 'A'	1.00
A623 Antenna, UHF Relay 'B'	1.00
A676 Multicoder	5.00
A628A Accelerometer, Impact	0.60
A683 Amplifier, Charge (3)	1.50
A684 Transmitter, 'S' Band	7.00
A685 Antenna, 'S' Band (2)	1.00
A686 Transponder, Exciter	22.00
A688 Antenna, 'S' Band Rec. (2)	0.40
A687 Decoder, Command	5.00
A689 Circulator 'S' Band (2)	1.40
A697 Altimeter, Radar	15.00
A698 Antenna, Radar Altimeter	0.50

TABLE 5.5.9-2. DETAILED WEIGHT BREAKDOWN ~ SUBSYSTEMS AND COMPONENTS (Continued)

Lander Subsystems	Weight (lb)
<u>Environmental Control</u>	(25.00)
1 in. Insulation	20.00
Installation Hardware	5.00
<u>Scientific Payload</u>	(48.30)
A807 Accelerometer, Tri Ax	2.00
A808 Transducer, Temp (2)	1.00
A809 Transducer, Press (2)	1.00
A810 Transducer, Press (2)	1.40
A817 Transducer, Temp (2)	1.00
A822 Camera, Facsimile A	2.00
A823 Camera, Facsimile B	2.00
A824 Camera, Facsimile C	0.40
A825 Camera, Facsimile D	0.40
A829 Sensors, Wind Velocity A-H (8) to A836	4.00
A837 Sensor, Moisture	10.00
A838 Spectrometer, Mass	8.00
A841 Inclinator (2)	2.60
A842 Instrument, Surface Comp.	9.50
A845 Sensor, Wind Velocity I	0.50
A846 Sensor, Wind Velocity J	0.50
A847 Transducer, Temp	0.50
A848 Transducer, Temp	0.50
A849 Detector, Water Vapor & Moisture	1.00

TABLE 5.5.9-2. DETAILED WEIGHT BREAKDOWN ~ SUBSYSTEMS AND COMPONENTS (Concluded)

Lander Subsystems	Weight (lb)
<u>Interface Equipment</u>	(0.88)
J2002 IFD, A/S Lander	0.13
J2003 IFD, T/C Lander	0.75
<u>Cable Assembly</u>	(12.80)
WL1 Cable Assembly, Command	2.10
WL2 Cable Assembly, Power	3.70
WL3 Cable Assembly, Instrument	3.00
WL4 Cable Assembly, Shield	0.80
WL5 Cable Assembly, Power	2.70
WL6 Cable Assembly, Co-Ax	0.50

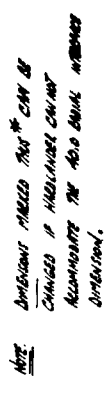
5.6 CONSTRAINTS IMPOSED ON ORBITER

The majority of constraints imposed by the Flight Capsule on the Orbiter are relatively independent of the mode of Capsule entry (direct or orbital) and the size or weight of the Capsule. Addition of the Flight Capsule, however, requires mechanical and electrical interfaces between the Orbiter and the Capsule. Fig. 5.6-1 shows the Capsule adapter which will provide the mechanical interface. In this study, it has been assumed that the MM '71 Orbiter will be modified for the combined Orbiter and Hard Lander mission in 1973. MM '71 is itself an adaption of the MM '69 flyby spacecraft. A complete description of the MM '73 Orbiter is contained in Appendix D. Table 5.6-1, excerpted from the appendix, highlights the major changes required of the MM '69 subsystems for conversion to an Orbiter in MM '71, and then to a Capsule bus (as well) in MM '73.

In addition to the changes summarized in the table, the Orbiter propulsion tankage must be expanded to insert the entire spacecraft into Mars orbit. The increased mass of the propulsion module, in turn, dictates that the rings, longerons, and shear panels of the MM '71 octagonal equipment module be increased in gauge to carry the increased loads. The details of the structural changes are discussed in detail in Appendix D. The details of the propulsion changes are tabulated in table 5.6-2.

TABLE 5.6-1. MAJOR SUBSYSTEM CHANGES

MM '69 Subsystem	Change For '71 Orbiter	Change For '73 Capsule
Power	<ul style="list-style-type: none"> • Solar Array Increase 	<ul style="list-style-type: none"> • Solar Array Increase
Radio	<ul style="list-style-type: none"> • New Maneuver Antenna • New High Gain Antenna • Modified Low Gain Antenna 	<ul style="list-style-type: none"> • New Maneuver Antenna • New High Gain Antenna • New Relay Receiver • New Relay Antennas
Attitude Control	<ul style="list-style-type: none"> • Cold Gas and Jet Size Increase • Modification of Autopilot Electronics 	<ul style="list-style-type: none"> • Cold Gas and Jet Size Increase • Modification of Autopilot Electronics • Relocated Sun Sensors • Possible Approach Guidance
Data Storage	<ul style="list-style-type: none"> • Additional Air • Additional DTR 	<ul style="list-style-type: none"> • New Relay Recorders
Command	<ul style="list-style-type: none"> • Possible Decoder Expansion 	<ul style="list-style-type: none"> • Probable Decoder Expansion
Telemetry		<ul style="list-style-type: none"> • Data Modes for Capsule Telemetry
Scan Control	<ul style="list-style-type: none"> • Removal of Mars Gates 	
Science	<ul style="list-style-type: none"> • Passive Cooling of IRS • Possible TV Field of View Changes 	No Estimate
Cabling		<ul style="list-style-type: none"> • Three Inflight Disconnects
Mechanical Devices	<ul style="list-style-type: none"> • High Gain and Maneuver Antenna Deployment • High Gain Antenna Articulation • Modified Separation Mechanics 	<ul style="list-style-type: none"> • Spacecraft Separation Mechanics • Modified Orbiter Separation Mechanics • New High Gain Antenna Deployment
Propulsion	<ul style="list-style-type: none"> • New 	<ul style="list-style-type: none"> • New Tanks and Supports for (Orbital Entry Capsule)
Structure	<ul style="list-style-type: none"> • Strengthened Adapter 	<ul style="list-style-type: none"> • Capsule Adapter • Spacecraft Adapter • Strengthened Octagon for (Orbital Entry Capsule)



SK56194-328
PROPOSED SPACECRAFT INTERFACES
OUT-OF-ORBIT VEHICLE SHOWN

SCALE AS NOTED

Figure 5.6-1. Capsule/Bus Interface

TABLE 5.6-2. ORBITER PROPULSION SUMMARY

ΔV (Total)	1525 mps
Weights -	
Capsule	1846 lb
Orbiter	963 lb
Adapter	70 lb
(1) Propulsion (Dry)	336 lb
(2) Residuals	85 lb
(3) Total propellant and pressurant	2404 lb
(1) + (2) Burnout	421 lb
(1) + (3) Propulsion system	2740 lb
Volumes* -	
Propellant tank diameter	22 in.
Propellant tank length	48 in.
Pressurant tank diameter	17 in.
Burn time (insertion)	2128 sec
Spacecraft Launch Weight	5619 lb
*Based on four propellant and two pressurant tanks	

5.7 PROBABILITY OF SUCCESS - POINT DESIGN 3

5.7.1 INTRODUCTION

A key factor in evaluating a design concept is the determination of the probability of success of the configuration. This determination is primarily beneficial at the early concept design state in performing tradeoff evaluations of several potential design configurations. As the design evolves from conceptual towards final, the merit of the quantitative value shifts from comparative to predictive.

A probability of success determination was performed for the conceptual mission as defined by Point Design 3. Due to the early stage of the design, it was necessary to perform this determination based on many assumptions. These are listed below. In general, it can be stated that failure rate data was based on information known concerning components of similar generic or complexity definition. It was also assumed that the new development items required for this mission will be developed, tested, and qualified before being flown.

Due to these assumptions, and the uncertainty of sterilization influence on some of the components, the predictive value of the determination may not be accurate. However, since the same assumptions and methodologies were used on all determinations during the study, the comparative value of the determinations are significant.

5.7.2 RESULTS

Probability of success values were determined for both the Capsule systems and for the Booster and Orbiter systems of the mission. The procedures used in performing these determinations are presented in Sections 5.7.3 and 5.7.4 below. A summary of the determinations, by major mission phase, is shown in table 5.7.2-1.

This tabulation indicates that the value obtained, under the study ground rules stated in the preceding paragraph for the probability of success of the total mission is 0.364. This is the probability of obtaining proper functioning of all mission equipment, as required, for the duration of the mission from launch to completion of the 90 day mission on the Martian surface.

TABLE 5.7.2-1. MISSION SUCCESS PROBABILITY, POINT DESIGN 3

Mission Phase	Booster and Orbiter		Capsule		Combined	
	Phase	Cumulative	Phase	Cumulative	Phase	Cumulative
Launch/Cruise	.748	.748	.945	.945	.707	.707
Mars Orbit	.945	.707	---	.945	.945	.668
Separation and Entry	.999	.706	.957	.904	.956	.638
Landed Operation	.997	.704	.572	.517	.569	.364

5.7.3 CAPSULE ANALYSIS

This section presents the procedure followed in analyzing the Mars Hard Lander System Point Design for the probability of successfully accomplishing its intended functions.

5.7.3.1 Assumptions

The assumptions and ground rules used in the analysis were as follows:

1. A component would not fail under non-operating conditions.
2. The probabilities of success of all components were considered to be statistically independent. This permitted the use of the product rule for assessing the system and subsystem success probabilities. In the case of redundant application, the above ground rule applied to the component function.
3. The success probability of the structure, aeroshell and impact attenuation was assumed equal to unity (1.0).
4. The probability of success of the system or its components was defined as being equal to the probability of zero (0) functional failures.
5. The mission phases and time of each phase upon which the analysis was based are as follows:

<u>Phase</u>	
Launch/Cruise	5,856 hrs
Pre-entry	2.0 hrs
Entry	0.18 hr
Landed Operation	90 days

6. The assessment for the success probability of a component during any given phase reflects only the time during the phase in which it operates.
7. If any portion of a component operated during a particular phase the entire component was assessed for its success probability.
8. The success probability of the various system components was based on failure data of components which were similar or identical in function or of equivalent complexity.

5.7.3.2 Procedure

5.7.3.2.1 Component Success Probability

The probability of success of time (or cycle) sensitive components was obtained using the following expression:

$$R_c = e - \lambda t \quad (1)$$

where:

R_c = probability of success

λ = Failure rate in failures/hr (or cycle)

t = Operating time (hr) or cycles

For redundant application of a component, the following expression was used to obtain the probability of success of the function:

$$R = [1 - (1 - R_c)^n] \quad (2)$$

where

R = probability of success of the function

R_c = probability of success of the component

n = number of components in the redundant group.

For components which are not time (or cycle) sensitive, such as squib valves, the success probability reflects the results of successes versus trials using appropriate statistical techniques.

5.7.3.2.2 Subsystem Success Probability

The probability of success of a subsystem for any given phase was obtained using the following expression:

$$R (S/S)_p = \pi_i R_i \quad (3)$$

where:

$R (S/S)_p$ = probability of success of the subsystem in the phase

R_i = probability of success of the i^{th} component or function (for redundant application) for the phase being considered

π = symbol for product

The probability of success of a subsystem over its entire mission was obtained using the following expression.

$$R(S/S)_M = \pi_j R(S/S)_j \quad (4)$$

where:

$R(S/S)_M$ = probability of success of the subsystem over the mission

$R(S/S)_j$ = probability of success of the subsystem for the j^{th} mission phase

5.7.3.2.3 System Success Probability

The probability of success of the system for any given phase was obtained using the following expression.

$$R(\text{System})_p = \pi_k R(S/S)_k \quad (5)$$

where:

$R(\text{System})_p$ = probability of success of the system in the phase

$R(S/S)_k$ = probability of success of the k^{th} subsystem for the phase being considered

The probability of success of the system over the entire mission was obtained using the following expression.

$$R(\text{System})_M = \pi_k R(S/S)_{M_k} \quad (6)$$

where:

$R(\text{System})_M$ = probability of success of the system for the mission

$R(S/S)_{M_k}$ = probability of success of the k^{th} subsystem for the mission

5.7.3.2.4 Orbiter Support Analysis

The probability of success of the Mars Hard Lander for the i^{th} mission phase, reflecting the success probability of the Booster and Spacecraft (in support of Capsule operations) and the Capsule system is given by:

$$R(\text{MHL})_i = R(\text{Booster})_i \times R(\text{Spacecraft})_i \times R(\text{Capsule})_i \quad (7)$$

The cumulative probability of success of the Mars Hard Lander for the i^{th} mission phase is given by:

$$R(\text{MHL}; \text{cumulative}) = \prod_{i=1}^i R(\text{MHL}) \quad (8)$$

where:

$R(\text{MHL})_{i-1}$ = independent probability of success of the MHL for the $(i-1)^{\text{th}}$ phase as obtained from eq (7)

$R(\text{MHL})_i$ = independent probability of success of the MHL for the i^{th} phase as obtained from eq (7)

The cumulative success probability for each of the systems are similarly obtained from eq (8)

5.7.3.3 Results

5.7.3.3.1 Component Success Probabilities

The success probability for the components (or functions in the case of redundant applications) comprising Point Design 3 for the Mars Hard Lander System is summarized in table 5.7.3-1 for each of the mission phases described in para 5.7.3.1.

The values appearing in the table were computed using expressions (1) or (2) described in para 5.7.3.2 as applicable, for time (or cycle) sensitive components. These values reflect failure rate data from the sources indicated in the table. Non-time (or cycle) sensitive component success probabilities were obtained directly from the indicated source.

5.7.3.3.2 System and Subsystem Success Probabilities

The success probabilities for the subsystems and system which define Point Design 3 are summarized in table 5.7.3-2 for each of the phases described in para 5.7.3.1 and the total mission. The values appearing in the table were obtained using expressions (3), (4), (5) and (6) described in para 5.7.3.2.

TABLE 5.7.3-1. RELIABILITY ESTIMATES, POINT DESIGN 3 COMPONENTS

Description	Reliability				Data Source
	Launch & Cruise	De-orbit	Entry	Landed Operation	
<u>EP&D Subsystem</u>					
Battery, Operational (1)	-	.9999	.9997	.9823	ERSR-TT Program
Battery, Entry (Dual)	-	.9999	-	-	↓
Battery, T/C (Dual)	-	.9999	-	-	REA-MBRV Program
Programmer, Lander (1)	-	.9999	.9995	.9137	RFMA-MK12 Program
Regulator, Voltage, A (1)	-	.9999	.9999	.9998	↓
Regulator, Voltage, B (1)	-	.9999	.9999	.9960	REA-Voyager Study
Regulator, Voltage, C (1)	.9999	.9999	-	-	RFMA-TT Program
Regulator, Charge (1)	.9999	-	-	-	↓
Module, Diode Block (2)	-	.9998	-	-	ERSR-TT Program
Module, Diode Block (1)	-	-	.9999	-	REA-MK12 Program
Battery, HR (Dual)	-	-	.9999	.9999	RFMA-TT Program
Module, Power Distribution	-	.9999	-	-	↓
Filter, EMC, A (1)	-	.9999	-	-	ERSR-TT Program
Filter, EMC, B (1)	-	.9999	-	-	REA-MK12 Program
Filter, EMC, C (1)	-	-	.9999	.9999	RFMA-TT Program
Module, Thermal Relay (2)	-	.9998	-	-	↓
Module, Thermal Relay (1)	-	-	.9999	.9999	ERSR-TT Program
Battery, Dual	.9999	.9999	-	-	REA-MK12 Program
Power Control, C	.9999	.9999	-	-	↓
Power Control, L	-	.9999	.9999	.9991	RFMA-TT Program
Programmer, Dual, C	-	.9999	-	-	FARADA
Switch, Hg (Dual)	-	-	-	.9999	FARADA
Switch, Breaker and Limit	-	.9999	-	-	REA-MBRV Program
Switch, Power Transfer	.9999	-	-	-	REA-Voyager Study
Solar Cell, Panel (2)	-	-	-	.9851	↓
Regulator, Charge, L (1)	-	-	-	.9987	RFMA-TT Program
Module, Diode Block	-	-	-	.9619	FARADA
Motor, Stepping (3)	-	-	-	.9999	↓
Controller, Motor	-	-	-	.9995	
<u>Telecommunication Subsystem</u>					
Transmitter, UHF	-	.9998	.9999	.9997	RFMA-MK12 Program
Conditioner, Signal Data	-	.9999	.9999	.9999	↓
Antenna, UHF (2)	-	.9999	.9999	.9999	FARADA
Core, Memory	-	.9999	.9999	.8782	↓
Processor, Data	-	.9999	.9999	.9946	RFMA-MK12 Program
Circulator, UHF (2)	-	-	.9999	.9999	FARADA
Communicator, Cruise	.9999	-	-	-	↓
Switch, Antenna (2)	-	-	-	.9989	RFMA-MK12 Program
Receiver, Beacon, UHF	-	-	-	.9813	FARADA
Sensor, Temperature (18)	.9961	.9982	-	-	↓
Sensor, Pressure (8)	.9982	.9992	-	-	
Sensor, Linear Velocity (12)	.9988	.9988	-	-	↓
Conditioner, Firing Circuit (1)	.9999	.9999	-	-	RFMA-MK12 Program
Sensor, Power Supply	.9999	.9999	-	-	MIL HDBK-217A

TABLE 5.7.3-1. RELIABILITY ESTIMATES, POINT DESIGN 3 COMPONENTS
(Continued)

Description	Reliability				Data Source
	Launch & Cruise	De-orbit	Entry	Landed Operation	
<u>Telecommunication Subsystem</u>					
Conditioner, Signal, C	.9999	.9999	-	-	RFMA-MK12 Program ↓ MIL HDBK-217A Accelerometer est. Sep. Switch est. RFMA-MK12-est. PCM est-MBRV Strain Gage est. FARADA ↓
Amplifier, Charge (3)	-	-	-	.9934	
Sensor, Voltage Regulator	.9999	-	-	-	
Detector, Separation Load (2)	-	.9999	-	-	
Indicator, A/S Rel (2)	-	.9999	-	-	
Conditioner, Linear Velocity Data	.9999	-	-	-	
Multicoder	-	.9999	.9999	.9999	
Sensor, Link Tensile (4)	.9996	-	-	-	
Impact Accelerater	-	-	.9999	-	
Transmitter, S-Band	-	-	-	.9892	
Antenna, S-Band Transmitter (2)	-	-	-	.9910	
Transponder/Exciter	-	-	-	.9892	
Decoder, Command	-	-	-	.9925	
Antenna, S-Band Receiver (2)	-	-	-	.9910	
Circulator, S-Band (2)	-	-	-	.9964	
Altimeter, Radar	-	-	.9998	-	
Antenna, Radar	-	-	.9999	-	
<u>Scientific Payload Subsystem</u>					
Transducer, Temperature, A (4)	-	-	.9997	-	FARADA ↓ FARADA ↓ FARADA ↓ MIL-HDBK-217A } MK12 } RFMA ↓ MIL-HDBK-217A ↓ FARADA ↓
Transducer, Temperature, L (4)	-	-	-	.9935	
Transducer, Pressure, A (6)	-	-	.9996	-	
Transducer, Pressure, L (1)	-	-	-	.9984	
Accelerometer, Tri-Axial (1)	-	-	.9983	-	
Camera, Facimile (4)	-	-	-	.9835	
Sensor, Wind Velocity (10)	-	-	-	.9248	
Sensor, Moisture (1)	-	-	.9999	.9925	
Spectrometer, Mass (1)	-	-	.9997	-	
Inclinometer (1)	-	-	-	.9779	
Surface Comp (1)	-	-	-	.9960	
<u>Electrical Interface</u>					
IFD, Cap - S/C	.9988	-	-	-	
IFD, A/S - Lander	.9988	.9999	.9999	-	
IFD, T/C - Lander	.9988	.9999	-	-	
Safe-Arm, Lander	.9988	.9999	.9999	.9999	
Safe-Arm, Aeroshell	.9988	.9999	-	-	
Safe-Arm, Canister	.9988	-	-	-	
Fitting, Coax Data	.9998	-	-	-	
Fitting, Coax Intfc	.9998	-	-	-	
Fitting, Coax VHF	.9998	-	-	-	
<u>Thermal Control S/S</u>					
Heater	.9846	.9999	-	-	
Thermostat	.9770	.9999	-	-	
Motor, Louver Dr	-	-	-	.9978	
Unit, Temperature Control	-	-	-	.9889	
Element, Temperature Detector	-	-	-	.9820	

TABLE 5.7.3-1. RELIABILITY ESTIMATES, POINT DESIGN 3 COMPONENTS
(Concluded)

Description	Reliability				Data Source
	Launch & Cruise	De-orbit	Entry	Landed Operation	
<u>Pressurization & Venting S/S</u>					
Valve, Vent	.9999	-	-	-	FARADA
<u>Separation S/S</u>					
Release, Hot Wire (4)	-	.9996	-	-	RFMA-MK12 Program
Nut, Explosive (4)	-	.9894	-	-	FARADA
Nut, Explosive (4)	-	.9894	-	-	↓
<u>Attitude Control & Propulsion S/S</u>					
Tank, N ₂	.9995	.9999	-	-	FARADA
Valve, Squib (8)	-	.9999	-	-	↓
Valve, Fill	.9994	.9999	-	-	↓
Tank, Hydrazine	.9995	.9997	-	-	↓
Disc, Burst	.9999	.9999	-	-	↓
Valve, Solenoid	-	.9999	-	-	↓
Gyro Rate	-	.9993	-	-	↓
Amplifier	-	.9997	-	-	↓
Detector, Threshold	-	.9994	-	-	↓
Generator RR	-	.9996	-	-	↓
Switch	-	.9995	-	-	↓
Rocket, Retro	-	.9999	-	-	↓
Ejector, Nozzle	-	.9975	-	-	FARADA
<u>Retardation S/S</u>					
G-Switch	-	-	.9991	-	MBRV Program
Mortar, Drouge	-	-	.9999	-	↓
Fitting, Main Release (3)	-	-	.9997	-	↓
Fitting, Drogue Release	-	-	.9999	-	↓
Switch, Impact	-	-	.9999	-	↓
Assembly, Parachute	-	-	.9999	-	↓
<u>Legend</u>					
RFMA - Reliability Figure of Merit Analysis					
REA - Reliability Estimate Analysis					
ERSR - Equipment Reliability Status Report					

TABLE 5.7.3-2. RELIABILITY SUMMARY, POINT DESIGN 3, CAPSULE SYSTEM AND SUBSYSTEM

Subsystem	Mission Phase				
	Launch and Cruise	De-orbit	Entry	Landed Operation	$R_M = \pi R_P$
EP & D	.9995	.9981	.9985	.8434	.8395
Attitude Control and Propulsion	.9983	.9934	-	-	.9917
Pressure and Venting	.9999	-	-	-	.9999
Separation	-	.9784	-	-	.9784
Telecommunications	.9921	.9950	.9988	.8038	.7925
Thermal Control	.9619	.9998	-	.9689	.9318
Scientific Payload	-	-	.9972	.8721	.8696
Retardation	-	-	.9984	-	.9984
Electrical I/F	.9924	.9996	.9998	.9996	.9914
$R_P = \pi R (S/S)$.9448	.9646	.9927	.5724	.5177

5.7.3.4 Redundancy Considerations

A Failure Mode Effects Analysis (FMEA) was performed as part of the Capsule analyses. Due to the conceptual state of the mission design, this was performed on a qualitative rather than a quantitative basis. The primary purpose of this analysis was to point out potential problem areas for redundancy considerations.

During the FMEA, it was learned that the items that had the greatest criticality and risk of failure were the canister heater and thermostat and the operational battery. The former were of high risk due to the long duty cycle during the interplanetary cruise. The latter was critical due to its requirement to perform all Capsule operations. Redundancy inclusions were provided for these items; a standby parallel thermal control system and internal cell redundancy in the battery.

In addition to these items, many other redundancy inclusions are provided in the Capsule design. A typical listing of some of these inclusions together with the type of redundancy used is shown below. Other redundancy provisions such as backup gate or switching signals and backup time signals are also provided but not included in the listing.

<u>Item</u>	<u>Type Redundancy</u>
Operational Battery	Internal
Canister Heater and Thermostat	Parallel
Dual Battery	Internal
Thermal Batteries	Parallel
Programmer - Lander	Internal
Charge Regulator	Internal
Blocking - Module	Internal
Power Distribution Module	Internal
Thermal Relay Module	Internal
Dual Programmer	Internal
Hg. Switch	Parallel
Unit, Breaker and Limit	Internal
Spin Initiator	Parallel Squibs
Despin Initiator	Parallel Squibs
Rocket Initiator	Parallel Squibs
Temperature Transducers	Parallel
Pressure Transducers	Parallel
UHF Antenna	Parallel

5.7.4 ORBITER SUPPORT ANALYSIS

5.7.4.1 Introduction

Probability of success determinations for the Booster and Orbiter systems were performed for those functions which support and/or contribute to the success of the Capsule and its mission. Flight operations were based on an out-of-orbit reference mission with a flight time of 244 days.

5.7.4.2 Assumptions

The assumptions made and the ground rules followed in the analysis were as follows:

1. Only those functions required for the success of the Capsule missions were included.
2. The Orbiter is assumed to use 1971 equipment/hardware with only minor modifications.
3. For the orbital entry mode, up to 30 days of orbital operations plus a trim maneuver have been assumed prior to Capsule release.
4. The Spacecraft support is required for 3 days of the landed mission.
5. The reliability or criticality of the ground support functions have not been included in the study.

5.7.4.3 Procedure and Data Sources

In arriving at the reliability estimates, the tools and failure rate data bases developed during the Voyager Task C redundancy and Task D Design studies conducted for JPL, as modified by more recent studies, were used. These procedures are described in detail in the reference documents shown in para 5.8. In summary, these can be stated as follows:

1. Minuteman level parts and Minuteman and Apollo failure rates were used to the greatest extent possible.
2. Curves developed during the studies showing the projected reliability growth for inertial components and integrated circuits were used.
3. Factors to reflect (1) parts reliability growth and (2) upgrading to a high reliability status were used to obtain failure rates for sources other than Minuteman and Apollo.

4. Where failure rate data was lacking, or inadequate, failure rates were derived by comparing the part in question with another part of similar construction or performance for which reliability information was available.

5.8 REFERENCES

- 5-1. "RF Transparent, Energy Absorbing, Structural Elements", Phase II Final Report Prepared for JPL under Contract No. 950964, August 1964, GE-MSD Document No. 64SD4329.
- 5-2. "Development of Energy Dissipating Plastic Honeycomb", Quarterly Progress Report Nos. 7 and 8, Contract No. 951172, JPL, GE-MSD Document No. 66SD4390.
- 5-3. "Failure Rate Data Base for Spacecraft Redundancy Study", VOY-C3-TR8.
- 5-4. "Reliability Characteristics of Voyager Components - Voyager Spacecraft Redundancy Study, VOY-C3-TR7.
- 5-5. Voyager Final Report, Phase IA, Tack C, Volume 4, Application of Redundancy Study, July 28, 1967, VOY-CO-FR, prepared for JPL under Contract 951112.
- 5-6. Voyager Spacecraft Final Report, Phase B, Task D, Volume II (Book 1 of 5), Systems Description, October 2, 1967, under Contract NAS 8-22603.

6. POINT DESIGN 4

6. POINT DESIGN 4

6.1 MISSION SEQUENCE

A sequence of events from launch to mission completion for this mission is shown by table 6.1-1. This is a direct entry mission with a nominal interplanetary flight time of 164 days before separation. Flight sequence from start of separation to impact is illustrated by fig. 6.1-1. The landed sequence is illustrated by fig. 6.1-2.

Separation occurs 24 hours prior to entry. The Lander Capsule is stabilized after separation by a spin-despin and roll control system. Deceleration is accomplished by parachute whose deployment is actuated by a radar altimeter at 20,000 ft. After separation, the spacecraft will go into synchronous orbit for three full diurnal cycles to support the Lander Capsule. Entry and surface science, and surface imaging is performed at the beginning of the first cycle with data transmitted real time to the Orbiter for relay to Earth. Surface science and surface composition measurements will be continued throughout the first cycle with data stored while Orbiter is not in periapsis communication range. Science data will be sent by direct S-band link to Earth on a daily basis. When Orbiter returns to periapsis range it will signal Lander, and stored data will be transmitted for relay to Earth. Imaging and surface science measurements will be repeated with real time transmissions to Orbiter. Solar cell deployment occurs 1-1/2 days after landing. Measurement and transmission modes will be repeated for the three days that Orbiter remains in support. Orbiter then goes into asynchronous orbit for separate mission activities.

Lander continues to perform surface meteorology measurement with direct transmission to Earth on S-band, for remainder of mission. Solar panels recharge the batteries for the operations after the third day. Lander includes a direct link command receiver to permit Earth to transmit variations in established sequence as desired.

TABLE 6.1-1. MISSION SEQUENCE OF EVENTS, POINT DESIGN 4

Item	Event	Time
A.	Launch to impact	
1.	Launch	TL
2.	First midcourse maneuver (if required)	TL + 30 days
3.	Second midcourse maneuver (if required)	TL + 154 days
4.	Mars arrival	TL + 164 days
5.	Start final Capsule diagnostic checkout	To (Entry - 48 hr)
6.	Complete diagnostic checkout	To + 120 min
7.	Update programmers complete	To + 20 hr

TABLE 6.1-1. MISSION SEQUENCE OF EVENTS, POINT DESIGN 4 (Continued)

Item	Event	Time
8.	Turn on Lander power, telemetry, sequencer and diagnostic data	T1 (To + 23.8 hr)
9.	Canister separation	T2 (T1 + 5 min)
10.	Spacecraft maneuvers to capsule separation attitude	T2 + 10 min
11.	Capsule separates from spacecraft	T3 (T2 + 10.1 min)
12.	Initiate spin stabilization	T3 + 0.5 sec
13.	Ignite deflection propulsion	T3 + 30 min
14.	Terminate deflection propulsion	T3 + 30.3 min
15.	Initiate de-spin	T3 + 30.5 min
16.	Separate thrust cone	T3 + 30.6 min
17.	Turn power and telemetry off	T3 + 30.7 min
18.	Turn on mass spectrometer for warm-up	T4 - 15 min
19.	Turn on telemetry (low data rate), initiate accelerometer and pressure sensor readings	T4 - 60 sec
20.	Entry	T4 (T3 + 24 hr 8.3 min)
21.	Mach 5 - Initiate mass spectrometer, water vapor, and temperature sensor readings turn on radar altimeter	<u>VM-8</u> <u>VM-9</u> T4+104 sec T4+97 sec
22.	Deployment parachute (20 kft)	T4+142 sec T4+325 sec (Mach 1.0) (Mach 0.38)
23.	Aeroshell separation	T4+152 sec T4+335 sec
24.	Jettison parachute	T4+301 sec T4+565 sec
25.	Impact - force sensed and transmitted to spacecraft (with redundant storage)	T5(T4+302 T5(T4+566 sec) sec)
B.	Landed operations	
1.	Diagnostic and stored entry data transmitted to Orbiter (low data rate)	T5 + 0.1 min
2.	Lander comes to rest - up direction sensed	T5 + 2 min
3.	Initiate hatch cover and boom deployments	T5 + 2.1 min
4.	Switch to high data rate transmission mode	T6(T5 + 2.5 min)
5.	Initiate stored diagnostic, entry, and impact data transmission to Orbiter	T6 + 0.1 min

TABLE 6.1-1. MISSION SEQUENCE OF EVENTS, POINT DESIGN 4 (Concluded)

Item	Event	Time
6.	Initiate imagery, meteorology, and inclinometer measurements and transmit to Orbiter for relay to Earth	T6 + 0.2 min
7.	Repeat items 5. and 6.	T6 + 13.3 min
8.	Turn off imagery and telemetry systems	T6 + 20 min
9.	Repeat surface science measurements (excluding imagery) at 20 min intervals and store data	-----
10.	Initiate surface composition (alpha scatter) measurement cycle and store data	T7(T5 + 1 hr)
11.	Complete initial surface composition cycle	T7 + 5 hr
12.	Repeat surface composition measurements every 3 hrs for one day period only	-----
13.	Transmit stored science data direct to Earth by S-band telemetry system	T8
14.	Receive signal that Orbiter is returning to range	T9(T6+ 24.5 hr)
15.	Turn on telemetry system (high data rate) and transmit stored science data to Orbiter	T10(T6 + 24.6 hr)
16.	Perform imagery and surface science measurements and transmit data to Orbiter for relay to Earth	T10 + 0.1 min
17.	Repeat items 15 and 16.	T10 + 13.3 min
18.	Turn off imagery and telemetry systems	T10 + 20 min
19.	Deploy solar array	T11 + (T5 + 36 hr)
20.	Repeat measurement and transmission cycles (items 3. through 18.) for 2 additional days while Orbiter is in support	-----
21.	Continue science measurement (no imagery) at 1 hr intervals with daily transmission direct to Earth for duration of mission*	-----

*Command receiver provides capability for Earth to signal variations in sequence.

FOLDOUT FRAME

FOLDOUT FRAME

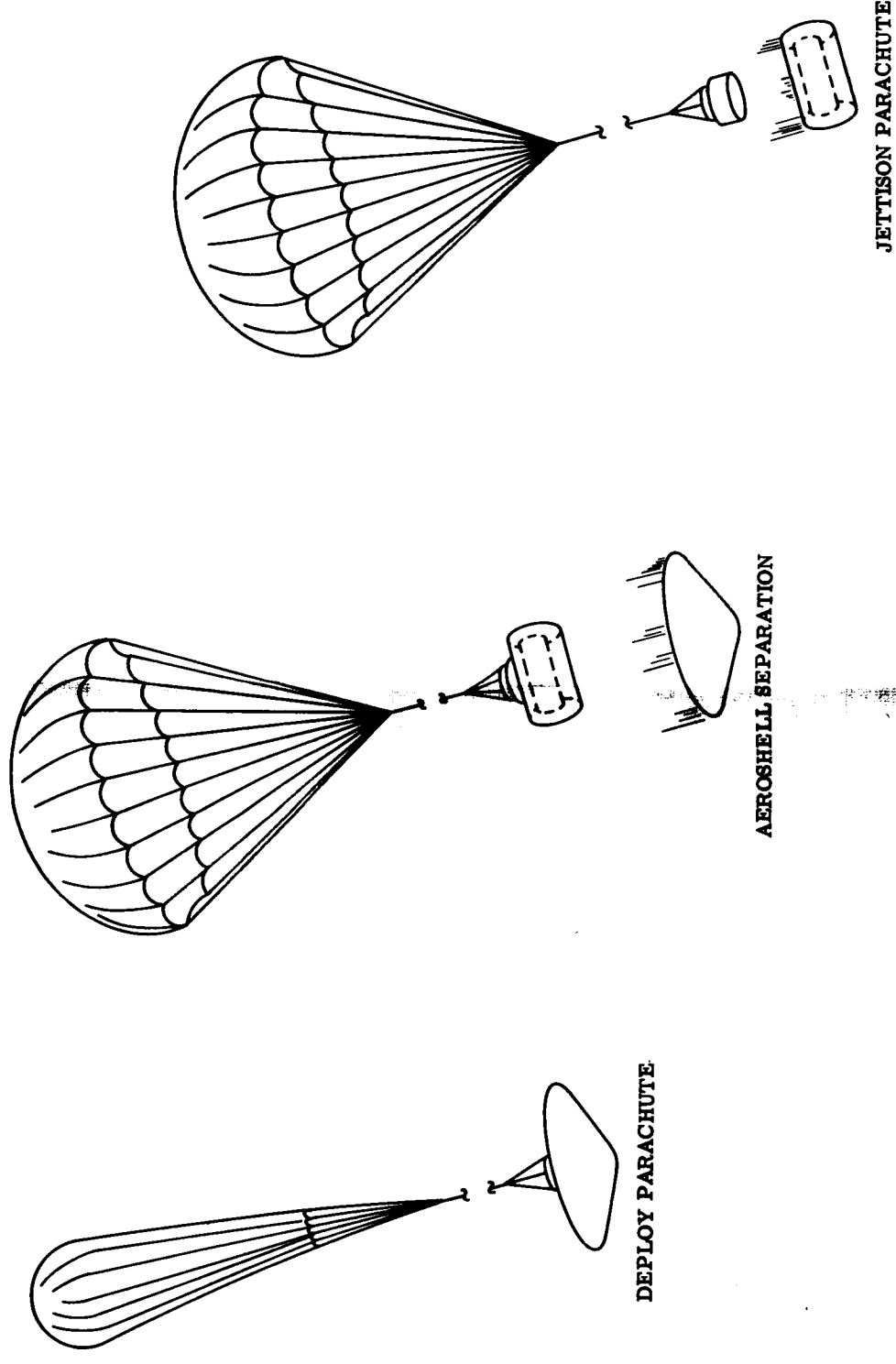
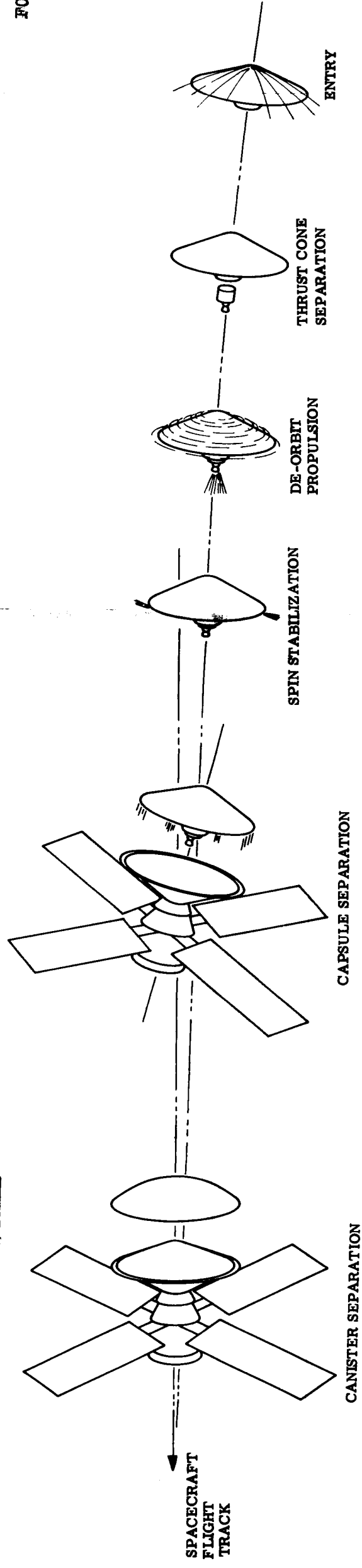


Figure 6.1-1. Operational Flight Sequence from Separation to Impact

FOLDOUT FRAME

FOLDOUT FRAME

FOLDOUT FRAME

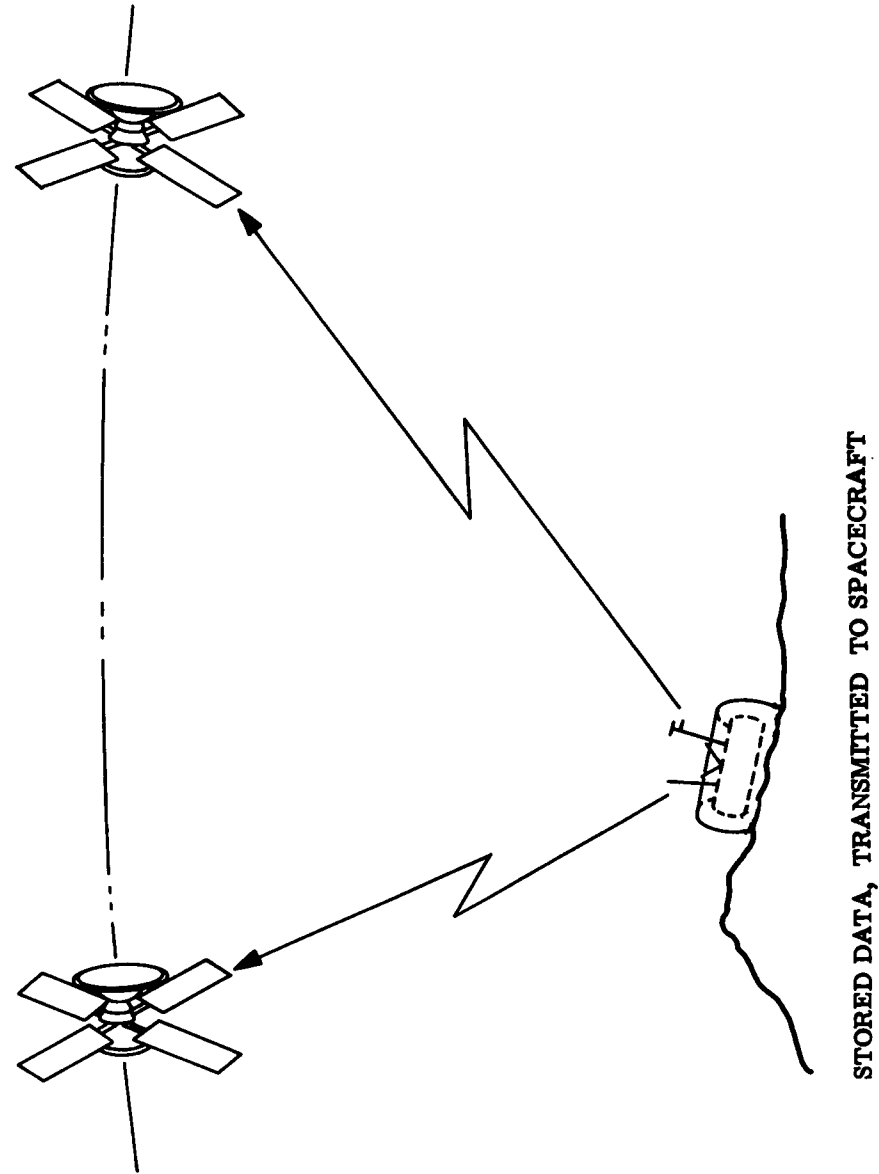
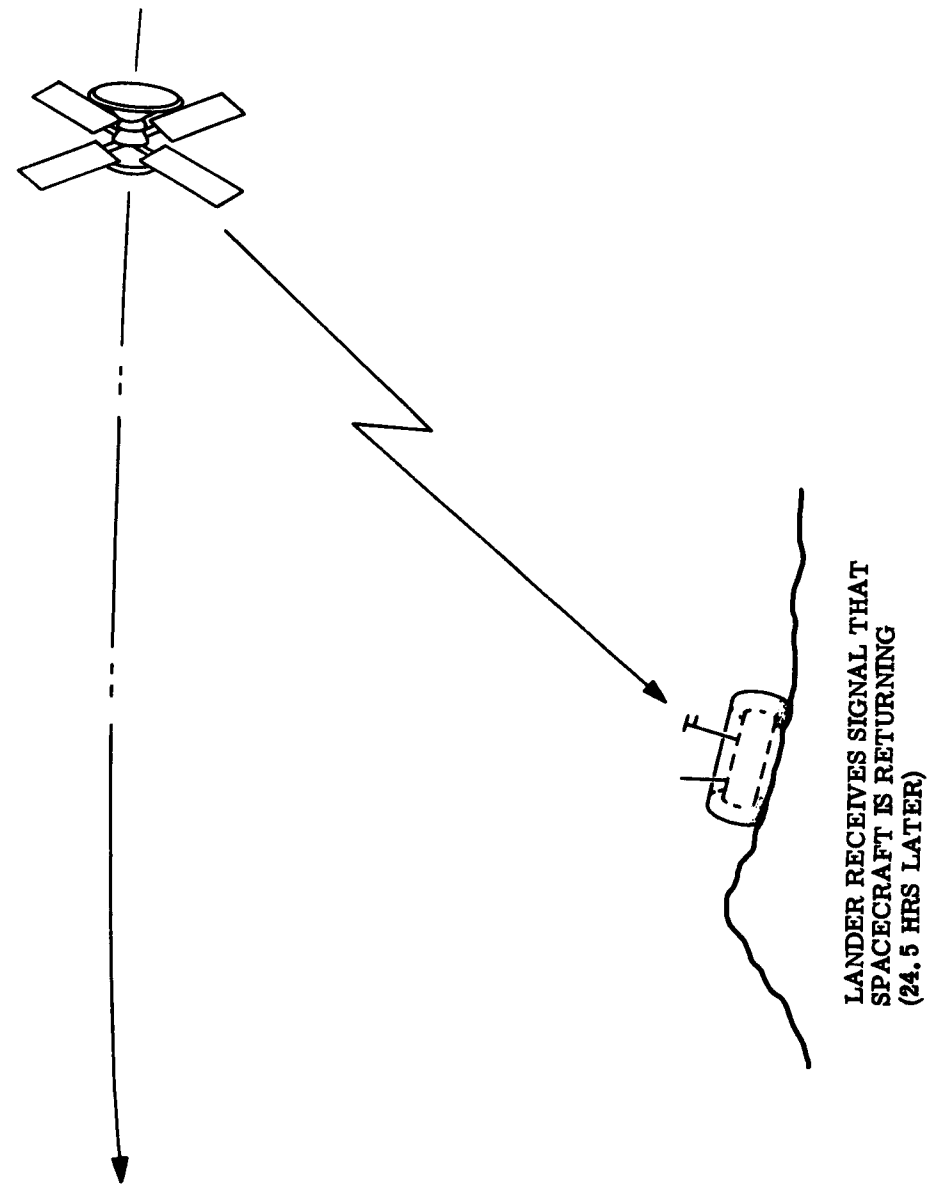
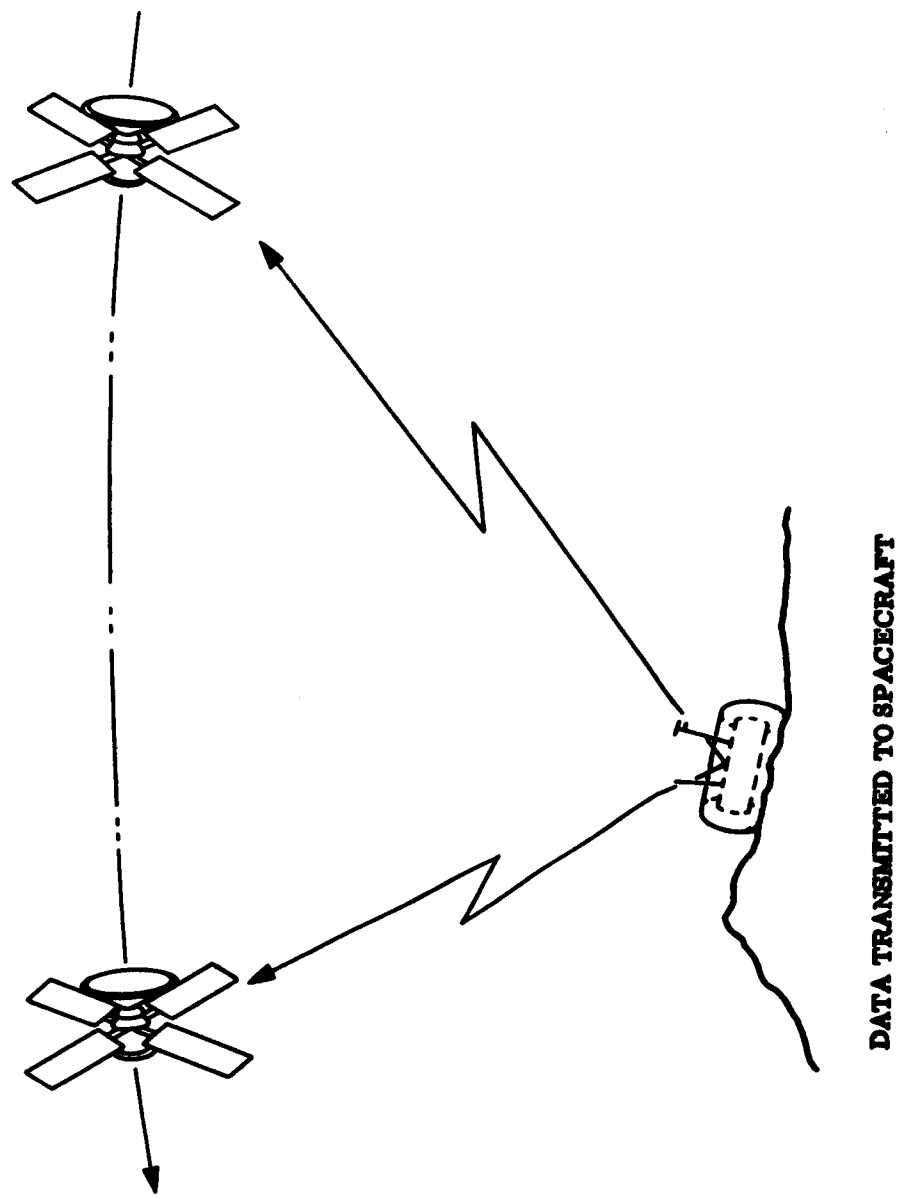


Figure 6.1-2. Landed Operations

6.2 CAPSULE SYSTEM DESIGN DESCRIPTION

A basic difference in the direct entry system and the out-of orbit entry system in a given point design pair is that the ballistic entry parameter ($W/C_D A$) for the direct entry vehicle (20,800 ft/sec entry velocity and 25° path angle) is approximately 0.75 the value appropriate for the out-of-orbit entry system (15,000 ft/sec and 16° at entry). Direct entry systems entering at a path angle increased to 40° require a ballistic parameter about 0.4 times smaller than the out-of-orbit vehicle.

The allowable or limiting ballistic coefficient is determined for the different entry mission modes by selecting the best combination of aeroshell drag area, parachute deployment, size, and landing load attenuation in the deceleration profile to Lander touchdown. The entry system velocity must be reduced to Mach 2 before parachutes are deployed and this deceleration increment must occur at a sufficiently high altitude that the Capsule Lander system can be decelerated by parachute to the acceptable touchdown velocity increment. In this study, the ballistic entry parameter limit is determined for each entry mode based on parachute deployment in the VM-8 Mars model atmosphere (lower altitude at Mach 2) and parachute sizing for descent in the VM-7 atmosphere, the model having the lowest atmospheric density at the surface.

The effect of the limiting ballistic coefficient is that the direct entry Capsules are designed with considerably larger base diameter and heavier aeroshells than the slower entry, out-of-orbit vehicle of the point design pair. The design approach taken for each vehicle in the particular design pair is the same and the system weight difference in the launch configuration, separation and entry is primarily due to the entry shell size because it directly affects the weight of aeroshell structure and heat shield, and the canister (larger size and inertial loading).

The aeroshell designs selected for each of the six Capsule point designs incorporate blunt body, sphere cone shell structures with ablative heat shields using elastomeric formulations such as GE's ESM 1004X at 16 lb/ft³ density for the out-of-orbit vehicles and ESM 1004 AP at 35 lb/ft³ density for the direct entry vehicles. The selected entry system structure and shield design is an extension of ICBM technology and the integrity of the approach in either soft bonded shields or film adhesive shields has been proved. The shield materials referenced are typical of the application but the exact formulation required would be specified in a more detailed engineering phase of a Mars mission program.

The Lander system of the Capsule is retained within the aeroshell by a tension strap arrangement and released by burning the wire wrap of the hot-wire bolts with 30 msec of 10 to 15 amp current. It is separated from the aeroshell by the parachute drag differential. The preferred release, separation and deceleration sequence is initiated with an altimeter. G-level switch and timing units as well as an axial g-level and base pressure measurements approach have been considered for the parachute deployment device. The altimeter approach is preferred because it can be used to delay parachute opening (below Mach 2) to match the descent time of the Lander to the view time available for communication with the Orbiter before and after landing. The requirement for shortening the descent time is most necessary if the flight was made in a VM-9 type atmosphere.

The Lander contains the instruments, power, sequencing, telemetry, and communication equipment to perform the surface science operations. The equipment is contained within a torroidal rim-stiffened cylinder that is equipped with a deep ring of phenolic glass, honeycomb structure that is sized and positioned to attenuate the landing loads by mechanical crush-up of the honeycomb material. The first point design pair developed for the minimum surface lifetime mission were prepared with both omni-directional and multi-directional Landers to develop the weight and size difference in the out-of-orbit and direct entry vehicles due to the design approach taken for impact attenuation. The difference in the weight of attenuation material between omni- and multi-directional landing (522 and 287 lb, respectively) is the difference in the omni- and multi-directional Lander total weights (weight suspended on parachute) of 858 and 623 lb.

The following weight statement (table 6.2-1) summarizes the comparison of the out-of-orbit and direct vehicles and the influence of Lander type for the minimum lifetime mission. The comparison is based on the first design pair data but the results are typical of like comparison studies of the other design pairs.

The pre-entry systems of the Capsule consist of the sterilization canister, adapter, attitude control, and the de-orbit maneuver hardware. The prime function of the canister is to encapsulate the Capsule system and maintain a physical, biological barrier to prevent contamination of the Capsule during:

1. The terminal sterilization cycle
2. Post sterilization operations in the ground environment
3. During launch and powered flight
4. During the cruise and up to the sequence for Capsule-Orbiter separation.

The canister design approach for the six Capsule designs is a semi-monocoque construction in minimum manufacturing gauge (0.012), 7075 aluminum. The rear shell of the canister assembly contains the Capsule-to-Orbiter adapter within the sterilized envelope and connections to the Orbiter are made outside this envelope. The forward shell is released by applying 24 amps for 30 msec to the four hot wire bolts of the V-ring type clamp segments. The shell is separated by two mechanical springs with a velocity of 2 ft/sec.

The adapter provides the structural transition between the Capsule and the Orbiter and contains the equipment for separating the flight systems. The Capsule is released by applying 48 amps to four explosive nuts and is separated at approximately 1 ft/sec by four springs.

Both spin de-spin and three axis control systems were studied for Capsule attitude control for the deorbit maneuver, for entry path angle control and for vehicle control up to Lander separation from the aeroshell. The six point designs have been detailed with spin de-spin for pre-entry and roll control during entry. The final system would be selected after more detailed error analyses are made and the principle trade-offs in landing site location; data communication and trajectory design are completed.

TABLE 6.2-1. COMPARATIVE WEIGHT SUMMARY OF MINIMUM MISSION SYSTEMS

Aeroshell Diameter	Out-of-Entry		Direct Entry	
	8.3 ft	8.3 ft	12.7 ft	11.4 ft
Lander type weight (lb)	Omni- 858	Multi- 623	Omni- 858	Multi- 623
Retardation weight (lb)	228	172	228	172
Aeroshell and Propulsion	329	329	465	389
Capsule weight at separation from spacecraft (lb)	1415	1124	1551	1184
Capsule weight at entry (lb)	1246	955	1480	1127
Ballistic entry coefficient (lb/ft ²)	15.2	11.7	7.9	7.3
Capsule weight at launch (lb)	1626	1335	1882	1463

Based on the baseline missions data, the out-of-orbit entry vehicles require a velocity increment of 235 meters/sec and the direct vehicles 45 meters/sec. Both solid propellant systems and liquid propulsion systems have been detailed in the point designs. The liquid systems are more easily adapted to de-orbit maneuver changes as weight and velocity requirements are modified. In the low impulse requirements range, the liquid systems have disproportionate weights for the propulsion hard parts compared to the total and generally, the liquid systems applicable to these study vehicles are about three times heavier and required considerably larger packaging volumes than the solids propulsion systems.

Both systems have been designed into the Capsules and the pertinent trades and the engineering details in each design application are given in Section 6.3 of this volume. In all six design applications the de-orbit maneuver system is arranged to be jettisoned before entry by release of preloaded, hot-wire bolts of the thrust cone and separation by mechanical springs.

The following sections give the engineering details of the direct entry Capsule of the second design pair prepared in this study. The surface lifetime is for more than 90 days, equipped with solar panel and battery electric power supply and with transmission capability for relay as well as direct to Earth. The Orbiter is assumed unavailable for data relay after the third day and thereafter data is transmitted to the Deep Space Network (DSN) directly. This is the fourth Capsule (Point Design 4) in the list of six point designs.

6.2.1 SCIENCE DATA REFERENCE

The weight of the sensors selected and a baseline reference of the atmospheric data acquired from entry to impact in the maximum flight time range of atmospheres is shown in table 6.2-2. Pressure and temperature readings are taken at both the stagnation and the base region of the aeroshell. The atmospheric density profile is determined from the vehicle aerodynamic data and the measured deceleration profile of the Capsule.

TABLE 6.2-2. SCIENCE WEIGHT SUMMARY

Entry Science	Weight (lb)	Data Load (Bits)		
		VM-8*		VM-9*
Pressure	3.0	1.0×10^4	-	2.6×10^4
Temperature	1.5	4.4×10^3	-	2.0×10^4
Composition	8.0	6.6×10^3	-	$10. \times 10^3$
Density	2.0	0.8×10^5	-	2.0×10^5
Water Vapor (Ducting)	1.0	5.7×10^1	-	3.7×10^2
	<u>15.5</u>	<u>1.01×10^5</u>	-	<u>2.56×10^3</u>
Landed Science				
Pressure	1.4	1.35×10^3		
Temperature	2.0	2.7×10^3		
Wind	5.0	4.9×10^3		
Moisture	10.0	1.77×10^3		
Photo Imaging	4.8	1.02×10^7		
Clinometer	2.6	7.0×10^1		
Soil Sampler	9.5	3.0×10^4		
	<u>35.3</u>	<u>1.02×10^7</u>		

*Time from entry to impact in VM-8 = 302 secs
in VM-9 = 566 secs

The landed science consists of meteorological data and surface imagery taken with (Philco) facsimile cameras that take four scenes of low resolution data and four nested scenes of high resolution data. The low resolution scenes are each $35^\circ \times 50^\circ$ segments imaged with $1/10^\circ$ Instantaneous Field of View (IFOV) and the high resolution scenes are $5^\circ \times 5^\circ$ segments imaged with $1/100^\circ$ IFOV. The total data acquired in four high and four low scenes (63 gray shades) is $6 \times 10 + 4.2 \times 10^6$ or 1.02×10^7 bits. A typical data summary for the surface operations is included in table 6.2-2.

A total of 4.08×10^7 bits of surface imagery are relayed to the Orbiter. The imagery is transmitted twice in the first day, after landing and at periapsis passage of the Orbiter. A third set of four scenes is transmitted at the next day's periapsis and a fourth set on the third day. Thereafter, the Orbiter changes to a new ephemeris and the relay link is discontinued. Meteorological data is sent direct on S-band to the DSN each day. An additional quantity of surface imagery is transmitted at a later date when the batteries have been charged by the solar power equipment. The Lander of this Capsule is the same as the one in the out-of-orbit Point Design 3 and if the landing sites are the same, the mission data retrieved is the same regardless of entry mode.

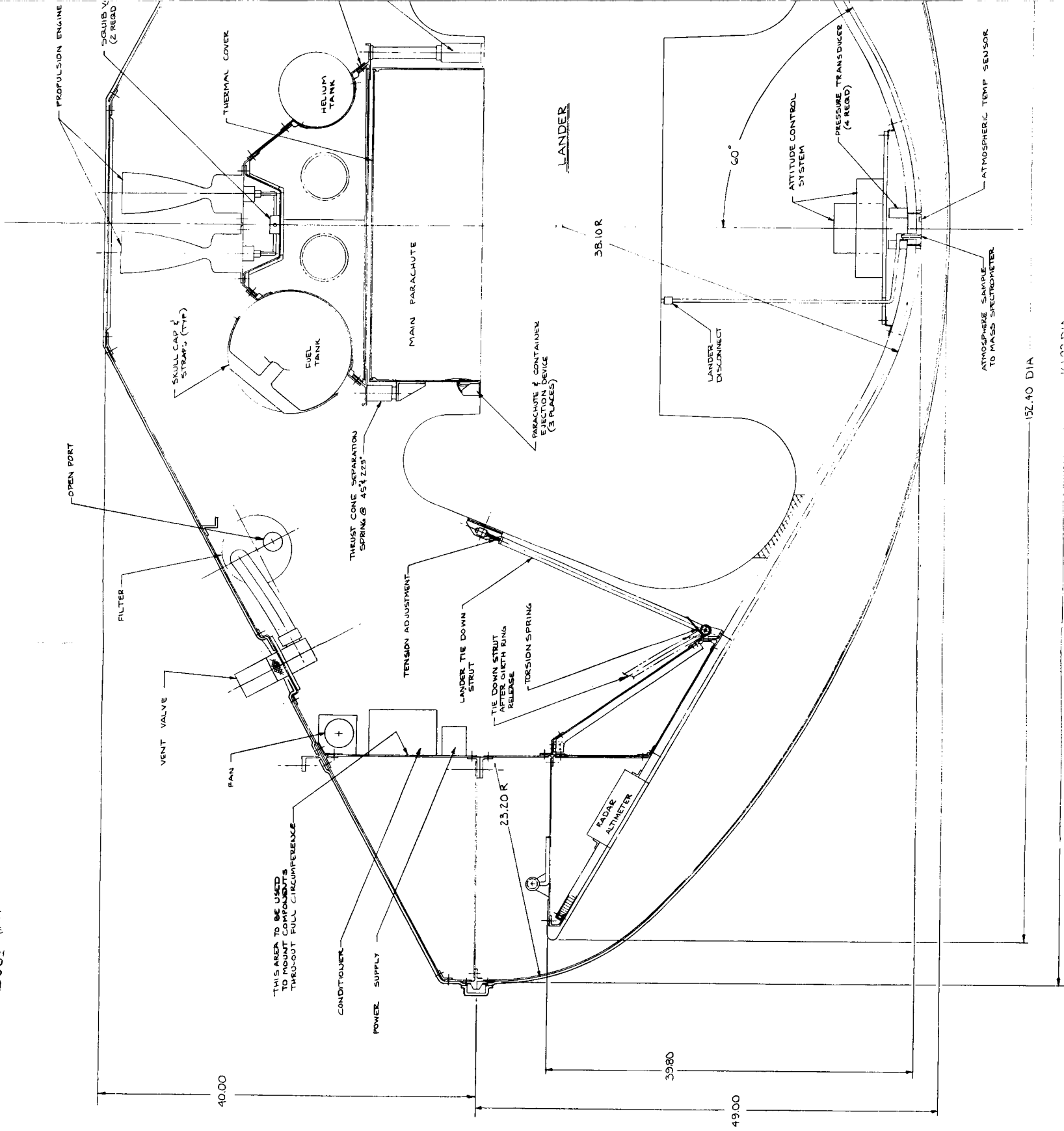
6.2.2 CAPSULE SYSTEM CONFIGURATION

The Capsule for Point Design 4 is a multi-directional Lander containing the minimum surface science with a surface lifetime of more than 90 days. It will be delivered to the Martian surface in a direct entry mode. Telecommunications initially will be accomplished by a UHF relay to the Orbiter and later by a direct link S-band system. A 25 ft^2 solar array will provide power for the extended lifetime period of performance. A liquid non-propellant propulsion system is used to de-orbit the entry vehicle. Parachute deployment will be initiated by a radar altimeter. Fig. 6.2.2-1 shows the configuration of the Point Design 4 Capsule.

6.2.3 CAPSULE SYSTEMS WEIGHT

The weight and inertials of this direct entry Capsule with a greater than 90 day surface lifetime is given in table 6.2-3. In this design approach, the Capsule is equipped with the same multi-directional Lander of 934 lb included in the out-of-orbit Capsule of Point Design 3. The entry drag area must be larger to match the baseline design requirement of approximately 8 lb/ft^2 ballistic coefficient. The weight at launch separation, entry, and landing are the same as those of the direct entry Capsule of the minimum lifetime mission. The Lander, however, is equipped with considerably more mission capability by utilizing the weight saving of multi-directional Lander crush-up material over the omni-directional design. The Capsule aeroshell base diameter is 12.7 ft and requires a hammerhead flight shroud configuration. A preliminary look at the potential application of an inflatable aft section to increase the aeroshell from 8.3 ft in diameter to 12.7 ft at entry is given in the report Section 9.

FOLDOUT



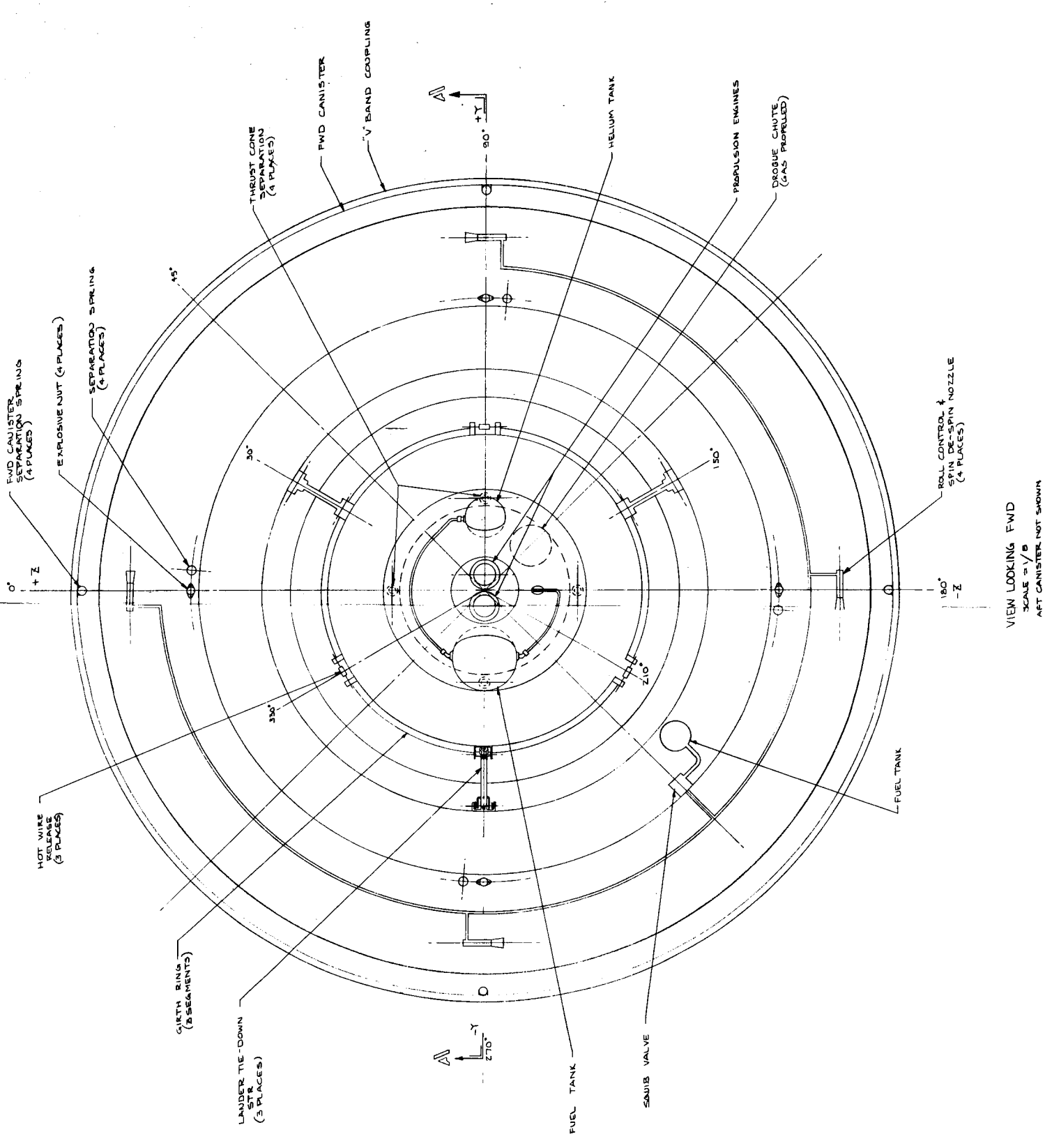
SECTION A-A

SCALE = 1/4

FOLD-out #1

FOLDOUT FRAME

FOLDOUT FRAME



VIEW LOOKING FWD
SCALE = 1/8"
AFT CANISTER NOT SHOWN

Figure 6.2.2-1. Mars Hard Lander, Point Design 4

FOLD-OUT #2

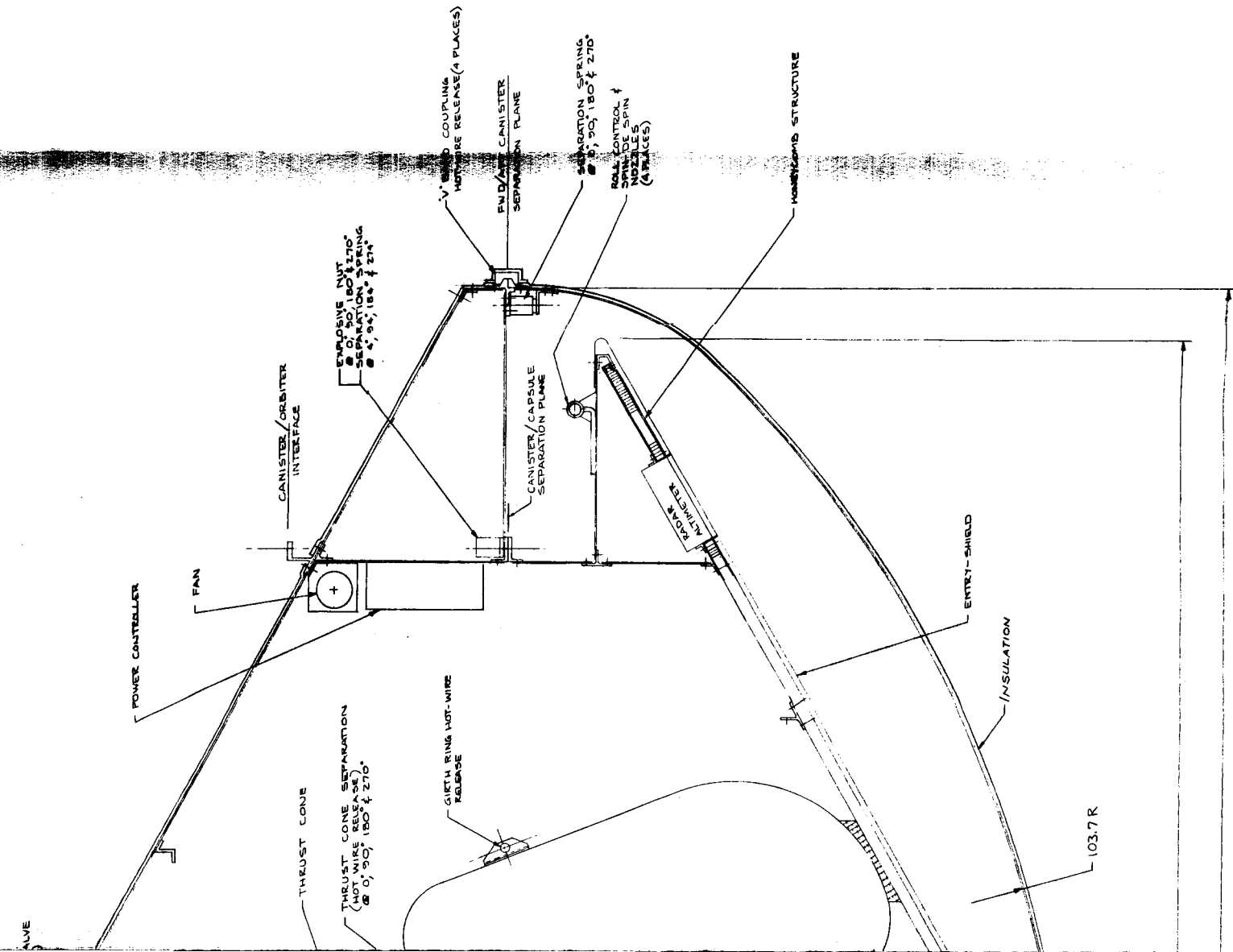


TABLE 6.2-3. WEIGHT AND INERTIA COMPOSITION, POINT DESIGN 4

Capsule Systems	Weight (lb)	Roll	Pitch slug/ft	Yaw
Lander	934			
Aeroshell	396			
Retardation	228			
Propulsion	89			
Canister and thermal blanket	330			
Capsule at launch	1977	434	376	376
Capsule at separation	1647	299	205	205
Capsule at entry	1558	298	195	195
Landed system	934	72	59	59

6.2.4 FUNCTIONAL BLOCK DIAGRAMS

The functional block diagram, fig. 6.2.4-1, is the complete system delineation of events from launch until the end of the mission. Each functional component is located with respect to functional criteria.

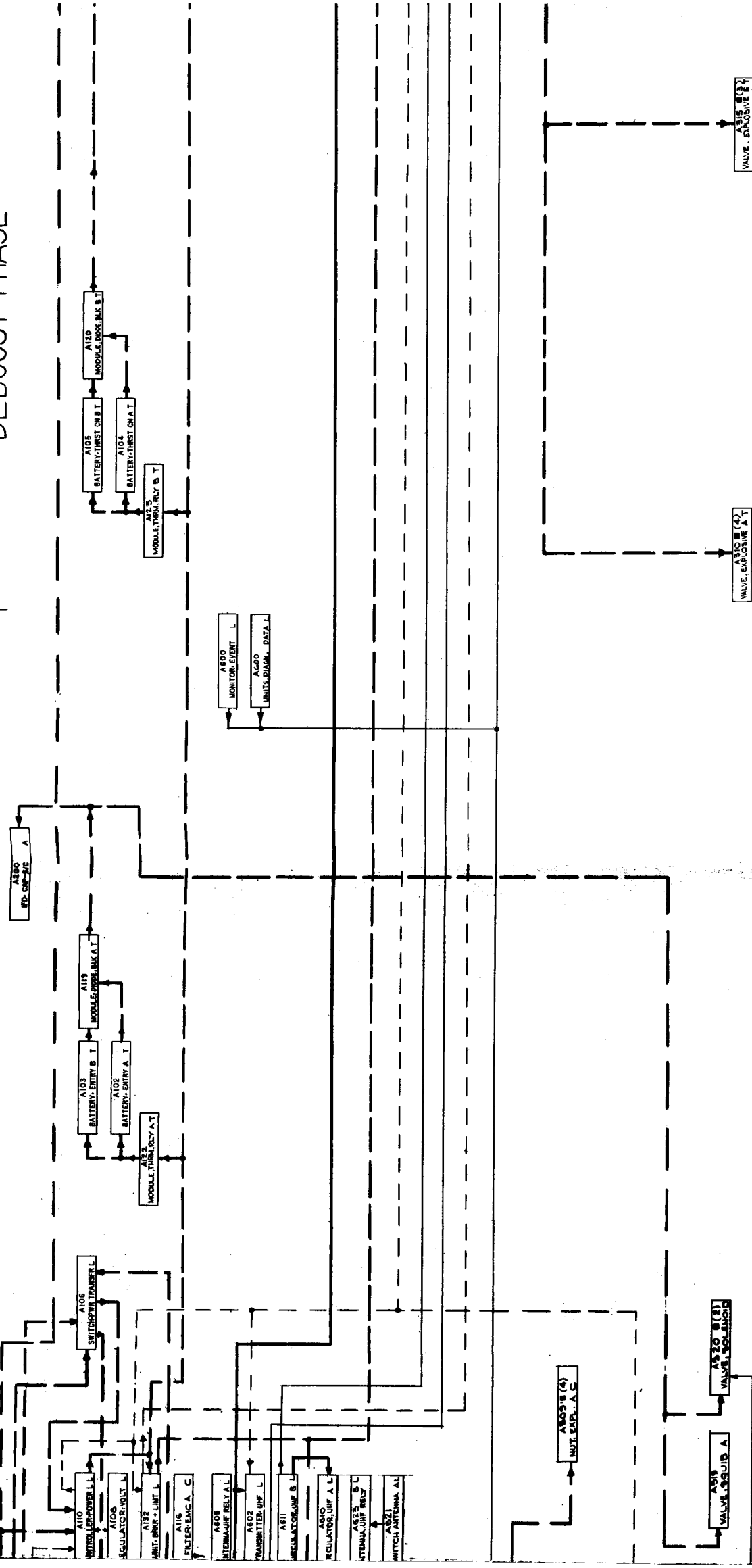
The horizontal axis can be considered a relative time axis with each mission phase occupying a discrete time segment, each segment, however, does not represent a linear time scale since the total cumulative length would become unreasonable. The time axis then, indicates the sequence of events rather than the time at which they occur. Whenever components operate in multiple events, either the primary event or the typical mode of operation is indicated. Although the component location indicates the relative beginning of the event, the duration, repetitive rate or the stop time of the event is not indicated.

The vertical axis is used to group the components by subsystem. The subsystem groupings, indicated on both the right and left hand borders, is maintained throughout the drawing. Therefore, for any given event, all components within the system used to perform that event will be shown within the same vertical time boundaries designated at the borders, and the components within a given subsystem are aligned from top to bottom in order of the first function of operation.

The inter-relationship of the components has been separated into four classifications as indicated on the drawing: (1) unregulated power; (2) regulated power; (3) signals; and (4) data. For clarity, components are shown with the most meaningful functions indicated. For example On/Off signals are often considered to originate by correct power switching and are thus designated by a power flow line rather than a signal line. Furthermore, each individual line may carry one or more similar functions such as different power levels.

DEBOOST PHASE

SEPARATION PHASE



LEGEND

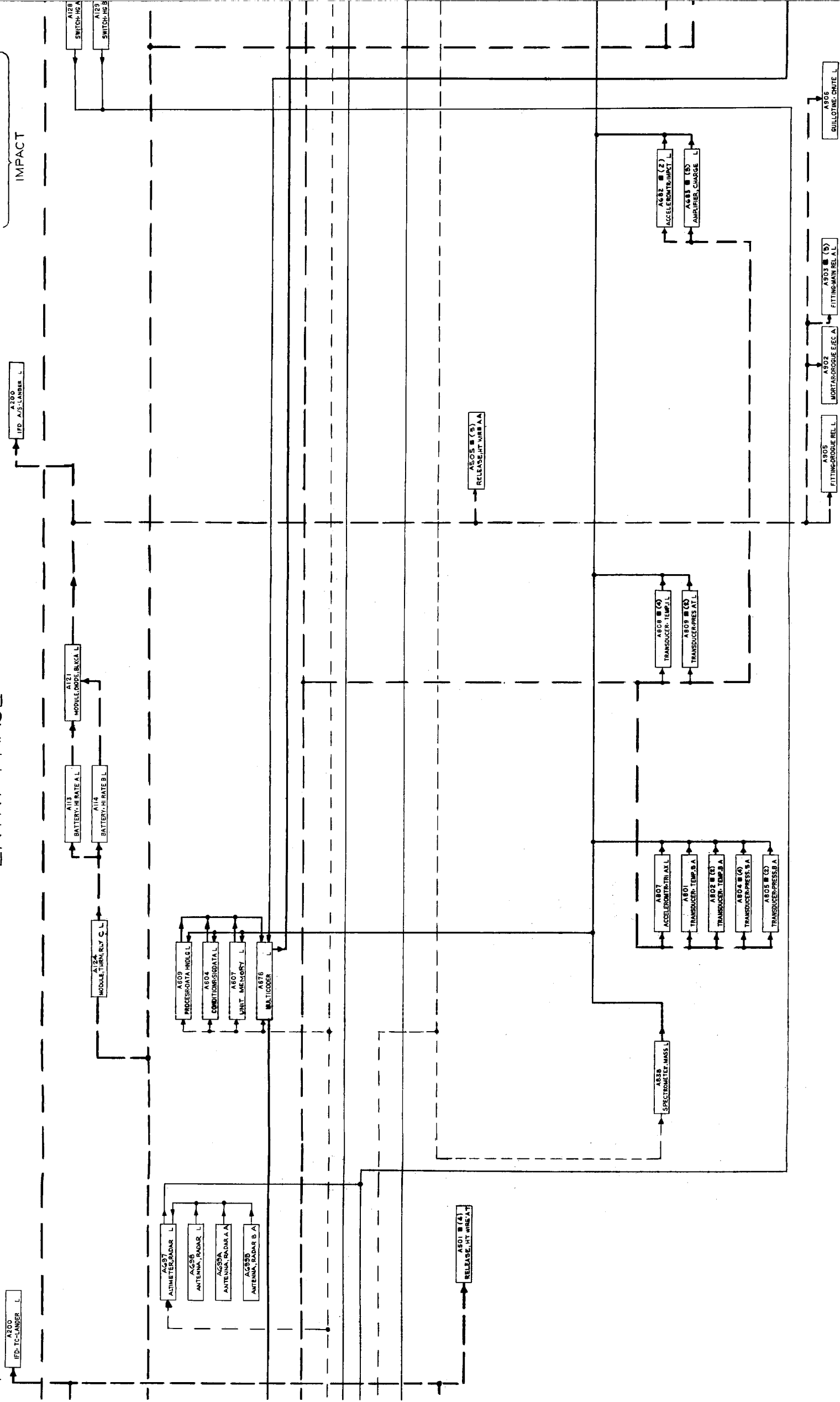
- ADDITIONAL UNITS NOT SHOWN
- UNREGULATED POWER FLOW
- - - REGULATED POWER FLOW
- ... SIGNAL PATH
- DATA PATH

SEPARATION PHASE

DEBOOST PHASE

FOLDOUT FRAME

ENTRY PHASE



ENTRY PHASE

FOLD-OUT #1

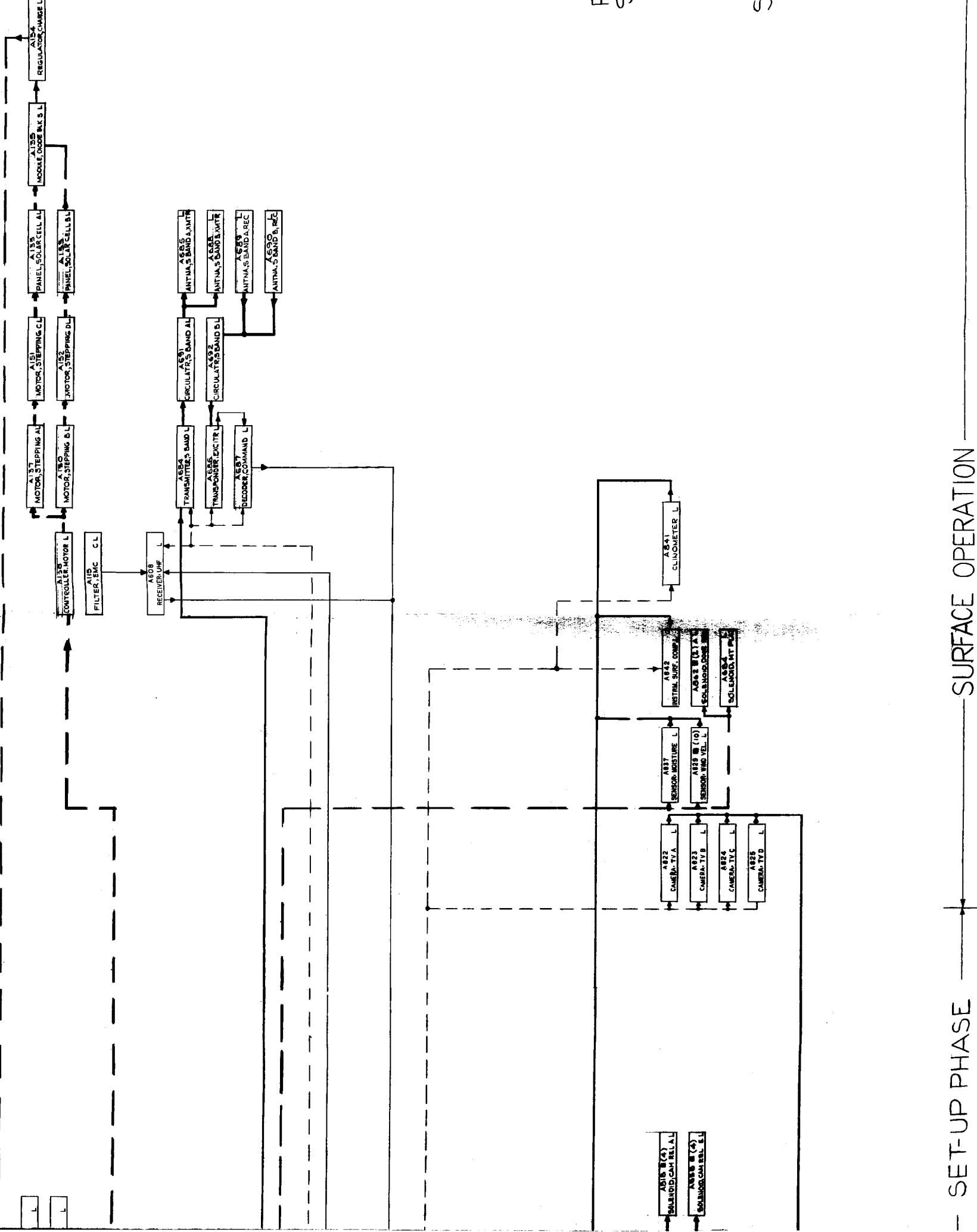
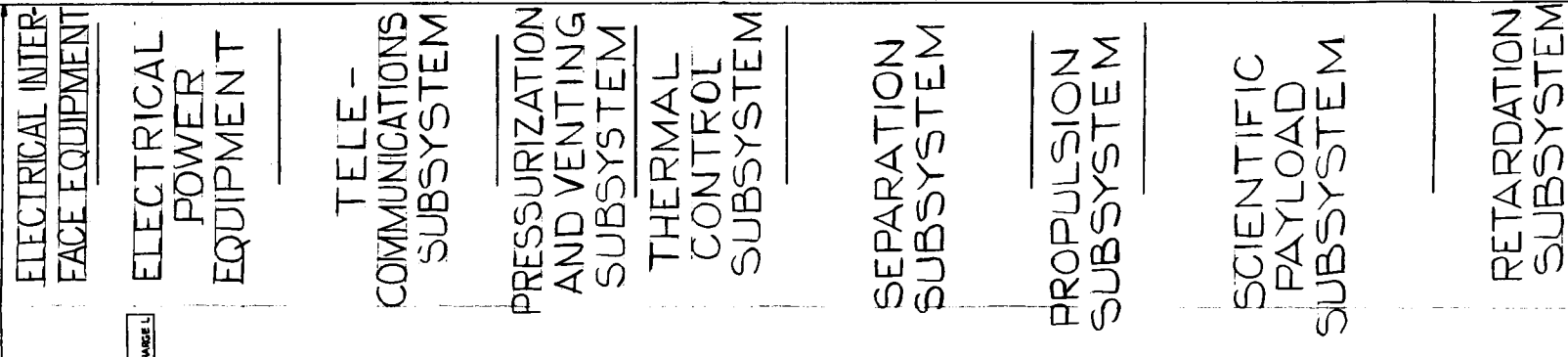


**Figure 6.2.4-1. Point Design 4
Functional Block Diagram
(Sheet 2 of 2)**

The components are represented by uniform blocks with a common notation. The electrical reference designator is assigned in accordance with MIL-STD-16. The component's name is listed below and the location of the component is noted by the appropriate letter abbreviation at the extreme right of the block.

The electrical connections between individual components and between subsystems is designed such that it allows the appropriate operations to be performed. By referring to Point Design 4 block diagram fig. 6.2.4-1, it can be seen that for a particular event, such as UHF transmission, there exists a specific group of components that must operate. These components are linked by several of the function lines. The sequence of events and flow of data can be traced as shown below. The appropriate type of power is switched through the power controller. This signal is supplied by the Lander programmer which initiates the power controller switching of all components required for the transmission of the data whether in the electrical, telecommunication or scientific payload subsystem. The correct interconnections then allow data flow from the science subsystem to the telemetry subsystem.

Although other events require a different series of components, the relationship of component functional line designations to events is similar. A separation event is preceded by the Lander programmer signalling the power controller which turns the stepping switch and connects the capacitor discharge circuit. These then supply the pulse loads as required.

Similar interconnections exist for all other events and the same scheme of functional operations is carried throughout the drawing. These component/subsystem relationships then become the foundation for the harnesses that physically supply the required electrical interconnections.

6.2.5 POWER PROFILE POINT DESIGN 4

The power profile as illustrated in fig. 6.2.5-1, represents the power demand sequence on the operational battery and solar array. By relating these demands to the event times, the curves reflect the mission sequence of events since each pulse is the power required by all the components operating at the event.

Superimposed on a continuous level of power are the various events. The operational battery is activated prior to Capsule/Spacecraft separation. It then supplies the required power for telemetry transmission during de-orbit and entry. In addition, entry science data is transmitted until impact. The radar altimeter also increases the power demands during this period.

After impact, the UHF link transmits the stored data with a real time imagery period. The meteorological sampling period begins at 20 minute intervals with clinometer readings every 6 hours. The surface composition instrument represents the relatively high continuous power level during the first day. The diurnal day concludes with another UHF relay transmission of stored data and real time imagery.

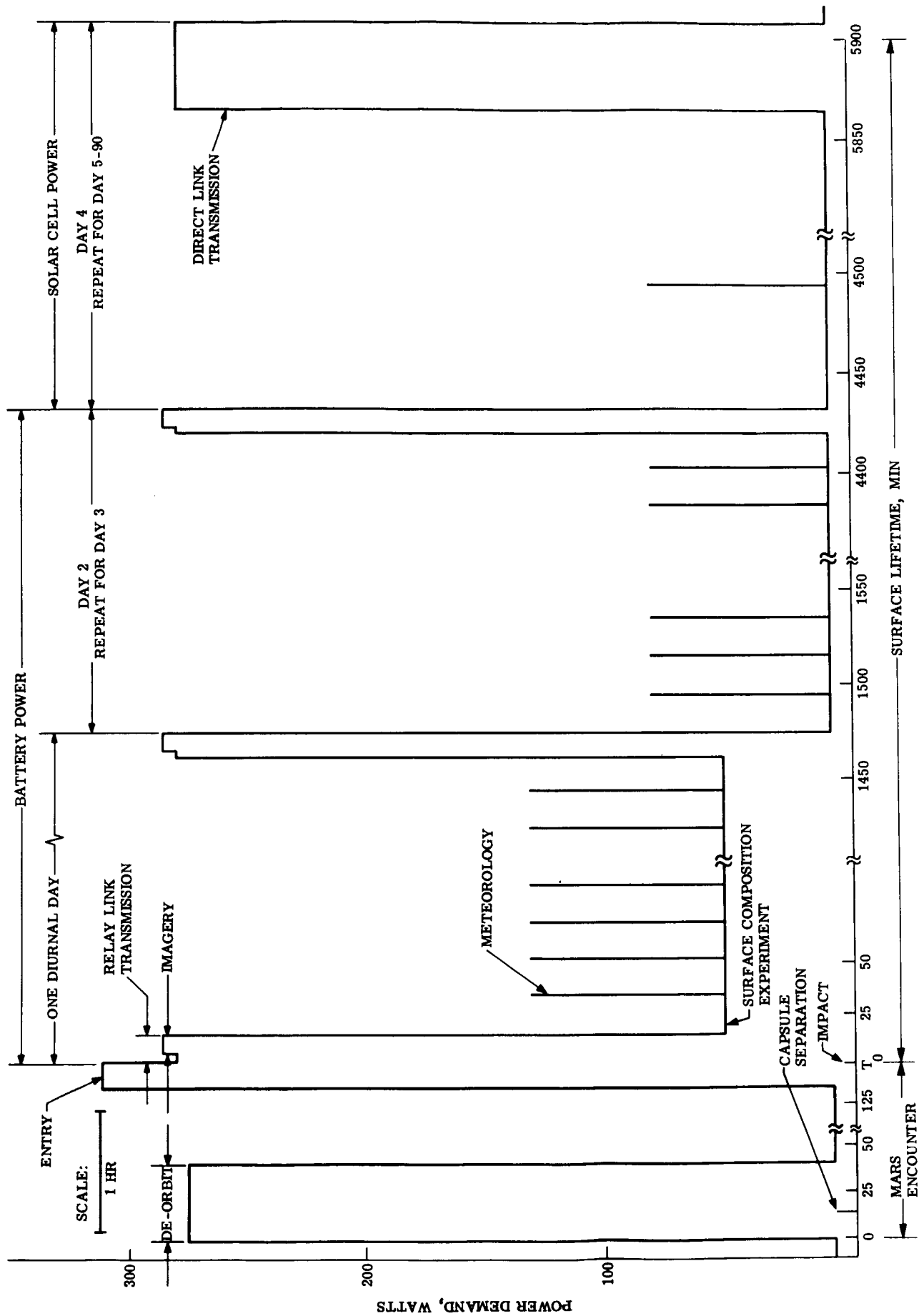


Figure 6.2.5-1. Power Profile, Point Design 4

Days 2 and 3 are identical with meteorological sampling every 20 minutes and a UHF relay link transmission of stored data and real time imagery.

After the fourth day and for the duration of the 90 day mission the solar array which has been deployed will supply the power during the day and charge the battery for night operation. This day 4 sequence can be seen to consist of a meteorological sampling period every hour with a direct link transmission period to Earth of both the stored data and real time imagery.

6.3 PRE-ENTRY SYSTEMS

6.3.1 CANISTER

6.3.1.1 Design Constraints

Canister design constraints for Point Design 4 were as follows:

1. Maximum diameter less than specified in Section 2.3.1 (171.6 in.)
2. Withstand an internal pressure
3. Withstand the inertial loads of launch and powered flight
4. Provide adequate clearance between the aeroshell heat shield and canister
5. Provide a separation and field joint as one and the same joint
6. Provide support for the entry system

Diameter constraints on the maximum allowable canister diameter were fully described in Section 2.3.1 and were imposed by the internal envelope available for the Capsule system installation.

Due to the requirement to maintain biological integrity within the internal portion of the canister it was necessary to evaluate the effects of an internal pressure on the shape, material and construction of both the forward and aft canisters. Inertial loading of the canister during flight and handling conditions, including equipment loadings on the aft canister, was a constraint which was traded off against the differential pressure to determine the more severe loading environment for the canister structure.

A driving influence on the canister size was the allowance necessary for clearances between the entry system and canister. This clearance has been estimated to be 2.0 in., as shown in fig. 6.3.1-1, to allow for Capsule System dynamic excursions.

The field joint for the canister could be combined with the device used for in-flight separation or it could be entirely separated. Maximum leak tightness was an overriding criteria in either case.

The entry system must be supported within the Capsule System and a means of support had to be designed. This design also considered that in addition to support it must have the capability of withstanding and transferring the entry system inertia loads through the structure and to the Capsule bus interface to the bus adapter ring.

6.3.1.2 Canister Structural Description

The forward canister for Point Design 4 is a hemispherically shaped minimum gauge aluminum shell making a tangent at its maximum diameter through a quarter torus section, fig. 6.3.1-2. This structure has been designed to act as a pressure vessel and the torus section provided to eliminate the inboard kick loads and minimize shell bending at the field joint ring due to the internal pressure. The minimum

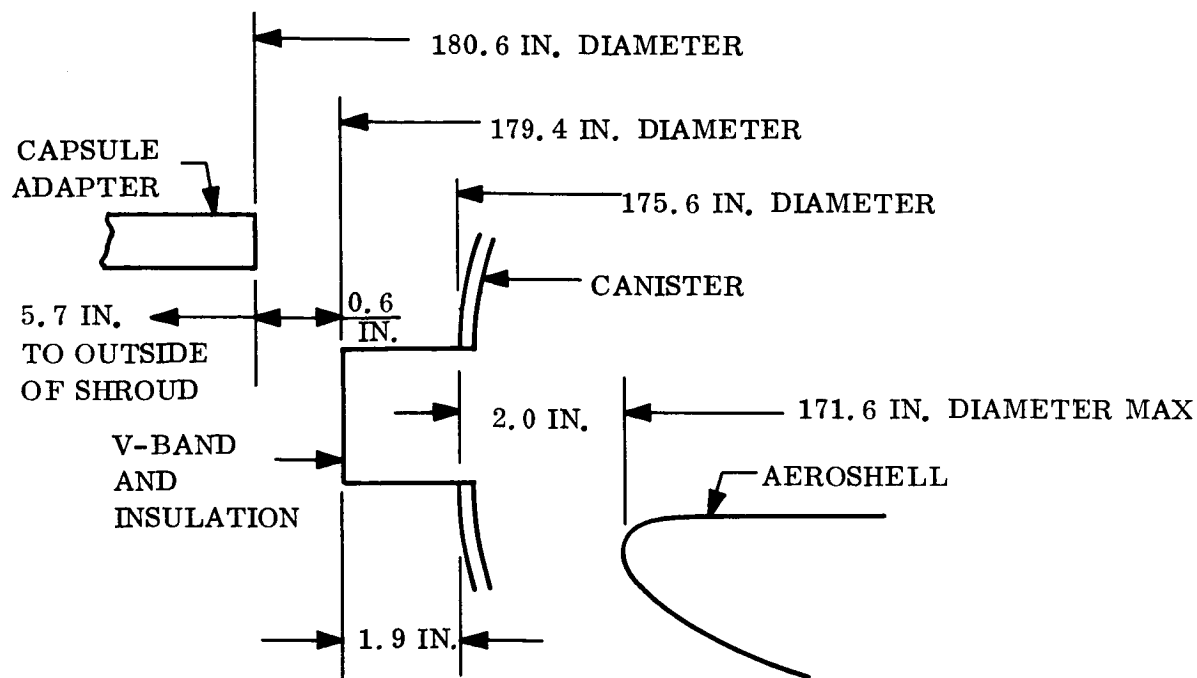


Figure 6.3.1-1. Aeroshell/Canister Clearances

gauge aluminum material is more than adequate to withstand the pressurization and inertial loads imposed on it. The hemispherical shape has been proven in previous analyses (Voyager Phase B Study) to be considerably stiffer from a dynamics standpoint than a conical shape.

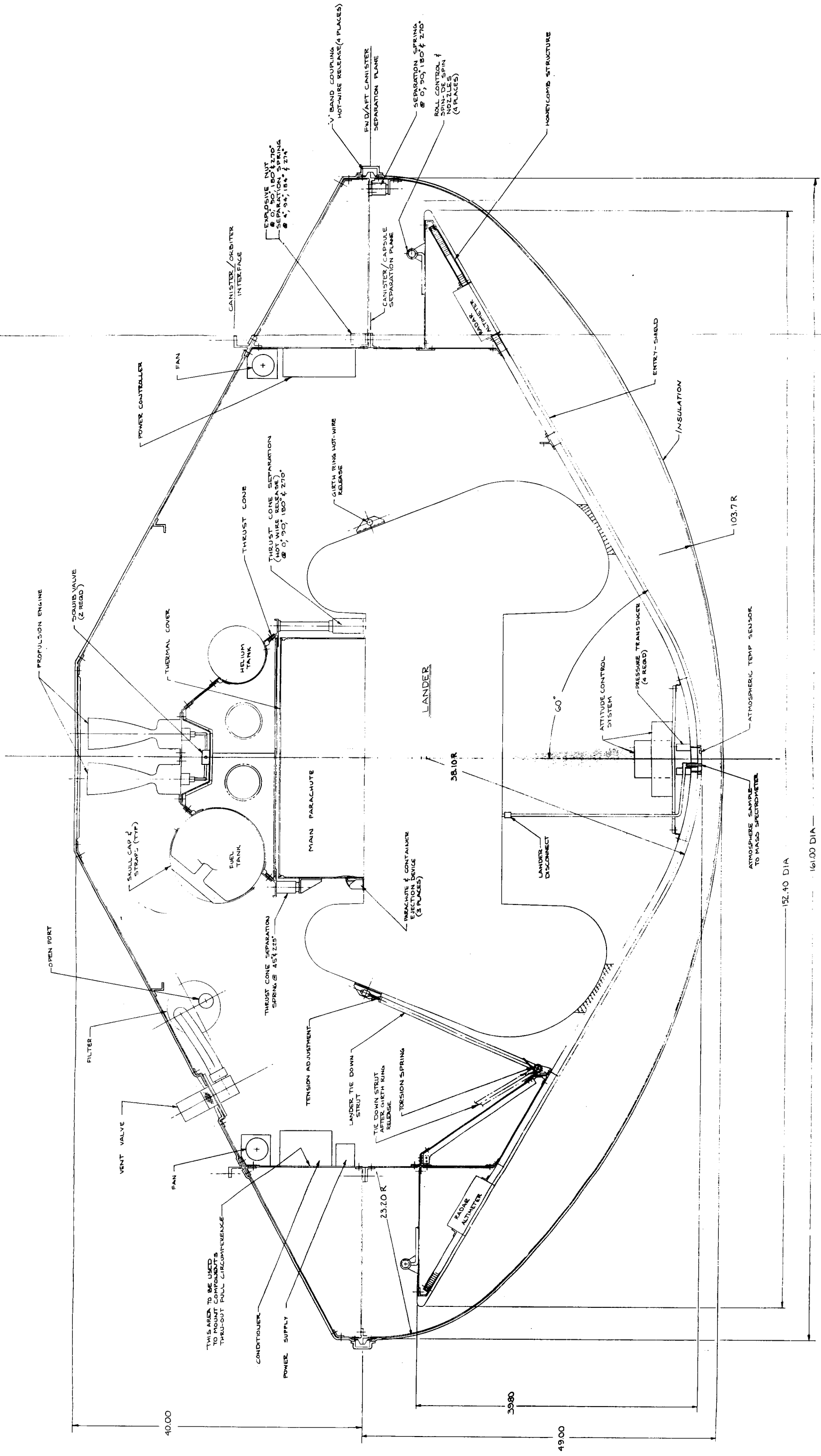
The forward canister has been designed such that there will be no yielding under design load conditions and no failure under ultimate design load conditions. This includes the transient and steady state loads encountered under the conditions of handling, transportation, sterilization, pre-flight, powered flight, transit and separation.

Inertial loading conditions were determined to be less severe than the internal pressurization condition in the design of the canister and the field joint ring. This can be seen in table 6.3.1-1 where the running loads on the interface ring are tabulated for both inertial and pressure loading conditions. As a result the pressure loading condition determined the desired construction, material and thicknesses to be used in the structural design of both the forward and aft canister.

Minimum gages were the over-riding constraint on the thicknesses selected for the canister design. Stiffeners to rigidize the shell for dynamic and ground handling loads have been provided. The limit pressure condition for the canister is 1.0 psia

FOLDOUT FRAME

FOLDOUT FRAME



SECTION A-A
SCALE = 1/4

Figure 6.3.1-2. Point Design 4
Inboard Profile

internal pressure and the structure is adequate to withstand a 1.7 psia burst pressure which results in a safety factor of 1.7 on the limit pressure.

TABLE 6.3.1-1. INTERFACE RING LOADS

Load Condition	W_V Vertical Load (lb/in)	W_H Inboard Load (horiz)	
C	1.59	0.57	
E	2.87	0	
F	0.45	2.87	
C&E	4.46	0.57	
C&F	2.06	3.39	
M	41.65	0	0.5 psi skin pressure
N	83.30	0	1.0 psi skin pressure

The field joint rings for the forward and aft canisters provide a seat for the band clamp, which holds the canister halves together, resist the loads imposed by the internal pressure and the band clamp and provide for the pressure tight sealing of the canister assembly. The aft canister ring slides under the forward mating ring and has an internal leg, as shown in fig. 6.3.1-3, which is connected to a bulkhead joining the ring with the internal adapter. This arrangement provides a torque box in the aft canister increasing both its stiffness and structural load carrying capability.

The combined inertia of the forward ring, aft rings and bulkhead is more than adequate to insure structural stability of the field joint under the critical load condition. Fig. 6.3.1-4 shows a plot of the required inertias for ring stability as a function of critical load in pounds per inch.

Structurally the aft canister is sized for the internal pressure which dictates the same minimum sheet gage as the forward canister. The aft canister is essentially conical in shape with the forward and a quarter torus making a tangent with the maximum diameter and the conical afterbody as shown in fig. 6.3.1-2. Stiffening members are located between the adapter to canister ring and the end bulkhead ring. These members also act as supports for the electrical equipment and vent system equipment in the aft end canister.

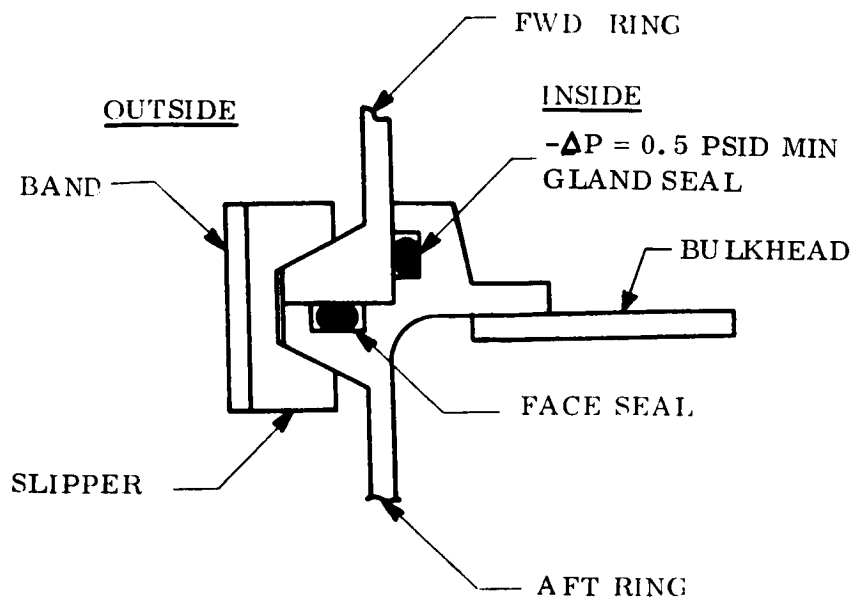


Figure 6.3.1-3. Canister Field Joint

6.3.1.3 Internal Adapter

The adapter for Point Design 4 is designed to support the entry vehicle and transfer loads introduced by the entry system to the capsule bus interface ring. This adapter is internal to the sterilization canister and interfaces with it at the aft canister ring. The adapter picks up the entry system at four points and attaches to the Capsule bus interface ring through the canister skin.

Structurally the internal adapter is a cylindrical aluminum shell with longitudinal stiffeners as shown in fig. 6.3.1-2. The shell and stiffeners have been sized such that the section modulus and working area are more than adequate to withstand the bending moment and axial loads which the structure will experience. The inertial loads used in determining the necessary section properties of the cylindrical skin and stiffeners were 6 g's limit in the axial direction and 2 g's limit in the lateral direction.

The forward ring, at the entry vehicle interface, attaches to a lateral interconnection to the aft canister interface ring. Lightening holes have been placed in the cylindrical structure to allow for free passage of heated gases between the canister and adapter during heat sterilization cycles. The lateral interconnection or bulkhead provides support for the aft canister ring as well as the adapter.

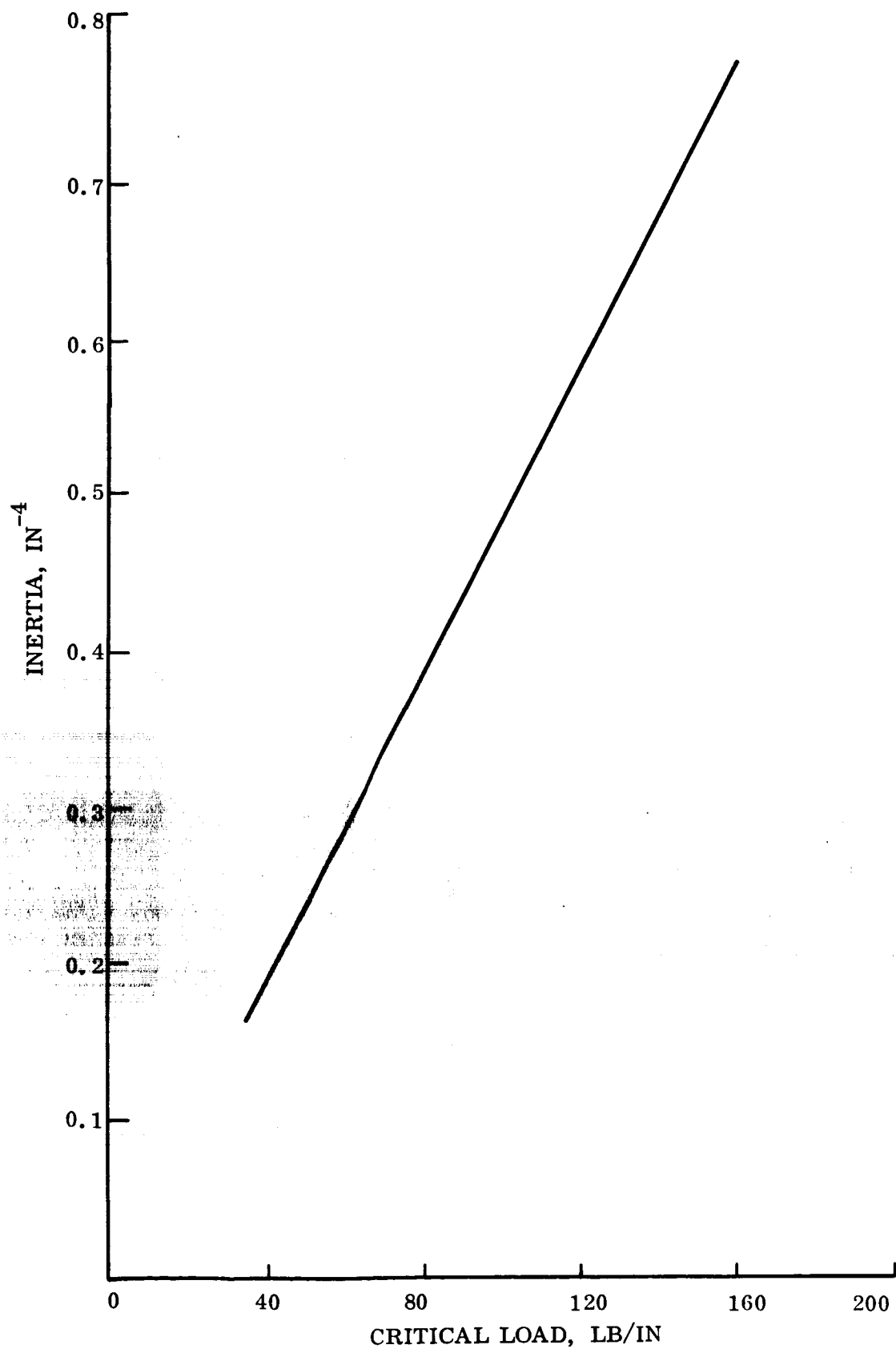


Figure 6.3.1-4. Required Ring Inertia for Stability as a Function of Critical Load

The spring-pusher housing is located on the inside of the adapter at the interface with the entry system. This device provides the separation force necessary to eject the entry system from the bus. Separation forces are needed through the adapter skin and stiffeners.

6.3.2 PRESSURE AND VENT SYSTEM

The basic function of the Pressure and Vent (P&V) System for Point Design 4 is to prevent recontamination of the capsule by maintaining a minimum specified differential pressure (ΔP) between the canister and the ambient environment. This positive ΔP is maintained from sterilization until prior to canister separation.

6.3.2.1 Design Constraints

The P&V system has been designed to meet the following constraints:

1. Provide inlet and outlet ports into the canister for sterilization
2. Provide circulation of air during sterilization
3. Provide pressure relief - due to temperature variations
4. Maintain a positive ΔP between 0.5 and 1.0 lb/in.² differential between the canister and ambient atmosphere from sterilization until exit from Earth's atmospheric
5. Vent 330 ft³ of internal air during ascent to maintain ΔP below 1 psid
6. Evacuate all entrapped gases to ambient space vacuum.

6.3.2.2 System Description

The primary function of the pressure and vent (P&V) system is to vent the internal canister during sterilization, after sterilization and during flight to prevent the internal pressure from exceeding 1 psid. This is accomplished using a combination relief valve with a solenoid override which opens at a nominal pressure of 15.6 psia with increasing pressure and closes at a nominal pressure of 15.3 psia with decreasing pressure. A biological filter is installed upstream of the valve to filter out any bacteria flowing upstream. Relief of a pressure build up due to a temperature increase is accomplished using the same valve described above.

The block diagram for Point Design 4 is shown in fig. 6.3.2-1. During sterilization, the P&V system provides for inlet and exit of sterilized gas (and decontaminating gases if used) by using a manually operated inlet valve connected to the sterile, filtered air supply, and electrically opening the vent valve for use as the outlet port. Since the gas will pass through the biological filter, it must be prefiltered to prevent clogging of the prime flight filter. Two circulating fans are used to speed up the heating and cooling cycles and to eliminate hot spots. These fans are used only during sterilization and their power will be provided by Ground Support Equipment. After sterilization, the make-up gas supply is connected to the manually operated valve. The canister is vented after launch and throughout powered flight until the canister reaches 0.5 psi.

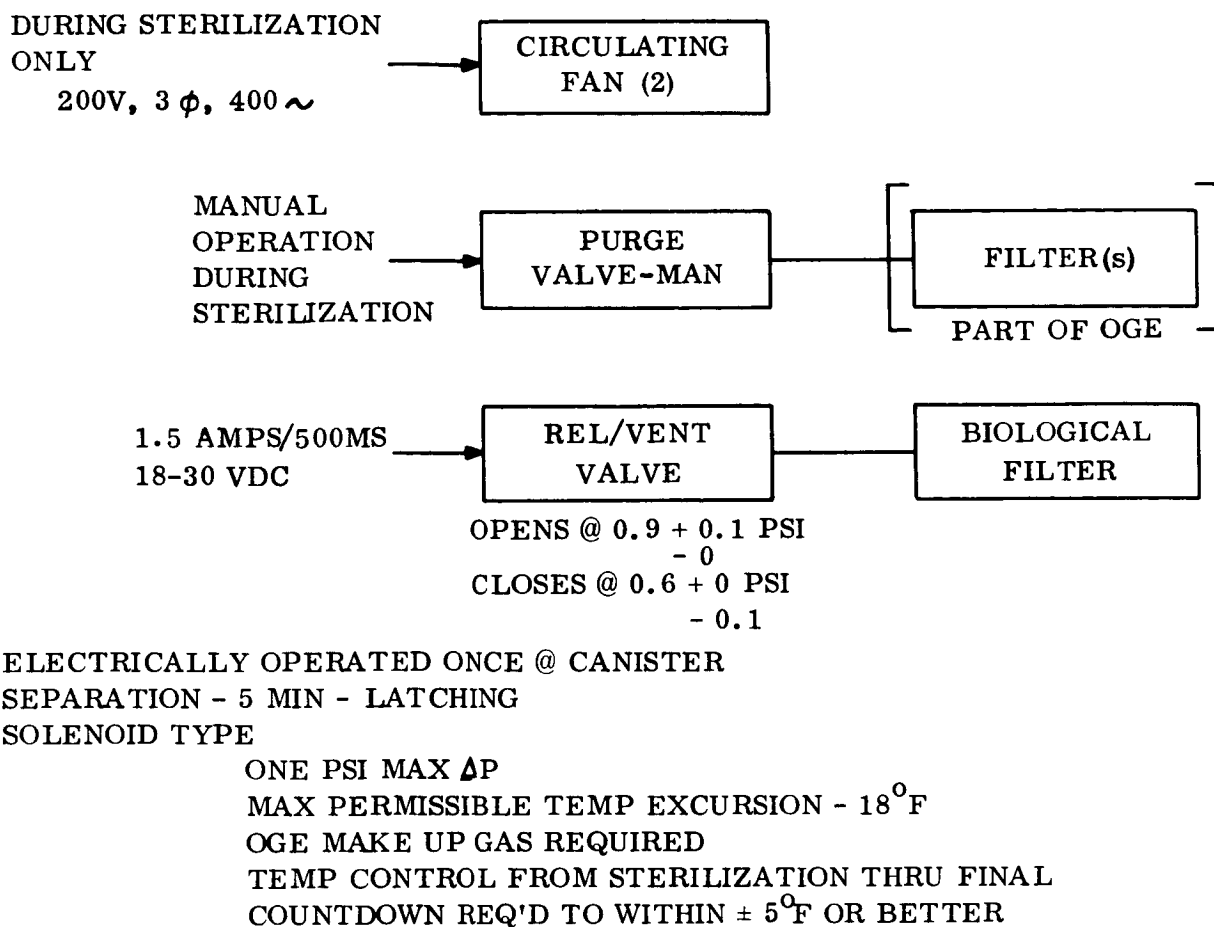


Figure 6.3.2-1. Pressure and Venting Subsystem Block Diagram

The canister remains pressurized at ~ 0.5 psia less leakage, after exiting the Earth's atmosphere until prior to canister separation; at which time, the vent valve will be electrically opened to evacuate the canister to near space vacuum.

To minimize the possibility of backflow during venting, the exit port from the canister is shaped as a convergent nozzle. It has been shown that in a convergent nozzle flow separation does not occur. Thus the possibility of gas flow upstream during venting is almost nil. This fact would preclude the entry of bacteria during the venting process when the valve is open.

6.3.2.2.1 Canister Venting

The vent valve is used to vent the canister during power flight. Its size is determined by the amount of gas and maximum permissible ΔP . For Point Design 4 there is an initial volume of 330 ft^3 of air and the maximum allowable ΔP is 1 psid. The nominal fill pressure will be 15.45 psia at 70°F . From the P&V parametric study, the vent area required for 330 ft^3 of air is 3.8 in.^2 ; and assuming a C_D for the valve of 0.7 gives a required valve aperture equivalent to a 5.34 in.^2 circular orifice.

The valve is a spring loaded, pilot operated relief valve with a latching, override solenoid, and a position indicating switch. This valve design permits its use for relief,

venting, purging and evacuation. The proposed design will be similar to Sterer P/N 19260, Pneumatic and Pressure Control Valve Assembly. The basic changes required to the valve relate to operating pressure and orifice area. The reference valve weighed 3.0 lb and it is estimated that the proposed valve will weigh 6.0 lb. Electrical power required for the solenoid is 1.5 amps at 30 vdc at 70° F for 1/2 sec maximum.

The outline of the proposed valve is:

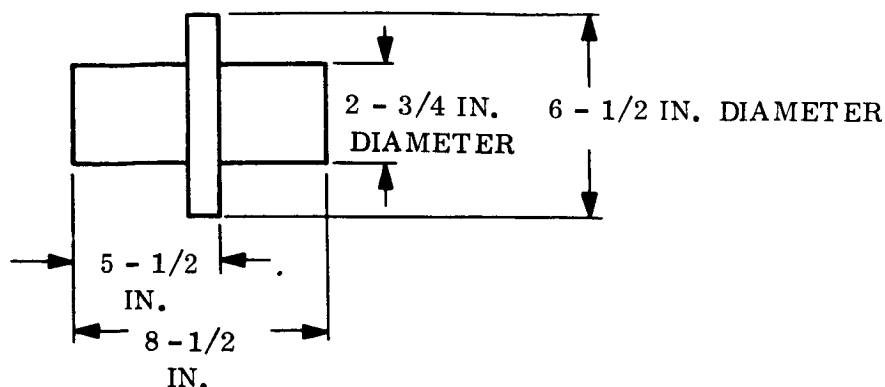


Figure 6.3.2-2 shows the approximate ΔP time history for a valve that opened and remained opened. Obviously, this method will not meet the requirement for maintaining the $\Delta P > 0.5$ psid. The relief valve will act not as a controller and it is expected that the valve will close in the cross hatched portion of the curve. The valve will be set to open at $0.9^{+0.1}_{-0}$ psid on increasing pressure and to close at $0.6^{+0}_{-0.1}$ psid on decreasing pressure. The valve will most likely cycle several times during the first 20 seconds and remain open until L. O. + 90, after which time it will remain closed until opened prior to canister separation.

The biological filter is used to prevent bacteria migration into the Capsule through the vent valve. The filter is installed in series with the valve and upstream of it. The filter is required then, to filter bacteria (0.3 microns) in the backward direction while presenting a low pressure drop to the air being vented. The filter size is governed by the maximum flow, the pressure drop and the differential pressure (ΔP). The maximum calculated flow for the point design (330 ft³ of air) was 0.50 lb/sec or 392 scfm. For the 1 psid ΔP system and a specified pressure drop of 0.1 psi, a filter area of approximately 12 sq ft² is required. Using Pall Corp's Ultipor 0.9 medium, an element size of 9.0 in. long x 6.2 in. diameter is obtained. The filter assembly will be 10.25 in. long x 7.5 in. diameter and would weigh approximately 4 lb.

The choice of Ultipor 0.9 was made because it presents a lower pressure drop than Ultipor 0.15, while satisfying the filtering requirements. It has a catalog rating of 100 percent removal of 0.08 micron particles in dry air. The filter can be decontaminated with ETO and has a temperature rating of 350° F in air.

To maintain the necessary flow, the filter housing requires 2-1/2 in. ports and will be connected to the vent valve with 2-1/2 in. aluminum tubing.

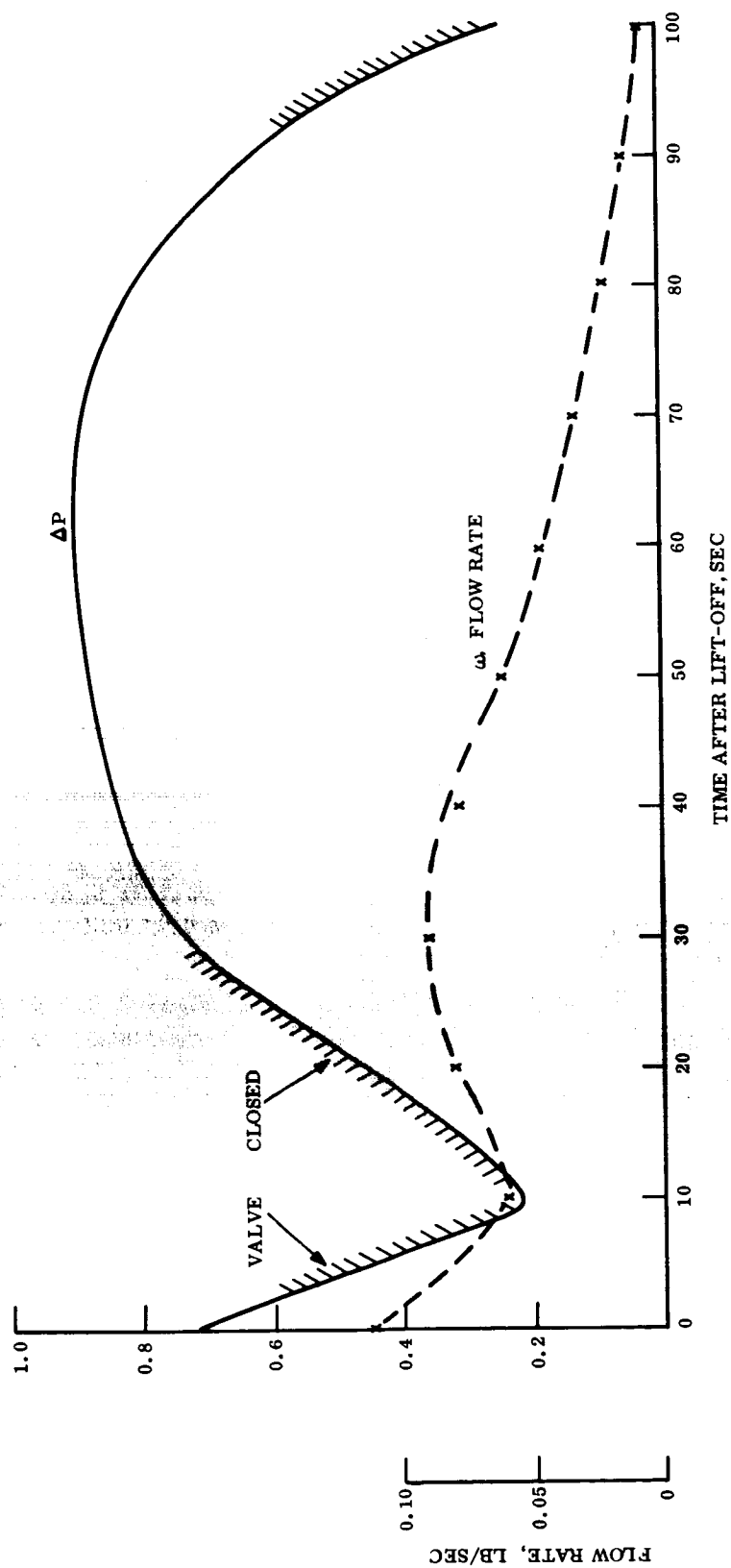


Figure 6.3.2-2. Flow Rate and Differential Pressure vs Time After Lift-off

6.3.2.2.2 Canister Sterilization

During canister sterilization, air will be introduced into the canister to speed up heating or cooling through the manually operated valve. Using 1-3/8 in. tubing and a valve with an area of 1.25 in.², 27 cfm of air can be introduced at 1 psid (15.7 psia), thus the canister air will be changed 4 + times in one hour.

Two fans, Rotron Mfg. Co. type AXIMAX 3, with a delivery of 150 cfm at 1 in. H₂O s.p. will be used to circulate air during sterilization, thus reducing warm up times, eliminating hot spots, and insuring that the entire Capsule reaches sterilization temperature.

Power required for the fans will be provided by OGE and shall be as follows: 200v, 3 ϕ , 400 ~, 0.41 amp line current per motor. Fan size is 3.0 in. diameter x 2-5/16 in. long and weight is 14 oz.

6.3.3 SEPARATION SUBSYSTEM

6.3.3.1 Design Constraints, Functions and Requirements - Point Design 4

The separation subsystem performs the following functions:

1. Separation of the forward canister
2. Separation of the Capsule assembly
3. Separation of the thrust cone assemble
4. Separation of the aeroshell.

The subsystem has been designed to meet the following requirements in addition to the usual environmental criteria.

1. Provide field and separation joints for the canister
2. Eject the forward canister at 2.5 ± 0.3 fps
3. Maintain a pressure tight joint from sterilization through exit from the Earth's atmosphere for a maximum internal pressure of 1.67 psid. Pressure tight is defined as leakage which results in less than 0.002 psi/hr drop at 70° F
4. Maintain maximum attainable pressure tightness during space cruise where outside temperature may be as low as -300° F
5. Maintain sterility of Capsule
6. Separation shall not produce debris or loose objects
7. Attach the Capsule at 4 points
8. Eject the Capsule at 1.5 ± 0.25 fps separation velocity from a bus with tip-off rates of $< 0.5^\circ$ /sec to the Capsule. Bus pitch inertia = Capsule's
9. Separation shall not cause collision with any of the remaining payload

10. Attach and separate the thrust cone at 1.0 fps minimum
11. Attach and release the aeroshell
12. Provide electrical separation as required
13. Optimum reliability and subsystem performance is paramount to mission success. Use proven concepts.

Other system constraints - electrical power, distribution, timing and signal lock-out shall be provided by the EP&D Subsystem.

6.3.3.2 General Subsystem Description

See block diagram, fig. 6.3.3-1. The canister halves are jointed by a V-band assembly consisting of independent slippers attached to a strap. The band is made in four equal segments joined by Hot-Wire Tension Bolts. The Hot-Wire Bolt is a non-pyrotechnic, mechanical device consisting of a turnbuckle coupling which separates when an electrical signal is applied to a hot-wire element which kept the turnbuckle together. The forward canister is ejected using four helical coil compression springs. The rings, to which the V-band clamps, perform double duty by providing the groove and sealing surfaces for the O-ring type pressure seal. After separation, the V-band segments remain attached to the aft canister via springs and lanyards. The canister is completely evacuated by the P&V subsystem prior to separation.

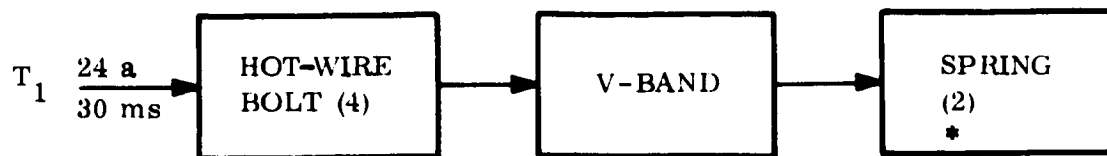
The Capsule assembly is separated from the Orbiter approximately 10 minutes after canister separation. The Capsule is attached to the adapter at four points by explosive nuts, but a hot-wire type of coupling is also being investigated. The Capsule is ejected at 1.4 fps nominally, by four helical coil compression springs.

The thrust cone assembly is attached to the Lander/Aeroshell assembly through four hot-wire bolts. Two helical coil compression springs identical to the ones used for canister ejection are used to eject the thrust cone at 3.3 fps, nominally. The thrust cone is separated after the de-orbit function is completed. The aeroshell is attached to the Lander by a strap assembly retained by 3 hot-wire tension bolts and released after parachute deployment. This system is described in more detail in Section 6.4.4.

The weight of the subsystem as described above based on a 13.4 ft diameter canister is

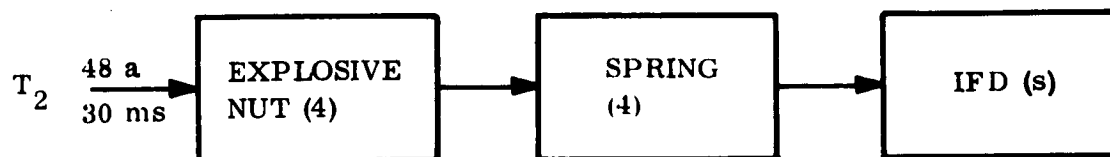
1. <u>Canister</u>	<u>lb</u>
V-band assembly	13.8
4 Hot-wire bolts	0.8
4 Springs	0.4
4 Spring housing, adj.	1.4

FWD CANISTER SEPARATION

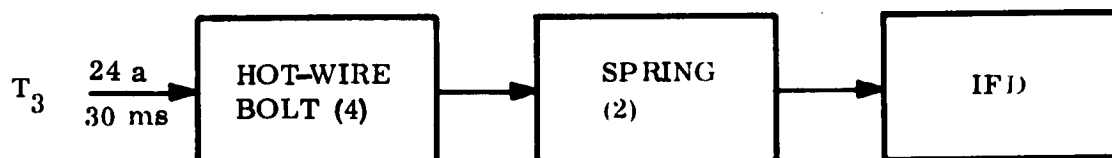


* 4 SPRINGS FOR POINT DESIGNS 2A, 2B, 4, 6

CAPSULE SEPARATION



THRUST CONE SEPARATION



AEROSHELL SEPARATION

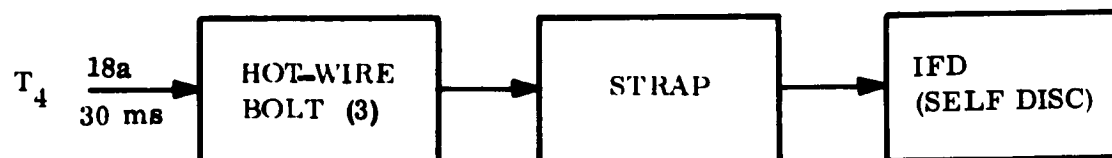


Figure 6.3.3-1. Separation Subsystem Block Diagram

2.	<u>Capsule</u>	<u>lb</u>
	4 Explosive nuts	1.0
	4 Springs	0.8
	4 Spring housings, adj	1.4
3.	<u>T/C Thrust Cone</u>	
	4 Hot-wire bolts	1.0
	2 Springs	0.2
4.	<u>Aeroshell</u>	
	1 Strap	1.2
	3 Hot-wire bolts	0.6
	TOTAL	<u>22.6</u>

The following paragraphs discuss the detail designs.

6.3.3.2.1 Canister Separation

The selection of the separation method for the canister is governed by the requirement for a sterile, pressure tight joint for a large, flexible structure. This basic requirement limits the separation joint design to one that can apply a continuous distributed force, such as, flexible shape charge, various types of MDC or primer cord, V-bands, closely spaced bolted joint, pyro fuze joint system or a thermal heat pad joint system. The V-band system was selected because of its simplicity, reliability, low separation shock, lack of debris, tolerance to temperature environment, eliminates need for a field joint, and it presents a tortuous path for microbial access to the separation interface.

The band must meet the following specific requirements:

1. Contain proof pressure without yielding,
2. Provide the necessary clamping force without yielding,
3. Contain the burst pressure without breaking,
4. Make allowance for creep at low temperature over a 9 month period.

The V-band assembly is made in four segments, with the strap material being 2024-T68 Aluminum, 1 in. wide x 0.072 in. thick. The slippers which are attached to the band by clips, are made of 7075-T73 Aluminum. The band is preloaded to 2300 \pm 230 lb in order to sustain all loads, allow for creep during cruise, and allow for tension variations during assembly. (See Vol. II, Appendix B for load and stresses in band.)

The V-band segments are held in tension by the four hot-wire bolt* assemblies. The choice of four points for attaching and torquing was made to maintain nearly uniform tension on the entire band and to facilitate band disengagement. The hot-wire bolt is a mechanical separation device which utilizes the reduction of tensile strength property of a material upon heating to actuate. Upon application of 6 amps for 30 msec the hot-wire element breaks and separation occurs. The hot-wire bolt consists of two separate studs connected by a segmented coupling. The coupling is held together by the hot-wire element, so that tension can be carried by the mechanism.

The required preload can be applied through 3/8 in. diameter thread and a 0.69 in. o.d. coupling (see fig. 6.3.3-2) made of 17-4 ph, Cond 1050 stainless steel, with an ultimate load capacity of 8,000 pounds tension. Nine turns of 0.014 in. diameter 302 stainless wire form the hot-wire element. The segments of the coupling are retained so that there is no debris. This unit is ideal for long service in space because of its all metal design. The band will separate if any of the four bolts operate.

The forward canister is ejected by four helical coil compression springs. The springs provide 35 lb of initial force each and have a working stroke of 2 in. They will impart a velocity of 2.5 ± 0.25 fps to the canister. The springs are of 302 stainless steel, stressed at 90,000 psi and are retained with the aft canister, in an adjustable subassembly. (See fig. 6.3.3-3.) Tip-off rates will be less than $2.0^\circ/\text{sec}$ about any axis. Center of gravity offsets are expected to be minimal since the forward canister is of symmetric construction.

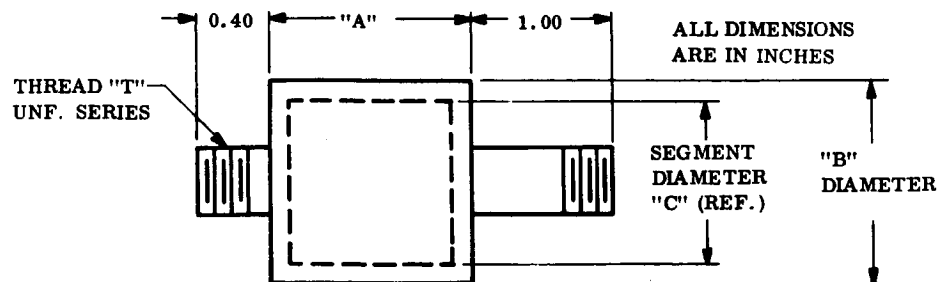
The canister separation joint seal utilizes two silicone rubber O-rings to attain a pressure tight seal. The O-rings are used in two different modes to enhance sealing capabilities, one O-ring being a face seal and the other a gland seal. This arrangement utilizes the axial and radial clamping forces of the V-band and closes off the clearances resulting from manufacturing tolerances, while retaining a machinable and structurally sound ring design. The basic cross section is depicted in the figs. 6.3.3-4, and 6.3.3-5 for the Point Design 4 ring. The face seal O-ring is nominally 0.139 in. diameter and is compressed from 0.014 in. to 0.041 in. The force necessary to compress this O-ring using 50 durometer silicone is from 1.2 to 12.0 lb/linear in. The gland seal is nominally 0.210 in. diameter and is compressed from 0.015 to 0.045 in., or 7 to 22 percent. The radial force to compress this ring is from 1 to 16 lb/linear in. The radial clamping force available if the nominal axial clamping force of 45.1 lb/in. is attained is,

$$FR = FN (\text{TAN}) = 45.1 (\text{TAN } 20^\circ) = 16.4 \text{ lb/in.}$$

which is adequate.

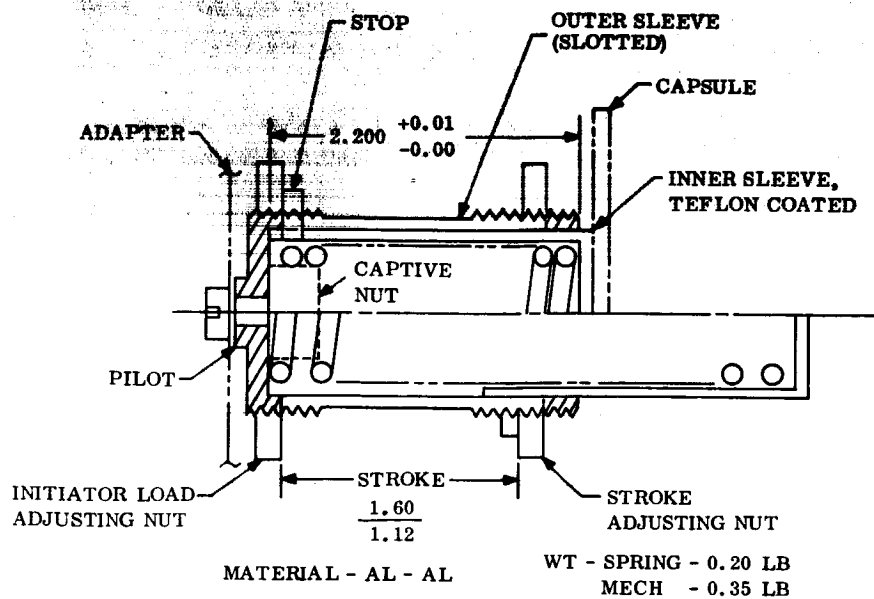
Silicone rubber material was selected because it has the best low temperature properties — rated to -80°F for seals, but doesn't harden until -150° to -180°F . Therefore, it is expected that the seal will degrade during the space cruise. If it is mandatory that a seal be maintained, then thermal insulation could be applied to the band to keep the temperature above -150°F .

* The hot-wire bolt is a GE/RS proprietary design.



MAX LOAD (LB)	PHYSICAL DATA				HOT WIRE DATA				
	A	B	T	C	WIRE DIA	NOTCH DIA	NO. OF TURNS	A. F. CURRENT	WT LB
8000	0.90	1.00	3/8	0.69	0.014	0.0040	9	6.0	0.20
12,000	1.15	1.32	7/16	1.00	0.020	0.0660	11	9.0	0.44
19,000	1.40	1.62	1/2	1.30	0.025	0.0075	13	12.0	0.81

Figure 6.3.3-2. Hot-Wire Tension Bolt



SPRING DATA

WIRE DIA	-	0.148 IN.
O. D.	-	1.034 IN.
SPS. CONST	-	75 LB/IN.
TOTAL TURNS	-	14.7
MAX LOAD	-	120 LB
NOM LOAD	-	108 LB
LS	-	2.19 LB
LF	-	3.79 IN.
NOMINAL STROKE	-	.128 IN.

Figure 6.3.3-3. Capsule Separation Adjustable Spring Assembly



6-44

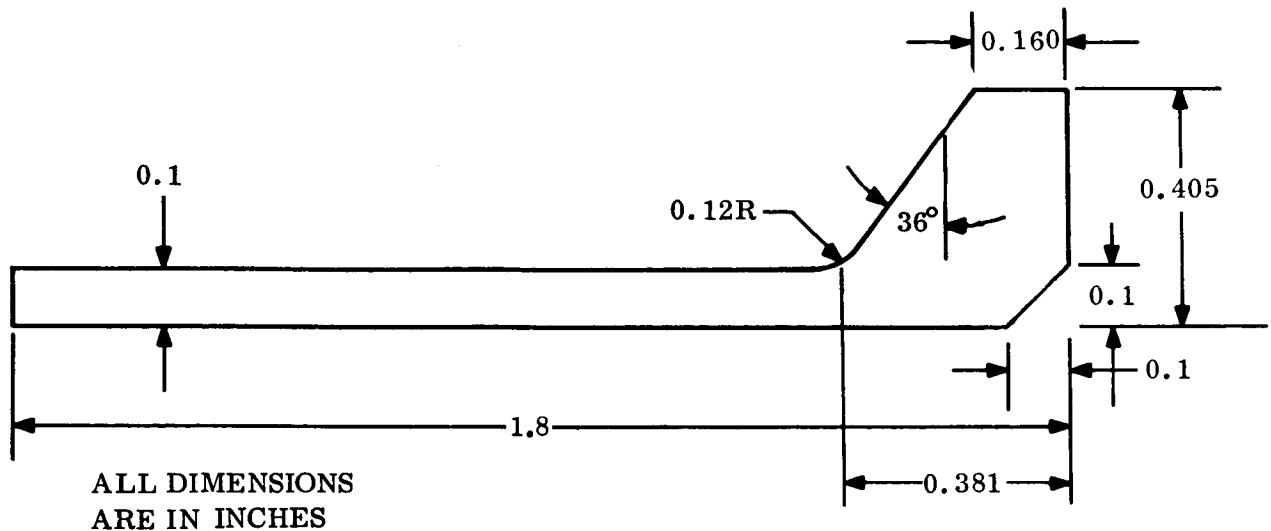


Figure 6.3.3-5. Forward Canister Ring

The ability of the separation joint to inhibit the penetration of bacteria is further enhanced by the tortuous path which they must follow to gain entry into the Capsule. The slipper is in full contact with the ring except for a 1/4-in. gap between the 5.75 in. long slippers, or a total of 96 percent of the circumference is covered by the slippers. The band, of course, covers the entire circumference except at openings for the hot-wire bolts, which probably will be about 1-1/2 in. long each, or 94.5 percent band coverage.

6.3.3.2.2 Capsule Separation

The main consideration for Capsule separation and ejection was the stringent tip-off rate requirement. To meet this requirement, it is necessary that the impulse generated by the separation device be either very low or nearly the same at all points. Likewise the ejection system must have controlled force and energy, with low variances; and lastly, center-of-gravity offsets, and ejection system force axes must be controlled.

Separation devices that meet the above needs are ball locks, collet releases, and explosive nuts. The latter was chosen because of their compactness and ease of use and installation. All of the above utilize pressure cartridges for operation, and for high reliability dual cartridges will be used. This introduces the problem of wide

impulse variance as a function of gas pressure (a function of cartridge design, simultaneity and number of cartridges firing).

A non-pyrotechnic device, similar to the hot-wire tension bolt discussed previously will be very seriously considered, because of its obvious advantages. Its main drawback is that it is new and needs to be developed.

The ejection systems that are available are pneumatic pistons, pyrotechnic thrusters, reaction systems and springs. Springs were selected for their obvious simplicity. To minimize tip-off rates, the energy and force of the ejection system must be controlled. A guide/roller system may also be required if rates are too high. The proposed solution uses preset springs in an energy package, with selective assembly and gives a maximum tip-off rate of $0.27^\circ/\text{sec}$ when the maximum and minimum spring forces are combined with the worst case center-of-gravity offset.

The Capsule is attached to the adapter by four 1/4-in. explosive nuts, each having dual cartridges. The explosive nut is of the captive type, with all loose pieces contained within the unit. The gas generated by the squibs is also contained. The choice of an explosive nut was made because of its reliability, capability for dual squib initiation, low weight, high load carrying ability. The 1/4 in. size nut can carry the full load of a 1/4 in. 160,000 psi UTS bolt, which is 3600 lb. The applied limit load is 2800 lb and therefore there is ample margin. Four nuts were selected based on the four pick up points on the structure.

Capsule ejection is accomplished by four helical coil compression springs. The springs exert a 108 lb force each, and have a working stroke of 1.28 in. The springs are stable ($L/D < 5$) and will impart a separation velocity of 1.4 ± 0.15 fps to the Capsule. Thus, the Capsule will require a positive ΔV of 0.70 fps, where as the forward canister was ejected at 2.5 fps. Tip-off imparted to the Capsule will be $0.27^\circ/\text{sec}$ obtained by trimming and selecting the springs. The Orbiter will acquire a negative or retrograde ΔV of 0.70 fps and a tip-off rate of $0.27^\circ/\text{sec}$ as a result of Capsule separation. It was assumed that this small motion was not detrimental to the mission. (See Vol. III, Appendix B for tipoff analysis.)

The spring assembly is shown in fig. 6.3.3-3. It provides for adjustment of initial load - one turn of the adjustment nut gives approximately a 2 lb load change - it provides for adjustment of total stroke, it retains the spring at the end of the stroke and provides a locating pilot. The inner sleeve is coated with Teflon on both inner and outer surfaces to reduce friction. Operation of the spring over the inner 80 percent of its total possible stroke assures nearly constant spring rate.

The following summarizes the recommended spring design. (See table 6.3.3-1 for spring detail data)

Spring Material - National Standard NS-355 stainless steel

Ultimate tensile strength - 330,000 psi for up to 0.159 in. wire

Torsional shear - 45 percent x UTS - 148,000 psi

Initial load - 108 lb at 0.16 in from solid

Final load - 12 lb at 1.44 in. from solid

Max load - 120 lb at solid height

Max stroke, X_m - 1.60 in.

Operating stroke - 1.60 - 20 percent (1.60) = 1.28 in.

Energy required - 25.5 ft-lb

Energy available - $\frac{(108 + 12)}{2} \frac{(1.28)}{12}$ (4 springs) = 25.6 ft-lb

Control spring rate - 75 ± 3 percent lb/in.

Adjust spring - 108 ± 2 lb Initial Load

Install springs, so that diametrically opposing springs have an initial load within 0.5 lb

TABLE 6.3.3-1. SEPARATION SPRING DATA

	Canister	T/C	Capsule
Wire diameter (in.)	0.107	0.107	0.148
Mean coil diameter (in.)	1.07	1.07	1.034
Number of springs	2	2	2
Comp. length (in.)	1.29	1.29	2.35
Solid height (in.)	1.09	1.09	2.19
Free length (in.)	3.29	3.29	3.79
Total weight (lb)	0.17	0.17	0.80
Number of active coils	8.4	8.4	12.7
Stress (psi)	90,000	90,000	110,000
Nominal ΔV (fps)	2.5	2.5	1.5

IFD's for electrical separation will be self disconnect type or electrically actuated, hot-wire type depending on size and location on the vehicle.

6.3.3.2.3 Thrust Cone Separation

The thrust cone is attached to the aeroshell/Lander through a hot-wire bolt to a male fitting which is internal and pinned to a female fitting on the Lander cover. The hot-wire separation is the same as described for the canister. The thrust cone is ejected at 3.3 fps using two helical coil compression springs identical to the ones used for canister separation. The springs remain with the thrust cone. IFD's for electrical separation will probably be of the spring-self disconnect type.

6.3.4 ENVIRONMENTAL CONTROL

Thermal control of the Lander components during interplanetary travel will be accomplished by insulating the Lander from the space environment and using heater power from the spacecraft to control the Lander temperatures. The insulated blanket will be multiradiation barrier type composed of a number of layers of either aluminized mylar or aluminum foils separated by an insulating material. An effective thermal conductivity of 1×10^{-4} Btu hr-ft- $^{\circ}$ R was selected for this type of insulation. Definition of the insulation details and heater power requirements will be dependent on the surface radiative properties, payload allowable temperatures and canister surface area. A low emissivity coating (EoS = 0.1) on the outside insulation surface will be utilized to maintain minimum heat loss through the canister. From fig. 6.3.4-1 insulation and heater power requirements can be determined on a unit surface area basis for a compartment temperature requirement of 310° R. Total heater power can be evaluated from fig. 6.3.4-2 at the design values.

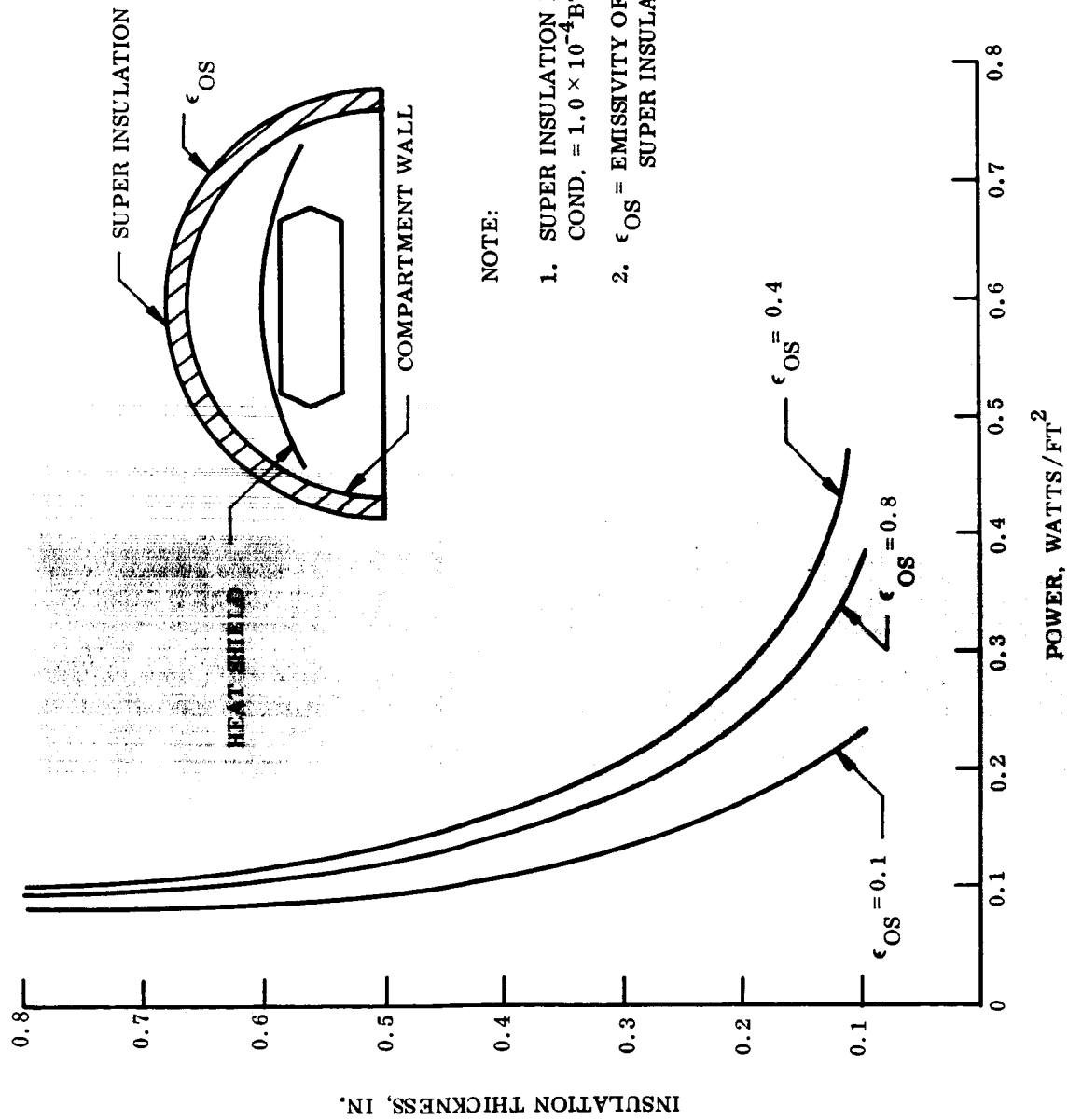


Figure 6.3.4-1. Super Insulating Requirements to Maintain 310°R on Compartment Wall and Heat Shield

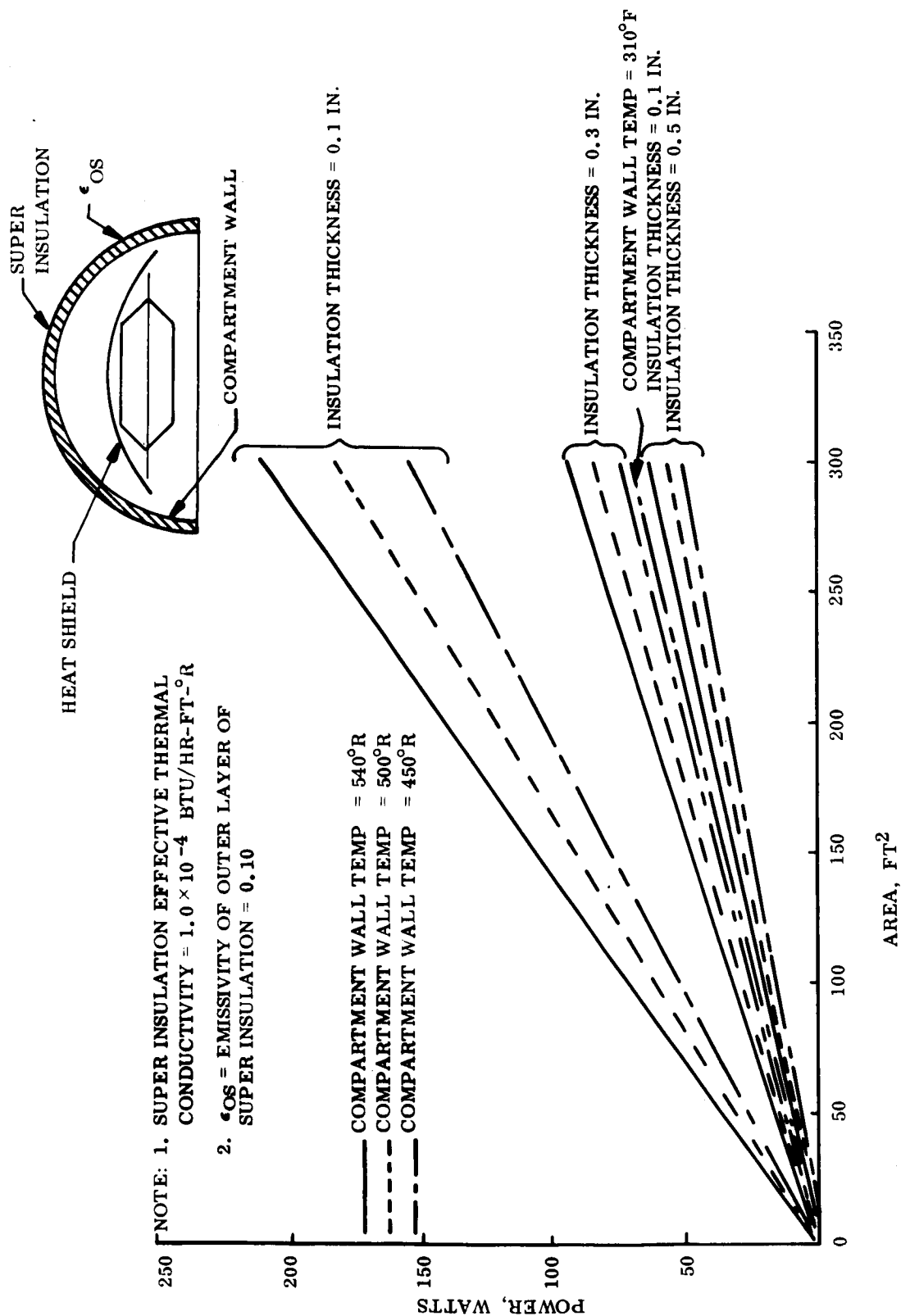


Figure 6.3.4-2. Transit Mode Power and Insulation Requirements for Various Canister Areas

6.3.5 DE-ORBIT PROPULSION SYSTEM

6.3.5.1 Design Constraints

The design constraints for the de-orbit propulsion system for Point Design 4 were as follows:

1. De-orbit weight of 1550 lb (less propulsion)
2. Velocity increment 45 meters/sec
3. Liquid monopropellant system
4. Burn time of approximately 60 sec.

6.3.5.2 Systems Description

6.3.5.2.1 De-Orbit Propulsion Equipment

The selected propulsion equipment for the Mars Hard Lander Point Design 4 is a liquid monopropellant system conforming to the requirements presented below. This portion of the report presents the performance data, and system description of the selected de-orbit propulsion equipment.

The de-orbit propulsion system must impart a velocity increment of 45 meters/sec to a 1550 pound vehicle for direct planet entry at 20,000 ft/sec a path angle of 25° . The vehicle weight does include the propulsion system weight, thrust termination is required and the system must be aligned to within $\pm 2^\circ$ with respect to the principal axis.

The performance, weight, and basic envelope data is presented in table 6.3.5-1. The propellant weight shown in the table is useful propellant weight. Inert weights consist of thrust chambers, valves, tanks, plumbing, residual propellants, gas, and structure.

Additional monopropellant systems were sized to show variability obtainable between burn time and weight, the weight change primarily due to an increase or decrease in quantity of thrust chamber assemblies. The 200 lb thrust system was selected because of the burn time constraint.

The monopropellant system will not require component development since it will use existing components. No significant changes to component function or reliability are anticipated due to the effects of the heat sterilization requirements. This is based on the heat sterilization program conducted by Martin-Marietta on a bipropellant liquid system and the assumption that similar components will perform similarly when exposed to sterilization cycles. However, the cost advantage of using existing components is offset by the sterilization requirements. This is because of the additional testing at the subsystem level, i. e., pressurization assembly, propellant feed

TABLE 6.3.5-1. PERFORMANCE, WEIGHT, AND ENVELOPE DATA

Parameter	Per requirements	F = 100 lb
ΔV (meters/sec)	45	45
Payload weight (lbm) (less propulsion)	1550	1550
Total propulsion system weight (lbm)	62	55
Propellant weight (lbm)	31	31
Propulsion inert weight (lbm)	31	24
TCA	11.8 ⁽¹⁾	5.9 ⁽¹⁾
Controls (valves, filters, lines, etc.)	8.8	8.3
Structure	4.1	3.1
Propellant tankage	2.4	2.4
Pressurant tankage and gas	3.3	3.3
Residual propellant	1.0	1.0
Mass fraction (propellant weight/total weight)	0.50	0.56
Propellants	Anhydrous Hydrazine	
I_{sp} , vacuum sec	240	
Nozzle expansion ratio	40	
Total impulse (lbf-sec)	7498	7491
Burn time (sec)	37	75
Thrust (lbf)	200	100
Number of thrusters	2	1
Max. chamber pressure (psia)	200	200
Approx. dimensions (spherical diameter inches)		
Fuel tank 1	12.6	12.6
Fuel tank 2	--	--
Gas tank	7.6	7.6

(1) Based on weight published Walter Kidde or Rocket Research Corporation

assembly, etc., and system level that is required for verification of the above assumptions. To date, no system subjected to heat sterilization has flown; therefore, the element of uncertainty involved requires additional testing.

A representative schematic diagram for a monopropellant propulsion system is presented in fig. 6.3.5-1. It is a regulated-gas pressure-fed system utilizing anhydrous hydrazine (N_2H_4) as the monopropellant. Helium gas, stored at 3600 psia, is used as the pressurant. Squib valves isolate the propellant and pressurant supplies until the system is required, at which time they are actuated. At maneuver completion, squib valves are again actuated to positively shut down the system.

Insofar as possible, components are grouped together and connections are welded to eliminate external leakage. Different functional groups are joined by field brazed points where welding is not practical. Squib valves are used, where feasible, to eliminate solenoid operated valves and thus assure high system reliability. Each of the major functional groups (pressurization, propellant feed, and thrust chambers) is described below.

The helium gas is stored at 3600 psia in a 6Al-4V titanium alloy spherical tank. Two parallel squib operated gas isolation valves are used to maintain the helium in the tank until the system is required for the de-orbit maneuver. Immediately downstream of the squib valves is a filter to remove particulate matter which might be generated by the squib valve actuation and be contained within the system. High pressure gas is fed to the pneumatic regulator providing regulated gas at a pressure of approximately 320 psia to the propellant feed system. A normally open squib valve is provided to positively shut down the gas system at maneuver completion. The propellant system is protected from over pressurization by a burst-disc and relief-valve unit. All pressurization system components, except the tank, will be a tray mounted as a single all-welded unit.

One propellant tank will be required. The tank is spherical, fabricated from 6Al-4V titanium alloy and contain butyl rubber bladders which collapse, when pressurized, around a standpipe to assure positive propellant expulsion. The tank discharge line feeds two parallel squib actuated isolation valves. A manually operated fill and drain valve is located in the common line. The squib valves are similar to those in the pressurization system in that they isolate the propellant until required and provide a redundant system. Downstream of the squib valves is a filter to trap particles generated by squib valve actuation. Normally open squib valves are provided in series to provide redundancy in the positive shut off mode. All valves and filter will be tray mounted and welded together to minimize leakage.

Two, 100 lb thrust chambers will be required since there are no qualified thrust cone assemblies between 100 and 300 lb thrust. Decomposition of the hydrazine is accomplished in a catalyst bed made from Shell 405 catalyst. Decomposed hydrazine at a temperature of approximately 1800° F discharges through the nozzle to provide the desired thrust.

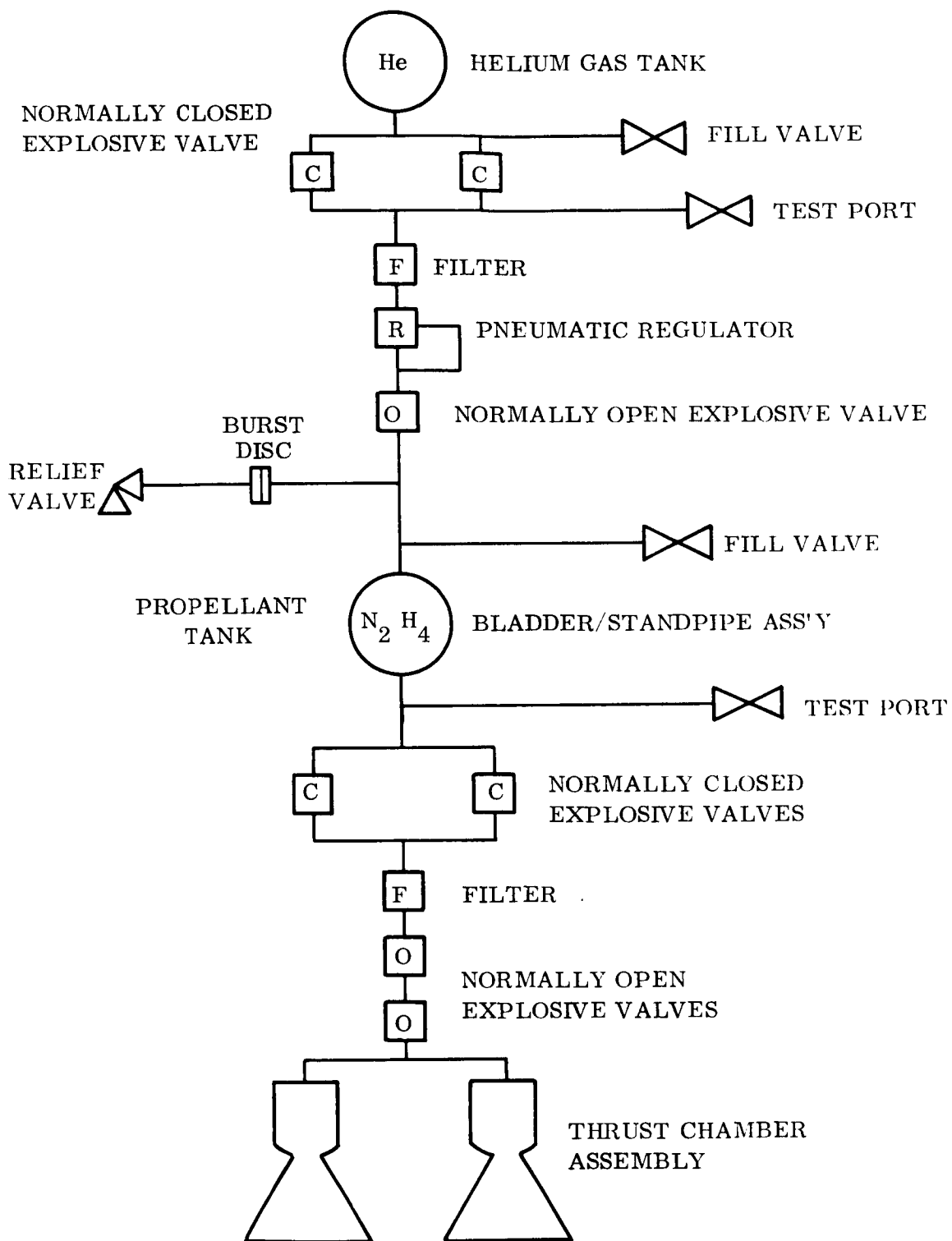


Figure 6.3.5-1. Monopropellant System

6.3.5.2.2 De-Orbit Structure

The de-orbit propulsion system for Point Design 4 is supported by an aluminum sheet metal thrust cone which is attached to the Lander cover by means of four tabular struts. Figure 6.3.5-1 depicts the complete assembly and the associated attachments.

The thrust cone structure is a built-up sheet metal structure designed to hold and support the fuel tank, gas tank and thrust chambers. Structurally it consists of sheet stiffened by full depth ribs and angles. Openings, which serve as saddles for the tanks, have been cut in the sheet. The tank is held in place by a skull cap as shown in fig. 6.3.5-2 which is fastened to fittings on the cone structure. The cone structure is attached to the four tubular struts through a T-shaped ring. This ring takes the shear loads due to lateral loading conditions and redistributes them to the tubular struts. The ring also tends to stiffen the cone for torsional forces which occur during spin and de-spin.

The four struts are aluminum tubes which act as short columns taking the loads introduced by the cone structure and propulsion engine redistributing them as four point loads into the Lander structure. The struts are attached to the Lander as shown in fig. 6.3.5-3, through a hot-wire bolt to a male fitting which fits into and is pinned to a female fitting on the Lander cover. The lower end of the column is threaded to match a threaded pre-load sleeve which when tightened puts tension in the hot-wire bolt. The de-orbit engine and all of the structure is released when the hot-wire separates.

6.3.6 ELECTRICAL EQUIPMENT - PRE-ENTRY

The canister is equipped with electrical/electronic equipment which provides status monitoring during cruise, preseparation checkout, arming, electrical disconnection, separation initiations and separation event monitoring.

Commands from the Orbiter CC&S are sent to the canister via hardwire where decoding takes place in the dual canister programmer. Signals from the programmer operate the power controller which contains redundant capacitor discharge energy storage units. Energy from these capacitors provide electrical initiation.

All canister equipment is powered from a sterilized dual silver-zinc secondary battery. This battery is similar in design to the Lander battery and its development is described in Section 4.3.1. This provides an independent energy source for operation when the Orbiter solar arrays are pointed away from the sun, e.g., maneuver and separation attitude, for separation event monitoring after Lander disconnection, and to avoid sending initiation energy across an interface.

The aeroshell for direct entry design is also equipped with a pre-entry silver-zinc battery which provides all power during the 24 hour coast period between separation and the onset of entry.

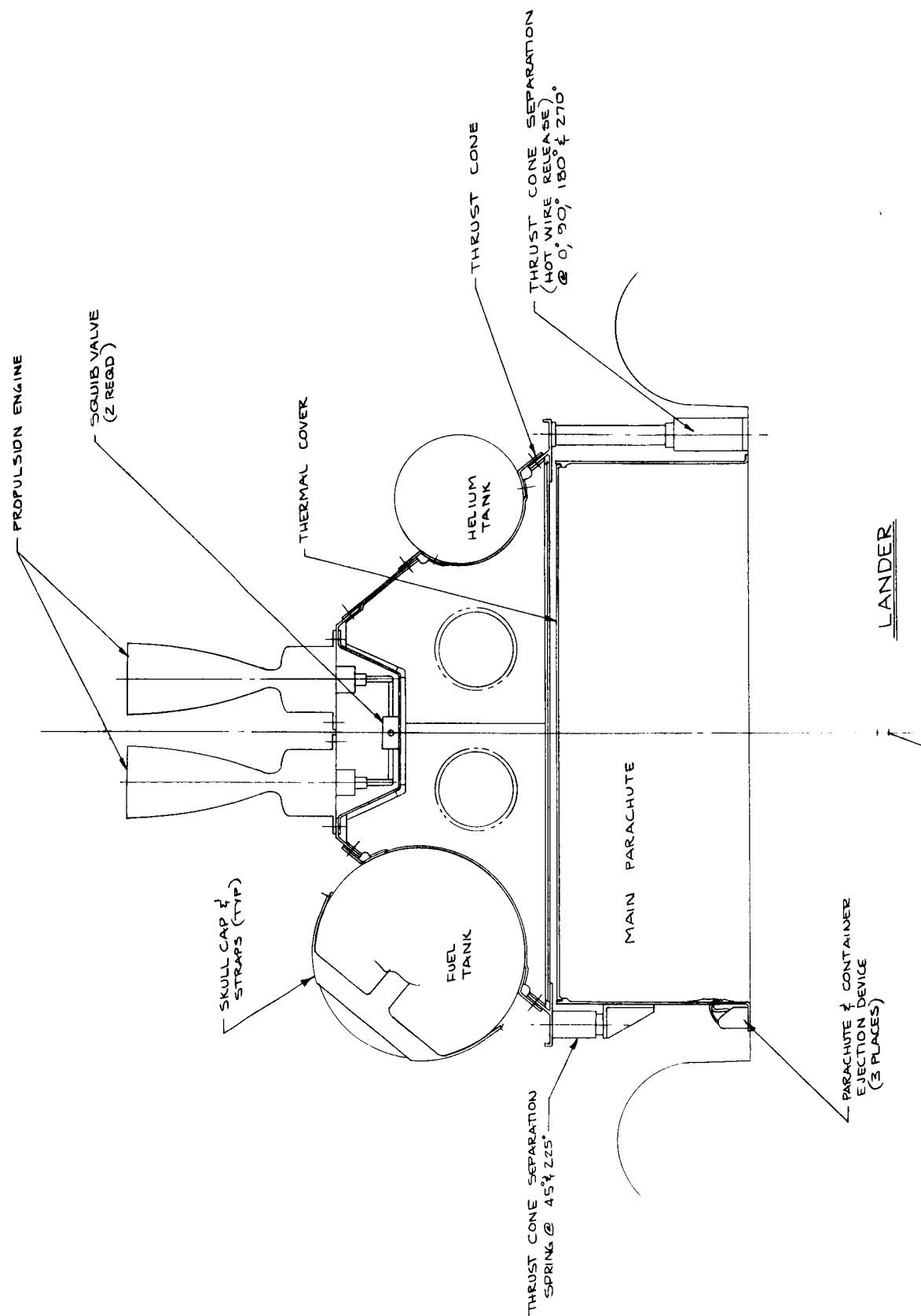


Figure 6.3.5-2. De-orbit Propulsion Installation

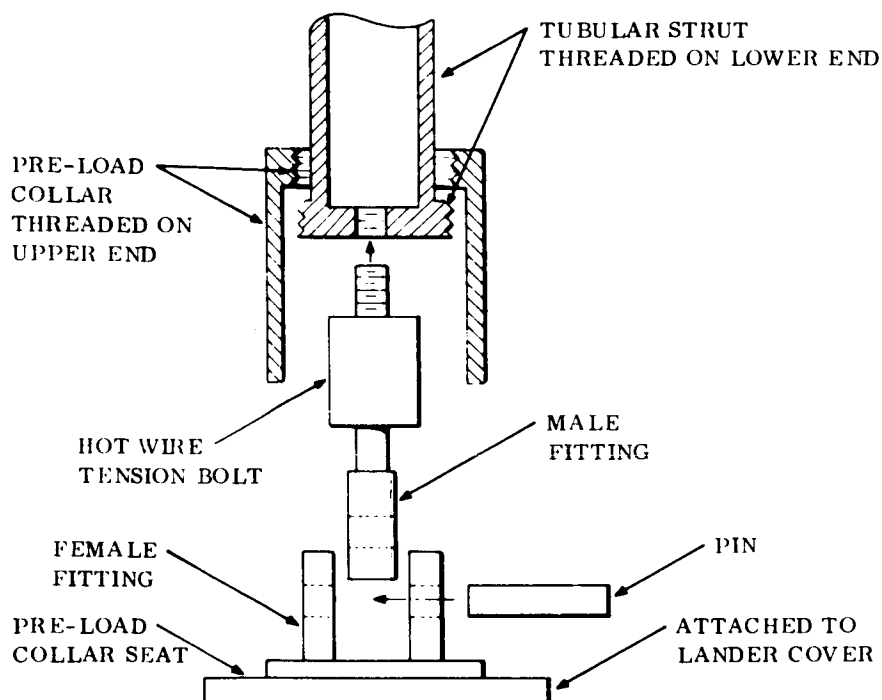


Figure 6.3.5-3. Thrust Cone Separation

Thermal batteries located on the thrust cone provide high level currents for the electrical initiation events associated with spin, deboost and de-spin. These are ignited from the Lander or pre-entry battery through thermal relay modules which protect the operational battery against initiation circuit faults. The thermal batteries are used in redundant pairs with diode blocking for isolation.

6.3.7 DE-ORBIT SYSTEM

6.3.7.1 Spin Control Subsystem

The subsystem configuration described here for Point Design 4 performs attitude control for the De-orbit System and roll control for the Entry System. By combining these functions, the overall equipment design is simpler, weighs less, and, since fewer components are needed, is more reliable. In the following discussion, reference will be made to the Entry System description, para 6.4.7.1, where appropriate.

6.3.7.1.1 Spin Requirements

The most important requirement for the spin control subsystem is to control the Capsule attitude during firing of the propulsion system so that the error in direction of the velocity increment (ΔV) will not cause excessive entry path angle or down range dispersions. Errors will be caused by thrust misalignment of the propulsion engine, center of mass offset of the Capsule, separation tip-off rates, and by other sources to be discussed later. The spin control subsystem provides

a combination of gyroscopic stability and cyclical averaging to reduce the effect of these error sources to less than 2.1° , 3-sigma error on the ΔV orientation.

Another requirement for the subsystem is to control the Capsule attitude at the beginning of entry into the atmosphere so that a large initial angle-of-attack, or even backward entry, is avoided. Since the initial angle-of-attack can be as large as 40° , the requirement is met by maintaining until entry the same inertial orientation established for de-orbit propulsion firing. Again, the gyroscopic stability of the spin control performs this function.

The requirements for roll control during entry are discussed in para 6.4.7.1 under entry systems. Additional requirements and constraints for the spin control are summarized in table 6.3.7-1. These requirements determine the required torque level and impulse.

6.3.7.1.2 Description of the Spin Control Subsystem

The spin control subsystem consists of a small monopropellant hydrazine reaction control, a single rate gyro, and an electronic assembly. A block diagram is shown in fig. 6.3.7-1. The rate gyro measures Capsule roll rate which is compared with the output of the roll rate generator. When the spin command is given, the high rate (50 rpm) mode is used for spin-up for engine firing. When the despin command is given, the low rate (5 rpm) mode is used for both de-spin and entry roll control. When the error voltage is larger than the preset threshold, the valve drivers operate the appropriate valve to generate corrective roll torques.

TABLE 6.3.7-1. SPIN AND ROLL CONTROL REQUIREMENTS,
POINT DESIGN 4

Capsule weight	1639 lb
Inertia, roll	299 sl-ft ²
Inertia, P/Y	205 sl-ft ²
Moment arm	72 in.
Separation rate	0.5 deg/sec
CM offset	0.3 in.
Nozzle align error	0.5 deg
Velocity increments	147.5 ft/sec
Time, separation to entry	86,400 sec
Entry spin rate	5 rpm
Entry roll torque	126 ft-lb
Entry roll impulse	1000 ft-lb-sec

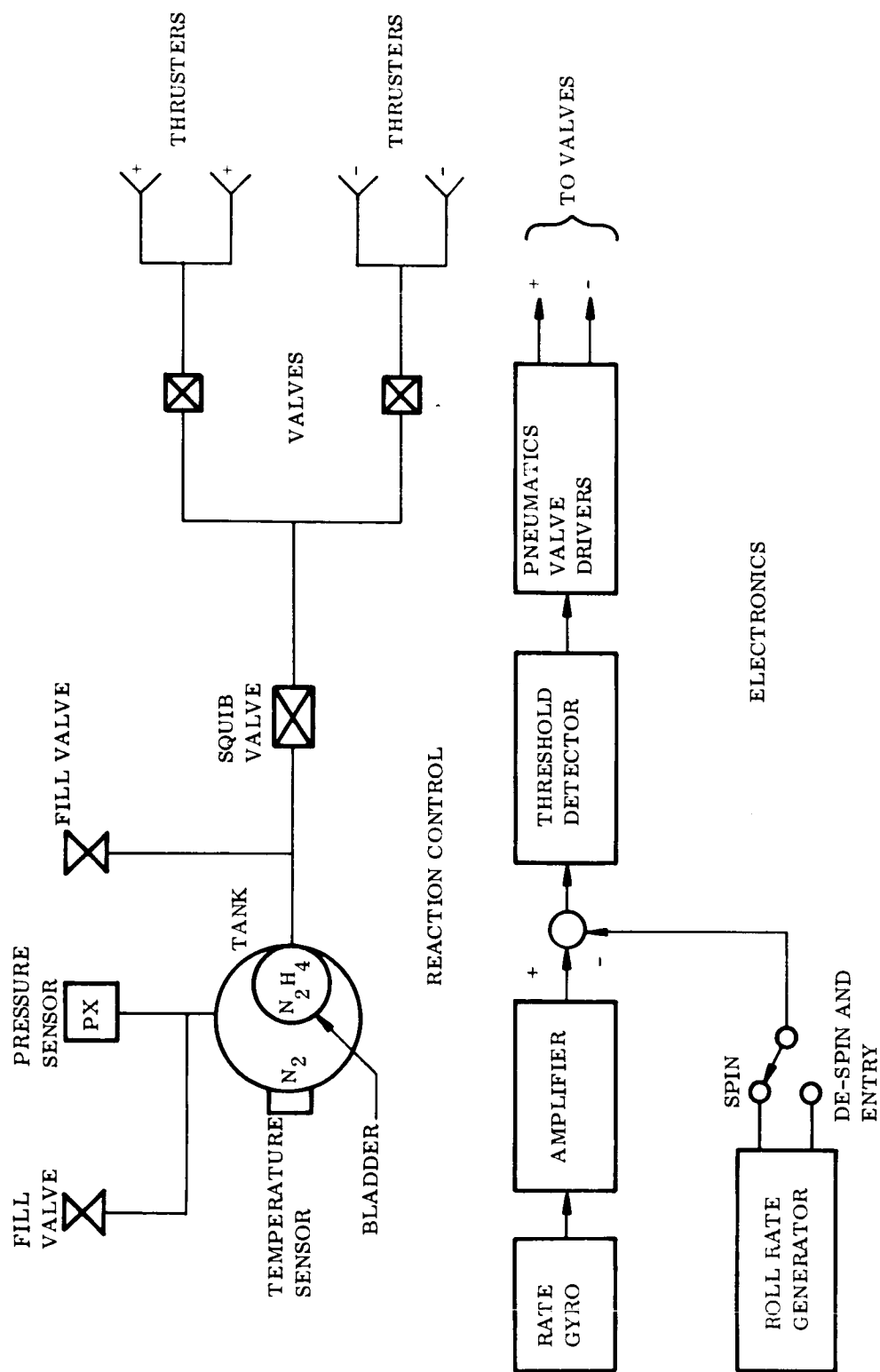


Figure 6.3.7-1. Spin and Roll Control Subsystem, Block Diagram

Reaction control is provided by a blow-down hydrazine system using nitrogen as a pressurant. An aluminum tank less than 8 in. in diameter is used. Its size is chosen so that the initial gas pressure of 400 psi is reduced to 300 psi when all of the hydrazine has been expelled. This limits the thrust decrease to approximately 25 percent. All control torques are provided as couples. The system is sealed off until Capsule separation by the explosive squib valve shown in fig. 6.3.7-1.

Power requirement for the gyros and electronic assembly is 5 watts. When one of the valves is energized, an additional 2 watts is required. The size of the combined gyro and electronics is $5 \times 6 \times 3$ in.

The operational sequence of the subsystem is as follows:

1. The spacecraft orients the Capsule in the proper direction for firing the de-orbit propulsion engine. The gyros and electronic are energized just prior to separation. The high rate mode of operation is commanded.
2. At 1.5 sec after separation, the explosive squib is fired, initiating spin-up.
3. A spin rate of 50 rpm is reached at 25 sec after spin-up started. This rate is maintained during propulsion firing.
4. After propulsion firing, and prior to entry, the low rate mode of operation is commanded. The subsystem remains in this mode throughout entry.

6.3.7.1.3 Spin Control Subsystem Performance

The pointing accuracy of the spin control subsystem is, of course, directly dependent on the accuracy the spacecraft orients the Capsule prior to separation. Two major additional errors are introduced by the Capsule separation subsystem and the spin control subsystem. These errors are the tip-off error and the coning error during propulsion firing.

The tip-off error is caused by the Capsule angular rate uncertainty at separation from the Capsule. This rate produces an attitude deviation from the separation spacecraft attitude proportional to the time interval from separation to spin-up command. It is estimated that the separation tip-off rate can be held to less than $0.5^\circ/\text{sec}$. For spin up occurring 1.5 sec from separation, this creates an angular error of 0.75° 3-sigma.

The coning error is caused by the upsetting torque created by the propulsion thrust not acting through the Capsule center of mass. Gyroscopic action reacts to the torque by producing spiraling increase in the attitude error. To maintain a required ΔV orientation error, the spin rate must be increased as the propulsion thrust level is made larger. For the selected spin rate of 50 rpm, the ΔV orientation error will be held to less than 0.75° , 3-sigma.

An error analysis, including these and other error sources, was described in Vol III, Section 5.2.5. The overall error in ΔV orientation is estimated to be 2.1° , 3-sigma.

The attitude error of the Capsule at entry into the atmosphere is dependent on the stability of the spinning Capsule from the time of propulsion burnout to entry. To use spin stabilization during this period, the problem of energy dissipation which could lead to attitude divergence must be considered. Since a vehicle is stable about the axis of maximum moment of inertia, even with energy dissipation, this point design will present no problem since its roll (spin) axis inertia is larger than that of the pitch/yaw axes.

6.3.8 PRE-ENTRY SYSTEMS WEIGHT

The weights of those items contained within the pre-entry systems for Point Design 4 are listed in table 6.3.8-1. The attitude control system is carried in the entry system weight summary Table 6.4.8-1. Total pre-entry system weight for this point design is 419 lb.

TABLE 6.3.8-1. PRE-ENTRY SYSTEM WEIGHT SUMMARY POINT DESIGN 4

Item	Weight (lb)	
Thrust Cone Assembly		88.7
Structure	25.0	
Propulsion System (Less Propellant)	24.0	
Propellant	31.0	
Separation system	1.2	
Electrical Equipment	7.5	
Canister		330.0
Shell	78.5	
Structure, Internal	61.2	
Separation Rings	39.1	
Separation System	19.6	
P&V System	13.5	
EP&D System	53.4	
Thermal Blanket	34.7	
Hardware & Misc	30.0	
Pre-entry System Total		418.7

6.4 ENTRY SYSTEMS

6.4.1 CONFIGURATION

6.4.1.1 Constraints

Constraints for Point Design 4 were placed on the following parameters:

1. Ballistic coefficient
2. Entry system weight
3. Maximum aeroshell diameter
4. Entry angle and velocity
5. Payload weight and volume
6. Powered flight and entry loads
7. Materials and construction techniques

The design goal was to achieve a vehicle design with a ballistic coefficient of 7 lb/ft². This had to be achieved within the envelope constraints discussed in Section 2.3.1 which limited the capsule system maximum diameter to 175.6 in. and the entry system diameter to 171.6 in. was as shown in fig. 6.3.1-1.

Entry system weight was an important parameter since along with the half cone angle and based diameter it determined that the final ballistic coefficient was the overriding criteria since it was this factor that had the most affect in heating rates, trajectories, loading and determined the retardation system deployment regime. Table 6.4.1-1 shows a tabulation from the CONfiguration SElection Program for the Point Design 4. It can be seen from looking at this table that for a fixed base diameter of 152 in. a varying half cone angle of 50° to 70°; the ballistic coefficient varies from 10.64 down to 7.03 for a change of greater than 25 percent while the weight change is only 62 lb. (less than 4 percent). This points up the fact that the ballistic coefficient is the important factor and must be held constant.

TABLE 6.4.1-1 CONSEP RESULTS FOR POINT DESIGN 4

$\frac{R_N}{R_B} = 0.5$			
Cone Angle	W/C_{DA} (lb/ft ²)	Entry Weight	R_B (in.)
50°	10.64	1566	76
60°	8.34	1530	76
65°	7.59	1516	76
70°	7.03	1504	76

Internal clearances between the canister and the aeroshell limit the aeroshell diameter to 171.6 in. Additionally the aeroshell could not be so small as to adversely affect the packaging of the Lander system. Working with both the 171.6 in. diameter and the packaging volume necessary for the Lander, Point Design 4 configuration was evolved.

The entry angle and entry velocity along with the ballistic coefficient, base diameter and bluntness ratio were important factors in determining the thickness of heat shield material necessary for this out-of-orbit mission.

The payload weight was an important factor for determining internal shell loads and for sizing the retardation system since it was this weight which contributed greatly to the total decelerator load.

The critical loading conditions for the entry system in the out-of-orbit mode were conditions J, K, O, and P as shown in table 6.4.1-2.

It was based on these conditions and the entry heating environment that the aeroshell structure was selected. Also important in selection of the material and construction of the aeroshell was its ease of fabrication, cost, and light weight.

6.4.1.2 Description

Geometrically, the Point Design 4 is a blunt sphere-cone vehicle with a bluntness ratio (R_N/R_B) of 0.5. The spherically shaped nose has a radius of 38.1 in. making a tangent with a frustum of a cone with a half angle of 60° and a base diameter of 152.4 in. as shown in fig. 6.4.1-1.

The heat shield is an elastomeric shield material (ESM) 1004 AP with a tapering thickness from the stagnation region to the end of the skirt. Density of this selected heat shield material is 35.0 lb/ft^3 . Corner heating effects were accounted for in the design and protection has been provided in the form of a peripheral edge protection. To protect against the possibility of backface heating around the edge of the entry vehicle, the backface, for a short distance, is coated with a heat shield material.

The aeroshell structure is an aluminum honeycomb shell with a core thickness of 1.50 in. and facing sheets 0.025 in. thick to form a total shell thickness of 1.55 in. In the aft end of the aeroshell is a torque box structure made up of webs and rings with periodic ribs to provide internal stiffness. This structure tends to stiffen the shell and minimize local shell bending and rotation as well as provide a load path for the Lander loads introduced by securing the Lander into the aeroshell. The combined spin, de-spin, and roll control nozzles are mounted on the aft web of the torque box. Separation forces, which occur at separation from the adapter and at Lander release, are taken in the longitudinal web of the box.

TABLE 6.4.1-2. POINT DESIGN LOADS

Letter	Condition	Limit Load Gx	Acceleration Gn	Remarks
A	Ground handling	2.0	2.0	83 lb/in. Radial
B	Band clamp	N/A	N/A	
C	First stage burnout	5.2	2.0	
D	Second stage burnout	4.0	2.0	
E	Axial vibration	+6.0 -3.0	---	
F	Lateral vibration	---	± 2.0	
G	Canister separation	Negligible	Negligible	
H	Entry systems separation	Negligible	Negligible	
I	Thrust cone separation	Negligible	Negligible	
J	Entry (max Gx)	5.5	Negligible	
		12.7	Negligible	Out-of-Orbit 320° Interface
		48.0	Negligible	Out-of-Orbit 250° F Interface
				Direct Entry 200° F Interface
K	Parachute opening	10.0	---	
L	Impact	1000.0	---	
M	Canister pressure	N/A	N/A	$\Delta P = 0.5$ psi at 275° F
N	Canister pressure	N/A	N/A	$\Delta P = 1.0$ psi at Ambient
O	Spin	N/A	N/A	50 rpm
P	Sterilization	N/A	N/A	

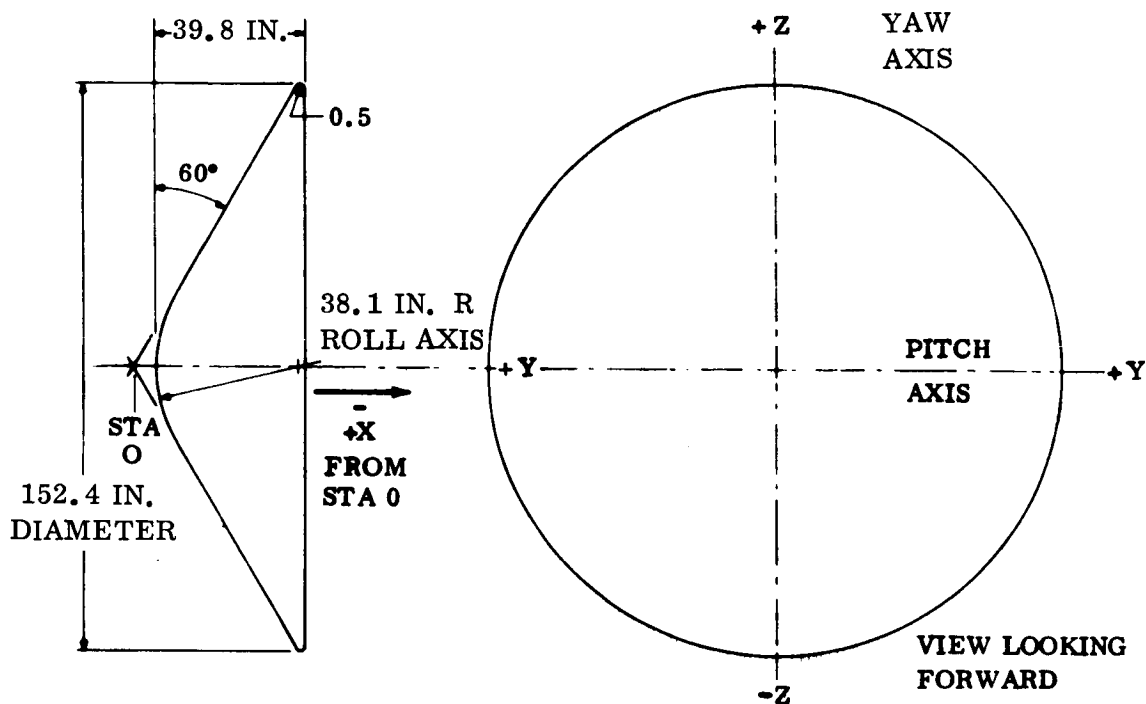


Figure 6.4.1-1. Aeroshell Geometry Point Design 4

The Lander is held in by a strap arrangement which consists of strap or belly-band, which runs completely around the Lander (see fig. 6.3.1-2), hot-wire device, T-bolt, tie-down strap, and torsion spring. The load in the tie-down strap is sufficient to overcome the rotational forces due to spin and de-spin and thus restrain the Lander from moving during these events.

The forward portion of the Lander sits in a phenolic glass honeycomb saddle which has a Teflon lining between it and the Lander to eliminate the possibility of adhesion of the saddle and Lander to each other during the long space flight while under the tie down load.

Pressure sensors and an air intake for temperature measurements, which also leads into the mass spectrometer located in the Lander, are located in the nose of the aeroshell.

6.4.2 HEAT SHIELD

At the heating rates expected for the direct entry Point Design 4 described in table 6.4.2-1, the most efficient materials on a weight basis are, in general, members of the low density charring ablator class. Thus, because of the relatively mild Martian entry environment where total surface recession is small in most cases and thermal insulation is of prime importance, the low density charring ablator, ESM 1004 AP, was selected to be a design solution for the Mars Hard Lander heat protection system for direct entry modes.

The basis for selection of this material was:

1. Minimum system weight
2. Maximum flexibility to accommodate non-design conditions
3. Fewer anticipated fabrication and development problems than with other approaches.
4. Sensitivity to the sterilization/decontamination and low temperature/hard vacuum environments can be circumvented by proper material formulation

For the direct entry missions where steep angle entry into the VM-8 atmosphere 25° nom. ($+7^\circ$) results in ESM surface melting, ESM 1004 AP (35 lb/ft³ density) is the preferred approach due to its good performance in relatively mild melting regimes.

It has been shown in Volume III, Section 3.1.2 that the maximum heat shield thickness requirement is dictated by the shallowest path entry angle attainable. The heating histories which include both convective heating and equilibrium and non-equilibrium radiative heating for Point Design 2B are shown in fig. 6.4.2-1 for the stagnation point and end of skirt locations and are used for Point Design 4 due to the similarity in requirements.

Employing the thermo-physical properties described in table 6.4.2-2 and the convective and radiative heat flux histories shown in fig. 6.4.2-1 the heat shield thickness requirements were generated using the techniques described in Vol III Section 3.1.2 and are shown for Point Design 2B in fig. 6.4.2-2. The shield thickness requirements are those required to hold the design bondline temperature to 600° F with a safety factor of 1.2 applied to the shield thickness requirements presented for Point Design 4. This would result in a margin of about 200° F on the backface temperature. Analysis has shown that one of the most significant factors which affects the estimation of the shield thickness is the tolerance on the entry path angle. Designing the heat shield thickness to the lower limit on entry angle results in a safety margin of about 10 percent for Point Design 4 when compared to the nominal entry condition.

TABLE 6.4.2-1. ENTRY CONDITIONS AND GEOMETRY OF POINT DESIGNS 1 THROUGH 6

Point Design	Mission Entry Mode	Entry Velocity (ft/sec)	Entry Angle (deg)	Ballistic Coefficient (lb/ft ²)	Aeroshell Base Dia. D _B (ft)	Half Cone θ ° C	Rn/Rb
1	Out of Orbit	15300	14	14	8.33	60	0.5
2A	Direct	20800	16	7	12.7	60	0.5
2B	Direct	20800	16	7	11.4	60	0.5
3	Out of Orbit	15300	14	14	8.33	60	0.5
4	Direct	20800	16	7	12.7	60	0.5
5	Out of Orbit	15300	14	14	10.0	60	0.5
6	Direct	20800	16	7	14.0	60	0.5

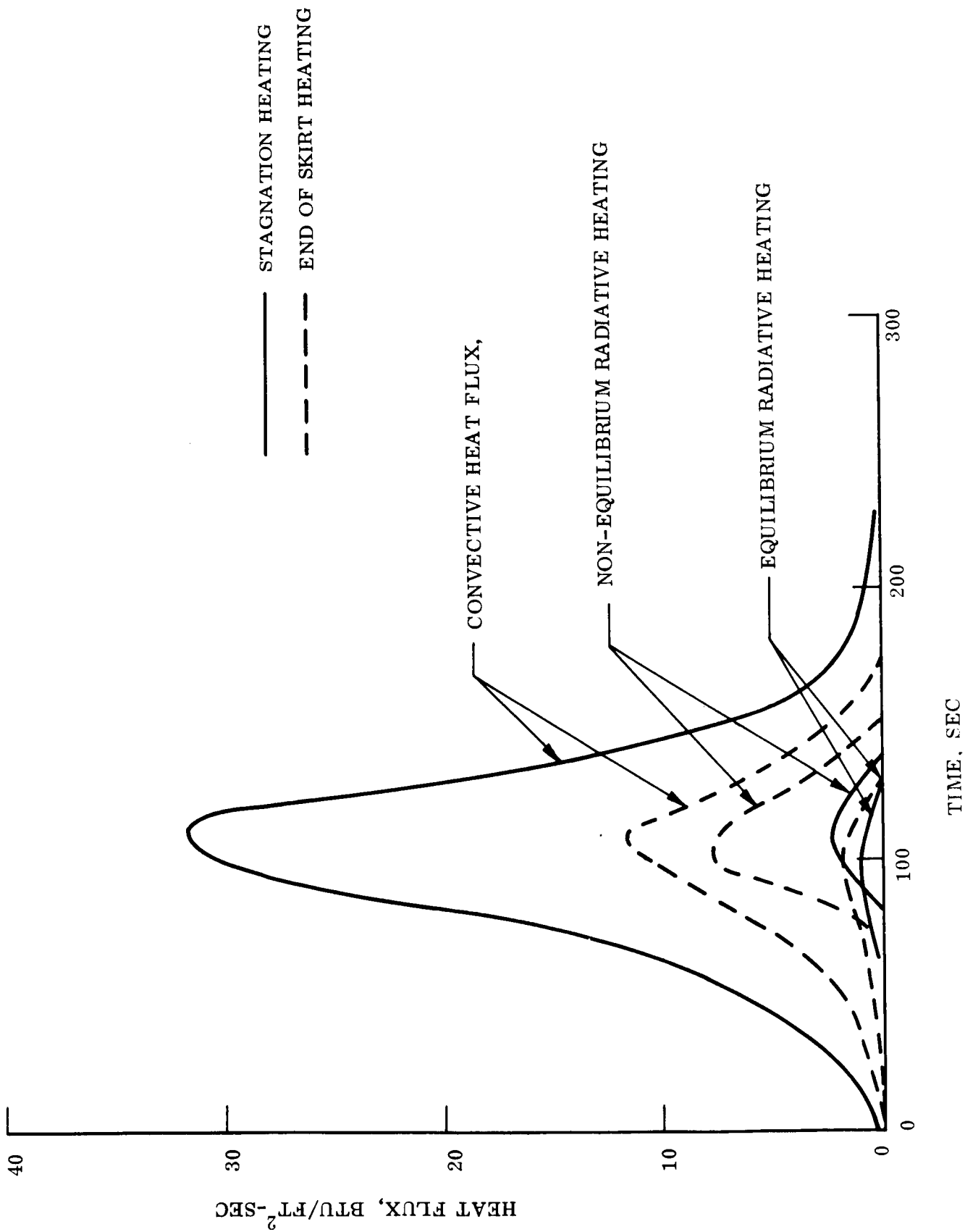


Figure 6.4.2-1. Cold Wall Convective and Radiative Heat Flux Histories Point Design 2B

TABLE 6.4.2-2. THERMOPHYSICAL PROPERTIES OF ESM MATERIALS

		ESM 1004X	ESM 1004AP
Virgin Density, ρ_v lb/ft ³		16.6	35.0
Char Density, ρ_c lb/ft ³		6.7	14.0
Pyrolysis gas specific heat, Cpg Btu/lb°R		0.4	0.384
Molecular weight of injected species, Mg		24.5	24.5
Order of reaction, N		2	2
Pre-exponential factor, A sec ⁻¹		15000	30000
Activation energy, E Btu/lb Mole		44700	47500
Heat decomposition, HGF	1335°R		50
(Btu/lb gas generated)	1460		45
	1710		1000
	1960		2610
Specific heat Cp			
Btu/lb°R	600°R	0.31	0.305
	710	0.33	0.360
	1210	0.44	0.44
	2075	0.44	0.44
Conductivity, k Virgin	610°R	0.0000115	0.0000237
Btu/ft - sec°R	800	0.0000170	0.0000220
	1335	0.0000220	0.0000210
	1710	0.0000260	0.0000231
Char	1335	0.0000740	0.0000777
	1710	0.0000850	0.0000855
	2210	0.0001000	0.000104

For the decomposition reaction described by the following Arrhenius type equation:

$$\frac{1}{W_o} \frac{dw}{dt} = \frac{(W-W_f)^N}{(W_o)^N} A e^{-AE/RT}$$

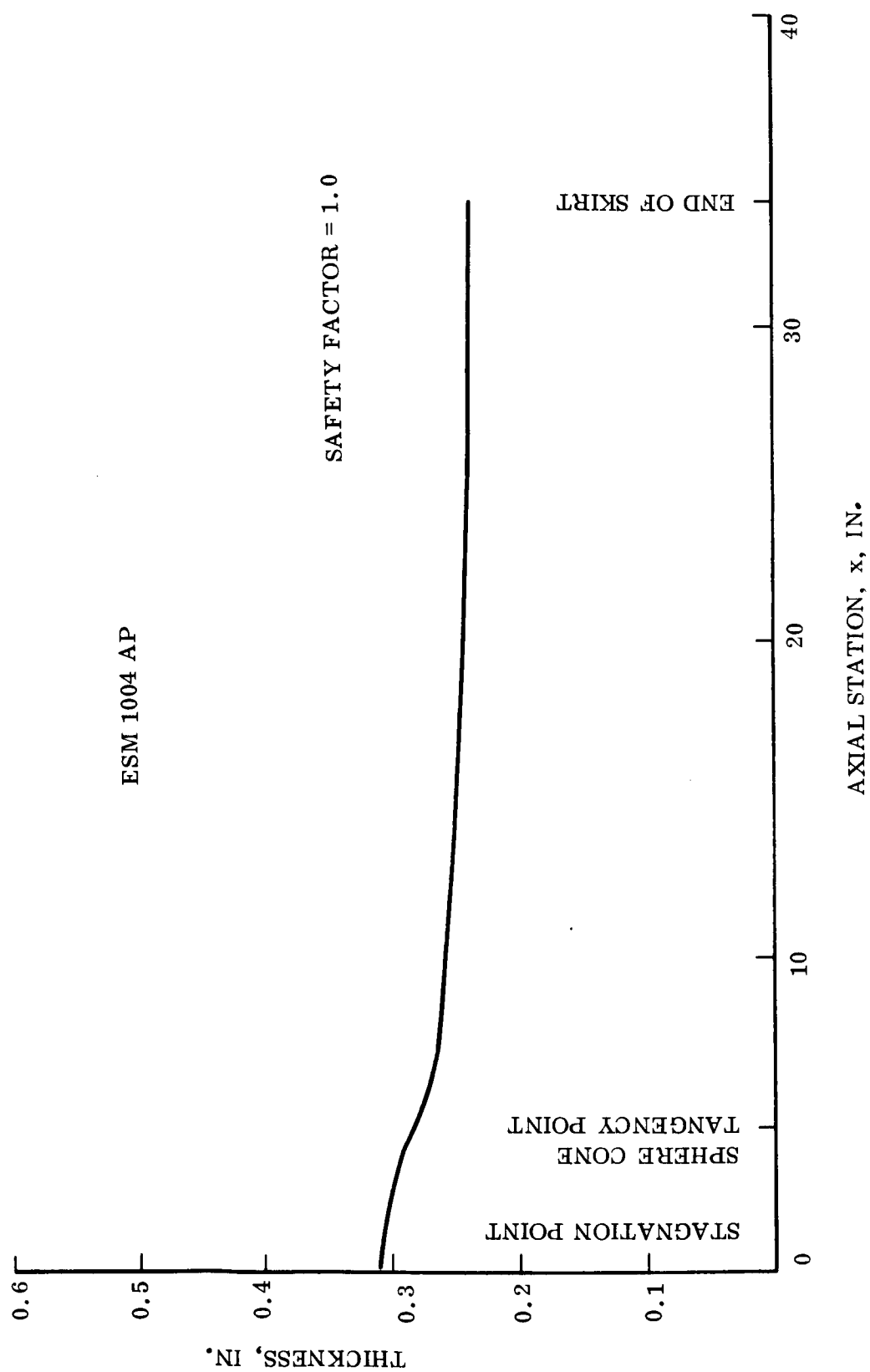


Figure 6.4.2-2. Heat Shield Thickness Requirements, Point Design 2B

The backface and frontface temperature histories of the shield material for Point Design 2B are shown in fig. 6.4.2-3. Fig. 6.4.2-4 shows the thermal gradients through the ESM material at selected times in the Martian entry corresponding to peak surface temperature and peak bondline temperature. These results are presented for entry into the VM-3 atmosphere. Shield thickness requirements for Point Design 4 are shown in table 6.4.2-3. Since entry conditions and shield requirements for Point Design 4 are very similar to those of Point Design 2B, then the thermal gradients and temperature histories presented for Point Design 2B, in figs. 6.4.2-3 and -4 are representative for Point Design 4.

Since the total heat load on the afterbody of the sphere-cone is expected to be small compared with the forebody, an ablating material for thermal protection is unnecessary, and a high emissivity coating would be an adequate protection. An analysis* indicated that for Voyager the peak cold wall heat flux on the afterbody was small, the resultant temperature rise being only 256°F.

The current design for the ESM 1004 AP heat shield allows for ease of fabrication, handling and final assembly. The heat shield material is designed to be fabricated in panel sections using maximum panel sizes, from a fabrication standpoint, of approximately 10 sq ft. Additional advantages of the segmented shield are that it allows for 100 percent inspection, does not require the aeroshell during manufacturing operations and allows for finish machining prior to its being bonded to the aeroshell.

Design considerations have also taken into account the necessity for steps between the segmented panels both longitudinally and circumferentially. These steps were determined by both the bond and heat shield thickness tolerances.

Corner heating effects have been taken into consideration at the base of the entry vehicle and a peripheral edge protection of ESM1004 AP is provided around the corner of the heat shield at the base of the aeroshell. To protect against the possibility of backface heating around the edge of the entry vehicle, the exposed aeroshell structure at the base and inboard on the vehicle is coated with ESM 1004 AP.

6.4.3 AEROSHELL AND STRUCTURE

The aeroshell for Point Design 4 is an aluminum honeycomb shell 1.55 in. thick. It is comprised of a 3 lb/ft³ core 1.50 in. thick with 0.025 in. thick 7075 aluminum facing sheets bonded with HT424 bond. This shell material has been selected for its light weight, ease of fabrication, and much lower cost than other types of honeycomb materials. It has been designed to take the axial, bending and shear loads encountered during powered flight and planetary entry.

*McDonnell Astronautics Voyager Capsule Phase B Final Report F694, Volume II, Part B, 31 August 1967.

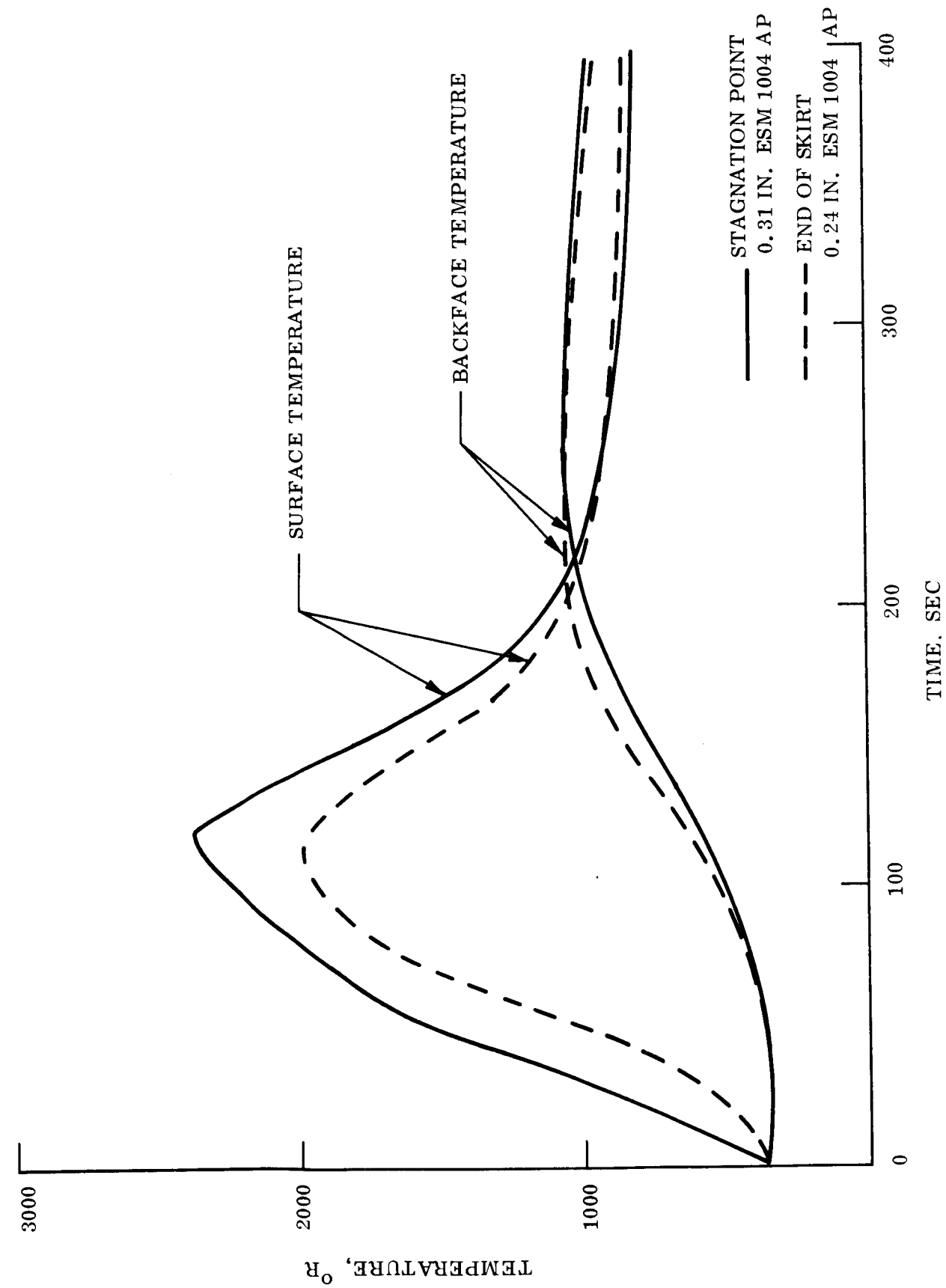


Figure 6.4.2-3. Surface and Backface Temperatures Histories, Point Design 2B

ESM 1004 AP

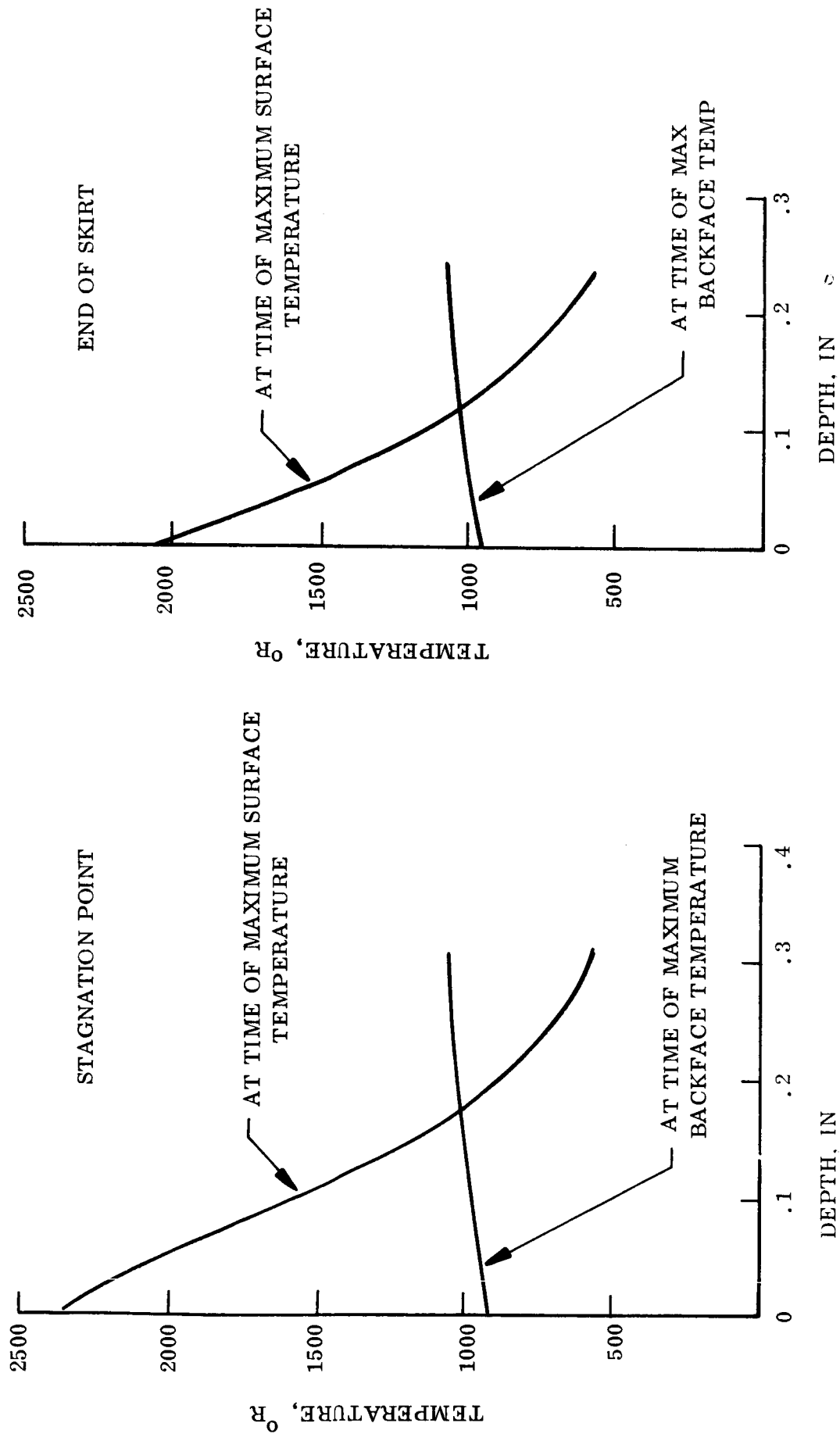


Figure 6.4.2-4. Temperature Gradients Through the Shield Point Design 2B ESM 1004 AP

**TABLE 6.4.2-3. SHIELD THICKNESS REQUIREMENTS FOR
POINT DESIGN 1 THROUGH 6**

Point Design	Entry Mode	Material Shield	Shield Thickness Requirements With 1.2 Safety Factor	
			Stagnation Point	End of Skirt
1	Out-of-Orbit	ESM 1004 X	0.624	0.415
2A	Direct	ESM 1004 AP	0.367	0.275
2B	Direct	ESM 1004 AP	0.372	0.288
3	Out-of-Orbit	ESM 1004 X	0.624	0.415
4	Direct	ESM 1004 AP	0.367	0.275
5	Out-of-Orbit	ESM 1004 X	0.617	0.407
6	Direct	ESM 1004 AP	0.360	0.263

The detailed analysis of the aeroshell to withstand the entry inertial loads and aerodynamic pressure loadings has been performed by MULTISHELL, a GE computer program. The inputs to this program to perform the analysis consist of the entire aeroshell configuration upon which are imposed the inertia and pressure loadings. Output from the program consists of the shell internal stresses, moments, shear, inplane shell loads and in addition the complete shell deformations. These deformations include all local discontinuity deformations of the shell. Figs. 6.4.3-1 through -5 present the deflection, moment, shear, in-plane load and stress distributions for Point 2A. The general distributions for Point Design 4 are similar.

Approximate structural analysis was performed to determine the initial core and facing thicknesses to be used in the computer program. Upon completion of the first MULTISHELL analysis, any necessary changes to the structural material gages are made to result in small positive margins of safety for all of the elements of the shell as shown in table 6.4.3-1.

Analysis of Point Design 4 indicates that the shell bending is critical and that aluminum honeycomb is just as efficient as titanium honeycomb, lighter than stainless steel honeycomb and easier to fabricate than both materials. The aluminum honeycomb is just as efficient as the titanium or steel honeycomb because local shell bending is the critical loading condition and the minimum gage is no longer the controlling factor. This local shell bending is induced by the loading of the aeroshell internally by the Lander and the aerodynamic pressure externally.

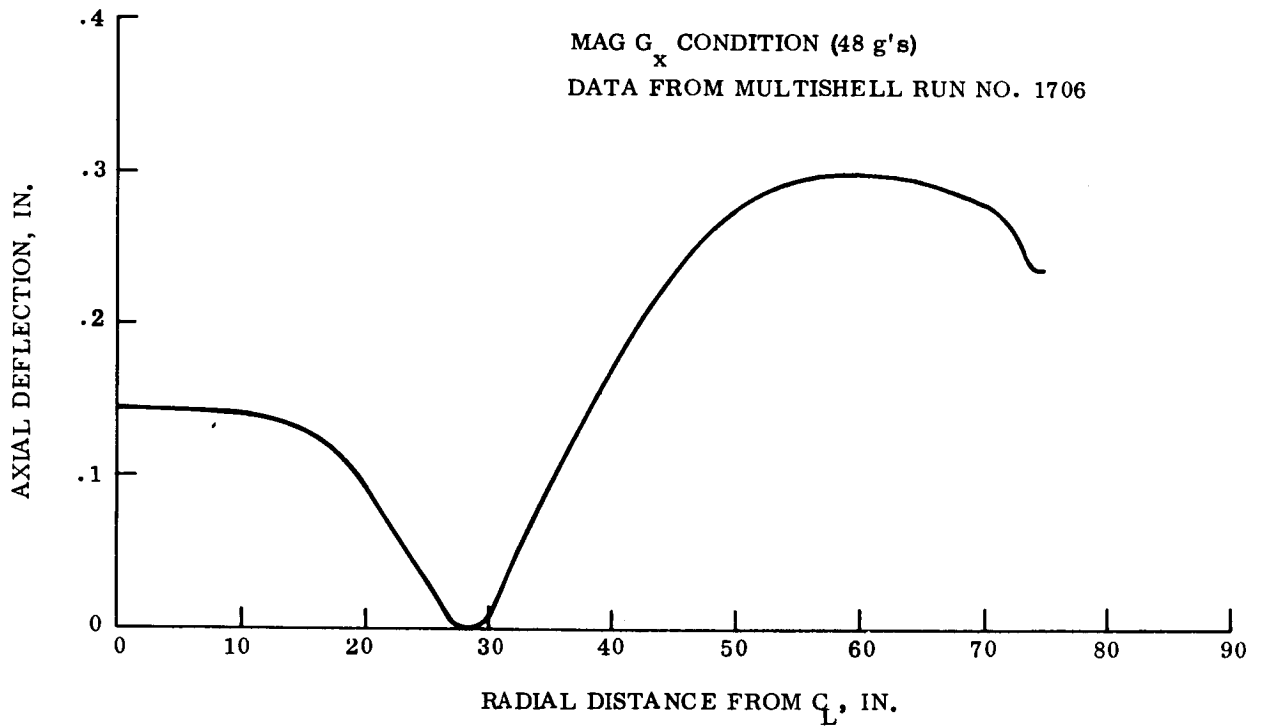


Figure 6.4.3-1. Axial Deflection-Aeroshell 2A vs Radial Distance

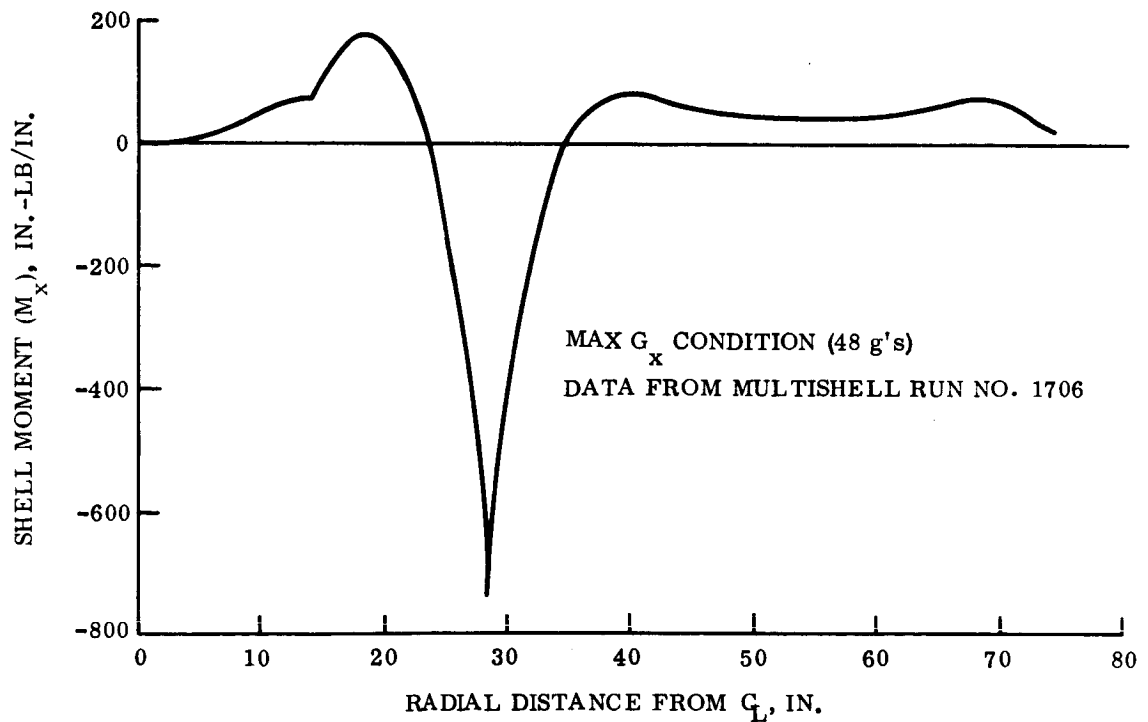


Figure 6.4-3-2. Axial Bending Moment (M_x)-Aeroshell 2A vs Radial Distance

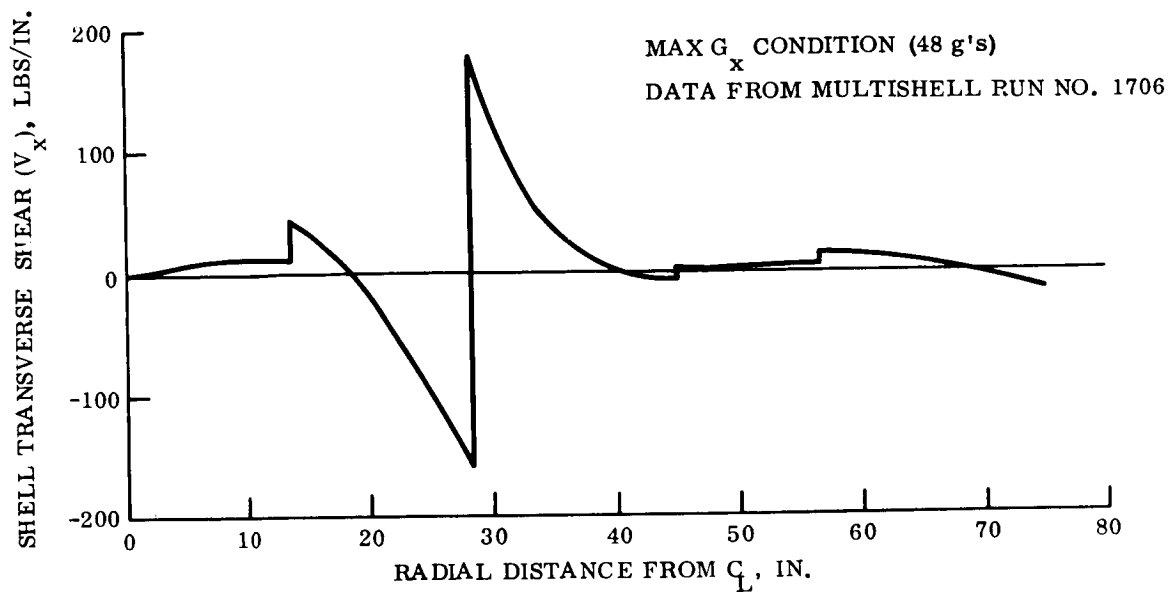


Figure 6.4.3-3. Shell Transverse Shear-Aeroshell 2A vs Radial Distance

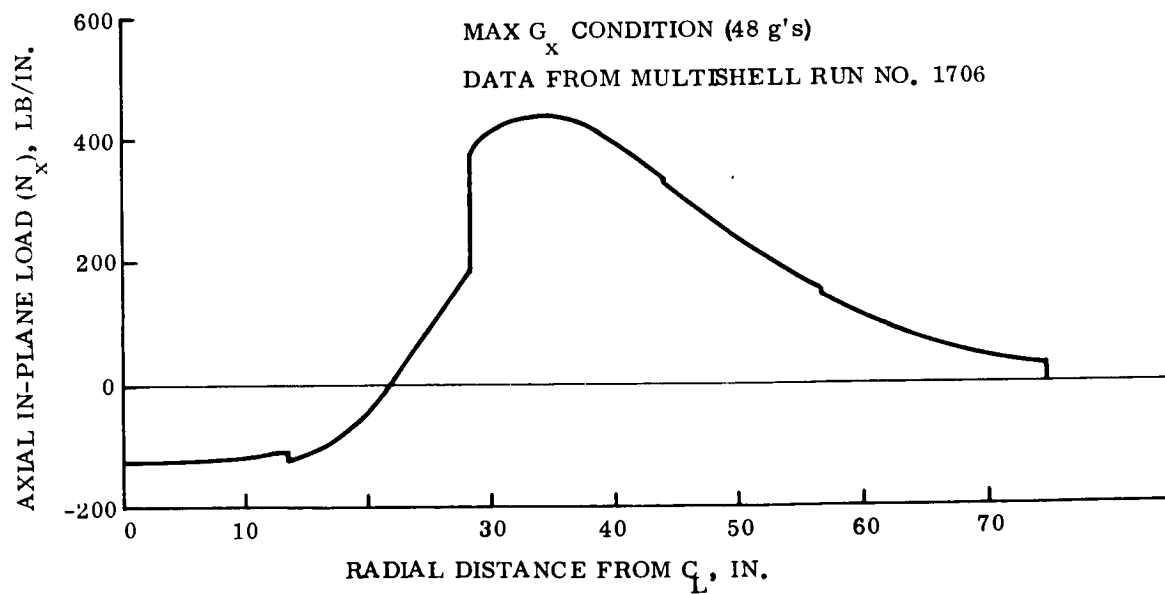


Figure 6.4.3-4. Axial In-Plane Load-Aeroshell 2A vs Radial Distance

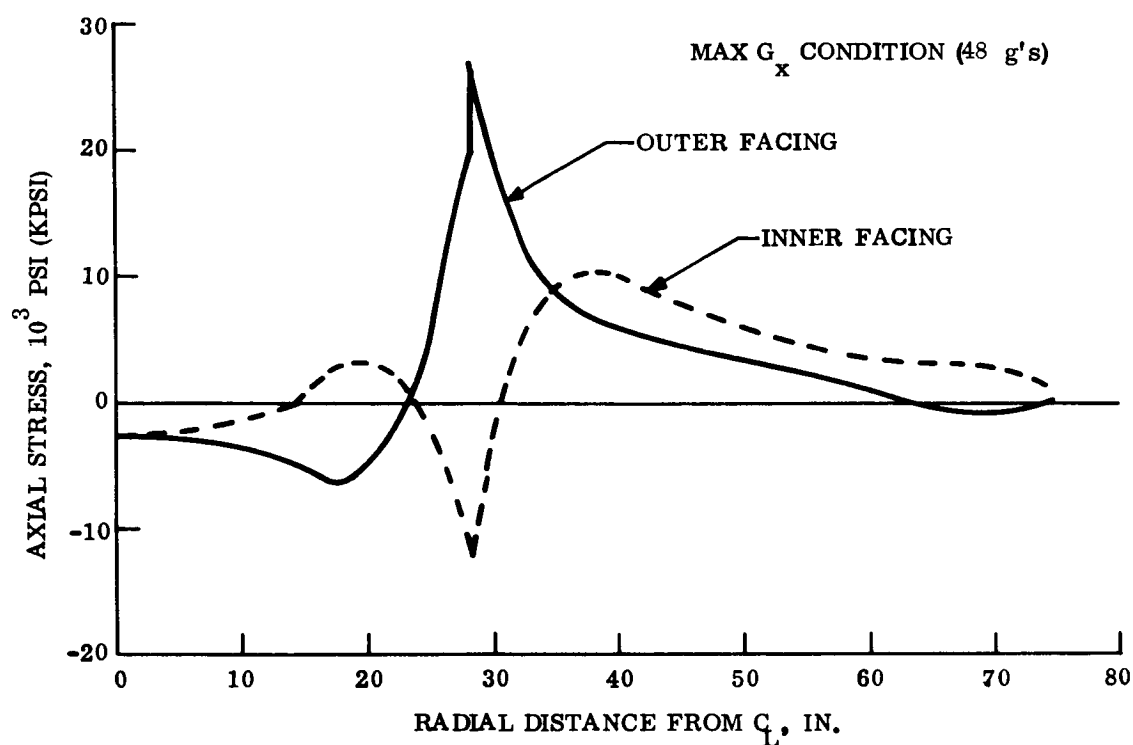


Figure 6.4.3-5. Axial Honeycomb Facing Stress Aeroshell 2A vs Radial Distance

TABLE 6.4.3-1. FINAL ALUMINUM HONEYCOMB REQUIREMENTS FOR AEROSHELLS

Point Design	Honeycomb		Min. M.S.	Facing Material
	Facing Thick	Core Thick		
No. 1	0.020	0.75	0.50	2024T4
No. 2A	0.025	1.50	0.09	7075-T6
No. 2B	0.025	1.50	0.15	7075-T6
No. 3	0.020	0.75	0.65	2024-T4
No. 4	0.025	1.50	0.09	7075-T6
No. 5	0.020	0.75	0.21	2024-T4
No. 6	0.030	1.50	0	7075-T6

The heat shield structure interface temperature is less than 200°F at the time of maximum loading (48.0 g's limit) and the loadings are lower at times of higher temperatures.

The temperature at parachute deployment, at the heat shield structure interface, can be 600°F since at this time the loading on the aeroshell is negligible.

Fig. 6.4.3-6 shows the time of maximum load imposed on the aeroshell and the interface temperature as a function of time from entry for the VM-3 environments. The maximum load occurs at a time when the heat shield structure interface temperature is 103°F. When parachute deployment occurs (230 sec from entry), the load has reduced to zero while the interface temperature has increased to 600°F. The total time at elevated temperature, prior to parachute deployment, is 125 sec or 2.0 min.

At an elevated temperature of 600°F the allowable stresses for a 20 min exposure indicate a compressive yield strength 37 percent of room temperature strength compared with loads that are negligible.

Point Design 4 configuration parameters are presented in table 6.4.3-2. The honeycomb core and facing thickness requirements and minimum margin's of safety are presented in table 6.4.3-1.

TABLE 6.4.3-2. POINT DESIGN ENTRY DATA

Point Design	Entry Weight (in.)	Diameter (in.)	Radius to Bearing Load (in.)	Radius to Box Structure "A" (in.)
1 (Out-of-Orbit)	1246	100.0	27.0	41.5
2A (Direct)	1480	152.4	32.0	44.0
2B (Direct)	1127	135.6	27.0	37.2
3 (Out-of-Orbit)	1324	100.0	31.0	41.5
4 (Direct)	1558	152.4	31.0	44.0
5 (out-of-Orbit)	1530	120.0	32.5	42.5
6 (Direct)	1766	168.0	31.0	46.6

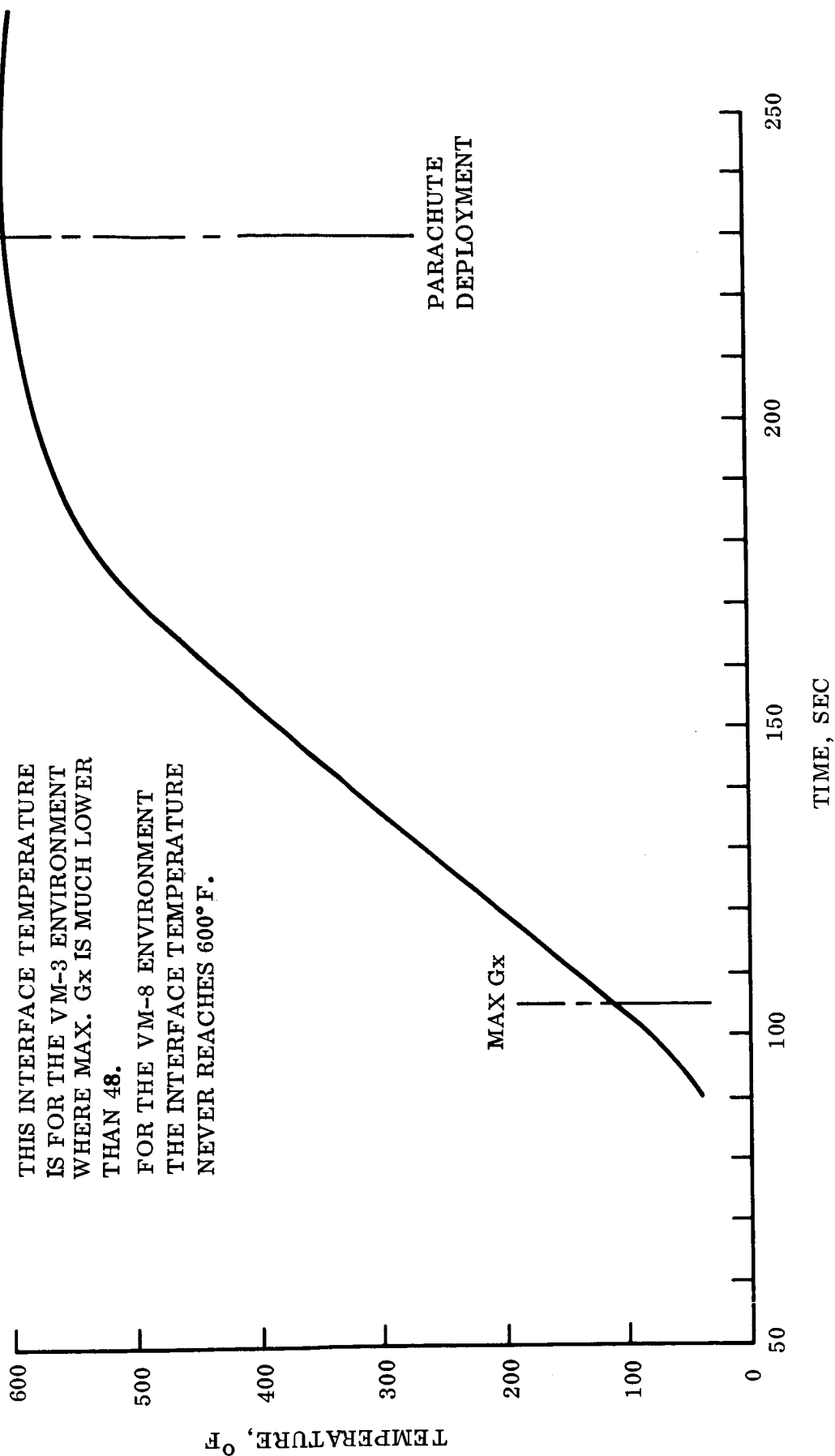


Figure 6.4.3-6. Point Design 2A Shield-Structure Interface Temperature

The aluminum honeycomb weight is 1.15 lb/ft^2 of surface area (including bond) compared with 1.25 lb/ft^2 for stainless steel honeycomb and 0.98 lb/ft^2 for titanium honeycomb.

At the maximum base diameter is a box structure which extends forward into the aeroshell. This box structure is made up of a circular radial web and cylindrical longitudinal web with periodic ribs joined together by a ring at the base and tied into the aft ring of the aeroshell and a frustum ring internal and forward in the aeroshell. The cylindrical longitudinal web extends beyond the maximum base diameter of the aeroshell to provide a support for the entry system separation device. At this point is the mating interface with the internal adapter.

This box like outer structure of the aeroshell acts as a torque box and restrains the rotation of the outer edge of the aeroshell. The construction of this torque box structure and the radial distance from the point of application of the load due to the payload bearing against the honeycomb shell determines the magnitude of the shell bending loads. With the torque box structure made very stiff, to allow very little torsional rotation, the maximum honeycomb shell bending moments and highest facing stresses would occur in the outer portions of the aeroshell. A reduction in the torsional box stiffness results in the maximum shell bending moments shifting to the center portion of the aeroshell. The ideal situation is then where some rotation is allowed such that the shell bending is reduced over the entire shell and the moments are of the same order of magnitude in the center and outer portions.

6.4.4 LANDER/AEROSHELL SEPARATION

The Lander is attached to the aeroshell by a strap assembly retained by 3 hot-wire tension bolts. The strap assembly, shown in fig. 6.4.4-1, consists of a strap or bellyband which runs completely around the Lander. As a part of the strap are cushioning pads and a Teflon spacer to eliminate the possibility of damage to the crush-up material. The strap is in three segments connected by 3 hot-wire tension bolts. In the middle of each segment is a fitting which is attained by a T-bolt to the tie-down strap. The tie-down strap is attached to a fitting on the box structure in the aft end of the aeroshell. A torsion (or "mousetrap") spring is also attached to this fitting and fits around the tie-down strap. Tension is placed in the entire assembly, to obtain the required restraining loads for the Lander, by torquing the T-bolt to a predetermined torque.

In order to separate the system, which occurs after parachute deployment, a current of 6 amps for 30 msec is fed to the hot-wire bolt causing them to separate. At this instant the torsion springs snap the tie-down strap and attached segments of the bellyband outboard and clear of the Lander which is extracted from the aeroshell by the parachute.

6.4.5 ENTRY SYSTEMS EQUIPMENT

With the exception of the 4 pressure and 1 temperature transducers for stagnation region measurements, all of the entry science instruments and support equipment

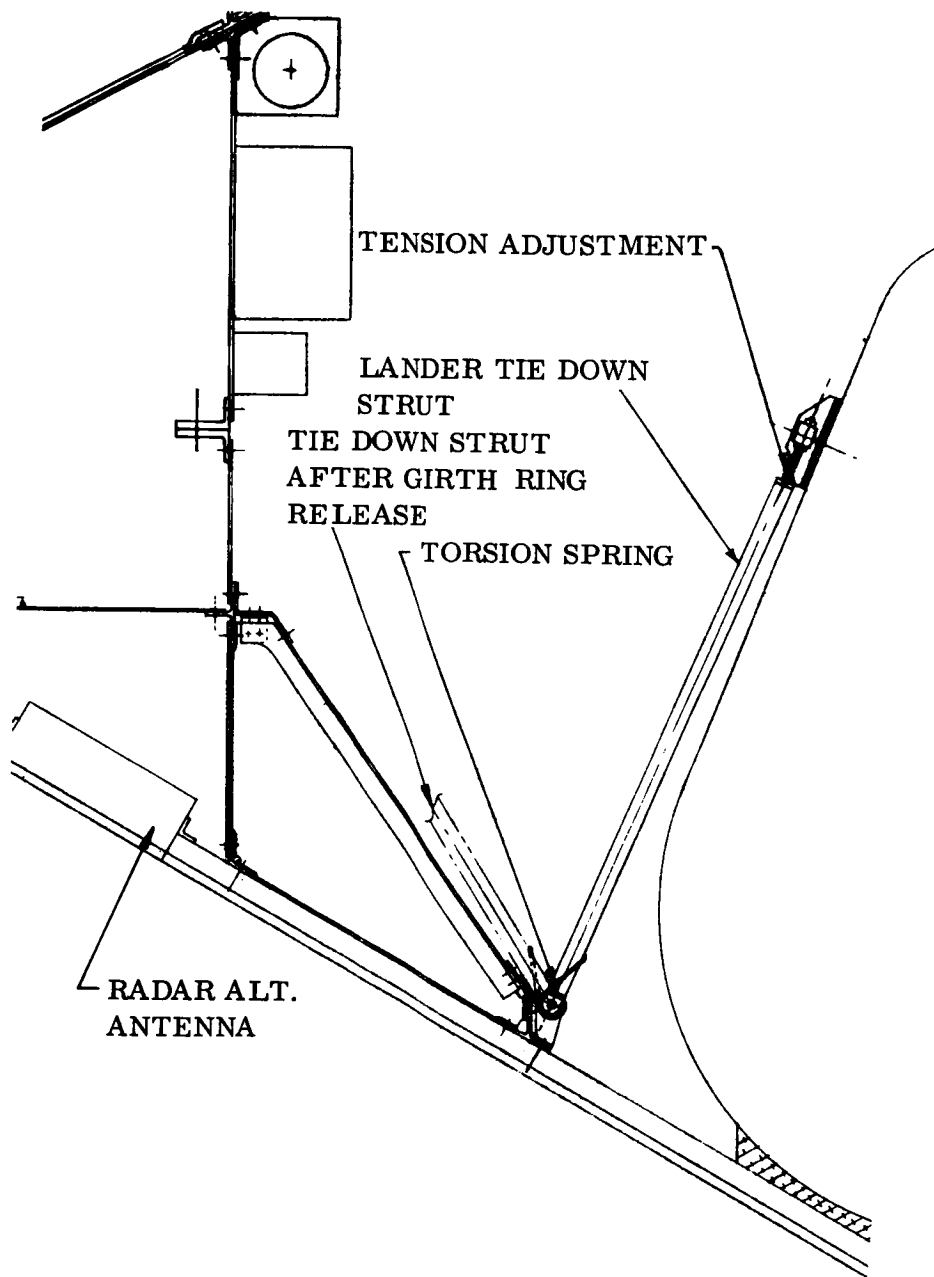


Figure 6.4.4-1. Lander Installation in the Aeroshell

(13.0 lb of the basic 15.5 package of instruments) is incorporated in the Lander module (fig. 6.4.5-1).

6.4.6 RETARDATION SUBSYSTEM

The retardation subsystem requirements are so similar for all of the point designs that a single subsystem design approach appears to be adequate. The design evolved for Point Design 4 will permit deployment and proper landing impact velocity to meet the required conditions of the mission. These are: deployment at speeds not greater than Mach 2 terminal velocity on main parachute at altitude not less than 6 kft; and a vertical descent velocity in least dense atmosphere (VM-7) of 100 fps.

6.4.6.1 Retardation Performance

6.4.6.1.1 Mortared Pilot Chute Selection

The use of a mortared pilot extraction parachute was selected over directly mortar ejecting the large main parachute. The size of mortar required to directly eject such a large mass from the decelerating vehicle would take more weight than the selected arrangement. Also, a more orderly deployment of the large diameter main parachute is ensured using the pilot parachute extraction technique.

6.4.6.1.2 Trajectory Considerations

It is desired for optimum Lander impact, to minimize descent time on the main parachute while insuring that the main parachute will be at equilibrium terminal velocity at the time of its separation. Combined sensing techniques can be used to provide this. Deployment based on the use of a radar altimeter alone to deploy at a set altitude does not accomplish this. For the case where Mach 2 occurs at 11 kft in the VM-8 atmosphere, deploying at 11 kft in the VM-7 or VM-1 atmospheres would result in reaching terminal velocity on the main parachute at a lower altitude than in the VM-8 case even though the initial deployment would be below Mach 2.

Deploying on Mach number alone would produce high altitude deployment and a long descent time on the main parachute if the atmosphere is dense (i.e. VM-9). If the deployment sensing coupled a Mach 2 gate with a time gate and an altitude gate then deployment below Mach 2 and minimum parachute descent time would be assured. The logic for this combination is discussed below. Further trajectory investigations would be necessary to optimize a particular point design.

Parachute deployment will be programmed to occur between 11 k and 20 kft. A 20 kft signal from the radar altimeter would enable parachute deployment. On receipt of the Mach 2 signal, the timer would be started. If the 20 kft signal were received before the preset time-out, parachute deployment would occur. This would indicate a rare atmosphere. If Mach 2 did not occur until the receipt of the 11 kft signal from the radar altimeter, this would indicate very rare atmosphere such as VM-8. If the Mach 2 signal were received and time-out of the timer occurred prior to the

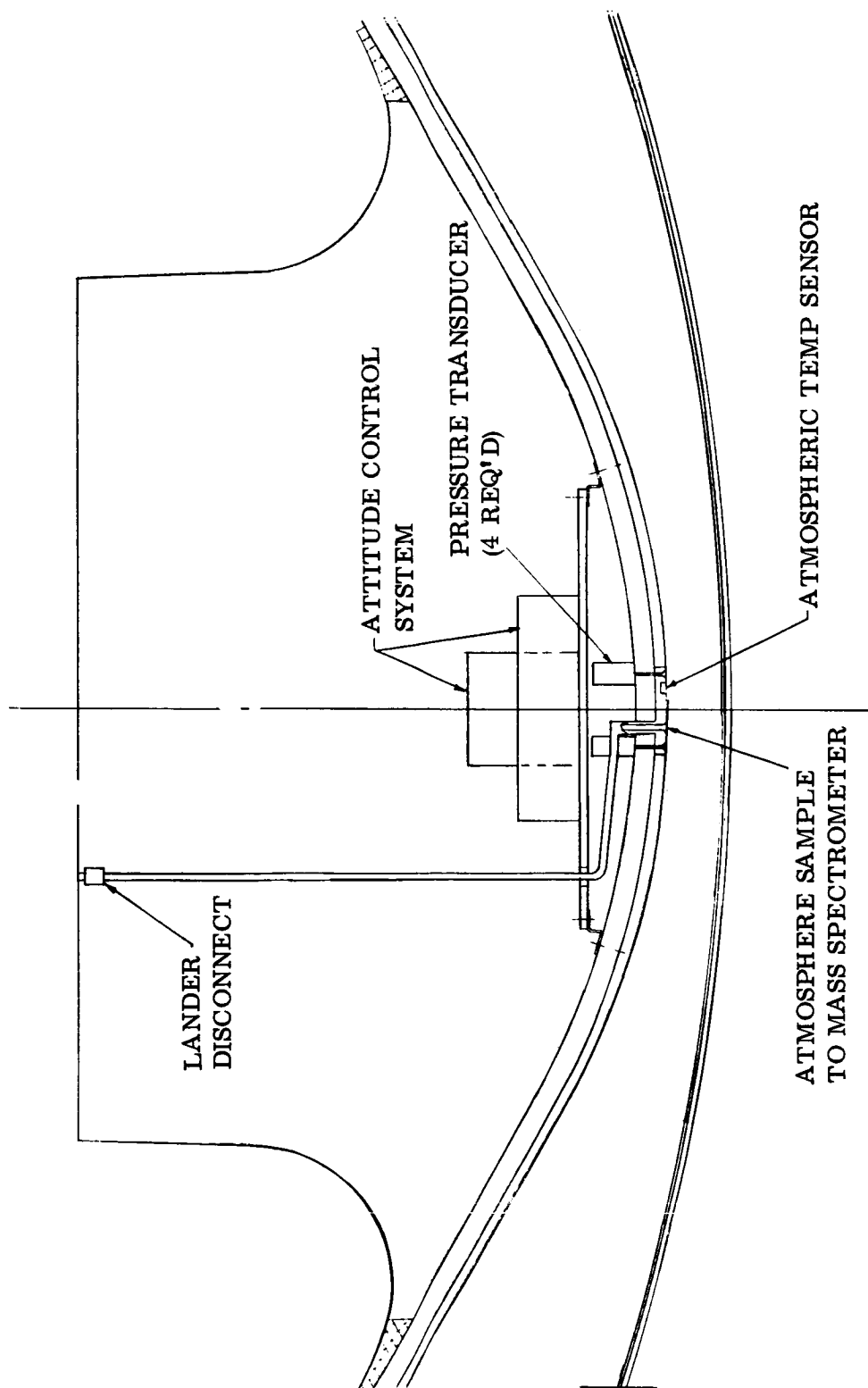
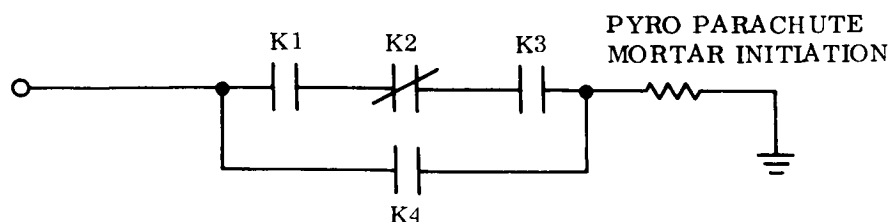


Figure 6.4.5-1. Entry System Instrumentation

20 kft signal from the altimeter, this would indicate a dense atmosphere such as VM-9 or -10. In this case, parachute deployment initiation is delayed until the 11 kft signal from the altimeter. In any case, deployment would be initiated at 11 kft.

The following schematic clarifies this deployment logic.



- K1 - closes at Mach 2 signal
- K2 - opens at end of timer time-out
- K3 - closes at 20 kft signal
- K4 - closes at 11 kft signal

6.4.6.2 Parachute Design

The modified ringsail parachute configuration, as tested in the PEPP program, was selected for the parachute design. To assure reliable deployment, a single large diameter main canopy deployed by an extraction pilot parachute was selected. The main parachute will be deployed with one stage of reefing to minimize opening loads and parachute weight. The technique of reefing is a proven and commonly used method of controlling parachute inflation and loads. It has been used in numerous applications in the past with complete success in all sizes of parachutes including ringsail parachutes of the size that would be required for the Hard Lander of this study.

The single large diameter main canopy was selected over a cluster of smaller parachutes. More complexity is involved in deploying clustered canopies. The use of a cluster would increase the development risk for this application. Providing reefing with clustered canopies is much more complex than in the case of a single canopy because of the inneractions of the clustered canopies. This inneraction problem created a great deal of difficulty in applying reefing to the clustered parachutes used in the Apollo development. None of the inflation problems encountered in the Apollo development should be experienced in applying reefing to a single main parachute design investigated here.

With a reefed stage, the development loads experienced by the main canopy will be low enough to allow the use of light weight parachute construction. Analyses substantiating the materials and construction selected are presented in Volume III under Parachute Deceleration. The parachute system weights used were calculated using the RESEP program, which is described in Vol. III, App. A.4.

Parachute design drag performance was based on results obtained in the PEPP Program. A constant value for C_D of 0.52 was used. Other test data on ringsail parachutes indicates a higher value for C_D should be obtainable. This would cause

a reduction in parachute size, weight and opening loads. The use of $C_D = 0.52$ should therefore be conservative.

Available test data indicates that the ringsail parachute inflation will follow the performance curve of fig. 4-49 and -50 of "Performance of and Design Criteria for Deployable Aerodynamic Decelerators", ASD-TR-61-579 (referred to as the parachute handbook). This data was used for this preliminary design analysis. The parachute inflation characteristic was assumed to be linear with time for each stage of deployment, i. e. C_{DS} increases linearly with filling time. This is a good assumption for a first cut design analysis and is fairly representative of test data.

6.4.6.3 Design Trajectory Example

The purpose of the trajectory study was to verify that the selected point design could function under the worst case deployment conditions and meet the established design requirements of parachute deployment at Mach ≤ 2.0 and reach main parachute full open terminal velocity at approximately 6 kft.

In some of the worst case point design trajectories investigated, the main parachute does not reach terminal velocity until altitude is down to almost 4 kft. When further work is done to finalize a planned vehicle design and the re-entry trajectory, the deployment altitude of the parachute system can be adjusted to reach terminal velocity at 6 kft.

The worst design conditions for the parachute occur in the rarest atmosphere represented by VM-8. The trade-off studies indicate that the vehicle will not decelerate to Mach 2 until approximately 11 kft altitude. For all other atmospheres, Mach 2 occurs at a higher altitude. Parachute performance was designed to meet the worst case deployment conditions of the VM-8 deployment. The study made included the extraction and deployment of the main parachute by the pilot parachute.

The pilot parachute deployment occurred at 11 kft, Mach 2 and $q = 20$ psf. The trajectory of the pilot parachute extracting the main parachute was examined and compared to the trajectory of the vehicle now minus the weight of parachutes. This study was used to determine the point of start of the main parachute reefed inflation where the main parachute skirt has been deployed. The results of this study are shown in fig. 6.4.6-1 and the parameters selected for use in the Point Design 4 study are listed in table 6.4.6-1.

6.4.6.3.1 Parachute Staging Design and Trajectory

Parachute reefing and duration of the reefed stage were optimized using existing computer programs to produce opening loads for both main parachute stages to be within the strength capability of the suspension lines and minimize altitude loss during deployment.

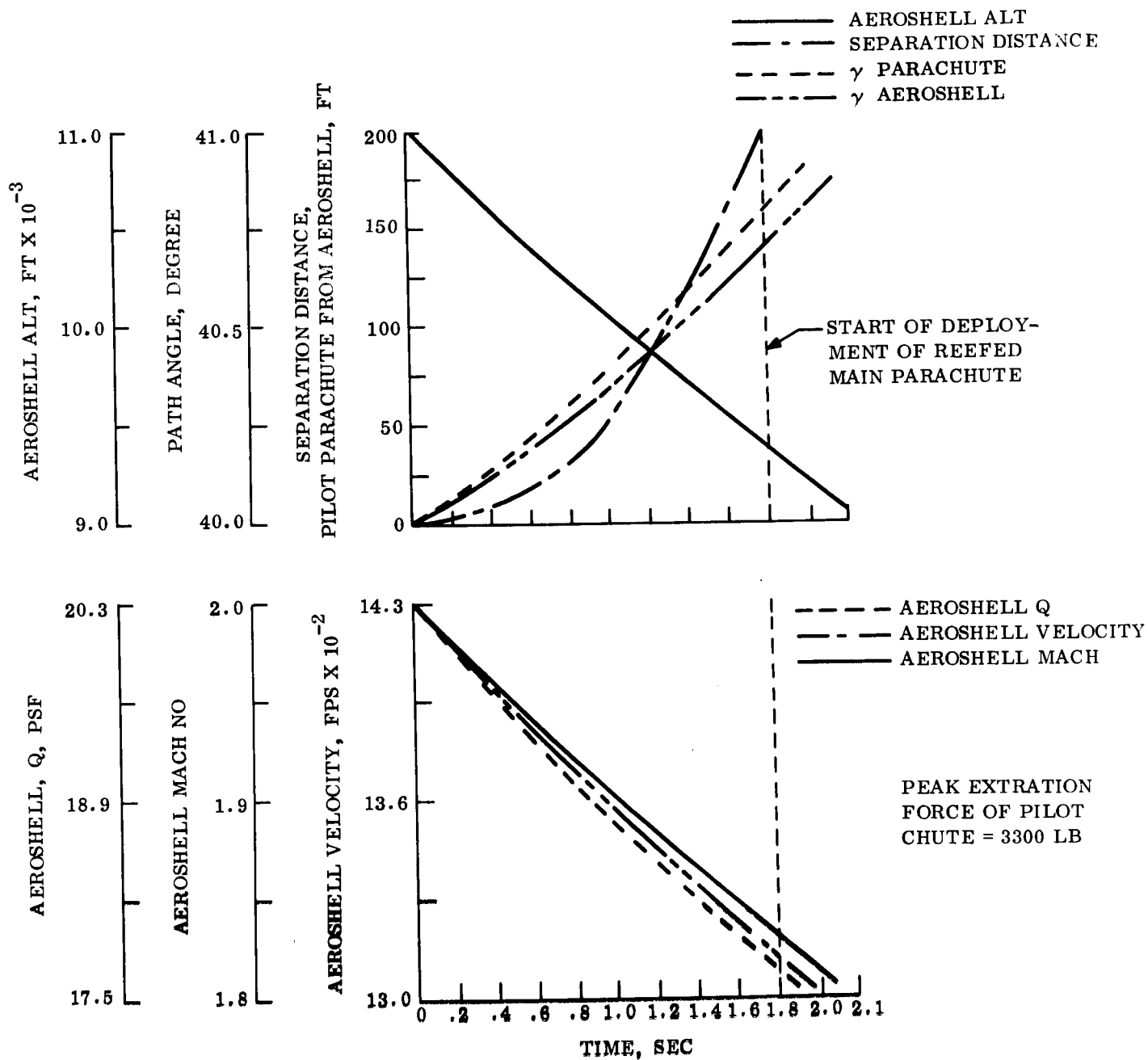


Figure 6.4.6-1. Point Design 4 Pilot Deployment Trajectory Study

TABLE 6.4.6-1. PILOT PARACHUTE DESIGN PARAMETERS

Atmosphere = VM-8
Initial deployment altitude = 11 kft
Weight being decelerated by pilot parachute = 193 lb
Vehicle weight minus the parachutes = 969 lb
Path angle below horizontal = 40.0°
Pilot parachute fill time = 0.24 sec
Linear pilot parachute inflation with time assumed.
Pilot parachute $D_o = 15.7$ ft
Pilot parachute $C_D = 0.52$
Pilot parachute $C_D S = 101 \text{ ft}^2$
Pilot parachute opening shock factor = 2.0
Average wake reduction effect during pilot parachute extraction = 0.85
Aeroshell $D_o = 12.7$ ft
Aeroshell $C_D = 1.46$

The analysis to establish reefing ratio is based on a simultaneous solution of the following equations for the two stage main parachute deployment.

$$F_1 = C_{D1} S_1 \cdot X_1 \cdot q_1$$

$$F_2 = C_{D2} S_2 \cdot X_2 \cdot q_2$$

$$q_2 = \frac{W_1 \cdot LF_1}{C_{D1} A_1}$$

Where:

$C_D S$	= effective drag, ft^2
F	= opening force, lb
X	= opening shock factor
q	= dynamic pressure, psf
W	= Weight in local gravity, lb
LF	= force along Z axis in local gravity, g's

Subscripts:

1	= stage one
2	= stage two

The quantities $C_{D2} S_2$, q_1 , X_1 , X_2 , LF_1 and W_1 must be known. Without accurate performance data on a given design, assumptions must be made for X_1 , X_2 , and LF_1 . If the correct characteristics are used, the performance can be verified in a computer trajectory analysis with a program designed to vary the $C_D S$ during parachute inflation.

Optimum reefing should produce equal opening load peaks for both stages. However, a reefed design can be satisfactory if other objectives are met and the peak loads are not balanced. In this case, if the opening forces are within the structural capability of the parachute and the total altitude loss during deployment is not excessive, the performance will meet the requirements.

In the staging study below values were selected based on past experience and data. Reefing ratio was selected, using the approach described above, to produce equal stage loads. In the trajectory study, fill time was based on data from the parachute handbook (ASD-TR-61-579) and $C_D S$ growth was assumed to be linear with time. The disreef opening force from the trajectory analysis (shown on fig. 6.4.6-2) came out lower than the reefed opening force. By iteration, the opening forces in the reefing ratio selection analysis and the trajectory analysis could be made to come out equal. However, at this point, the exercise would be academic. Slight changes in the disreef fill time, or some nonlinearity in $C_D S$ growth, or a combination of the two could significantly affect the resulting disreef open force. At this point, there is higher confidence that the reefed opening force is correct than there is in the disreef opening force.

In the hardware development program, the reefing line length to produce the desired reefing ratio will be selected based on the best existing data available. After first test data is obtained necessary adjustments would be made to obtain the desired reefed performance based on data from the actual system. There is high confidence that required reefed performance can be achieved with little difficulty.

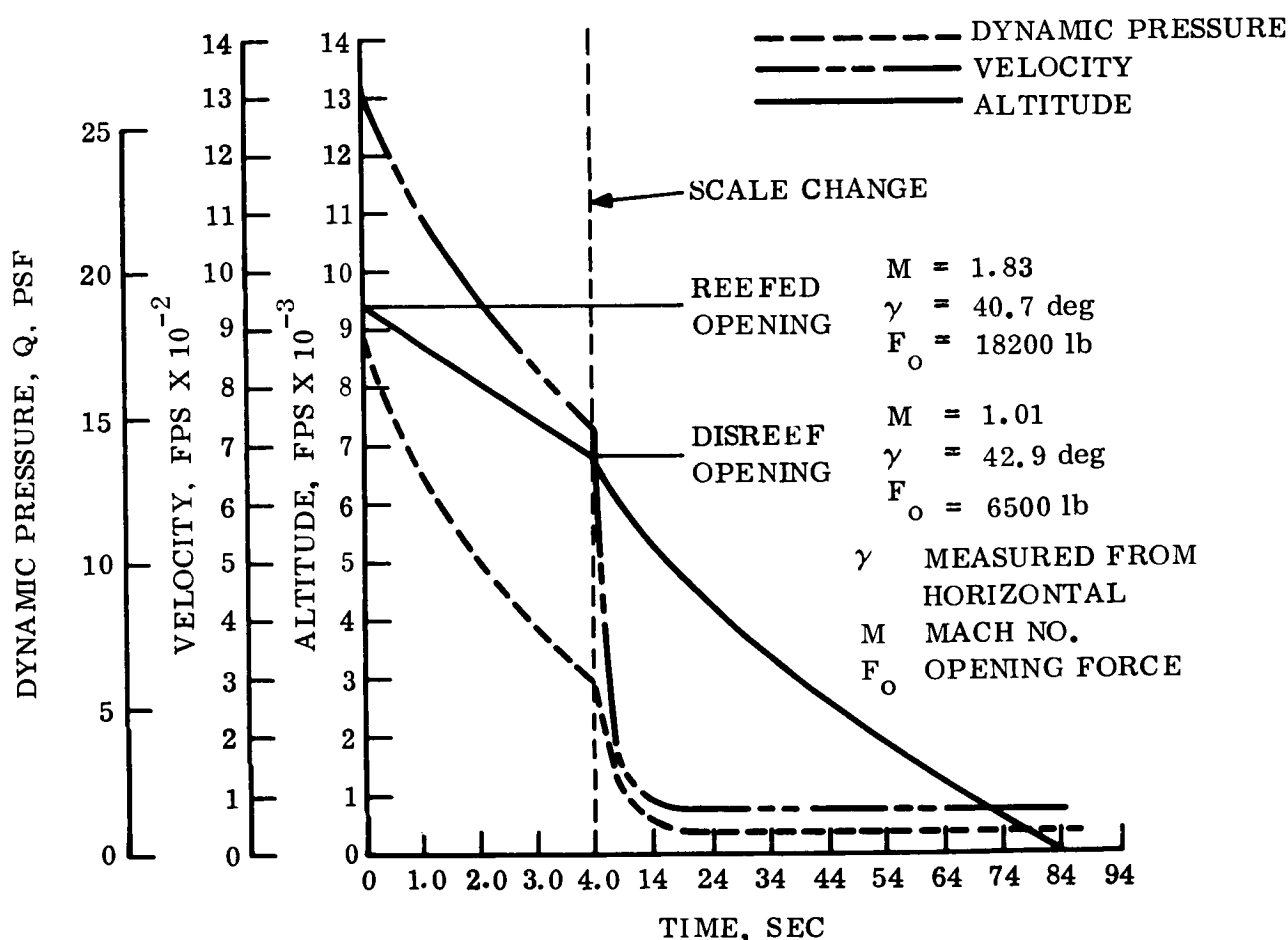


Figure 6.4.6-2. Point Design 4 Main Parachute Trajectory in VM-8 Atmosphere

The PEP program demonstrated satisfactory inflation characteristics in Mach 2 deployment in a rare atmosphere. With reefing, inflation will proceed in the same manner as without reefing until the point where the reefing line restricts and delays full inflation. In all cases, a reefing design must be verified in the parachute development test program.

The parameters selected for the staging study are shown for Point Design 4 in table 6.4.6-2.

The parachute trajectory was calculated by computer using the established or calculated parameters shown in table 6.4.6-3.

The results of this trajectory study are shown on fig. 6.4.6-2. These calculations are conservative in as much as the aeroshell or Lander drag area is not considered as part of the retardation drag area after main parachute deployment.

6.4.6.4 Hardware Description and Function

The basic hardware concepts selected for Point Design 4 have been previously used, tested and proven in other programs. The mortared parachute deployment is a commonly used, proven technique and the thermal cover concept and deployment arrangement has been used by GE on the 698 BJ program and the Maneuvering Ballistic Re-entry Vehicle program. The method of main parachute release has also been verified on these programs using explosive nuts. The parachute designs selected for the point designs of this study are based on the designs and results to date of the NASA PEP Program. The aeroshell release and fall-away is similar to the re-entry heat shield separation used by GE in the A45 program.

6.4.6.4.1 Pilot Parachute Mortar Thermal Cover

The thermal cover provides the means for securing the pilot extraction parachute in the mortar prior to mortar deployment. It also anchors one end of the main parachute thermal cover and provides thermal protection from wake heating to the pilot parachute, mortar gas source and the pull away electrical disconnect. The cover will be secured to the mortar tube by a break cord or shear pins until mortar firing. A bag handle on the pilot parachute deployment bag will be secured to the thermal cover in a recess within the cover. Thus, the thermal cover will also provide a mass to assist in stripping the deployment bag from the pilot parachute during deployment.

6.4.6.4.2 Pilot Extraction Parachute

The pilot extraction parachute will be similar in design to modified ringsails tested in the NASA PEP Program. All parachute lines and materials will be dacron that is sterilizable. Presently, lightweight construction is envisioned using 1.1 oz cloth and 300 lb suspension lines. In a development program, an investigation would be made to determine the suitability of utilizing 0.8 oz material in the lower panels near the skirt to save weight. The pilot parachute will be pressure packed to a 40 lb/ft³ density or slightly higher.

TABLE 6.4.6-2. MAIN PARACHUTE DESIGN PARAMETERS

Main parachute full open $C_D S = 6587 \text{ ft}^2$
 Initial reefed deployment $q = 17.74 \text{ psf}$
 Reefed stage opening shock factor = 2.0
 Disreef opening shock factor = 0.5
 Axial deceleration at disreef $\approx 7 \text{ g's Martian}$
 Total weight being decelerated = 1162 lb
 Main parachute $C_D = 0.52$

TABLE 6.4.6-3. POINT DESIGN 4 PARACHUTE TRAJECTORY PARAMETERS

Atmosphere = VM-8
 Total Weight being decelerated = 1162 lb
 Initial deployment altitude = 9397 ft
 Initial velocity, reefed deployment = 1312 fps
 Initial path angle = 40.7°
 Linear reefed opening inflation with time assumed
 Reefing ratio = 8.06%
 Reefed filling time = 0.16 sec
 Total time of reefed stage = 4.0 sec
 Main parachute $D_o = 127 \text{ ft}$
 Main parachute $C_D = 0.52$
 Main parachute full open $C_D S = 6587 \text{ ft}^2$
 Main parachute full open fill time = 3.16 sec
 Linear Full opening inflation with time assumed.

6.4.6.4.3 Pilot Parachute Riser Line

The pilot extraction parachute will be provided with a riser line to provide a minimum length of 6 aeroshell base diameters to the skirt at parachute inflation. This line will also be used to provide a mouth lock for the pilot parachute bag and to extract the main parachute bag for main deployment. It will attach to two fittings one at each end of the main parachute thermal cover, for extraction and deployment of this cover. The end of this line, at the main parachute bag, will be used to form a tuck bight

through a locking loop of the three tie-down straps securing the main parachute in its compartment.

6.4.6.4.4 Main Parachute Compartment Thermal Cover

The main compartment thermal cover provides thermal protection for the main parachute pack from re-entry wake heating. It is deployed by the pilot extraction parachute and permanently attached to the pilot parachute riser. This cover can also serve as a mounting point for spring pushers to jettison the de-orbit propulsion and thrust structure. The cover will be aluminum with necessary reinforcement to sustain the loads of deployment. All edges will be well rounded to prevent damage to the pilot parachute riser line. The outside surface will be covered with thermal protective coating to preserve the cover's structure and control main parachute temperature from re-entry wake heating.

6.4.6.4.5 Main Parachute, 2 Stage Deployment, Modified Ringsail - 15 Percent Geometric Porosity

The main parachute will be a single large diameter parachute. It will be provided with one stage of reefing. Existing design hermetically sealed reefing line cutters, manufactured by Technical Ordnance Products Co., will be used. The parachute will be made of dacron material that can be sterilized, in light weight construction similar to the constructions tested in the PEP program. At present the parachute would be made of 1.1 oz cloth with 300 lb suspension lines since deployment q will be 20 psf or less. In a development program to optimize weight and volume, the use of 0.8 oz cloth in the lower panels near the skirt would be investigated. A higher weight, lower mechanical porosity material is needed in the crown area to facilitate initial reefed deployment. 1.6 oz material will be used in the crown area if added strength is required. The main parachute will be pressure packed to 38 to 40 lb/ft³ density. Parachute reefing will be established to produce approximately equal opening loads at each stage of deployment to a level that utilizes the full structural strength capability of the suspension lines considering appropriate design operating factors. The reefed stage time will be set as short as possible to minimize altitude loss during this stage and provide a high opening velocity for rapid full open inflation. The trajectory in the VM-8 atmosphere, where Mach 2 occurs at the lowest altitude, will be used to determine staging time and reefing ratio. The opening loads in any other atmosphere will be lower than those for the VM-8 atmosphere as the deployment is presently envisioned.

6.4.6.4.6 Main Parachute Attachment Riser

The attachment risers will connect the main parachute at the suspension line confluence to the three tie-down fittings at the bottom of the parachute compartment. At main parachute release, the parachute compartment including the mortar will remain with the main parachute, attached by the risers, for removal.

6.4.6.4.7 Parachute Compartment Including Mortar

The parachute compartment will be an aluminum sheet metal fabrication to confine the parachute and provide thermal protection from re-entry wake heating. The outside surface of the compartment will be provided with the required thermal protective coating. The attachment and tie-down fittings will be attached to the rim at the bottom of the compartment. The pilot parachute mortar will be built into one side of the compartment. It will consist of a mortar tube and a sabot for the pilot parachute to seat against. The gas for mortar ejection will enter through tubing at the bottom of the mortar under the sabot. The area on each side of the mortar will be used for mounting the gas source for mortaring and the pull-apart electrical disconnect to separate the power supply from the mortar pyrotechnic. The side of the parachute compartment opposite the mortar will provide a slotted projection to receive a tang on the main thermal cover that secures that end of the thermal cover.

6.4.6.4.8 Parachute Attachment and Tie-Down Fittings

Three fittings, one for each of the three risers, are attached to the parachute compartment at the bottom flange and will be provided with two pins for webbing attachment. One pin will attach the main parachute risers (3), and the second pin will attach tie-down straps that secure the main parachute in a position such that it does not put a load in the main parachute thermal cover by pressing against it. The three tie-down straps will secure the main parachute using a locking loop and a tuck bight formed by the pilot parachute riser.

6.4.6.4.9 Mortar Pyro Gas Generator or Compressor Gas Supply

The gas for mortar ejection can be provided by either a pyro gas generator or a compressed gas supply. The compressed gas supply can be provided at a slight weight increase over the gas generator. Standard components are available from Conax Corp. (The Conax Eager Paks) for the compressed gas supply. It would consist of a small hermetic cylinder (10 to 15 in. capacity) containing compressed nitrogen at 3000 psi and a pyro valve that fires, piercing the cylinder allowing flow out through a connecting tube. This arrangement offers several advantages. There is no hot gas that could damage fabrics or components used for mortaring. There will be less of a problem of pyro development for the Mars mission in that the valve uses a standard squib and does not need the special gas generating materials. Reaction forces and performance will be more predictable. The compressed gas can be sterilized readily where this may be a problem with the gas generator materials.

6.4.6.4.10 Pull-Apart Electrical Disconnect

This component consists of an electrical connector, half of which is mounted captive to the main parachute compartment. At main parachute release, when the parachute compartment is pulled away, the two halves of the connector are separated. This component has been used successfully in a number of GE vehicle designs in the past.

6.4.6.4.11 Parachute Compartment Separation Device (3 Required)

The parachute compartment will be secured to the payload by three explosive nuts, each having dual cartridges, attached to bolts passing through the attachment and tiedown fittings. These will be similar to the explosive nuts used for Capsule separation and described in Vol IV, Section 6.3.3. The main parachute tie-down and deployment loads will be carried by these separation devices.

6.4.6.4.12 Radar Altimeter

A radar altimeter described in 6.4.6.6 will be used to sense altitude for parachute deployment and main parachute release above the surface. Where altitude sensing alone may not be adequate for all possible atmospheres, the altimeter would be coupled with the Mach 2 sensor providing gates to establish the correct point for parachute deployment.

6.4.6.5 Sequence of Retardation Subsystem Events

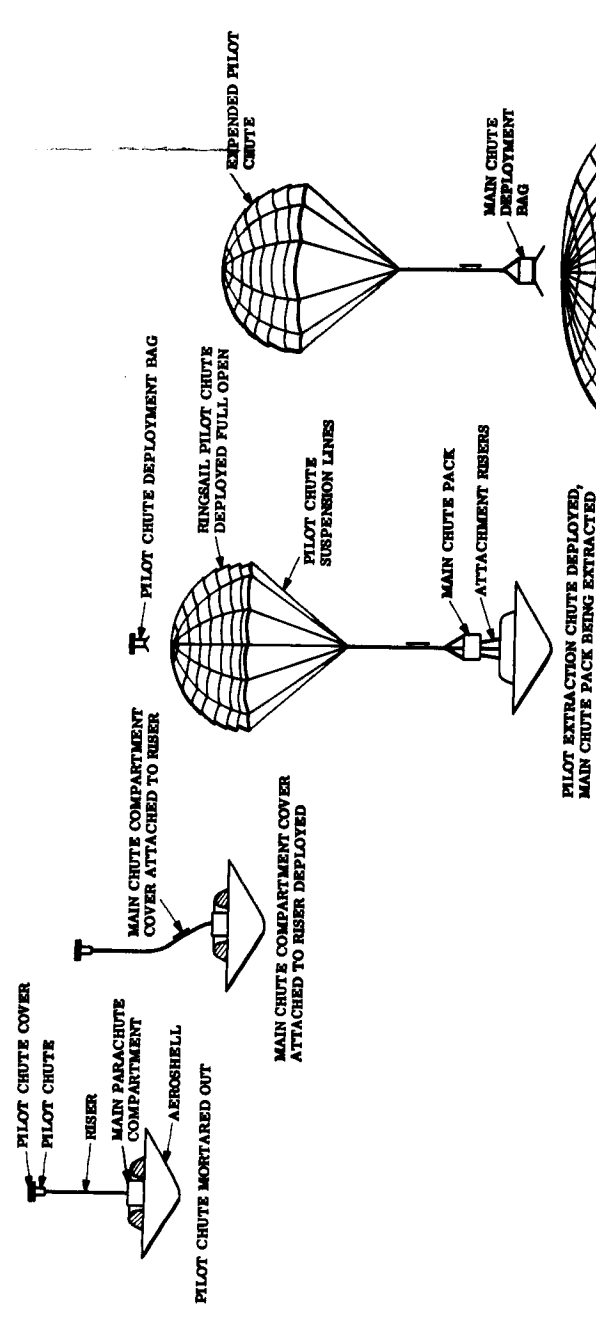
The series of deployment events described are depicted in fig. 6.4.6-3.

On receipt of the signal from the radar altimeter for parachute system deployment, power from the vehicle power supply will be applied to the mortar pyro initiation. Mortar firing will release and deploy the pilot parachute thermal cover and the pilot parachute. After stripping off the pilot parachute, the pilot parachute deployment bag and attached thermal cover free-fall away.

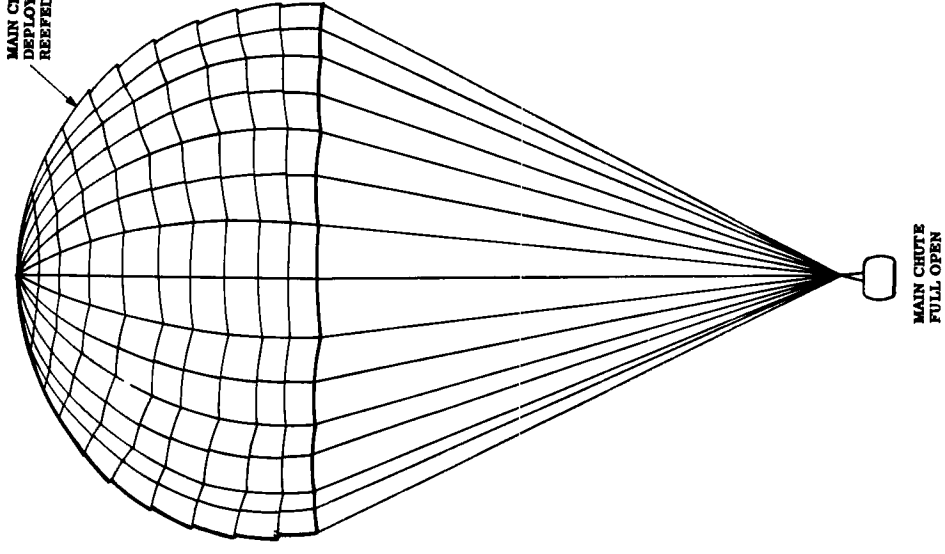
As the pilot parachute is being deployed, the main compartment thermal cover will be deployed by the snatch force of the pilot parachute. One end of the main thermal cover is released by the pilot parachute cover separation. The main cover is attached to the pilot parachute riser at two points for deployment and retention to the riser. As the cover is rotated out by the pull from the pilot parachute, the hold down tang on the edge of the cover opposite the mortar will rotate out of a slot in the main parachute compartment completely releasing the cover.

The snatch force of the main compartment thermal cover on the pilot parachute riser will pull out the tuck bight securing the main chute tie-down straps. This releases the main parachute pack for deployment. Further pull force on the pilot parachute riser will be applied to the main parachute bag handles for main parachute extraction and deployment.

The main parachute is extracted and deployed in a reefed condition by the pilot parachute. During this deployment, the mechanically initiated pyro time delay reefing line cutters are actuated. As the drag of the reefed main parachute develops, the aeroshell is released and allowed to free-fall away. After time-out of the redundant reefing line cutters, the cutters actuate severing the reefing line. This event permits main parachute full open deployment.



MAIN CHUTE DEPLOYED REEFED



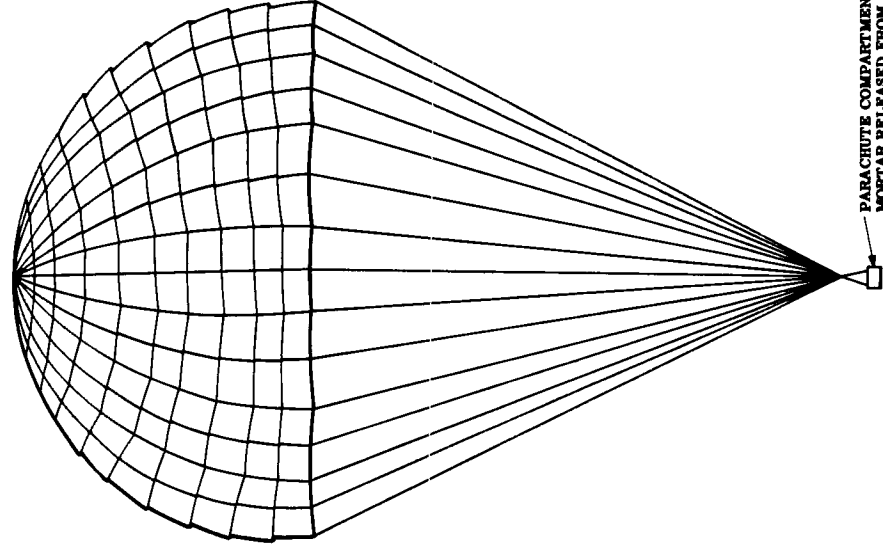
MAIN CHUTE FULL OPEN

MAIN CHUTE SUSPENSION LINES

LANDER PAYLOAD

RELEASED AEROSHELL

MAIN CHUTE DEPLOYED REEFED, RELEASED AEROSHELL FALL AWAY



PARACHUTE COMPARTMENT WITH MORTAR RELEASED FROM LANDER

RELEASED LANDER PAYLOAD



MAIN CHUTE RELEASE AT 150 ± 50' FOR LANDER IMPACT

MARS SURFACE

Figure 6.4.6-3. Retardation System Sequence of Events

When the descending Lander is 150 ± 50 ft from the surface, a signal will be sent from the radar altimeter to apply power from the vehicle power supply to the explosive nuts. This will cause release of the parachute compartment/mortar assembly from the Lander. The Lander will free fall to surface impact. The jet-tisoned main parachute will collapse and spill to one side due to the sudden release of leading from the suspension lines while the parachute was fully inflated.

6.4.6.6 Radar For Deceleration Events

The function of the radar altimeter is to mark the altitude (about 20 kft) to deploy the Lander deceleration parachute and the altitude (150 ± 50 ft) at which the parachute is separated from the Lander before touchdown. In addition to providing these essential marks, the radar provides a continuous altitude signal for correlation with atmospheric profile measurements.

6.4.6.6.1 Altitude Marking Radar (AMR) Description

The AMR is a time domain radar. That is to say, it is a non-coherent, pulse type radar which utilizes an early-late gate range tracking method. Figure 6.4.6-4 shows a functional block diagram of the AMR. None of the redundancy is shown.

The transmitter, a triode oscillator operating at 1 GHz, is pulsed by the modulator with a pulse length which depends on altitude. Initially in Mode 1, the pulse length is 0.7μ sec. and remains so until about 5 kft altitude, whereupon, in Mode 2, the pulse length is changed to 0.18μ sec. This will give an accuracy of approximately 45 ft on the remaining ranges.

The duplexer is provided along with the proper gating to enable the use of one antenna for both transmission and reception.

After translation in frequency by the local oscillator the return signal is amplified, filtered, detected and enters the range tracking circuits. Because of the extent of the target and the width of the radar antenna, pattern, the return is much wider than the transmitted signal; tracking of the leading edge of the return is desirable to determine altitude. To facilitate the early-late tracking approach, the target return is passed through a leading edge differentiator (delay line) whose output is a pulse of approximately the transmitted pulse width and whose position corresponds to the nearest point of the target return. Figure 6.4.6-5 shows how the return pulse is formed. In that idealized diagram the time intervals correspond to:

t_1 = time that leading edge of pulse hits the surface

t_2 = time that trailing edge of pulse hits the surface

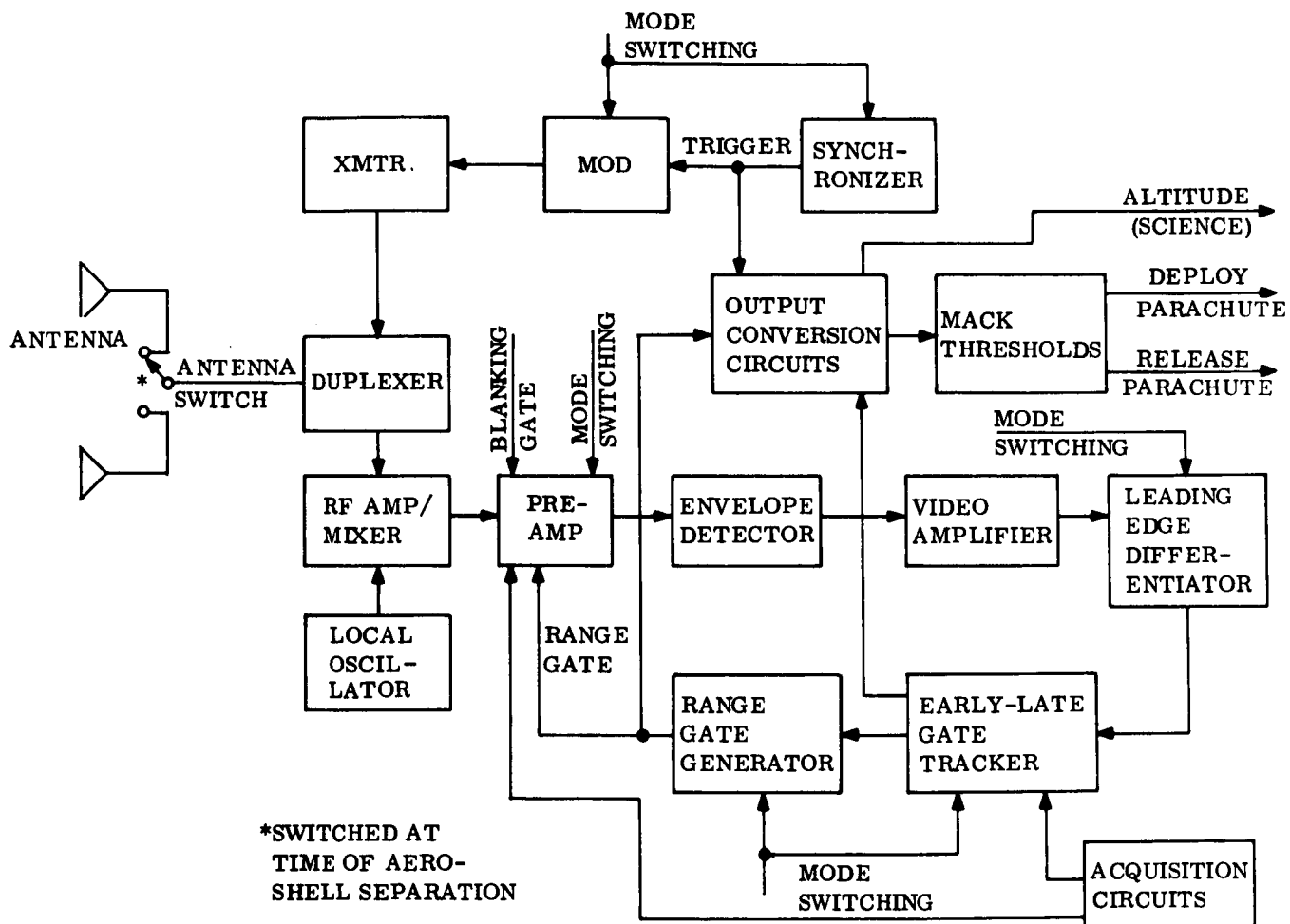


Figure 6.4.6-4. Altitude Marking Radar Functional Block Diagram

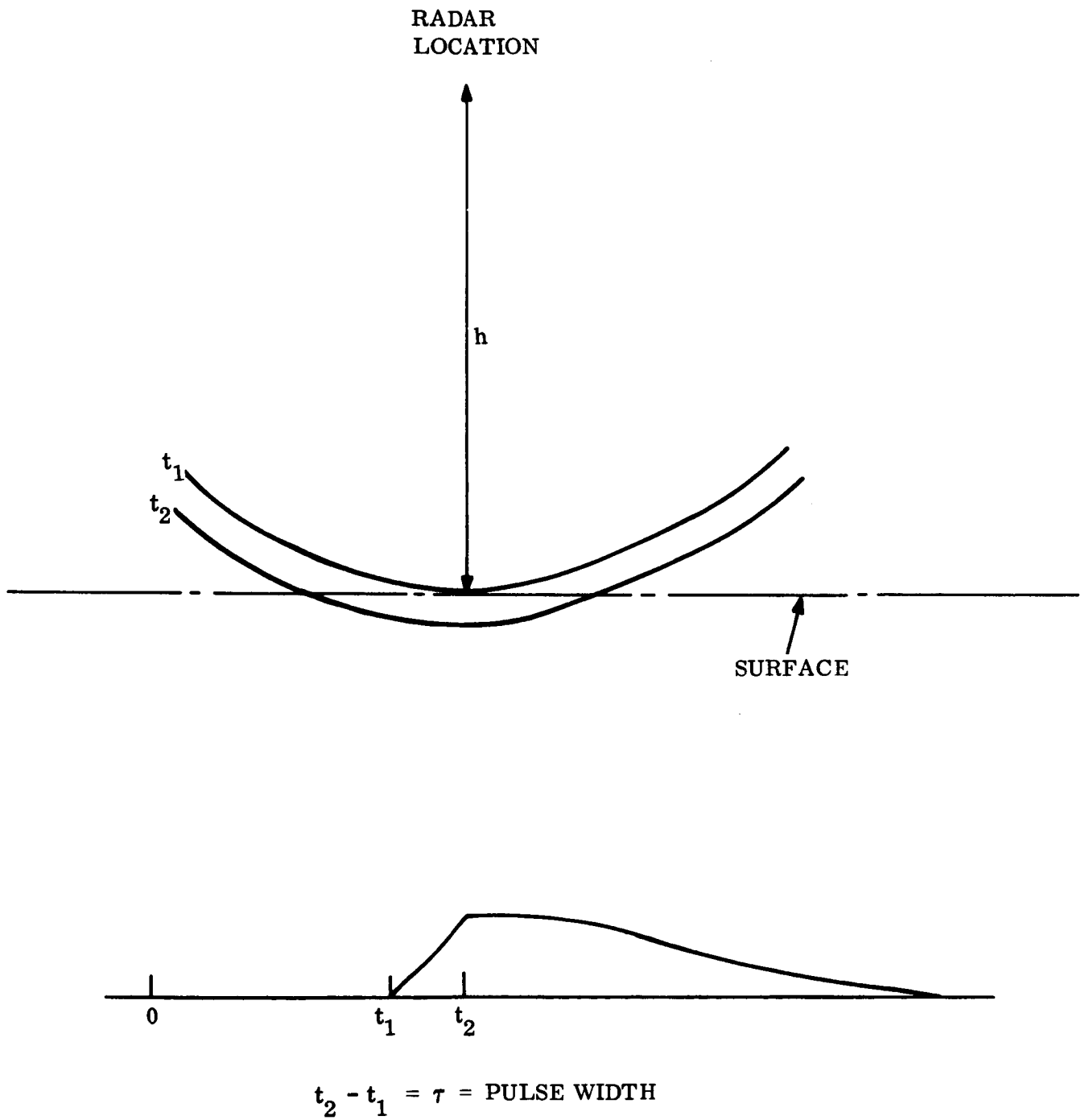


Figure 6.4.6-5. Geometry of AMR Return Signal

During this time the reflected power increases linearly until the entire pulse illuminates the surface. The returned power then decreases from this level due to reflection from more distant points within the beam. If this pulse shape, passed through a μ sec delay line, is subtracted from the original, ideally one gets a non-zero output during the leading edge buildup with a negligible output (and the opposite polarity) for the trailing edge. The resulting narrow pulse is time discriminated in a split gate range tracker whose output controls the time position of the range gate.

The range gate is used to gate the preamplifier on at the proper range, enhancing the signal-to-noise ratio.

In the output conversion circuits, the time delay between the trigger and the range gate is determined, and converted to an analog voltage to give continuous altitude signal.

6.4.6.6.2 Antennas

The AMR is used both prior to and after separation from the aeroshell. The attitude of the Lander can vary over a wide range requiring a broad beam antenna to obtain signal returns for the expected orientations. This is accomplished before aeroshell separation by an antenna with a torroidal pattern (roll symmetrical) pattern.

The 1GHz radar antenna system on the aeroshell will consist of a two antenna array. The two antennas will be identical, but they will be located 180° apart on the shell on an 88 in. diameter. They will be fed in phase with equal amplitude signals from a hybrid. Each antenna, in turn, will be a two slot element array. The slots will be oriented with their long (4 in.) dimensions along a cone element and they will be end to end. The slot closest to the vehicle nose will be fed a signal that is advanced by 60° in phase but equal to amplitude to that which feeds the rear slot. This will cause the peak amplitude of the pattern to occur at an angle of 60° with respect to the vehicle axis (see fig. 6.4.6-6). The polarization will be linear and orthogonal to the vehicle axis. The gain, which is optimized for a 15 to 40° re-entry angle, will average 0 dB or greater over any cone of 10° half-angle within the range of angles from 50° to 75° with respect to nose-on (see fig. 6.4.6-7). The element will be dielectric loaded, cavity backed, slots 2 in. wide and 2-1/2 in. deep. The cavities will be probe fed by a hybrid power divider with an additional length of transmission line in one output leg to account for the required 60° phase shift. An 8 x 2 in. quartz window will be required through the ablation shield to permit proper operation after the re-entry charring of the shield. The antenna system will weigh 5-1/2 lb exclusive of the cable feed system. The input VSWR will not exceed 3:1 for this antenna system for all ablation and re-entry plasma conditions. It will handle 50 watts of input power.

The antenna system for the body of the Lander will be a simple, single slot located on the downward facing surface. It will be 6 in. long by 1 in. wide with a 3 in. deep backing cavity. It will be loaded with dielectric and weigh 1 lb. It will produce a pattern with linear polarization and a major lobe of about 5 dB of gain in the downward

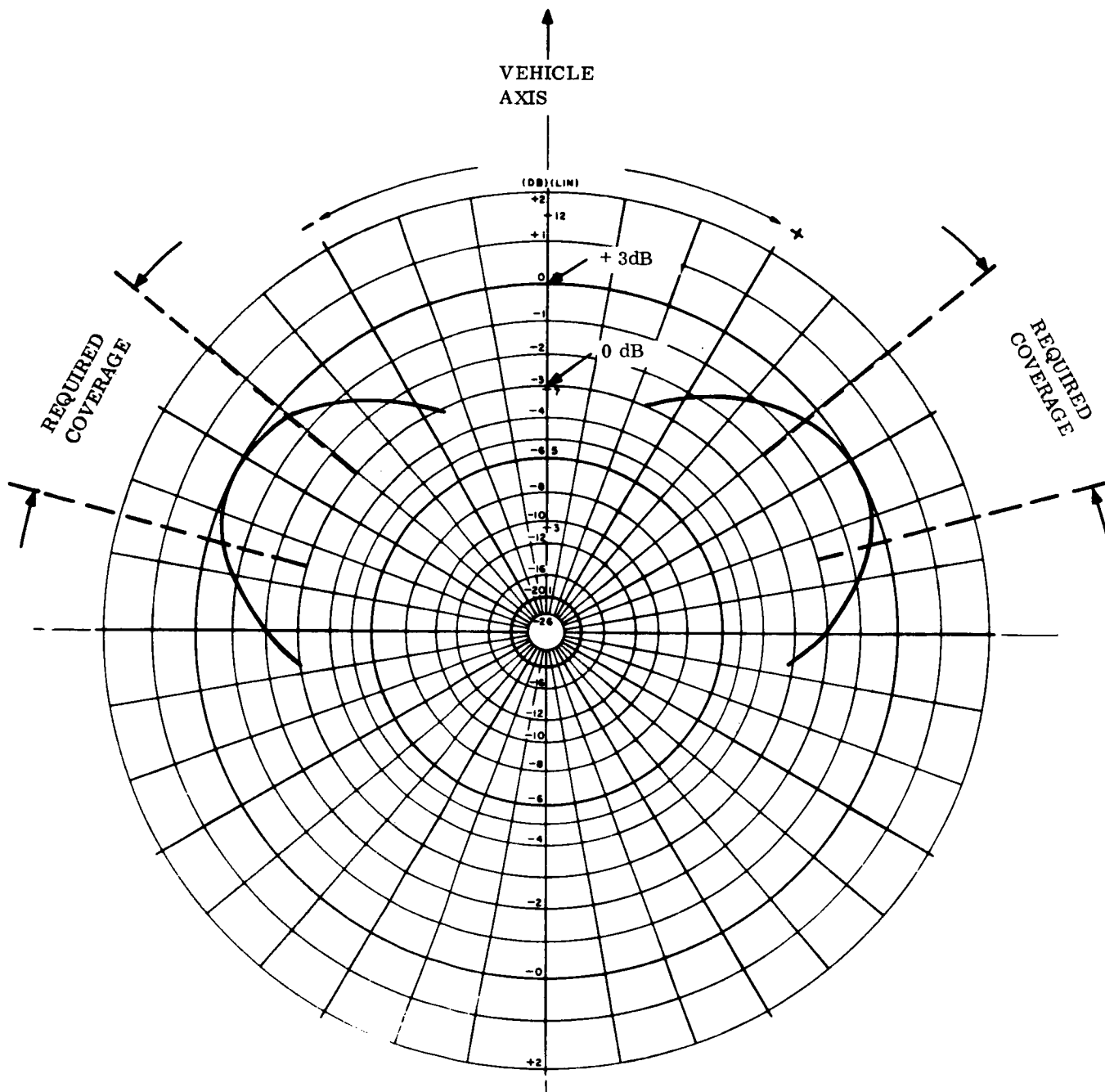


Figure 6.4.6-6. Pattern Thru Axis and Plane of Antennas on Aeroshell

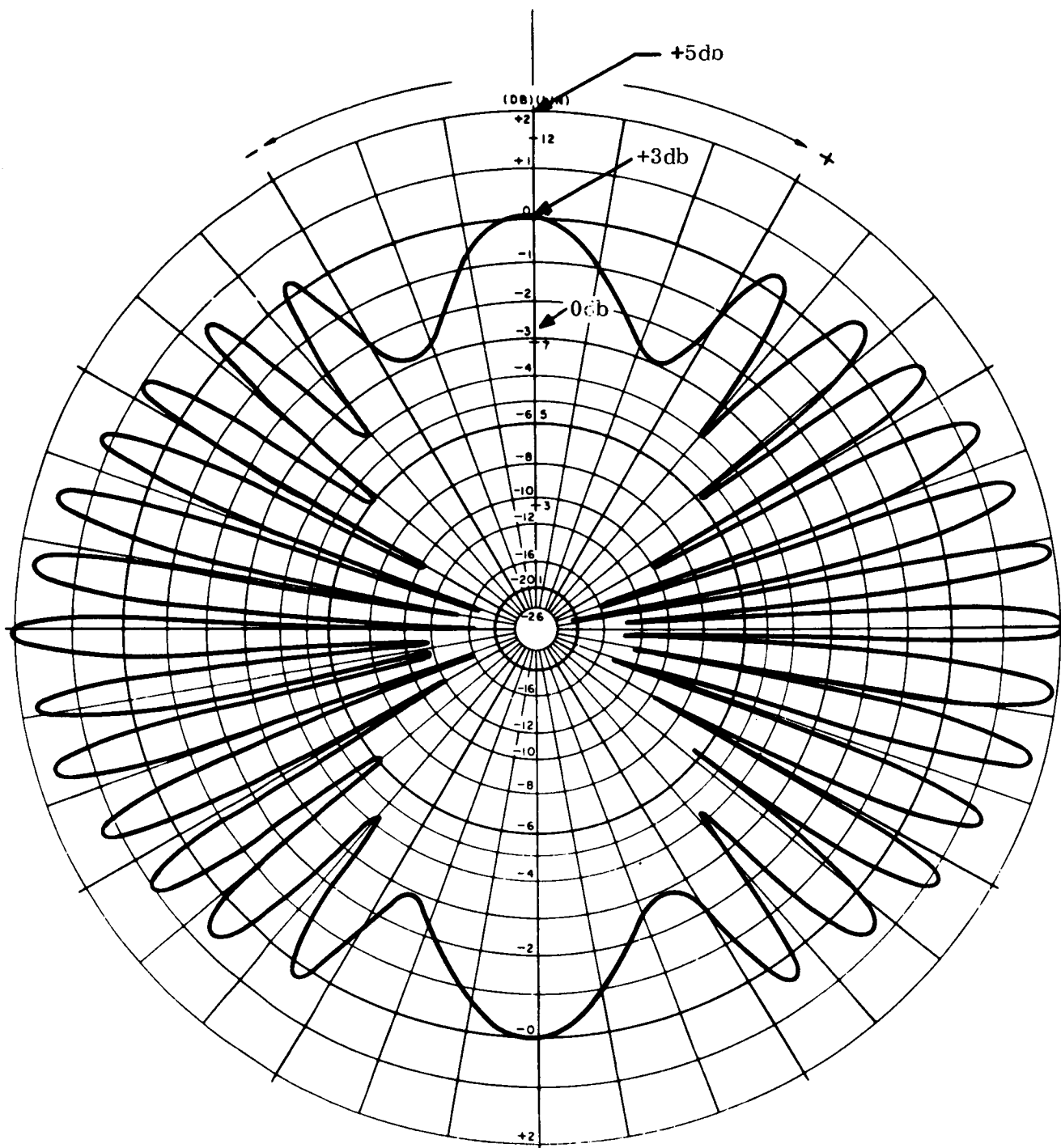


Figure 6.4.6-7. Roll Pattern Radar Antenna on Aeroshell

direction (see fig. 6.4.6-8). Everywhere within the required coverage angle (within 40 degrees of the vehicle forward axis) the gain is +2 dB or greater. The input VSWR will be less than 1.5:1 for this antenna and it will handle 50 watts of input power.

Switch over from one antenna to the other occurs at aeroshell separation and requires a signal from the guidance and control sequence to shut down the transmitter, switch the antennas and repower the transmitter. The radar begins functioning again about 4 to 6 sec after aeroshell release. At this time the aeroshell will be near in range and must be discriminated against during the reacquisition of the desired target return. This is accomplished with a receiver blanking gate of 5-6 μ sec duration effectively blanking out any target within 2500-3000 ft of the vehicle. This blanking gate is removed after the surface is reacquired and the normal range gate is functioning.

6.4.6.6.3 Parameters of the AMR

Table 6.4.6-4 lists the functional and physical parameters of the radar.

The calculation for SNR is based on the assumption that the surface reflectivity coefficient is $\sigma_o = -10.0$ dB.

$$SNR = \frac{\sigma_o P G_{\lambda}^2 C_{\tau}}{64 \pi^2 L H^3 R T_o F B}$$

where:

C = speed of light

k = Boltzman's constant

T_o = 290°K

Other symbols are defined in table 6.4.6-5

6.4.6.6.4 Radar Altimeter Parameters

Table 6.4.6-5 shows the weight, volume and location of the components of the Radar Altimeter. These weights are excluded from the retardation weight table but are included in the Entry Systems and Lander Weights.

6.4.6.7 Retardation Subsystem Weight

The subsystem equipment weights for Point Design 4 is given in table 6.4.6-6.

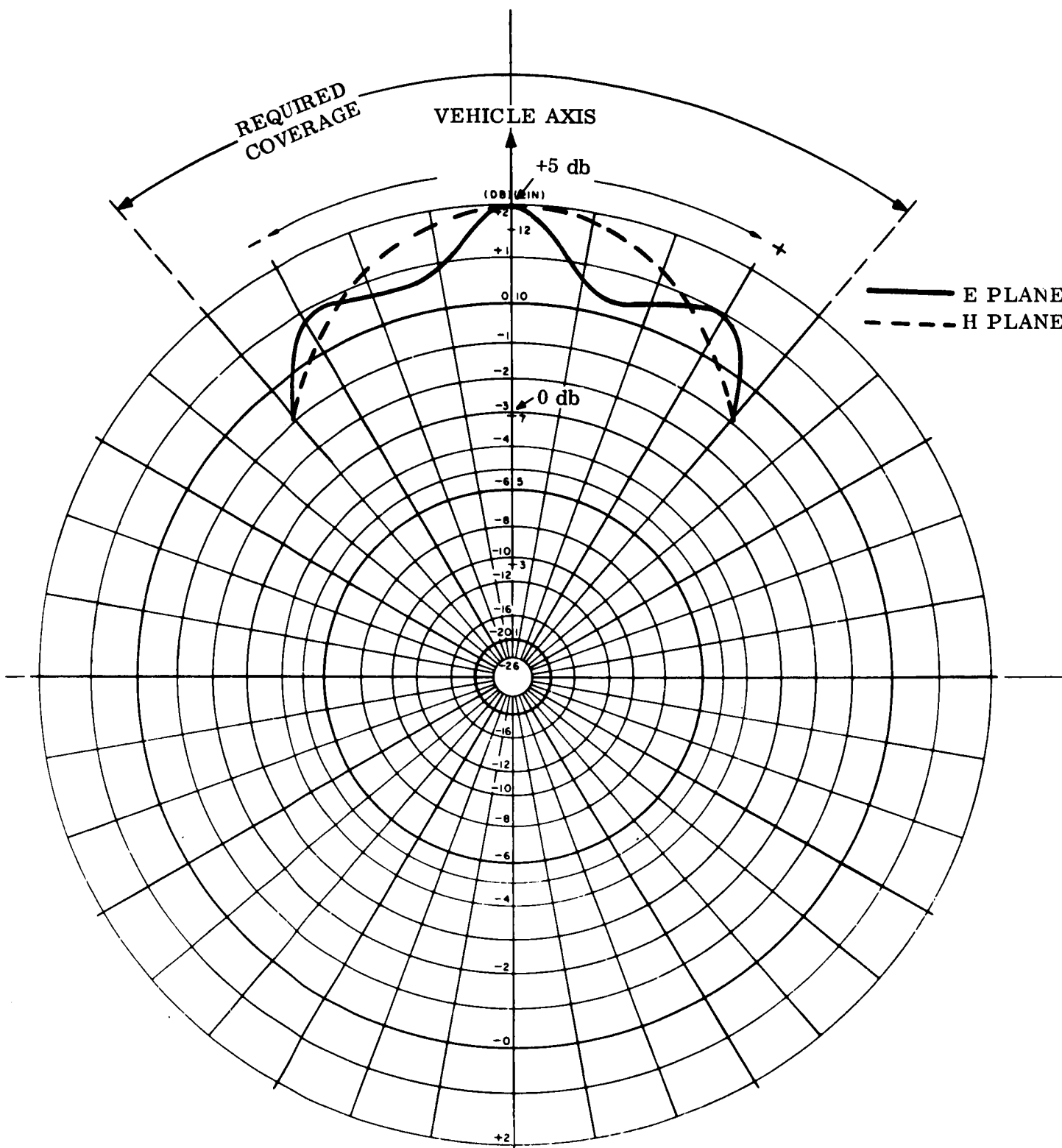


Figure 6.4.6-8. E and H Plane Patterns of Antenna on Vehicle Body

TABLE 6.4.6-4. FUNCTIONAL PARAMETERS

	Symbol	
Peak power	P	50 watts
Frequency	f	1.0 GHz
Wavelength	λ	0.3 meters
Antenna gain	G	0.0 db
Pulse length	τ	0.7 μ sec (long range) 0.18 μ sec (short range)
Repetition frequency	PRF	1000 Hz
Noise figure	F	6 dB
System losses	L	6 dB
I-F Bandwidth	B	2.1 MHz (long range) 8.2 MHz (short range)
Acquisition sweep time	T _{aq}	2 sec
Single pulse signal-to-noise	SNR	+7.1 dB (long range @ 20,000 ft) 13.1 dB (short range @ 5000 ft)
Probability of Detection single sweep	P _d	> 0.95
Accuracy		1% \pm 175 ft (long range) 1% \pm 45 ft (short range)

TABLE 6.4.6-5. RADAR ALTIMETER PARAMETERS

Item	Location	Weight, (lb)	Volume (in. ³)	Power (watts)
Electronics	Lander	15.0	500	20
Antenna (1) (parachute release)	Lander	0.5	18	-
Antenna (2) (atmospheric profile)	Aeroshell	5.5	80	-

TABLE 6.4.6-6. RETARDATION SYSTEM WEIGHT BREAKDOWN

	Weight (lb)
Pilot parachute mortar thermal cover	1.5
Pilot extraction parachute (modified ringsail)	7.0
Main parachute compartment thermal cover	7.0
Main parachute, 2 stage deployment (modified ringsail)	188.0
Main parachute attachment riser (3 legs)	2.0
Parachute compartment including mortar	15.0
Parachute attachment and tie-down fittings (3)	2.0
Mortar pyro gas generator or compressed gas supply	3.0
Pull-apart electrical disconnect	0.2
Explosive nuts (3)	2.5
Total Subsystem Weight	228.2

6.4.7 ROLL CONTROL SUBSYSTEM

The roll control function for Point Design 4 is performed by the de-orbit equipment described in para 6.3.7.1, "Spin Control Subsystem." A single monopropellant hydrazine control is used, in conjunction with a rate gyro, to perform both the functions of spin and entry roll control.

6.4.7.1 Roll Control Requirements

At very low dynamic pressures, blunt bodies can be made unstable at zero angle-of-attack by spin. This phenomenon occurs after peak pressure where the pressure is decreasing with time. The effect here is that in the terminal steady state condition the vehicle will diverge to a trim angle-of-attack (dependent on configuration, spin rate, ballistic coefficient, and inertia properties) and follow a helical flight path.

The effects of this divergency may or may not be significant depending on requirements. Specific items that would be affected are base pressure measurements, radar altimeter measurements, vehicle ballistic coefficient (increases at angle-of-attack) and communication aspect angle.

In order to insure stability in this region a maximum roll rate must not be exceeded, however, roll torques will develop during entry due to built-in and ablation induced asymmetries. An estimate of this roll torque and the total roll impulse during entry is listed in table 6.3.7-1.

The capsule will tend to spin up under the action of this roll torque and it is necessary to provide sufficient roll control torque and impulse to prevent capsule roll rate from exceeding a maximum limit. Note, however, that it is not necessary to provide roll control torque greater than the peak disturbance torque since there is no requirement for roll attitude control in a non-lifting vehicle and the peak torque occurs for a very short period. The list of fixed hardware is given in Table 6.4.7-1 for a total fixed weight of 10.6 lb. The weight of the remainder of the subsystem (hydrazine, pressurant, and tankage) also is included in Table 6.4.7-1. Total subsystem weight is 16.7 pounds. The control torque and impulse provided for roll control is listed in table 6.4.7-2.

6.4.8 ENTRY SYSTEMS WEIGHT

A summary weight statement for the items comprising the entry system weight (less Lander and pre-entry systems weight) for Point Design 4 is shown in table 6.4.8-1. Total entry system weight for this point design 624 lbs.

TABLE 6.4.7-1. SPIN AND ROLL CONTROL SUBSYSTEM FIXED
HARDWARE WEIGHT, POINT DESIGN 4

Component	Quantity	Weight (lb)
Rate gyro	1	1.0
Spin electronics	1	2.4
Fill valve	2	0.5
Squid value	1	5
Pressure sensor	1	0.5
Temperature sensor	1	25
Valves	2	6
Thrusters	4	1.0
Tubing, fittings	-	1.05
Supports		<u>2.8</u>
Total weight		10.6

TABLE 6.4.7-2. SPIN AND ROLL CONTROL SUBSYSTEM
PARAMETERS, POINT DESIGN 4

Time, separation to spin-up	1.5 sec
Spin rate	50 rpm
Spin-up time	25 sec
Roll thrust	5.2 lb
Roll torque	62.4 Ft-lb
Impulse requirements	
Spin/design	506 lb-sec
Roll control	167 lb-sec
Weight of hydrazine	
Spin/de-spin	2.2 lb
Roll control	0.7 lb
Tank weight	2.6 lb
Pressurant weight	0.6 lb
Fixed hardware weight	10.6 lb
Total subsystem weight	16.7 lb

TABLE 6.4.8-1. ENTRY SYSTEM WEIGHT SUMMARY, POINT DESIGN 4

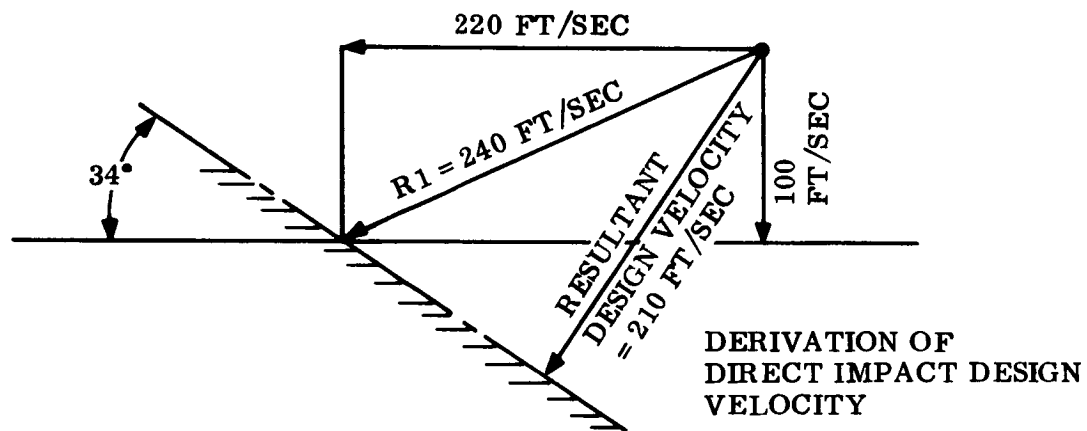
Item	Weight (lb)
Aeroshell	116
Misc structure	52
Heat shield	182
Separation system	1.8
Attitude control	16.7
Retardation	228.2
Harness and cabling	19.5
Entry science	2.5
Radar altimeter	5.5
Total entry system weight	624.2

6.5 LANDER SYSTEMS

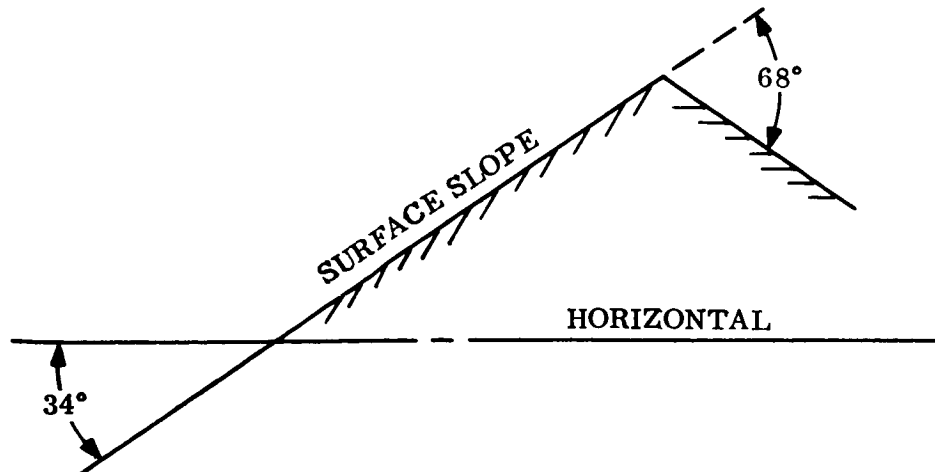
6.5.1 CONFIGURATION CONSTRAINTS AND DESCRIPTION

6.5.1.1 Constraints and Design Parameters for Vehicle Point Design 4

1. Maximum horizontal velocity of Lander at impact due to winds: 220 ft/sec.
2. Maximum vertical velocity of Lander at impact: 100 ft/sec. This was selected based on the optimization of the deceleration and impact attenuation subsystems.
3. Maximum resultant direct impact design velocity: 210 ft/sec.



4. Surface characteristics (to Langley requirements)
 - a. Surface slopes: zero to $\pm 34^\circ$ relative to horizontal, with abrupt slope changes of $\pm 68^\circ$ forming hills (or valleys), as shown in the following sketch:



- b. Continuous slopes: as long or longer than the base diameter of the Lander.
- c. Maximum surface rock diameter: 5.0 inches.
- 5. Maximum total Lander design g level: 1000. This was selected for point design, as a compromise between conflicting influences of structure and impact attenuation system design: volume for aeroshell packaging and weight.
- 6. Vehicle attitude and impact design: Multi-directional design with attenuation capability for the maximum design velocity and g-level, on the prime impact side and round the edge to approximately 70° . The remainder of the impact attenuation system on the back face and edges has been designed for 100 ft/sec impact velocity at maximum g-level. The geometry of the system is shown in Section 6.5.8.
- 7. Landed temperature conditions assumed for environmental control design.
 - a. Ambient: -152° F to $+114^\circ\text{ F}$ (to specification*)
 - b. Component tolerance (non operating): -40° F to $+160^\circ\text{ F}$. Except for battery where the allowable temperature range is $+50^\circ\text{ F}$ to $+80^\circ\text{ F}$.
- 8. Surface mechanical properties:
 - a. Bearing capacity six psi to infinity
 - b. Coefficient of friction up to 1.0

(Infinite strength surface assumed as the limiting design case for impact attenuation.)
- 9. Geometrical, weight and c. g. constraints:
 - a. Packaging objective - approximately 40 lb/ft^3 in central cylinder of payload container
 - b. Center of gravity - on or forward of horizontal center line of Lander container.

6.5.1.2 Lander Description

6.5.1.2.1 Configuration

The Lander concept is a doughnut shaped vehicle, with a central circular flat pack payload container. Either side of the vehicle may be face up after landing.

*Mars Engineering Model Parameters for Mission and Design Studies. Langley Research Center, May 1968.

It utilizes a completely passive landing system. The configuration of Point Design 4 is illustrated in fig. 6.5.1-1, general assembly of Lander.

The central container, a short large diameter cylinder with a D-shaped edge structure, houses all the science and supporting subsystem equipment. A deep ring phenolic glass impact attenuation system is bonded to the edge structure of the payload container. Provision is made for science instruments and other equipment to be deployed from the lander. The degree and type of deployment necessary varies between point designs and is discussed in detail in deployment Section 6.5.6 for Point Design 4.

Depending upon the vehicle mission, electrical power and telecommunication subsystems vary between point designs and these subsystems and other vehicle equipment for Point Design 4 are discussed in detail in the following Lander sections.

Point Design 4 carries a minimum science payload and subsystems and equipment for an operation surface lifetime in excess of 90 days. It is designed with a multi-directional landing capability.

6.5.1.2.2 Science Payload

Science instrument payload installed is listed and is discussed in Section 6.5.2. The Lander carries the majority of the entry science as well as the surface science, to avoid duplication of supporting subsystems and instruments and for flexibility of data acquisition and storage.

Provision is made for deployment of cameras, wind measuring instruments, temperature transducers, the alpha back scatter instrument head and solar arrays. The cameras, wind velocity and temperature instruments are housed in a central bay, which is the full width and depth of the Lander payload container. They are mounted on short spring loaded swinging booms primarily provided for camera deployment. The wind velocity instrumentation requires secondary spring loaded arms which unfold at right angles to a spring loaded extension of the camera booms when the booms are deployed, to provide correct relative location. Deployment of equipment from this bay is substantially automatic following selection and jettison of the bay door on the uppermost and exposed side of the Lander. With the current provision of four separate cameras and deployment booms and the capability to deploy all four from either side of the Lander for high and low resolution imaging, some boom deployment sequencing will be necessary, but can be kept relatively simple.

A gravity sensing device determines the uppermost side of the Lander and releases the upper door. Doors are spring loaded and secured with bolts incorporating hot-wire devices.

The alpha back scatter instrument is located in a separate full depth bay and the instrument head can be deployed downward onto the planet surface, through whichever side of the Lander constitutes the underside. To facilitate this operation with a minimum of rotational movement of the instrument head, the alpha back scatter is installed on its side in the bay. Sensing for operation of inward hinging doors enclosing the alpha back scatter bay is by the gravity device provided for the camera bay doors.

Each of the solar arrays, also located in individual bays, can be deployed in either direction from the flat surfaces of the Lander container. Sensing door release and direction of operation is again controlled by the gravity device.

A full detailed description of the deployable instrument and equipment installation and mechanical operations, with illustrations, is given in Section 6.5.6.

The remainder of the payload (science and support subsystems) is housed in other compartments formed by the inner framework of the payload container. Access to this equipment is available through either the top or bottom bolted covers of the container, or by removal of the inner framework from the Lander, complete with all equipment. The installation is compact to achieve low weight and volume, but consistent with requirements for assembly, service and operational functions.

6.5.1.2.3 Lander Support Subsystems

To perform the 90 Day plus mission of Point Design 4, a telecommunications link is designed to provide a relay link for transmission of imagery data for the periapsis passage of the Orbiter immediately after impact on the surface of the planet and at the end of each succeeding diurnal cycle for a period of three days. The telecommunications system consists of a 400 MHz transmitter with a dual power amplifier output stage, memory with 180,000 bit storage capacity and the appropriate signal conditioning and data handling equipment.

For the extended mission time for this point design a direct link telecommunications system and a command link with its associated decoding and data handling capability has been incorporated in the design. The direct link provides the capability has been incorporated in the design. The direct link provides the capability for obtaining meteorological data for the extended mission time. A radar altimeter has been included to provide a more accurate altitude sensing for parachute deployment and subsequent parachute release prior to Lander impact. The antenna for parachute release is located in the base of the Lander whereas the antenna for parachute deployment is located in the aeroshell.

The electrical power and distribution equipment, located in the Lander provides all primary power required of the Lander and the appropriate programming and sequencing functions. The main power source for this mission is a solar array/

battery system. The battery was sized for a three day mission and weights approximately 68 lb. This battery was sized based on a 30 watt-hr/lb rating. The solar array is 25 ft² and provides the required power for the telecommunication and science equipment.

Surface science equipment consists of the minimum science package including equipment to measure wind velocity, surface temperature, and pressure, alpha back scattering, imagery, a clinometer and moisture detector. Imagery data will be taken and transmitted to the Orbiter during the periapsis passage for each of the four available transmission periods, and will be transmitted real time. Additionally, stored entry and surface science data, diagnostic, and real time surface science data is alternately transmitted between the picture taking sequence.

Environmental control, primarily an insulation problem, is achieved by the use of honeycomb panels with fiberglass core for the outer shell of the Lander container; coupled with the application of thick layers of foam on exposed surfaces, such as the sidewalls of the camera bay. Batteries, which are the component most sensitive to the cold environment, are maintained at a working temperature by a combination of heat dissipated from other components and an individual electric heater.

A complete description of science and Lander subsystems including structural and mechanical components is given in the sections following, together with detailed weight information.

6.5.2 SCIENCE PAYLOAD EQUIPMENTS

6.5.2.1 General

The various instruments carried by the hard Lander to Mars may be classified into two general categories. They are the entry phase instruments, which require no special compatibility with unusually high deceleration loading, and the landed phase instruments which must survive the extreme loads and shocks encountered during impact and maintain their calibration and state of operability. In most cases, the entry phase instrumentation can be rather well defined in terms of the state-of-the-art, however, certain devices, such as the water vapor detector, will require some development before a device is available that will fulfill the scientific requirements of the measurement. The landed phase instrumentation includes a minimum science payload and certain other devices that may feasibly be carried by the Lander. In this group of instruments there are several devices that do not physically exist at the present. Others in this group are at some point in their development that provides sufficient confidence in their design to consider them in this mission even though serious doubts exist concerning their ability to withstand the high g impact of the hard Lander. For these designs, additional shock attenuation can be considered for isolating the instrument from the extreme environment. However, this additional weight and volume appears prohibitive at the present time.

The section provides a brief summary of the scientific instrumentation selected for inclusion in the point designs. Detailed descriptions of the equipment and the

studies performed in their selection have been given in previous Sections (2.3.3 and 2.3.4) of this volume. Considerations used for identifying the implementation approaches best suited for the missions have been discussed in Volume II, Sections 4.

6.5.2.2 Entry Science Payload

6.5.2.2.1 Tri-axial Accelerometer

The tri-axial accelerometer is mounted at the entry system center of gravity. Several varieties are currently available, however, the magnetic force balance type seems to have the most desirable characteristics. Table 6.5.2-1 shows the mechanical and electrical characteristics of an accelerometer that is currently being used on various military programs. Also shown are the sequencing, sampling and data format requirements for the accelerometer. No significant problems are foreseen in sterilizing the device.

6.5.2.2.2 Temperature Transducers

Atmospheric temperature measurements during the entry phase are performed by three temperature transducers. These are platinum resistance thermometers. One is located in the stagnation region of the aeroshell and measures the stagnation temperature from the beginning of entry down to aeroshell ejection. The other two thermometers are located on the base of the lander system and are used during the subsonic region of flight primarily during parachute descent. Table 6.5.2-1 shows the physical and electrical characteristics of the resistance thermometers and its data collection profile. The exact configuration and design of the stagnation transducer will depend upon a large number of variables. The definition of the transducer design parameters will require preflight testing of the thermal characteristics of either scale model or prototype vehicles.

6.5.2.2.3 Pressure Transducers

Variable capacitance pressure transducers located on the aeroshell and on the base on the entry system measure atmospheric pressure profiles. The four transducers arrayed about the stagnation region perform the dual function of measuring pressure and angle of attack. These transducers are located just behind the heat shield and are exposed to the external environment via ducting leading through the beryllium cap of the heat shield. The pressure transducer located on the base of the Lander system measures base pressure from supersonic through subsonic flight regimes. Table 6.5.2-1 lists the characteristics of these transducers and also shows the sampling schedule and data format.

6.5.2.2.4 Mass Spectrometer

The measurement of atmospheric composition by mass spectrographic techniques requires acquisition of a sample from the atmosphere. This acquisition must be performed without exposure to contamination from gaseous materials exuded by the heat shield or other sources. The ducting leading from the mass spectrometer to

TABLE 6.5.2-1. ENTRY SCIENCE PAYLOAD

Instrument (Lander)	Weight	Volume	Power Requirements	Location	Sampling Schedule	Data Format
Mass Spectrometer	8 lb	2 x 7 x 14 in.	7 watts	Internal near surface. Requires port through heat shield	Initiates near Mach 5. Terminates at impact	50 (8) bit words per sample (2 sec scan, 8 sec readout) 50 bits/sec readout
Resistance Thermometer	0.5 lb each	1 in. dia x 2 in. long	1 watt ea	Two on base of vehicle	Initiates at Mach 5. Terminates at impact.	one nine bit channel each 1 sample/sec
Variable Capacitor Pressure Transducers	0.5 lb each	2 in. dia x 2 in. long	1 watt ea	Two on base of vehicle	Initiates at beginning of entry. Terminates at impact.	one nine bit channel each 1 sample/sec
Tri-Axial Accelerometer (1 Dual Scale)	2 lb	2.8 x 1.8 x 2 in.	4 watts	Located at body c. g. with one axis aligned to vehicle vertical axis	Initiates at beginning of entry. Terminates at impact.	8 bits/sample/axis 10 samples/sec 72 bits/sec total Automatic scale switching
Water Vapor	1 lb (ducting only)	Detector located in surface science package	N/A	Ducting located same as mass spectrometer ducting	Initiates near Mach 5. Terminates at impact.	1 sample/15 sec 2 seven bit (parallel) channels 1 eleven bit (parallel) channels

TABLE 6.5.2-1. ENTRY SCIENCE PAYLOAD (Concluded)

Instrument (Aeroshell)	Weight	Volume	Power Require- ments	Location	Sampling Schedule	Data Format
Stagnation Temperature Transducer (1)	0.5 lb	1 in. dia x 2 in. long	1 watt	See text	Initiates at beginning of entry. Terminates at aeroshell ejection	1 nine bit channel 1 sample/sec
Stagnation Region Pressure Trans- ducer (4)	0.5 lb each	2 in. dia x 2 in. long each	1 watt each	Behind nose of aeroshell (See text)	Initiates at beginning of entry. Terminates at aeroshell ejection	4 nine bit channels 1 sample/sec

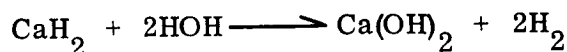
the external environment terminates in the nose area that contains the beryllium plug which serves to minimize the probability of contamination from heat shield outgassing products. This same ducting also delivers atmospheric samples to the water vapor detector located in the entry payload and must be disconnected when the aeroshell is separated from the Lander at parachute deployment.

Table 6.5.2-1 shows the physical, electrical, and data collection characteristics of the mass spectrometer.

6.5.2.2.5 Water Vapor Detector

At present the chemical/radiological water detector is in the concept development stage. Since this device will also be used during landed operations it must be designed for high shock survival. Fig. 6.5.2-1 shows, in block diagram form, the design of the water vapor detector. Table 6.5.2-1 shows the physical and electrical characteristics of the detector. The ducting leading from the nose for entry data is disconnected at aeroshell separation and a second port is open for landed operations.

The basic operating principle is that when calcium hydride comes in contact with water (in either liquid or vapor form) the following reaction takes place:



When the hydride is labelled with tritium, the gaseous effluence contains the radioactive tritium. This element may be quantitatively detected by its radiation and thus the amount of water entering into the reaction may be determined. Radiation shielding of this system will present no problems since tritium emits 18 kev beta particles that are stopped by the chamber walls. Present laboratory tests have demonstrated the device at 1 part per million with definite indications of feasibility for operation of 1 part per billion.

6.5.2.3 Surface Science Payload

6.5.2.3.1 Pressure Transducer

Unlike the pressure transducers included in the entry payload, the surface pressure transducer must be able to withstand high level shock loading. This requirement necessitates either an extension to the state-of-the-art in low pressure transducers or provisions for reducing impact loading much below 1000 g. The added weight and volume for this shock compatibility or attenuation is not included in the component weight or volume shown in table 6.5.2-2.

6.5.2.3.2 Temperature Transducer

Atmospheric temperature is measured by a set of platinum resistance thermometers. They are deployed following impact with the camera booms to obtain free stream data with minimum Lander induced perturbations. Such devices have been designed to withstand rather high 'g' loading and thus no serious problems are expected as a result of a "rough" landing. The ultimate physical design of the

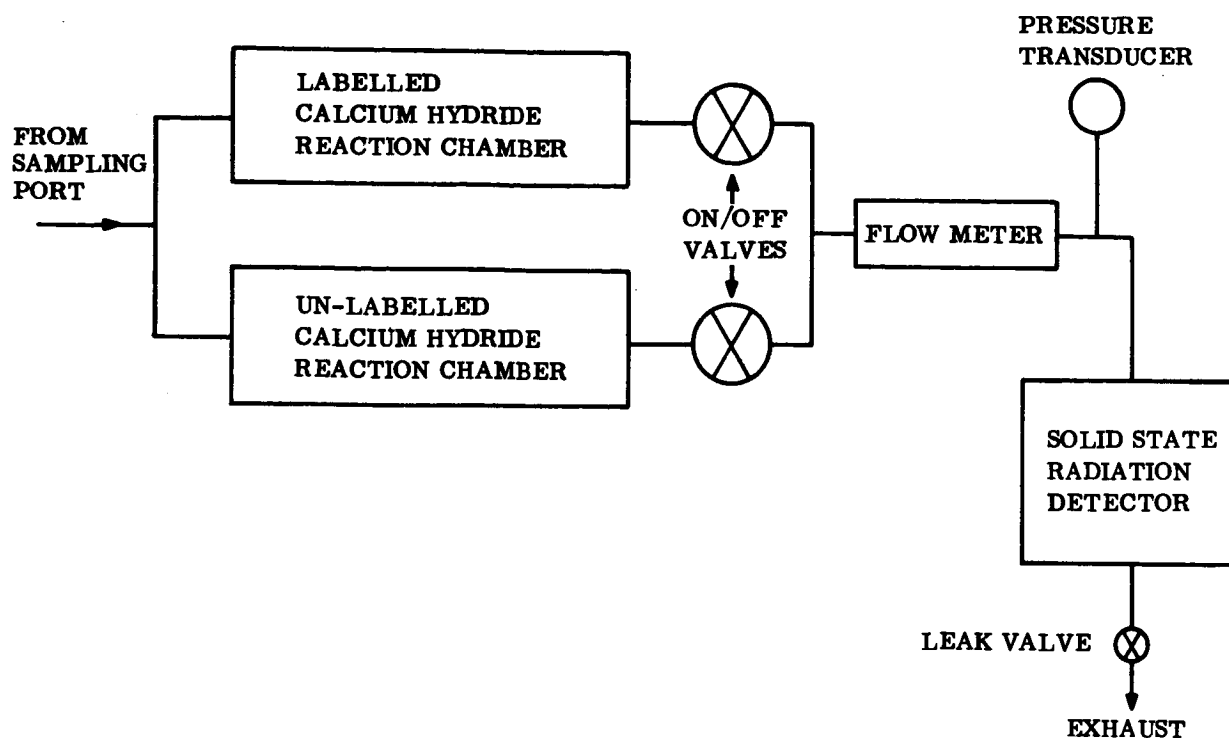


Figure 6.5.2-1. Water Vapor Detector Block Diagram

thermometers will deal with minimization of direct solar heating since this can be a serious measurement problem. A solar shield is required to accomplish the task of decoupling the resistance element from the solar flux. See table 6.5.2-2 for transducer characteristics.

6.5.2.3.3 Wind Velocity Sensor

Although an acoustic velocity sensor has not yet been built for planetary exploration application, the changes required to modify existing designs intended for terrestrial applications appears straightforward. The design approach used for point design evaluation consists of five magnetostrictive transducers (fig. 6.5.2-2) mounted on the boom supporting the TV camera system. A microminiaturized electronics package produces the necessary ultrasonic pulses that drive the transducers and also measures the transit time for each pulse to travel from one transducer to the next. No problem is foreseen in fabricating the required electronics and transducers to meet the sterilization and shock environment requirements. Care must be taken, however, to assure reasonably good rigidity in the transducer supporting arms during the measurement since motion of the transducers may be misinterpreted to signify motion of the medium (atmosphere). Table 6.5.2-2 shows the anticipated physical and electrical characteristics of the wind velocity sensor.

6.5.2.3.4 Water Vapor (Moisture) Detector

The chemical/radiological water vapor detector has not been hardened for the extreme environments that will be encountered during the entry and landing phases

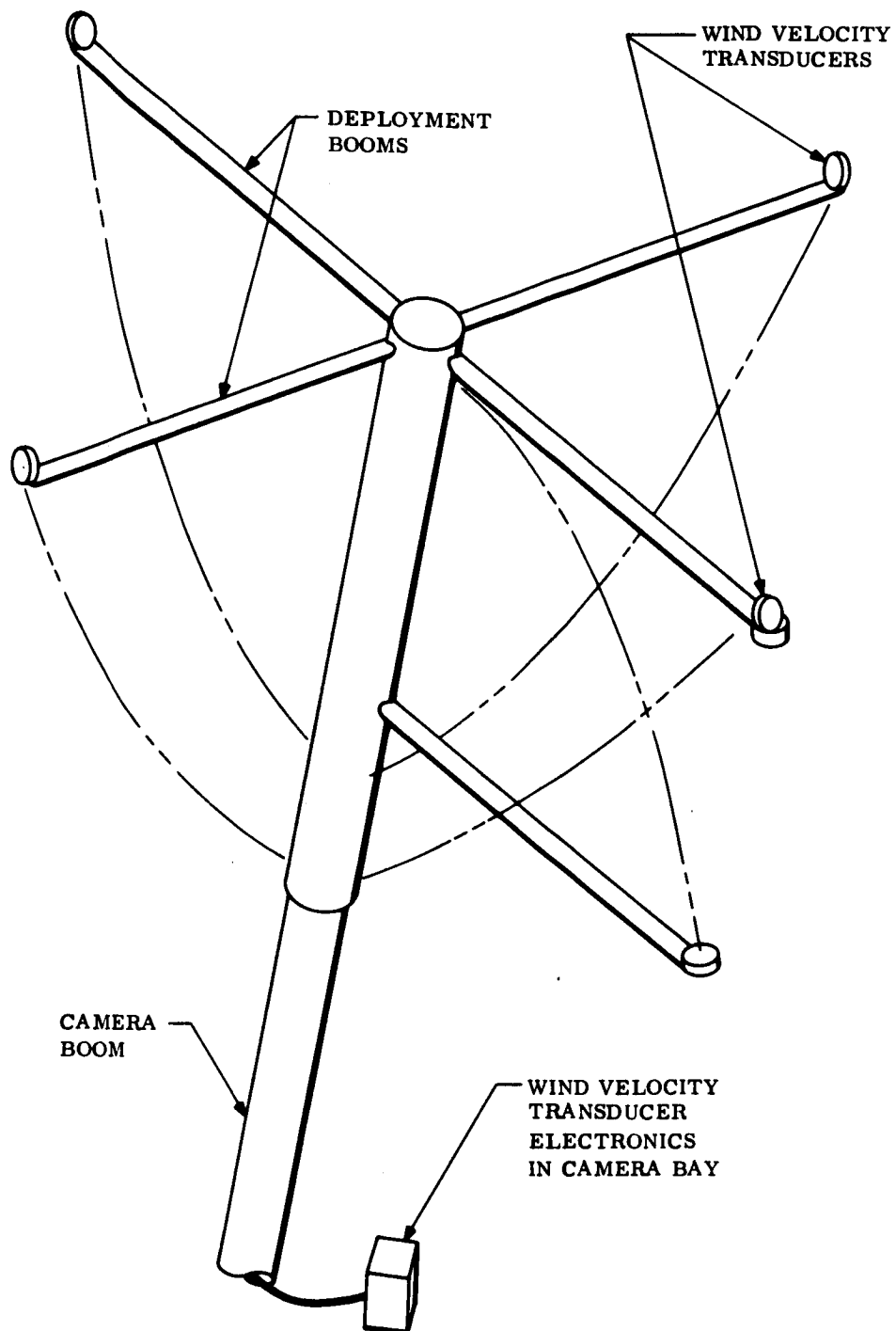


Figure 6.5.2-2. Wind Velocity Sensor

of the mission. However, since the design is inherently mechanically simple, it is expected that a device with the physical characteristics shown in table 6.5.2-2 can be developed and tested in time for a 1973 missions to Mars. Operating experience (laboratory) in the low parts/million and high parts/billion range has demonstrated that water vapor sorption-desorption by materials used in the sampling system could be the major factor toward limiting the response and detection sensitivity in this and lower concentration regions. This would also be of special importance for water detectors based on physical principles especially at lower operating pressures, where sorption-desorption by the detector supporting hardware could contribute significantly to a non-representative water environment around the detector. It is felt that water sorption-desorption can be controlled by appropriate materials selection, by minimizing exposed surfaces, and by operating these surfaces at temperatures consistent with the level of water concentration to be sensed.

The device will remain in the Lander during operation and gas sampling will occur through a vent tube in a camera boom. The key interface requirements are shown in table 6.5.2-2.

6.5.2.3.5 Alpha Back Scatter Spectrometer

An alpha back scatter spectrometer suitable for operation on Mars is being considered for development by the University of Chicago (Turkevitch). Such a device will most probably not use the isotope source (Cm^{242}) used in the Surveyor spectrometer and the source selection will be one of the prime considerations for any future designs. Mechanically, with the possible exception of the deployment mechanism, the spectrometer will probably be able to meet the requirements of a rough landing. Fig. 6.5.2-3 shows the Surveyor alpha-spectrometer for reference purposes. Reduction of the

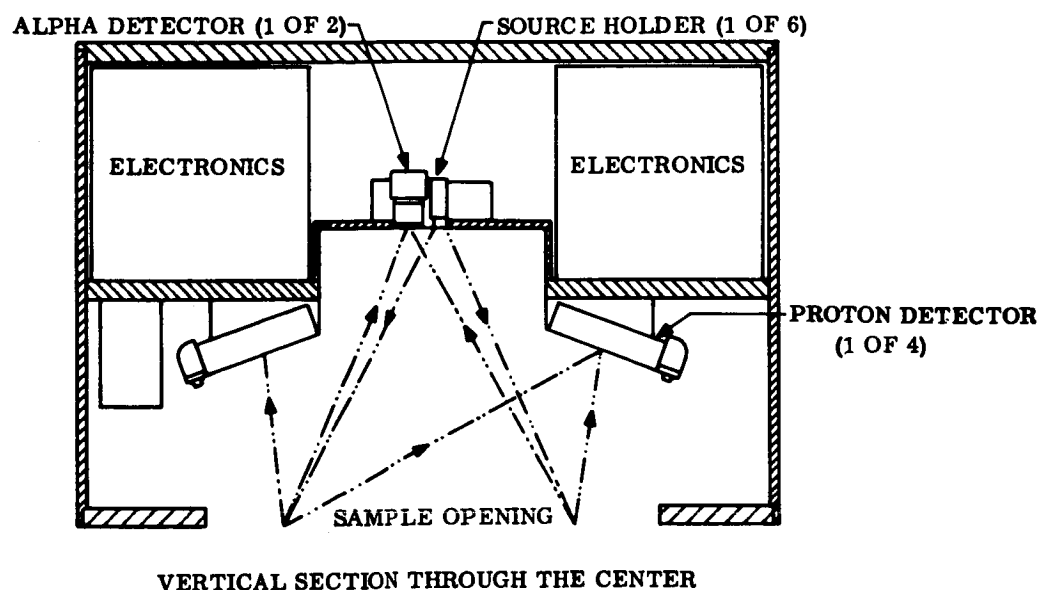


Figure 6.5.2-3. Alpha Backscatter Instrument

overall dimensions of the sensor head are anticipated since the Martian atmosphere will interfere with the measurement. This reduction will result in shorter particle path lengths and correspondingly smaller interference with the measurement.

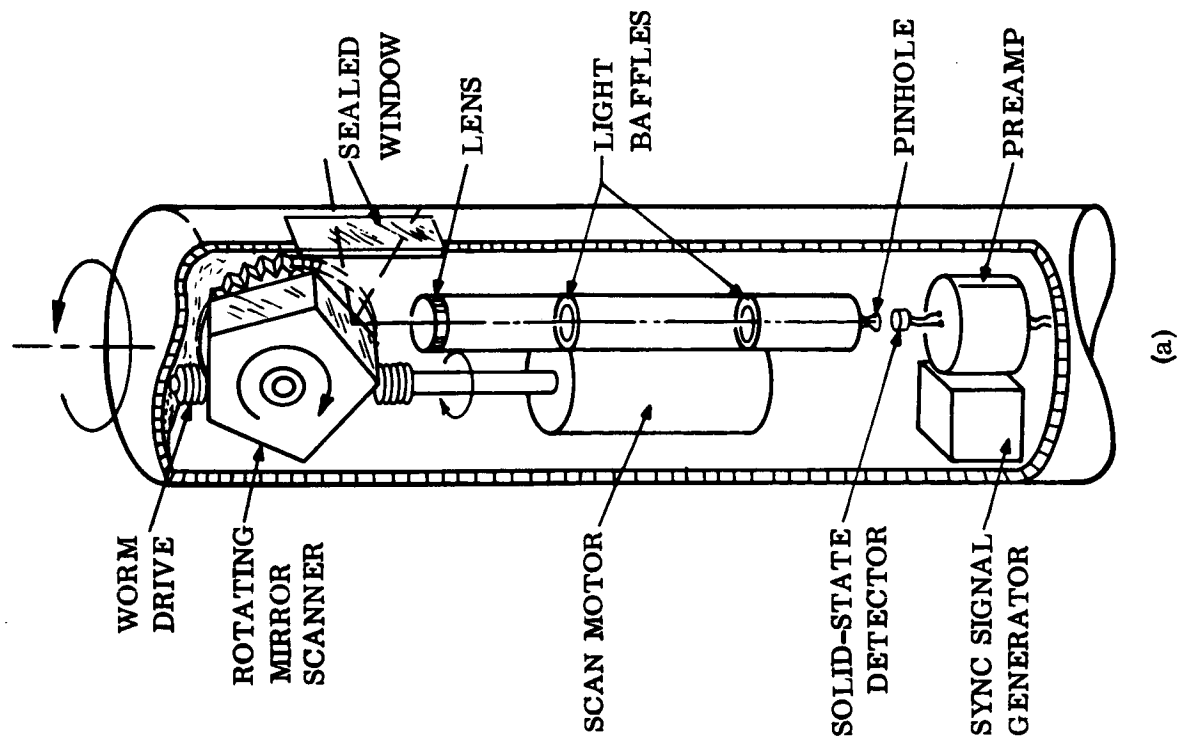
The head, which must be deployed to come in contact with the surface of the planet, is mounted on a swivel bracket so that deployment either up or down will be possible. The existence of surface protuberances in the field of view will introduce errors. A calibration sample is exposed to the bottom of the sensor head when in the stowed position thus providing a reference source for data interpretation. Table 6.5.2-2 gives the physical and electrical parameter estimates for the proposed device. The deployment will be carried out in two stages: i. e. , partial deployment toward surface for background counting and full deployment for composition measurements.

6.5.2.3.6 TV Cameras

The high and low resolution cameras are installed on individual hinged masts although it may be possible to combine them within one casing. Fig. 6.5.2-4 shows the basic elements that each contains. Neither of the two versions shown contain the azimuthal drive motor. The high speed version (fig. 6.5.2-4) has a 5-sided mirror that rotates unidirectionally, the preferred video rate for this version is not well defined and can be from 10 kHz to 100 kHz depending on circumstances. The incident light passes through the window and is reflected from the mirror onto the silicon cell detector. The solid state amplifier amplifies the resulting electrical signal to $\pm 5v$ maximum, the output signal leads from the camera housing carry this signal to the processing electronics. The slow speed version (that can take up to 4 hr for a full panoramic sweep) has a nodding mirror activated by a cam. The light beam is deflected via this mirror onto the silicon cell after being chopped by a small light chopper placed in front of the cell. This latter addition enables the same basic amplifier to be used for both the high speed and low speed versions. The silicon cell response is shown in fig. 6.5.2-5. The dimensions of the camera unit that contains all the mechanical drive mechanisms and all the electronics for the video and synchronizing signals varies with the full design specification, normally however, these will be between 1 and 3 in. diameter and between 5 and 16 in. long. Total weights of the cameras as described can again vary from $1\frac{1}{2}$ lbs to $6\frac{1}{2}$ lb. (See table 6.5.2-3.)

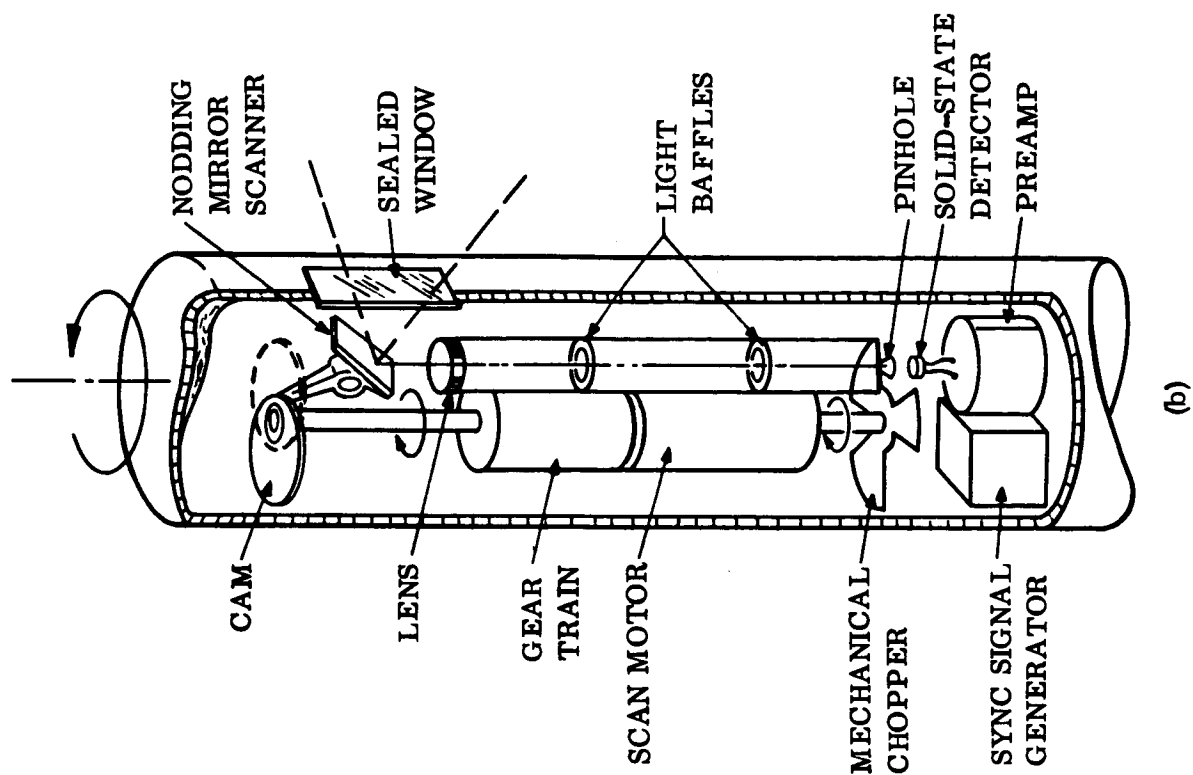
6.5.3.7 Clinometer

The clinometer proposed for the 1973 Hard Lander will require development. Specifications for the design are not complete; however, the parameters shown in table 6.5.2-2 are based on engineering estimate for the conceptual design shown in fig. 6.5.2-6. The potentiometer housings could also include any electronics required to operate the system. Location of the instrument in the Lander is not critical.



ROTATING MIRROR FOR
RAPID SCANNING MODE

(a)



NODDING MIRROR FOR
SLOW SCANNING MODE

(b)

Figure 6.5, 2-4, High and Low Speed TV Cameras

TABLE 6.5.2-2. SURFACE SCIENCE PAYLOAD (LANDER)

Instrument	Weight	Volume	Power	Location	Deployment/ Orientation	Mission Profile	Data Format/ Requirements
Pressure Transducer (2)	0.7 lb each	2 in. dia 2 in. long each	1 watt each	Internal near skin of vehicle	Port through skin to ambient environment either top or bottom. No deployment	Operates continuously after impact	3 samples/hr each 1 percent accuracy. Two channels total
Resistance Thermometer (4)	0.5 lb each	1 in dia 2 in. long each	1 watt each	One on each camera boom	Deployed above lander on camera booms. One on each boom.	Same as above	3 samples/hr each 1 percent accuracy. Four channels total
Wind Velocity Transducer (2)	2.5 lb each	25 in. ³ prior to deployment each	3 watts each	One on each of two camera booms	Boom deployment above vehicle on camera booms	Same as above	3 samples/hr 6 channels Each channel consisting of 11 parallel bits. Total of 66 bits/sample
Moisture Detector (1)	10 lb	60 in. ³	5 watts	Mounted internal to Lander	Pneumatic tubes deployed as part of camera booms	Same as above	3 samples/hr 2 seven bit (parallel) channels 1 eleven bit (parallel) channels

TABLE 6.5.2-2. SURFACE SCIENCE PAYLOAD (Continued)

Instrument Lander	Weight	Volume	Power	Location	Deployment/ Orientation	Mission Profile	Data Format/ Requirements
Surface Composition (Alpha-Scatter) (1)	9.5 lb	5.5 in. x 7.5 in. x 4.5 in.	5 watts	Internal to vehicle	Must be deployed so that sensor head rests on surface of planet. Top of bottom deployment controlled by clinometer	Deploy 3 hours after impact. First readout 1 hour after impact 2nd readout 3 hours after impact then readouts every 3 hours thereafter	1 sample/3 hrs 130 channels 14 bits (parallel) each 130 channels 12 bits (parallel) each 3 channels 7 bits (parallel) each
Photo Imaging (4)	4.8 lb total	1 in. - 2 in. dia 9 in. - 12 in. long each	6-10 watts total	One on each of four booms deployed above Lander	Boom deployment 36 in. > Height > 18 in. One boom/camera	4 Frame sweeps on high resolution and 4 frame sweeps on low resolution in sequence. Operation time coincident with transmissions	Flexible to meet maximum transmission capability of lander. Period from one second to eight hours per picture. Total bits between 10^7 and 10^8
Clinometer (2)	1.3 lb each	2 in. dia x 3 in. long	3 watts	Two internal to lander mounted with long dimension parallel to vertical axis of Lander	N/A	Sampled immediately after impact. Then once every three hours.	1 sample/3 hrs 2 channels 7 bits (parallel) per channel

TABLE 6.5.2-3. TYPICAL CAMERA SPECIFICATIONS

Model Identification	CM	SL	NP	SS	SM
Special Feature	Small Size Small Power	Rugged	High Speed	Adjustable Performance	High Resolution
Field of View	9° x 360°	50° x 360°	25° x 360°	10° x 10° to 90° x 360°	1° x 1°
Resolution	0.1 in @ 6 ft	0.1 in. @ 6 ft	0.1 in. @ 100 ft	0.1 in. @ 1 ft to 0.1 in. @ 60 ft	1 micron @ 3/4 in.
Frame Time	1/2 min	7 min	2-1/2 sec	30 sec to 10 hr	1 sec
Sensitivity Range	0.1 - 1000 ft-L	0.3 - 3000 ft-L	1 - 5000 ft-L	0.001 - 5000 ft-L	10 - 10,000 ft-L
Size	1 in. D x 6 in. L	1.5 in. D x 10 in. L	2.5 in. D x 11 in. L	3 in. D x 18 in. L	3 in. D x 15 in. L
Weight	0.4 lb	3.5 lb	5.5 lb	6.5 lb	6 lb
Power	1 W	10 W	150 W	15 W	4 W
Temperature (of the Environment)	-10°F to +150°F	-40°F to +180°F	-10°F to +125°F	-45°F to +145°F	-45°F to +145°F
Pressure(External)	1 atm	10 ⁻⁹ Torr	1000 psi	1 mb	1 mb
Shock and Vibration	1000 g	3500 g	100 g	300 g	50 g

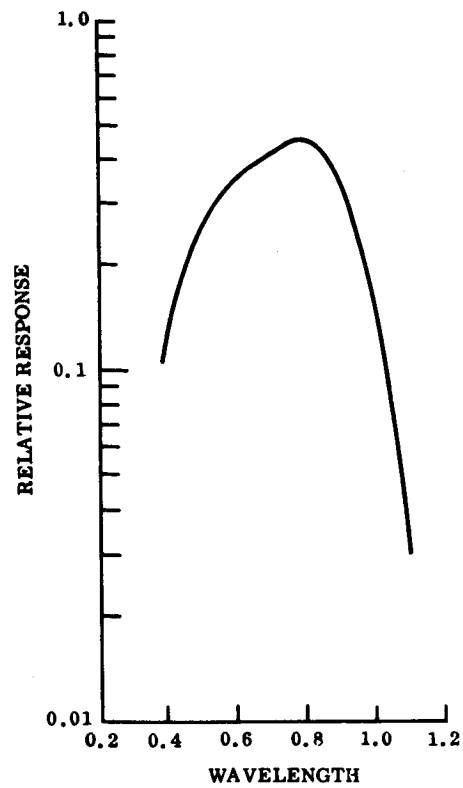


Figure 6.5.2-5. Silicon Photo-Voltaic Cell Spectral Response

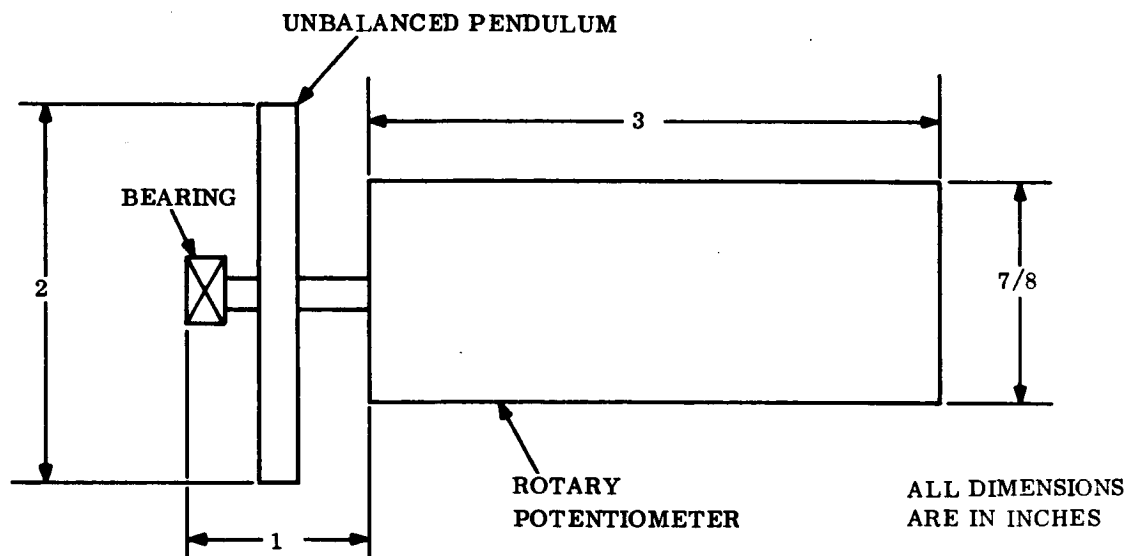


Figure 6.5.2-6. Rotary Potentiometer Clinometer

6.5.3 TELECOMMUNICATIONS

6.5.3.1 Summary

The telecommunications subsystem consists of:

1. A hardware data link for Capsule checkout prior to separation from the Spacecraft,
2. A relay communications link to provide Lander entry data and high data rate imagery after landing,
3. A direct S-band data link to provide engineering and scientific data during the extended mission via the Deep Space Net (DSN),
4. A UHF beacon link to detect Orbiter presence for relay communications, and,
5. An S-band command link for detecting and decoding commands for control of the Lander subsystems.

A functional block diagram of the telecommunication subsystem is shown in fig. 6.5.3-1. The communication link characteristics are summarized in table 6.5.3-1.

TABLE 6.5.3-1. DESIGN SUMMARY

Phase	Link	Data Rate (BPS)	Transmission Time	Total Data (Bits)
Post separation	400 MHz FSK, relay	1090	30 min	2.0×10^6
Entry	400 MHz FSK, relay	1090	302 to 566 (1) 566 min (1)	0.33 to 0.62 $\times 10^6$ (1)
Post impact, set-up	400 MHz FSK, relay	1090	2.5 min (2)	0.16×10^6 (2)
Entry pass,	400 MHz	31×10^3	-	See table 6.5.3-7
1 Orbiter pass	FSK, relay	31×10^3	800 sec (3)	2.5×10^7
2 Orbiter pass	FSK, relay	1090	1400 sec	1.5×10^6
3 Orbiter pass	FSK, relay	-	-	(7)
Post-relay (daily)	S-band, PSK direct	11	4.2 hr (4) 1580 sec (5) 290 sec (6)	166320 17000 3184

(1) Atmosphere dependent.
 (2) Data during this period may be lost because entry antenna may be underneath Lander.
 (3) Minimum effective transmission interval.
 (4) Antenna beamwidth limited.
 (5) Based on average daily transmission time limit imposed by solar array size.
 (6) Nominal time required for data.
 (7) No communication in extreme cases.

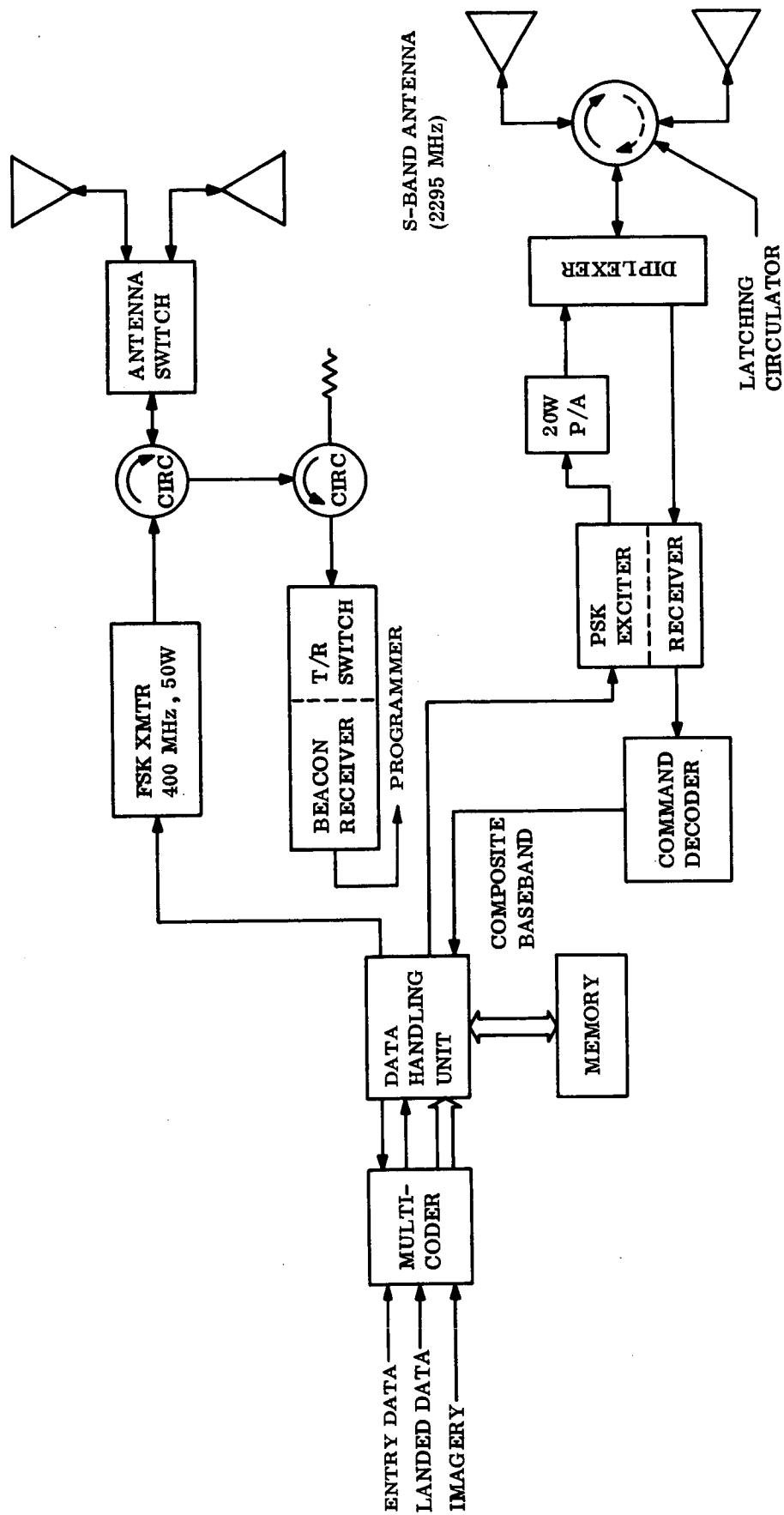


Figure 6.5.3-1. Telecommunications Subsystem, Functional Block Diagram

To support the high data requirement for imagery, the data will be relayed to Earth via the Orbiter, with communication to the Orbiter taking place during a peri-apsis pass to take advantage of the relatively short line-of-sight range. Data is stored in the Orbiter and subsequently transmitted to Earth. Non-coherent frequency shift keying with Manchester coding is chosen as the modulation technique to minimize acquisition time. After landing (for the entry pass and the first Orbiter pass) the link is designed to operate at 31 kbps data rate. The performance under maximum adverse tolerance, 46° worst case Lander tilt and worst case Orbiter-Lander line of sight parameters is shown in table 6.5.3-1. To accomplish this data transfer requires 50 watts of transmitter power, the maximum allowable to avoid antenna breakdown at Mars surface pressure. It is assumed that the Orbiter will be provided with the capability to record data at this high rate. If this is not the case, the total data transferable (and the required transmitter power) scale down approximately proportional to the actual recording rate.

Data requirements prior to and during entry are relatively modest, but communication ranges are more severe. It was determined that the same transmitter and receiver used for imagery data after landing can be used at a lower data rate for entry data. This minimizes equipment and complexity on both the Orbiter and Lander.

The turn-on of the data transmission for the direct entry mission is complicated by the large uncertainties in the orbit period. The two approaches previously considered, a pre-programmed turn-on of the data link and a beacon link to sense the Orbiter presence, can result in early turn-on time of 6.8 hr and about 2 hr, respectively. From an energy consideration, these early turn-on times are not reasonable. The alternative is to update the turn-on information based upon Earth tracking of the Orbiter. Both the Lander and Orbiter have command links. Redundancy is provided by utilizing both of the command systems to update the turn-on time. The Lander command system is used to modify the programmed data link turn-on time. The Orbiter command system controls the beacon transmitter turn-on. In this case, the beacon link is used to sense the presence of the Orbiter and to initiate data transmission.

When the Orbiter is no longer available, data is transmitted directly to Earth via DSN facilities. The nominal data load for this phase is 3184 bits. By using a 20 watt (minimum) S-band transmitter and receiving with the 210 ft dish in the listen only mode, with a 4 Hz receiver bandwidth, the direct link can support this nominal data load with reserve capacity throughout the 90 day mission. (The 4 Hz DSN receiver is not currently available.) This is accomplished using a vertically oriented helix antenna which provides about 4.2 hr Earth coverage time (at 11 bits/sec) with maximum adverse tolerance and the worst case pointing error of 30° at the nominal 10°N latitude. That is, irrespective of power supply limitations, the daily capacity is 166,320 bits while about 4.8 min are required to transmit the nominal data. Latitude errors of 12° can be accommodated with no loss in nominal data. If errors in excess of 12° are expected, the antenna must be designed with wider beamwidth and a corresponding degradation in available bit rate will result.

An S-band command link is provided. Commands at the rate of 0.5 bits per sec are feasible throughout the 90 day mission by using an 85 ft DSN antenna and a 100 kw transmitter. (To share the 210 ft dish would disastrously degrade the direct data link because of losses in additional r-f equipment.) For command reception, a vertically oriented antenna will be used to provide a 4.2 hour Earth command window daily.

The landing orientation uncertainty dictates the use of two antennas for both the relay and direct links. The S-band command receiver and data transmitter share the same antennas through a diplexer. Antenna selection is accomplished by semi-conductor switches, in the 400 MHz system and by electrically controlled latching circulators in the S-band system.

6.5.3.2 Telecommunications Sequence

Prior to separation, Lander power is turned on for final checkout (table 6.5.3-2). Except for a momentary check of transmitter power, transmitter operation within the canister is avoided. During this interval, data is transferred via hardwire to the spacecraft. Immediately after separation r-f transmission is initiated for event monitoring and engineering diagnostic measurements.

TABLE 6.5.3-2. TELECOMMUNICATIONS SEQUENCE

Phase	Duration	Communications
Pre-separation	15 min	Low rate/hardwire
Post-separation	30 min	Low rate
Entry	302-566 min	Low rate
Post impact	2.5 min	Low rate
Post-landing Entry pass	See table 6.5.3-7	High rate
Orbit period	~25 hours	None
Beacon turn-on	Periapsis uncertainty	None
Beacon early trigger	0-12 min	High rate
Orbiter pass	800-1400 sec	High rate
Post-relay	~4 hr	Receive commands
Post-relay	4.8 min	Direct link

During entry and for 2.5 min after impact, scientific and engineering diagnostic data are transmitted at the low data rate. The high data rate is then used to transmit imagery for a period of 800 sec. (See para 6.5.3.4).

The beacon receiver is turned on prior to nominal Orbiter pass by a time interval equal to the Orbiter arrival time uncertainty. The beacon transmitter turn-on is initiated upon command to include updated orbit period information. The beacon link will trigger high rate transmission of stored scientific and engineering data and imagery.

The command receiver and direct link transmitter are turned on by stored command with the nominal data transmission time being 4.8 minutes.

6.5.3.3 Data Requirements

Table 6.5.3-3 is a list of measurements for the entry, landed (relay) and post-relay mission phases. Table 6.5.3-4 gives the corresponding data transmitted. During entry, real time data is interleaved with data delayed by 70 sec to avoid loss of data during blackout. The combined data dictates a 1.09 kbps data rate. Prior to entry, only engineering diagnostic data is transmitted. Immediately after landing, imagery is transmitted at the high data rate. Imagery and surface science data are transmitted at the high data rate on subsequent Orbiter passes if the Orbiter is within range. During the entry pass and subsequent Orbiter passes, scientific, engineering and imagery data are transmitted to the Orbiter. Total nominal scientific and engineering diagnostic data requirement is 68850 bits. In the post-relay phase, data requirements are reduced to a nominal 3184 bits with some flexibility available via commands.

TABLE 6.5.3-3. MEASUREMENTS LIST

	Pre-impact	Post-impact (relay)	Post-relay
Diagnostic data (50 channels)	X	X	
Scientific data (6 channels)			X
Pressure	X	X	X
Stagnation pressure	X		
Temperature	X	X	X
Stagnation temperature	X		
Water vapor	X		
Tri-Axial spectrometer	X		
Wind velocity		X	X
Moisture		X	X
Surface composition		X	
Clinometer		X	X
Imagery		X	
Stored data		X	

TABLE 6.5.3-4. DATA TRANSMITTED

	Entry	Landed (Relay)	Post-Relay
Science	$194\frac{2}{3}$ bps	34600 bits	2134 bits (3)
Diagnostic	350 bps	26250 bits	1050 bits (3)
Stored	$544\frac{2}{3}$ bps (1)	100,000 bits(2)	---
Imagery	---	$\sim 2.5 \times 10^7$	---
Total data/day	---	2.5×10^7 bits	3184 bits (3)
Data transmission time	302 to 506 sec	800 sec (4)	4.8 min
Data rate	1.09 kbps	31 kbps	11 bps

(1) Science and diagnostic data delayed by 70 sec.
 (2) Data stored during entry.
 (3) Based on a 1/hr sampling rate.
 (4) Entry pass. Communication time on subsequent orbits is dependent upon orbit accuracy.

6.5.3.4 Link Designs

6.5.3.4.1 Landed (Relay)

The fundamental constraints for the landed telecommunication imagery and stored data relay links are that (1) maximum data is to be transferred, (2) maximum allowable power is 50 watts to avoid antenna breakdown and (3) the permissible bit error probability is 4×10^{-3} . (Orbiter to Earth link is 10^{-3} giving an overall bit error probability of 5×10^{-3}). Additionally the link must be tolerant of Lander attitude (tilt) uncertainty due to surface slopes and crush-up variance and tolerant of landing site uncertainty. Finally, the Lander size requires that the antenna be physically small.

These constraints are satisfied by the non-coherent, frequency shift keyed (FSK), Manchester coded, 400 MHz link. The use of non-coherent FSK with Manchester coding minimizes acquisition time. The antenna is made small physically by sacrificing bandwidth (with essentially no degradation in link performance). The need for pointing or steering mechanisms is avoided by using an antenna with beamwidth wide enough to accommodate Lander tilt uncertainties.

The data optimization procedure is related in Volume III and summarized here. Resulting available data rates vs time for the nominal Orbiter/Lander line-of-sight parameters, figure 6.5.3-2, are repeated in fig. 6.5.3-3 for worst case adverse link tolerances. Figures 6.5.3-4 and -5 relate the available data rates vs time for the 30° Orbiter period errors, ± 3.4 hr. These results do not consider possible antenna distortion resulting from ground reflections or specific Lander configuration. Fig. 6.5.3-6 is the relay/beacon block diagram, and table 6.5.3-5 contains the design

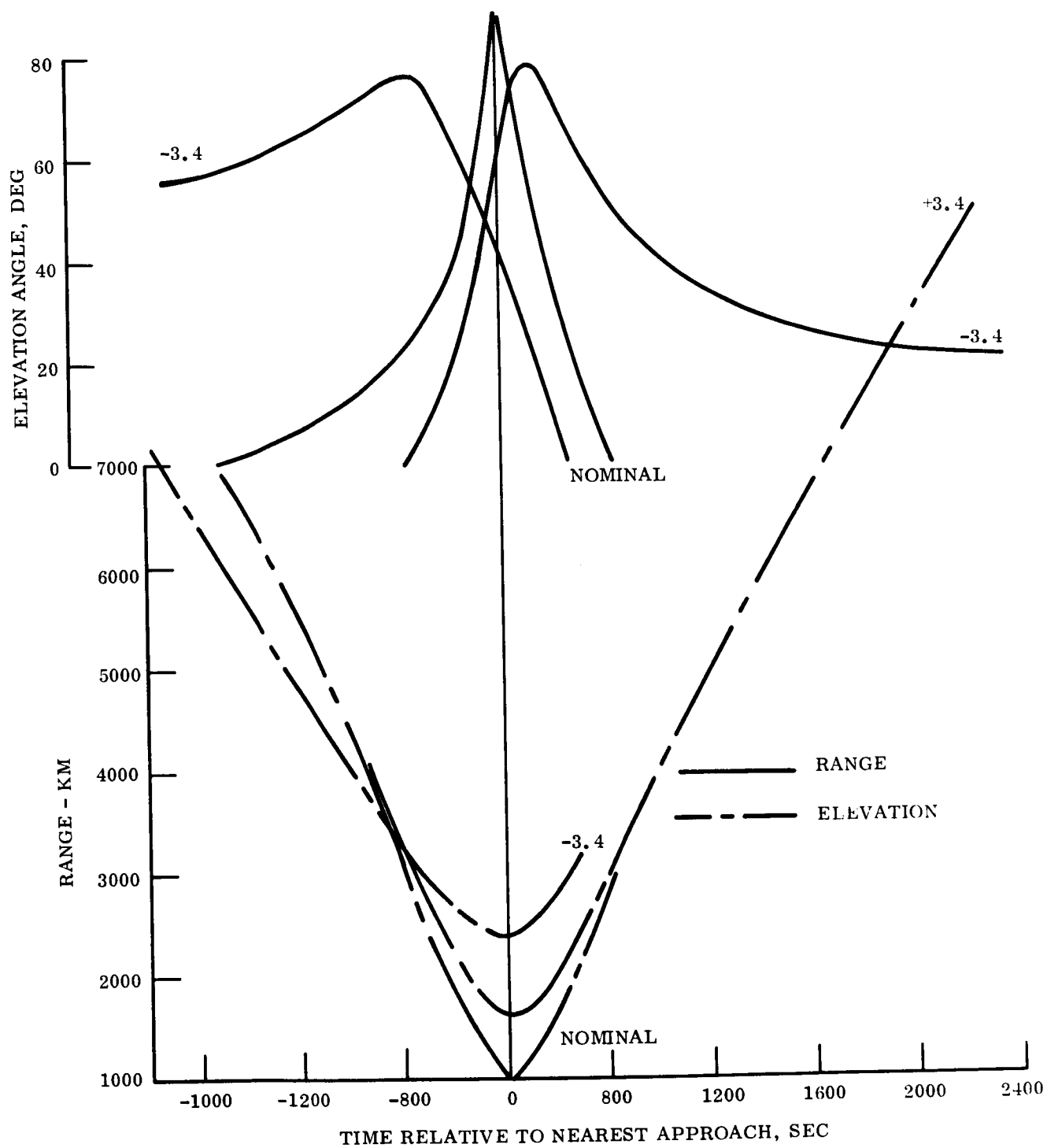


Figure 6.5.3-2. First Orbit Pass Communication Parameters

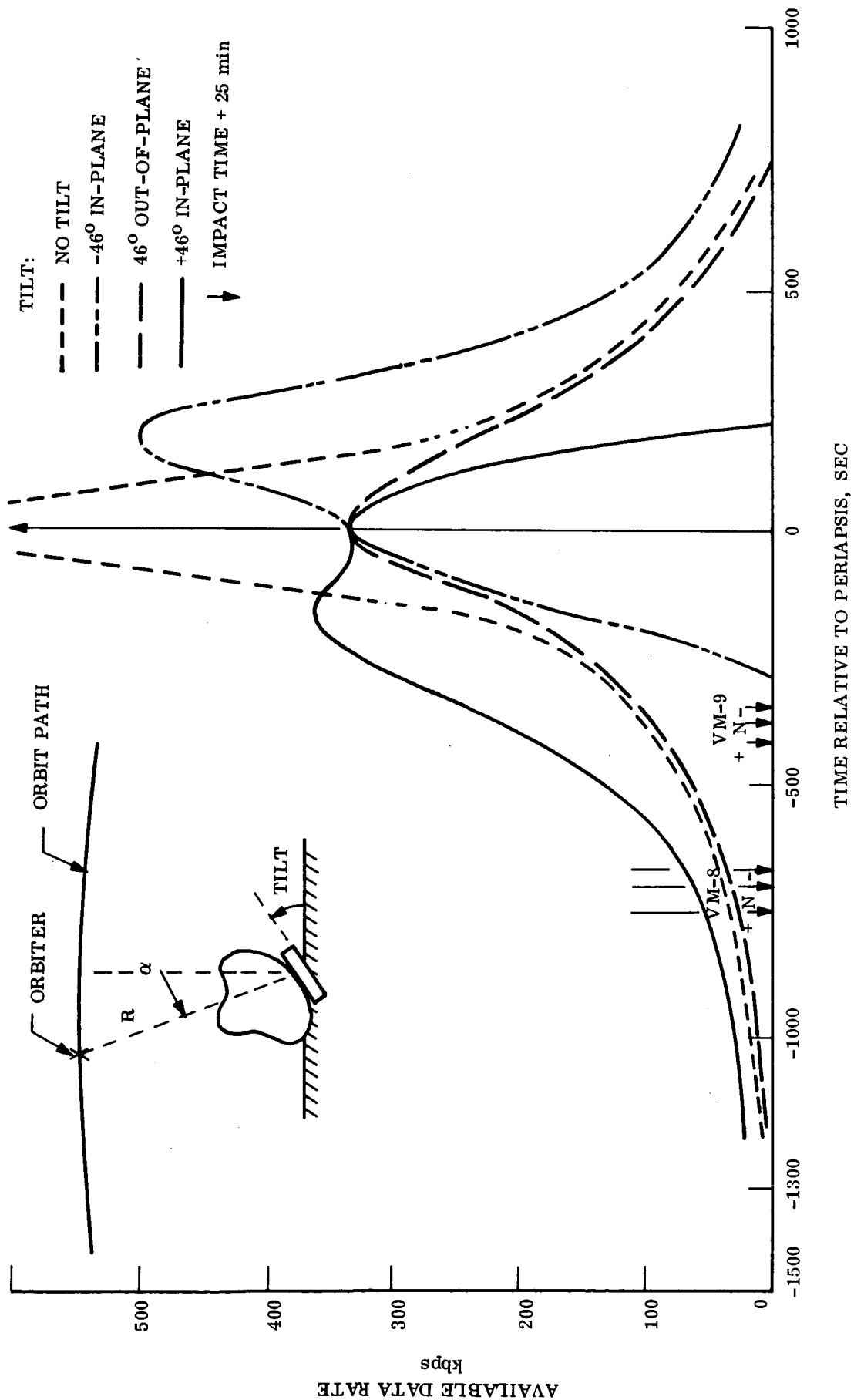


Figure 6.5.3-3. Available Data Rate vs Time with Adverse Tolerances, Entry Pass and Nominal Orbital Passes

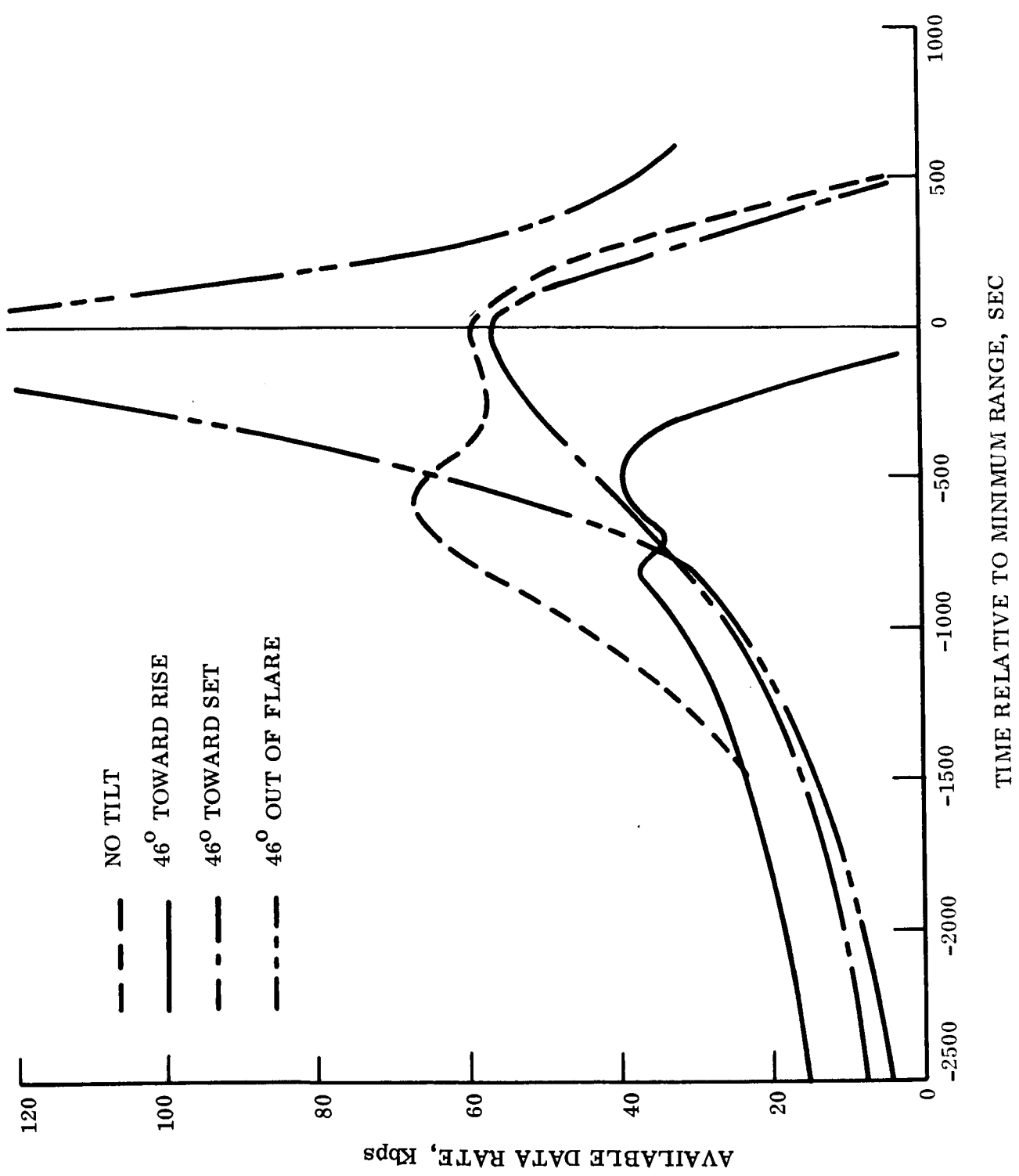


Figure 6.5.3-4. Available Data Rate vs Time with Adverse Tolerances, First Orbiter Pass, -3.4 hr Period Error

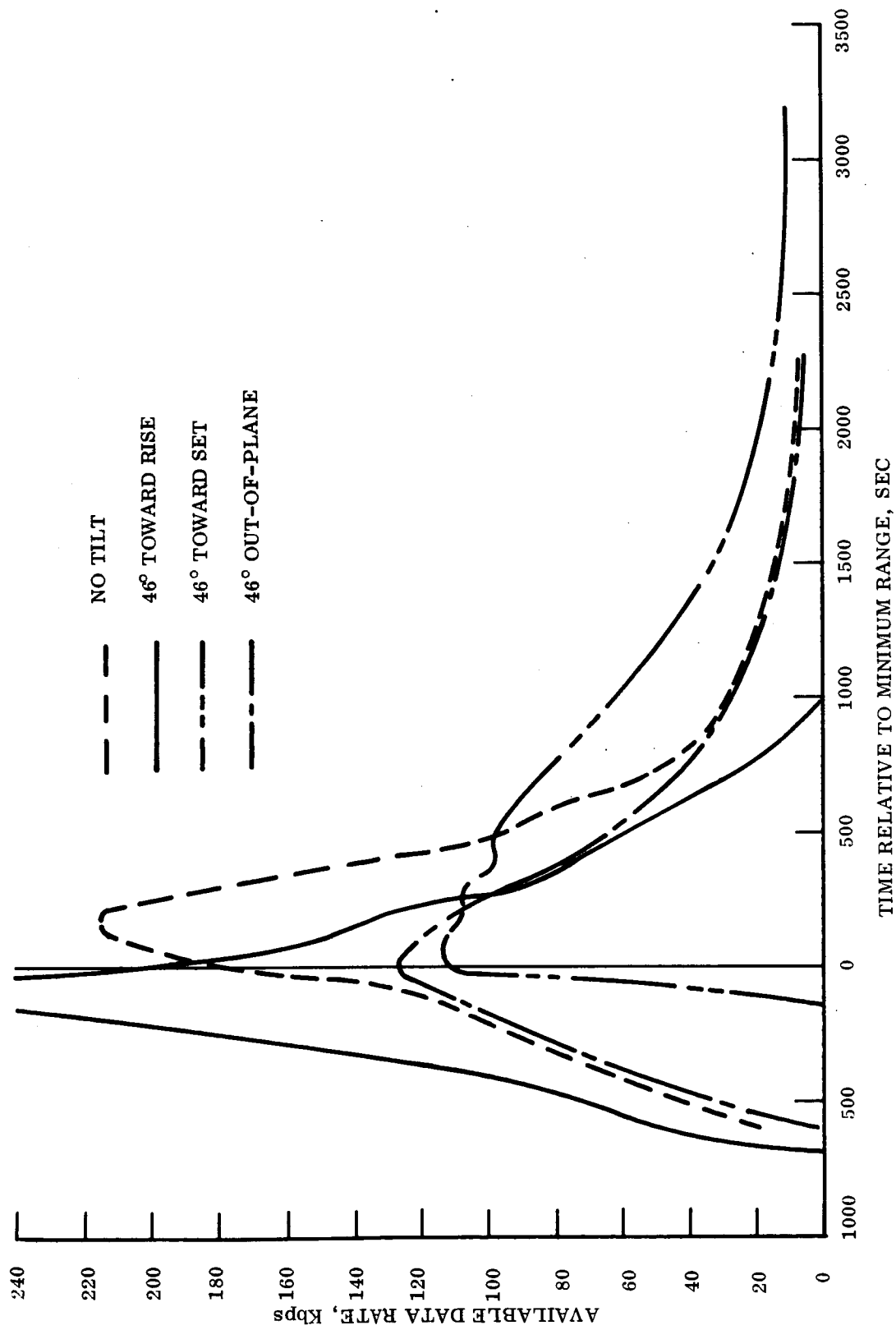


Figure 6.5.3-5. Available Data Rate vs Time with Adverse Tolerances, First Orbiter Pass, +3.4 hr Period Error

TABLE 6.5.3-5. DESIGN CONTROL TABLES -

RELAY (LANDED) AND BEACON

Parameter	Nominal Values and Worst Case Tolerances					
	Relay (Landed)			Beacon Link		
	Nom	+tol	-tol	Nom	+tol	-tol
Modulation technique	FSK	--	--	AM	--	--
Frequency (MHz)	400	--	--	400	--	--
Transmitter power (watts)	50	--	--	4.1w	--	--
(dBm)	47.0	0.0	1.0	36.1	0.0	1.0
Transmit circuit loss	-1.5	0.2	0.4	-1.5	0.2	0.4
Transmit antenna gain (dB)	2.0 ⁽⁵⁾	0.5	0.5	2.0 ⁽⁵⁾	0.0	0.5
Transmit antenna pointing loss	0.0	0.0	0.0	-1.0	1.0	0.0
Range (km)	3000 ⁽⁵⁾			3000 ⁽⁵⁾		
Space loss	-154.1	--	--	-154.1	--	--
Polarization Loss	-1.0	1.0	0.5	-1.0	1.0	0.5
Receiving antenna gain	2.0 ⁽⁵⁾	0.0	0.5	2.0 ⁽⁵⁾	0.5	0.5
Receiving antenna pointing loss	-1.0	1.0	0.0	0.0	0.0	0.0
Receiving circuit loss	-1.0	0.2	0.4	-2.0	0.2	0.4
Total received power (S)(dBm)	-107.6	2.9	3.3	-117.7	2.9	3.3
Effective noise temperature(^o K)	650	--	--	724	--	--
Receiver noise power						
spectral density (N/B)	-170.5	0.0	1.0	-170.0	0	1.0
Bit rate, 1/T (bps/dB)	31 k1	--	--	--	--	--
	44.9					
Frequency uncertainty (kHz)	20.0 ⁽²⁾	--	--	16.0 ⁽⁴⁾	--	--
I-F bandwidth (kHz)	145.0	--	--	25.0	--	--
Required S/N/B	56.3 ⁽³⁾	0.0	2.0 ⁽³⁾	47.0	1.0	1.0
Required ST/N/B	11.7 ⁽³⁾	0.0	2.0 ⁽³⁾	3.0 ⁽¹⁾	1.0	1.0
Threshold data power (dBm)	-113.9	0.0	3.0	-123.0	1.0	2.0
Margin	6.3	2.9	6.3	5.3	3.9	5.3
<p>(1) Signal-to-noise ratio in i-f bandwidth.</p> <p>(2) Transmitter stabilizer ± 10 ppm; Receiver stability ± 5 ppm; Doppler ± 4 kHz.</p> <p>(3) Nominal signal-to-noise ratio is theoretical value. 2 dB adverse tolerance is allowed to account for practical performance degradation, e.g., non-ideal bit sync. Value from Volume III, Section 4.2.2.</p> <p>(4) Same as (2) except only one sided doppler shift needs to be considered.</p> <p>(5) Values shown are typical and correspond to the G/R^2 ratio required to support the 31 kbps data rate.</p>						

control table. In this table, the 3000 km range and 2 dB transmit antenna gain are reference values and yield an allowable data rate of 31 kbps with worst case adverse tolerances. For such high data rates relative to the frequency uncertainty, the available data rate is proportional to the gain over range squared ratio, G/R^2 , which is the basis of fig. 6.5.3-3. Fig. 6.5.3-3 includes gain and range as determined from Lander to Orbiter line-of-sight range and look angle and Lander tilt. Tilts in the direction of Orbiter set and Orbiter rise and tilt perpendicular to the Orbiter plane are considered. The reference condition of zero tilt (nominal case) shows a very sharp peak as the Orbiter passes overhead. This is the result of minimum communication range and maximum antenna gain. When the Lander is tilted toward Orbiter rise (set), the peak gain is pointed off vertical and tends to counteract the bit rate loss resulting from increasing range. The net effect of in-plane tilt is a lower peak data rate and longer available transmission time at near peak data rates. On the other hand, pure out-of-plane tilt lowers the gain and, hence, available data rate at all times.

Optimization is accomplished by examining the communication time as a function of bit rate for positive and negative in-plane tilt and for out-of-plane tilt. The maximum total data that can be transmitted with confidence at a specific bit rate is the product of bit rate and minimum communication time for the three tilt conditions considered. The bit rate yielding the largest maximum total data transmitted is the optimum bit rate.

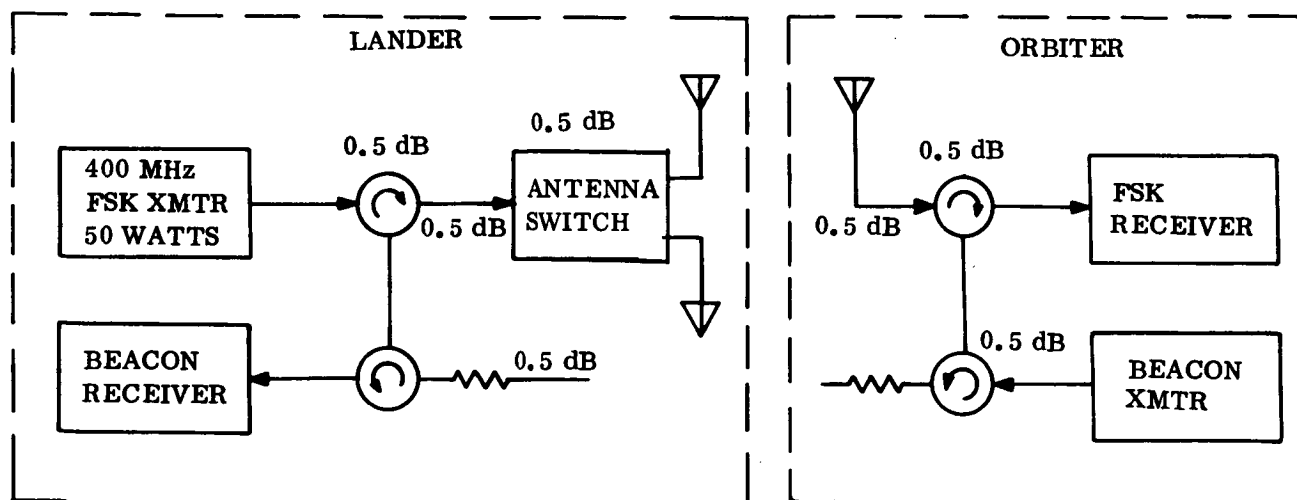


Figure 6.5.3-6. Relay and Beacon Link, Block Diagram

Times (relative to time of nearest Orbiter approach) of impact plus 2.5 min for the extreme atmospheres, VM-8 and VM-9, are indicated in fig. 6.5.3.2 for trajectory uncertainties leading to nominal and ± 3.4 hr Orbiter period errors. The data transferable after impact at a specific bit rate is the product of the bit rate and the time available at that bit rate. Maximum data occurs at high bit rates on the order at 160 kbps. Requirements for transmission during the 1st Orbiter pass and the desire to use a single data rate for entry and 1st Orbiter passes will constrain the data rate to a lower value.

For the nominal Orbiter period, the maximum data transferable for worst case tilt of 46° and maximum adverse link tolerances is 8.1×10^7 bits at an optimum bit rate of 160 kbps. When Orbiter period errors are considered, the data transferable during the first Orbiter pass is significantly reduced. In fact, for the 3-sigma case at a -3.4 hr period error, the maximum data rate that can be supported for all tilt conditions is about 40 kbps and the optimum is 21 kbps yielding a total data of 3.1×10^7 bits. A data rate of 31 kbps is recommended as a compromise with the entry pass communications and to be consistent with the electrical system described in this report. At 31 kbps, the worst case data transferable during the first Orbiter pass is 2.5×10^7 bits, i.e., at least 800 sec or more transmission time at this rate is available. For the entry pass, the data transferable at 31 kbps during the entry pass is indicated in table 6.5.3-6.

In fig. 6.5.3-3, transmission at a given rate is allowable when the available data rate is equal to or greater than that rate. To be certain of transmitting the 2.5×10^7 bits the transmission interval must include at least 800 sec having allowable rates greater than 30 kbps for each and every tilt and period error condition. The minimum period is 1040 sec to cover tilt uncertainties for the -3.4 hour period error. An additional 360 sec is required because of atmosphere uncertainty thus, the transmission interval must be 1400 sec (about 23.5 min) plus the uncertainty in Orbiter time of arrival.

TABLE 6.5.3-6. DATA TRANSFERABLE AFTER IMPACT PLUS 2.5 MIN⁽¹⁾

Atmosphere (Adverse Link Tolerances)	(Bits/ 10^7)	-46° Tilt ⁽²⁾	46° Out-of-Plane ⁽³⁾	$+46^\circ$ Tilt ⁽⁴⁾
	No Tilt			
VM-8	4.0	4.4	3.9	2.7
VM-9	3.0	3.4	2.9	1.7
<p>(1) Data shown is for nominal Orbiter parameters. Data transferable for 3-sigma tolerances in Orbiter parameters is within $\pm 0.3 \times 10^7$ bits.</p> <p>(2) Lander tilted 46° in direction of Orbiter set.</p> <p>(3) Lander titled 46° perpendicular to and away from the Orbiter plane.</p> <p>(4) Lander titled 46° in direction of Orbiter rise.</p>				

For the second Orbiter pass the extreme period uncertainties have drastic effects on communication parameters. For example, with -3.4 hr period error the minimum range of about 5100 km occurs at 0° elevation and the range at 34° set is about 6300 km. A reasonable approach is to reduce the bit rate to the entry value of 1090 bits/sec. From table 6.5.3-8, the margin over adverse tolerances is 18.6 dB at 1000 km range, indicating a range limitation of 8500 km. To get a feel for communication capability, data transferable was computed by finding the time between the 8500 km range and 34° rise or set. For -3.4 hr period error 0.15×10^7 bits can be transferred (1400 sec). For $+3.4$ hour period error, 0.33×10^7 bits can be transferred (3000 sec available). (These data capacities do not consider battery energy limitations.) The command capability could be used to transmit at higher rates in the case of near nominal Orbiter period.

For the third Orbiter pass with extreme period errors, the Orbiter appears only at less than 6° elevation angle. Clearly no communication is feasible under these conditions.

6.5.3.4.2 Beacon Link

A beacon transmitter on the Orbiter and a beacon receiver on the Lander comprise the beacon link. The beacon and data links are diplexed on the same antenna so that r-f path losses will be nearly identical and weight and space conserved. The narrowband antenna characteristic forces the beacon link to operate at essentially the same frequency as the relay link so that the two links must time share the antennas. To accomplish this the Orbiter beacon transmitter must transmit, for example, for an interval of one sec and then listen for 10 sec to see if the Lander is transmitting. When the Lander received signal strength is above a preset threshold level, data transmission will be initiated after a 1 sec delay. The Orbiter will sense Lander transmission and cease beacon transmission.

The beacon link received signal strength is proportional to link antenna gain divided by range squared and, hence, is indicative of relay link available data rate. Ideally the link could detect exactly when the high data rate can be supported which would lower the required transmission time to just that necessary to transmit the data. Unfortunately, the beacon link does have a range of tolerances which must be considered. To aid in minimizing the range of tolerance, the beacon transmitter power will be closely controlled, i.e., within 1 dB and its signal will be AM modulated to eliminate the noise bias uncertainty. The maximum beacon link uncertainty is 9.2 dB, a factor of 2.9 in range (see table 6.5.3-5). This uncertainty would normally cause the transmitter to turn-on early since the link is designed such that transmission will be triggered in time to complete data transfer under worst case adverse tolerance conditions. If the beacon link was allowed to operate continuously, serious early turn-on, on the order of 2 hr, could occur for the -3.4 hr period uncertainty. The possibility is eliminated by inhibiting beacon transmitter turn-on until the Orbiter is near the Lander. This function is controlled from Earth. The beacon transmitter turn-on time is updated to reflect the orbit period as determined from tracking information.

6.5.3.4.3 Entry

Although, there is a wide variation in the line-of-sight range and look angle during the entry phase due to the uncertainty of the atmosphere, communications can be maintained throughout entry.

Entry data is transmitted via the same link as landed data by keying at the low data rate (1090 bits/sec) to minimize weight and complexity. (This requires the Orbiter receiver be capable of receiving either data rate.) The design control table for the entry link is shown in table 6.5.3-7. The link has a margin over adverse tolerance of 18.6 dB at the reference range, 1000 km, with 2 dB transmit antenna gain, or a worst case range limitation of 8500 km. The antenna provided has a gain greater than zero dB over a range of $\pm 70^\circ$ with respect to the rear-looking Lander roll axis. The mission range and look angle profiles indicate an approximate maximum range of 5200 km and maximum look angles of about 60° . (Here look angle is angle to Orbiter with respect to the velocity vector. Any variation between the velocity vector and roll axis, e.g., due to coning or swing on the parachute, will degrade the communication angle.) Swing in excess of 20° at this time could cause the link margin to decrease momentarily below the adverse tolerance level. As the Lander descends and the Orbiter begins to overtake the Lander, the look angle improves and more swing is allowable.

During the entry phase, signals transmitted from the Lander may be reflected from the planetary surface toward the Orbiter. These multipath signals may interfere with the desired signal which is received on the line-of-sight path from the Lander. As shown in Volume III, Section 4.2.3, the slow fading environment is most detrimental to the communication link performance. The conditions for slow fading occur near impact. Based upon the maximum range during entry, the minimum margin over worst case tolerances is 4.3 dB. The tolerable signal to interference level to allow fading loss for less than 99 percent of the time is about 12.0 dB for the 4.3 dB margin. If this level proves to be a problem, another Orbiter receiver can be added with an i-f bandwidth to match the transmitted data rate yielding an additional margin of approximately three dB.

6.5.3.4.4 Direct

The direct link was constrained to a power of 20 watts (minimum) to capitalize on the available high shock TWT. Steered antennas were ruled out because of complexity and size/deployment limitations. To establish direct communications throughout the 90 day mission with a 10 January '74 landing date, requires use of a 210 ft DSN receiving facility. A vertically oriented antenna is used which results in a maximum pointing error of 90° less the minimum Earth elevation angle. For the nominal case of 10°N latitude, this is 30° . The antenna provides a gain and beam-width approximately equivalent to the optimum in the sense of maximum daily data transfer. See parametric data, Volume III.

For the direct link, split phase data phase modulates the S-band carrier for transmission to the DSN station. The 210 ft antenna with the listen only feed is utilized and a receiving system temperature of 28° achieved by restricting operation to Lander elevation angles exceeding 20° (rather than the worst case temperature of 55°).

The modulation index is selected so that carrier and data channel thresholds occur at the same input power. The carrier channel threshold is set by the carrier phase lock loop bandwidth ($2B_{LO}$) and the required signal to noise ratio (SNR) in that

TABLE 6.5.3-7. ENTRY LINK DESIGN CONTROL TABLE

Parameter	Relay (entry) nominal	Adverse Tolerance
Modulation technique	FSK	--
Frequency (MHz)	400	
Transmitter power (watts)	50	
(dBm)	47.0	1.0
Transmit circuit loss	-1.5	0.4
Transmit antenna gain	2.0(1)	0.5
Transmit antenna pointing loss	0.0	0.0
Reference range (km)	1000(1)	
Space loss	-144.5	
Polarization loss	-1.0	0.5
Receiving antenna gain	2.0	0.5
Receiving antenna pointing loss	-1.0	0.0
Receiving circuit loss	1.0	0.4
Total received power (S), dBm	-98.0	3.3
Effective noise temperature ($^{\circ}$ K)	650 ⁰	
Receiver noise power spectral density (N/B)	-170.5	1.0
Modulation loss	N/A	
Data power (dBm) S_D	-98.0	3.3
Bit rate, 1/T (bps/dB)	1090/30.4	--
Frequency uncertainty	20.	--
I-F bandwidth (KHz)	145.0(3)	--
Required S/N/B	47.6 (2)	2.0(2)
Required ST/N/B	17.2 (2)	2.0(2)
Threshold data power (dBm)	-122.9	3.0
Margin	24.9 (4)	6.3
<p>(1) Reference values.</p> <p>(2) Nominal signal-to-noise ratio used is theoretical value. 2 dB adverse tolerance is allowed to account for practical performance degradation, e.g., non-ideal bit sync.</p> <p>(3) Bandwidth required for high bit rate.</p> <p>(4) This margin, less the adverse tolerances, is available as protection against multipath. At the maximum range during entry, this margin is reduced to 4.3 dB.</p>		

bandwidth while the data channel threshold is set by the product of the data rate (R_b) and the ratio of data energy per bit to noise spectral density (E/N_0). As the mod index is adjusted so that the carrier channel power is decreased, the power in the data channel increases, allowing a higher data rate to be achieved, however, as the SNR in the carrier loop is reduced, the VCO phase jitter is increased, thereby degrading the data channel performance. For a given set of values of carrier loop bandwidth and data rate, there is an optimum modulation index which will result in the best performance. For the link under consideration the optimum modulation index results in a modulation loss (data power/total power) of 2.8 dB.

The required data channel E/N_0 was taken to be 7.4 dB based on the following assumptions:

Theoretical E/N_0 for $P_e^b = 5 \times 10^{-3}$	5.2 dB
Filter loss	0.5
Carrier jitter loss	0.8
Subcarrier jitter loss	0.2
Bit sync jitter loss	0.2
Margin	$\frac{0.5}{7.4 \text{ dB}}$

Table 6.5.3-8 summarizes the direct link design. The range shown is the worst case for the 90 day mission. The transmit circuit loss includes 0.5 dB for the latching circulator (used as an antenna switch - see fig. 6.3.5-1), 0.4 dB transmit (diplexer) loss, and 0.4 dB cable losses.

The link can support a data rate of 11 bits/sec and is able to transmit the nominal data load of approximately 3184 bits in 4.8 min. The total daily capacity is limited by the 4.2 hr Earth viewing time to 166,320 bits.

6.5.3.4.5 Command

The command link utilizes the DSN S-band command capability at a one sub-bit/sec rate. To provide coverage for the 90 day mission duration requires the use of a 100 kw transmitter and an 85 ft antenna.

Table 6.5.3-8 contains the command link design control table. It shows that the link is capable of operation at maximum range in the presence of maximum adverse tolerance. A receiver noise figure of 8.0 dB is used with receive circuit loss allowances as follows.

TABLE 6.5.3-8. S-BAND DESIGN CONTROL TABLE

Parameter	Data		Command	
	Nominal	Adverse Tolerance	Nominal	Adverse Tolerance
Modulation technique	PSK	-	PSK	
Frequency (MHz)	2295		2115	
Transmitter power (W/dB)	20/43	0.7 (dB)	100 kw/80	
Transmit circuit loss (duplexer)	-1.3	0.4	0.0	
Transmit antenna gain	7.0	0.4	51.0	0.5
Transmit antenna pointing loss	-3.0		-0.1	
Maximum range (km)	270x10 ⁶		270x10 ⁶	
Space loss	-268.3		-267.7	
Polarization loss	-0.1		-0.1	
Receiving antenna gain	61.0		0	0.5
Receiving antenna pointing loss	0.0	0.3	-3.0	
Receiving circuit loss	0.0		-2.1	0.5
Total received power(s), (dBm)	-161.7	1.8	-134.5	1.5
Effective noise temp (^o K)	28		1750	
Receiver noise power spectral density (N/B)	-184.1		-166.2	1.1
Carrier Performance				
Carrier modulation loss (dB)	-4.6		-0.9	0.1
Received carrier power	-166.3	1.8	-135.4	1.6
Carrier APC noise BW(2B _{LO})(Hz/dB)	4/6		20/13	0.2
Threshold SNR in 2B _{LO}	10.0		8.5	1.0
Threshold carrier power	-168.1		-144.7	2.3
Performance margin	1.8	1.8	9.3	3.9
Data Performance				
Data modulation loss (dB)	-2.8		-12.0	0.4
Data power (dBm)	-164.5	1.8	-146.5	1.9
Bit rate, 1/T (bps/dB)	11/10.4		1SBPS/O	
Required S/N/B (total power)	20.6		11.3	
Required ST/N/B (data power)	7.4		11.3	
Threshold data power (dBm)	-166.3		-154.9	1.1
Performance margin	1.8	1.8	8.4	3.0

Latching circulator	0.4 dB
Receiver filter (duplexer)	1.2 dB
Cable	0.4 dB
Total	<u>2.1 dB</u>

The signal to noise ratio used in the table yields a bit error probability of 10^{-5} . The time available for transmission of commands is the same as the telemetry transmission time, i. e., 4.2 hr. This minimum time occurs during the early portion of the mission.

6.5.3.5 Equipment Descriptions

6.5.3.5.1 Antennas (400 MHz)

The configuration of the wide beam 400 MHz antenna is that of a pill box eight in. in diameter and two in. deep. The top surface of the box is flush with the vehicle outer surface and has two orthogonal slots, two in. wide and eight in. long (dividing the top of the box into four quarters). The slots are tuned with capacitors to match the input and provide circular polarization. The bandwidth of this antenna is about 2 MHz. The estimated pattern is shown in fig. 6.5.3-7. Since the Lander diameter is of the order of a wave-length, the available ground plane is not large indicating that the actual antenna pattern will vary somewhat from that shown.

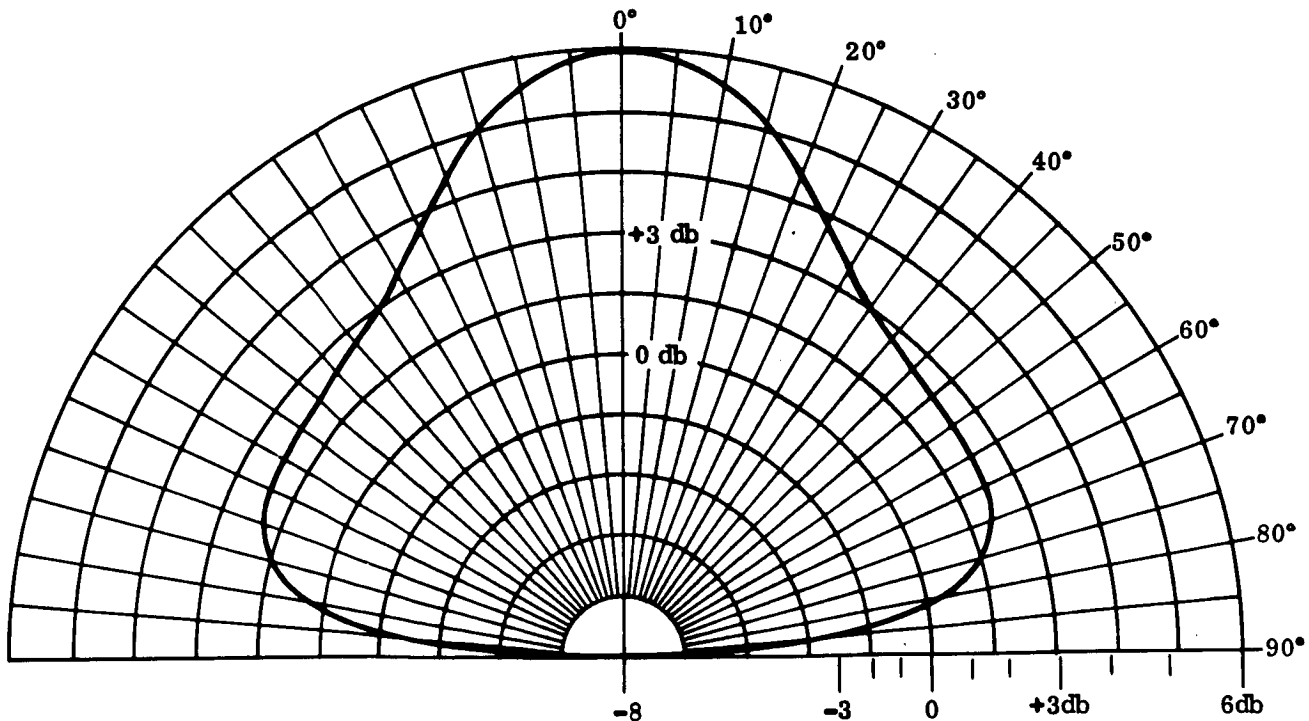


Figure 6.5.3-7. 400 MHz Antenna Pattern

6.5.3.5.2 S-band Antenna

The S-band receiver and transmitter are diplexed on one of two vertically oriented, 90° beamwidth antennas having a peak gain of 7 dB. The antenna is automatically selected and vertically oriented by sensing the attitude of the landed vehicle; it consists of a two turn helix mounted in a conical cup as shown in fig. 6.5.3-8 and has the pattern shown in fig. 6.5.3-9. Its selection was based on near optimum data transfer.

6.5.3.5.3 400 MHz FSK Transmitter

A block diagram for the FSK transmitter is shown in fig. 6.5.3-10. The frequency shift keyed modulation is produced by switching between two stable crystal oscillators operating at 25.0375 MHz and 24.9625 MHz, respectively. Multiplying these signals by a factor of 16 produces transmitter output signals at 400.6 MHz and 399.4 MHz, respectively. The multiplier chain will be constructed at a low signal level in order that filtering and multiplier inefficiencies do not adversely affect the overall efficiency.

The power amplifier chain consists of amplifier stages to produce a total gain of about 47 dB; approximately 10 dB of this will be excess gain to be used for AGC. The final amplifier stage consists of two 2N5178's operating in push-pull; these transistors are each rated for 50 watts output at 500 MHz with a dissipation rating of 70 watts at 25°C .

The output power level of the transmitter will be controlled at 50 watts $\pm 0, -1$ dB throughout the temperature environment by means of an AGC circuit consisting of a detector for output sampling, a high gain amplifier and a voltage variable attenuator located at the low level input to the 400 MHz power amplifier chain.

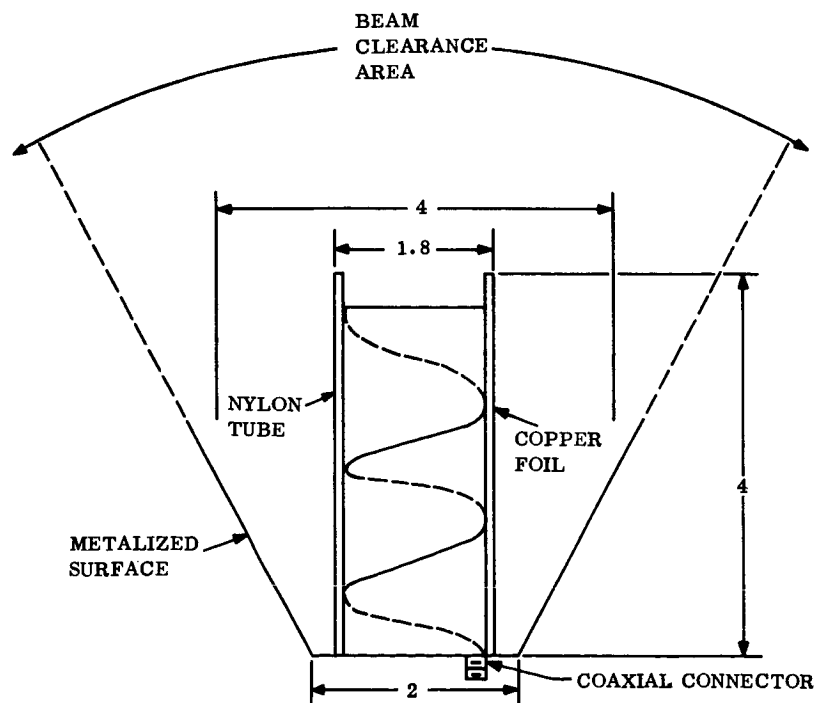


Figure 6.5.3-8. Circularly Polarized S-band Antenna (90° Coverage)

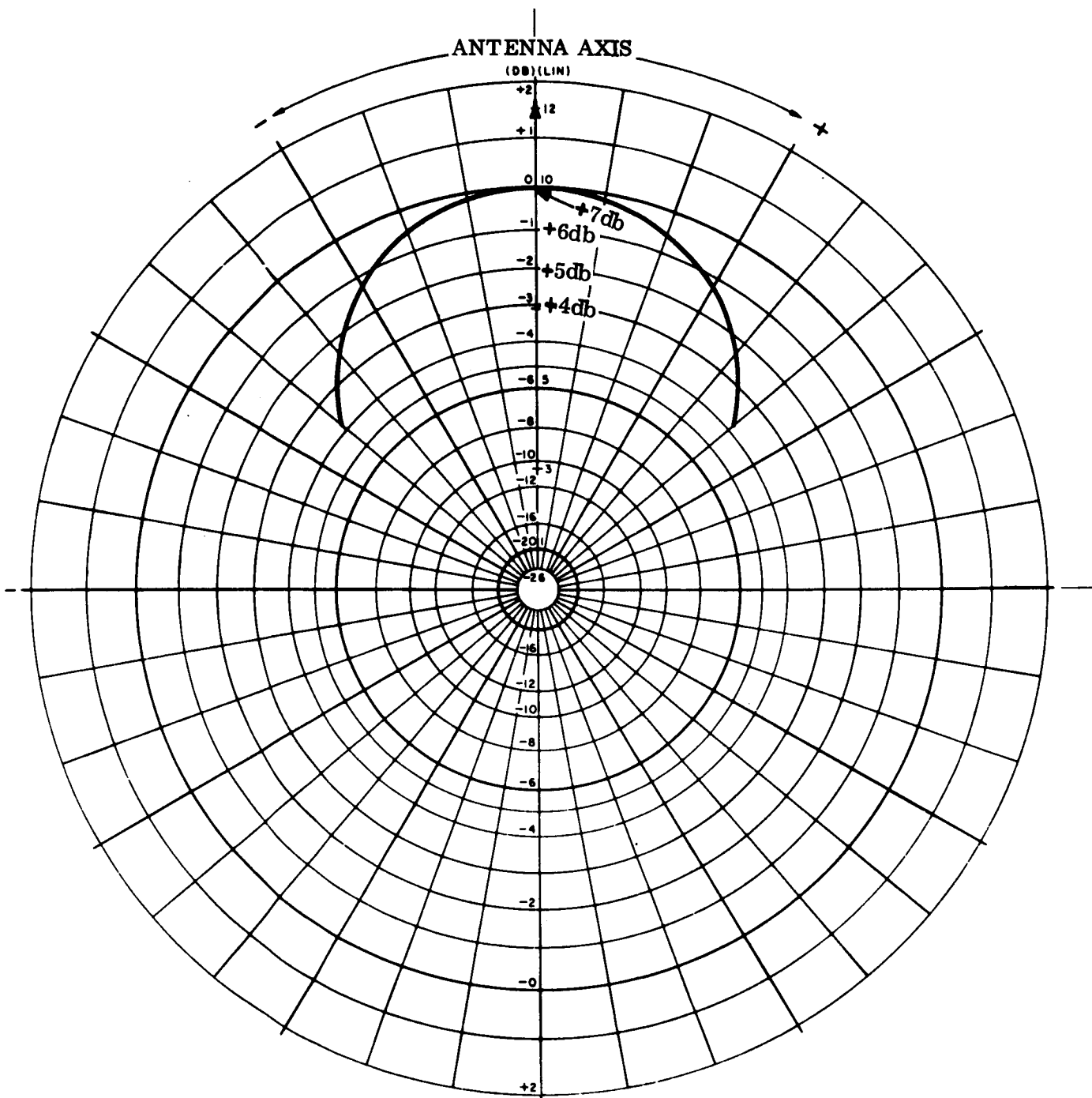


Figure 6.5.3-9. Calculated Approximate 90° S-band Antenna Pattern

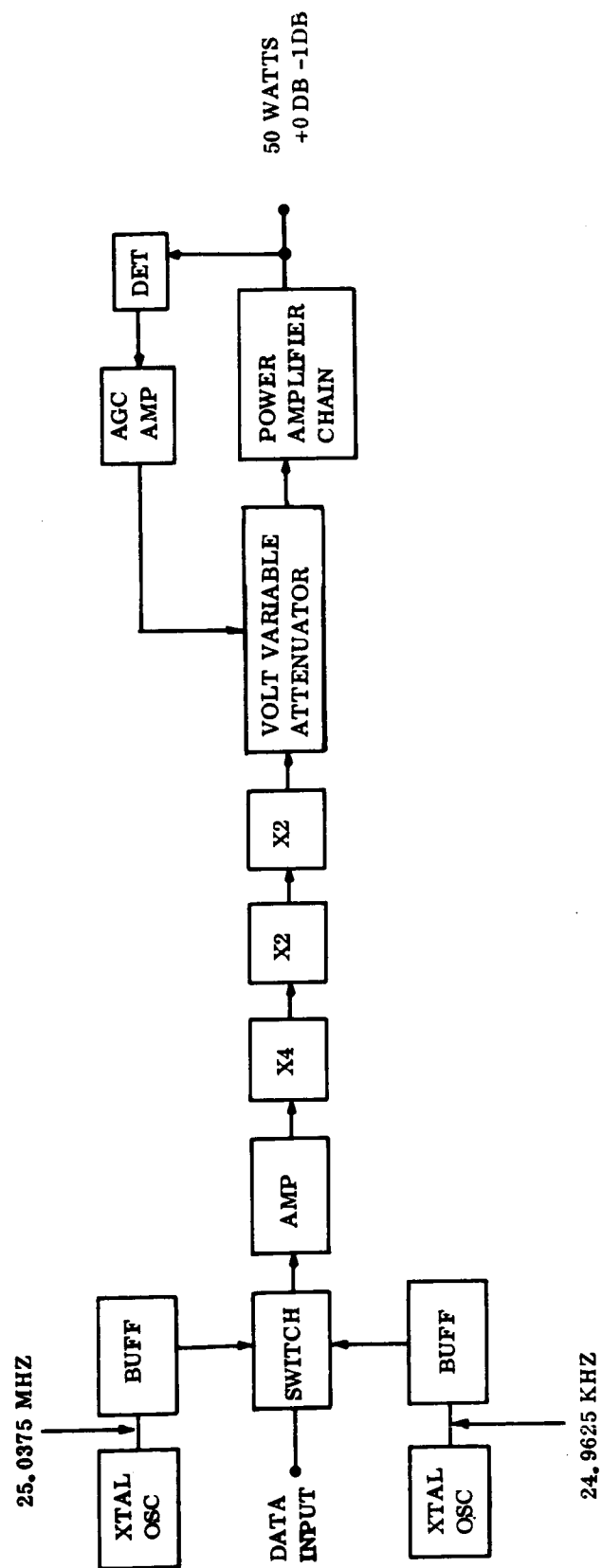


Figure 6.5.3-10. 400 MHz Transmitter, Block Diagram

The transmitter oscillator stability will be 10 ppm over a temperature range of -40°C to $+70^{\circ}\text{C}$ with negligible warmup time at any temperature. Aging will be 1 ppm per year. The state-of-the-art in temperature compensated crystal oscillators has reached a point where stabilities in the order of 1 ppm or better can be achieved for considerable periods of time, however, to account for degradation which may result from shock such as deformation of the crystal structure or holder, a stability of 10 ppm is considered conservative.

No serious problems are anticipated in the sterilization of the transmitter or in the high shock levels expected. Several years ago RSD designed and constructed a VHF 50 watt transmitter which was successfully sterilized and subjected to multiple shock impacts at levels of 5000 g's for approximately 500 μsec . The transmitter was potted with Dow Corning XR-6-3700 silicon potting compound. (The complete results of these tests are reported in GE, TIS 66SD2002 entitled "Fifty Watt Solid State FM Transmitter for Deep Space Communication", by Julius Shatas.

6.5.3.5.4 Duplexing Circuit

The duplexing arrangement used for the 400 MHz transmitter and receiver shown in fig. 6.5.3-11. It consists of two circulators connected as a 4-port circulator and a receiver T/R switch. The circulators protect the transmitter against large reflections and provide receiver isolation. In the normal receive mode the T/R switch is biased to pass the received signal. When the transmitter is turned on the circulator provides 20 dB receiver isolation, and the T/R switch is biased to reflect the leakage power back into the circulator where it is dissipated in a load. The T/R switch will be located in the receiver and the 4-port circulator near the transmitter.

The T/R switch considered is a Hylelectronics model SU175, and the circulators are similar to the Melabs HB5 series.

The antenna terminal of the duplexing circuitry is connected to the antenna switch as shown in the block diagram. This solid state switch is used to select one of two antennas according to Lander orientation. A solid state switch is selected because of its reliability and potential to withstand the shock environment. The switch considered is Hylelectronics model SU176.

6.5.3.5.5 400 MHz Beacon Receiver

The purpose of the beacon receiver is to sense when the relay link can support the high data rate. This is accomplished by looking for reception of a preset signal level. When the expected signal level is detected the 400 MHz transmitter is energized after a one second delay.

The receiver shown in fig. 6.5.3-12 receives an amplitude modulated signal of 400 MHz which is amplified in the low noise pre-amplifier and converted to the first i-f frequency. After amplification a second conversion takes place resulting in a second i-f signal at 3 MHz. The second mixer is fed to a band pass filter which reduces the overall noise level at that point to prevent limiting in the 3 MHz i-f amplifiers

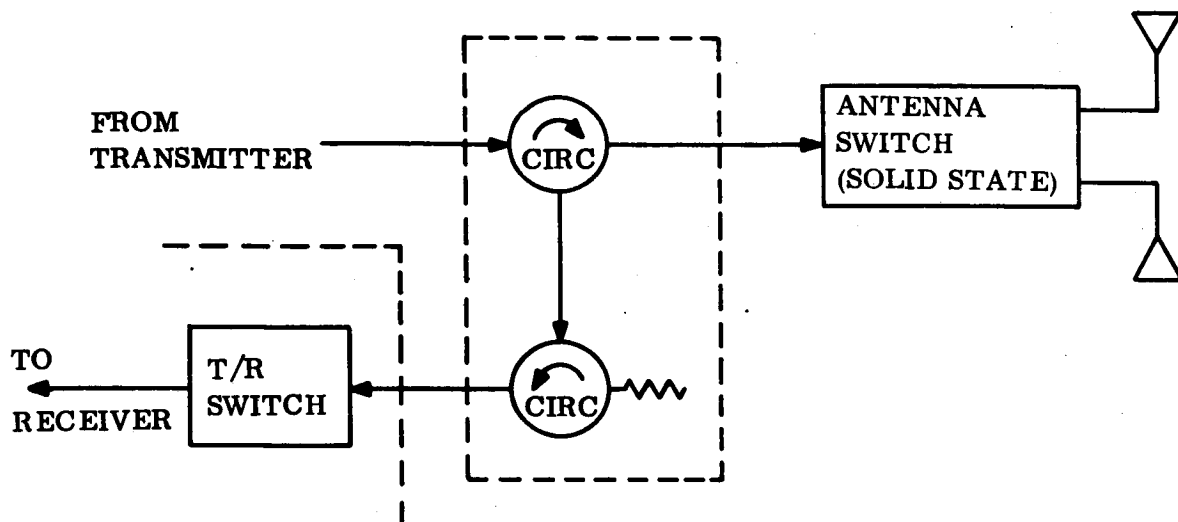


Figure 6.5.3-11. Duplexer and Antenna Selector

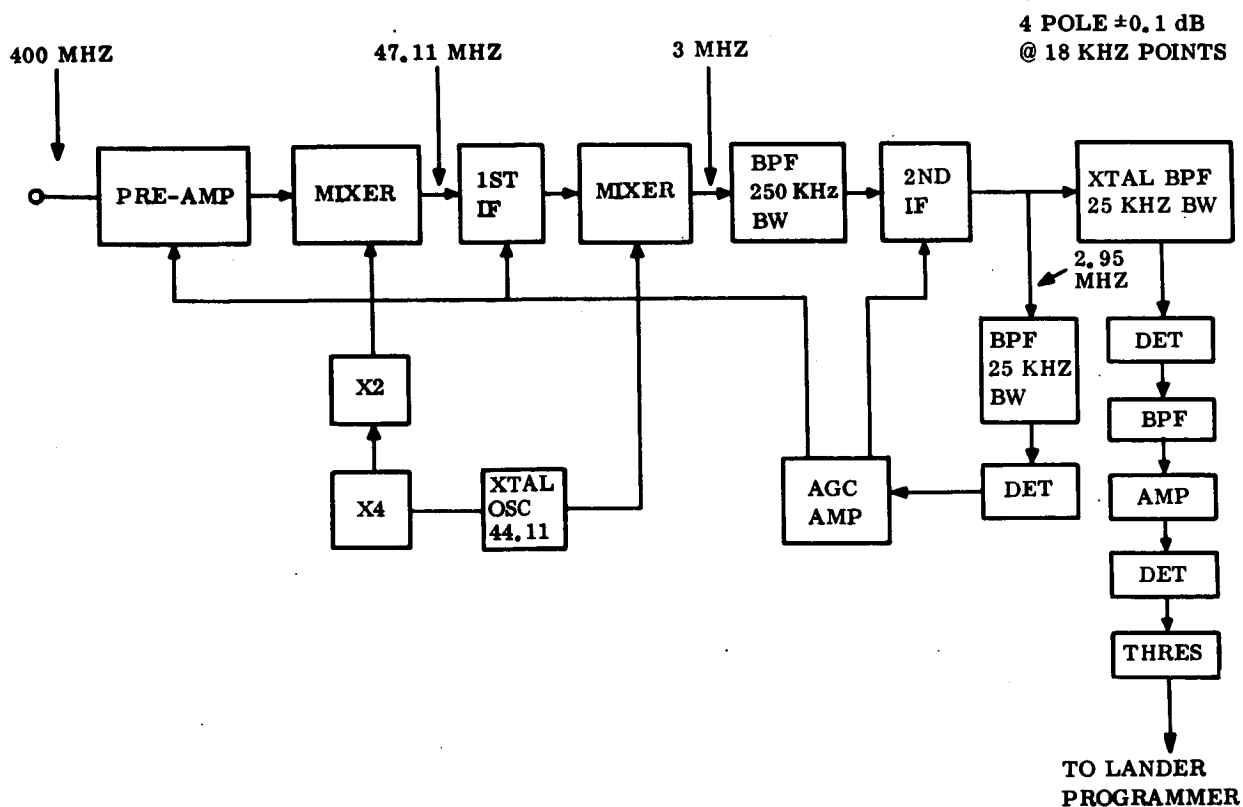


Figure 6.5.3-12. 400 MHz Receiver, Block Diagram

which follow. The signal is then filtered in a band pass filter with a noise bandwidth of 25 kHz. The filter is a 4-pole crystal filter with variations of not more than ± 0.1 dB across the 18 kHz passband. After filtering the signal is detected and the demodulated signal filtered again in a tone filter with a pass band of about 100 Hz. At this point the signal is fed to a threshold detector.

The threshold is set for a nominal signal-to-noise ratio of 3 dB in the 25 kHz bandwidth which is equivalent to 27 dB in the 100 Hz final detection bandwidth. Allowing 3 dB for modulation loss and 6 dB for detection loss leaves a signal-to-noise ratio at threshold of 18 dB with a corresponding probability of false alarm on the order of 10^{-26} , implying false alarm is essentially impossible.

In order for the receiver to provide indication of signal strength the total gain of the receiver must be stable over a wide temperature range. This is achieved from the receiver front end to the output of the second i-f by means of an AGC circuit referenced to the receiver noise generated in the receiver front end. With a high gain AGC loop it is felt that gain variations with temperature can be kept to ± 0.5 dB excluding effects of changes in the referenced noise level.

The remaining gain of the receiver which falls outside the AGC loop, that is, from the output of the second i-f to the threshold detector must be kept within ± 0.5 dB for a total receiver gain variation of ± 1 dB. This includes ripple (± 0.1 dB) in the pass band of the 25 kHz bandwidth crystal filter, changes in the detectors and threshold circuit and variations in gain of amplifiers used outside the AGC loop.

The noise figure of the receiver is 5 dB referenced to the input of a pre-selector filter at the pre-amplifier front end. Since the receiver AGC circuit is referenced to front-end receiver noise, variations in noise figure will cause the receiver gain to vary. Thus the noise figure will be required to remain constant to within ± 0.5 dB over the operating temperature range. The transistor anticipated for use in the pre-amplifier circuit is a KMC-K5001 specified at a noise figure of 1.4 dB at 400 MHz. If the noise figure of the transistor circuit is optimized at room temperature, the noise figure increased 0.4 dB at both temperature extremes. Since the optimum noise figure for this transistor is obtained with a 3:1 mis-match at the input, any temperature effects on the circuit affect the overall noise figure.

If the device noise figure changes from 1.4 to 1.8 dB, then 0.6 dB variation allowance remains for the rest of the front end circuit if the overall noise figure is to remain at a fixed value $-0, +1$ dB. This is accomplished by temperature compensating the front end circuitry and having sufficient gain at the front end to over-ride noise contributed by the following stages such as the first mixer.

The effective receiver temperature is given by:

$$T_e = (N-1)290^\circ + \frac{T_a}{L} + \left(1 - \frac{1}{L}\right) T_L$$

where N is the receiver noise figure, T_a is the antenna noise temperature, T_L is the temperature of the receiving circuit loss components, and L is the numeric loss factor (greater than one). The receiver loss is 2 dB (two circulators at 0.5 dB, one antenna switch at 0.5 dB, and 0.5 dB of cable losses). Using an antenna temperature of 70°K , a loss temperature of 200°K , and $N = 5$ dB yields

$$T_e = (3-1) 290 + \frac{70}{1.51} + \left(1 - \frac{1}{1.51}\right) 290^\circ = 724^\circ\text{K}$$

6.5.3.5.6 Orbiter 400 MHz Radio Subsystem

Fig. 6.5.3-13 shows a simplified block diagram of the 400 MHz equipment. The duplexing circuitry including the two circulators and T/R switch is identical to that in the Lander vehicle.

The beacon transmitter consists of a stable crystal oscillator operating at 25 MHz, a times 16 multiplier chain to 400 MHz, and amplifiers to achieve the desired output level. The square-wave tone oscillator 100 percent amplitude modulates the transmitter output.

The receiver, with an overall noise figure of 4 dB, is similar to the beacon receiver used on the Lander except the output detectors. The second i-f output drives the FSK demodulator having two wideband filters followed by independent opposite polarity detectors which are summed to form the Manchester coded signal.

In the Lander transmitter binary data having a NRZ format and bit rate R_b is bi-phase modulated on a square-wave subcarrier with frequency R_b to produce a Manchester coded signal; this signal modulates the frequency shift key (FSK) transmitter. The reconstructed signal (detected by the Orbiter FSK detector) is fed to the bit sync detector which generates a square-wave subcarrier at frequency R_b to convert the reconstructed signal back to the NRZ format. This signal is detected in a matched filter.

6.5.3.5.7 S-band Transponder

The transponder consists of a phase-lock receiver, and a solid-state exciter, and performs the following functions:

1. Receives and demodulates and r-f signal from the DSIF via the Lander antenna.
2. Provides coherent translation of the frequency and phase of the received signal by a 240:221 ratio for coherent two-way Doppler tracking.
3. Provides a turnaround ranging channel which demodulates the range code to baseband and conditions it for modulation on the transmitted signal.*

*The question of whether or not the link can support the ranging signal to noise ratio requirement was not considered, but the transponder has the capability to provide this function.

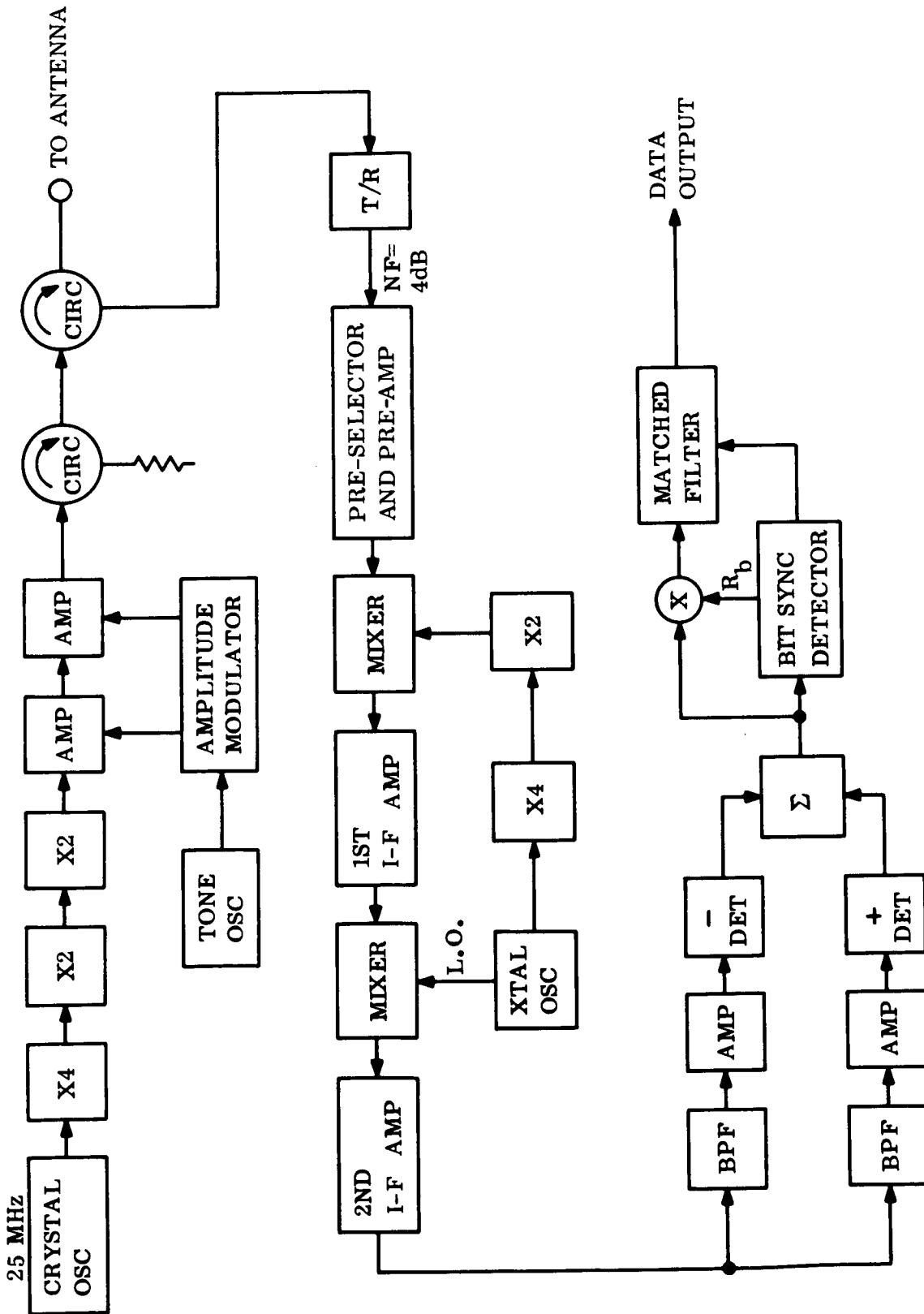


Figure 6.5.3-13. Orbiter 400 MHz Radio Subsystem

4. Generates a stable r-f carrier at a level suitable for driving the power amplifier.
5. Modulates the carrier with the telemetry (and ranging) signal.

The transponder has the same basic configuration as the Mariner C transponder; however, minor modifications directed at obtaining greater reliability and improved performance have been considered. The basic Mariner C design is selected for its proven reliability and demonstrated performance. A complete description of that design is presented in the Motorola document "Final Report, S-Band Transponder, Mark I, 20-Cycle Bandwidth" dated July 31, 1964.

A condensed description of transponder operation and brief discussion of modifications under consideration are presented in the following paragraphs. Improvements in these areas are being made in the updating of the transponder design for MM '69 by Philco. Fig. 6.3.5-14 is a block diagram of the transponder for reference during the ensuing discussion.

A. Receiver Description

The receiver is the familiar phase-lock design with a nominal noise figure of 8 dB and a carrier threshold sensitivity of -153 dBm. The characteristics are essentially those of the Mariner C receiver. The noise bandwidth of the carrier tracking loop is adaptive to the received signal level, and varies from 20 Hz at receiver threshold to 233 Hz for strong signal inputs. This provides capability for tracking high Doppler rates at strong signal strength, and preserves the narrow bandwidth desirable near threshold. The loop transfer characteristics at threshold are patterned after the mathematical model:

$$H(s) = \frac{1 + \left(\frac{3}{4\beta_L}\right) S}{1 + \left(\frac{3}{4\beta_L}\right) S + \left(\frac{9}{32\beta_L^2}\right) S^2}$$

where $2\beta_L$ is the two-sided loop noise bandwidth.

A coherent AGC system which responds only to the received carrier level provides an accurate analog of received signal strength for telemetry purposes. In addition, it serves as an indication of receiver lock, and as such, controls the selection of the signal source for the transponder exciter. When the receiver is phase-locked to a signal from DSN, the exciter derives its source from the coherent receiver voltage controlled oscillator (VCO). Alternately, when the receiver is out of lock, as indicated by the absence of receiver AGC, the exciter is automatically switched to derive its source from a stable auxiliary crystal oscillator.

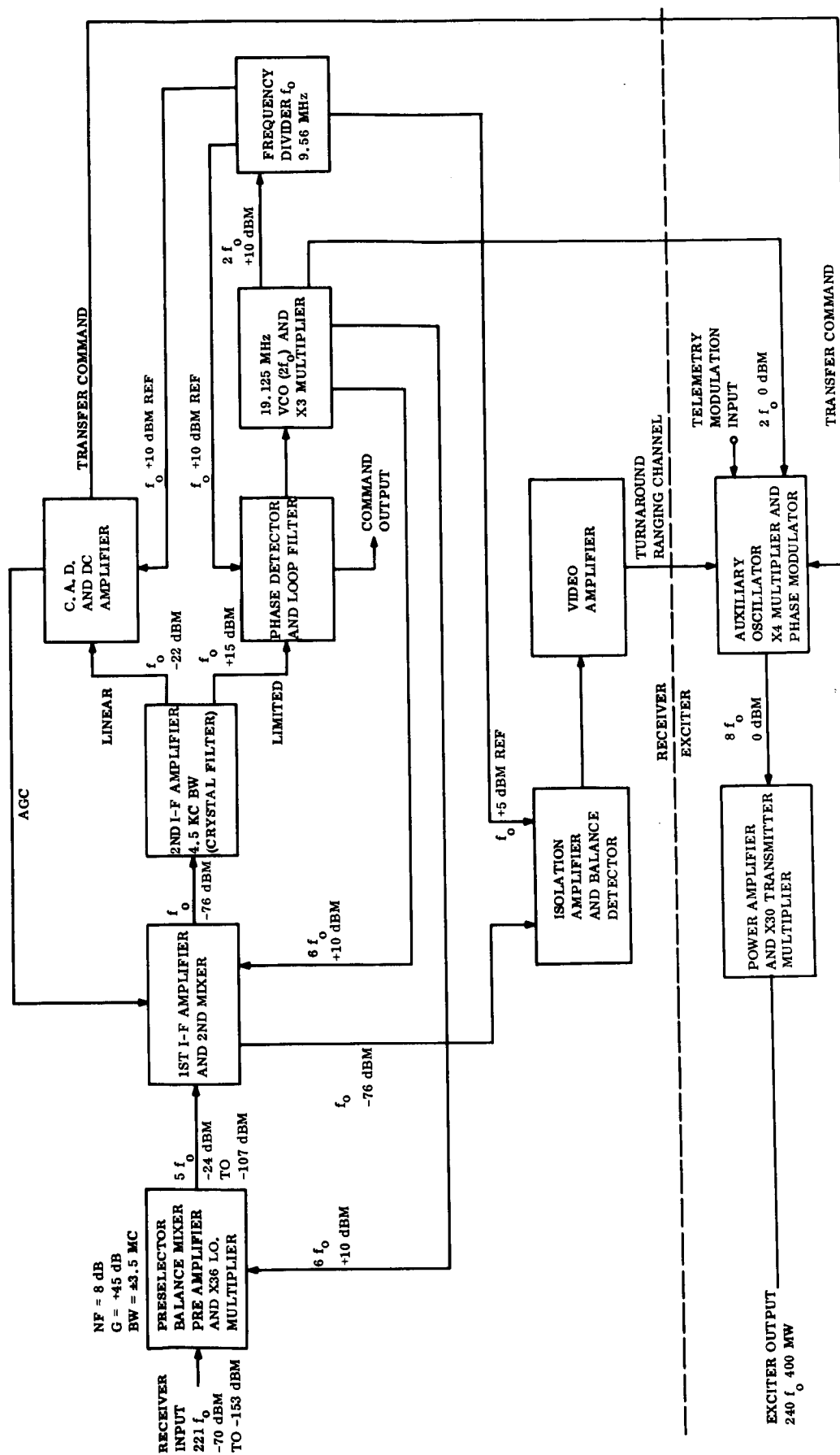


Figure 6.5.3-14. S-band Transponder, Functional Diagram

Demodulation of command information on the received signal is an auxiliary function of the phase detector in the carrier tracking loop. By virtue of the phase relationships necessary for receiver lock and the bandwidth established, the command subcarrier appears at the carrier loop error point. After suitable conditioning, this information is passed on to the command subsystem.

Because of the position of the command spectrum and the adaptive characteristic of the transponder carrier loop, some filtering of the command signal can occur when the received signal strength is high. Distortion of the command spectrum introduced by the proposed carrier loop design does not adversely affect the performance of the command subsystem. Also, analysis has shown the command spectrum will not adversely affect the transponder performance or the performance of the DSN receiver, Doppler, or ranging subsystems.

B. Receiver Modifications

The most significant modification under consideration for the receiver is the development of a low noise r-f mixer with a nominal noise figure of 8 dB. Advances in the state-of-the-art since completion of the Mariner design indicate this goal can be obtained along with a substantial improvement in reliability. The diode contacts used in the present mixer package are recognized as a weak area. The X36 local oscillator (LO) multiplier would be redesigned as part of the mixer package in a configuration which reduced LO spurious outputs.

Other minor modifications which would be made include:

1. Modification of the first i-f amplifier to extend its dynamic range and reduce its noise figure.
2. Modification of its frequency divider to eliminate potential instabilities in the current design.
3. Modification of the AGC dc amplifier to improve the temperature stability of the current design.
4. Modifications when necessary to withstand high shock environment.

C. Exciter Description

The exciter portion of the transponder generates a stable S-band modulated carrier at a level which is suitable for driving the power amplifiers. The signal source for the carrier may be either the coherent receiver VCO or the stable self-contained auxiliary crystal oscillator. Two modules, the auxiliary oscillator and the X30 multiplier, are used. The auxiliary oscillator module contains the alternate crystal oscillator, an X4 multiplier, and the exciter phase modulator. The modulator accepts pre-conditioned telemetry and ranging signals and modulates them on the carrier at indices up to 4.0 radians peak when converted to S-band. The modulator bandwidth extends from dc to 2 MHz. The X30 multiplier module amplifies the modulated signal and multiplies it by a factor of 30 to provide the S-band output.

D. Exciter Modifications

The development of a new X30 multiplier for the exciter is considered essential. The current design exhibits excessive nonharmonic spurious outputs under certain conditions of temperature and supply voltage. These spurious outputs can cause false lock when the turnaround ranging channel is open. An alternate approach which does not exhibit these instabilities has been under development at Motorola for some time. Its operation is essentially as follows.

The X30 multiplier is required to convert a 0 dBm signal at 76.5 MHz to a 26 dBm signal at 2295 MHz. Fig. 6.5.3-15 is a block diagram of the alternate design being considered. The input signal is coupled through an isolation amplifier to an X3 varactor multiplier chain. The varactor multiplier chain requires a nominal input of 2 watts at 153 MHz to produce 0.5 watt of output power at 2295 MHz. The X5 varactor multiplier is a lumped constant circuit with a 3-section helical resonator filter at the output. The X3 varactor multiplier is a distributed constant, strip transmission line circuit which contains a three-section interdigital bandpass output filter. The basic configuration has been successfully employed in the LEM transponder to produce 1.4 watts at S-band, and the Apollo Block II transponder to deliver 0.6 watt. A similar design produces 0.2 watt in the FM transmitter of the Apollo Block II system. This design has demonstrated reliable, stable, and efficient operation over extended temperature ranges. A 3 dB bandwidth of 90 MHz at the output frequency is being realized on the Apollo hardware with a dc to r-f efficiency of nearly 15 percent.

All spurious harmonic outputs are down 60 dB at the transmitter output terminals with no evidence of the parametric instabilities which can cause "ring-around" or "false-lock" problems in the transponder.

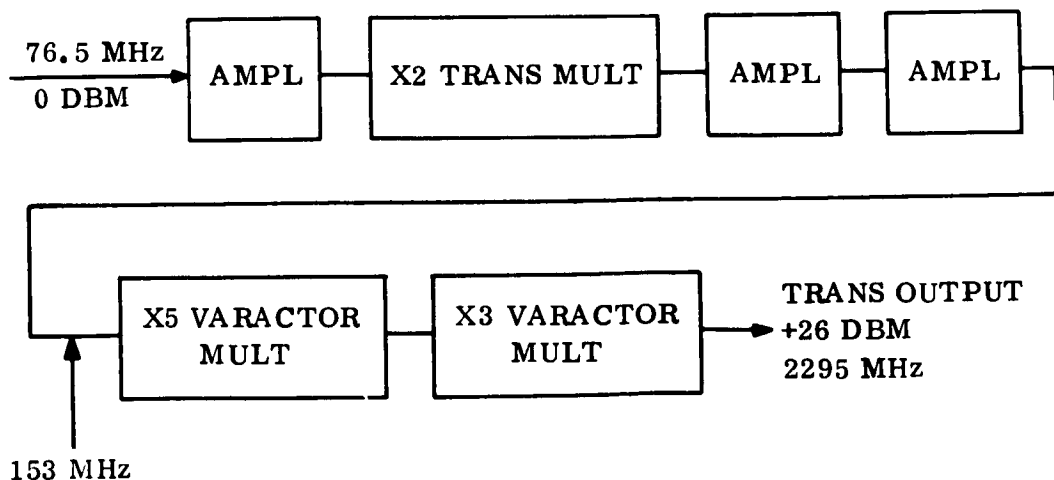


Figure 6.5.3-15. X30 Module of the Transmitter Exciter, Block Diagram

Additional modifications to the exciter would include changes in the auxiliary oscillator module to obtain improved oscillator stability and to reduce the variations in sensitivity of the phase modulator. This transponder module has already been redesigned for the Lunar Orbiter transponder and the improvement verified. The development of low noise oscillators for both the auxiliary oscillator and the VCO is also planned. These oscillators would allow the use of narrower tracking bandwidths in both ground and flight receivers. Performance parameters of the receiver and exciter are listed in tables 6.5.3-9 and -10.

E. S-band Power Amplifier

The power amplifier consists of a TWT/power supply package designed by Watkins Johnson/JPL for high shock environment. This high impact tube was shock tested at 9600 g's for 0.5 msec duration.

F. Advantages of the TWT

1. The most significant argument in favor of the TWT over other power amplifiers is the fact that it is presently being used in nearly all the major space programs and has been flight proven. It shows a MTBF in excess of 50,000 hours which enhances the reliability of the telecommunication system.
2. The TWT has a nominal gain of 30 dB which eliminates the requirement for high output powers from the exciter.
3. The efficiency of a TWT is greater than 40 percent at the present and is being continually improved. Efficiencies higher than 45 percent now appear feasible.
4. The TWT is essentially a wideband device; i.e., at S-band frequencies, bandwidths well in excess of 10 mc are possible. This provides good phase linearity over the bandwidth needed for turnaround ranging.
5. The physical size and weight of the TWT lend the device to high density packaging. The sizes of present devices are being reduced to the extent that the dimensions of an overall power amplifier package are determined by the size of the power supply and not the device.
6. The TWT is capable of stable operation at elevated temperatures which might occur in the absence of r-f drive. Without r-f drive all the dc power is dissipated through the collector.

G. Disadvantages of the TWT

1. Of most concern to the radio subsystem is the noise generated by the tube. Since the TWT has a wideband circuit, it generates noise at the receiver frequency. This is troublesome in diplexed configurations as the noise from the TWT degrades the equivalent noise figure of the receiver connected to the diplexer. Therefore, to use the TWT a filter must attenuate this noise to a sufficiently low level.

TABLE 6.5.3-9. RECEIVER PERFORMANCE PARAMETERS

Parameter	Value
Center frequency	2113 MHz nominal (see Section 3.2.1)
Noise figure	8 dB \pm 1 dB
Strong signal carrier tracking bandwidth	233 cps ($2\beta_{LSS}$)
Threshold carrier tracking bandwidth	20 cps ($2\beta_{Lo}$)
Threshold sensitivity	-153 dBm \pm 1 dB
Dynamic range	-70 dBm to threshold
Tracking range	± 3.0 parts in 10^5 (for r-f signals > -120 dBm)
Carrier tracking loop threshold transfer function (model)	$H_{(s)} = 1 + \left(\frac{3}{4\beta_{Lo}} \right) S$
Carrier tracking loop pre-detection filter bandwidth	4.5 kHz $1 + \left(\frac{3}{4\beta_{Lo}} \right) S + \left(\frac{9}{32\beta_{Lo}^2} \right) S^2$
AGC loop bandwidth	0.33 Hz to 0.83 Hz
Ranging channel i-f bandwidth (3 dB)	3.3 MHz
Video limiter rise and fall time	70 nsec
Ranging channel video bandwidth (3 dB)	100 Hz to 2 MHz
Input VSWR	1.3:1 maximum

TABLE 6.5.3-10. EXCITER PERFORMANCE PARAMETERS

Parameter	Value
Output frequency	2295 MHz nominal (see Section 3.2.3)
Output power	+26 dBm \pm 0.5 dB
Output VSWR	1.3:1 maximum
Auxiliary oscillator frequency stability	1 part in 10^5 per year
Phase stability	Residual PM less than 9 deg peak in a 20 Hz phase coherent receiver
PM modulator dynamic range	0 to 4 radians peak
PM modulator linearity	Within \pm 7 percent of straight line
PM modulator sensitivity	1 radian per volt \pm 2 percent
PM modulator bandwidth	0.5 dB BW dc to 1 MHz 3.0 dB BW 1.8 MHz min
PM modulator input impedance	1000 ohms resistive

2. To minimize the external magnetic field of the TWT, complicated field balancing techniques are required to cancel the effects of the beam-forming magnetic field along the full length of the tube.

6.5.3.5.8 Data Handling System

A. Functions

The data handling and storage subsystem provides encoding, time multiplexing, sequencing information and storage of the Capsule's engineering and science data, and storage and execution of on-board command functions. The data handling and storage subsystem controls the programmer, data collection, formatting, and data transmission as a function of the mission phase from interplanetary cruise through post impact operations. The subsystem also detects the composite command baseband from the receiver and stores these commands or transfers them to the programmer.

B. Summary Description

The functional block diagram of the data handling subsystem is presented in fig. 6.5.3-16. All analog signals (0-5v) are multiplexed by the analog gates. The formatting of the data is determined by the data handling unit. The fixed formats are selected, as a function of mission phase, by a mode select command from the random access memory.

The A-to-D encoders sample the analog signals and perform the digital conversion many times faster than the word rate. Using the fast conversion and a nine bit ADC, the transmitted number of conversion bits per scientific data source can be made nine bits or less depending on the source's accuracy requirements. The engineering signals are encoded to 7 bits.

Multicoder - The multicoder will have four modes of operation, each controlled by the data handling unit pulse lasting the duration of each mode. The number of data channels per mode are defined below: All analog inputs are high level (0 to +5 VDC).

1. Entry Mode

- a. 60 analog inputs, 9 bit resolution, 1 sample/sec
- b. 3 analog inputs, 9 bit resolution, 3 samples/sec
- c. 50 digital groups, 8 bit parallel occurring in 50 serial words on command from the multicoder at the rate of 5 groups/sec
- d. 2 digital words, 7 bit parallel, 1 sample/10 sec
- e. 1 digital word, 11 bit parallel occurring in two words, 1 sample/10 sec

2. Landed Mode No. 1

- a. 58 analog inputs, 7 bit resolution, 1 sample/20 min
- b. 6 digital words, 11 bit parallel, 2 lines, 3 words/line. 1 sample/20 min
- c. 1 digital word, 11 bit parallel, 1 sample/20 min
- d. 130 digital words, 14 bit parallel sequential on multicoder command, 1 sample/20 min
- e. 130 digital words, 11 bit parallel sequential on multicoder command, 1 sample/20 min

Figure 6.5.3-16. Data Handling System

- f. 3 digital words, 7 bit parallel sequential on multicoder command, 1 sample/20 min
- g. 2 digital words, 7 bit parallel, 1 sample/20 min
- 3. Landed Mode No. 2
 - a. 14 analog inputs, 7 bit resolution, 1 sample/20 min
 - b. digital inputs, b, c, and g of Landed Mode No. 1
- 4. Landed Mode No. 3
 - a. One of four TV inputs, 6 bit resolution, 27,000 sps (160,000 bps).

Data Handling Unit - The data handling unit (DHU) accepts commands from the command storage control unit to determine in which mode the multicoder will operate, fig. 6.5.3-16. It decodes these commands and controls the multicoder functions by supplying pulses on one of four mode lines. The data from the multicoder is routed by the DHU either to the random access memory unit to the VHF transmitter or to the S-band transmitter. During entry, data from the multicoder is interleaved with delayed data from the random access memory unit.

The DHU also conditions the signals from the multicoder and memory going to the transmitters.

Commands from the Spacecraft via hardwire are routed through the DHU to the command storage unit and then to the memory.

Random Access Memory Unit - The random access memory unit (RAMU) is used to provide storage for digital words from the multicoder (7 bits/length) and to store command words (21 bits length).

The telemetry storage has two modes:

- 1. Store data serially and read out serially 70 sec later.
- 2. Store data and read out at a fixed rate at some later time.

Both of these modes are used in entry data collection as shown in fig. 6.5.3-19. Mod 2 is also used for collection of landed serial and engineering data and playback during Orbiter passes.

Data will be inputted and outputted in a 21 bit format. Read out will be destructive with a restore mode option for Mod 1 as required.

Command Storage Unit - The command storage unit (CSU) (part of the DHU) accepts commands from the Spacecraft via hardwire and from the command detector. The commands and time labels are stored in the memory. The unit examines sequentially each command location in the memory. It does pass a command time word until that time agrees with the vehicle clock time. When agreement occurs it jumps to the next location which should be a command and outputs it to the Lander Programmer (see para 4.5.4.2).

The commands in the memory can also control the sequence of examination of the CSU. Thus, a fixed sequence of operations can be addressed by commanding the CSU to that memory location. At the end of this sequence (e.g., data gathering) a command would be present which would send the CSU back to the memory location following the jump command. By using auxiliary registers (part of the random access memory) and decoding functions to control the CSU, the CSU became a versatile general purpose program machine.

For a mission of 24 hr with experiments requiring data gathering every 20 min, 3 hr and 6 hr, the specific actions at each sampling time need be stored only once with time increment and return commands at the end of these sequences.

The timing signals for the CSU are provided by the Lander programmer.

The actions on the vehicle can be controlled by the parallel output from the command storage control unit. The unit scans the memory and executes the commands stored therein when the time of the commands agrees with the vehicle time. This is shown in fig. 6.5.3-17.

The presence of a lock signal from the command detector causes the command storage control unit to cease sequential search of the memory and accept command sub bits. The command words as shown in fig. 6.5.3-18 include a 6 sub-bit preamble which is used for word sync purposes. The 6 sub-bit sequence is 111,000; it is impossible for this sequence to occur in any other place without at least two errors. The command storage control unit checks the command bits after conversion from sub-bits for parity, if parity checks, the word is stored or executed and the word is transmitted to Earth via the direct link. If parity does not check, a unique 21 bit word is transmitted to Earth and nothing is stored.

The command detector, the command storage control unit, and the random access memory comprise the command group of the data handling subsystem. The command detector accepts the modulated subcarrier signals from the transponder, determines sub-bit sync and sub-bit values which are inputted to the command storage control unit. The command storage control unit (if a real time command is decoded) outputs a parallel word of 8 bits to the programmer or stores the word (if a stored program command is decoded) in the random access memory unit.

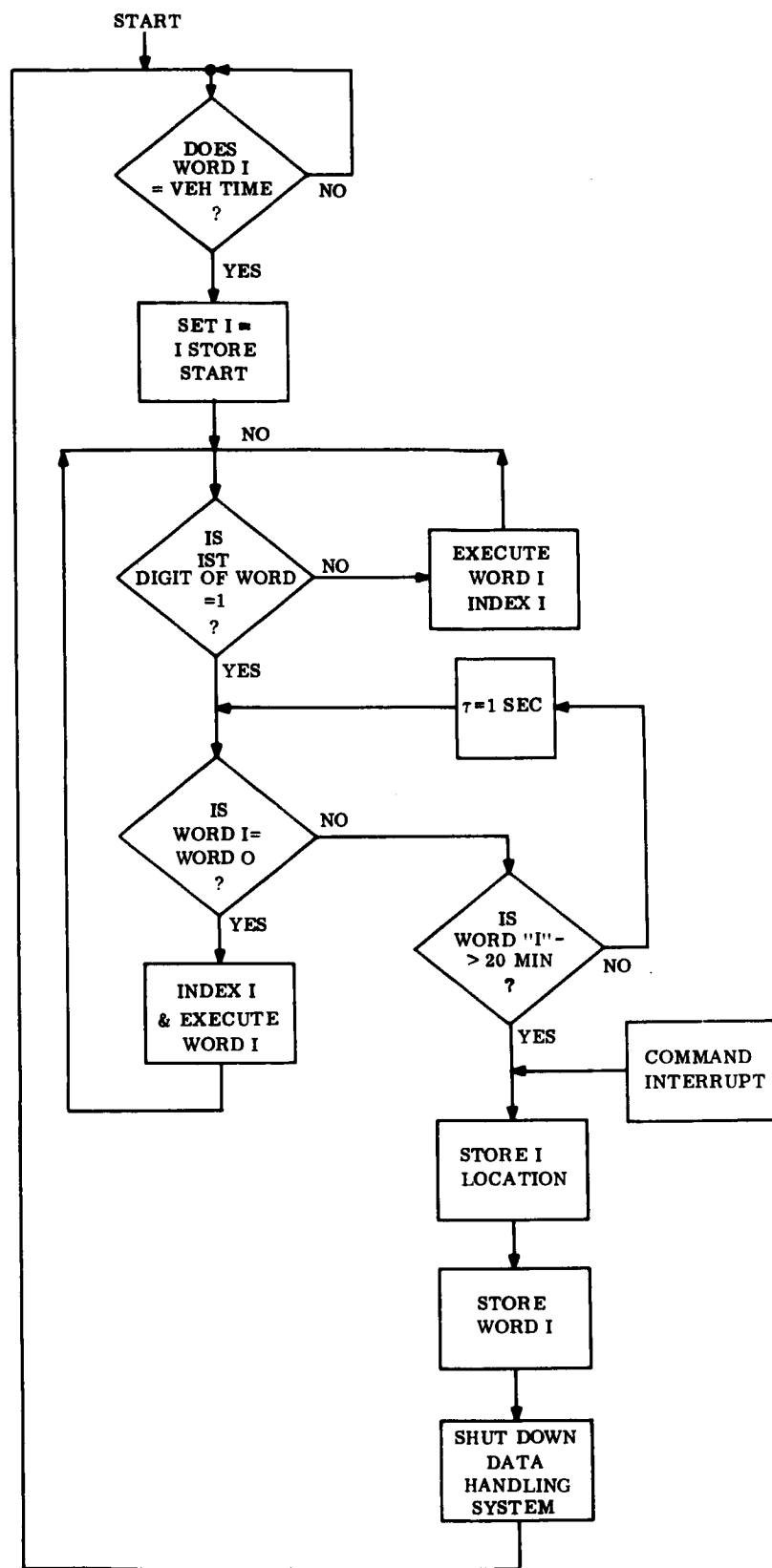


Figure 6.5.3-17. Operation of Command Storage Control Unit

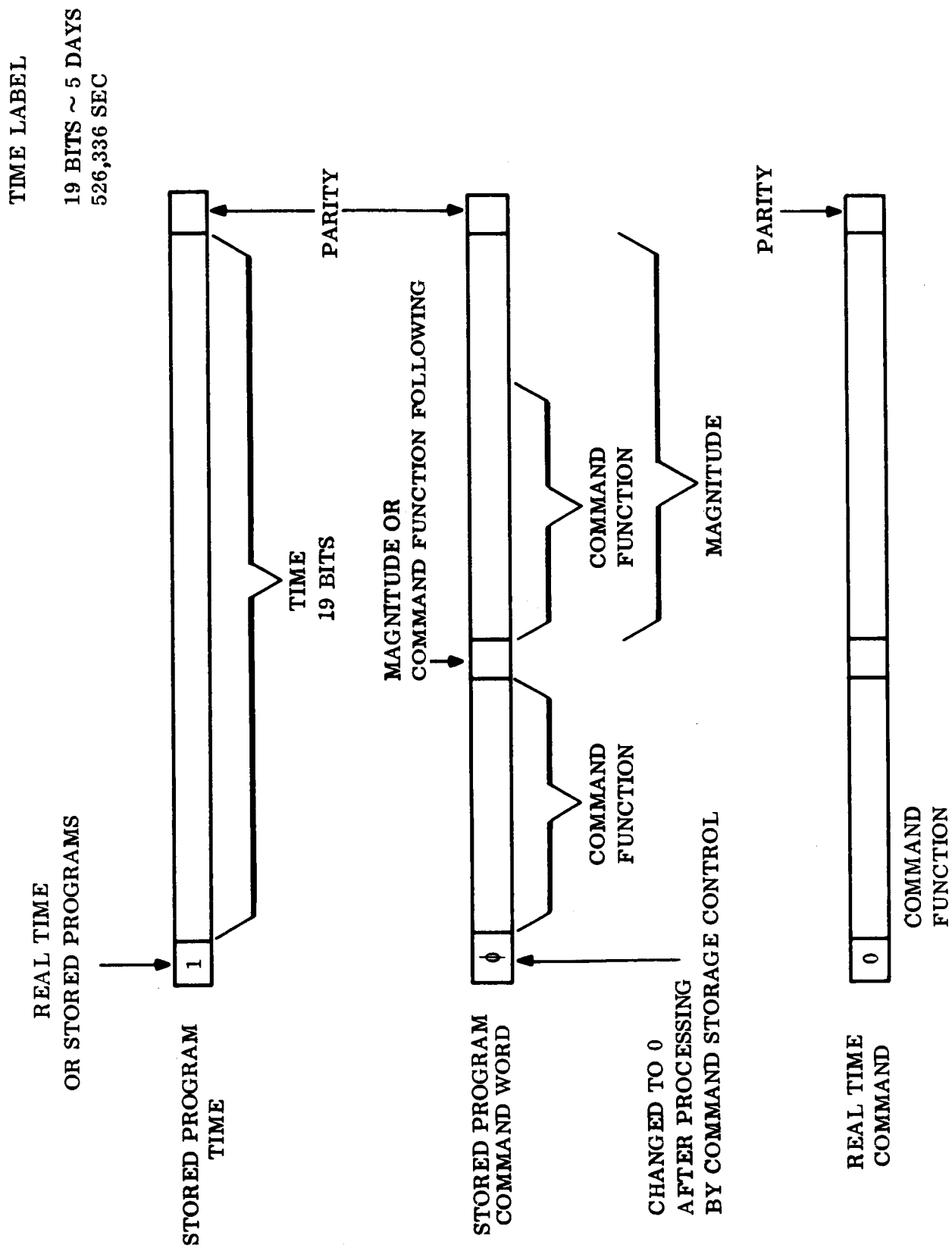


Figure 6.5.3-18. Command Word Format

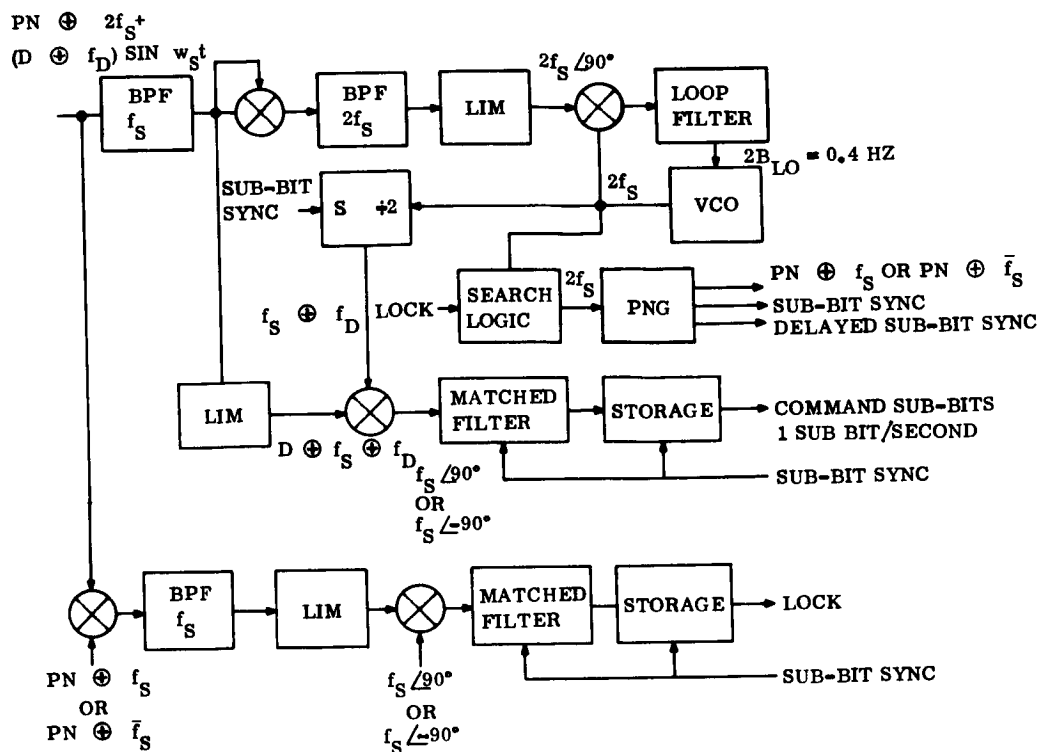


Figure 6.5.3-19. Command Detector, Block Diagram

A block diagram of the command detector is shown in fig. 6.5.3-19. Note that the output of the command detector is sub-bits, each command bit being composed of two sub-bits. When the execute word is received that word is decoded. If it is a RT command it is shifted out to the programmer. If it is an SP command it is stored in the memory (usually in a location given by a previous RT command).

This subsystem will be shut down to conserve power when the time between commands is more than one hour. A separate set of registers will be used to store the time at which the data handling system shall begin functioning and also the memory location of the next command. The flow chart in fig. 6.5.3-17 shows how the command storage unit checks the time until next command execute and shuts the system down until this time is reached on the vehicle clock.

C. Data Handling Versus Mission Phase

Interplanetary Cruise - The Capsule's data handling equipment is assumed deenergized during interplanetary cruise. Monitoring of thermal control and the Capsule's electrical power subsystem is performed by the Spacecraft's data handling subsystem.

Capsule Checkout - The Capsule checkout mode is initiated sufficiently prior to separation to determine the status of the Capsule and its payload and to allow for corrective action. Under control of the programmer and command storage unit, Capsule checkout is accomplished with data being transferred to the Spacecraft via hardware.

Capsule Separation and Engine Fire - From Capsule separation to engine fire (approximately 20 min), the Capsule is transmitting at 1090 bps. Only engineering data is monitored. The received data on the Spacecraft is detected and stored for delayed transmission to Earth over the high data rate link.

Capsule Cruise - Capsule cruise lasts for approximately 24 hr for the direct entry delivery mode. During this period the data handling subsystem will be dormant except for two registers which will store the time of entry and the memory location at which to resume sequence at this time.

Capsule Entry - Upon initiation of entry (g-switch or timer) data transmission is resumed at 1090 bps composed of 544-2/3 bps real time and 544-2/3 bps delayed. The entry data rate requirements are shown in table 6.5.3-11. A rate of 350 bps is assumed for engineering data. The data is stored in the random access memory at a 544-2/3 bps rate. Essentially, the memory will act in two modes; one as a delay line with a 70 sec delay, and two, as a memory in which 100 k bits of entry data are stored. Each word in the memory is 7 bits. The operation of the random access memory during entry is shown in fig. 6.5.3-20.

Post Impact Relay - Upon impact the buffer readout is temporarily halted. The buffer will contain 100 kbits of entry data. Engineering data is read out at 190 bps until completion of the set up period. Upon completion of the set-up period, the imaging data collection and transmission begins. The low and high resolution frames are alternated, allowing time for one of the cameras to be turned while the other camera is readout. The landed measurement requirements are given in table 6.5.3-12.

Landed Operations - The picture taking operation performed after impact is repeated one Martian day later when the Orbiter is in view. Camera operation can be repeated in later days by commanding such activity from Earth.

Data for the first several days will be collected on a twenty minute period with the data collection routine loaded into the memory, controlling these actions. For direct link operation 6.4 kbits science and 3.1 kbits engineering data will be collected each day. This data will be read out by command (RT or SP) each day when the Earth is within the transmitting antenna beamwidth.

If the relay link is used, 34.6 kbits of science and 26.3 kbits of engineering data will be accumulated and transmitted.

To conserve power and extend the life of the Lander, the system can be shut down except for the two registers, clock and time comparison circuitry which requires 1/4 watt. During this time (~5 days), no transmission or data gathering functions will be performed.

TABLE 6.5.3-11 ENTRY DATA

Sensor	Accuracy (%)	Sampling Rate (sps)	Bits/Sample	No. of Channels	BPS	Time
Pressure transducer (2) 0 -0.3 psia	1	1	9	2	18	Post parachute deployment
Resistance thermometer (2) 100° - 300° K	0.2	1	9	2	18	
Mass spectrometer (readout 8 bits at a time)	---	N/A	8	N/A	40	1 hr before entry to impact
Triaxial accelerometer (dual scale)	1	3	8	3	72	1 hr before entry to impact
Stagnation temperature	0.25	1	9	1	9	1 hr before entry to impact
Stagnation pressure (4)	0.25	1	9	4	36	1 hr before entry to impact
Water vapor	N/A	1/15	7 (parallel)	2	14/15	1 hr before entry to impact
		1/15	11 (parallel)	1	11/15	1 hr before entry to impact
Engineering measurement	---	1	7	50	350	

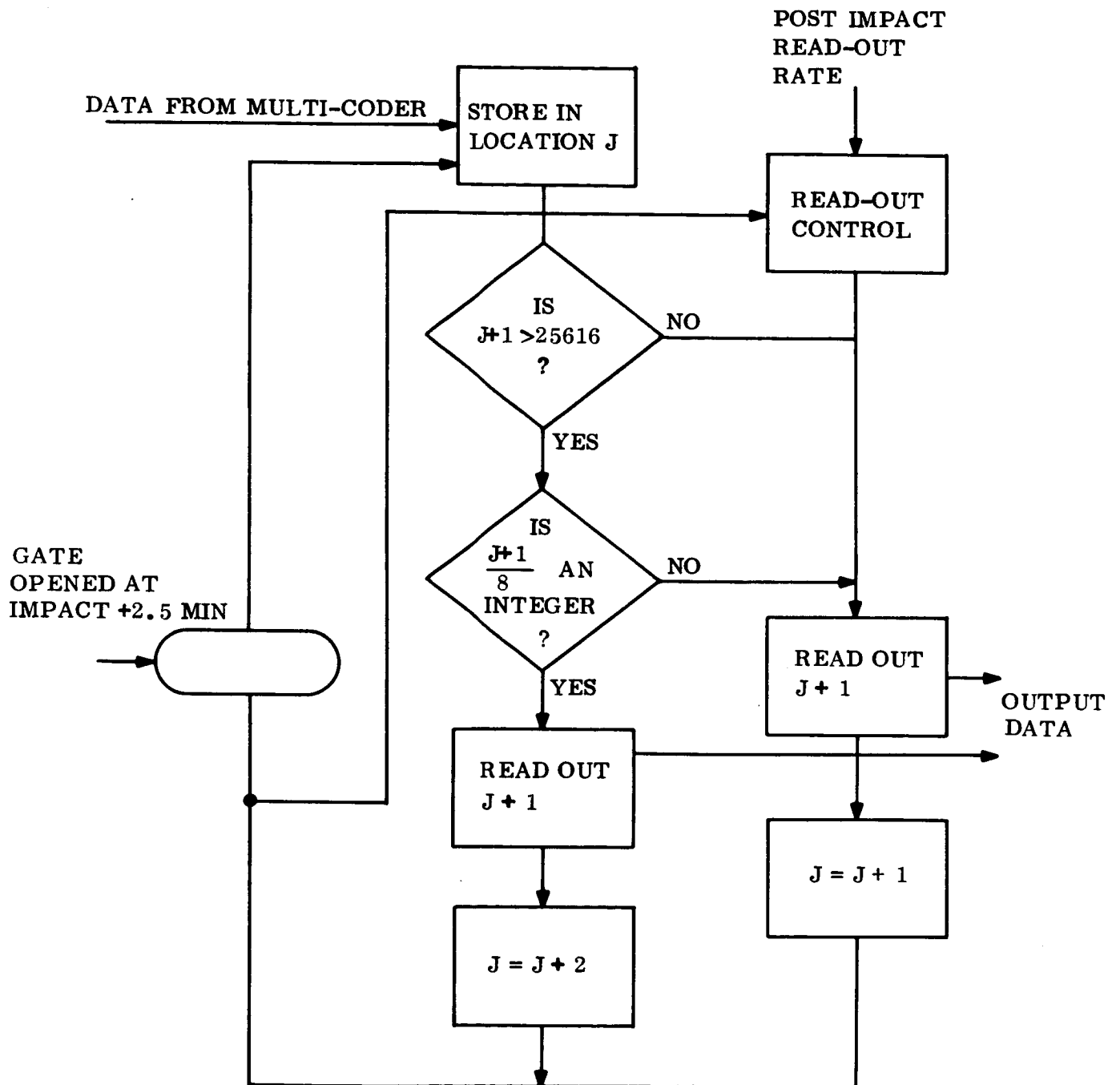


Figure 6.5.3-20. Entry Data Storage Routine

TABLE 6.5.3-12. LANDED SCIENCE (NON-IMAGING)

Sensor	Accuracy	Sampling Rate	Bits/Sample	No. of Channels/Sensor	No. of bits/hr
Pressure transducer (2)	1%	1/ hr* 3/ hr**	6	2	36* 12**
Thermometer (4)	1%	1/ hr* 3/ hr**	6	2	72* 24**
Wind velocity (2)	3%	1/ hr* 3/ hr**	11 (parallel)	6	66* 22**
Moisture	--	1/ hr* 3/ hr**	7 (parallel)	2	75* 25**
			11 (parallel)	1	
Surface composition	Less than 256 counts per energy slot in 3 hr	1/3 hr	14(P) 12(P) 7(P)	130 130 3	1133*
Clinometer (2)	1%	1/6 hr	7(P)	2	14/6
Engineering measurements	--	3/ hr*	7	50	1050*
--	--	1/ hr** 3/ hr*	7	6	42** 126*

*Relay Mode

**Direct Link Mode

6.5.3.5.9 Physical Characteristics

Table 6.5.3-13 summarizes the physical characteristics of telecommunications equipments. The key to development status is:

1. No modification required (off-the-shelf)
2. Modify (e.g., for high shock)
3. Redesign (basic equipment exists but redesign for new frequency, detection technique, etc.)
4. New design (specify new design using established techniques)
5. New development (employs near-future state-of-the-art techniques)

TABLE 6.5.3-13. PHYSICAL CHARACTERISTICS

Component and Quantity	Size (in.)	Weight (Based on 1000 g's) (lb)	Power	Sterilizable (125°C)	Max Shock (present information)	Development Status	Remarks
UHF Transmitter	30 in. ³ 1.5 x 4 x 5	2.5	150 w	yes		4	
UHF Antenna (2)	8 dia. x 2	1	-	yes		4	2 required 1 will be used
UHF Circulators (2)	6 in. ³ 2.5 x 2.5 x 1	0.4	-	yes		3	2 required in close proximity
UHF Antenna Switch	1.1 in. ³ 2 x 1.5 x 0.375	1.0	0.25A @ 3.5 V and 10 micro- A @ 28V	yes	3000 g's, 3 ms	1	Interchange voltages to switch antenna - Power during xmit and receiver
Beacon Receiver and T/R Switch	21 in. ³ 5.4 x 3.6 x 1.1	1.3	0.5 watts and 0.06A @ 1.2V	yes		4	0.06A @ 1.2V required during 400 MHz transmit periods
Multicoder	104 in. ³ 3.5 x 4.3 x 7	5	15 watts	yes		3	Power required during data sampling periods only (see text)
Data Handling Unit	100 in. ³ 4 x 5 x 5	4	3 w	yes		4	
Thin Film Memory	88 in. ³ 4 x 4 x 5.5	5	6 w	yes		4	180000 bit capacity, random access
Signal Conditioner	4 x 5 x 7	4	8 w	yes		2	50 channels only
Three Axis Impact Accelerometer	1.3 x 1.3 x 0.8	0.6		yes	10,000 g's	1	
Charge Amplifier (3)	1.25 x 2 x 3	0.5	1.2 w ea.	yes	representative unit passed 2000 g test	1	2 required connected to in accelerometer by coax cables
S-Band P/A	300 in. ³ 10 x 12 x 2.5	7	89 w	yes	9600 g's	2	
S-Band Antenna, receive (2)	4 dia. x 4	0.2	-	yes		4	2 required - 1 used
S-Band Antenna, trans (2)	8 dia x 3	0.5	-	yes			
S-Band Latching Circulator (2)	2 x 2.5 x 1.25	0.7	pulse 2A, 28V, 1ms	yes	3000 g's for 3 ms	3	must be vertically oriented pulse to switch antennas
Transponder: Exciter Receiver	700 in. ³	22	15 w 12 w	yes		2	
Command Decoder	153 in. ³	5	2 w	yes		2	

6.5.4 ELECTRICAL POWER EQUIPMENT

The power equipment provides electrical energy, power switching, charge control, voltage control and electrical distribution. Fig. 6.5.4-1 illustrates this equipment. Note that the electrical energy flow, power, signals and data which takes place between subsystems is shown in the Functional Block Diagram, Section 6.2.4.

6.5.4.1 Operation

Commands are received via hardwire connection to OSE for post sterilization check, via hardwire from the spacecraft through the telecommunications subsystem during interplanetary cruise and from the telecommunications subsystem after landing. These commands enter the programmer as a 21-bit word where they are decoded into operation signals for the relays which switch the power feeder lines. The programmer also contains a multichannel hardwire program section which provides an additional independent operation of the spin, de-boost, and landing sequences for mission assurance. These programs have programmable start times and, once initiated, proceed with the execution of a fixed program sequence. A single command, regardless of origin, may signal the operation of either a single load or a group of loads as required.

All operation signals from the programmer go to the power controller where power switching takes place. The components which require independent switching, such as the payload scientific instruments, have separate electrical power feeders. Other components which are always used as a group, such as the engineering diagnostic instrumentation, share a single feeder. The power controller can accept energy from the operational battery, from the high rate batteries, from the spacecraft or from ground power, and switch this power to the appropriate load or loads. The line contactor is used to select and control which of these power sources supplies the power controller.

The operational battery supplemented by the pre-entry battery during coast, provides all Lander electrical energy except the high rate pyrotechnic and hot-wire initiations. This secondary silver-zinc battery is charged from raw spacecraft power prior to separation. Power from the operational battery feeds the unregulated loads directly. This battery is equipped with extra cells and semiconductor bypass for redundancy.

6.5.4.1.1 Battery Redundancy Considerations

To enhance reliability three alternatives have been investigated.

If two batteries were flown, each capable of providing the minimum mission duration objectives, a considerable weight penalty would be suffered. An alternative route would be to provide two batteries which would each provide half the desired output. This method would increase the battery weight, about 25 percent, because of the lower power to weight ratios of smaller batteries, and ensure that half the mission objective would be achieved.

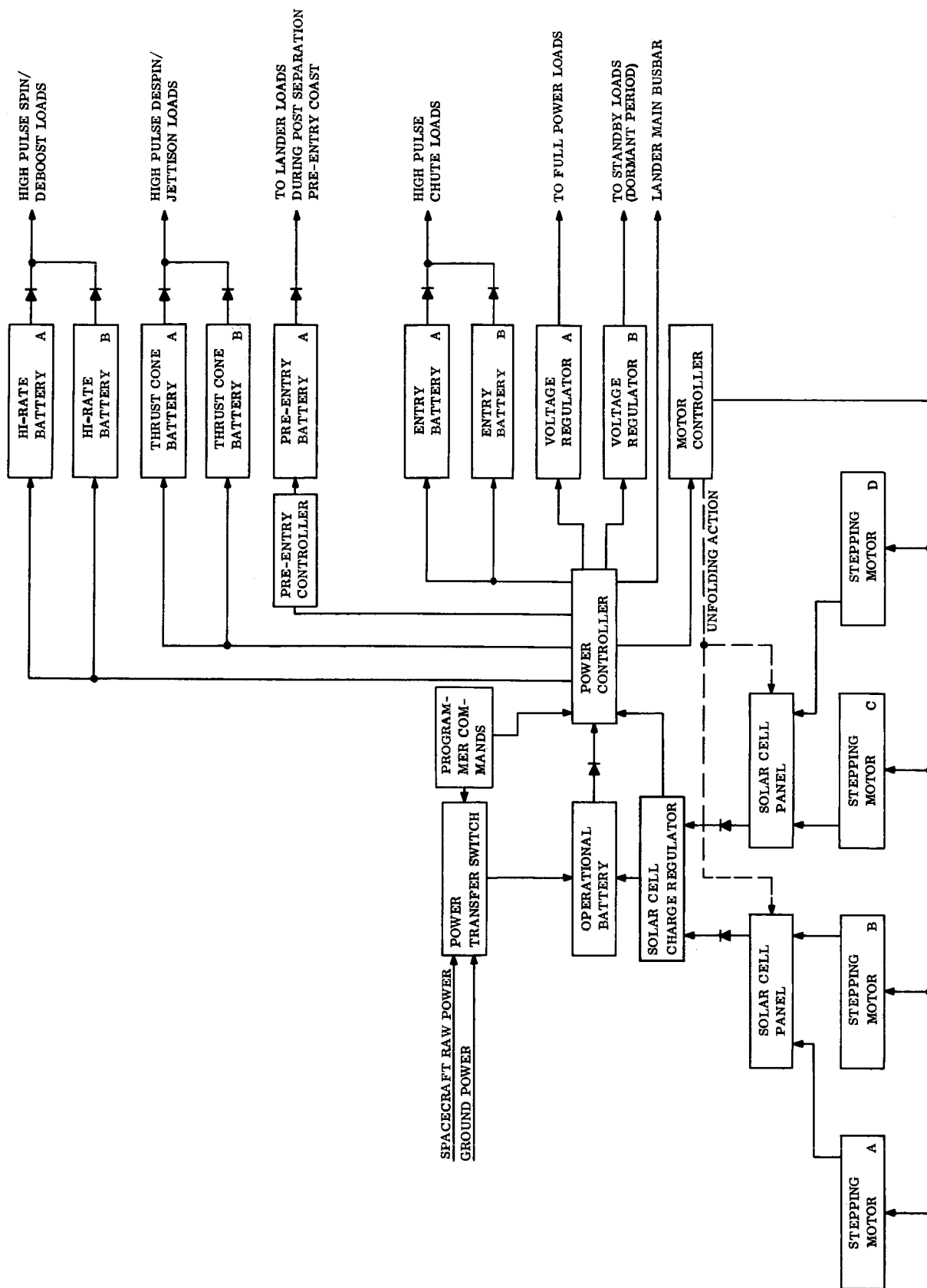


Figure 6.5.4-1. Electrical Power Subsystem Block Diagram Point Design 4

The method adopted to provide adequate redundancy is to carry redundant cells. The logic in this approach is that it is usual if failure should occur for only one or at most two cells to fail. If these can be replaced by reserve cells considerable savings will result.

The circuit shown in fig. 6.5.4-2 incorporates diodes on the charging side having a tightly controlled Zener regulating level, e.g., 2.05 volts, and very low dynamic impedance. The diode on the discharge side of the circuit has a low forward voltage. Three redundant cells in the battery are connected through the controller to be added in series when needed as directed by the programmer.

If, during charge, a cell fails open circuit or high resistance, the Zener voltage of that cell will be exceeded and the cell will be bypassed. If the cell fails short circuit or low resistance then the cell will carry the charge current. A slight loss may result in charging a bad cell. Because each Zener protective voltage level will be equal to its cutoff voltage, the arrangement gives added protection against overcharging.

If a cell fails on discharge, the diode in the discharge circuit will conduct and bypass the failed cell, avoiding driving the cell negative. Whichever way the cell fails it will always be bypassed.

Switching in new cells through the controller is achieved by low voltage sensing in the programmer. The low voltage is caused by the loss of a cell plus the diode drop as it switches in. Two cells would therefore be switched in for the first cell failure to compensate for diode voltage drop. A nominally higher voltage than the original battery would then result. If a second cell failed only one other cell would be switched.

A redundant system has been provided which allows for the failure of two cells in a battery. The additional weight approximates 20 percent of the original battery. This includes cells, diodes, programmer and controller modifications.

The need for high current capability during initiation operations is met by three pair of thermal batteries. These provide power for spin/de-boost operations, despin/entry operation and parachute/aeroshell operations. In each case two batteries are available for redundancy. The batteries are activated separately from the canister or operational battery and the output is switched to the initiators via the power controller. These activation circuits are equipped with thermal relays to protect the operational battery.

During the extended mission electrical energy is obtained via the conversion of solar energy through photovoltaic semiconductor arrays. These solar cell panels are stored under tension to provide shock hardening and are unfolded as described in Section 6.5.6 for use after the completion of a days photo imagery. During illumination, the solar array powers the loads and recharges the secondary silver-zinc battery used during entry and prior to solar cell deployment. Since the battery is large, as required to meet the first few days operating requirements, a high charging efficiency results.

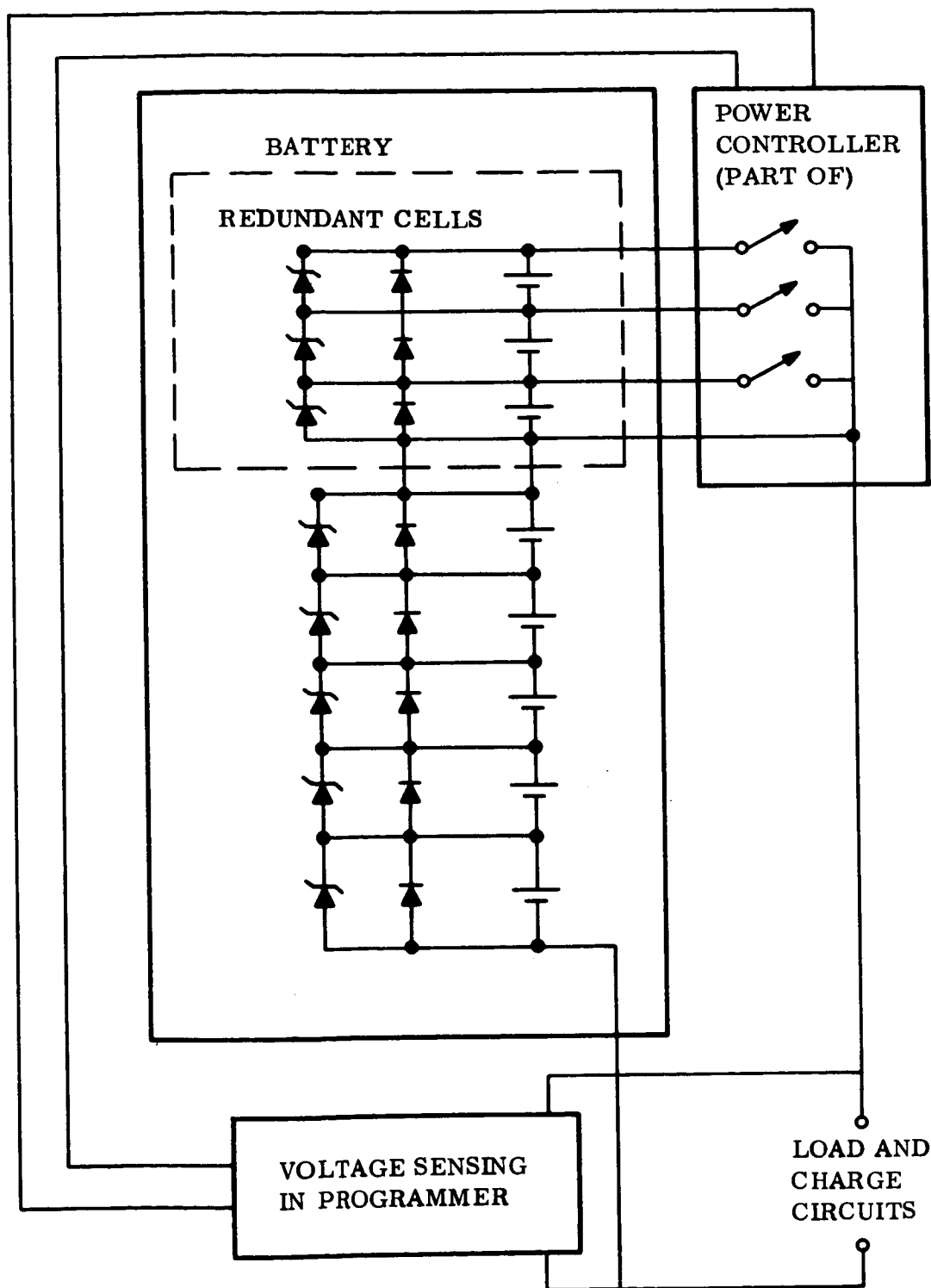


Figure 6.5.4-2. Battery Redundancy Circuit

A buck-boost regulator is used to assure the fullest possible utilization of the available solar power.

The scientific payload, r-f equipment, diagnostic instrumentation, data processing equipment, and sequencing components will require voltage regulation. To minimize weight, to obtain the high efficiency needed on the extended mission and to permit noise control, a single central voltage regulator should be used. However, the high degree of energy conservation required would not permit stand-by losses of such a large regulator on a continuing basis. For this reason two regulators are used, a small unit for the timer and receiver which are operated through the dormant periods and a larger unit which handles all other loads. In addition, it is recognized that selected small loads in the scientific instruments may require special high accuracy regulation.

Battery charging on the spacecraft is controlled by redundant equipment located in the canister. This equipment uses solid state switching circuitry with time ratio control for high efficiencies on the spacecraft.

The Mars Hard Lander electrical system utilizes direct current power sources and distribution as well as steady-state sensing of pressure and temperatures. Programming, sequencing and power switching are performed for durations of a minute or longer with synchronization accuracies in the order of 0.1 sec. Safing and arming are performed manually. Conditioned and regulated powers are processed at a low audio frequency. Initiation and electromechanical operations are performed with the application of electrical energy for durations of a few msec to a few hundred milliseconds.

Electromagnetic compatibility equipment is designed to provide protection over a broad spectrum. This includes low repetition rate pulse-transients through the r-f frequencies used for telemetry.

Data processing, encoding, and multiplexing involve kilocycle and higher frequencies. The camera electronics with imagery represents the highest data bit rate.

UHF and S-band are used for telemetry, providing the highest frequency equipment aboard the Probe system.

These needs describe the spectrum of electrical energy which must be distributed by the cables and harnessing.

Since the Lander will carry a number of different scientific equipments as payload, it is desirable to make arrangements permitting the mission to continue should electrical difficulties arise in a limited area. This feature is provided through a breaker and limiter unit which provides electrical protection to each payload item. Should an electrical fault develop, the load element is disconnected or current limited so that the remainder of the mission may continue.

6.5.4.2 Component Description

Each component is described in detail in this section. Table 6.5.4-1 lists the electrical equipment of Point Design 4 by name, location, weight, size and power level together with electrical reference designators. The equipment situation is indicated by capability to withstand 125°C sterilization temperature, prior shock level accomplished, and development status. The development status is shown by the same numerical code as defined in para 6.5.3.5.9.

6.5.4.2.1 A101, Operational Battery

Function: Provides energy source for all aeroshell and Lander electrically operated equipment, except high rate initiation loads, from the time of aeroshell release through the mission completion.

Type: Manually-activated heat-sterilizable silver-zinc secondary battery sealed with high pressure emergency rupture disk.

Rating: 1816.1 watt hours each, 28v nom, ± 18 percent
Load profile per Section 6.2.5

6.5.4.2.2 A113, A114 High Rate Batteries

Function: Provide energy source for multiple high rate initiation type loads.

Type: Remotely activated, electrically initiated, thermal type primary battery.

Rating: Peak power output 1000 watts
Maximum activated stand 3 min

6.5.4.2.3 A106 Line Contactor

Function: Power transfer of aeroshell Lander systems from ground power to spacecraft power to internal batteries and solar cells.

Type: Electromechanical latch type line power contactor.

Rating: Contact rating 20 amp
Interrupt capacity 250 amp
Pull-in time 100 msec max
Pull-in power 0.3 watt max
Contact configuration later
Operating life 100,000 cycles
Dielectric withstand capability 1500v for 1 min

TABLE 6.5.4-1. POINT DESIGN 4 ELECTRICAL EQUIPMENT HARDWARE MATRIX

Component and Quantity	Size (in.)	Weight (lb)	Power (watts)	Sterilizable (125°C)	Mass Shock (g's) (present information)	Development Status
Operational Battery (A101)	12.2 × 6.1 × 12.2	67.6	Source	Yes	2,000	5
Power Transfer Switch (A106)	2.5 × 2.5 × 5.0	2.0	5.6	Yes	400	3
Lander Programmer (A107)	8.8 × 7.7 × 3.5	7.2	12.6	Yes	400	4
Voltage Regulator A(A108)	5 × 6 × 8	7.0	250.0	Yes	1,000	3
Power Controller L(A110)	3.5 × 5 × 7	5.5	15.0	Yes	700	5
High Rate (A114) Battery A & B (A113)	2 dia. × 3	0.5	Source	Yes	15,000	1
EMC Filter C(A115)	3 × 3.75 × 5.5	1.9	--	Yes	5,000	2
Diode Blocking Module C(A121)	1.5 × 1.5 × 2.5	0.2	13.6	Yes	20,000	2
Thermal Relay Module C(A124)	1.5 × 1.5 × 2.5	0.15	3.0	Yes	50	4
Hg Switch (A128) A and B (A129)	1 dia. × 2.5	0.1		Yes	50	4
Voltage Regulator B(A130)	2.5 × 3 × 4	0.9	27.0	Yes	1,000	3

TABLE 6.5.4-1. POINT DESIGN 4 ELECTRICAL EQUIPMENT HARDWARE MATRIX (Continued)

Component and Quantity	Size (in.)	Weight (lb)	Power (watts)	Sterilizable (125°C)	Mass Shock (g's) (present information)	Development Status
Breaker and Limit Unit (A132)	2 × 2 × 3	0.6	1.0	Yes	10,000	2
Solar Cell Panel A(A133)	18 × 4.5 × 16.5	20.0	Source	Yes	50	4
Charge Regulator (A134)	4 × 5.4 × 10	7.8	2644	Yes	1,000	3
Diode Blocking Module S(A135)	2 × 2 × 3.5	0.5	83	Yes	20,000	2
Drive Mecha- nism A and B (A155) (A136)	4 dia. × 6	4.0		Yes		
Stepping Motor A, B, C, (A150) and D(A152) (A151)	2.5 dia. × 3.5	2.0	0.36	Yes	2,000	3
Motor Controller (A138)	3 × 4 × 4.5	1.3	0.72	Yes	700	5
Solar Cell Panel B(A153)	18 × 4.5 × 16.5	20.0	Source	Yes	100	4
Pin Puller (A158) (A159)		0.3		Yes		
Aeroshell/Lander IFD (J2002)	1.83 dia. × 1.52	0.16	--	Yes	2,000	3

TABLE 6.5.4-1. POINT DESIGN 4 ELECTRICAL EQUIPMENT HARDWARE MATRIX (Concluded)

Component and Quantity	Size (in.)	Weight (lb)	Power (watts)	Sterilizable (125°C)	Mass Shock (g's) (present information)	Development Status
Thrust Cone/ Lander IFD (J2003)	2.5 dia. × 2	0.75	--	Yes	2,000	3
Command Cable Assembly (WL1)	14C × 8 ft	2.1	--	Yes	2,000	3
Power Cable Assembly (WL2)	16C × 28 ft	3.7	--	Yes	2,000	3
Instrumentation Cable Assembly (WL3)	50C × 40 ft	3.0	--	Yes	2,000	3
Shielded Cable Assembly (WL4)	1C × 24 ft	2.1	--	Yes	2,000	3
Power Cable Assembly (WL5)	10C × 20 ft	2.7	--	Yes	2,000	3
Coaxial Cable Assembly (WL6)	1C × 24 ft	0.5	--	Yes	2,000	3

6.5.4.2.4 A107 Lander Programmer

Function: Provide all sequencing, timing, signals, synchronization and clock functions within the Lander and aeroshell.

Type: Solid-state digital circuitry using majority logic and redundancy backup features.

Rating: Channels
In-flight check-out
Powered flight program
Diagnostics cycle
Maneuver mode control
Preseparation program
Coast sequence (Point ϕ only)
Deboost sequence
Entry sequence
Set-up mode control
Surface science sequence
Photography cycle
Solar array unfolding and leveling
Vehicle clock

6.5.4.2.5 A108 Voltage Regulator

Function: Provide control and correction for electrical potential variations. Also, provide various potential levels required to operate aeroshell and Lander electronics.

Type: D-C isolate solid-state inverter transformer-rectifier with time ratio control and feedback regulation.

Rating:

Output	250 watts
Voltage levels	Regulation - See Vol III, table 4.3.1-4
Transient recovery time	later
Regulation	later
Input	23 to 33 v dc

6.5.4.2.6 A110 Power Controller (Lander)

Function: Provide distribution center equipment and all power switching for the aeroshell, thrust core, and Lander electrical loads. Receives commands with proper time sequences and synchronization from the Lander Programmer A107.

Type: Electromechanical relay, switch and contactor construction.

Rating:	Number of switched loads	100
	Contract rating	40 amps max
	Pull-in time	10 to 100 msec
	Pull-in power	0.5 watt each
	Feeder buses	50

6.5.4.2.7 A121, A135 Diode Blocking Modules

Function: Present reverse power flow between various energy sources.

Type: Solid-state single crystal silicon semiconductor diode with redundancy.

Rating:	PIV	75 v
	Recovery time	NA
	Forward current	10 to 75 amp

6.5.4.2.8 A115 Electromagnetic Compatibility Filters

Function: Suppress spurious and conducted electromagnetic interference.

Type: Lumped parameter networks with non-linear and lossy type circuit elements.

Rating:	A115	r-f band pass rejection
	Number of bands	later
	Center frequencies	later (UHF)
	Attenuation	later
	Dielectric withstand	1500 v

6.5.4.2.9 A124 Thermal Relay Module

Function: Provide system protection against faulted squib firing circuits.

Type: Bimetallic heat operated latch type switching element.

Rating:	Interrupt capacity	10 amp
	Trip level I Rt	later

6.5.4.2.10 A128, A129 Switch Hg

Function: Detect upwards direction and enable proper deployment circuits.

Type: Potted mercury switch, 3 pole

Rating:	Current rating	1 amp
	Voltage rate	250 vdc
	Dielectric withstand	1500 v, 1 min

6.5.4.2.11 A130 Voltage Regulator

Function: Provide control and correction for electrical potential variation at high efficiency for standby usage. Also, provide various potential levels required to operate the standby Lander electronics.

Type: Dc isolated solid-state inverter transformer rectifier with time ratio control.

Rating:	Output	27 watts
	Input	23 to 33 vdc

6.5.4.2.12 A132 Breaker and Limiter Unit

Function: Protect the electrical system against non-vital load faults.

Type: Circuit breaker, thermal relays, and limiting resistors in selected groups.

Rating:	Circuits	20
	Trip levels	30 ma to 2 amp

6.5.4.2.13 A133, A153 Solar Cell Panels

Function: Conversion of solar photon energy into electrical energy for the extended mission. Powers Lander loads and recharges batteries during the illuminated period.

Type: Flat stacked panels containing N/P silicon 2 ohm-cm photovoltaic cells 8 mils thick, 1 x 2 cm. Each panel unfolds to 12.5 ft² including frames. The subpanels are joined through a series of spring loaded pantograph links.

Rating:	P _{initial}	100 watts/panel at AM028 and 1AU
	P _{ave}	19.1 watts/panel in application
	V _{out}	42.4 vdc
	I _{out}	0.454 amp

6.5.4.2.14 A134 Charge Regulator

Function: Controls the flow of power from the solar array to the storage battery and electrical system during illumination.

Type: Buck-boost inverter regulator which power optimizes for different illumination levels together with battery temperature and pressure compensations to the charge regime.

Rating: VA_{max} 110 volt-amperes
Voltage Control $\pm 1/2\%$

6.5.4.2.15 A136, A155 Drive Mechanism

Function: Provides translational motion of the solar panel so the unfolding base is level with the top of the flat-pack vehicle and panel clears the crush-up material.

Type: Rack and pinion gear with brushless d-c motor drive.

Rating:

6.5.4.2.16 A137, A150, A151, A152 Stepping Motor

Function: Move or release mechanical stops which control limits on the solar panel unfolding. Enables approximate leveling of the solar array in two axes.

Type: d-c torque motor

Rating:

6.5.4.2.17 A138 Motor Controller

Function: Switches and applies power to the drive mechanism and stepper motors in the proper direction and amount to achieve the desired deployment.

Type: Electromechanical relay, switch and contactor construction

Rating: Number of loads 6
Contractor rating 5 amp max
Pull in time 50 msec
Pull in power 0.3 watt each

6.5.4.2.18 A159, A160 Pin Pullers

Function: Release the stowed solar array to initiate unfolding.

Type: Pyrotechnically operated

Rating:

6.5.4.2.19 J2002, P2002 Inflight Disconnect Aeroshell/Lander (connector, electrical: electromechanically disconnected)

Function: Provide remotely operable, electrical disconnection between the aeroshell and the Lander vehicle during Martian entry flight.

Type: Hot wire operated push-off type collet lock-unlock connectors with crimp insertable cuperic contacts and 360° RFI shielding.

Rating:

Circuits	15 pins
Wire sizes	later
Operate time	less than 100 msec
Operated signal	3.5 amp for 50 msec
Safe level	1 amp, 1 watt, for 5 min
Release impulse	later
Reliability	0.995 at 90 percent confidence each device.

6.5.4.2.20 J2003, P2003 Inflight Disconnect - Thrust Cone/Lander (Connector, electrical; electromechanically disconnected)

Function: Provides remotely operable electrical disconnection between aeroshell and the Lander vehicle during Martian entry flight.

Type: Hot wire operated push-off type collet lock-unlock connectors with crimp insertable cuperic contacts and 360° RFI shielding.

Rating:

Circuits	59 pins
Wire sizes	later
Operate time	less than 100 msec
Operated signal	3.5 amp for 50 msec
Safe level	1 amp, 1 watt, for 5 min
Release impulse	later
Reliability	0.995 at 90 percent confidence each device.

6.5.4.2.21 WL1 - Lander Command Cable Assembly

Function: Provides command and signal distribution from the Lander programmer to various receiving equipment.

Type: Copper conductor electrical cable insulated with Kapton and Teflon (H + 1/2 T) in a wrapped construction. Cable connectors of NAS 1599 type and modified in selected cases to permit high density inserts and rear insertion construction.

Rating: Later

6.5.4.2.22 WL2, WL5 - Lander Power Cable Assemblies

Function: Provide electrical power distribution throughout the Lander, from the power controller and batteries to the various loads.

Type: Copper conductor electrical cable insulated with Kapton and Teflon (HF + 1/2 T) in a wrapped construction. Cable connectors of NAS 1599 type and modified in selected cases to permit high density inserts and rear insertion construction.

Rating: Later

6.5.4.2.23 WL3 - Lander Instrumentation Cable Assembly

Function: Distributes data from sensors and payload instruments to data conditioners, encoders and telecommunication equipment in the Lander.

Type: Copper conductor electrical cable insulated with Kapton and Teflon (HF + 1/2 T) in a wrapped construction cable connectors of NAS 1599 type and modified in selected cases to permit high density inserts and rear insertion construction.

Rating: Later

6.5.4.2.24 WL4 - Shielded Lander Cable Assembly

Function: Provides coaxial transmission of signals and high frequency energy through the Lander.

Type: Copper conductor electrical cable insulated with Kapton and Teflon (HF + 1/2 T) in a wrapped construction Cable connectors of NAS 1599 type and modified in selected cases to permit high density inserts and rear insertion construction.

Rating: Later

6.5.4.2.25 WL6 - Coaxial Cable Assemblies

Function: Carries i-f power to the antenna and signals from the antennas to the receiver.

Type: RG

Rating: Zc 50 ohms

6.5.5 ENVIRONMENTAL CONTROL

The mission weight and reliability constraints are such that the environmental control system complexity and design margins must be the minimum possible. In line with this objective, a semi-passive method of thermal control utilizing an insulated payload, optimum surface radiative coatings, and local electrical heaters was selected to satisfy the thermal control requirements.

The Lander configurations present an ideal approach for providing the necessary payload thermal insulation. The 1.5 in. thick honeycomb container structure will be utilized thereby eliminating any additional space requirements for the insulating material. A low thermal conductivity core material (phenolic glass) with foam insulation packed cells will be utilized to control the Lander temperature response. Detailed insulating tradeoffs are presented in the parametric data (Vol IV Section 4.4). By adding the foam insulation the heat transfer losses are reduced to a conduction mode only with a relatively high thermal resistance. This is desirable since the radiative and convective heat losses between the honeycomb face sheets could be considerable based on:

1. Radiation across the cell ends could be significant with a possible outside surface temperature of -60°F and an inside structural temperature of 50°F .
2. Although a reduced atmosphere exists, minimizing the heat transfer coefficient, some convection losses could be present in the air space thereby contributing to the overall heat loss.

This conceptual design produced a shell around the payload which has a thermal conductance value of $0.36 \text{ Btu/hr} - ^{\circ}\text{F ft}^2$. Therefore, the payload has sufficient thermal isolation that its minimum temperature will not fall below -40°F , the lower allowable limit for all of the payload components except the battery. To maintain the battery at or above its minimum operation temperature of 50°F , it is thermally isolated from the payload with an insulated package which contains an electrical heater. This heater is thermostatically controlled to turn on when the battery falls below 50°F .

A transient solution was performed to determine the temperature response of an isothermal payload and battery in the Martian environment. Appropriate conduction and radiation was considered based on the Lander configuration. For minimum heat leak, a low surface emissivity of $E_{\text{OS}} = 0.1$ was assumed. Results of this analysis are shown in figs. 6.5.5-1, -2, -3, and -4. Figs. 6.5.5-1 and -2 shows the battery temperature response and heater power necessary to maintain the battery at 50°F . The temperature response of the payload for the minimum and maximum environments are shown in figs. 6.5.5-3 and -4 respectively. These show that no heater power is required to maintain the payload temperature above -40°F .

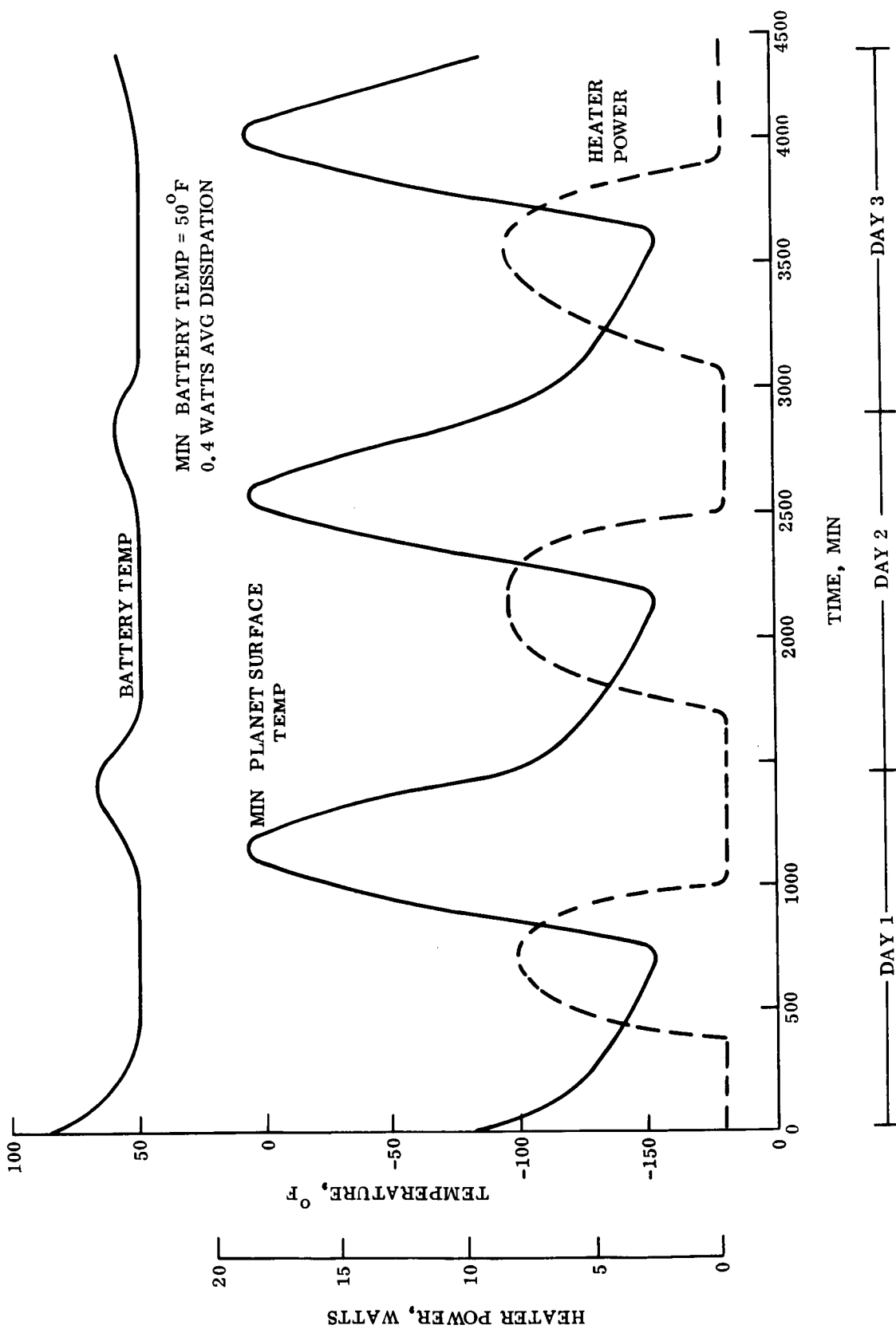


Figure 6.5.5-1. 90-Day Lander Heater Power Requirements for Thermal Battery Control, Minimum Environment

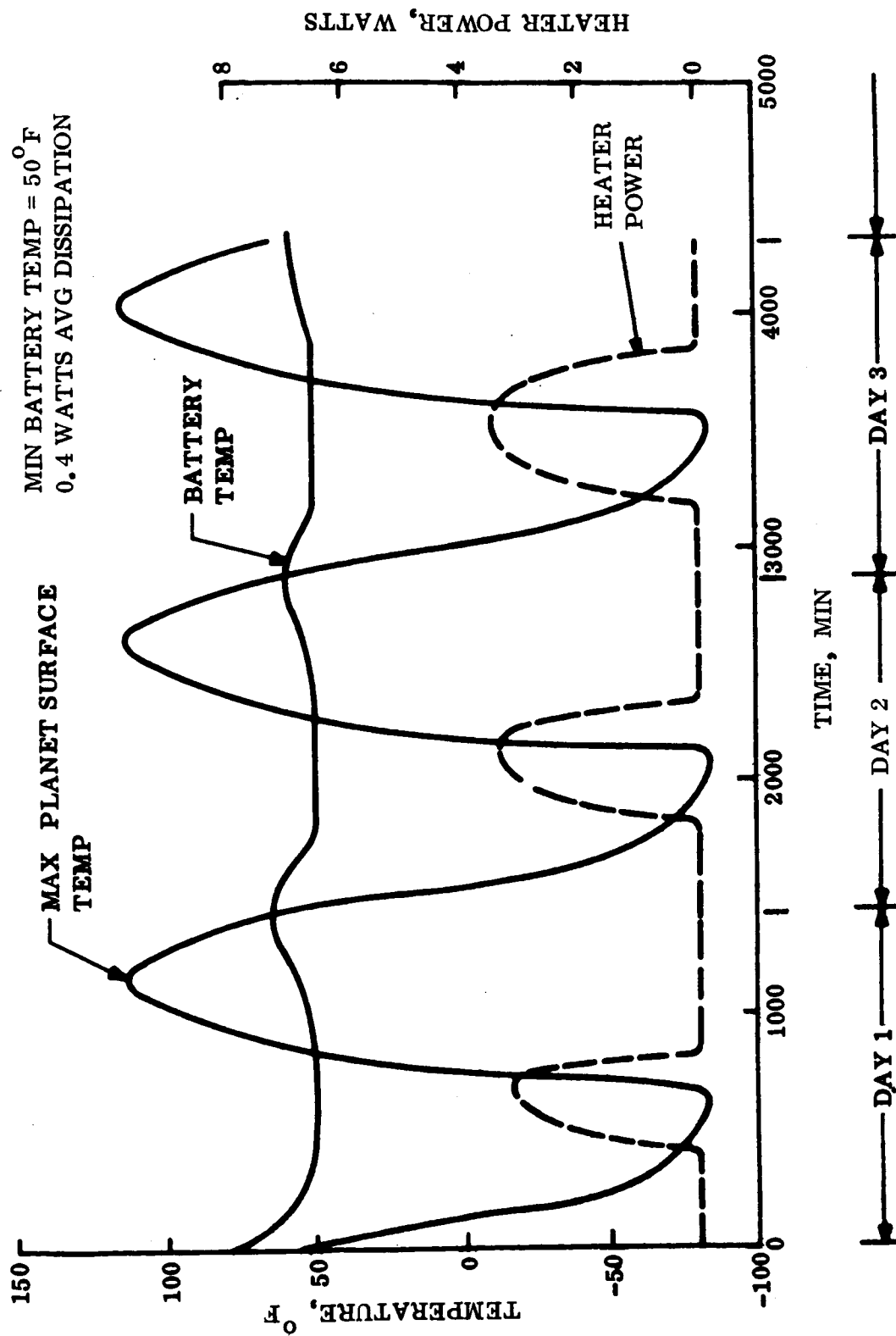


Figure 6.5.5-2. 90-Day Lander Heater Power Requirements for Thermal Battery Control, Maximum Environment

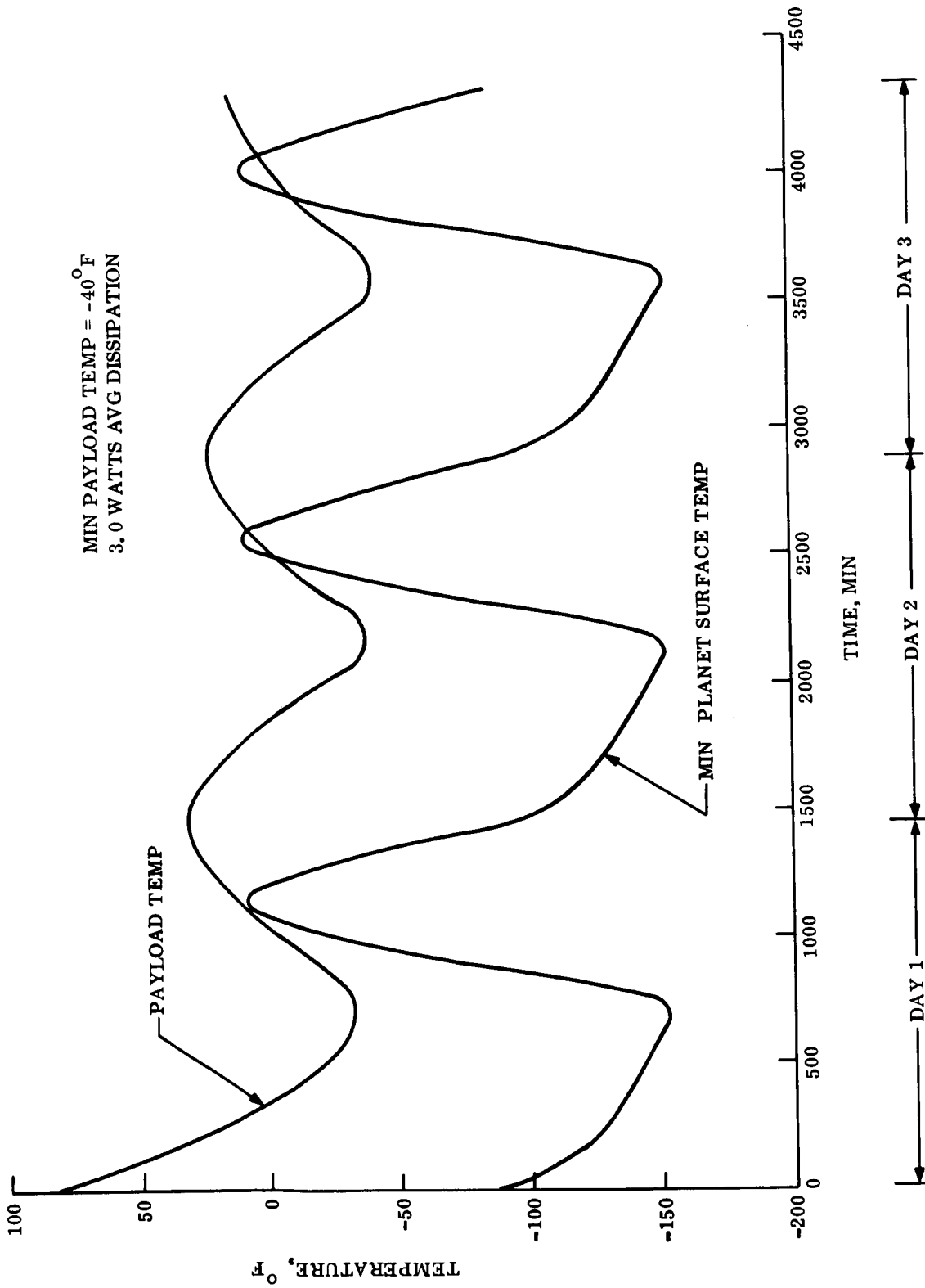


Figure 6.5.5-3. 90-Day Lander Payload Temperature Response,
Minimum Environment

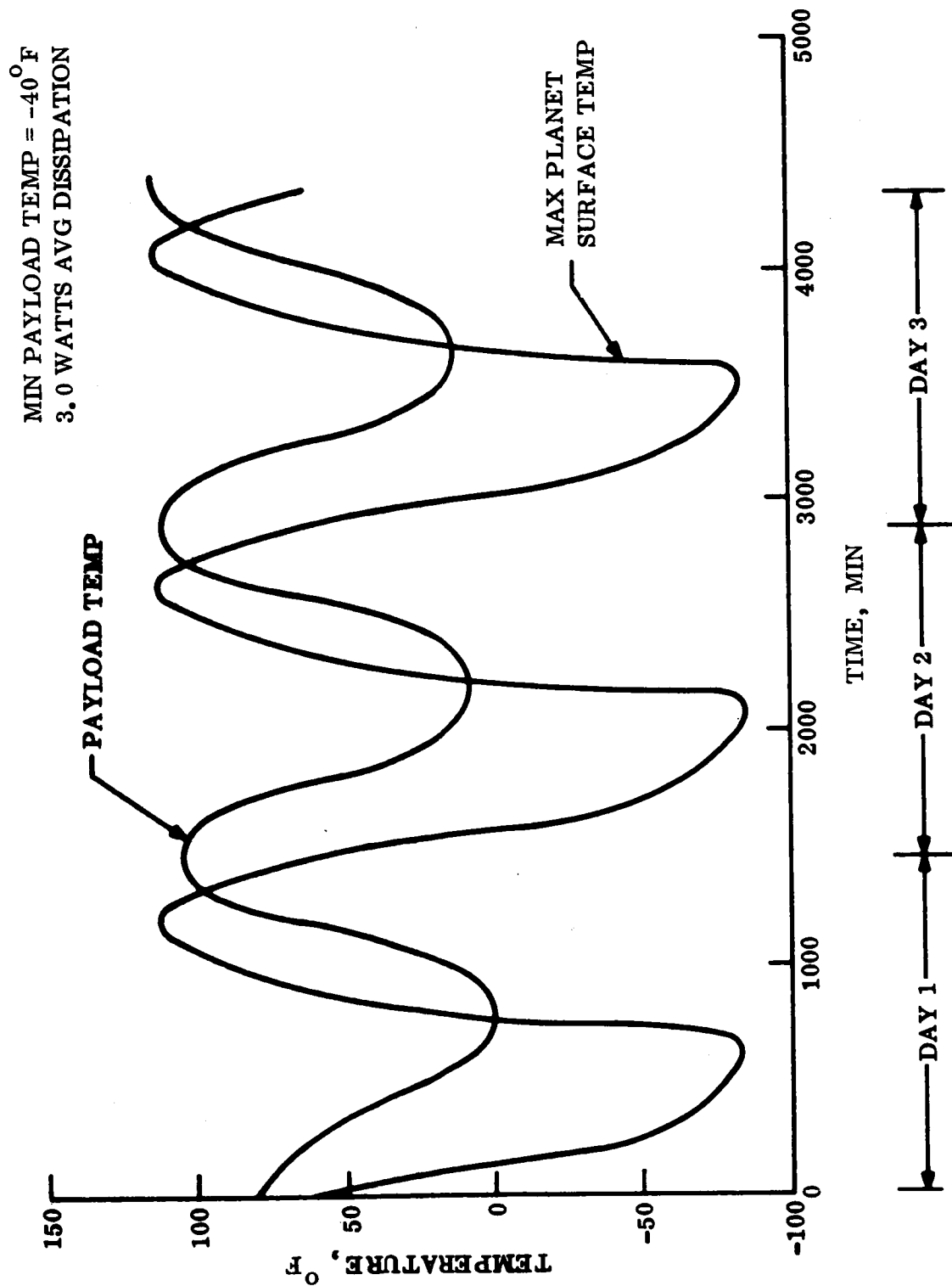


Figure 6.5.5-4. 90-Day Lander Payload Temperature Response, Maximum Environment

The transmitter temperature response was studied as a function of daily transmission power with the resulting analysis indicating that no protection in the form of thermal storage material is required to prevent overheating. The specified power level of 32.5 watt-hr/day will only produce an 18°F temperature rise resulting in a peak temperature of 138°F.

6.5.6 DEPLOYMENT MECHANISMS

In the landed position, either side of the vehicle may be uppermost, so provision has been made for the deployment of instruments and equipment from both sides of the flat pack container. However, to avoid unnecessary duplication of the instruments, the actuating mechanisms have, in general, been designed for two way operation. A 'g' sensing device will determine the direction of deployment operation.

Instruments deployed in Point Design 4 are: four cameras (two high and two low resolution), 10 wind velocity transducers (two sets of five), four temperature transducers and one surface composition (alpha back scatterer) instrument head. All except the alpha back scatterer are located in a central bay the full width and depth of the Lander container, as shown in fig. 6.5.6-1. The alpha back scatterer is located in an individual full depth bay, also shown on the drawing.

6.5.6.1 Camera Installation, Deployment and Mechanism

The camera(s) and swinging boom(s) installation and associated mechanism is shown in detail in fig. 6.5.6-1.

Each of the four cameras is mounted on the free end of pivoted tubular booms. The booms are aluminum alloy material approx. 36 in. long and 2 in. outside diameter. They rotate through approximately 90° in either direction, as shown, from the installed horizontal position so that when erected, two are side by side at opposite edges of the Lander, one with a high and one with a low resolution camera. This arrangement of relatively short swinging booms, with the capability to erect four cameras on either side of the Lander and take pictures over the edge of the Lander in segments shown in the insert on the drawing, was selected as the most satisfactory compromise between the need for simple and stable erection devices and mechanism and the requirement for adequate azimuth and vertical angles of uninterrupted vision. Deployment design with telescoping (not hinged) tubes, cannot easily be made to work in two directions, and investigations proved that unless the number of cameras was doubled, the telescopes had to be many feet in length, to provide adequate vertical angles of vision over the edge of Lander impact attenuation system. Deployment booms of such length pose serious problems regarding camera stability. Stowed, the cameras and booms lie horizontally across the Lander in a block of four. Saddles on the inside of the jettisonable doors covering the camera bay, clamp the booms securely to withstand the 'g' forces imposed, in particular during the landing phase. The booms are spring actuated to move through 90° in either direction from the stowed position, by a single torsion spring around the hinge pivot, which is restrained in a neutral setting when the bay doors are assembled. Release and jettison of the camera bay door from the uppermost exposed side of the

FOLDOUT FRAME

FOLDOUT FRAME

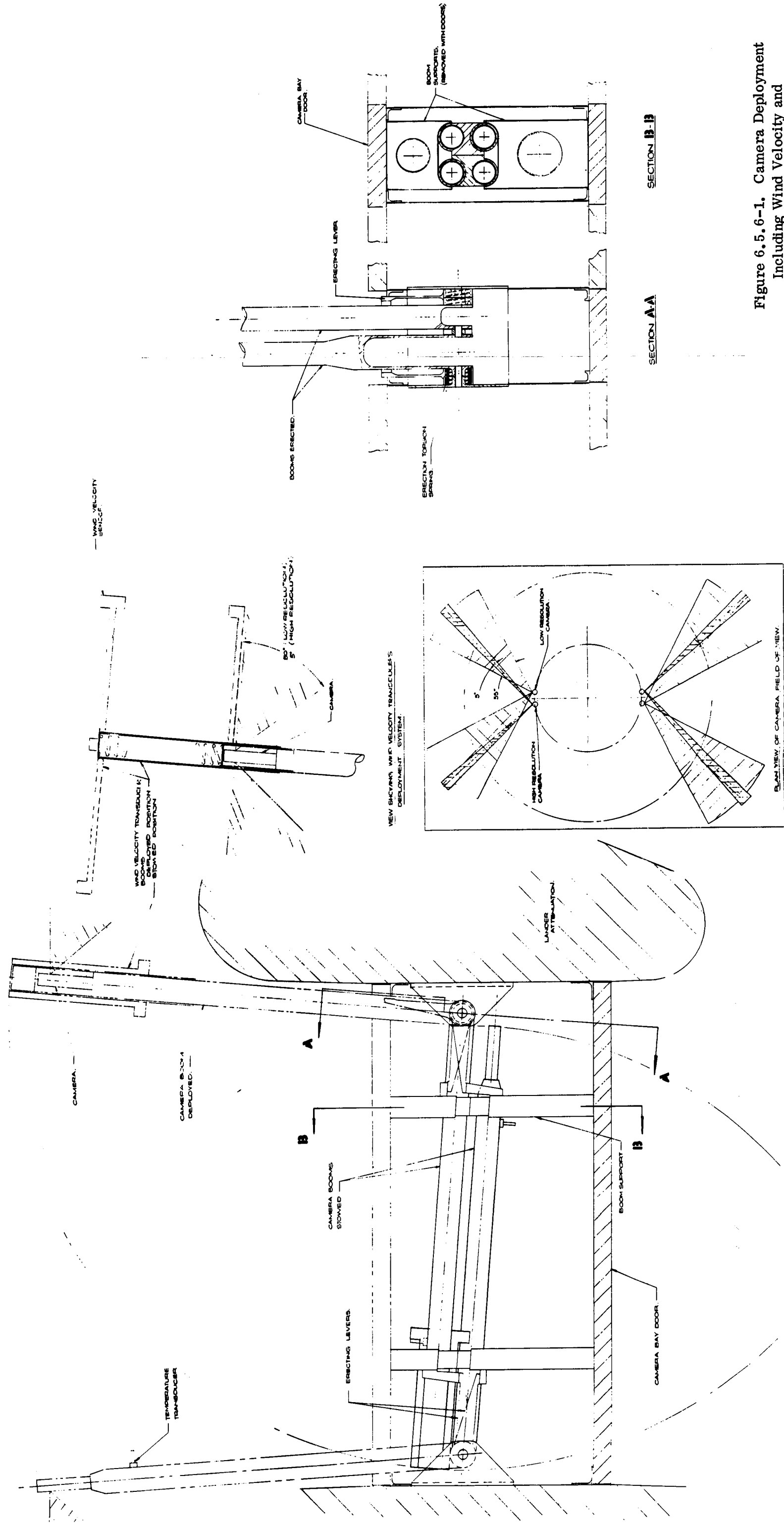


Figure 6.5.6-1. Camera Deployment Including Wind Velocity and Temperature Transducers

Lander, unclamps the boom(s) and releases one end of the torsion spring to pick up a lever on the boom and effect its rotation. Thus boom operation is automatic once the appropriate cover door has been jettisoned. All four booms are individually operated by the same spring loaded principle, the two lying deepest in the Lander from the exposed side are restrained to move until the two uppermost ones are deployed and are unlocked by the final motion of the upper booms. This is a simple and automatic sequencing for the four boom arrangement. The cover door(s) are secured with bolts incorporating a hot wire release and jettisoned by springs with sufficient force to ensure that they fall clear of the Lander.

6.5.6.2 Wind Velocity and Temperature Transducers

Five wind velocity transducers constitute a set necessary to obtain wind measurement data. Four are mounted in a plane at 90° to each other on a two feet pitch circle diameter, the fifth is mounted below one of the other four to provide a vertical reading. As stated in Section 6.5.2 the instruments are acoustic devices requiring unimpeded line of sight between each sensor. In the arrangement shown in fig. 6.5.6-1 the transducers are attached to the ends of spring loaded arms, which are mounted on a telescoping extension of the camera booms and unfold when the boom triggers a release mechanism as it locks into the erected position.

The weight involved in the installation of a set of wind velocity transducers is very small and two sets have been provided on two camera booms for redundancy.

A temperature transducer is mounted directly on each of the four camera booms at the base of the camera.

6.5.6.3 Surface Composition (Alpha Back Scatterer)

Although this instrument has not been completely designed, analysis has provided preliminary weight, volume, deployment and other requirements. The installation and deployment approach herein is based on a conceptual design which is illustrated in fig. 6.5.6-2. The Surveyor alpha back scatter instrument has been referred to and utilized to some extent.

The instrument sensor head is installed on its side in the bay provided in the Lander container. The head will be firmly clamped against a pivot bar, in the stowed position, by a soil calibration sample holder extended across the bay and secured to the vertical side walls. When the calibration phase of the alpha back scatter instrument head either linearly along the bay or by rotation. The function will be performed by a pin pulling device and spring loaded mechanism. The instrument head is now free to rotate through 90° due to its offset c.g. and the force of gravity and drop through the bottom side of the Lander attached by the control cord and wire bundle provided.

Low friction guides will be installed on either side of the instrument head from the bay sidewalls to ensure that the head rotates and exits from the Lander with a smooth controlled motion.

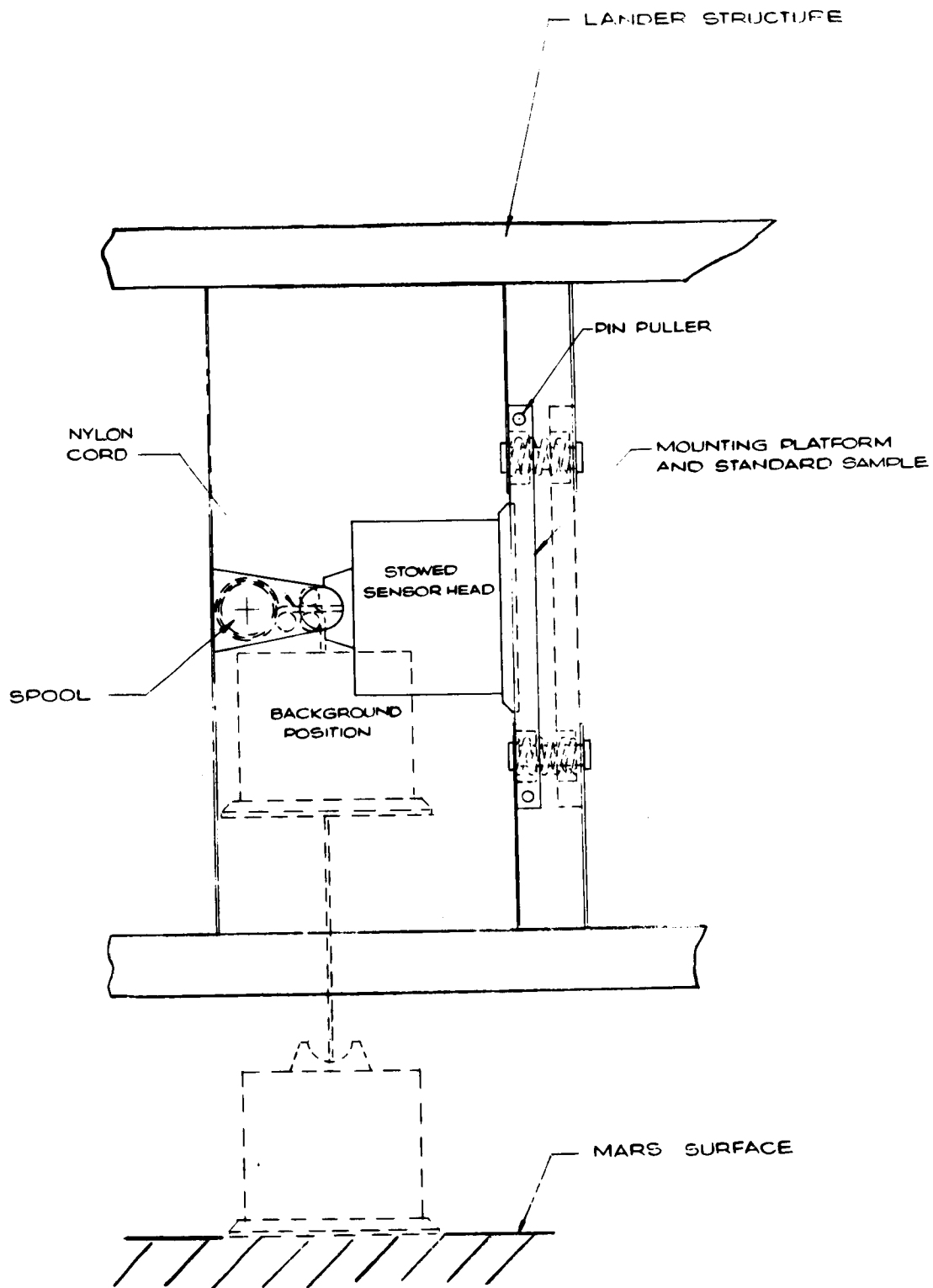


Figure 6.5.6-2. Operation of Alpha-Back Scatter Deployment Mechanism

Assuming that the head is prevented from being lowered completely clear of the Lander, it can operate equally well within the bay provided the surface is in good contact with the ground.

Covers over the bay provided in the Lander have been studied, but jettisonable or sliding doors are not desirable because of possible interference with the instrument head or jamming in the event of landing damage. Consequently, two inward opening hinged doors will be provided on either side of the Lander.

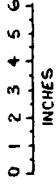
6.5.6.4 Solar Panels

Solar arrays have been installed in blocks in individual bays in the Lander. The combined deployed area of the arrays is 25 ft². Two installed arrangements are discussed which have been investigated to a preliminary design stage and have promise regarding feasibility. Other designs will continue to be investigated. Considering the two arrangements currently suggested, the basic scheme illustrated in fig. 6.5.6-3 utilizes two blocks of solar panels which are mounted in a compressed and locked condition vertically in approximately the center of full depth bays in the Lander container. The design is such that each block of solar panels can be deployed from either side of the Lander, whichever is uppermost. Deployed in either direction; the pantograph linkage between the solar panels in a stack, coupled with levers and a set of lazy tongs at each end of the stack, ensures that the solar cells on each panel face uppermost. Solar cells on one side of a panel only permit a shock cushioning material to be bonded to the other side; this separates the solar panels and protects the cells in the stacked condition, against the rigorous conditions imposed during landing. Stacked panels seem to be the most convenient arrangement for compact stowage and good deployment potential with the flat-pack Lander and selected impact attenuation system and this basic design offers a two directional deployment capability from each stacked pack.

To minimize the size of the bay required in the Lander for each pack and to facilitate the deployment of the array over the deep ring impact attenuation to a substantially horizontal position, deployment of the pack is in two stages. First, when the door on the exposed side of the Lander has been selected by the 'g' sensing device and released, the array is free to move to the surface of the Lander still in the stacked condition. The motive force is a compression spring. Compression springs are located on both sides of the stacked pack, between the pack and the cover doors. These springs can also function to jettison the door when the door attachments have been released.

When the stacked solar array is at the end of its vertical movement, locked and protruding from the surface of the Lander, a clamp compressing the panels into the stack is released with a hot-wire device. A 1/12 horsepower electric motor mounted on the bottom of the stack drives through a gear box to actuate the lazy tong linkage at the bottom of the stack. This second stage action both raises and deploys the set of solar panels in one movement sideways over the impact attenuation to the final horizontal deployed position. Two motors are installed, one for each direction of deployment of the stack; thus, either one is operative to drive the solar array through this second stage to full deployment.

FOLD OUT



IV

An assembly of 20 panels constitute a stacked array and each panel is approximately seven in. by eleven in. Each panel complete with structural backing is 0.025 in. deep based on the assumption that 0.025 in. maximum thickness solar cells with insulation will be bonded to a flanged metal base plate. The side links of the pantograph system are also 0.25 in. deep and require to be 0.20 in. thick at the center pin joint where bending is at maximum. It is intended that these links shall be in steel probably forgings. Pins are 1/8 in. diameter. It is recognized that this basic arrangement of solar array extends some distance over the edge of the Lander, however, it can be made quite rigid and if necessary the free end can be provided with extending feet to rest on the ground.

The second arrangement of solar array presented as an alternative provides the same total area of deployed solar array divided into four stacked blocks of panels of reduced depth on each side of the Lander container. The advantages are that each array deployed would not extend so far over the edge of the Lander; arrays can be deployed at 90° to each other in plan instead of 180° as for the basic scheme, with the possibility of increased electrical efficiency; that other equipment could be mounted underneath a solar array stack in the Lander, in other words, there is the possibility of more flexibility between solar arrays and other equipment in a tightly packed Lander; that loads on the solar arrays could be reduced giving a potential saving in array weight. The severe disadvantage is that for a given total area deployed from one side of the Lander the installed area of solar cells doubles with a consequent appreciable increase in cost weight and volume. With this alternative proposal, which is only illustrated as a sketch scheme in fig. 6.5.6-4, the design principals, methods of actuation and deployment can be virtually the same as for the basic design.

6.5.6.5 Direct Link Telecommunication Antennas

With the installation of a direct link telecommunication subsystem, additional antennas are required. These have been located in the body of the Lander as shown in fig. 6.5.1-1. Details of the antennas are specified in section 6.5.3.

Consistent with the principle that the Lander can settle on either side, duplicate S-band antennas have been provided to operate from both surfaces of the flatpack container. The location and installation is preliminary and subject to verification based on the antenna design and pattern definition which is beyond the scope of the present program. If deployment is required the design can incorporate this capability.

6.5.7 LANDER CONTAINER STRUCTURE

The flatpack configuration for the landed payload container illustrated in fig. 6.5.7-1, was selected on the basis that it offers a good compromise between structural efficiency and all other design constraints, notably packaging and deployment of experiments. The following requirements and criteria were imposed for the design of this structure:

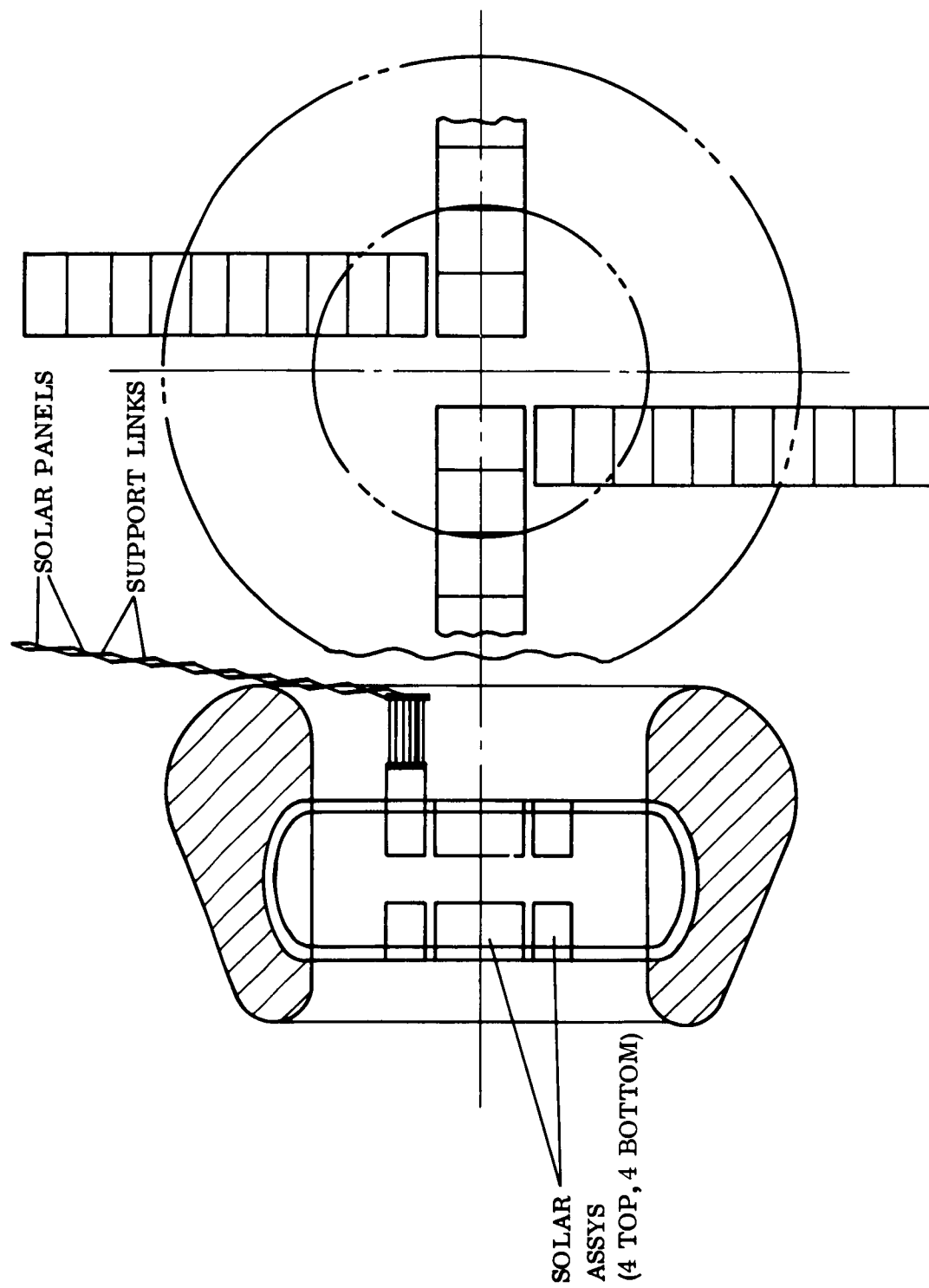
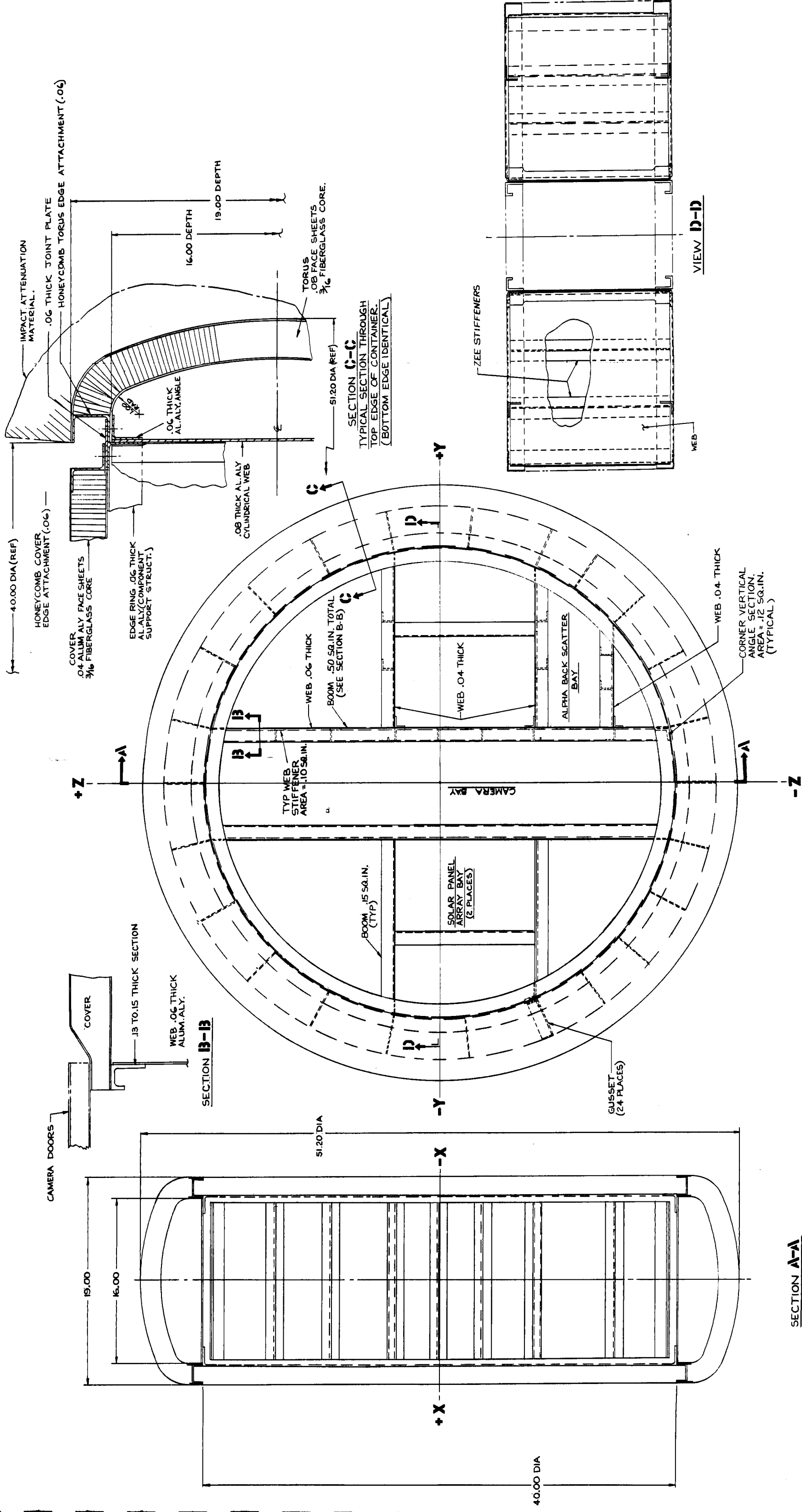


Figure 6.5.6-4. Solar Array (Alternate Scheme)

FOLDDOUT FRAME

FOLDDOUT FRAME



PLAN VIEW (COVERS REMOVED FOR CLARITY)

SECTION A-A

Figure 6.5.7-1. Structure

1. Design weight - 900 lb. This is used for structural design purpose and is based on a total Lander weight less the material which is crushed during primary impact.
2. Local pressures and inertia loads resulting from impact up to 1000 g's.
3. Limit design factor - 1.0.
4. Ultimate design factor - 1.25.

Based on the requirements and constraints which are present, a design has been evolved which has the following significant features:

1. A full-depth inner space frame module containing most instrumentation and subsystems. This module can be removed from or inserted into the flatpack as a bench subassembly.
2. Individual components can be added or removed from the top or bottom of the space frame while installed in the container.
3. Dual purpose space frame which acts as primary structure and component support.
4. Jettisonable and hinged doors for deployment of camera and alpha back scatterer respectively.
5. Primary structure consisting of a D-shaped toroid section supporting the impact attenuator, combined with the inner space frame.

The container consists of three basic elements: the D-shaped toroidal edge structure, the inner space frame, and the top and bottom covers and doors. (See fig. 6.5.7-1). This complete assembly is designed to withstand the forces generated by initial impact at 1000 g's and any forces resulting from subsequent impact after rebound.

The D-shaped edge structure acts as a primary load path for distribution of impact attenuator loads. The outer shell of this section is tied to the cylindrical wall with radial aluminum sheet nose ribs, stiffened and spaced approximately every five inches around the circumference. These radial members transfer some of the loading to the internal cylindrical web and allow the section to act as a heavy ring frame, transferring load into the upper and lower cylindrical edge rings. Local loading up to 950 psi imposed by the crushing honeycomb is resisted by the outer shell of the D-shaped section which is a 1-1/2 in. thick fiberglass honeycomb (3/16 in. cells) core with 0.08 in. aluminum face sheets. The cylindrical section is an 0.08 in. lightened and stiffened cylindrical shell. Except for items such as cable harnesses, it is not proposed to utilize the edge structure for packaging, and therefore some structural deformation is tolerable.

The full depth cross members of the inner space frame stiffen the container against deformation from the cylindrical shape and resist bending of the flatpack, as well as providing component support. Two main cross members form the camera bay. These beams have 0.06 in. aluminum alloy webs, extruded alloy channel beams, and section vertical stiffeners. There are seven secondary cross beams at right angles to the main beams. These are of similar but lighter construction in aluminum alloy. Top and bottom angle rings, 0.06 in. thick, and vertical angles at the junctions of the main and secondary beams and at the free ends of these beams complete the assembly. The inner space frame is attached to the D-section through the vertical flanges of top and bottom angles.

The top and bottom covers are considered secondary structure. They are 1.35 in. thick fiberglass honeycomb panels with 0.04 in. aluminum face sheets. A Z edge section is inserted for attachment. The edge members of the D-section, the inner space frame, and covers, when bolted together form strong rings at the top and bottom surface of the container.

Thick honeycomb panels with fiberglass core have been selected for the construction of the outer shell of the container as a means of satisfying both structural and thermal requirements. A possible alternative for the container outer shell generally, could be reduced depth honeycomb panels with foam on the inner side. Additional investigation will consider fiberglass facing sheets for all honeycomb panels used as a strength-to-weight trade-off. Surfaces of the full depth cross beams, which are exposed when the camera and alpha back scatter bay doors are jettisoned, are thermally insulated with a layer of foam to the full depth of the beam vertical stiffeners. The foam is covered with plastic coating to maintain integrity on landing impact.

A preliminary analysis, for critical loading points of three conditions shown in fig. 6.5.7-2, has been made and used to formulate the estimated weight of the container. Typical torus cylinder interface loads, for the edge impact condition are shown in figs. 6.5.7-3, -4, and -5.

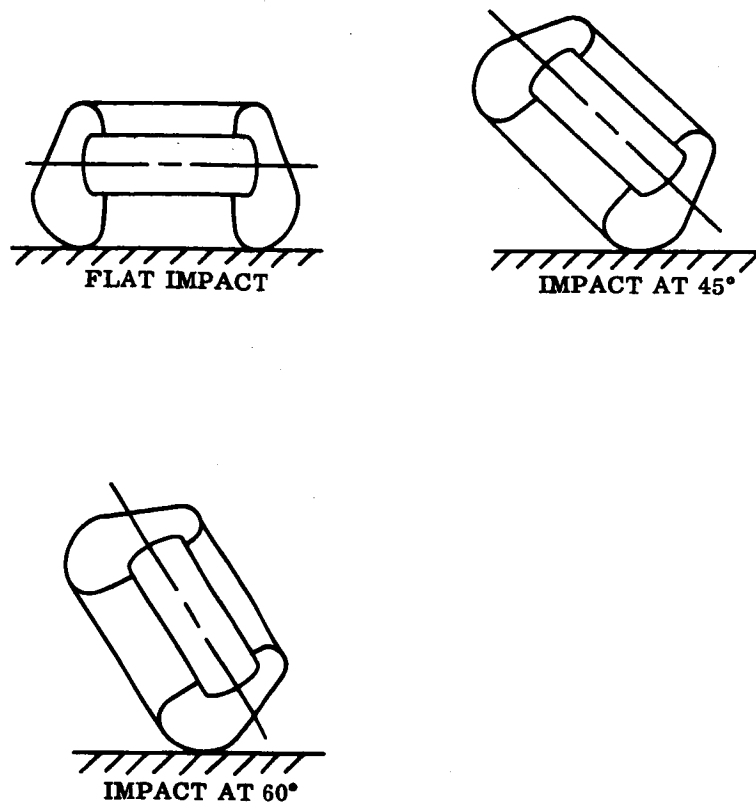


Figure 6.5.7-2. Three Conditions Used for Preliminary Loading Analysis

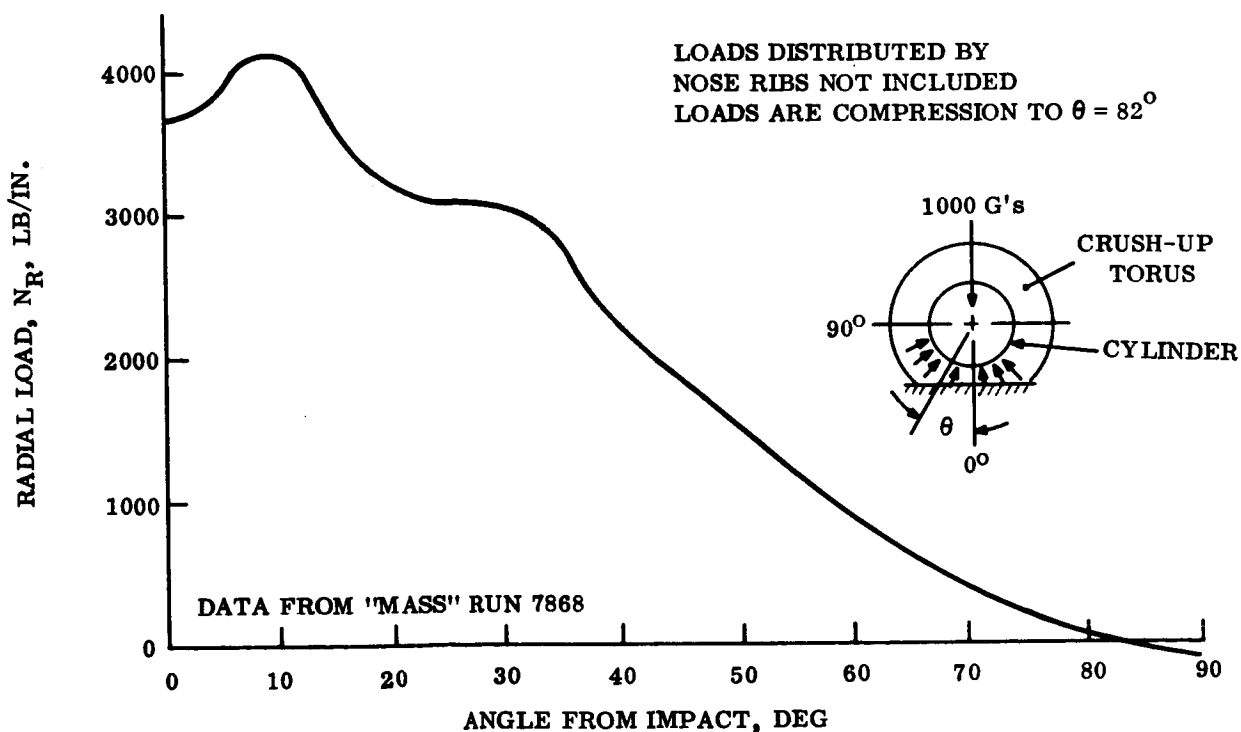


Figure 6.5.7-3. Typical Interaction Radius Loads between Torus and Cylinder, Edge-on Condition

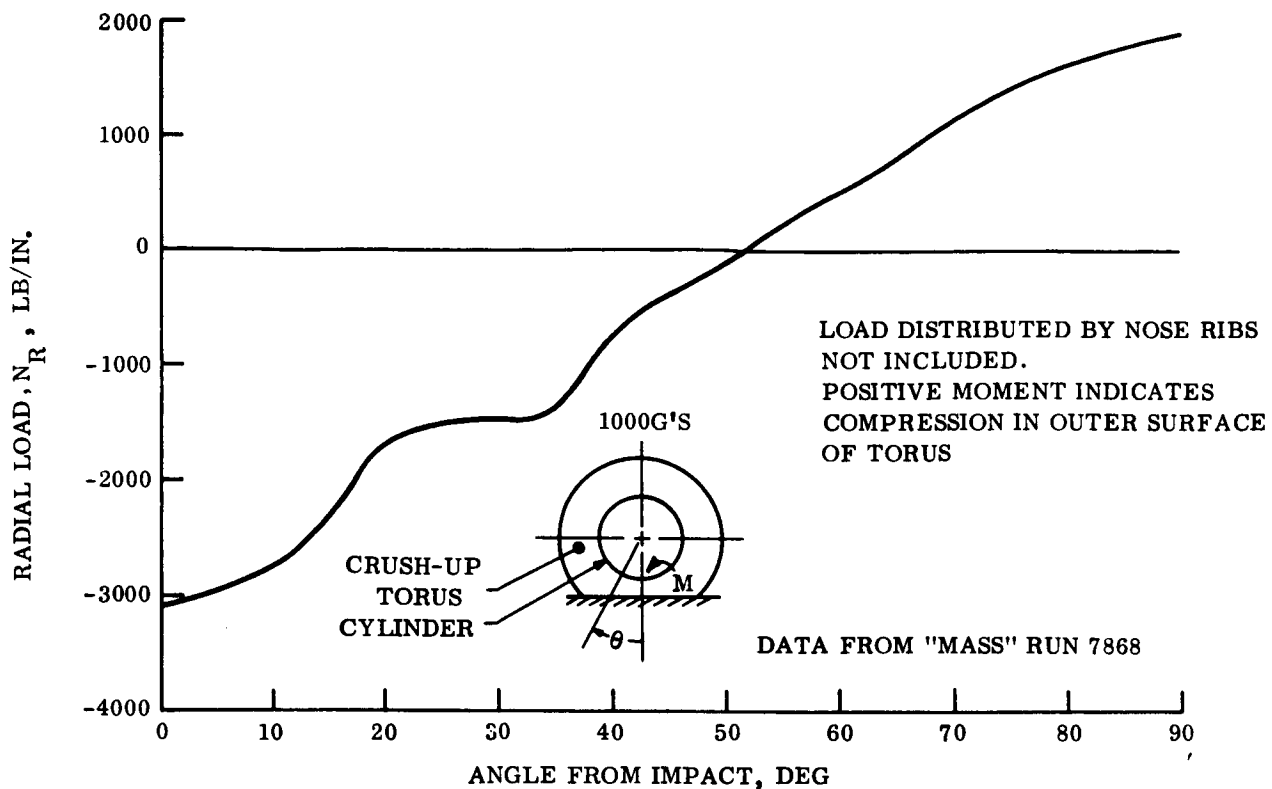


Figure 6.5.7-4. Typical Interaction Moment Between Torus and Cylinder, Edge-on Condition

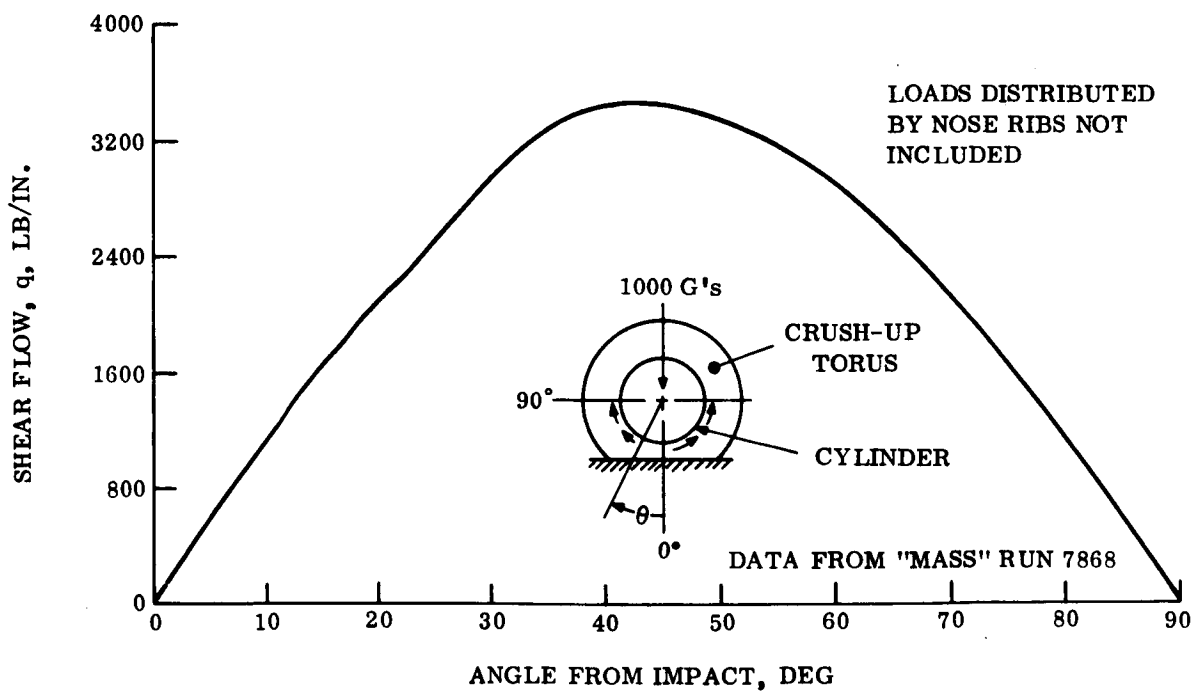


Figure 6.5.7-5. Typical Interaction Shear Flow Between Torus and Cylinder, Edge-On Condition

6.5.8 IMPACT ATTENUATION AND STRUCTURE

6.5.8.1 Attenuation Requirements and Criteria

6.5.8.1.1 Gross Vehicle Response

The mechanical crush-up impact attenuation system is designed to provide sufficient stopping distance to decelerate the Lander within the allowable g-limits while dissipating the impact kinetic energy. At the same time the acceleration pulse must have a sufficient rise time and be essentially broad and flat. The honeycomb phenolic fiberglass material inherently behaves in a manner which produces this behavior.

6.5.8.1.2 Response of Individual Components

Initial studies have been performed to determine the feasibility of further attenuating the impact acceleration levels experienced by individual components carried by the Lander. These are reported in Vol. IV, App. A. The conclusions drawn from this appendix indicate that it does not appear feasible to obtain significant reductions with shock mounts or by component mounting stiffness tailoring. These devices are of primary use in minimizing g-level amplification effects.

6.5.8.1.3 Angular Accelerations: Their Effect on Components

It appeared that if the Lander impacts on one edge, there was the possibility that high angular accelerations might produce high loading on components located at the outer extremity of the container. This situation is studied in Vol. IV, App. A. The conclusion reached is that such high angular acceleration g's will not occur.

6.5.8.1.4 Selection of Phenolic Honeycomb as the Reference Material for Impact Attenuator Design

Phenolic honeycomb was selected as the reference material for this study for the following reasons. Both balsa wood and phenolic honeycomb are feasible materials for the size and weight of vehicles being examined herein. Both materials can function at the operating g-levels anticipated with a hard Lander System. However, the balsa wood can be adversely affected by exposure to the sterilization cycle. In past tests, balsa wood has split after being subjected to dry heat sterilization. Careful control of the wood moisture content can, however, probably eliminate this problem. Balsa wood has the added disadvantage that its material properties have been known to vary from ± 15 to ± 50 percent. This is significant since balsa, being a natural material, cannot be further developed to a significant extent. Phenolic honeycomb, on the other hand, has been improved in the past and this trend can be expected to continue.

6.5.8.2 Environmental Definition and Interpretation

Vol. IV App. B contains the detailed account of the specification used in the point design. Included are discussions of surface strength, friction, slopes and rocks. The wind specification for the point designs is also elaborated upon.

In brief, the point design is capable of impacting an infinitely hard surface with friction, five in. rocks and slopes up to and including 34° from the horizontal. The prevailing wind, blowing against the surface slope is the extreme value of 220 fps. Should the surface strength be less than attenuator stress, some penetration will be experienced, but this is estimated as a few inches by the analysis in Vol. IV App. B.

The important effect of a parachute sway angle (of up to 40° from the local vertical) was also examined. The chief result is that the sway angle couples with the surface sloper to require higher angles of the Lander to be analyzed for the initial impact condition. The significance is that an increment in honeycomb attenuator thickness over that thickness necessitated by a non-swaying vehicle must be incorporated on the Lander sides to allow for the swaying effect on vehicle orientation at touchdown. Details are given in Vol. IV App. B.

6.5.8.2.1 Secondary Impacts of the Lander Vehicle

The combined environmental conditions of extreme wind, parachute sway and varying surface slopes warranted an investigation of post impact vehicle motion. In particular, the probability and significance of secondary impacts was reviewed. Vol. IV App. B contains the dynamic analysis for the secondary impact problem as well as an initial probability estimate of the likelihood of occurrence of this event.

The statistical analyses were performed for the purpose of ascertaining the probability of experiencing a secondary impact velocity less than or equal to a chosen value. In particular, the value of 100 fps was investigated because this was the velocity used to size the top side of the multidirectional Lander. Based upon the limited first order approximation used, the following trends are indicated. For the extreme wind velocity of 220 fps the Lander flips over about 92 percent of the time and hits the second time on its top side.

In light of the new Mars Mission Specification (1968) of a design wind velocity of 110 fps, another probability estimate may be made. For this wind velocity, (but the same slope and sway angle variations) the Lander will flip over only about 25 percent of the time. Given that the Lander does flip, the secondary velocity will be 100 fps or less 81 percent of the time. If the analysis were adjusted to account for the new definition of surface slope of 20° (as contained in the Mars Mission Specification - 1968) this 81 percent figure would improve considerably. The foregoing brief summary identifies the surface wind specification as a critical design parameter.

6.5.8.3 Effect on Point Design Due to Perturbation in the Design Parameters

Vol. IV App. C delineates the effects on the impact attenuation system design due to variations in the reference condition. These parameters in which perturbations are especially significant are also identified.

In general, lower wind and descent velocities, flatter slopes, softer surfaces, smaller rocks, lessened parachute sway, higher component g-tolerance and lower Lander weights than the corresponding design value enhance the point design integrity.

Increases in velocities, slopes and parachute sway angle tend to compromise the design integrity. Higher Lander weights than in the design condition, and lower component g-tolerance tend to compromise the adequacy of the design.

Small increments in effective rock size are deleterious but, after a point, the rock becomes a large outcrop and is more of a hard surface than a penetrating hazard. It is noted that since the design is based on an infinitely hard surface no problem arises with an increase in surface hardness above that used in design computations.

Vol. IV App. C also encompasses variations in honeycomb material properties. Specific comments identify the effects of variations in crushing density, specific energy, stroke efficiency, effective geometry and crush-up behavior.

6.5.8.4 Impact Attenuation Design Approach

The attenuation system design approach for Capsule Point Design 4 is now described. Fig. 6.5.8-1 is a sketch of the nominal deep ring geometry for the point design, multidirectional Lander. In the design, the attenuation material is phenolic fiberglass honeycomb (3/16 in. cell size) of the type developed by GE-MSD under contract to the JPL. This material is of the hexagonal cell variety with parallel cells which can be wrapped with (R/t) radius to thickness ratios of greater than five. It is the reference material selected for use in this study and is currently used in the JPL drop testing program. This material is readily available from Honeycomb Products, Inc. in densities of 4 to 12 pcf. The particular density used in the point design will be determined by the design conditions, especially Lander weight and allowable rigid body g-level. The performance of this thin dipped phenolic material varies depending upon its axial orientation with respect to the impact load vector. This is a key design factor investigated in the point design computation. The requirements of multidirectionality results in analyses of the Lander for various cutting plane orientations ranging from forward-flight onto aft-end-first (for a secondary impact). Requirements of multi-directionality lead to some weight penalties since material which is fully effective in one touchdown orientation may be of less or no value when other orientations are examined. Past analyses and judicious application of the specifications have indicated that three critical crush-up condition must be analyzed. There are 0° (forward) impact, 90° (side-on) impact, and an intermediate surface slope impact. The intermediate slope has been taken as 34° for point design purposes. It is apparent that to adequately handle all of the highly probable impact conditions special attention must be directed toward the crush-up lay-up because of the material's variable effectiveness. For point designs this honeycomb lay-up is produced by cutting and segmenting the attenuator material to produce near-radial cell axis orientation with respect to the internal toroidal container structure. At the same time this segmented approach allows more efficient wrapping of the container. (Refer to Section 6.5.8-5 for details. The same varying effectivity is also complicated by a geometric effect produced by the curvature of the Lander as seen in plan. The net result is that the area-stroke characteristics are direction dependent in a complex relationship (fig. 6.5.8-2). This means that the force stroke history is direction dependent and that, depending on the direction of impact the stroke (and thus the thickness) required will be different.

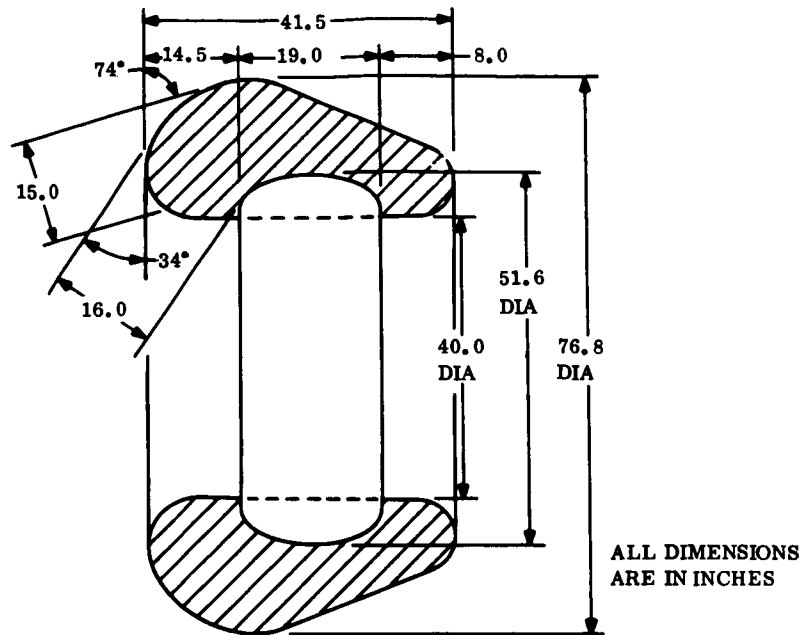


Figure 6.5.8-1. Lander Attenuation Point Design 4

An additional geometric effect, distinct from that of crush-up directionality also enters the analysis. This is, for a given direction of impact a variable amount of honeycomb material is actively being crushed. Some material may be oriented in such a way that it experiences shearing forces. Because of this localized condition bond line shear failures can result with little or no crush-up action. Such failures could occur without providing sufficient stroke capability. For this effect detailed design must ensure that sufficient material is working in each specific direction. Finally, attention must be directed toward the location of crush-up propagation. It is desired that the fracturing progress from the outside in and not from the payload to the extremity of the attenuator. Design details of the container/honeycomb interface and slight precrushing of the attenuator can eliminate this problem.

6.5.8.4.1 Analytical Details

With the above background, point design analysis takes the following form. A series of CRUSH (geometrical program) runs were made for each prototype point design. The results were made of the form of gross crushed cross sectional area against stroke for various angles encompassing the operational map as defined in the specification. The geometric results were used to perform a direct graphical analysis of several multidirectional prototype shapes. The conclusions drawn from this thorough study provide the underlying logic for a computer assisted procedure to size the attenuator for point design purposes.

In fig. 6.5.8-2, plots of crushed area against stroke for a nominal size deep ring multi-directional Lander are produced. It is emphasized that this figure is for gross area with no directionality effects included. In fig. 6.5.8-3, plots of effective sectional area are provided. These latter plots were generated in the following manner. The phenolic material loses two percent of its strength per degree of obliquity between the longitudinal cell axis and the normal to the crushing plane.

The design guide for this reduction is fig. 6.5.8-4. This design guide is based upon test results summarized in fig. 6.5.8-5.

The data to support this procedure are reported in ref. 6-1 in addition, a 20 percent reduction is incorporated to account for the effect of curvature (in plan). The analysis also assumes that the active area encompasses all cells lying within 30° of the normal to the impacting plane examined and that all others are not actively crushed.

After examining various cutting planes for the Lander prototypes it was found that for the multi-directional Lander three principal strokes need be computed: dead on, side-on (90°) and 45° angular cutting plane. Actually for sizing purposes there is small difference whether the cutting plane passes at 34° or 45°. This is shown in fig. 6.5.8-2.

From data similar to that fig. 6.5.8-2 the principal strokes can now be computed by equating Lander normal kinetic energy to the absorbed energy due to crushing. For the prime (0° impact) case, it was found from analyzing several prototype multi-directional Landers that

$$\begin{aligned} \text{energy absorbed} &= 1/2 \frac{W}{g} (V_N)^2 = 0.77 \text{ WGS} \\ S_{(0^\circ)} &= 0.65 \frac{(V_N)^2}{gG} \approx \frac{0.6 (V_N)^2}{gG} \end{aligned}$$

where V_N is the impact velocity component normal to the plane, 'g' is the earth gravitational constant and G is the allowable deceleration level in g-units. As described in Vol. IV App. B it is assumed that the velocity component parallel to the plane is absorbed by surface sliding. This is why the normal velocity computations. For the 45° and 90° (side-on) cases the same procedure applied to several cases yields on the average to several cases yields on the average

$$\begin{aligned} S_{45^\circ} &= \frac{(V_N)^2}{gG} \approx \frac{0.6 (V_N)^2}{gG} \\ S_{90^\circ} &= \frac{0.5 (V_N)^2}{gG} \end{aligned}$$

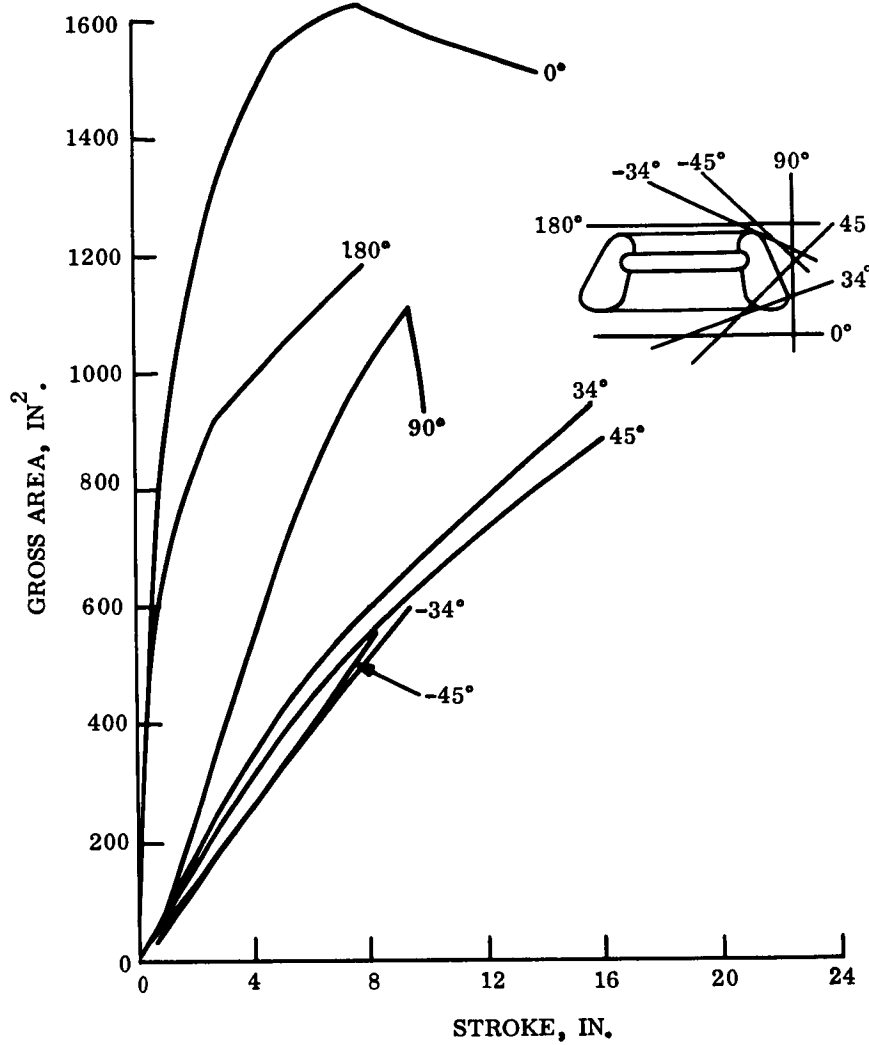


Figure 6.5.8-2. Gross Cross Sectional Area vs Stroke for the Multi-directional Lander

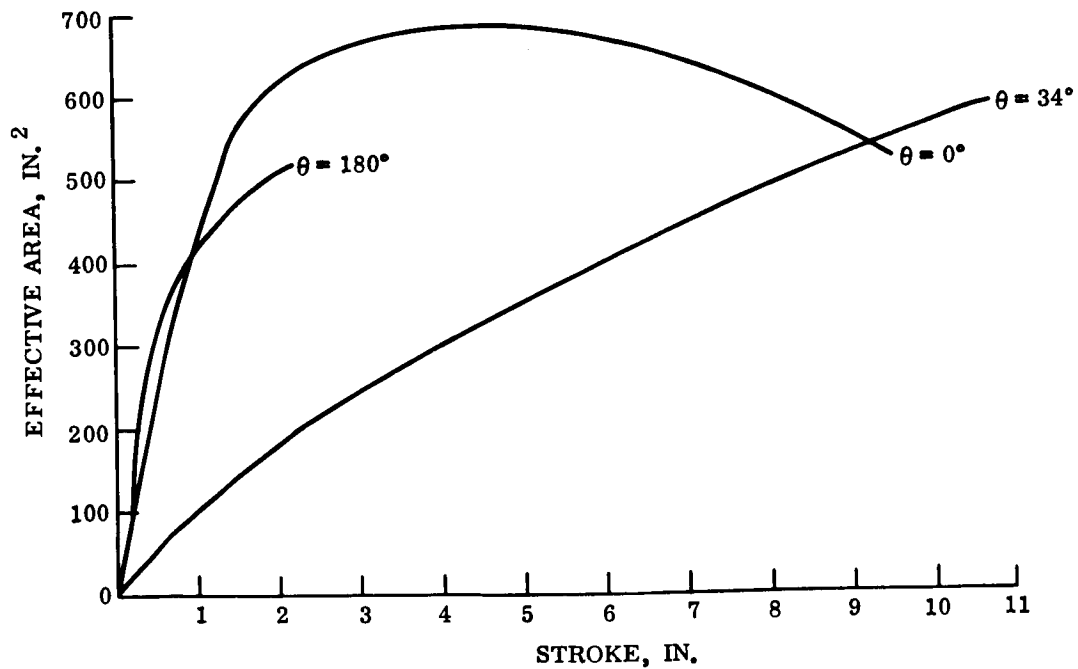


Figure 6.5.8-3. Effective Cross-section Area vs Stroke

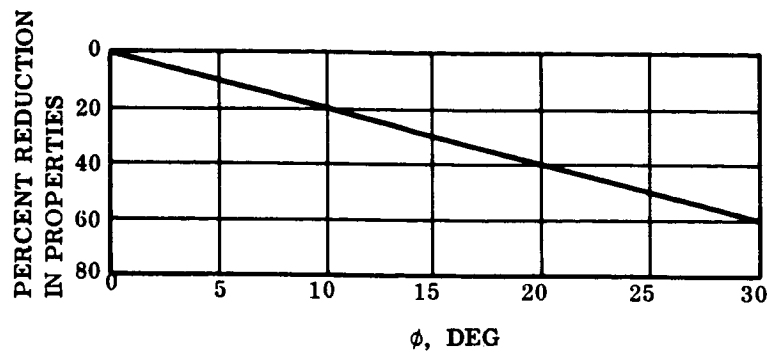


Figure 6.5.8-4. Design Guide for Reduction in Honeycomb Properties for Non-axial Impacts

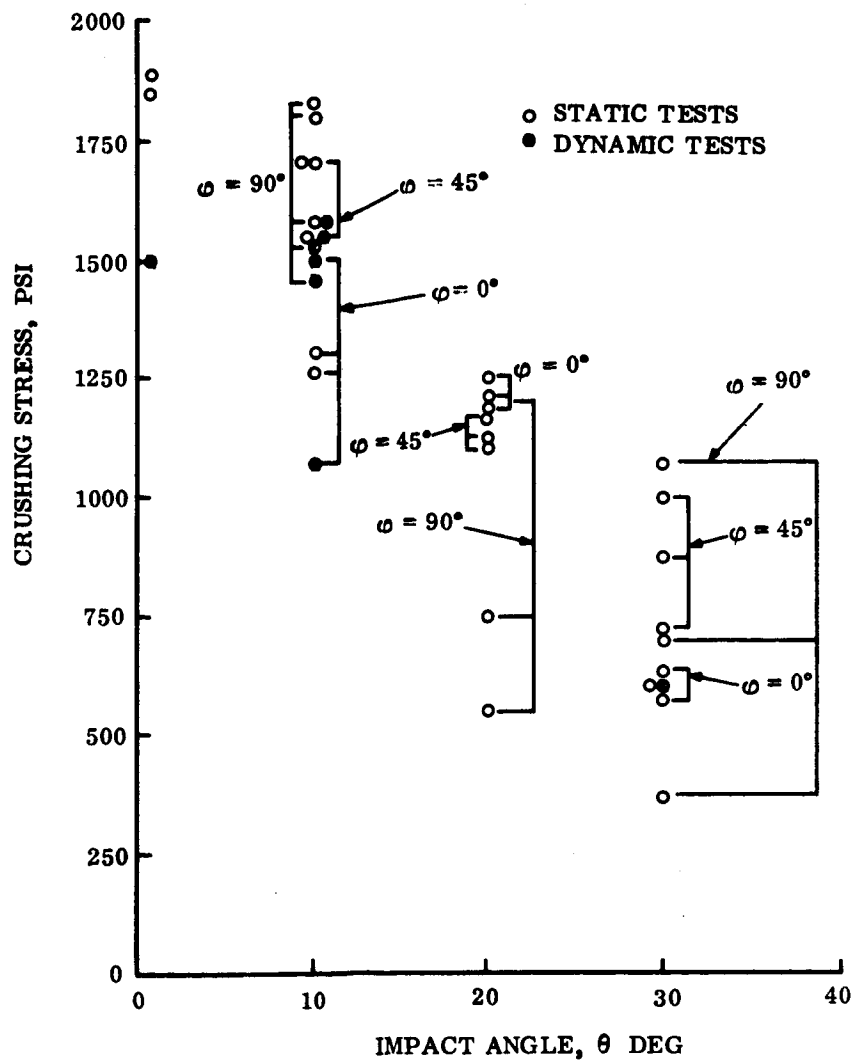


Figure 6.5.8-5. Comparison of Crushing Stress vs Angle of Impact for Static and Dynamic Loading

It should be realized that although these strokes are sufficient to limit the deceleration they will not necessarily be experienced. The reasoning for this statement is as follows. For the moment neglect parachute sway. The multi-directional Lander is operational for slopes up to and including 34° . See fig. 6.5.8-7. This means that crushing planes from 0° through 34° must be examined. From this viewpoint only a crushing plane at 90° does not enter the analysis. If parachute sway is introduced, the sketch of fig. 6.5.8-8 is appropriate. From this last figure extreme conditions of slope and sway angle are apparent. The net effect is that more crushing planes must be investigated. When it is recalled that the Lander will experience a rotational motion during crush-up, it is likely that the theoretical strokes provided around the circumference which are conservatively based, on a continuing direct constant, penetration will not be expended. With the three principal strokes known one has the principal contributing factors to the attenuator thickness computation. Provision must still be made for stroke efficiency, a factor of safety, and rock protection dimensions. These are handled as follows. Ref. 6-1 contains data on honeycomb stroke efficiency. For the point design this efficiency is about 0.8 (see fig. 6.5.8-6 for data). Stroke efficiency is defined as that fraction of total honeycomb thickness which will actually crush-up when impacted. This effect occurs because some of the total thickness provided is lost as accumulated crushed material builds up. See fig. 6.5.8-9. Therefore corresponding to the three stroke values (S_i for $i = 0^\circ, 45^\circ, 90^\circ$) just derived one must provide associated thicknesses (t_i) of

$$t_i = \frac{S_i}{0.8}$$

However, due to the possibility of rock or other outcroppings these thicknesses must be compared to $S_i + 5$ inches and the larger value used in design. Therefore the design thickness is the greater of the following two expressions (ref. Vol. IV App. B)

$$t_i = \frac{S_i}{0.8}$$

$$t_i = S_i + 5$$

With the three thicknesses known, the attenuation system may be sized and the volume of crush-up material computed. For multi-directional point designs this was accomplished by fitting a smooth curve through the three key points and considering that the upper side is sized by the following expression.

$$t_{AFT} = \frac{V^2}{gG} \times 12 + 5''$$

which is valid for a triangular 'g' versus stroke history. For purposes of the point design the velocity used in this expression was 100 fps. The implications of using this velocity, which may be produced in a secondary rebound impact are discussed in Vol. IV App. B.

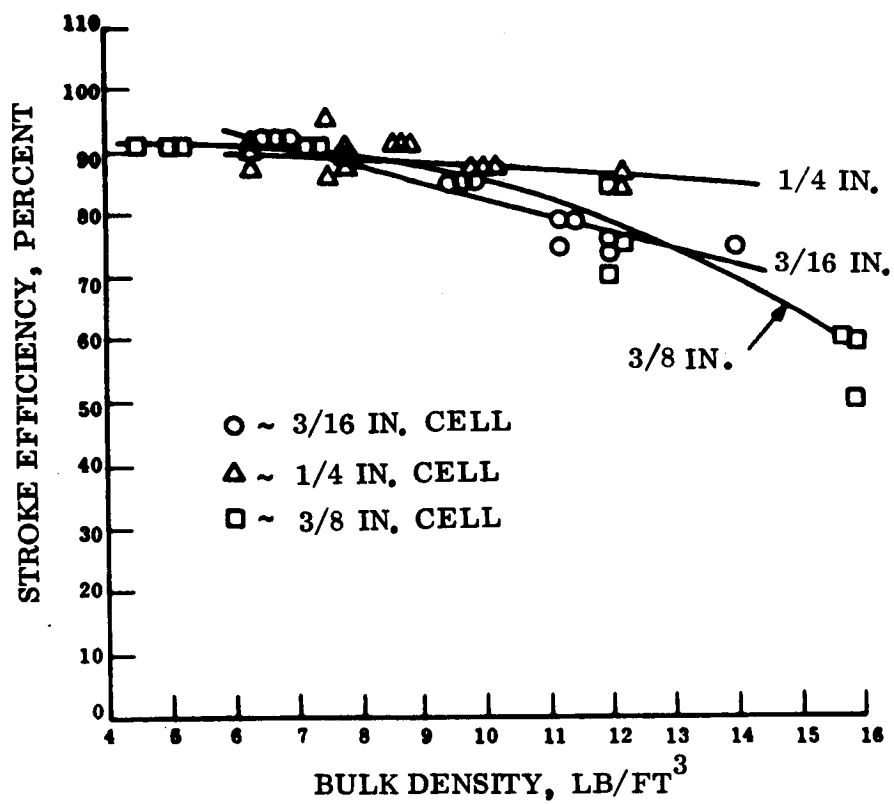


Figure 6.5.8-6. Stroke Efficiency vs Bulk Density

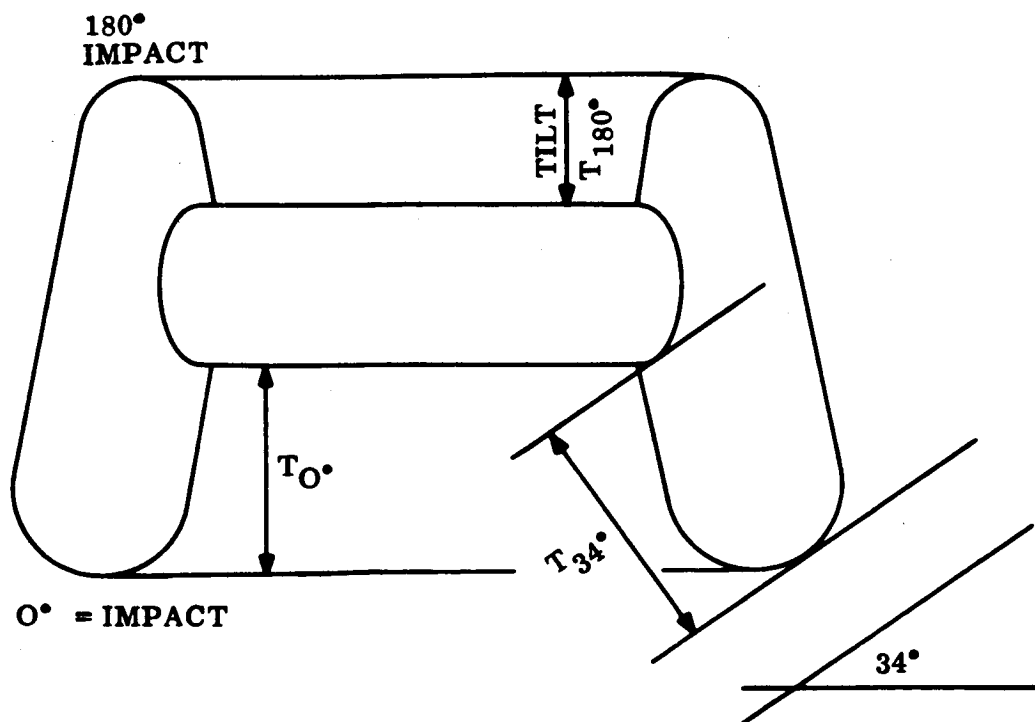


Figure 6.5.8-7. Crushing Planes for Stroke Analysis

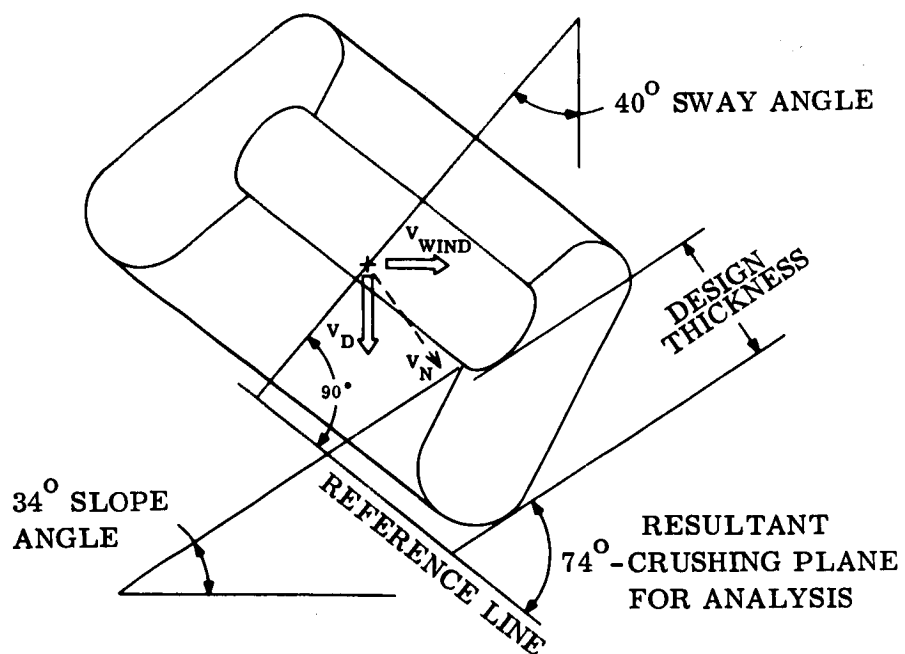


Figure 6.5.8-8. Typical Crush-up Condition Analyzed for Multi-directional Lander Showing Sway and Slope Angle Effects

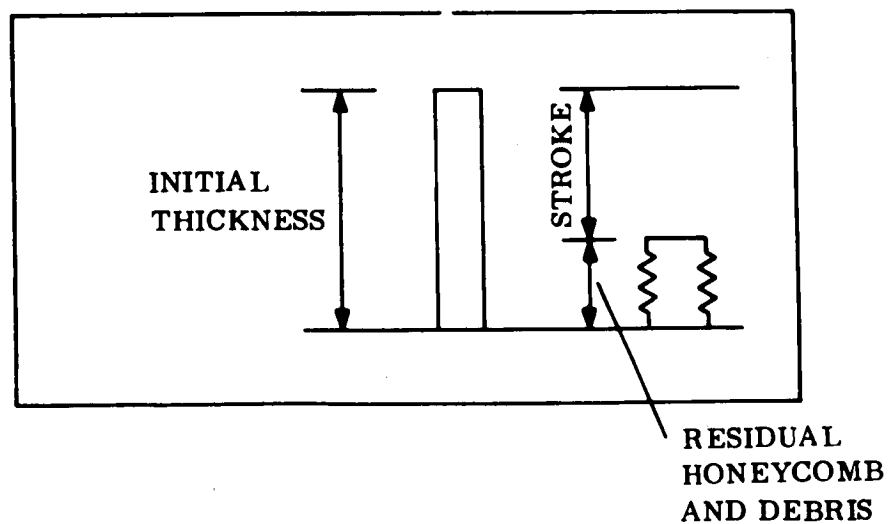


Figure 6.5.8-9. Illustration of Stroke Efficiency

Another design quantity is the material density to be used to limit the g-loading to the desired values. This density for the 3/16 phenolic honeycomb is related to the specific energy and crushing stress as shown in fig. 6.5.8-10. For minimum attenuator weight a density greater than 11.85 pcf should not be used since the maximum specific energy and crushing stress occur at this value. This establishes an upper limit on the useful density. A lower bound on the density is determined from previously reported experimentation in ref. 6-1. It is shown that honeycomb densities below four pcf are erratic in behavior and this density is consequently a lower bound on the feasible materials for design use.

The density selection for use in point designs is made by selection of a crushing stress according to the formula

$$\sigma = \frac{WG}{A}$$

where W is Lander weight, G is allowable deceleration level and A is the cross sectional area corresponding to the progression of the stroke to that point at which the peak g-loading is experienced. The area A is determined via a computer code and used to find the corresponding crushing stress. With this crushing stress the appropriate density from the relation in fig. 6.5.8-10 is read off and used in the attenuator design. Options in the two different computer design codes were constructed based on this information. The codes allow one to input the point design conditions of touchdown velocity, size, landed subsystem weight g-tolerance and surface rock specification in order to obtain attenuation sizing, volume and weight, crushing stress and material density for a given point design. The computer calculated volume and weight are then verified by planimeter computations using the exact cross-sectional areas. The geometry used in the program is sketched in fig. 6.5.8-11, the input geometry includes interior and exterior diameter and inside container height. A program option yields complete sizing dimensions of the Lander as well as geometric checks for compatibility with aeroshells of different cone angles for initial installation feasibility computations.

6.5.8.3.2 Point Design 4 Particulars for Impact Attenuation System

When the foregoing criteria were applied to Point Design 1 the impact attenuation system was defined as 406 lb of 3/16 in. cell size phenolic fiberglass honeycomb. The honeycomb volume was 50.8 ft³; the density was 8 pcf. The other conditions were:

- V_D = 100 fps descent velocity
- V_H = 220 fps wind velocity
- directional capability
- clearance and protection for 5 in. rocks
- 1000 g (rigid body) capability

The honeycomb thicknesses are shown in outline form in fig. 6.5.8-1.

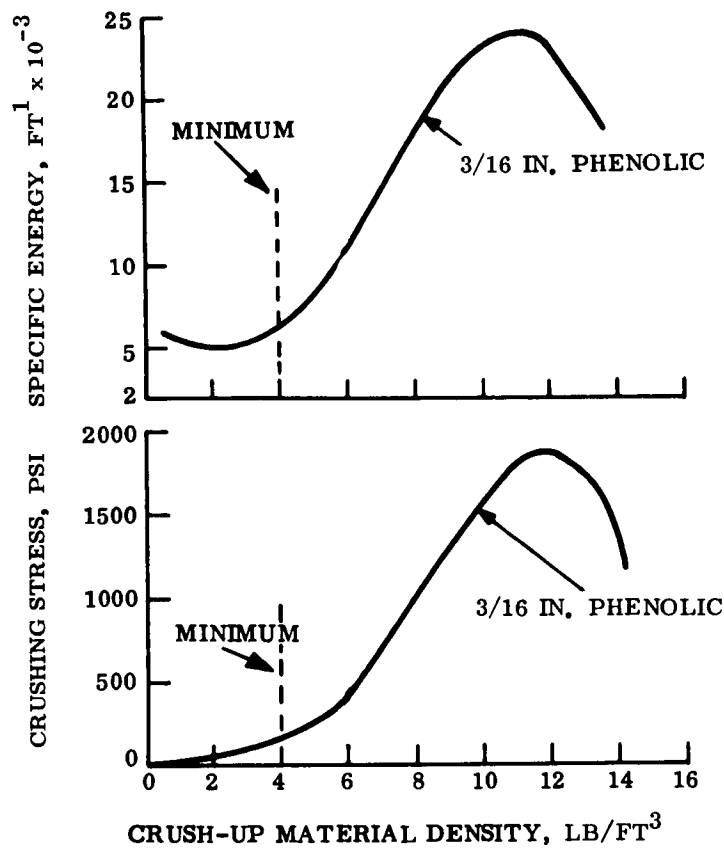


Figure 6.5.8-10. Crushable Honeycomb Properties

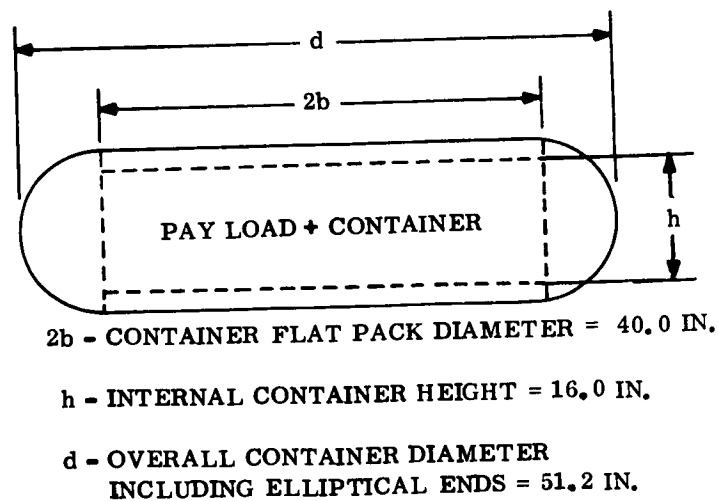


Figure 6.5.8-11. General Internal Geometry for Point Design 4

6.5.8.5 Detailed Design

Another detail in the point designs is the utilization of a face sheet over the honeycomb to encapsulate it. The potential factors which could necessitate this facing are five:

1. Prevention of the honeycomb cells from filling with loose surface debris.
2. Facilitation of sliding. The sliding mechanism is used to absorb the impact velocity component parallel to the surface.
3. Enhancement of the structural integrity of the attenuator.
4. Distribution or spreading of concentrated loads produced by surface protrusions.
5. Confinement of crush-up fragment which might provide an undesirable background for surface measurements.

Experimentation has shown that loose surface (sand, loam, dust, etc.) tend to fill up the impacting cells quite quickly. This filling will interfere with pure crushing action and for this reason is undesirable. However, for surfaces presenting this potential hazard, the major energy absorber is the ground with a reduced amount of honeycomb attenuator crushing or no crush-up at all. From this viewpoint, therefore, the first consideration for a cover may not produce a compelling argument.

The smooth surface presented by a cover would certainly provide better sliding behavior than the exposed open cells of a honeycomb. On anything less than a very hard terrain of low relative roughness this is an important factor. Moreover, in the point design analyses lateral sliding motion are counted on to absorb the horizontal component of the impact velocity vector.

The structural strength of the attenuator is favorably affected by use of a facing plate. The facing lessens the tendency to shear off entire chunks of the attenuator thereby thwarting the desired crush-up behavior. A wrap-around membrane also allows more of the attenuator to participate in the energy absorbing process than if no cohesive member was used.

More important than this last argument, however, a face sheet produces a spreading action of possible localized loads produced by rocks and other surface protrusions. This lessens the possibility of local punctures or intrusions which could circumvent the crush-up process. The spreading of loads is important if the design assumptions are to be reasonably accurate. Moreover, a thin cover protects the outermost cell edges and minimizes local shear deformations which could cause lateral failure produced by the surface friction.

Finally, encapsulation of the honeycomb prevents stray honeycomb fragments from reaching the surface and interfering with surface science measurements and other scientific experiment (alpha back scattering, for example).

If an encapsulation device is used, the determination of its thickness can be made as follows. Strength will not govern the design since the facing is not required to perform a major structural function. Instead the facing must be designed to be sufficiently thin so that it can be contoured to fit the doubly curved Lander geometry. The actual lay-up is a detailed design manufacturing problem. A piece wise lay-up of extremely light gauge material is one possible design choice. The lower limit on gauge is determined by the criteria that the membrane itself must not be so light that it is easily punctured by surface abrasion.

Finally, two other design details remain. First, cross deformation effects are investigated for two conditions. The first is excessive stroke requirements which produce thickness sufficiently large (> 24 in.) to lead to impulsive buckling of the honeycomb cells without crushing behavior. If such strokes are indicated the attenuator is segmented further to eliminate buckling and promote crushing of the attenuator. Second, gross shear failures must also be considered. This possible mode involves the breaking off of an entire piece of material without crushing deformation. Where analysis indicates that gross shear is a possibility, radial metallic strips welded to the payload container can be used to take out the shear in excess of what can be carried laterally by the honeycomb cells. These elements, while resistant to shear, are sufficiently slender that they buckle when impacted along their length and thereby crush-up with the phenolic honeycomb materials.

Past experience indicates that the double curvature introduced in this Lander concept can be wrapped effectively by segmenting the honeycomb into pieces which are then bonded together. In this way the longitudinal axis of the honeycomb cells can be made near-radial with the payload contained structure. The wrapping proceeds around the Lander circumference and then outward until the desired thicknesses are provided.

6.5.8.6 Honeycomb Lander Fabrication

The principal operations involved in the fabrication of the honeycomb crush-up system include the segmenting and cutting of the honeycomb material so that it may be properly oriented, as shown on fig. 6.5.8-12, the bonding of the honeycomb segments to one another, and the bonding of the honeycomb to the aluminum substructure and the external protective covering.

6.5.8.6.1 Adhesive Selection

For proper bond action suitable adhesives must be selected. Adhesive bond systems are required for two distinctly different joints: honeycomb to honeycomb and metal to honeycomb. While these configurations present separate joining problems the bonded joints must nevertheless have the same cure cycle. There are however modified epoxy-phenolic adhesives suitable for temperatures of -200°F to 900°F . A representative example of such a product is the HT 424 adhesive manufactured by the Bloomingdale Department of the American Cyanamid Corporation. These adhesives may be formulated to be r-f transparent as required. The properties of this class of adhesive are such that the bonds formed are stronger than the weakest material comprising the joint. In fact, shear and bending tests will fail the honeycomb interface of the bond.

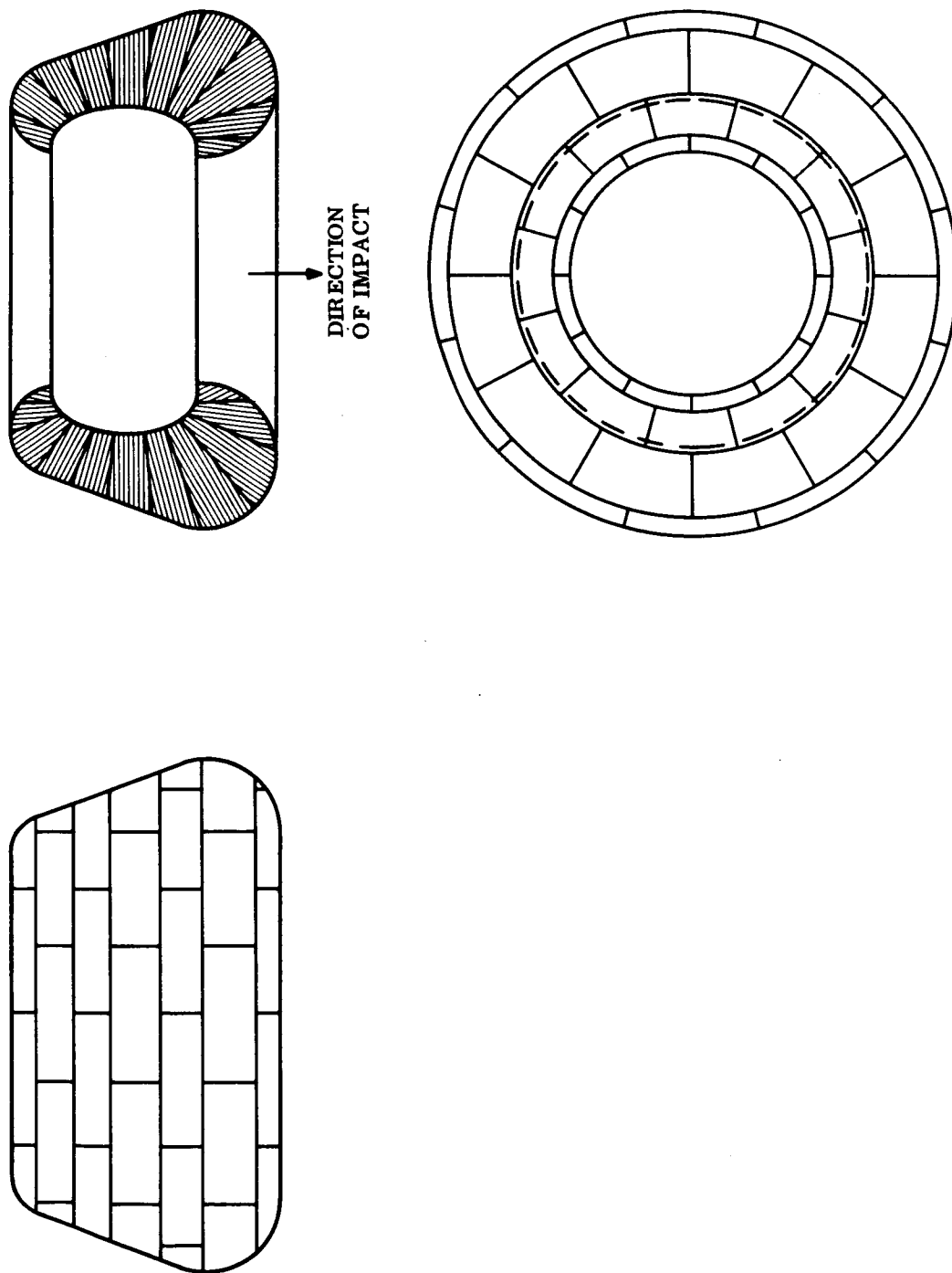


Figure 6.5.8-12. Layout of Honeycomb Attenuator (Multi-directional)

6.5.8.6.2 Honeycomb to Honeycomb Joints

In fabricating the Lander, there are a large number of possible variations at the interface between the honeycomb segments. The selected desirable approach is to bond flat surfaces of honeycomb together utilizing a space - filling adhesive as needed to fill gaps between points contacts.

6.5.8.6.3 Honeycomb to Aluminum Joints

Previous development testing (ref. 6-2) has identified adhesive suitable for bonding phenolic fiberglass honeycomb to aluminum.

Previous GE-MSD efforts have, furthermore, identified adhesives for this bond which have cure cycles compatible with the adhesives used for honeycomb to honeycomb joints. As an example, adhesives of the H424 high-temperature resin family produced by the Bloomington Department of the American Cyanamid Corporation are feasible. (For aluminum to honeycomb joints HT 424 F, in particular, has been tested by GE-MSD as reported in ref. 6-2.)

For honeycomb to honeycomb bonds HT 424 is indicated.

6.5.8.6.4 Tooling and Fixtures

Phenolic fiberglass honeycomb material of the densities used in this Lander point design can be cut to size and shape with moderate ease. Heavier densities or lighter ones should also work well. Standard shop equipment with metal cutting tools may be used throughout.

Tool steel routers and mills may be used, for rough cutting the honeycomb segments a carbide tipped band saw blade is preferred. For final thickness and taper large inertia sanding wheels are used. Specialized wood fixtures can be designed for many of the sizing and contour cutting operations. For curing operations a standard circulating air furnace provides a rotating spit fixture for the assembly cure cycle.

6.5.8.6.5 Lander Fabrication

The Lander fabrication sequence proceeds according to the following steps:

1. Preparation of container structure surface. This includes final finishing to produce proper dimensional tolerances and special treatment of apertures and holes. After all finishing the structure is surface - treated with a chemical reagent (such as Alodine 1200) to promote good adhesive bonding.
2. Preparation of exterior shell inner surface this includes final shaping of the impact attenuator encapsulating structure (skin). This surface is also treated prior to adhesive bonding.

3. The raw honeycomb crush-up material is then rough cut to size with proper attention to the designed lay-up and resultant cell wall orientation.
4. The rough cut surface is then checked for dimensional accuracy and secondary trimming or sanding is performed.
5. A preliminary fit-up of the honeycomb to the subsystems container is made. This is done by using shims to allow for adhesive bond thicknesses.
6. The epoxy adhesive is then prepared according to the manufacturer's specifications.
7. The bonding of the honeycomb segments to the container structure and to one another is then begun. For this purpose a rotating spit device to hold the container, along with the associated jigs and fixtures for temporary support during curing must be used. The exact fixture details must be determined during the manufacturing development period. However, in general, these are wooden forms which can be snapped in and out of position.
8. The assembly, which is now fully mated is subjected to the proper cure cycle determined by the adhesive and also the specified strength level to be attained. The lay-up of the honeycomb is shown in fig. 6.5.8-12.
9. The exterior facing plate is now attached, held in position by jigs, and cured. Because of the double curvature of this element it must be laid up in pieces in a manner comparable to the lay-up of conventional toroidal metallic shells.

6.5.9 MASS PROPERTY AND INERTIA DATA

Following is a summary weight statement for the complete Lander, table 6.5.9-1, and a detailed weight breakdown of the payload subsystems and components, table 6.5.9-2.

TABLE 6.5.9-1. WEIGHT SUMMARY

Lander Systems and Equipment - Point Design 4			Weight (lb)		
<u>Lander Complete</u>					
Structure			180.0		
Attenuation			406.0		
Electric power equipment			160.5		
Telecommunications			80.0		
Environmental control			25.0		
Scientific payload			48.3		
Interface equipment			0.9		
Cables and harness			12.8		
Deployment-cameras			10.0		
Deployment-alpha backscatter			<u>10.0</u>		
			Total 933.5		
C. G. 's ('X' CG Datum- Apex of Heat Shield Cone)			<u>Gross Inertias in Slug/ft²</u>		
<u>X</u>	<u>Y</u>	<u>Z</u>	<u>Roll</u>	<u>Pitch</u>	<u>Yaw</u>
39.0"	0.22"	0.59"	72.3	58.9	58.7

TABLE 6.5.9-2. DETAILED WEIGHT BREAKDOWN,
SUBSYSTEMS AND COMPONENTS

Lander Subsystems	Weight (lb)
<u>Electrical Power Equipment</u>	(160.45)
A101 Battery Operational	67.60
A106 Line, Contactor	2.00
A107 Programmer, Lander	7.20
A108 Regulator, Voltage	7.00
A110 Controller, Power	5.50
A113 Battery, High Rate 'A'	0.50
A114 Battery, High Rate 'B'	0.50
A115 Filter, EMC	1.90
A121 Module, Diode Block	0.20
A124 Module, Thermal Relay	0.15
A128 Switch, Hg 'A'	0.10
A129 Switch, Hg 'B'	0.10
A130 Regulator, Voltage	0.90
A132 Unit Breaker and Limiter	0.60
A133 Panel Solar Cell and Linkage	20.00
A134 Regulator, Charge	7.80
A135 Module, Diode Block	0.50
A136 Mechanism, Drive	4.00
A137 Motor, Stepping	2.00
A138 Connector, Motor	1.30
A150 Motor, Stepping	2.00
A151 Motor, Stepping	2.00
A152 Motor, Stepping	2.00
A153 Panel, Solar Cell and Linkage	20.00
A155 Mechanism, Drive	4.00
A159 Pin Puller	0.30
A160 Pin Puller	0.30

TABLE 6.5.9-2. DETAILED WEIGHT BREAKDOWN,
SUBSYSTEMS AND COMPONENTS (Continued)

Lander Subsystems	Weight (lb)
<u>Telecommunications</u>	(80.0)
A602 Transmitter UHF	2.50
A604 Conditioner, Signal Data	4.00
A605 Antenna, UHF Relay 'A'	1.00
A607 Unit, Memory	5.00
A608 Receiver, UHF Beacon	1.30
A609 Processor, Data Handling	4.00
A610 Circulator, UHF 'A'	0.40
A611 Circulator, UHF 'B'	0.40
A621 Switch, Antenna 'A'	1.00
A623 Antenna UHF Relay 'B'	1.00
A676 Multicoder	5.00
A682A Accelerometer, Impact	0.60
A683 Amplifier, Charge (3)	1.50
A684 Transmitter, S-band	7.00
A685 Antenna, S-band (2)	1.00
A686 Transponder, Exciter	22.00
A689 Antenna, S-band Receiver (2)	0.40
A687 Decoder, Command	5.00
A691 Circulator, S-band (2)	1.40
A697 Altimeter, Radar	15.00
A698 Antenna, Radar Altimeter	0.50
<u>Environmental Control</u>	(25.00)
1 in. Insulation	20.00
Installation Hardware	5.00
<u>Scientific Payload</u>	(48.30)
A807 Accelerometer, Tri Ax	2.00
A808 Transducer, Temp (2)	1.00

TABLE 6.5.9-2. DETAILED WEIGHT BREAKDOWN,
SUBSYSTEMS AND COMPONENTS (Continued)

Lander Subsystems	Weight (lb)
A809 Transducer, Press (2)	1.00
A810 Transducer, Press (2)	1.40
A817 Transducer, Temp (2)	1.00
A822 Camera, Facsimile A	2.00
A823 Camera, Facsimile B	2.00
A824 Camera, Facsimile C	0.40
A825 Camera, Facsimile D	0.40
A829 Sensors, Wind Velocity A-H (8) to	
A836	4.00
A837 Sensor, Moisture	10.00
A838 Spectrometer, Mass	8.00
A841 Inclinator (2)	2.60
A842 Instruments, Surface Comp	9.50
A845 Sensor, Wind Velocity I	0.50
A846 Sensor, Wind Velocity J	0.50
A847 Transducer, Temp	0.50
A848 Transducer, Temp	0.50
A849 Detector, Water Vapor and Moisture	1.00
<u>Interface Equipment</u>	(0.88)
J2002 IFD A/S Lander	0.13
J2003 IFD T/C Lander	0.75
<u>Cable Assembly</u>	(12.80)
WL1 Cable Assembly, Command	2.10
WL2 Cable Assembly, Power	3.70
WL3 Cable Assembly, Instr	3.00
WL4 Cable Assembly, Shield	0.80
WL5 Cable Assembly, Power	2.70
WL6 Cable Assembly, Co-Ax	0.50

6.6 CONSTRAINTS IMPOSED ON ORBITER

The majority of constraints imposed by the flight Capsule on the Orbiter are relatively independent of the mode of Capsule entry (direct or orbital) and the size and weight of the Capsule. Addition of the flight Capsule however requires mechanical and electrical interfaces between the Orbiter and the Capsule. Fig. 6.6-1 shows the Capsule adapter which will provide the mechanical interface. In this study, it has been assumed that the MM '71 Orbiter will be modified for the combined Orbiter and Hard Lander mission in 1973. MM '71 is itself an adaption of the MM '69 flyby Spacecraft. A complete description of the MM '73 Orbiter is contained in Appendix D of this volume. Table 6.6-1, excerpted from the appendix, highlights the major changes required of the MM '69 subsystems for conversion to an Orbiter in MM '71', and then to a Capsule bus (as well) in MM '73. No other changes are required of the Orbiter to accommodate this specific Capsule point design.

TABLE 6.6-1. MAJOR SUBSYSTEM CHANGES

MM'69 Subsystem	Change for MM '71 Orbiter	Change for MM '73 Capsule
Power	<ul style="list-style-type: none"> • Solar Array Increase 	<ul style="list-style-type: none"> • Solar Array Increase
Radio	<ul style="list-style-type: none"> • New Maneuver Antenna • New High Gain Antenna • Modified Low Gain Antenna 	<ul style="list-style-type: none"> • New Maneuver Antenna • New High Gain Antenna • New Relay Receiver • New Relay Antennas
Attitude Control	<ul style="list-style-type: none"> • Cold Gas and Jet Size Increase • Modification of Autopilot Electronics 	<ul style="list-style-type: none"> • Cold Gas and Jet Size Increase • Modification of Autopilot Electronics • Relocated Sun Sensors • Possible Approach Guidance
Data Storage	<ul style="list-style-type: none"> • Additional Air • Additional DTR 	<ul style="list-style-type: none"> • New Relay Recorders
Command	<ul style="list-style-type: none"> • Possible Decoder Expansion 	<ul style="list-style-type: none"> • Probable Decoder Expansion
Telemetry		<ul style="list-style-type: none"> • Data Modes for Capsule Telemetry
Scan Control	<ul style="list-style-type: none"> • Removal of Mars Gates 	
Science	<ul style="list-style-type: none"> • Passive Cooling of IRS • Possible TV Field of View Changes 	No Estimate
Cabling		<ul style="list-style-type: none"> • Three Inflight Disconnects
Mechanical Devices	<ul style="list-style-type: none"> • High Gain and Maneuver Antenna Deployment • High Gain Antenna Articulation • Modified Separation Mechanics 	<ul style="list-style-type: none"> • Spacecraft Separation Mechanics • Modified Orbiter Separation Mechanics • New High Gain Antenna Deployment
Propulsion	<ul style="list-style-type: none"> • New 	<ul style="list-style-type: none"> • New Tanks and Supports for (Orbital Entry Capsule)
Structure	<ul style="list-style-type: none"> • Strengthened Adapter 	<ul style="list-style-type: none"> • Capsule Adapter • Spacecraft Adapter • Strengthened Octagon for (Orbital Entry Capsule)

6.7 PROBABILITY OF SUCCESS - POINT DESIGN 4

6.7.1 INTRODUCTION

A key factor in evaluating a design concept is the determination of the probability of success of the configuration. This determination is primarily beneficial at the early concept design state in performing tradeoff evaluations of several potential design configurations. As the design evolves from conceptual towards final, the merit of the quantitative value shifts from comparative to predictive.

A probability of success determination was performed for the conceptual mission as defined by Capsule Point Design 4. Due to the early stage of the design, it was necessary to perform this determination based on many assumptions. These are listed below. In general, it can be stated that failure rate data was based on information known concerning components of similar generic or complexity definition. It was also assumed that the new development items required for this mission will be developed, tested, and qualified before being flown.

Due to these assumptions, and the uncertainty of sterilization influence on some of the components, the predictive value of the determination may not be accurate. However, since the same assumptions and methodologies were used on all determinations during the study, the comparative value of the determinations are significant.

6.7.2 RESULTS

Probability of success values were determined for both the capsule systems and for the Booster and Orbiter systems of the mission. The procedures used in performing these determinations are presented in Sections 6.7.3 and 6.7.4 below. A summary of the determinations, by major mission phase, is shown in table 6.7.2-1.

This tabulation indicates that the value obtained, under the study ground rules stated in the preceding paragraph for the probability of success of the total mission is 0.412. This is the probability of obtaining proper functioning of all mission equipment, as required, for the duration of the mission from launch to completion of the 90 day mission on the Martian surface.

TABLE 6.7.2-1. MISSION SUCCESS PROBABILITY, POINT DESIGN 4

Mission Phase	Booster and Orbiter		Capsule		Combined	
	Phase	Cumulative	Phase	Cum.	Phase	Cum.
Launch/Cruise	.807	.807	.958	.958	.773	.773
Separation & Entry	.998	.805	.949	.909	.947	.732
Orbit Achievement	.989	.796		.909	.989	.724
Landed Operation	.997	.794	.572	.520	.570	.412

6.7.3 CAPSULE ANALYSIS

This section presents the procedure followed in analyzing the Mars Hard Lander System Point Design for the probability of successfully accomplishing its intended functions.

6.7.3.1 Assumptions

The assumptions and ground rules used in the analysis were as follows:

1. A component would not fail under non-operating conditions.
2. The probabilities of success of all components were considered to be statistically independent. This permitted the use of the product rule for assessing the system and subsystem success probabilities. In the case of redundant application, the above ground rule applied to the component function.
3. The success probability of the structure, aeroshell and impact attenuation was assumed equal to unity (1.0).
4. The probability of success of the system or its components was defined as being equal to the probability of zero (0) functional failures.
5. The mission phases and time of each phase upon which the analysis was based are as follows:

<u>Phase</u>	
Launch/Cruise	3,936 hours
Pre-entry	24.1 hours
Entry	0.16 hours
Landed Operation	90 days

6. The assessment for the success probability of a component during any given phase reflects only the time during the phase in which it operates.
7. If any portion of a component operated during a particular phase the entire component was assessed for its success probability.
8. The success probability of the various system components was based on failure data of components which were similar or identical in function or of equivalent complexity.

6.7.3.2 Procedure

6.7.3.2.1 Component Success Probability

The probability of success of time (or cycle) sensitive components was obtained using the following expression:

$$R_c = e^{-\lambda t} \quad (1)$$

where:

R_c = probability of success

λ = Failure rate in failures/hour (or cycle)

t = Operating time (hours) or cycles

For redundant application of a component, the following expression was used to obtain the probability of success of the function:

$$R = [1 - (1 - R_c)^n] \quad (2)$$

where:

R = probability of success of the function

R_c = probability of success of the component

n = number of components in the redundant group.

For components which are not time (or cycle) sensitive, such as squib valves, the success probability reflects the results of successes versus trials using appropriate statistical techniques.

6.7.3.2.2 Subsystem Success Probability

The probability of success of a subsystem for any given phase was obtained using the following expression:

$$R (S/S)_p = \pi_i R_i \quad (3)$$

where:

$R (S/S)_p$ = probability of success of the subsystem in the phase

R_i = probability of success of the i^{th} component or function (for redundant application) for the phase being considered

π = symbol for product

The probability of success of a subsystem over its entire mission was obtained using the following expression.

$$R (S/S)_M = \pi_j R (S/S)_j \quad (4)$$

where:

$R (S/S)_M$ = probability of success of the subsystem over the mission

$R (S/S)_j$ = probability of success of the subsystem for the j^{th} mission phase

6.7.3.2.3 System Success Probability

The probability of success of the system for any given phase was obtained using the following expression.

$$R (\text{System})_p = \pi K R (S/S)_k \quad (5)$$

where:

$R (\text{System})_p$ = probability of success of the system in the phase

$R (S/S)_k$ = probability of success of the k^{th} subsystem for the phase being considered

The probability of success of the system over the entire mission was obtained using the following expression.

$$R (\text{System})_M = \pi_k R (S/S)_{M_k} \quad (6)$$

where:

$R (\text{System})_M$ = probability of success of the system for the mission

$R (S/S)_{M_k}$ = probability of success of the k^{th} subsystem for the mission

6.7.3.2.4 Orbiter Support Analysis

The probability of success of the Mars Hard Lander for the i^{th} mission phase, reflecting the success probability of the booster and spacecraft (in support of capsule operations) and the Capsule system is given by:

$$R (\text{MHL})_i = R (\text{Booster})_i \bullet R (\text{Spacecraft})_i \bullet R (\text{Capsule})_i \quad (7)$$

The cumulative probability of success of the Mars Hard Lander for the i^{th} mission phase is given by:

$$> R (\text{MHL}; \text{cumulative}) = \pi \prod_{i=1}^i R (\text{MHL})_i \leq \quad (8)$$

where:

$R(\text{MHL})_{i-1}$ = independent probability of success of the MHL for the $(i-1)^{\text{th}}$ phase as obtained from eq 7

$R(\text{MHL})_i$ = independent probability of success of the MHL for the i^{th} phase as obtained from eq 7

The cumulative success probability for each of the systems are similarly obtained from eq 8

6.7.3.3 Results

6.7.3.3.1 Component Success Probabilities

The success probability for the components (or functions in the case of redundant applications) comprising Point Design 4 for the Mars Hard Lander System is summarized in table 6.7.3-1 for each of the mission phases described in para 6.7.3.1.

The values appearing in the table were computed using expressions eq 1 or eq 2 described in para 6.7.3.2 as applicable, for time (or cycle) sensitive components. These values reflect failure rate data from the sources indicated in the table. Non-time (or cycle) sensitive component success probabilities were obtained directly from the indicated source.

6.7.3.3.2 System and Subsystem Success Probabilities

The success probabilities for the subsystems and system which define Point Design 4 are summarized in table 6.7.3-2 for each of the phases described in para 6.7.3.1 and the total mission. The values appearing in the table were obtained using eq. 3 through 6 described in para 6.7.3.2.

6.7.3.4 Redundancy Considerations

A Failure Mode Effects Analysis (FMEA) was performed as part of the Capsule analyses. Due to the conceptual state of the mission design, this was performed on a qualitative rather than a quantitative basis. The primary purpose of this analysis was to point out potential problem areas for redundancy considerations.

During the FMEA, it was learned that the items that had the greatest criticality and risk of failure were the canister heater and thermostat and the operational battery. The former were of high risk due to the long duty cycle during the interplanetary cruise. The latter was critical due to its requirement to perform all Capsule operations. Redundancy inclusions were provided for these items; a standby parallel thermal control system and internal cell redundancy in the battery.

TABLE 6.7.3.1. RELIABILITY ESTIMATES, POINT 4 DESIGN COMPONENTS.

Description	Reliability				Data Source
	Launch & Cruise	De-orbit	Entry	Landed Operation	
<u>EP&D Subsystem</u>					
Battery, Operational (1)	-	.9999	.9997	.9823	ERSR-TT Program
Battery, Entry (Dual)	-	.9999	-	-	↓
Battery, T/C (Dual)	-	.9999	-	-	REA-MBRV Program
Programmer, Lander (1)	-	.9999	.9944	.9137	RFMA-MK12 Program
Regulator, Voltage, A (1)	-	.9999	.9999	.9998	↓
Regulator, Voltage, B (1)	-	.9999	.9999	.9960	REA-Voyager Study
Regulator, Voltage, C (1)	.9999	.9999	-	-	RFMA-TT Program
Regulator, Charge (1)	.9999	-	-	-	↓
Module, Diode Block (2)	-	.9998	-	-	ERSR-TT Program
Module, Diode Block (1)	-	-	.9999	-	REA-MK12 Program
Battery, HR (Dual)	-	-	.9999	.9999	RFMA-TT Program
Module, Power Distribution	-	.9999	-	-	↓
Filter, EMC, A (1)	-	.9999	-	-	ERSR-TT Program
Filter, EMC, B (1)	-	.9999	-	-	REA-MK12 Program
Filter, EMC, C (1)	-	-	.9999	.9999	RFMA-TT Program
Module, Thermal Relay (2)	-	.9998	-	-	↓
Module, Thermal Relay (1)	-	-	.9999	.9999	ERSR-TT Program
Battery, Dual	.9999	.9999	-	-	REA-MK12 Program
Power Control, C	.9999	.9999	-	-	↓
Power Control, L	-	.9999	.9999	.9991	RFMA-TT Program
Programmer, Dual, C	-	.9999	-	-	FARADA
Switch, Hg (Dual)	-	-	-	.9999	FARADA
Switch, Breaker and Limit	-	.9999	-	-	REA-MBRV Program
Switch, Power Transfer	.9999	-	-	-	REA-Voyager Study
Solar Cell, Panel (2)	-	-	-	.9851	↓
Regulator, Charge, L (1)	-	-	-	.9987	RFMA-TT Program
Module, Diode Block	-	-	-	.9619	FARADA
Motor, Stepping (3)	-	-	-	.9999	↓
Controller, Motor	-	-	-	.9995	RFMA-MK12 Program
<u>Telecommunication Subsystem</u>					
Transmitter, UHF	-	.9998	.9999	.9997	↓
Conditioner, Signal Data	-	.9999	.9999	.9999	FARADA
Antenna, UHF (2)	-	.9999	.9999	.9999	↓
Core, Memory	-	.9999	.9999	.8782	RFMA-MK12 Program
Processor, Data	-	.9999	.9999	.9946	FARADA
Circulator, UHF (2)	-	-	.9999	.9999	↓
Communicator, Cruise	.9999	-	-	-	RFMA-MK12 Program
Switch, Antenna (2)	-	-	-	.9989	FARADA
Receiver, Beacon, UHF	-	-	-	.9813	↓
Sensor, Temperature (18)	.9961	.9982	-	-	RFMA-MK12 Program
Sensor, Pressure (8)	.9982	.9992	-	-	FARADA
Sensor, Linear Velocity (12)	.9988	.9988	-	-	↓
Conditioner, Firing Circuit (1)	.9999	.9999	-	-	RFMA-MK12 Program
Sensor, Power Supply	.9999	.9999	-	-	MIL HDBK-217A

TABLE 6.7.3-1. RELIABILITY ESTIMATES, POINT DESIGN 4
COMPONENTS (Cont'd)

Description	Reliability				Data Source
	Launch & Cruise	De-orbit	Entry	Landed Operation	
<u>Telecommunication Subsystem</u>					
Conditioner, Signal, C	.9999	.9999	-	-	RFMA-MK12 Program ↓ MIL HDBK-217A Accelerometer est. Sep. Switch est. RFMA-MK12-est. PCM est-MBRV Strain Gage est. FARADA ↓ ↓ FARADA ↓ FARADA ↓ MIL-HDBK-217A } MK12 } RFMA ↓ MIL-HDBK-217A ↓ FARADA ↓
Amplifier, Charge (3)	-	-	-	.9934	
Sensor, Voltage Regulator	.9999	-	-	-	
Detector, Separation Load (2)	-	.9999	-	-	
Indicator, A/S Rel (2)	-	.9999	-	-	
Conditioner, Linear Velocity Data	.9999	-	-	-	
Multicoder	-	.9999	.9999	.9999	
Sensor, Link Tensile (4)	.9996	-	-	-	
Impact Accelerater	-	-	.9999	-	
Transmitter, S-Band	-	-	-	.9892	
Antenna, S-Band Transmitter (2)	-	-	-	.9910	
Transponder/Exciter	-	-	-	.9892	
Decoder, Command	-	-	-	.9925	
Antenna, S-Band Receiver (2)	-	-	-	.9910	
Circulator, S-Band (2)	-	-	-	.9964	
Altimeter, Radar	-	-	.9998	-	FARADA ↓ FARADA ↓ FARADA ↓ MIL-HDBK-217A } MK12 } RFMA ↓ MIL-HDBK-217A ↓ FARADA ↓
Antenna, Radar	-	-	.9999	-	
<u>Scientific Payload Subsystem</u>					
Transducer, Temperature, A (4)	-	-	.9997	-	
Transducer, Temperature, L (4)	-	-	-	.9935	
Transducer, Pressure, A (6)	-	-	.9996	-	
Transducer, Pressure, L (1)	-	-	-	.9984	
Accelerometer, Tri-Axial (1)	-	-	.9983	-	
Camera, Facimile (4)	-	-	-	.9835	
Sensor, Wind Velocity (10)	-	-	-	.9248	
Sensor, Moisture (1)	-	-	.9999	.9925	
Spectrometer, Mass (1)	-	-	.9997	-	
Inclinometer (1)	-	-	-	.9779	
Surface Comp (1)	-	-	-	.9960	
<u>Electrical Interface</u>					FARADA ↓ FARADA ↓ FARADA ↓ MIL-HDBK-217A } MK12 } RFMA ↓ MIL-HDBK-217A ↓ FARADA ↓
IFD, Cap - S/C	.9988	-	-	-	
IFD, A/S - Lander	.9988	.9999	.9999	-	
IFD, T/C - Lander	.9988	.9999	-	-	
Safe-Arm, Lander	.9988	.9999	.9999	.9999	
Safe-Arm, Aeroshell	.9988	.9999	-	-	
Safe-Arm, Canister	.9988	-	-	-	
Fitting, Coax Data	.9998	-	-	-	
Fitting, Coax Intfc	.9998	-	-	-	
Fitting, Coax VHF	.9998	-	-	-	
<u>Thermal Control S/S</u>					FARADA ↓ FARADA ↓ FARADA ↓
Heater	.9846	.9999	-	-	
Thermostat	.9770	.9999	-	-	
Motor, Louver Dr	-	-	-	.9978	
Unit, Temperature Control	-	-	-	.9889	
Element, Temperature Detector	-	-	-	.9820	

TABLE 6.7.3-1. RELIABILITY ESTIMATES, POINT DESIGN 4
COMPONENTS (Cont'd)

Description	Reliability				Data Source
	Launch & Cruise	De-orbit	Entry	Landed Operation	
<u>Pressurization & Venting S/S</u>					
Valve, Vent	.9999	-	-	-	FARADA
<u>Separation S/S</u>					
Release, Hot Wire (4)	-	.9996	-	-	RFMA-MK12 Program
Nut, Explosive (4)	-	.9894	-	-	FARADA
Nut, Explosive (4)	-	.9894	-	-	↓
<u>Attitude Control & Propulsion S/S</u>					
Tank, N ₂	.9995	.9999	-	-	FARADA
Valve, Squib (8)	-	.9999	-	-	↓
Valve, Fill	.9994	.9999	-	-	↓
Tank, Hydrazine	.9995	.9997	-	-	↓
Disc, Burst	.9999	.9999	-	-	↓
Valve, Solenoid	-	.9999	-	-	↓
Gyro Rate	-	.9993	-	-	↓
Amplifier	-	.9997	-	-	↓
Detector, Threshold	-	.9994	-	-	↓
Generator RR	-	.9996	-	-	↓
Switch	-	.9995	-	-	↓
Rocket, Retro	-	.9999	-	-	↓
Ejector, Nozzle	-	.9975	-	-	FARADA
<u>Retardation S/S</u>					
G-Switch	-	-	.9991	-	MBRV Program
Mortar, Drouge	-	-	.9999	-	↓
Fitting, Main Release (3)	-	-	.9997	-	↓
Fitting, Drogue Release	-	-	.9999	-	↓
Switch, Impact	-	-	.9999	-	↓
Assembly, Parachute	-	-	.9999	-	↓
<u>Legend</u> RFMA - Reliability Figure of Merit Analysis REA - Reliability Estimate Analysis ERSR - Equipment Reliability Status Report					

TABLE 6.7.3-2. RELIABILITY SUMMARY, PD 4 CAPSULE SYSTEM AND SUBSYSTEM

Subsystem	Mission Phase				
	Launch & Cruise	De-orbit	Entry	Landed Operation	$R_M = \pi R_P$
EP & D	.9995	.9981	.9904	.8434	.8332
Attitude Control and Propulsion	.9977	.9934	-	-	.9911
Pressure and Venting	.9999	-	-	-	.9999
Separation	-	.9784	-	-	.9784
Telecommunications	.9921	.9950	.9988	.8038	.7925
Thermal Control	.9740	.9998	-	.9689	.9435
Scientific Payload	-	-	.9972	.8721	.8696
Retardation	-	-	.9984	-	.9984
Electrical I/F	.9949	.9996	.9998	.9996	.9939
$R_P = \pi R (S/S)$.9586	.9646	.9846	.5724	.5216

In addition to these items, many other redundancy inclusions are provided in the Capsule design. A typical listing of some of these inclusions together with the type of redundancy used is shown below. Other redundancy provisions such as backup gate or switching signals and backup time signals are also provided but not included in the listing.

<u>Item</u>	<u>Type Redundancy</u>
Operational Battery	Internal
Canister Heater and Thermostat	Parallel
Dual Battery	Internal
Thermal Batteries	Parallel
Programmer - Lander	Internal
Charge Regulator	Internal
Blocking - Module	Internal
Power Distribution Module	Internal
Therm. Relay Module	Internal
Dual Programmer	Internal
Hg Switch	Parallel
Unit, Breaker and Limit	Internal
Spin Initiator	Parallel Squibs
Despin Initiator	Parallel Squibs
Rocket Initiator	Parallel Squibs
Temperature Transducers	Parallel
Pressure Transducers	Parallel
UHF Antenna	Parallel

6.7.4 ORBITER SUPPORT ANALYSIS

6.7.4.1 Introduction

Probability of success determinations for the booster and Orbiter systems were performed for those functions which support and/or contribute to the success of the Capsule and its mission. Flight operations were based on a direct entry reference mission with a flight time of 164 days.

6.7.4.2 Assumptions

The assumptions made and the ground rules followed in the analysis were as follows:

1. Only those functions required for the success of the Capsule missions were included.
2. The Orbiter is assumed to use 1971 equipment hardware with only minor modifications.
3. The spacecraft support is required for 3 days of the landed mission.

4. The reliability or criticality of the ground support functions have not been included in the study.

6.7.4.3 Procedure and Data Sources

In arriving at the reliability estimates, the tools and failure rate data bases developed during the Voyager Task C redundancy and Task D Design studies conducted for JPL, as modified by more recent studies, were used. These procedures are described in detail in the reference documents shown in Section 6.8. In summary, these can be stated as follows:

1. Minuteman level parts and Minuteman and Apollo failure rates were used to the greatest extent possible.
2. Curves developed during the studies showing the projected reliability growth for inertial components and integrated circuits were used.
3. Factors to reflect (1) parts reliability growth and (2) upgrading to a high reliability status were used to obtain failure rates for sources other than Minuteman and Apollo.
4. Where failure rate data was lacking, or inadequate, failure rates were derived by comparing the part in question with another part of similar construction or performance for which reliability information was available.

6.8 REFERENCES

- 6-1 R-F transparent, Energy Absorbing, Structural Elements, Phase II Final Report, Prepared for JPL under Contract No. 950964, Aug. 1964, GE-MSD, Doc. No. 64SD4329.
- 6-2 Development of Energy Dissipating Plastic Honeycomb, Quarterly Progress Report Nos. 7 and 8, Contract No. 951172, JPL, GE-MSD Doc. No. 66SD4390.
- 6-3 Failure Rate Data Base for Spacecraft Redundancy Study, VOY-C3-TR8.
- 6-4 Reliability Characteristics of Voyager Components - Voyager Spacecraft Redundancy Study, VOY-C3-TR7.
- 6-5 Voyager Final Report, Phase IA, Task C, Volume 4, Application of Redundancy Study, July 28, 1967. VOY-CO-FR, prepared for JPL under contract 951112.
- 6-6 Voyager Spacecraft Final Report, Phase B, Task D. Volume II (Book 1 of 5), Systems Description, October 2, 1967, under contract NAS 8-22603.